FINAL REPORT

Storm Bay Biogeochemical Modelling and Information System

Supporting sustainable aquaculture in Tasmania.
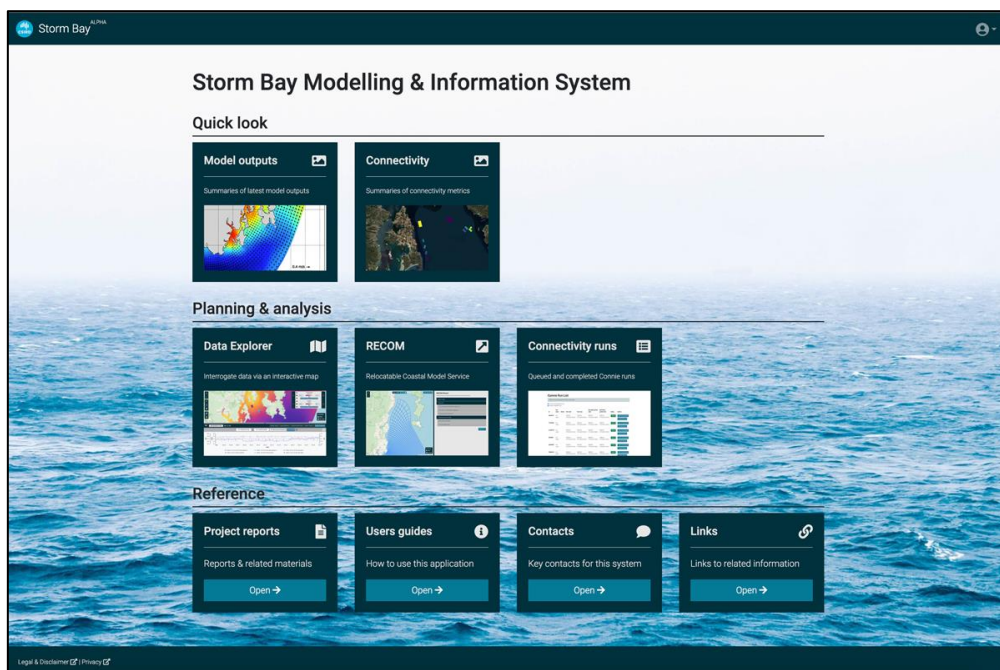
Karen Wild-Allen, John Andrewartha, Mark Baird, Jack Beardsley, Elizabeth Brewer, Lev Bodrossy, Ruth Eriksen, Rob Gregor, David Griffin, Mike Herzfeld, David Hughes, Pete Jansen, Clothilde Langlais, Nugzar Margvelashvili, Andrew Martini, Merinda McMahon, Andrew Revill, Farhan Rizwi, Jenny Skerratt, Cassie Schwanger, Kendall Sherrin, Sascha Frydman, Dan Wild.

March 2023

ISBN **[Insert ISBN/ISSN – researcher to obtain]**

Storm Bay Biogeochemical Modelling and Information System: supporting sustainable aquaculture in Tasmania
FRDC Project No. 2017-215

March 2023

Ownership of Intellectual property rights

Creative Commons licence

Disclaimer

The authors do not warrant that the information in this document is free from errors or omissions. The authors do not accept any form of liability, be it contractual, tortious, or otherwise, for the contents of this document or for any consequences arising from its use or any reliance placed upon it. The information, opinions and advice contained in this document may not relate, or be relevant, to a reader's particular circumstances. Opinions expressed by the authors are the individual opinions expressed by those persons and are not necessarily those of the publisher, research provider or the FRDC.

The Fisheries Research and Development Corporation plans, invests in and manages fisheries research and development throughout Australia. It is a statutory authority within the portfolio of the federal Minister for Agriculture, Fisheries and Forestry, jointly funded by the Australian Government and the fishing industry.

CSIRO advises that the information contained in this publication comprises general statements based on scientific research. The reader is advised and needs to be aware that such information may be incomplete or unable to be used in any specific situation. No reliance or actions must therefore be made on that information without seeking prior expert professional, scientific and technical advice. To the extent permitted by law, CSIRO (including its employees and consultants) excludes all liability to any person for any consequences, including but not limited to all losses, damages, costs, expenses and any other compensation, arising directly or indirectly from using this publication (in part or in whole) and any information or material contained in it. CSIRO is committed to providing web accessible content wherever possible. If you are having difficulties with accessing this document please contact csiroenquiries@csiro.au

Researcher Contact Details		FRDC Contact Details	
Name:	Dr Karen Wild-Allen	Address:	25 Geils Court
Address:	CSIRO Oceans & Atmosphere, GPO Box 1530, Hobart		Deakin ACT 2600
Phone:	+61 3 6232 5222	Phone:	02 6122 2100
Fax:	+61 3 6232 5000	Email:	frdc@frdc.com.au
Email:	Karen.wild-allen@csiro.au	Web:	www.frdc.com.au

Contents

Acknowledgments

Further details of data agreements in place are included in Appendix A1.

Executive summary

The objectives of the FRDC 2017-215 project Storm Bay Modelling and Information System were to:

1. Evaluate the performance of the existing hydrodynamic model of Storm Bay

2. Characterise the primary sources of nutrients into Storm Bay from ocean currents, sediment resuspension, river inputs.

3. Deliver a validated model of water quality in Storm Bay suitable for assessing future salmon farm expansion.

4. Provide an information system comprising model results, observations, and synthesis analyses, with links to parallel projects (e.g. monitoring program, decision support tools, seasonal predictions).

This final technical report documents the project achievements in detail and is accompanied by 8 Appendices of supplementary information and analysis.

Hydrodynamic Model

The CSIRO hydrodynamic model STORM developed in 2009-2011 has been assessed against observations with a detailed report provided to stakeholders in December 2018. The model was found to reproduce the main dynamical structure including seasonal warming, cooling, stratification and mixing although overall there was a warm and fresh bias in the model results. Surface river plumes were too diffuse in winter and too stratified in summer; their spatial extent was approximately correct, but their seaward trajectory was sometimes inaccurate. Non-tidal variability of sea level was greater than observed and intrusions of ocean water were not always well modelled. The most significant error appeared to be the fresh (low salinity) bias, although this did not appear to cause large errors in the residual circulation.

In this project the former Storm Bay model (STORM) has been updated with a new model grid (TASSE) to meet stakeholders needs (35 vertical layers from 0.5m at the surface to 20m at depth; 200-300m spatial resolution around the Acteon Islands, Port Arthur, Fredrick Henry Bay, and the Derwent and Huon Estuaries; ocean boundary ~50km south of Storm Bay) and accurately resolve the key hydrodynamic processes impacting water quality in Storm Bay.

The new Storm Bay (TASSE) hydrodynamic model has been calibrated using observations collected in the hindcast period 2014-16. The model reproduces observed mooring, glider, and remotely sensed observations with a high degree of skill; observed variation in sea level are also well simulated indicating accuracy in the simulation of local currents and circulation. Complex mesoscale eddies and filaments of offshore water enter Storm Bay particularly from the East Australia Current (EAC) system in summer, and on occasion, the simulated position of a local front may be offset in space and time. Neighbourhood techniques have therefore been employed in the calibration procedure which demonstrates the model to have a good skill, sufficient for the simulation of sediment transport and biogeochemical processes. The calibrated hydrodynamic model run was extended to 2021 for further validation against additional independent observations, analysis of connectivity and reinitialization of the near real time model. Outputs necessary for sediment transport and biogeochemical model simulations have been made available and final production runs are complete. Hindcast and near real time hydrodynamic model results are currently displayed on the Storm Bay Modelling & Information System Dashboard.

Connectivity analysis for the Storm Bay area shows a coherent circulation eastwards with flow from the Huon directed mostly north through the D'Entrecasteaux Channel and joining Derwent flow to form a strong jet travelling southeast across Storm Bay and around the southern tip of the Tasman Peninsula. Less often, flow from the Huon travels southeast and around the southern tip of Bruny Island. Flows are stronger in winter whilst in summer three water masses (coastal water, EAC, sub-Antarctic) create highly variable frontal regions in the bay. EAC water enters Storm Bay intermittently as sub-mesoscale turbulent eddies move southwest past Tasmania. Sub-Antarctic water enters the mouth of the bay from the southeast and can form deep water intrusions under the EAC eddies. Flushing analysis, passive tracer release studies and age tracers all show longer residence times for tracers released in Port Arthur, Nubeena, and Fredrick Henry Bay.

Sediment Model

The CSIRO sediment model has been configured to resolve mud, sand, gravel, and bedrock (rocky reef) over the upper 1 m of bottom sediment (1cm of bedrock) in 12 vertical layers. Data from the Geoscience Australia Marine Sediment database (MARS) and the Derwent Estuary field programs has been sourced to partition the 3 sediment size classes into carbonate and mineral fractions and initialise the model. The sediment model simulates the resuspension, settling and benthic processes including consolidation, pore water dynamics and bioturbation for all particulate components in the sediment and biogeochemical model. The sediment transport is driven by waves and currents simulated by the hydrodynamic model (SHOC) and the wave model (SWAN - Simulating WAves Nearshore). The SWAN model has been implemented for Storm Bay to adequately resolve the inshore wave field modified by the coast and reproduces the observed wave field with a high level of accuracy. For model calibration, observed turbidity and backscatter from the lander deployments were scaled against lab analysed samples of total suspended solids. The sediment model was able to reproduce the timing and magnitude of observed resuspension events at the lander sites, particularly those associated with stormy weather. Observed turbidity due to biological activity, local sources of sediment unresolved by the model or advection of stochastic patchiness was not always well reproduced. The near real time model has been updated to include the sediment model and hindcast and near real time wave and sediment model results are available on the Storm Bay Modelling & Information System Dashboard.

Sediment model results show that bottom shear velocity is greatest along coastlines exposed to ocean waves, particularly in winter months, due to storms and ocean-swell. Inside estuarine channels and coastal embayments, bottom shear velocity is lower and, in winter is lower than in summer. Simulated sediment mobility maps are consistent with the distribution of the bottom shear stress. The lowest probability of sediment resuspension occurred within estuarine channels, inside coastal embayments and behind land features that provided shelter from ocean swell. A map of cumulative erosion shows plausible broadscale features but is aliased at small scales by variation in the thickness of the bottom water column layer with bathymetry. The model shows high levels of suspended sediment concentration in the upper reaches of the estuaries, inside Fredrick Henry Bay, and in shallow coastal regions of Storm Bay. Catchment loads contributed to suspended sediments in the Derwent and Huon Estuaries, in the northern part of the Storm Bay, in North-West Bay and in the southern part of the D'Entrecasteaux Channel.

Biogeochemical Model

The CSIRO biogeochemical model resolves the cycling of carbon, nitrogen, phosphorous and dissolved oxygen through multiple phytoplankton, zooplankton, macrophyte, detritus and dissolved organic and inorganic nutrient pools. Recent innovations in the biogeochemical model include the resolution of inorganic carbon chemistry for investigations into ocean acidification and the inclusion of spectral optics

for direct comparison of simulated sea leaving radiance with remotely sensed sea surface colour. Boundary conditions for the Storm Bay biogeochemical model were generated from statistical relationships of observed nutrients and water mass properties matched to simulated hydrodynamic conditions on the model boundary. Spatially and temporally resolved plankton concentrations on the model boundary were estimated from remotely sensed ocean colour. The input of biogeochemical concentrations from rivers, anthropogenic point source loads from wastewater treatment plants, industry outfalls and fish farms were estimated from observations and discharge compliance data. The biogeochemical model runs at ~52:1 (52 model days in 1 real day) with all forcing data available for the hindcast period Dec 2014 - May 2020. The model transitioned to a pilot near real time deployment in mid-2020 which defaults to repeated cycles of biogeochemical variable concentrations in rivers, and discharge loads of sewerage, industry outfalls and fish farms (currently from the year 2020 in the absence of more up-to-date data).

The biogeochemical model hindcast was quantitatively assessed against satellite ocean colour, glider observations, in-situ monitoring data and benthic lander observations. The model reproduced the observed interannual, seasonal and event scale variability in dissolved inorganic nutrients, plankton, dissolved oxygen and optical conditions with mostly good or very good statistical skill. Observed spatial gradients (including vertical distributions) were also well simulated. Simulated levels of denitrification, broadscale nutrient ratios, sediment distributions of organic matter and macrophyte distributions were consistent with literature values and current expert knowledge. The biogeochemical model was deemed fit for the purpose of simulating the water quality in Storm Bay for assessing future salmon farm expansion and to characterise the primary sources of nutrients into Storm Bay from ocean currents, sediment resuspension, river and anthropogenic inputs.

The biogeochemical model hindcast demonstrated that regional water quality varies considerably from year to year due to variation in river outflow and the influx of nutrient rich ocean water. In Storm Bay peak surface nitrogen occurred in winter due to seasonally high river discharge and anthropogenic inputs; in summer surface nitrogen tended to zero due to plankton and macrophyte uptake. Nitrogen concentrations in bottom water were augmented by the influx of sub-Antarctic ocean water in summer, during intrusion events associated with passing EAC eddies, and in late winter following the relaxation of the Zeehan Current. The model simulated a spring phytoplankton bloom in October and a smaller autumn bloom in April. Bottom water dissolved oxygen concentrations were generally > 80% saturation and analysis of water clarity showed that in summer at least 1% surface light (often recognised as minimum required for photosynthetic growth) reached the seabed for 20% of the area of Storm Bay. The simulated nitrogen budget for Storm Bay showed considerable interannual variability. On average for 2016-2019 49% of the nitrogen supply to Storm Bay came from from the open ocean, 31% from the Derwent and D'Entrecasteaux Channel system, 16% from Fredrick Henry Bay and 4% from local fish farms; while nitrogen loss terms were 53% to the ocean, 22% to the Derwent and D'Entrecasteaux Channel, 12% to Fredrick Henry Bay and 13% to local denitrification.

Scenario Simulations

Five scenarios defined in terms of anthropogenic nutrients loads were investigated: #2 *Pre-Development* (no anthropogenic load), #3 *Pre-Storm Bay Development* (2015 STP+Industry load; 2013 fish farm load), and 3 Post-Storm Bay development scenarios with 2020 anthropogenic loads plus increasing fish farm loads in Storm Bay as *#4 2020+2ktN in SB*, *#4.5 2020+3ktN in SB* and *#5 2020+4.5ktN in SB*. With increasing nutrient load the model scenarios show an increase in water column nitrogen and chlorophyll, along with a small decline in bottom water dissolved oxygen and light. In all scenarios Storm Bay surface nitrogen levels tended to zero in summer indicating full utilisation by plankton and macrophytes. Nitrogen budget

analysis of the scenarios showed that with increasing nutrient load the export of nitrogen from Storm Bay to the ocean and adjacent waterways increased, with only a very slight increase in denitrification (as temperature and oxygen conditions which regulate denitrification rate were largely consistent across scenarios). Storm Bay is mostly oligotrophic with the area classified as mesotrophic (annual mean chlorophyll between 1-3 mg m^{-3}) increasing from 34% in the #2 *Pre-Storm Bay Development* scenario to 45% in the *#5 2020+4.5ktN in SB* scenario; no areas of Storm Bay became eutrophic in any simulation. Preliminary analysis of change in water quality at monitoring program sites in Storm Bay found that most sites showed some change with increasing farm loads, with the greatest change observed at sites close to farm lease locations. Interannual variability in water quality in Storm Bay is high and it will be difficult to distinguish changes in water quality due to increased fish farms from natural variability using monitoring data alone. The use of continuous sensing systems, model output and ongoing scenario simulations with- and with-out anthropogenic loads could help to distinguish natural variability from fish farm induced change in water quality.

New Observations

The project achieved 6 glider missions in Storm Bay; 3 winter deployments characterised the Zeehan Current and 3 summer deployments characterised the East Australia Current (unfortunately in January 2021 the glider was damaged and lost during a storm). The Zeehan Current was observed to travel down the west coast of Tasmania and across outer Storm Bay heading east. The Zeehan Current is warm, saline, low in nitrate concentration, and extends from the surface to the seabed (~100 m), with higher nutrient conditions observed in offshore waters beyond the core current. The East Australia Current is also warm and saline with low nitrate content and extends from the surface to ~ 50 m depth, with elevated nutrient concentrations observed in deep water beneath the EAC and offshore from the core current.

Benthic landers instrumented with water quality sensors and current meters were deployed for 6 month periods in the east, west, middle, and north of Storm Bay to investigate resuspension processes. Sensors and sampling quantified the transition from summer to autumn water masses, nutrient concentrations, and phytoplankton assemblages. The landers recorded several periods of sediment resuspension that correlated with enhanced wave height (> 2m); some resuspension events also had elevated nitrate concentration. Phytoplankton analysis found a rich diatom-dominated assemblage in spring, abundant small heterotrophic ciliates in late summer, and dinoflagellates prominent in autumn; biodiversity and abundance were greater in inshore waters. A laboratory resuspension process study showed a systematic decline in nutrients in overlying water and a rapid increase in microbial activity, during stimulated resuspension; this demonstrated that microbial assimilation during resuspension events can be an important pathway for nutrient transformation.

A final lander deployment was made in southeast Storm Bay (68 m depth) Jan-Jun 2021 in an attempt to observe nutrients in a deep water intrusion. Benthic lander sensors and field data show elevated nutrients at depth and during short periods when cooler water with reduced salinity and oxygen passed the lander site. Optical backscatter at the lander also showed episodic sediment resuspension during storm events.

Two sensor systems (located at the CSIRO wharf and in the northern D'Entrecasteaux Channel) have delivered water quality data in near real time since 2018, for ongoing evaluation of the near real time models. Three Australian Integrated Marine Observing System (IMOS) profiling mooring trials have been achieved in outer Storm Bay (>100m deep) in 2019 and 2021. The moorings transmitted profiles of temperature, salinity, dissolved oxygen and chlorophyll (0 - 80m) in near real time and additional delayed mode CTD and optical nitrate data were obtained from sensors located at 100m on retrieval. These mooring trials demonstrate the technology and data delivery for operation of potential sentinel monitoring

stations in offshore waters for ongoing validation of near real time modelling systems; such a system is particularly important in Storm Bay which is subject to seasonally variable influx of deep ocean water masses that are difficult to sample by other means.

Outer Storm Bay and the southern Tasmanian shelf was sampled from the RV Investigator over 2 weeks in November 2020. CTD casts, water samples, underway systems, and an undulating towed platform (Triaxus) characterised inshore waters, offshore sub-Antarctic waters and a turbulent jet of EAC water moving southwestwardly along the shelf edge. Preliminary analysis of this extensive data set shows elevated nutrient concentrations and plankton biomass in the sub-Antarctic water mass, and low nutrient concentrations in the surface EAC water down to ~ 50 m depth. Offshore phytoplankton in the sub-Antarctic water mass were dominated by a few Southern Ocean diatom species, whilst inshore Storm Bay samples featured a highly diverse community of diatoms and dinoflagellates. Ongoing analysis of a Triaxus transect across a swirl of EAC water south of the Tasman peninsula has the potential to characterise the mixing of deep nutrients onto the shelf associated with these transient mesoscale features.

Communication of Results

The outputs of our project are made available via the Storm Bay Modelling & Information System Dashboard at: https://stormbaymodelling.csiro.au (access valid March 2023). This system now provides model hindcasts and near real time estimates of hydrodynamics, waves (sufficient for simulation of resuspension), sediment and biogeochemical fields. These are delivered in the form of: 1) a curated collection of pre-generated graphics and animations to communicate results with the general public in a readily comprehensible format; 2) a Data Explorer tool that supports high-level analysis for government and industry decision-makers, allowing them to bring together a variety of data sources to gain a holistic view of the Storm Bay region; and 3) data services that allow researchers to access data for bespoke research and analysis. The system is integrated with the FRDC Projects, 'Storm Bay Decision Support Tools' and 'Storm Bay Monitoring Program' with pilot links to connectivity decision support tools, the relocatable model, the marine ecological emulator and observations.

The project team have been involved in a number of communications to stakeholder groups and a briefing to the Tasmanian Legislative Assembly; publications to date include project reports, conference abstracts and information sheets. In June 2021 a day of science talks hosted by the FRDC informed a broad group of stakeholders (including EPA, NRE, FRDC, BE CRC, Environmental Groups, Industry, CSIRO and University Researchers) of science achievements to date; in June 2022 an 'Open House' event organised by the FRDC communicated our science findings to the public through a series of interactive displays and conversations. Project information is also available on the CSIRO Coastal Environmental Modelling Team's website: https://research.csiro.au/cem/projects/current-projects/storm-bay/ (access valid March 2023).

1 New understanding and project recommendations

1. This project delivers a hindcast and near real time Storm Bay Modelling and Information System that is fit for the purpose of simulating water quality and characterising nutrients in Storm Bay from ocean currents, sediment resuspension, river and anthropogenic (including fish farm) inputs. The project has been subject to internal and external peer review, who note: *'The authors are to be congratulated on an impressive and comprehensive modelling study and report. The work follows or exceeds current best practices in marine biogeochemical modelling and model evaluation.'*

    - We recommend that the model, observations, analysis, knowledge and information dashboard created in this project are used to inform ongoing research and resource management throughout the region.

2. The residual circulation in Storm Bay is generally clockwise, and primarily driven by freshwater input; tracers released in some side bays and at some farm sites have relatively long residence times.

    - We recommend that this information is considered when selecting fish farm lease site locations and production levels, to minimise persistent deleterious impacts to water quality.

3. In summer, instabilities in the East Australia Current result in sub-mesoscale eddies and filaments entering Storm Bay with highly intermittent intrusions of warm oligotrophic water in the upper 50 m that can initiate or reinforce Marine Heat Waves, and cold nutrient-rich water at the bottom that can result in nutrient spikes. Fronts associated with 3 water masses continually move and cause large fluctuations in water quality at monitoring sites.

    - We recommend ongoing operation of the near real time Storm Bay Modelling and Information System, to inform the interpretation of sparse monitoring data of contemporary river plume and oceanic influence.

    - We recommend research funding supports further development of the Storm Bay Modelling and Information System to include near real time data assimilation to improve the stochastic resolution of EAC eddies.

4. In winter, extension of the Zeehan Current delays influx of nutrient rich sub-Antarctic water into Storm Bay, with strong interannual variability.

    - We recommend further glider or profiling mooring observations in late winter to confirm this finding and identify any correlation with ENSO cycles that are known to influence the intensity of the Leeuwin-Zeehan Current system.

5. Broad-scale simulated sediment features (kilometres and more) showed plausible sediment resuspension during extreme weather in Storm Bay; some stochastic variability was not reproduced in the model due in part to unresolved small-scale spatial variability in the hydrodynamic and/or sediment fields.

    - For sub-regions of Storm Bay requiring highly resolved sediment dynamics (e.g. characterisation of specific fish farming areas), we recommend deployment of the high resolution relocatable

model (RECOM - implemented in the FRDC Storm Bay Decision Support Tools project) informed by fine-scale sediment observations.

6. Simulation of nitrogen cycling in Storm Bay shows peak surface nitrogen occurs in winter due to seasonally high river discharge and anthropogenic inputs augmented by ocean influx in late winter; in summer highly variable bottom water intrusion events bring nutrient rich sub-Antarctic water into Storm Bay. There is considerable interannual variation in nitrogen supply to Storm Bay. For the period 2016-19 on average 49% of nitrogen input to Storm Bay was from the ocean and 4% from local fish farms; loss terms included 53% exported to the ocean and 13% to local denitrification.

   - We recommend further research be undertaken on the processes of denitrification as, whilst simulations are consistent with literature values, few observations have been made in this region.

7. Scenario simulations of increasing anthropogenic nutrient load predict an increase in Storm Bay water column nitrogen and chlorophyll, a small decline in bottom water dissolved oxygen and light and an increase in mesotrophic area (from formerly oligotrophic). Nitrogen budget analysis showed increasing export of nitrogen from Storm Bay to the ocean and adjacent waterways. Small systematic changes in water quality due to anthropogenic nutrient enrichment would be difficult to identify at monitoring stations due to high natural variability.

   - We recommend extending the nitrogen budget analysis to encompass the whole region to quantify the contribution of river, sewerage and industrial discharge, in addition to fish farm waste to the regional nitrogen budget.

   - We recommend annual scenario projections to anticipate water quality change with evolving anthropogenic discharge; also downscaled climate projections to anticipate the likely future impact of any change in river, atmosphere or oceanic influence on water quality.

   - We recommend the ongoing use of scenario simulations with- and with-out anthropogenic loads to help distinguish natural variability from anthropogenic induced change in water quality and assist in the interpretation of monitoring data.

8. New observations collected from multiple observation platforms (gliders, benthic landers, profiling moorings, small and large research vessels) at a range of spatial and temporal scales, often in locations that were difficult to sample frequently by traditional means, were fundamental to our new understanding of the influence of water masses and resuspension on water quality in Storm Bay, and essential for the demonstration of the model as fit for the purpose of simulating the water quality in Storm Bay.

   - We recommend future applied modelling projects invest in similar high quality multi-scale data sets to target key research unknowns and provide multiple lines of evidence to ensure models are fit for their designated purpose.

   - We recommend that monitoring programs incorporate continuous sensor data for more complete understanding of the spatial and temporal evolution of water quality.

   - We recommend that continuous sensors are rigorously calibrated and also quality controlled against in situ samples to confirm accuracy.

9. A laboratory resuspension process study showed a rapid increase in microbial activity and systematic decline in nutrients in overlying water during resuspension; this suggested that microbial assimilation during resuspension events can be an important pathway for nutrient transformation.

- We recommend further research to quantify nutrient transformation by microbial activity during sediment resuspension across a range of sediment types, particle size and sites, including analysis of samples from fish farm leases.

10. Outputs from this project are made available via the Storm Bay Modelling & Information System Dashboard which has been designed with stakeholder input to meet their need for ready access to information and tools for strategic and tactical decisions.

- We recommend ongoing funding for the Storm Bay Modelling and Information System, to enable continued operation (and upgrade) of the near real time models, to support ongoing update of key data sets, scenarios and evolving analysis, and to provide ready access to information, tools and training to inform arising strategic and tactical decisions.

2   Reporting Milestones

This final technical report documents the project achievements in detail and is accompanied by 8 Appendices of supplementary information and analysis. Specifically, for this reporting period we have addressed the milestones detailed in bold in Table 2.1 and provided sufficient background information to understand these project achievements in the context of the overarching project objectives.

Table 2.1 FRDC Table of project milestones [specific items addressed in this report are highlighted in bold].

Due Date	Deliverables Type (Deliverable Type)	Deliverables Status	Detail
31/07/2018	Signing of Agreement	Achieved	• Project commencement • Staff deployed • Consumables ordered • Documents signed
8/02/2019	Progress report	Achieved	Written report detailing progress and interim results for period including: • Assessment of current Storm Bay hydrodynamic model against observations • Benthic lander deployment; winter Zeehan glider deployment; summer EAC process study plan • Storm Bay model updated with latest hydro, sediment, biogeochemistry & optical model
1/08/2019	Progress report	Achieved	Written report detailing progress and interim results for period including: • 1st winter Zeehan process study completed; summer EAC analysis underway; 1st benthic lander analysis underway; 2nd winter Zeehan process study plan • Storm Bay model calibration underway • Visualisation dashboard demonstration platform Provision of access to the developmental Visualisation dashboard for relevant stakeholders
10/08/2020	Progress report	Achieved	Written report detailing progress and interim results for period including: • 1st summer EAC process study completed; 1st benthic lander deployment complete; 2nd Zeehan analysis underway; 2nd benthic lander deployment underway; 2nd EAC study plan • Storm Bay model calibration of hydro finalised; pilot sediment, biogeochemistry & optical model • Visualisation dashboard displays hydrodynamic model results; links to decision support tools & monitoring program established
3/02/2021	Progress report	Achieved	Written report detailing progress and interim results for period including: • 2nd Zeehan study complete; 2nd EAC analysis underway; 2nd benthic lander analysis underway • Storm Bay model calibration of sediment finalised; biogeochemistry & optics calibration underway • Hydrodynamic model characterisation of Storm Bay • Visualisation dashboard displays hydrodynamic & sediment model results; user feedback sought
10/08/2021	Progress report	Achieved	Written report detailing progress and interim results for period including: • 2nd EAC study complete; 2nd benthic lander deployment complete • Storm Bay calibration of biogeochemistry & optics finalised • Scenario simulations commenced • Visualisation dashboard displays biogeochemistry & optics model results; user feedback incorporated
30/06/2022	Draft final report	Achieved	Written report detailing progress and interim results for period including: • Biogeochemistry & optics characterisation of Storm Bay including influence of EAC and Zeehan • Scenario simulations completed Provision of access to the completed and fully operational Visualisation dashboard for relevant stakeholders
30/11/2022	Final report	Achieved	Final report with review comments addressed

31/03/2023	Final Report	Achieved	**Final report with additional EPA Scenario and analysis added**
31/03/2022	Final Deliverable	In progress	• Project proposal for sustainable operation of Storm Bay Model and Information System

3 Legacy Storm Bay hydrodynamic model assessment

CSIRO developed a hydrodynamic model STORM for Storm Bay and adjacent estuaries in 2009-2011 as part of the "Linking models and sensor networks" project (Figure 3.1). The accuracy of this model has now been assessed by comparison of this model with a suite of ocean observations made as part of the federally-funded Integrated Marine Observing System (IMOS). The comparison period was June 2014 - July 2015. The observations available for comparison with the model included sea level, temperature and salinity; quantitative assessment of the model's performance used standard time series metrics (root mean square error (RMSE), mean absolute error (MAE) correlation coefficient (cc), bias, Willmott scores (d)).   A summary of the assessment is provided here with the full report available as:

Langlais C, Herzfeld M, Griffin D, Wild-Allen K (2018) Assessment of the CSIRO Storm Bay Hydrodynamic Model Against Observations. FRDC 2017-215 Progress Report Work Package 1.1, CSIRO Atmosphere, Hobart.
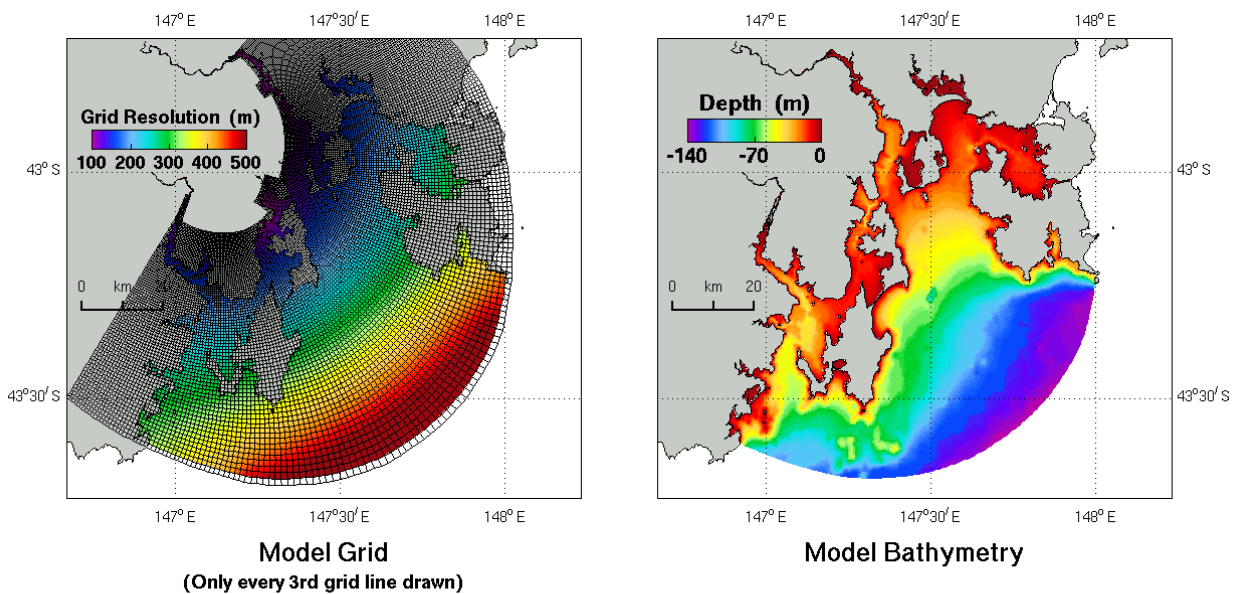

Figure 3.1 STORM model domain: grid configuration (left) and bathymetry (right).

Whilst the STORM model had an overall warm and fresh bias, the main dynamical structures were present (Figure 3.2). The model simulated the seasonal variability of the fresh river plume quite accurately, with seasonal cooling and warming, and coming and going of vertical stratification. The surface layer of river-affected water was too diffuse in winter and too stratified in summer, but its spatial extent appeared to be approximately correct. The seaward trajectory of the plume was sometimes but not always correct in the model (e.g. Figure 3.6).
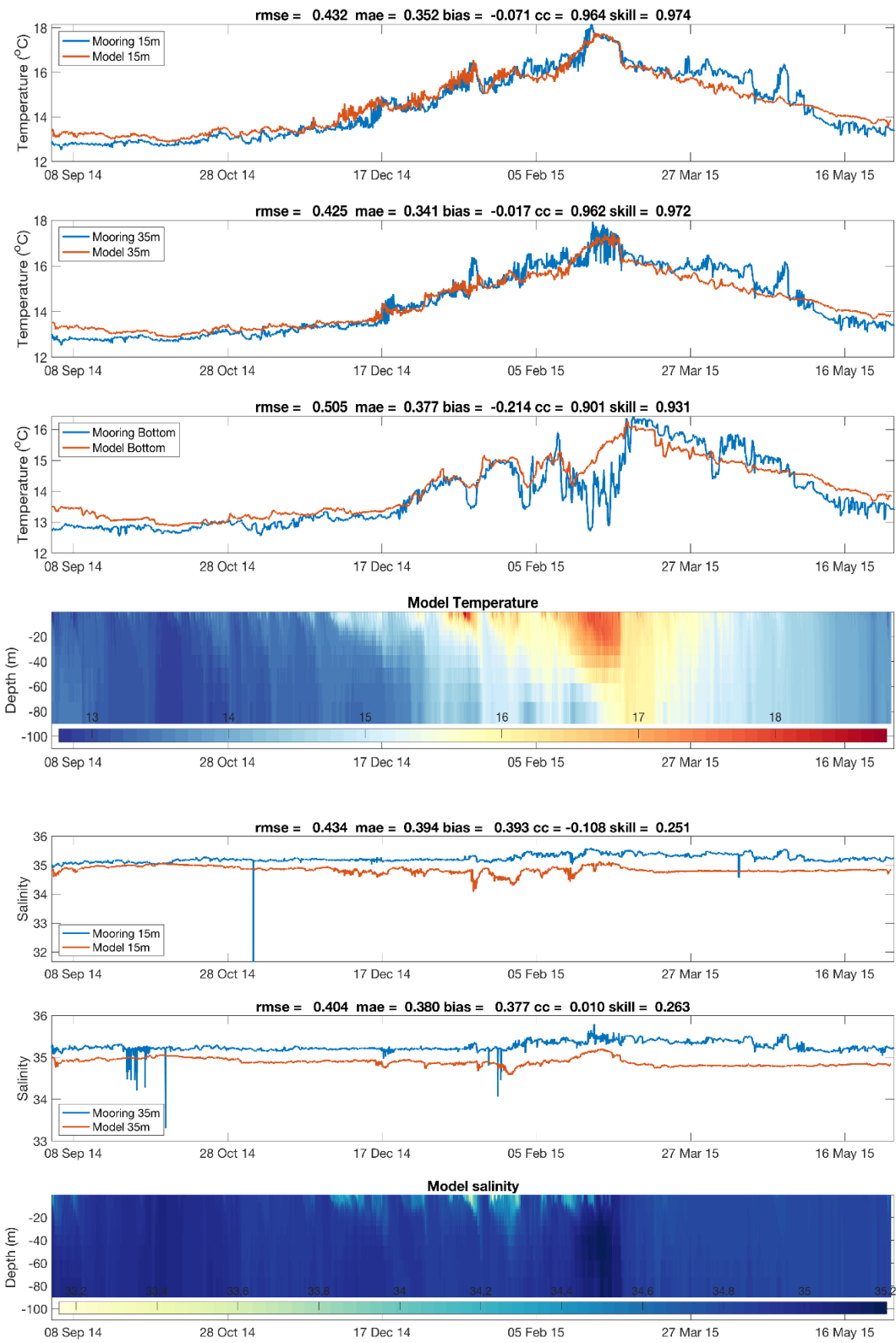
Figure 3.2 Comparison of hourly observed (blue) and modelled (red) time series at the Storm Bay IMOS mooring located at (147.66°E, 43.3°S) over a 9-month period for temperature (top 4 panels) and salinity (lower 3 panels). Skill metrics are detailed in panel headers, scales vary between plots to clearly illustrate features.

Tidal variability was accurately modelled but the simulated non-tidal variability of sea level was greater than observed (e.g. Figure 3.3). The reason for this is not known, but could potentially be due to an issue with boundary forcing of sea level.
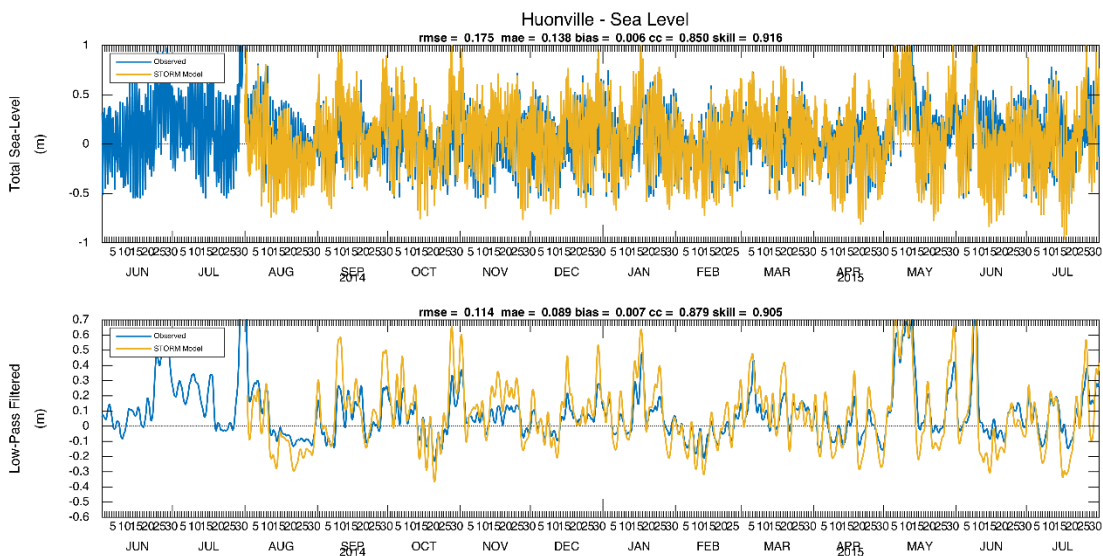
Figure 3.3 Tidal sea level (top) and low-pass filtered sea-level (bottom) for June 2014 -July 2015.

Intrusions of cold water associated with interactions of the EAC with the continental shelf (Figure 3.4) were sometimes but not always well modelled (e.g. Figure 3.5). This would have had consequences for the accuracy of models of the biogeochemistry as injections of ocean nutrients may have been missing.

The most significant error of the 2009-11 STORM model appeared to be the fresh (low salinity) bias, but because the offset tended to be uniform throughout the water body, it did not cause any significant errors in the simulated residual circulation (Figure 3.6).
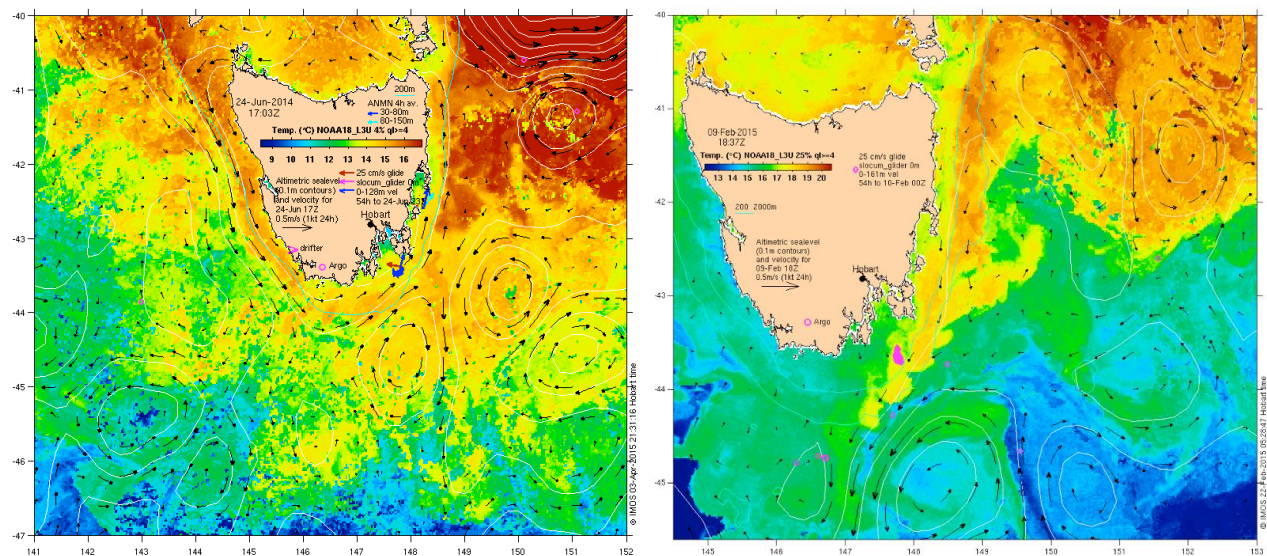
Figure 3.4 Surface temperature and circulation from satellite images (IMOS ocean current http://oceancurrent.imos.org.au/index.php (access valid Nov 2022)). Left - 24 June 2014 showing warm Zeehan Current to the south and west of Storm Bay; right - 9 Feb 2015 showing warm East Australia Current to the south and east of Storm Bay
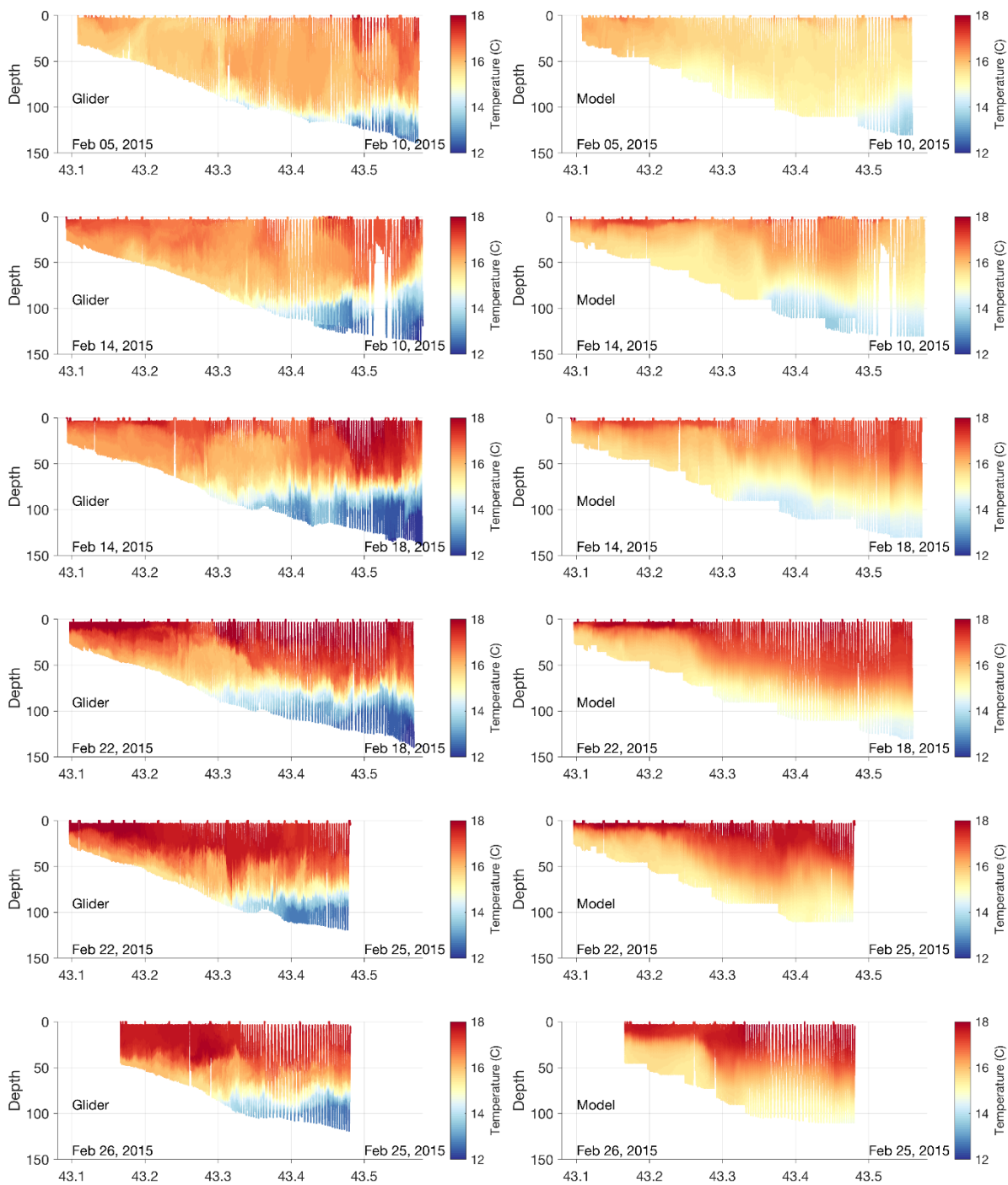
Figure 3.5 Observed (left) and modelled (right) temperature sections in Storm Bay during the 2015-02 glider deployment showing a cold subsurface intrusion into Storm Bay.
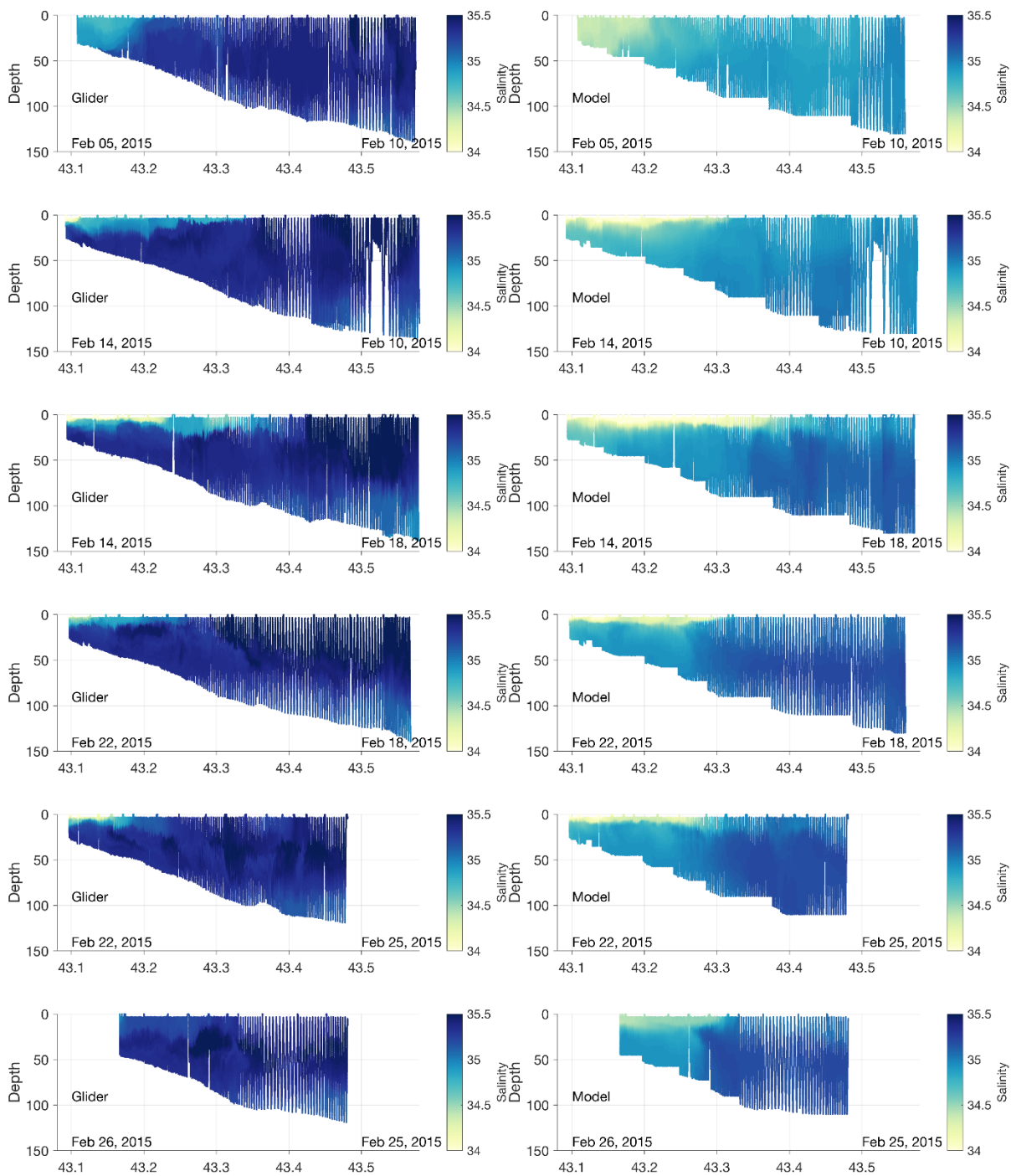
Figure 3.6 Observed (left) and modelled (right) salinity sections in Storm Bay during the 2015-02 glider deployment showing the surface freshwater river plume.

4 Storm Bay model update

4.1 Background context

The new Storm Bay hydrodynamic model (TASSE) replaces two operational hydrodynamic models developed during the LMSN project ("Linking models and sensor networks" project 2009-2011), one being the South-East Tasmania continental shelf region model (the SETAS model) and the second being a higher-resolution model of Storm Bay and the Derwent and Huon Estuaries (the STORM model). The performance of the STORM model during the June 2014 - July 2015 period was assessed against observations in work package 1.1 of the project (Langlais et al., 2018 "Storm Bay hydrodynamical model assessment"). The two main limitations were issues with the flood plume response and the shelf break response. The former suggests that there would have been uncertainty in the simulation of connectivity during flood events. The impact of the latter on the simulation of connectivity is unknown and could have been important for offshore nutrient supply.

The new Storm Bay model has been developed using the latest version[1] of the CSIRO Environmental Modelling Suite (Herzfeld et al., 2006, Baird et al., 2020) https://research.csiro.au/cem/software/ems/ - access valid Nov 2022). It has been run for the hindcast period Dec 2014 – June 2020, and is now running in near-real time, predicting three-dimensional fields of temperature, salinity and currents, suspended and bed sediments, biogeochemistry and spectral optics in Storm Bay and environs. Calibration and performance of the models has been quantitatively assessed by repeatedly running the model for a specified period of time in the past (i.e. performing a hindcast), and fine-tuning the free parameters in the model until errors between the model predictions and available observations are minimised.

Geography

Storm Bay is near Hobart in south-eastern Tasmania. It is a large and deep bay about 26 km long and 40 km wide. Storm Bay is bounded by the Tasman Peninsula on the eastern side of the bay and Bruny Island on the western side. The main freshwater inflow is the River Derwent, entering the bay from the north-western boundary. Storm Bay extends south-eastward to the shelf-edge where it connects to the Tasman Sea. The shelf-edge is the region of the seafloor where the flat continental shelf drops away rapidly to form the continental slope. The depth of the shelf edge is between 150 and 400m.

Regional Circulation

Storm Bay is a moderately-tidal, region of freshwater influence (ROFI) with significant freshwater inflow from the Derwent and Huon rivers, opening onto a continental shelf that is strongly influenced either by

---

[1] SHOC: Sparse Hydrodynamic Ocean Code EMS Version: v1.3.0 rev(6527)

eddies of the East Australian Current, the Zeehan Current from the west or other dynamical features of the Tasman Sea and Southern Ocean (Figure 4.1). The ocean circulation in Storm Bay is a complex relationship between coastal, shelf and open ocean currents which transport water masses, nutrients and microplankton communities from three different oceans (Buchanan et al., 2014). Inshore, Storm Bay is characterized by large fluctuations in temperature and salinity on many temporal and spatial scales.
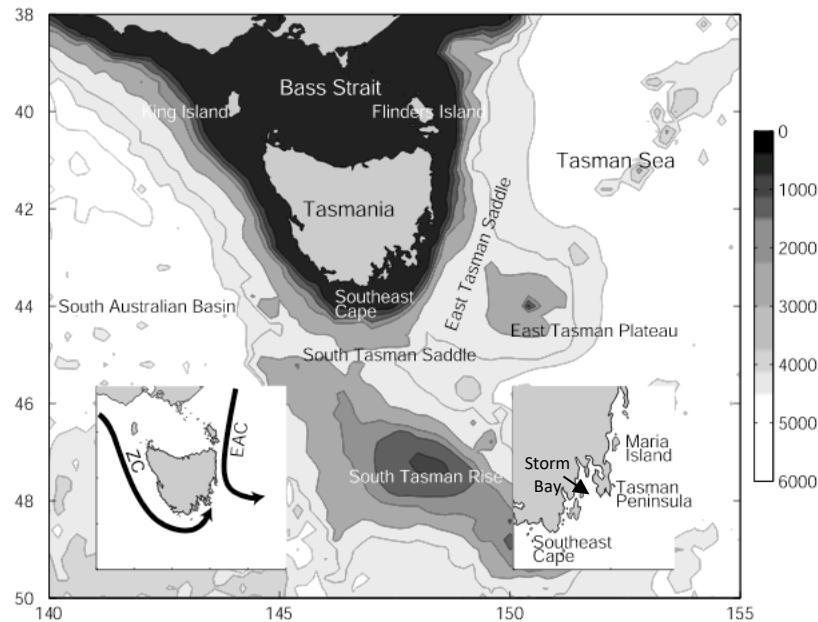

Figure 4.1 Waters around Tasmania showing both the main bathymetric features (depth in m) and other geographic features. The inset on the right shows the southeast coast in greater detail. The inset on the left shows a schematic of the major current systems in the region.

Source: Figure1 from Ridgway 2007

Offshore, the eastern Tasmanian shelf lies at the boundary between two ocean currents (Ridgway, 2007; Figure 4.1). From the north, the East Australian Current (EAC) brings relatively warm and salty nutrient-depleted sub-tropical water down the east coast of Australia to Tasmania (Pilo et al., 2015). The EAC extension consists of sporadic eddies reaching Tasmania. It peaks in February and is weakest in winter. From the south, relatively cool and fresh water from the Zeehan Current (ZC) reaches the eastern Tasmanian shelf with a peak in May-June. The ZC is a shelf break current and is the downstream part of a larger Southern Australia Current System which extends from the Leeuwin Current Extension upstream to the ZC (Duran et al., 2020). Note that while tropical water may be found in the ZC, the inertia of the Leeuwin Current dissipates around the head of the Great Australian Bight (Herzfeld, 1997). The ZC flows down the west coast of Tasmania, before turning around the southern tip of Tasmania.

The strong seasonality of the EAC eddies/ZC system means that the eastern Tasmanian continental shelf is dominated by the ZC in winter, while in summer, two thirds of the shelf is dominated by the EAC eddies that oppose the ZC and push it to the southern part of the eastern continental shelf. Autumn and spring are periods of transition between these two states (Oliver et al., 2016).

To the south, the subtropical convergence is the transition between warm, saline subtropical water and cool, fresher subantarctic water. This transition is characterised by enhanced meridional temperature and salinity gradients, and is referred to as the Subtropical Front (STF, Stramma et al., 1995). Whilst this front is

a continuous feature in the Atlantic, Indian and Pacific Oceans, south of Tasmania it occupies the trough between Tasmania and the South Tasman Rise, around 47ºS (Rintoul et al., 1997). Szymanska and Tomczak (1993) report in the southern Tasman Sea the STF is identified by the 34.8 isohaline, or more approximately by the 13ºC isotherm. Although the STF lies well south of the Tasmanian continental shelf, we see that at times the mesoscale eddy activity present at the frontal boundary may advect intrusions of subantarctic water onto the shelf and into Storm Bay. This is particularly evident when the Zeehan Current is absent in summer.

Within Storm Bay in summer there exists the possibility for three water masses to interact; warm and relatively fresh water originating from the Bays and Estuaries surrounding northern Storm Bay (Storm Bay water), warm and salty water originating from the East Australian Current (EAC water) which flows along the shelf edge past Tasman Peninsula in the east, and cool and relatively fresh subantarctic water that intrudes from the west as a consequence of eddy activity at the STF further south. This situation is illustrated in Figure 4.2 for SST on 26 Jan 2015, where warm EAC extension water flows down the east coast of Tasmania, continuing south-westward to ~46ºS. Cold water originating from the STF at ~47ºS is transported northward by eddy activity to the south-west coast of Tasmania, where in this instance it bifurcates with some cooler water flowing eastward along the shelf and into Storm Bay. The northern waters of Storm Bay also have elevated temperature. It should be noted that the core of the EAC does not enter Storm Bay, rather, as the EAC core flows past the Tasman Peninsula it generates sub-mesoscale turbulence in the form of eddies and filaments, which may advect into Storm Bay to increase surface temperatures.
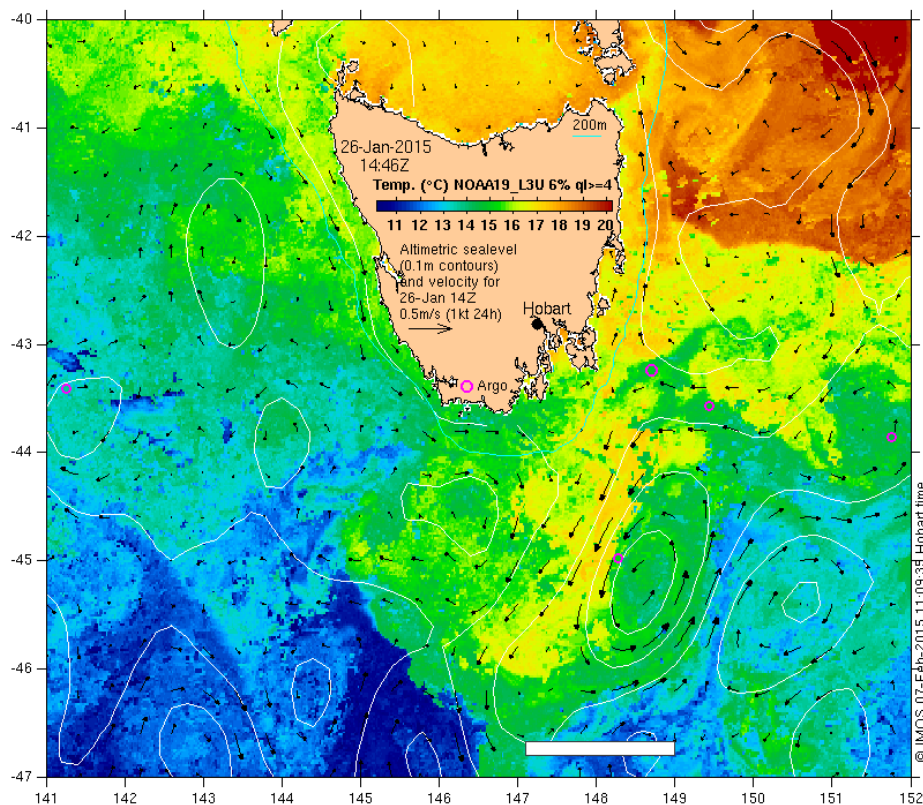

Figure 4.2 **IMOS Ocean Current image of southern Tasmania for 26 Jan 2015 (http://oceancurrent.imos.org.au/product.php - access valid Nov 2022).**

4.2 Hydrodynamic model

The hydrodynamic model SHOC (Sparse Hydrodynamic Ocean Code; Herzfeld et al., 2006, https://research.csiro.au/cem/software/ems/hydro/strucutured-shoc/ - access valid Nov 2022) is employed for this study. SHOC is the hydrodynamic component of the broader Environmental Modelling Suite (EMS), which includes libraries for sediment transport, biogeochemistry (BGC), waves and tracer statistics (https://research.csiro.au/cem/software/ems/ - access valid Nov 2022). SHOC is a general-purpose model based on the paper of Blumberg and Herring (1987), applicable on spatial scales ranging from estuaries to regional ocean domains. It is a three-dimensional finite-difference hydrodynamic model, based on the primitive equations. Outputs from the model include three-dimensional distributions of velocity, temperature, salinity, density, passive tracers, mixing coefficients and sea-level. Inputs required by the model include forcing due to wind, atmospheric pressure gradients, surface heat and water fluxes and open-boundary conditions such as tides and low frequency ocean currents (Figure 4.3). The model is based on the equations of momentum, continuity and conservation of heat and salt, employing the hydrostatic and Boussinesq assumptions. The equations of motion are discredited on a finite difference stencil corresponding to the Arakawa C grid.

The model uses a curvilinear orthogonal grid in the horizontal and a choice of fixed 'z' coordinates or terrain-following σ coordinates in the vertical. The 'z' vertical system allows for wetting and drying of surface cells, useful for modelling regions such as tidal flats where large areas are periodically dry. The current implementation of the model uses z-coordinates. The bottom topography is represented using partial cells. SHOC has a free surface and uses mode splitting to separate the two-dimensional (2D) mode from the three-dimensional (3D) mode. This allows fast moving gravity waves to be solved independently from the slower moving internal waves allowing the 2D and 3D modes to operate on different time-steps, resulting in a considerable contribution to computational efficiency. The model uses explicit time-stepping throughout except for the vertical diffusion scheme which is implicit. A Laplacian diffusion scheme is employed in the horizontal on geopotential surfaces. Smagorinsky mixing coefficients may be utilized in the horizontal. The ocean model can invoke several turbulence closure schemes, including k-ε, k-ω, Mellor-Yamada 2.0 & 2.5 and Csanady type parameterizations. A variety of advection schemes may be used on tracers and 1st, or 2nd order can be used for momentum. The model also contains a suite of open boundary conditions, including radiation, extrapolation, sponge, and direct data-forcing. A generous suite of diagnostics is included in the model.

The 'sparse' coordinate system (Herzfeld, 2006) employed by SHOC facilitates the use of highly complex curvilinear grids that allow resolution optimization. This sparse system allows the removal of dry land cells in the gridded domain, thus reducing the computational burden. It has been shown that runtime, as in wall time, decreases exponentially as wet cells decrease using the sparse system (Herzfeld, 2006). The sparse system also presents several other advantages, including arbitrary domain decomposition for distributed processing, reduced file sizes for storage and compatibility with finite volume approaches which are generally faster (than unstructured models).

Detailed Science and User Manuals for SHOC can be downloaded from https://research.csiro.au/cem/software/ems/ems-documentation/ (access valid Nov 2022).
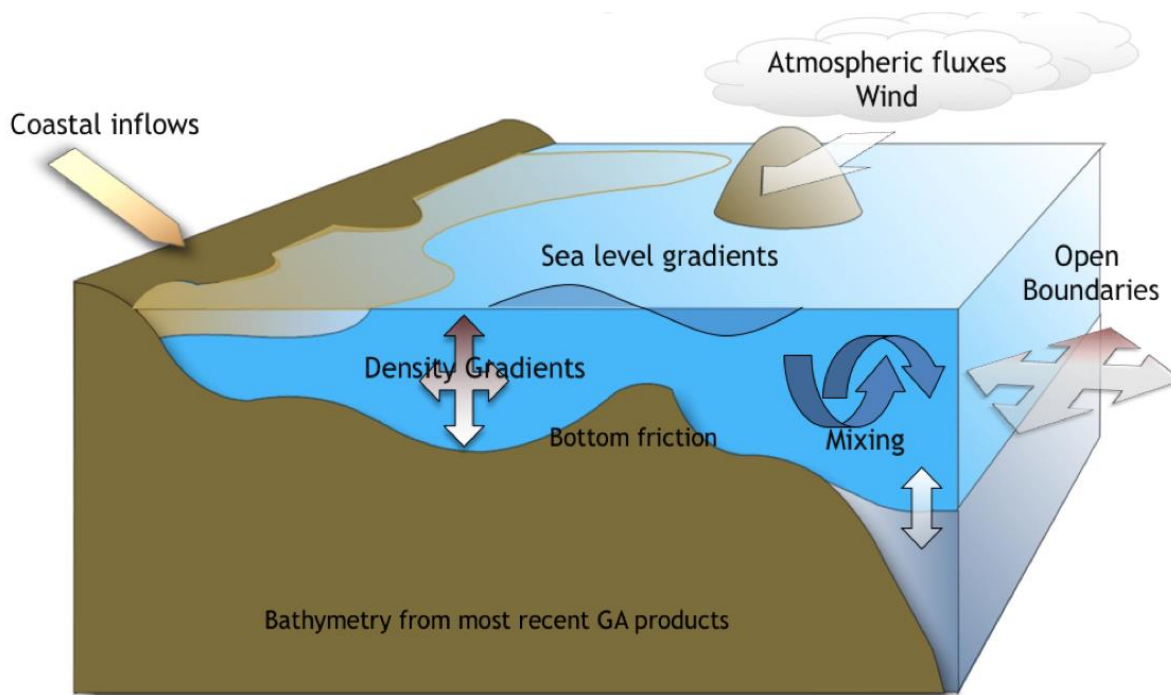
Figure 4.3 Schematic representation of major forcing inputs for the SHOC hydrodynamic model.

4.2.1   Numerical Model Configuration

Downscaling grid configuration

The target resolution of a numerical model in Storm Bay is of the order of several hundred metres. It is standard practice to nest regional and local applications within global ocean models (e.g. OceanMAPS, http://wp.csiro.au/bluelink/global/oceanmaps/ - access valid Nov 2022) so that all modes of forcing are introduced into the target domain. However, the resolution of these global products is ~10 km, and there are limitations as to the amount of resolution that can be increased across nesting boundaries, with a rule of thumb that 5:1 is an acceptable upper bound. This means that a downscaling nesting strategy must be implemented, with an intermediate resolution model 'bridging' the scales between the global model and the high-resolution local model (TASSE). In this case we use the existing SETAS model, which was similarly used as the parent model for the STORM model assessment. The SETAS model has a resolution at the open boundary of ~ 2km, thus allowing acceptable boundary nesting ratios to be achieved for both upscaling to the global model and downscaling to the local model (Figure 4.4). However, the SETAS model's open boundaries only just encompass the local model domain, hence we do not expect the interior dynamics as represented by the SETAS model to add significant skill to boundary information used to force the local model, and this model is predominantly an interpolation vehicle from global to local scales used to satisfy nesting ratios. As such, detailed calibration of the SETAS model is not expected to improve the local model boundary forcing, and we use the SETAS model in its pilot form.
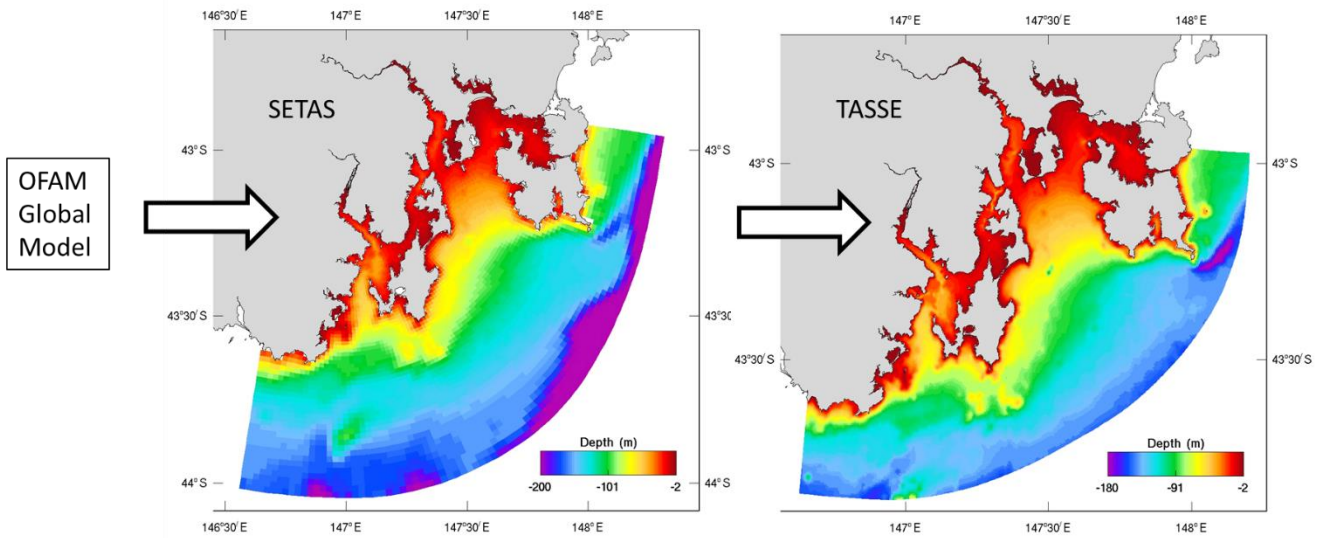
Figure 4.4 Downscaling nesting strategy

The TASSE model grid is curvilinear with 490 x 400 horizontal grid cells. A quasi-polar configuration is utilized where resolution increases away from the boundary, with grid resolution ranging from around 450 m on the offshore boundary (~1/5 of the SETAS resolution of 2km), to around 130 m in the upper reaches of the Huon and Derwent Estuaries. Storm Bay receives a resolution ranging from ~250 m in the north to ~400 m in the south.
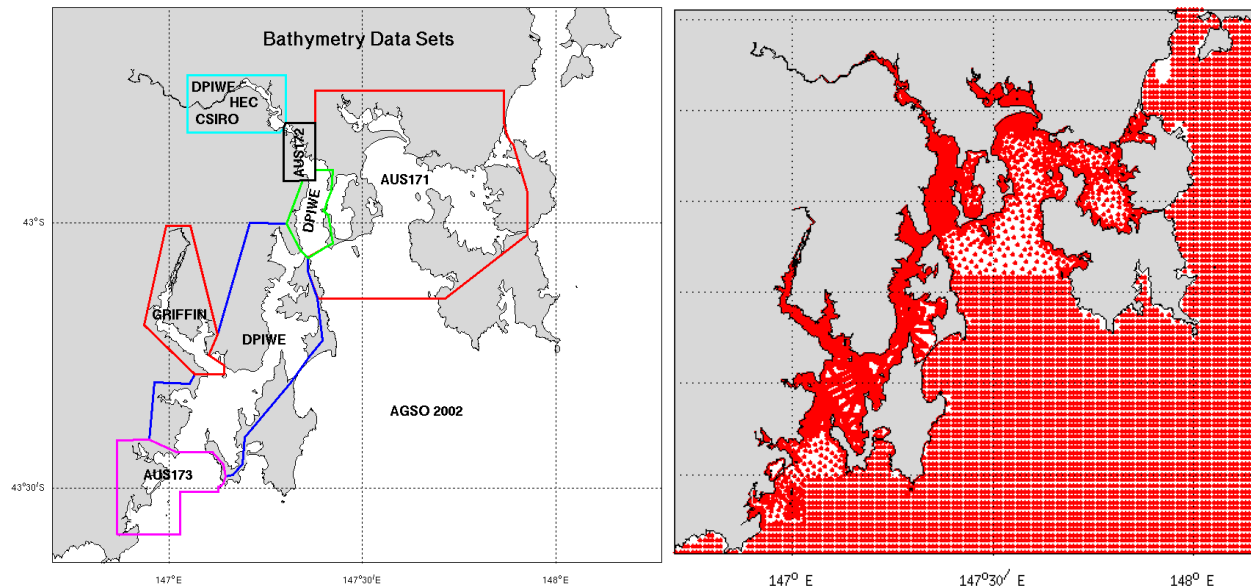

Figure 4.5 Various sources from which bathymetry data was extracted (left), and scatter plot of actual data (right).

Bathymetry data were merged from several pre-existing datasets from NRE, Hydro Tas., CSIRO, plus further data was digitised in-house from naval charts AUS171, AUS172 and AUS173. The remaining offshore region was infilled with data from Geoscience Australia (2002) (Figure 4.5). Survey dates ranged from 1964 (or earlier) for AUS171, 2002 for the GA data, 2004 (or earlier) for the NRE data (Alan Jordan's surveys), to 2004 for the CSIRO data. The water depth over the model domain ranges from 2 to 180 m, with the minimum depth imposed to reduce gradients and assist with model stability. There are 36 model layers

with a vertical resolution of 0.5 m at the surface to 20 m at depth[2]. The model 3D time step is 20 seconds and the 2D time-step is 2.5 s.

Within the complementary project 'Next generation decision support tools to support sustainable aquaculture in Storm Bay' (FRDC project 2018-104), the CSIRO relocatable model will be configured to allow high resolution models to be deployed in sub-regions of interest within the TASSE model domain.

Forcing and initial conditions

The ocean boundary forcing consists of daily fields of three-dimensional velocities, sea level, temperature, and salinity. For SETAS, open ocean boundary forcing and initial conditions were from the global OceanMAPS model (Oke et al., 2008), operated by Bureau of Meteorology (BoM) (http://www.bom.gov.au/oceanography/forecasts/site-help.shtml - access valid Nov 2022) while TASSE uses output from SETAS for open boundary information. Low frequency sea-level from the global model is superimposed with 8 tidal constituents (M2 S2 N2 K2 K1 O1 P1 Q1) from the TPXO global model (Egbert et al, 2002) and applied at the boundary of the SETAS model. The local model is subsequently nested within the regional model, and therefore inherits both low frequency and tidal signals. The open boundary condition used to specify the boundary forcing is that of Herzfeld and Andrewartha (2012).

Surface fluxes are derived from the Australian Bureau of Meteorology's operational atmospheric models (ACCESS-R and ACCESS-VT; Puri et. al., 2012, http://www.bom.gov.au/nwp/doc/access/NWPData.shtml - access valid Nov 2022) at a resolution of 12 km. Heat fluxes applied at the surface boundary condition were computed from standard meteorological variables provided by ACCESS-R (wet and dry bulb temperature, air pressure, wind speed and cloud amount) using short and longwave calculations outlined in Zillman (1972) and the bulk method for sensible and latent heat using bulk coefficients of Kitaigorodskii et al., (1973). For the surface freshwater fluxes, precipitation was provided by ACCESS-R and evaporation was computed from the latent heat flux. Wind speed was converted to stress using the bulk scheme of Large and Pond (1981).

Runoff from 8 rivers (Huon, Derwent, Jordan, North West Bay, Snug, Esperance, Coal and Carlton Figure 4.6 and 4.7 is included in the TASSE model by specifying the flow rate and temperature of freshwater input. The flow rate is provided by NRE except for the River Derwent at Meadowbank Dam which is supplied by Hydro Tasmania. The freshwater flows were implemented using the method described by Herzfeld (2015).

---

[2] Grid layer depths are 0.5, 1.0, 1.5, 2.0, 2.5, 3.0, 3.5, 4.0, 4.5, 5.0, 5.6, 6.3, 7.1, 8.0, 9.0, 10.2, 11.7, 13.7, 16.0, 18.5, 21.5, 25.0, 29, 34, 40, 47, 55, 65, 77, 90, 105, 120, 140, 160, 180 m.
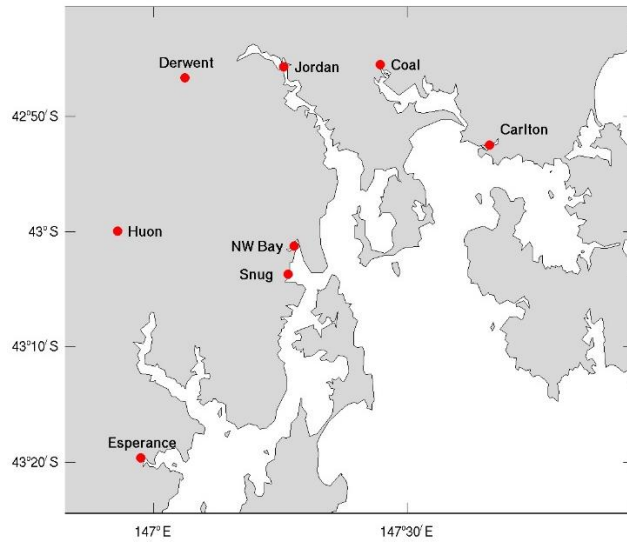
Figure 4.6 Location of freshwater inputs in the local Storm Bay model.

Figure 4.7 River flows into the Storm Bay model from Dec 2014 – Dec 2020.

Both temperature and salinity in the global model, and therefore inherited as the initial condition in TASSE, were observed to contain biases in comparison to a glider mission in December 2014. To overcome this, we additively scale the OceanMAPS temperature and salinity distributions interpolated onto the glider trajectory and use a nearest neighbour interpolation to distribute these unbiased fields throughout the domain. This correction has the potential to modify the dynamically consistency of the initial condition, so results should be ignored for the first few days of spin-up while the model reaches dynamic equilibrium.

The forcing data used in the TASSE model is summarized in Table 4.1.

Table 4.1 Data requirements for the TASSE model.

Forcing	Data	Source
TASSE		
Open boundary conditions	SETAS hindcast - 2014-12 to 2020-09 SETAS NRT – 2020-09 to 2020-12	CSIRO
Initial conditions	SETAS	CSIRO
Meteorological surface fluxes	ACCESS-R - 2014-12 to April 2020-03 ACCESS-VT3 - 2020-04 to 2020-12	BoM
River flow	Gauged	NRE
River temperature	Low pass filtered 2m atmospheric temperature observation	BoM station
SETAS		
Open boundary conditions	BRAN – 2014-09 to 2018-12. OFAM(OceanMAPS) – 2019-01 to 2020-12	CSIRO and BoM
Initial conditions	BRAN	CSIRO
Meteorological surface fluxes	ACCESS-R ACCESS-VT	BoM
River flow	Gauged	NRE
River temperature	Low pass filtered 2m atmospheric temperature observation	BoM station

Configuration summary

The TASSE model runs in both hindcast and near-real time modes, predicting three-dimensional fields of temperature, salinity and currents in Storm Bay and environs. The model runs at approximately 20 x real-time using 16 processors (i.e. a 1-year simulation takes approximately 18 days to complete). Key model parameters are summarized in Table 4.2. The calibration period is 1 year from December 2014 to Jan 2015.

Table 4.2 Key parameters for the TASSE hydrodynamic model.

Parameter	Value
Grid size	490 x 400
# layers	36
Turbulence closure	k-ε (Burchard et al., 1998)
Background vertical viscosity	1×10^{-4} m^{2}s^{-1}
Background vertical diffusivity	1×10^{-5} m^{2}s^{-1}
Background horizontal viscosity	15 m^{2}s^{-1}
Horizontal diffusivity & viscosity	Smagorinsky, (1963) c=0.1
Horizontal advection	ULTIMATE QUICKEST (Leonard, 1991)
Time steps (3D/2D)	20 / 2.5 s
Bulk scheme	Kitaigorodskii et al (1973)
Short wave attenuation	Variable
Short wave transmission	Variable
Short wave bottom absorption	1.0
Open boundary scheme	Herzfeld & Andrewartha (2012)
Boundary relaxation timescale	4 seconds

Table 4.3 Storage and access to boundary conditions for TASSE hydrodynamic model H1p5

SETAS hindcast	Bowen storage	NCI storage
2015	/bowen/etas/data/setas/runs/run1	/g/data/et4/data/forcing_tasse/obc/
2015	/bowen/etas/data/setas/runs/run2	/g/data/et4/data/forcing_tasse/obc/
2017	/bowen/etas/data/setas/runs/run3	/g/data/et4/data/forcing_tasse/obc/
2018	/bowen/etas/data/setas/runs/run4	/g/data/et4/data/forcing_tasse/obc/
2019	/bowen/etas/data/setas/runs/run20	/g/data/et4/data/forcing_tasse/obc/
2020 (Jan-Sep)	/bowen/etas/data/setas/runs/run21	/g/data/et4/data/forcing_tasse/obc/
SETAS NRT		
2020(Sep-Dec)	/bowen/etas/data/setas/nrt	/g/data/et4/data/forcing_tasse/obc/

Table 4.4 Storage and access to TASSE hydrodynamic model hindcast H1p5 outputs Dec 2014 to Dec 2020

	Bowen storage	NCI storage
Transport files tran.nc	/bowen/etas/data/tasse/hindcast/tasse_hydro1.5/tran	/g/data/et4/projects/cel599/tasse_hydro_hindcast_v1.5/outputs_v1.5/tran
All files		/g/data/et4/projects/cel599/tasse_hydro_hindcast_v1.5/outputs_v1.5/
Simple files		/g/data/et4/projects/cel599/tasse_hydro_hindcast_v1.5/outputs_v1.5/simple
Surface files		/g/data/et4/projects/cel599/tasse_hydro_hindcast_v1.5/outputs_v1.5/
Profiler/mooring /landers parray files		/g/data/et4/projects/cel599/tasse_hydro_hindcast_v1.5/outputs_v1.5/
Ts files (glider , mooring, lander)		/g/data/et4/projects/cel599/tasse_hydro_hindcast_v1.5/outputs_v1.5/
Sections files		/g/data/et4/projects/cel599/tasse_hydro_hindcast_v1.5/outputs_v1.5/

The Storm Bay model runs in hindcast and near-real time modes, predicting three-dimensional fields of temperature, salinity and currents in Storm Bay and environs. The final hindcast archive H1p5 extends from December 2014 to December 2020 and the version control project area is : https://svnserv.csiro.au/svn/CEM/projects/eTas/model/tasse/tasse_hydro_hindcast/ - access valid Nov 2022. Storage and access details are in Table 4.3 and Table 4.4. A pilot near real time implementation has been running since October 2018 with daily updates to model output (subject to timely provision of all forcing data).

The development of the Storm Bay near real time (NRT) modelling system is complete and includes the SWAN wave model in the automated workflow. The framework has been developed in Python with a web based front end in Cronicle. The purpose of this system is to automate the collection of the various forcing data sets and the setting of values within the model parameter file as well as to monitor and report on the status of active SHOC runs (Figure 4.8). This framework supports all NRT models for Tasmania including regional and local models as well as biogeochemical simulations. The NRT hydrodynamic, wave, sediment

and BGC transport models are all currently running within this Cronicle framework and delivering output to the prototype visualisation dashboard.
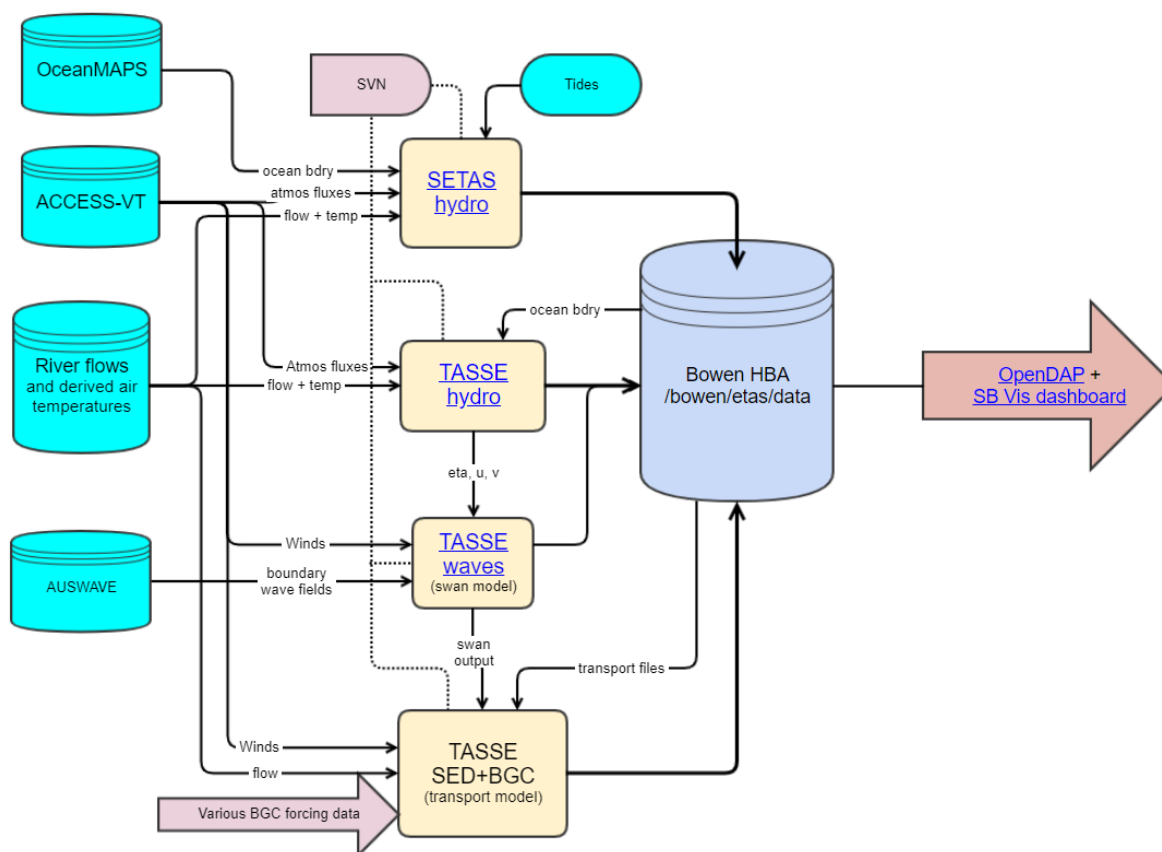

Figure 4.8 Model flow chart for scheduling the near real time modelling system and delivering model output to the visualisation dashboard.

4.2.2   Observations to constrain hydrodynamic model

Calibration of hydrodynamic models is best served through assessment against high frequency conservative variables, such as sea level, salinity, or temperature. A data record that captures seasonality is required, so at least an annual cycle is useful, or at a minimum, winter and summer seasonal records.

During 2015 repeat glider transects were undertaken from the mouth of the Derwent Estuary to the shelf edge across Storm Bay (Table 4.5). Each glider mission included multiple transects containing many profiles from surface to bottom, providing an excellent dataset with which to calibrate the model. This was supplemented with data from the IMOS mooring located at 43.315°S, 147.623°E with T/S observations at 15, 35, 70 and 97 (T only) m, and tide gauges at Battery Point Hobart and Southport. Additionally, we use the Group for High Resolution Sea Surface Temperature (GHRSST) data to benchmark the model sea surface temperature against remotely sensed observation.

Following calibration over the 2015 period, other data were obtained to subsequently allow validation of the model. These data include:-

- Lander data (salinity & temperature) from CSIRO deployments on the sea-bed at 4 locations around the perimeter of Storm Bay during the periods Nov 2018 – May 2019 and Dec 2019 – May 2020.

- Mooring data from a CSIRO/IMOS deployment of a McLane profiling crawler (PRAWLER) (salinity and temperature profiles) from 90m to the surface during the period Oct -Nov 2019.
- Industry data (surface salinity, temperature, waves) from a Tassal Wave buoy near Wedge Is. and Huon Aquaculture moorings (YB2, SB1, CCD) near Bruny Is. during the period Dec 2018 – present.

The locations of the observational platforms are shown in Figure 4.9.

Table 4.5 Glider missions 2014 - 2015

Mission	Start date	End date
1	20 Nov 2014	10 Dec 2014
2	5 Feb 2015	26 Feb 2015
3	29 Apr 2015	11 May 2015
4	16 Jun 2015	8 Jul 2015
5	5 Oct 2015	27 Oct 2015
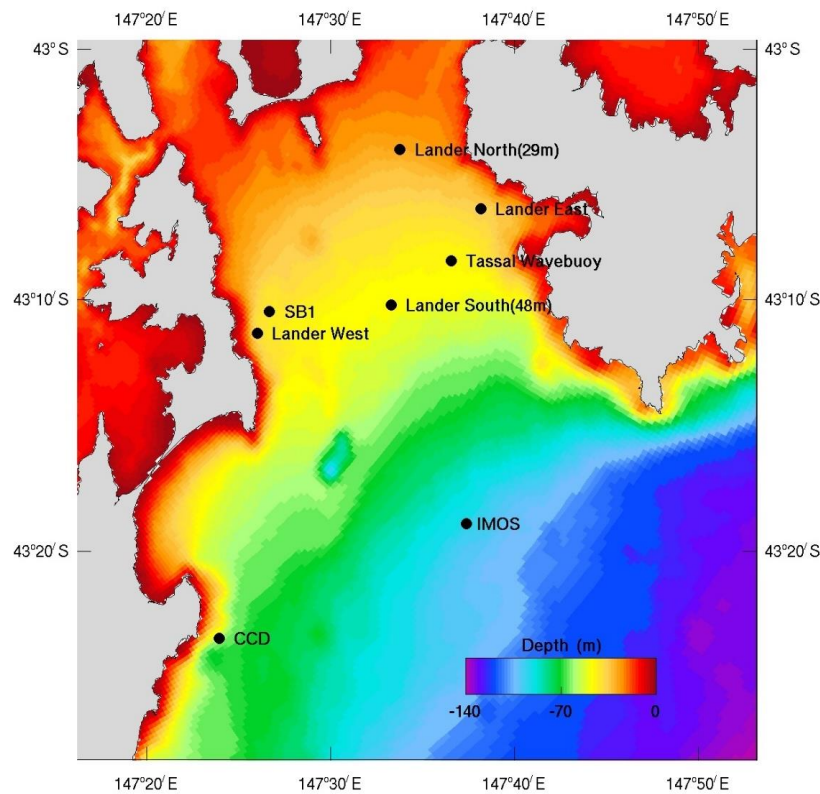
Figure 4.9 Locations of observation platforms used for calibration and validation.

Comparisons of glider observations to model data is not straightforward; a methodology for doing so is presented in Herzfeld et al., (2020) and we follow the same approach here. Glider profiles are sampled at higher resolution than the model and therefore resolve finer scale dynamics which are absent in the model. This makes quantitative comparison difficult, and to overcome this we 'bring the glider toward the model' by sub-sampling the glider data onto the model grid, as opposed to interpolating the model output onto the glider trajectory. The glider observations are averaged into model volumetric cells at discrete time intervals and subsequently viewed as a time series, allowing quantitative assessment of the model's

performance using standard time series metrics (root mean square error (RMSE), mean absolute error (MAE) correlation coefficient (cc), bias, Willmott scores (d)). In addition to coincident model and glider variables, a horizontal neighbourhood can be defined around the glider location in the model, and fuzzy verification techniques (Ebert, 2008) may be used to assess the extent of any double penalty issues. For this study, a simple bound is placed around the glider variable representing minimum and maximum values of the variable in the model within the neighbourhood. If the glider observation falls within these bounds, we can assume the model is reproducing observed dynamics within a length scale representing a tolerable displacement of features. In terms of Ebert's decision model definition: 'Useful forecast predicts the observed variable within an area having a length scale that represents a tolerable displacement of a feature in the model.'

The net heat flux in the model consists of shortwave radiation (SWR), longwave (incident and upward) radiation and turbulent (sensible and latent) heat fluxes. There latter components are computed using the bulk scheme of Kitaigorodskii et al., (1973). While the longwave, sensible, and latent heat fluxes impact on the first layer of the model, the SWR is depth distributed, impacting multiple layers of the model, and potentially reaching the bottom in shallow areas. The specification of the attenuation and transmission parameters in the model dictate how heat due to SWR input is distributed within the water column. Whilst the total heat in the water column due to SWR is fixed, these parameters do determine how much heat remains in the surface layer, hence is available as heat loss due to long wave output and latent (and to a lesser degree sensible) heat loss. The transmission parameter sets the fraction of the SWR that will be depth distributed, the remaining part being input at the surface boundary. The attenuation coefficient sets how the transmitted part of the SWR is distributed with depth. This partitioning of SWR approximates the preferential absorption of longer wavelengths within the first few metres and deeper penetration of the blue end of the spectrum (Simpson and Dickey, 1981).

Where SWR penetrates to the sea floor, the surplus radiation can either be absorbed by the sea floor, or bottom reflectance can provide extra heat to the bottom layer. The bottom absorption parameter sets the fraction of SWR that is absorbed into the seabed; in the TASSE model we allow all SWR reaching the bottom to be absorbed.

SWR attenuation and transmission may be used as tuning parameters to balance the heat budget due to uncertainties in the bulk fluxes. Additionally, and perhaps more importantly, the vertical distribution of heat has a profound effect on the stability of the water column, and hence the magnitude of vertical mixing. These SWR parameters must therefore be carefully set to tune the balance of buoyancy production to shear production in the source terms for the vertical closure scheme. This is somewhat analogous to tuning the c_{e3} parameter that scales buoyancy production in the dissipation equation. Note that Burchard et al., (1998, section 4.1) report this parameter is dependent on the stability functions and is used as a calibration parameter. In order to optimize the SWR parameters, we employ an inline approach where an ensemble (of 100 members in this case) capturing the range of the SWR parameters is created, and the vertical mixing of temperature (using the differing distributions of SWR as source terms) is advanced forward for a prescribed time-step (3 hours in this case) for every member of the ensemble to generate vertical profiles of temperature. These profiles may then be compared to observation to identify the most accurate parameterisation in the ensemble; we compare to SST derived from the OSITA GHTSST L4 product (THREDDS access at https://www.ghrsst.org/ghrsst-data-services/services/ - access valid Nov 2022). This delivers a spatial and temporally varying SWR attenuation and transmission specification that minimizes error when compared to observation.

4.2.3   Hydrodynamic model calibration and validation

A number of skill metrics to assess the model: the root-mean-square error (RMSE), the mean absolute error (MAE), model bias, correlation coefficient (cc), and model skill (d2) described by Willmott (1981). This latter skill metric is a dimensionless index between 0 (zero skill) and 1 (perfect skill) that weights the model errors relative to the known amplitude of local variability. It is computed as the difference between the model and observation anomalies relative to the time-average observations, divided by the sum of observed anomalies relative to the time-average observations. While the temperature and salinity comparisons give us information on water mass properties, seasonal and synoptic variability in these properties can be linked with known dynamical processes (flood plumes, intrusions at the shelf break) and inform us on the performance of the model in representing the complex circulation in Storm Bay.

In early summer there can be a complex interplay between the water masses present in Storm Bay, with highly variable frontal boundaries evident. Unfortunately, the IMOS mooring is located in the middle of these competing water masses, making comparison to the model difficult due to double penalty issues if frontal boundaries lie at the mooring location. This is illustrated in Figure 4.10 for situations in 17 Dec 2014 (Figure 4.10 a and b) and 29 Jan 2015 (c and d) for model temperature and salinity. It is seen that the location of the IMOS mooring (black dot) lies on a frontal boundary between cooler subantarctic water and warmer Storm Bay water. If this frontal boundary were to migrate a small distance north or south, then the mooring data would be correlated to quite different water properties in the model. Although the water masses in Storm Bay described above are correctly simulated by the model, their exact location at the precise time may not be correct, and standard error metrics will penalize this situation as severely as if the water masses were altogether absent, i.e. the double penalty issue. It is unreasonable to expect the model to maintain such a level of frontal position accuracy without data assimilation (e.g. Jones et al., 2012), and to address the issue during assessment we employ neighbourhood techniques (Ebert, 2008) in the same manner as is used for glider comparisons. In this case we use a neighbourhood of 30 km (approximately the de-correlation length scale of temperature and salinity in the model at the IMOS location).
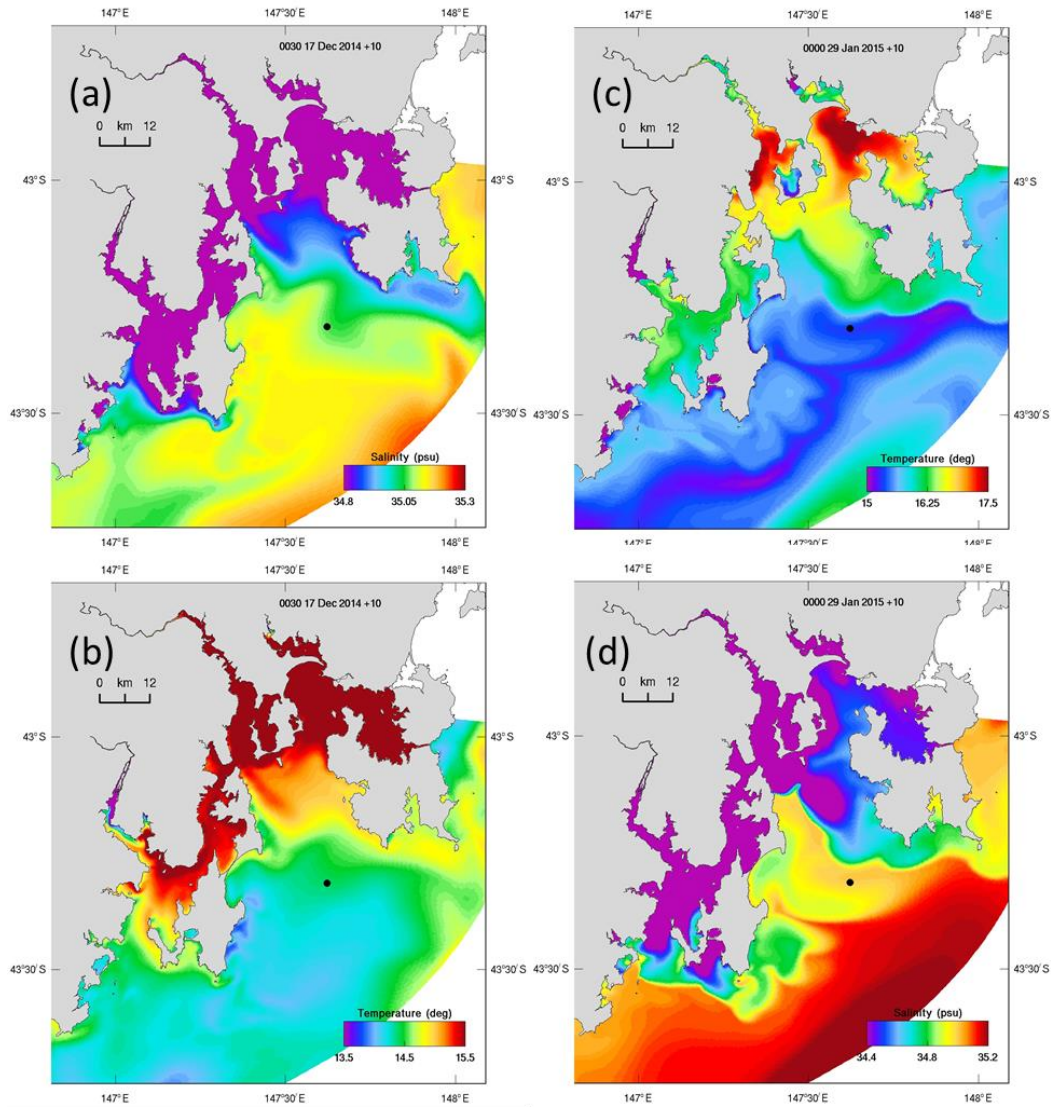
Figure 4.10 Surface temperature (a) and salinity (b) for 17 Dec 2014, and temperature (c) and salinity (d) for 29 Jan 2015. The IMOS mooring is at the location of the black dot.

Such a situation also occurs with sub-mesoscale eddies shed by the EAC. Figure 4.11 shows such an eddy on 17 Feb 2015, with the trajectory of the glider overlaid. A sub-mesoscale filament of warm water has detached from the warm shelf edge core and is propagating into Storm Bay. Such a feature is also evident in SST imagery. However, the glider trajectory lies on the frontal boundary of this feature, and again small shifts in spatial position can lead to large changes in interpretation of standard quantitative metrics. The use of neighbourhood techniques in this situation is again warranted to address any double penalty issues.
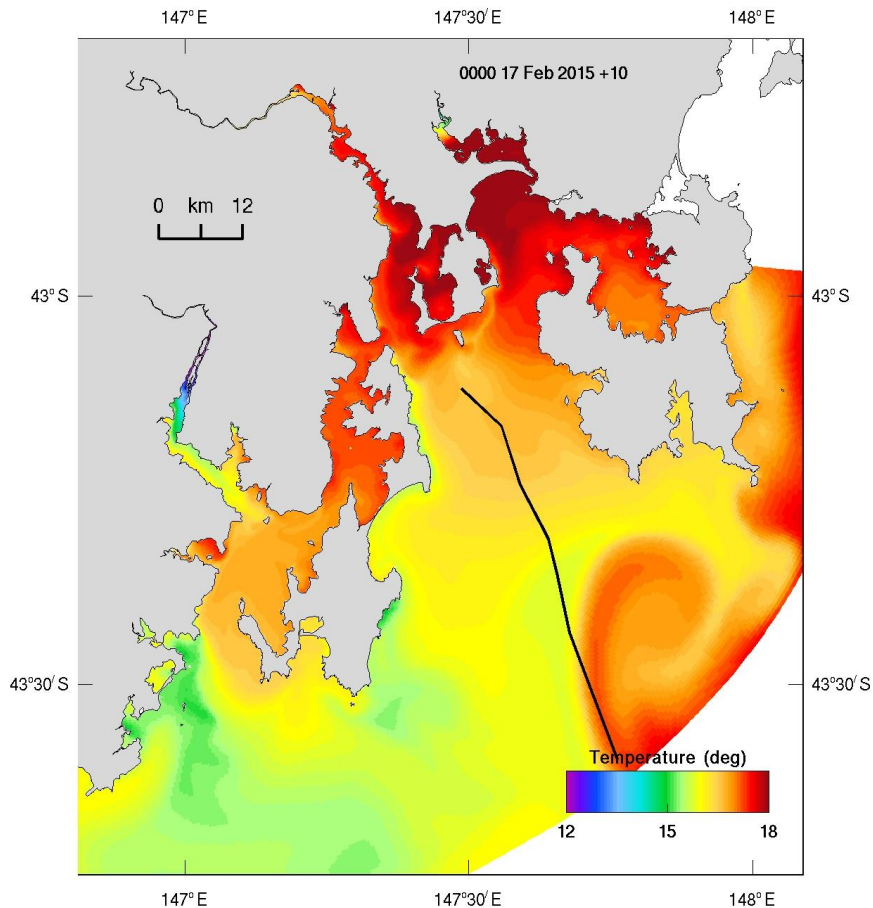
Figure 4.11 Surface temperature on 17 Feb 2015. The black line is the glider transect.

The Dec 2014 glider mission is compared to model output in Figure 4.12 using the glider assessment methodology described above. For the whole mission, high levels of model skill are achieved with a Willmott skill of 0.94 for temperature and 0.92 for salinity. Samples of the trajectory when the glider is offshore (Figure 4.12 b) and inshore (Figure 4.12 c) show the model is accurately representing the stratification. Note that these plots also show the depth of the glider, and the number of glider samples that were averaged onto a model cell. The small range of glider depths (< 30m) corresponds to when the glider is inshore at its northern extent in Storm Bay, and the large range corresponds to instances when the glider is in deeper water near the shelf edge. In Figure 4.12 the data comparison starts when the glider is in deep water and subsequently travels inshore, turns on 4 Dec to travel again to the shelf edge, and again turns once more to travel inshore where the mission ends on 10 Dec. Note that at times there are > 100 samples taken by the glider while it traverses a single model cell. Further comparisons for the Feb, Apr and Jun missions are shown in Figure 4.13.

Comparison to the IMOS mooring is displayed in Figure 4.14 for the first 9 months of 2015. Included in this plot are the minimum and maximum bounds within a 30 km neighbourhood in the model; ideally the observations should lie within these bounds. We see that in late summer and early autumn the model becomes cooler than observations, even within the neighbourhood.
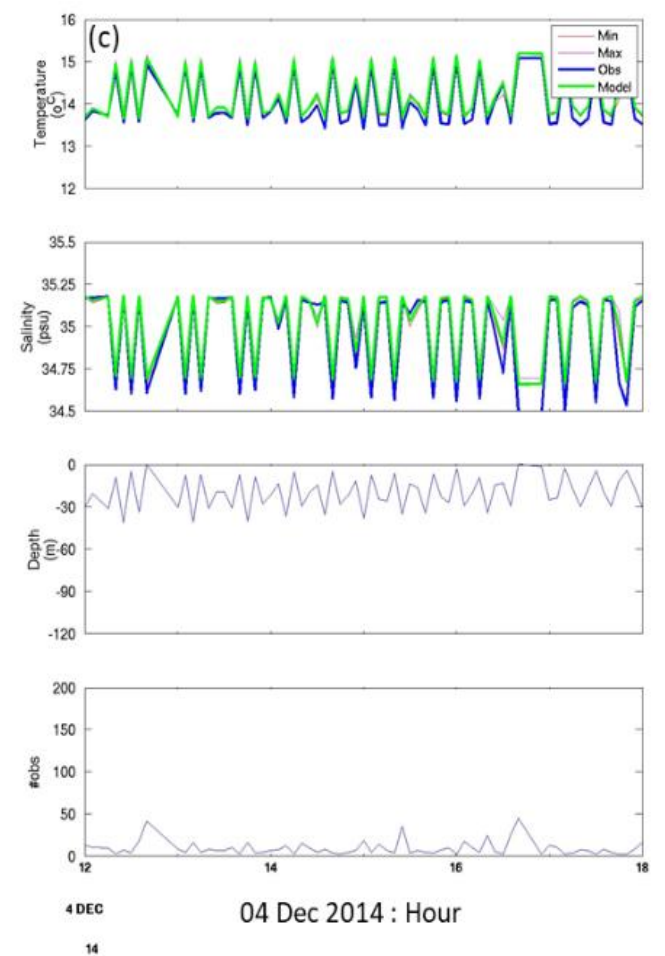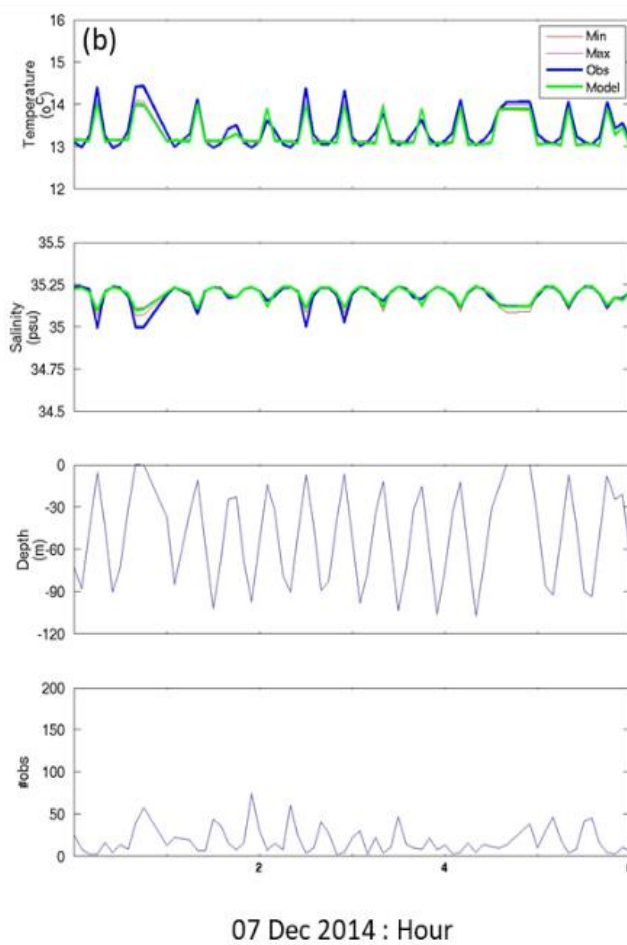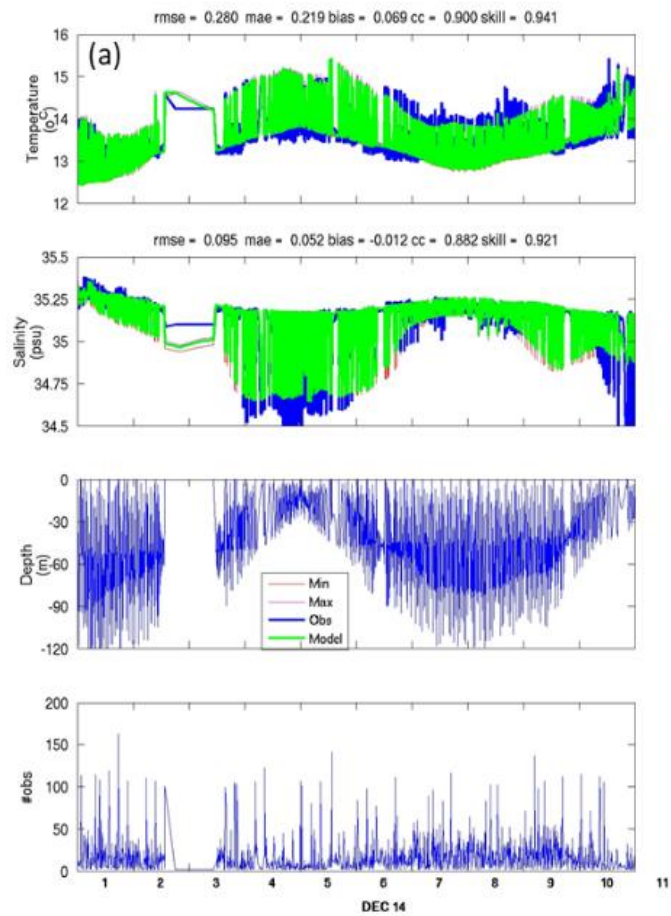
Figure 4.12 December 2014 glider mission (a) whole mission, (b) offshore sample, (c) inshore sample. Glider observations are in blue and model output is in green. The minimum (red) and maximum (magenta) model values in a 3 km neighbourhood of the glider position are included.
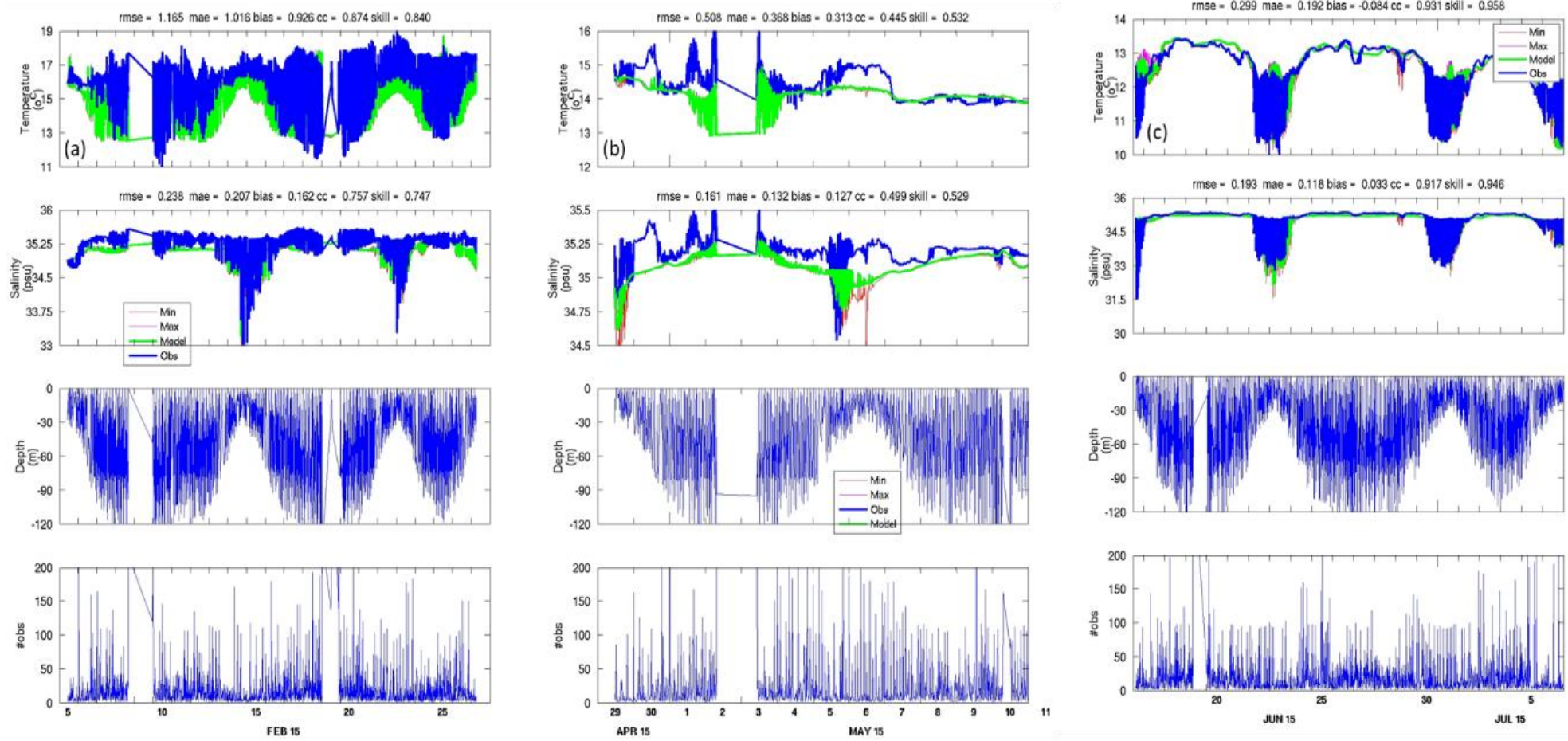
Figure 4.13 Glider mission comparisons to model for (a) February, (b) April and (c) June 2015.

Around this time there is also large variability in the observations, indicative of the water masses in Storm Bay competing for position over the mooring location. While the model does predict the presence of these water masses in their mean state, as stated above, it is unlikely the model can skilfully reproduce the exact location of these water masses without data assimilation (e.g. Jones et al., 2012). This deterioration in model skill is also seen in the April glider comparison. In early summer, late autumn, and winter when the presence of subantarctic water is not as prevalent, the model accurately predicts temperature at all depths at the IMOS mooring location. This is also seen in the February and June glider comparisons, which show good skill with T/S Willmott scores of 0.84 and 0.75 in February and 0.96 and 0.95 in June. The model captures particularly well a freshwater plume from the Derwent Estuary which intrudes into Storm Bay freshening surface water in June. Salinity shows a fresh bias of ~0.15 throughout, likely due to biases in the global model boundary forcing. This will be attempted to be compensated for using boundary scaling for salinity.
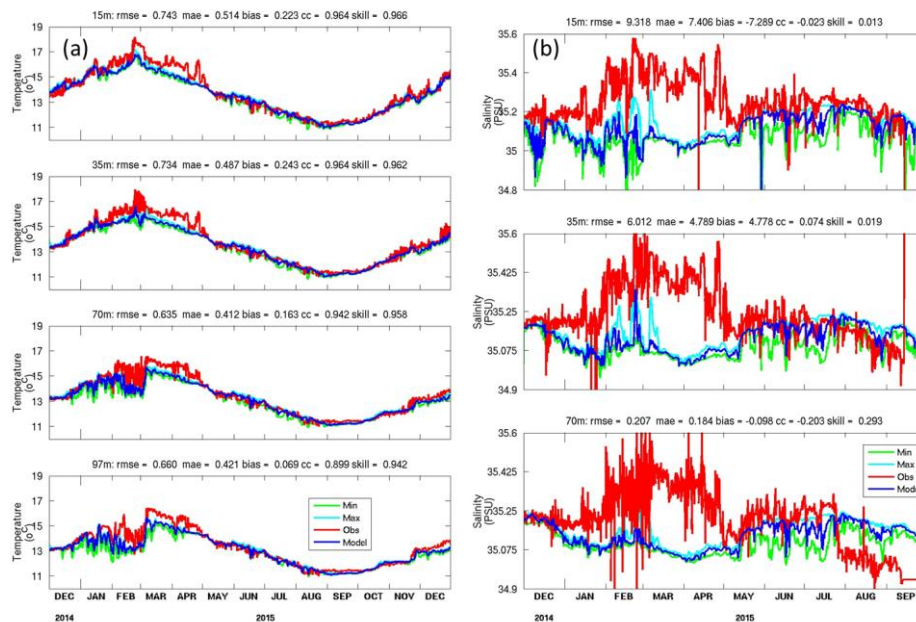
Figure 4.14 Model comparison of (a) temperature at 15m, 35m, 70m, 97m, (from top panel to bottom) and (b) salinity at 15m, 35m 70m (from top panel to bottom) to the IMOS mooring.

The model sea-level is assessed against observation at Battery Point and Southport (Figures 4.15 to 4.18). The skill metrics were computed for the total signal and low frequencies over 13 months December 2014 to January 2016, and also for a 2-month period January-February 2015. The low-pass filtered signal determines the long term barotropic fate of material. For visualisation purposes, a 2-month period allows us to clearly observe whether the model is accurately capturing the key characteristics of tidal amplitude, phase, and form factor.

The model shows good skill at tidal and low frequencies. The model tidal magnitude and phase compares very well to observation (RMSE = 0.07 m, MAE = 0.04 m), the tide is in phase with observation (cc = 0.98) and overall, the model exhibits very high skill (d2=0.91). The neap-spring cycle is also well resolved. Skill metrics for the low frequency component also show good skill

(RMSE = 0.03 m, MAE = 0.02 m, cc = 0.97 and d2=0.86). It is important to note that skill is slightly degraded occasionally, with some smaller amplitude of the model in the low frequency (10-01-2015 to 22-01-2015 and 05-02-2015 to 15-02-2015 for examples).

Overall, the comparison of the model with sea level measurements indicates a good tidal forcing at the open boundary and a good propagation of the tidal signal inside the model, which reflects an adequate representation of the bathymetry. Low frequency motion is also well represented which indicates a good residual circulation.
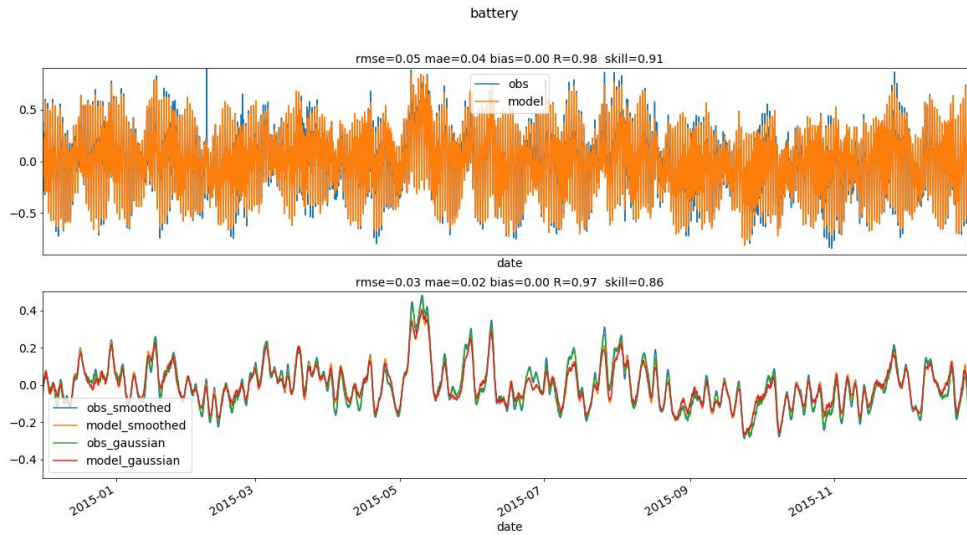
Figure 4.15 Total sea-level (top) and low-pass filtered sea-level (bottom) at Battery Point for Dec 2014 to Jan 2016.
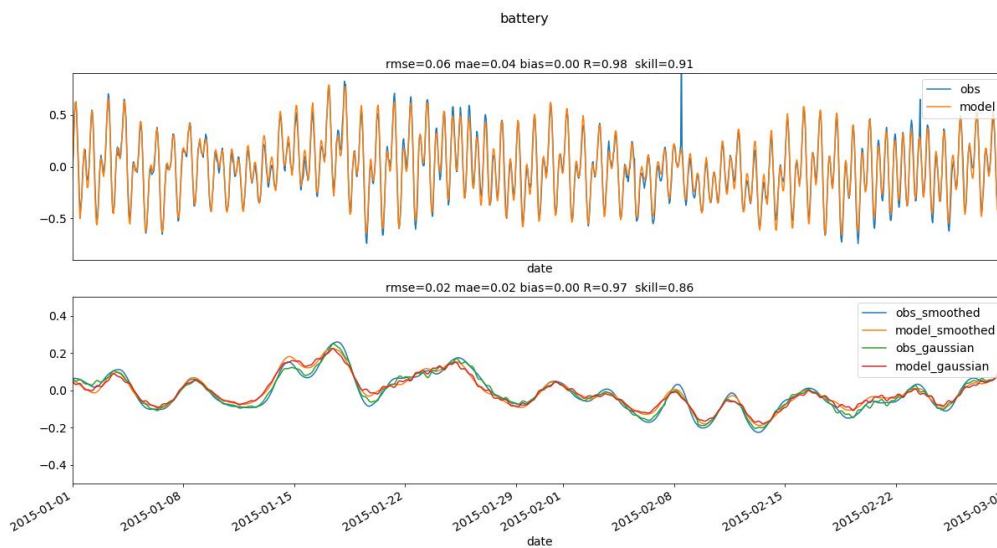
Figure 4.16 Total sea-level (top) and low-pass filtered sea-level (bottom) at Battery Point for Jan and Feb 2015.
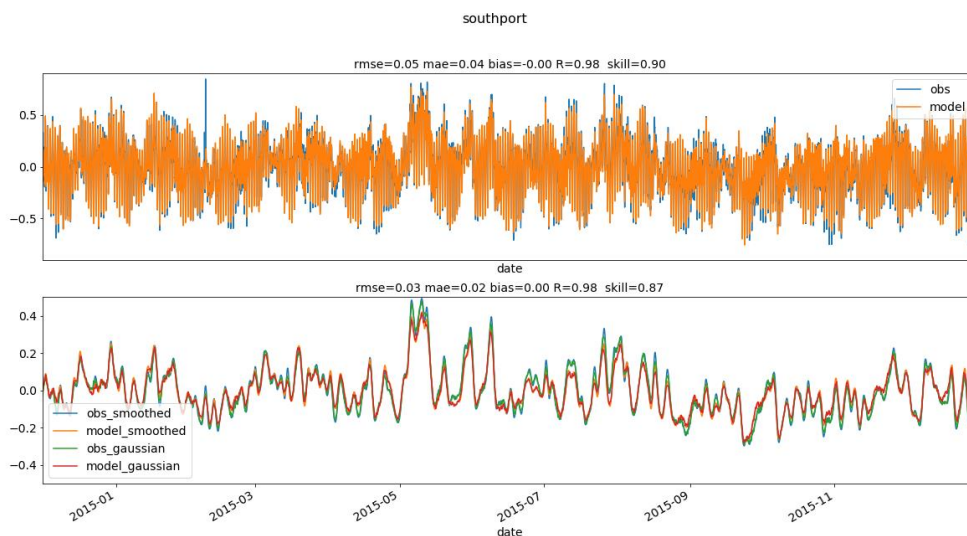
Figure 4.17 Total sea-level (top) and low-pass filtered sea-level (bottom) at Southport for Dec 2014 to Jan 2016.
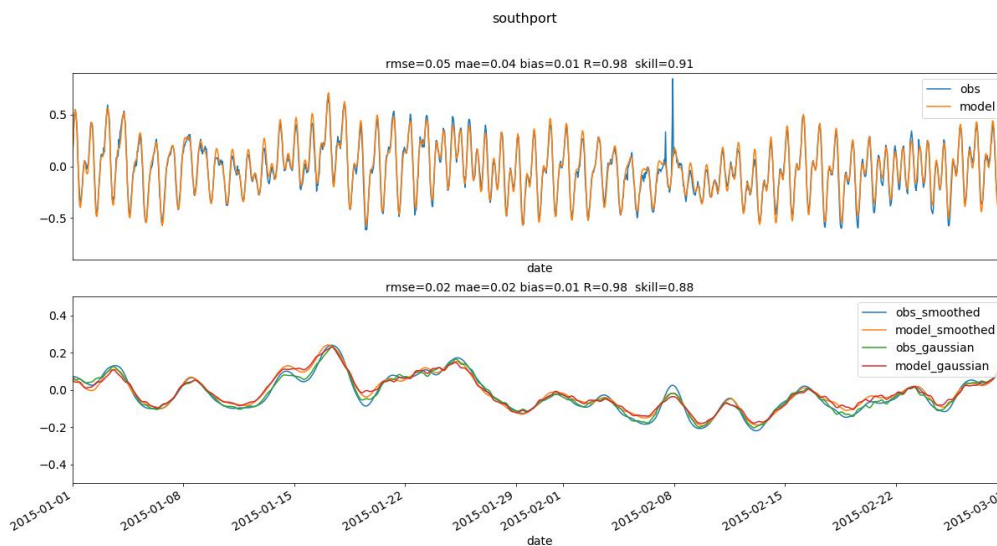
Figure 4.18 Total sea-level (top) and low-pass filtered sea-level (bottom) at Southport for Jan and Feb 2015.

The model allows the import of GHRSST products (https://www.ghrsst.org/ghrsst-data-services/services/ - access valid Nov 2022), interpolated onto the same grid the model uses. Here we use the GHRSST OSITA global L4 product. Close to land the satellites samples may be contaminated by land pixels, hence areas within the shallower regions within the Huon and Derwent Estuaries, and Pittwater should be treated with caution. Elsewhere the SST product is likely accurate. Inline RMSE can be computed; here we show the yearly RMSE in Figure 4.19. The GHRSST SST compares favourably with the model, exhibiting errors less than 0.5^{o}C, except at the offshore boundary where there is influence of the EAC during the summer months, and in the shallower inshore regions.

Calibration Summary

The model is currently showing acceptable performance when compared to observational data and is considered fit for purpose to transport sediment and biogeochemical variables. Validation of the model to additional independent observations is underway for later years. The hindcast period from December 2014 – January 2021 has been completed including the outputs necessary for sediment transport and biogeochemical model.
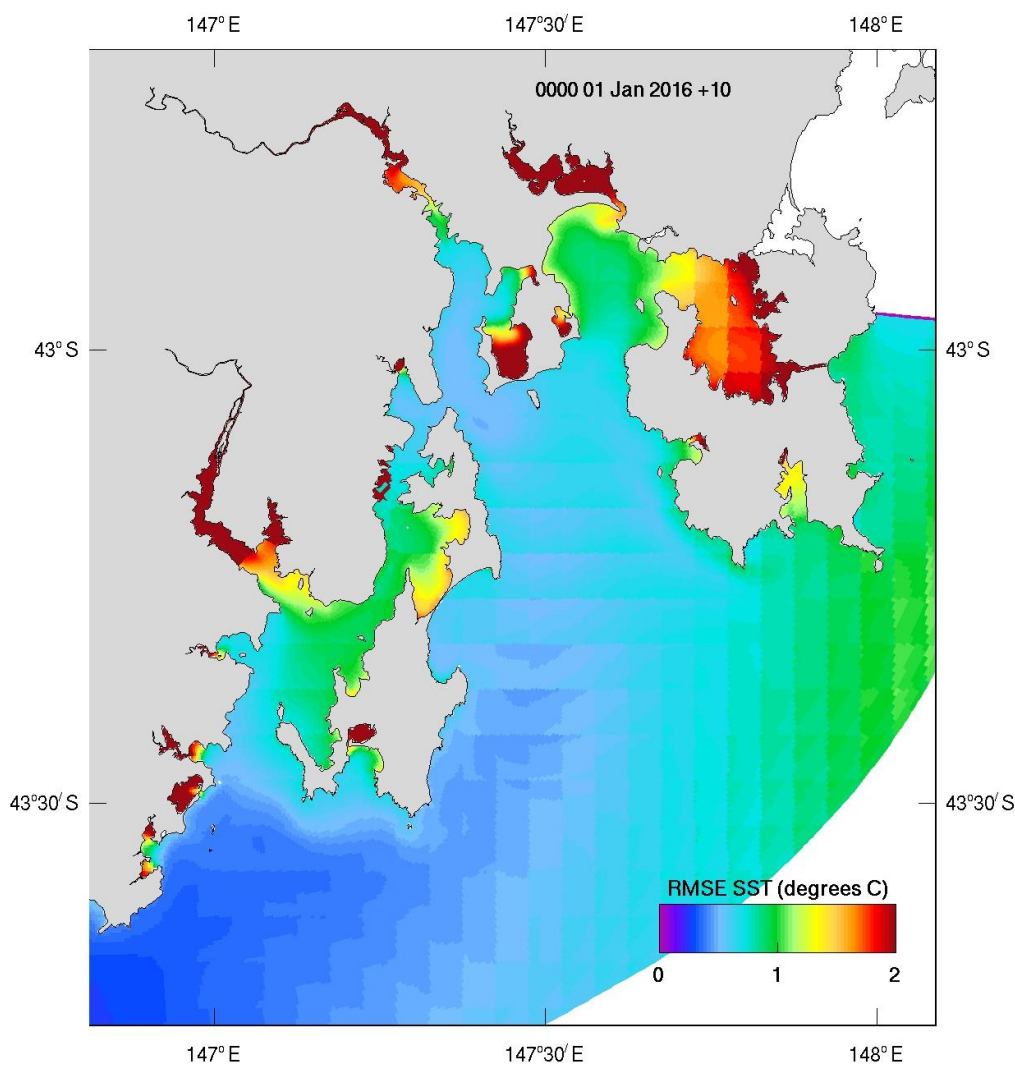
Figure 4.19 Yearly RMSE of model surface temperature compared to GHRSST L4 for 2015.

4.3   Connectivity Analyses

The hydrodynamic model produces predictions of sea-level, temperature, salinity, and currents within Storm Bay, which may be used to produce connectivity analyses. Various metrics describing how long a dissolved substance is available within a regional water body may be produced, viz. maps of residual flow, passive tracer distributions, age tracers and flushing times.

The different techniques, their advantages and limitations are described in this section.

4.3.1   Residual flow

The seasonal mean of 3D and 2D currents provides an indication of the long-term fate of tracers within the domain. The difference between summer and winter conditions usually provides the largest contrast in residual flow, which may be represented by seasonal means. Monthly means

may provide further insight into variability within seasons. The summer means are shown in Figure 4.20 and winter means in Figure 4.21; bottom mean flows are shown in Figure 4.22.
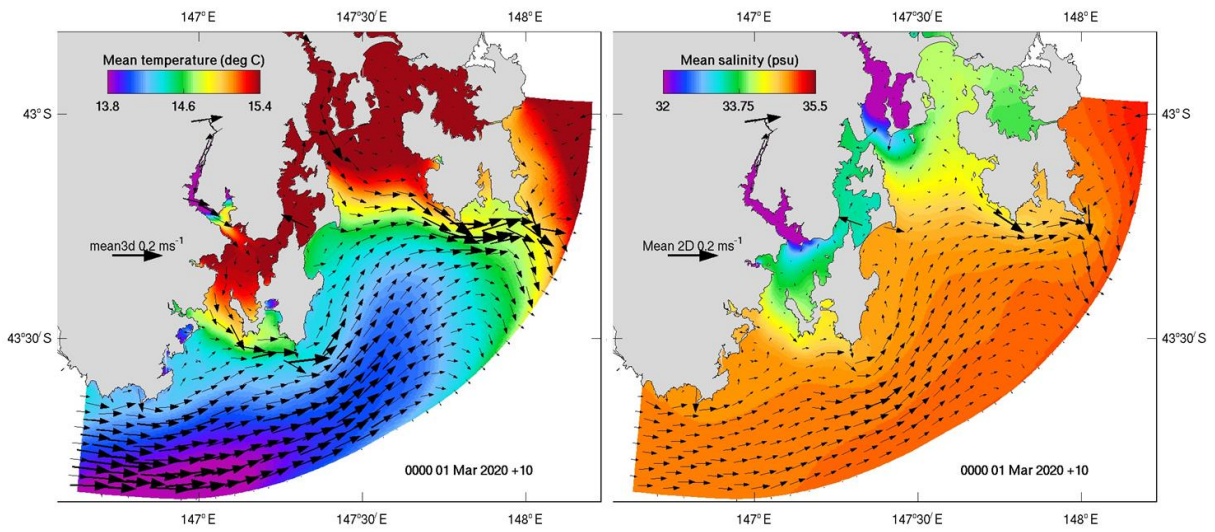
Figure 4.20. Summer surface temperature and surface currents (left) and surface salinity and depth averaged currents (right).
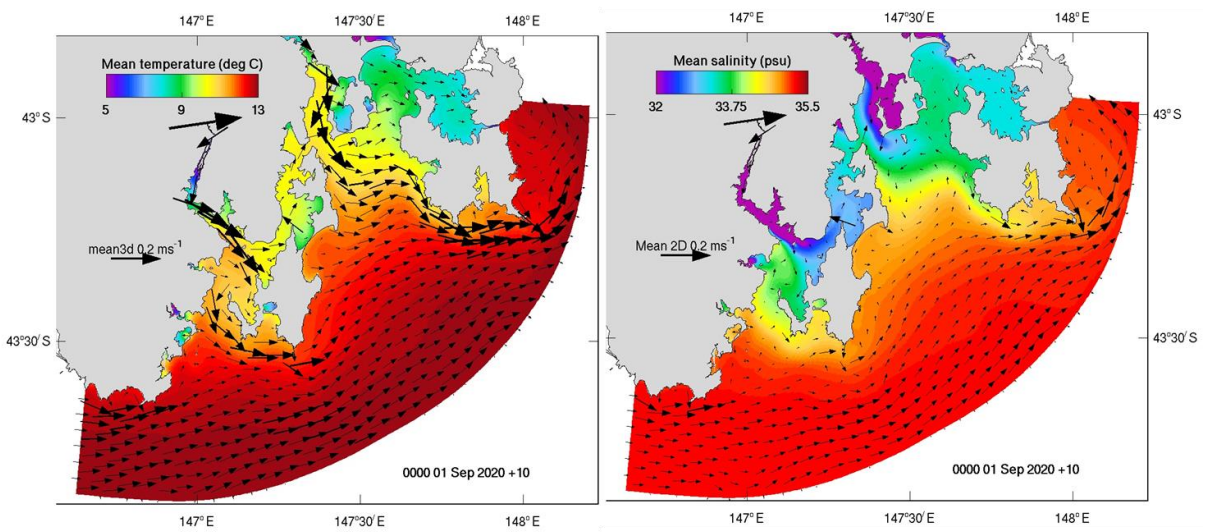
Figure 4.21. Winter surface temperature and surface currents (left) and surface salinity and depth averaged currents (right).
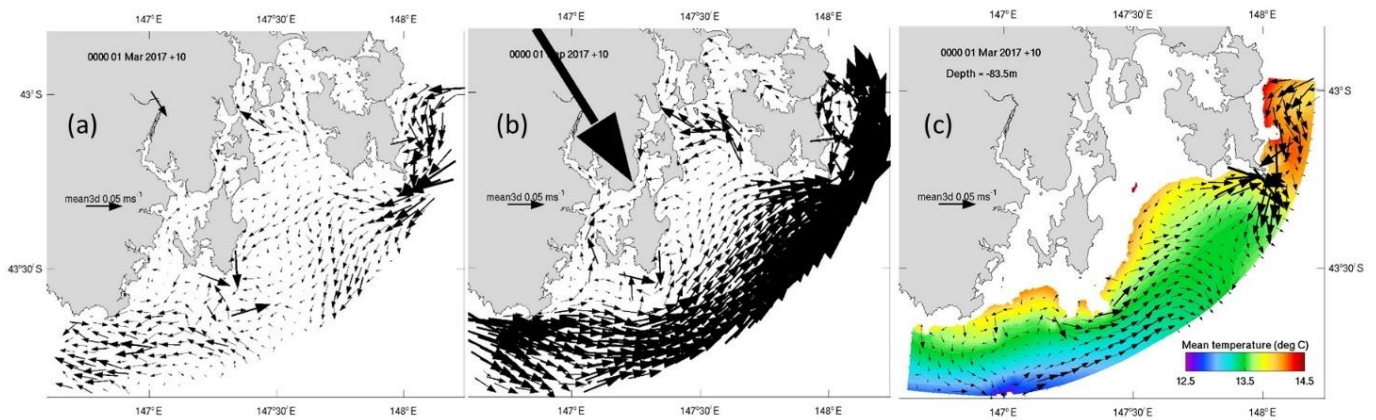
Figure 4.22. Summer (a) and winter (b) bottom currents [the large arrow is the mean flow from the Huon River input, which is huge owing to flood events]. The summer temperature and currents at ~80 m are displayed in (c).

Storm Bay and D'Entrecasteaux Channel

The flow in Storm Bay is generally directed eastward, with a strong jet flowing out of the Derwent Estuary and south-east across Storm Bay, to exit the region around the southern tip of Tasman Peninsula. Similarly, strong flow exits D'Entrecasteaux Channel around the southern tip of Bruny Island. However, more freshwater makes its way northward in D'Entrecasteaux Channel, with low salinity in winter indicative of the flood plume acting under the influence of rotation (Herzfeld, 2010). Flows are stronger in winter than in summer. This circulation is characteristic of a buoyant plume whose dynamics are dominated by Earth's rotation, with the far-field buoyant plume forming a geostrophic coastal current following the coast towards the left in the southern hemisphere (Horner-Devine et al., 2015). Note that winds and ambient currents might also contribute to this averaged circulation pattern.

Large flows are seen entering the head of the Huon and Derwent Estuaries at the surface and bottom, particularly in winter. Bottom flows in winter mirror the surface flows, with the exception that water is entrained into the mouths of Huon and Derwent Estuaries by the salt wedge circulation. These inflows originate in Storm Bay (Derwent) and southern D'Entrecasteaux Channel (Huon). Bottom flow is also seen into Frederick Henry Bay.

Shelf circulation

In winter flow follows the shelf break eastward across the domain. In summer the surface temperature shows three water masses within Storm Bay; warm water > 16.5°C in the northern part of the Bay, cool 15-15°C sub-Antarctic water intruding from the west, and warm > 16.5°C EAC extension water along the shelf edge in the east. These water masses can create highly variable frontal regions within the Bay (e.g. see Figure 4.10), with the approximate summer latitude of the front between Storm Bay and sub-Antarctic water residing at ~-43.2S. A horizontal slice of mean temperature and currents at ~80 m is shown in Figure 4.22c, from which it is seen that during summer a confluence of colder eastward moving sub-Antarctic water with warmer EAC extension water moving south-west occurs at the southern tip of the Tasman Peninsula. This averaged circulation acts to bring cold sub-Antarctic rather than EAC water onto the shelf at depth in the mouth of Storm Bay.

The residual flow analysis reveals that there is no averaged seasonal flow from the EAC extension entering Storm Bay. An EAC anti-cyclonic eddy is seen off the eastern coast of Tasman Peninsula, likely a lee eddy due to instability at the southern tip. But on the western coast of the Tasman Peninsula, the surface flow is dominated by the relatively thin jet emanating from the Derwent, and only in deeper layers does the EAC feature in summer.

In summer some bottom water flows westward past the southern tip of Tasman Peninsula into Storm Bay and follows a general westward trajectory along the shelf break. Note that the bottom flow can be misleading owing to the large range of depth spanned. In Section 4.2.3 it was shown that any EAC water entering Storm Bay is the result of sub-mesoscale turbulence (e.g. see Figure 4.10). This makes the transport of EAC water into Storm Bay periodic, unsustained, and relatively unpredictable.

Offshore forcing

Figure 4.23 shows the summer monthly means of surface temperature, sea level and surface currents computed from BRAN. Offshore from Storm Bay a cold intrusion is seen to extend from the west, gradually weakening throughout summer and replaced with warmer EAC extension water further offshore. Surface currents are eastward south of Tasmania, supported by low sea level to the west of Tasmania with higher sea level to the east. We hypothesize the low sea level is due to cold core mesoscale eddy activity originating from the sub-tropical front further south, and advected eastward in the West Wind Drift. This eastward flow does not appear to be associated with uplift, as the West Wind Drift south of Tasmania is a downwelling favourable flow. The confluence of this eastward flow and south westward EAC extension is consistent with the TASSE model at depth (Figure 4.22c); this is expected as these flows are inherited from the global model on the open boundary.
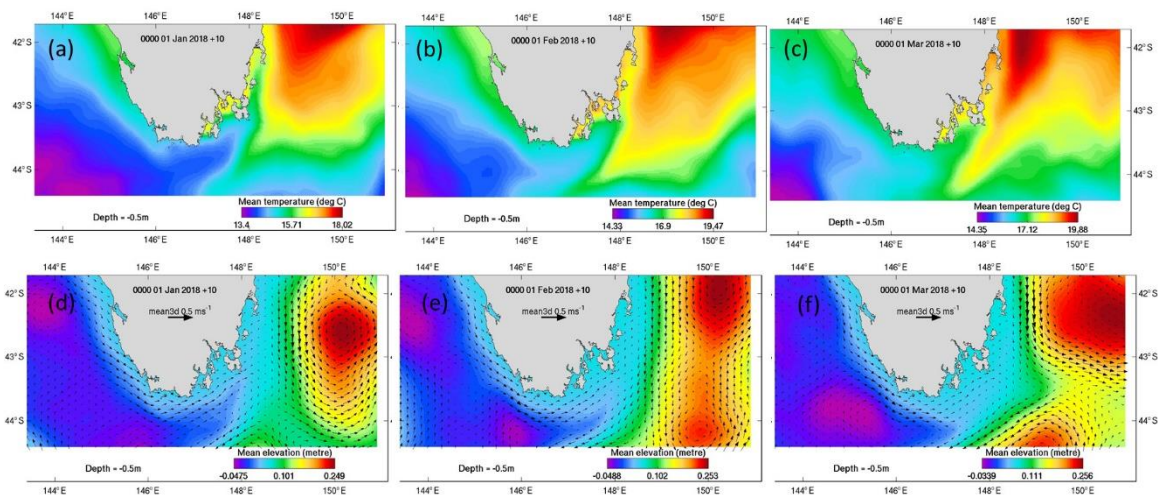

Figure 4.23. Mean monthly SST for (a) Dec, (b) Jan and (c) Feb. mean sea level and surface currents for (a) Dec, (b) Jan and (c) Feb. Means were computed from BRAN for 2015 – 2018.

Herzfeld (2008) noted the existence of quasi-stationary anti-cyclonic eddies south of Tasmania during spring and summer (2002 – 2005) associated with positive sea surface anomalies, which

drove south-westward flow along the shelf edge during those seasons. This flow was capable of supporting uplift in the bottom boundary layer and was hypothesized as a mechanism to bring nutrients from depth over the slope into Storm Bay (Figures 4.17 and 4.18 in Herzfeld, 2008). In winter cyclonic eddies south of Tasmania supported north eastward flow (Figure 4.19, Herzfeld, 2008). Large variability was noted in these sea surface anomalies. There is little evidence of such south westward flow along the shelf break (> 100 m) in the spring seasonal mean (not shown) for the years 2015 – 2019. The October IMOS sea level anomalies and October mean of BRAN show low sea level off southern Tasmania associated with eastward flow (Figure 4.24). The uplift identified in Herzfeld (2008) due to anticyclonic mesoscale eddies may be valid, however, in the years modelled here there does not appear to be any such eddies in close proximity to the shelf-break that could drive such uplift.

The monthly mean sea surface anomalies do not provide an unambiguous view of circulation south of Tasmania. While they largely correlate with depth averaged flow (Figures 4.20 and 4.21), flow reversals are seen at depth compared to the surface. This indicates baroclinic forces play a role and is an area that requires further investigation.
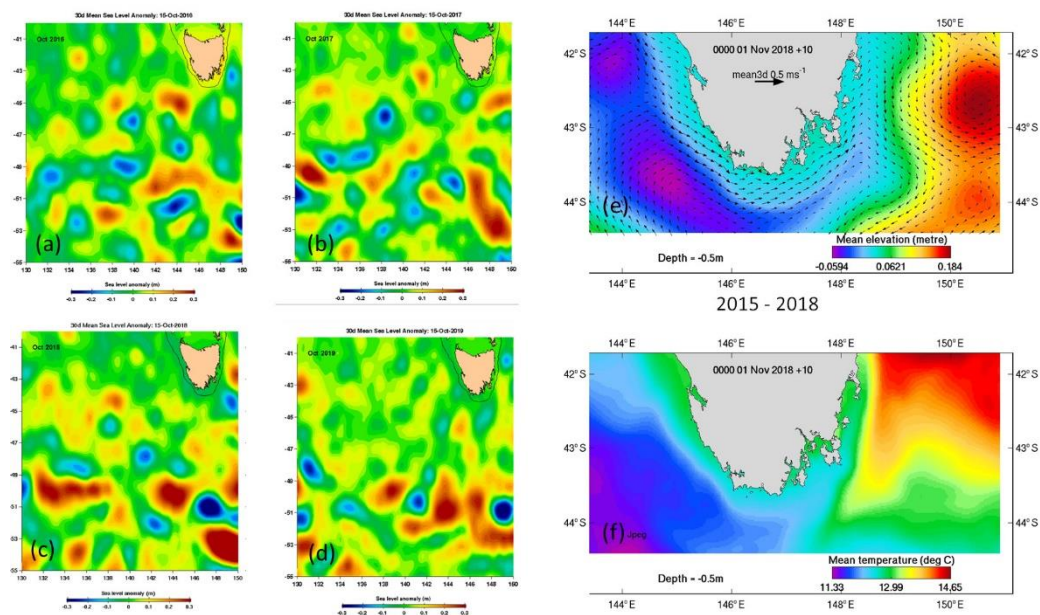
Figure 4.24. (a) – (d) IMOS Ocean Current mean sea surface anomalies for Oct 2016 – 2019. (e) October mean sea level and currents from BRAN and (f) October mean SST from BRAN, 2015 – 2018.

A schematic summarising the mean flow described above in Storm Bay, D'Entrecasteaux Channel and the offshore shelf break is shown in Figure 4.25.
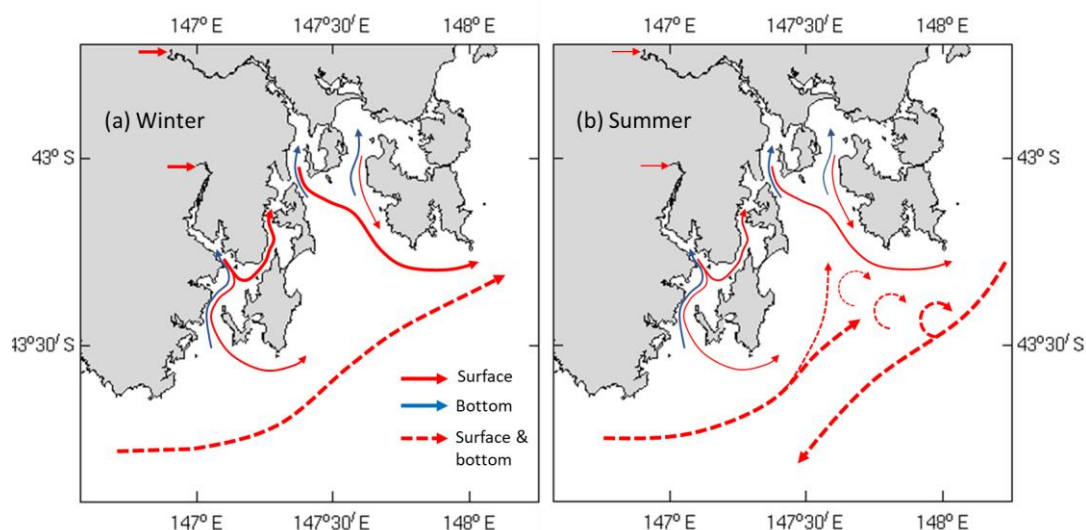
Figure 4.25. mean flow schematic in (a) winter and (b) summer. Solid red arrows are surface flows, and blue arrows are bottom flows. Depth averaged flows are shown as dashed red arrows.

4.3.2   Point sources - passive tracers at designated locations

From a management perspective, the fundamental outcome of connectivity analysis is to describe where material released at certain locations goes, in what quantities it goes there and what the variability of those quantities are. The most informative method to diagnose the fate of a pollution source is to supply order statistics of spatial distributions of passive tracer concentration as a result of input at designated locations. In this case the release locations have been selected at salmon lease sites.

The passive tracer is continuously injected with a unit flux (e.g. 1 kg/s) of material into a layer of the model at a prescribed grid point. The resulting material is advected and diffused by ambient conditions to provide a spatially and temporally varying distribution of passive tracer (with concentration units kg/m^3). The resultant distributions of the passive tracer concentration provide information on where, and in what concentrations water is transported. By providing order statistics (5th, 50th (median) and 95th percentile distributions) of the resultant distributions captured at high frequency (1 hour) based on multi-year simulations, we integrate over most forcing conditions the region is subject to, and provide a measure of variability that is experienced. Then, for example, the 95 percentile distribution will show the concentrations in the domain that will only be exceeded for 5% of the time (i.e. concentrations will be less than the provided distribution for 95% of the time). In areas of high connectivity, the concentration distributions will attain larger values than those areas where connectivity is poor.

The conservation equations describing tracer movement are linear with respect to tracer concentration, so if the actual flux is known the corresponding distributions can be scaled accordingly. For example, it the actual flux was 100 kg/s then all the concentrations in the percentile distributions would need to be multiplied by a factor of 100.

In this case the unit tracer was continuously released in the top 1 m of the water column at the locations depicted in Figure 4.26, and surface percentile distributions were computed from Dec

2014 to Sep 2019. Median tracer distributions are presented for Storm Bay sites in Figure 4.27. This shows that site SB055 is poorly connected with Storm Bay, with little concentration leaving Port Arthur Bay. Concentrations are 0.005 – 0.01 south of the release site in the Bay, and higher than 0.02 in Stewarts Bay. The SB117 site has concentrations confined to Norfolk Bay and eastern Frederick Henry Bay, with smaller concentrations in Pittwater. Little concentration enters Storm Bay; that which does follows the mean flow down the western coast of Tasman Peninsula. Concentrations are 0.001 – 0.002 in Norfolk Bay.

Site SB190 shows better connectivity with the surrounds, with median tracer distributions showing a band of higher concentration (1×10^{-4} – 5×10^{-4}) in the mean flow alongside Tasman Peninsula, and lower concentrations (4×10^{-5}) in Frederick Henry Bay. The latter tracer would be delivered to this region by bottom currents after vertical mixing throughout the water column. Lastly the site SB261 shows a band of high concentration (1×10^{-4}) stretching eastward from the release site, transported with the mean surface flow, and another band of the same concentration in the mouth of the Derwent up to South Arm, transported by the bottom mean flow. Concentration is fairly evenly distributed in the northern part of the domain (including northern D'Entrecasteaux Channel and mid-Derwent), but little tracer is found in southern Storm Bay, Huon Estuary, and upper Derwent.

The 5th and 95th percentile tracer distributions are provided in Figures 4.28 and 4.29 respectively for reference.
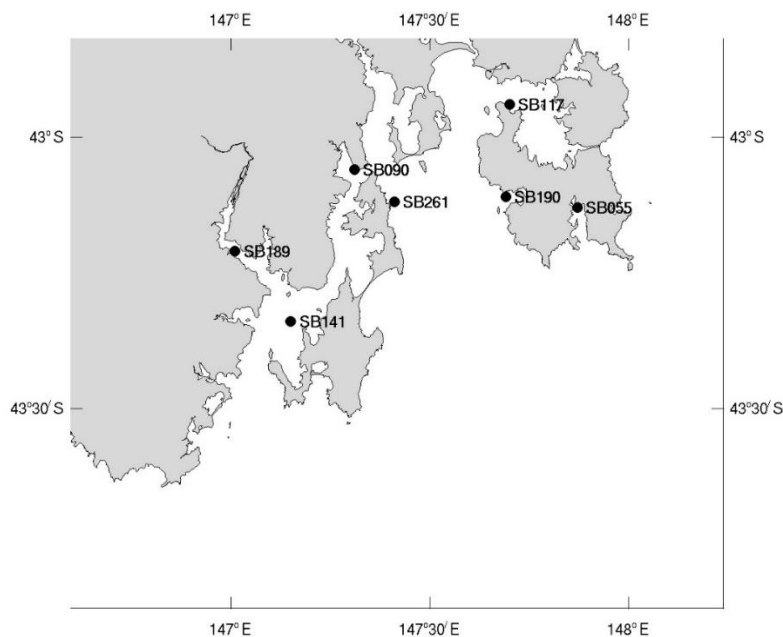
Figure 4.26. Release sites for tracer distribution analysis.
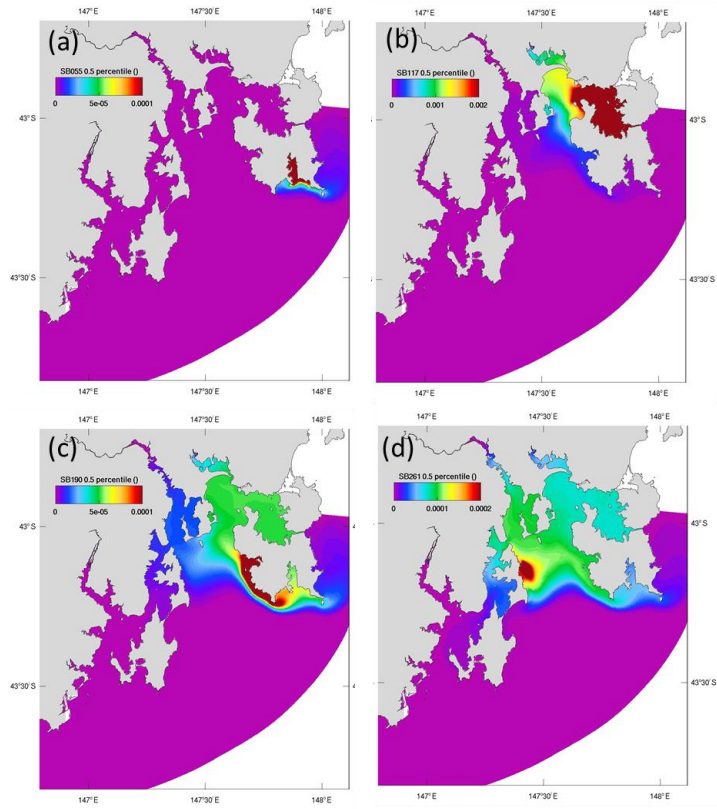
Figure 4.27. Median tracer distributions from sites (a) SB055, (b)SB117, (c) SB190 and (d) SB261.
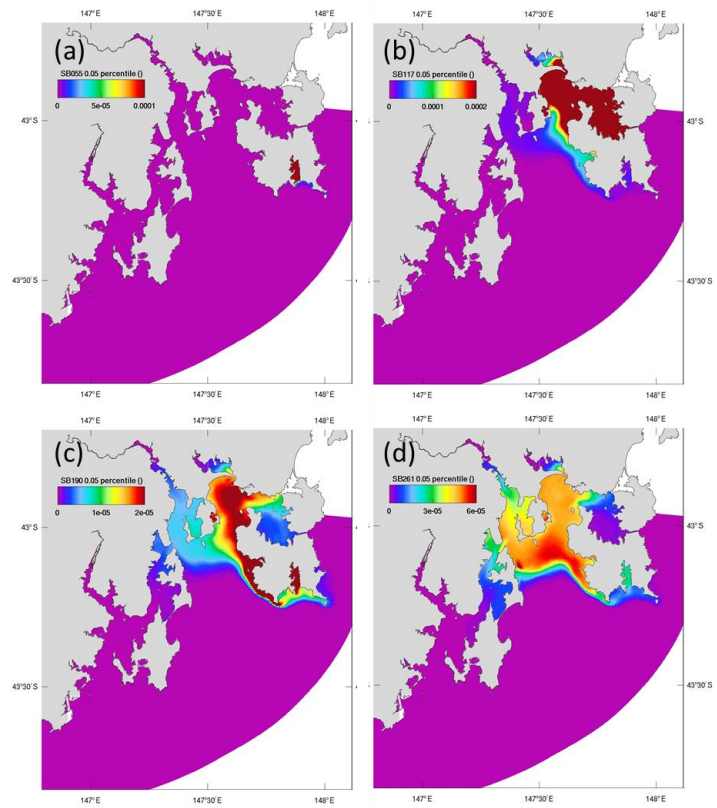
Figure 4.28 5th percentile tracer distributions from sites (a) SB055, (b)SB117, (c) SB190 and (d) SB261.
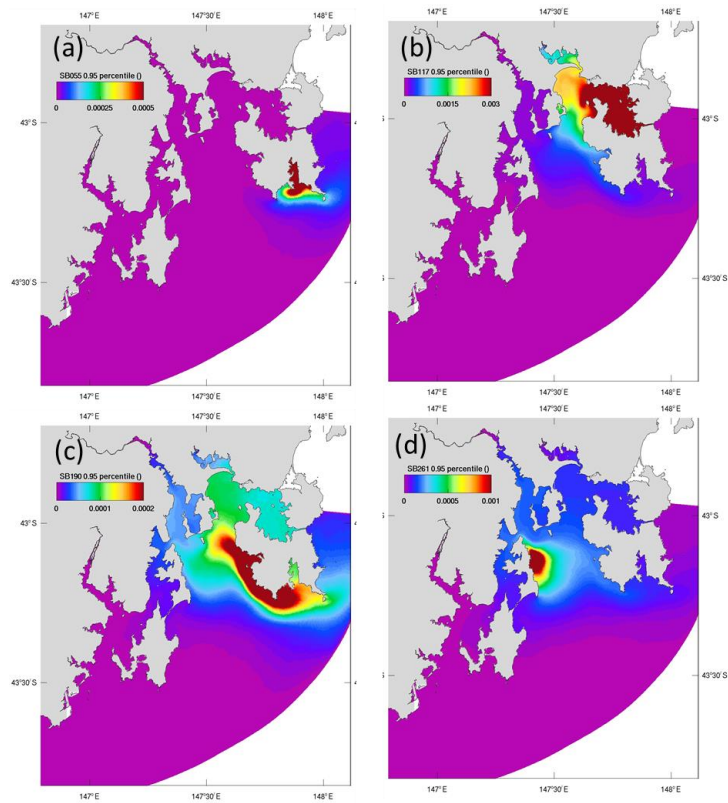
Figure 4.29 95th percentile tracer distributions from sites (a) SB055, (b)SB117, (c) SB190 and (d) SB261.

4.3.3   Regions analysis

Flushing times provide a measure of how long material is expected to reside in a certain area. They do not, however, provide integrated estimates of the destinations, concentrations, or variability of that material. Flushing times (the non-stationary method, Tartinville et al., 1997), residence times (batch reactor approach, Bailey and Ollis, 1986) and age tracers (Baird et al., 2006) metrics rely on the definition of sub-regions in the domain. We decompose the study area into five regions for this purpose (Figure 4.30) and for which these metrics may be computed. These regions consist of the Storm Bay region out to the 100 m isobath, and the connecting areas of the Derwent and Huon Estuaries, D'Entrecasteaux Channel and Frederick Henry Bay and Pittwater.
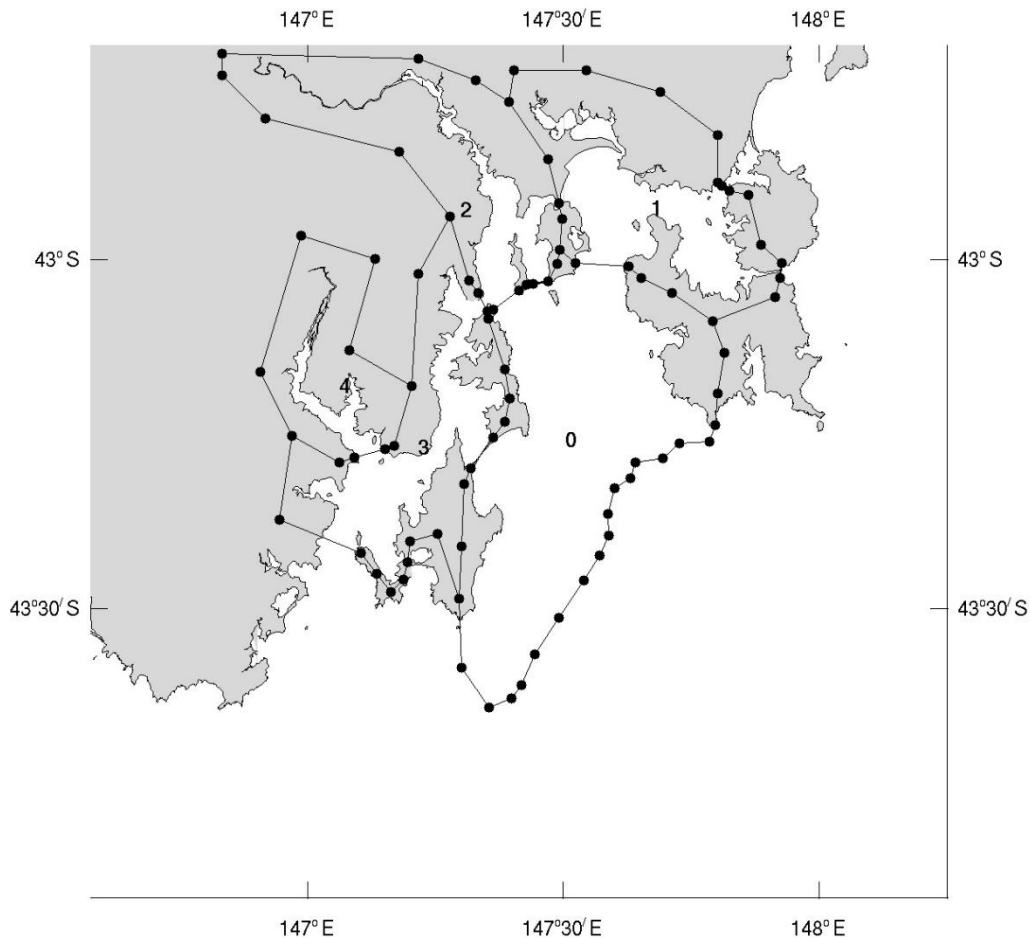
Figure 4.30 Sub-regions used in the connectivity analyses.

Flushing and residence metrics may not always produce reliable results, typically delivering a range of values which may span up to an order of magnitude. These metrics are influenced by the forcing conditions in effect at the time of computation and the size of the region chosen to compute the metric. Moreover, the assumptions upon which the method is based are often violated, and the presence of tides can unduly bias results.

Caution must be taken when quoting flushing / residence times for a region as they are not always reliable indicators of the absolute time it takes a substance to remain within or exit a region. For example, a strong ebb tide may effectively flush a small region on a semi-diurnal timescale, however, on the flood tide the material is returned to its original position at approximately the same concentration. Also, material may be removed from a designated flushing region to be deposited in a neighbouring region - material remains in the system but this cannot be revealed by a flushing time alone.

4.3.4 Flushing times - non-stationary method, Tartinville et al. (1997)

To compute the flushing time in Storm Bay, the sub-region 0 is initialized with a given concentration and the concentration is set to zero outside of the sub-region. The flushing time is defined as the time for the total mass in the sub-region to decrease by a factor of 1/e (~38%, i.e. the e-folding time).

This representation of the flushing time assumes that tracer is well mixed in the sub-region and the total mass is assumed to decrease exponentially according to:

$$M(t) = M_0 e^{-t/\tau}$$

where M_0 is the initial mass and τ is the flushing time scale. When $M = M_0/e$ then $t = \tau$, and the flushing time is recovered. This diagnostic is highly sensitive to the size of the region chosen and forcing in effect at the time.

The flushing time for region 0 (Storm Bay) is displayed in Figure 4.30, from which it is seen that flushing can be as little as 5 days but as long as 25 days.
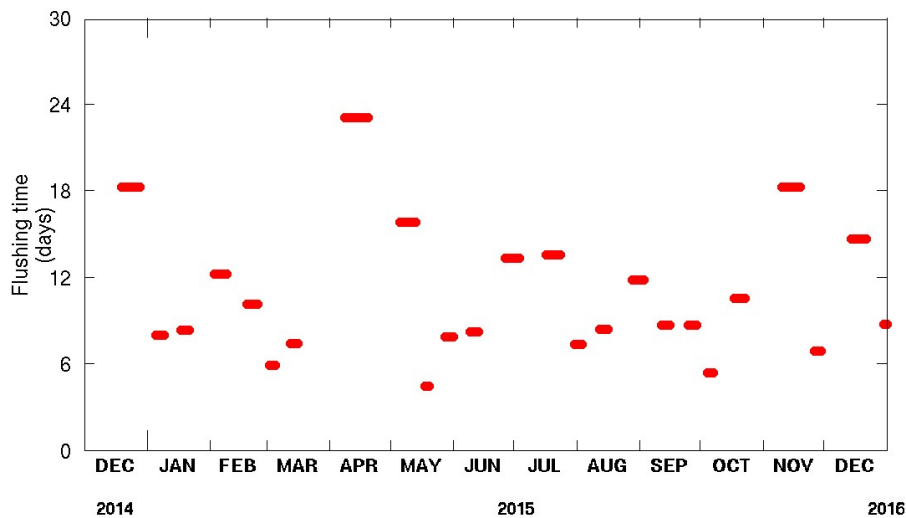
Figure 4.31 Flushing times of Storm Bay (1 Dec 2015 – 31 Jan 2016).

4.3.5   Residence time

The residence time may also be computed using the well-mixed batch reactor approach (Bailey and Ollis, 1986), where the residence time is defined as the time it takes a given flux of water through the boundaries of a region to replace its volume. There exist two possibilities when computing total fluxes between a given region and its neighbours: 1. the instantaneous (one-way) flux may be used; the presence of large tides can create very large oscillating fluxes that turn the region volume over quickly, or 2. the net (incoming plus outgoing) flux. In this case it is possible that simultaneous inflow and outflow through some boundaries exist, so that even though large volumes of new water are entering the region, the net exchange is small and consequently computed residence times may be very long. Additionally, the residence time is dependent on the size of the region, and location of adjoining boundaries between regions relative to the circulation. The resulting residence time is many 100s of days for region 0 using these methods, which is considered an unreliable estimate of the time it takes for dissolved substances to exit the nominated region.

4.3.6   Age tracer

An 'age tracer' may also provide an indication of the time that material resides in a certain region. The 'age tracer' is incremented at a rate of 1 day^{-1} within the region, and the rate is set to zero elsewhere. Tracer within the region is transported out of the region until quasi-steady state is achieved. The value of the age tracer within the region provides an indication of how long it has remained within the region.

Achieving steady state depends on the forcing in effect, and order statistics of the age tracer can provide an indication of the variability of the age of tracer within the region. For example, a median tracer distribution provides an estimate of the 'middle' age within the region. The age is again dependent on the location and size of the region boundaries but is considered a better measure of connectivity than the flushing metrics. The 5th percentile age reflects tidal exchanges and the 95th percentile reflects the age resulting from residual circulation. Age tracer order statistics were computed at the surface for the years 2015 – 2016, based on hourly outputs. The median tracer distribution of surface age is shown in Figure 4.32b. The largest median tracer ages of ~40 days are seen in eastern Storm Bay, alongside Tasman Peninsula, with a band of ~30 days stretching westward to Bruny Island. South of the frontal zone separating Storm Bay from sub-Antarctic water the median tracer age decreases to < 10 days. This response basically indicates that the northern part of Storm Bay is flushed 3x slower than the southern half. Note that age distributions are computed for the whole water column (although only surface distributions are shown in Figure 4.32), and while surface mean flow may exit age tracer from the region along Tasman Peninsula, bottom mean flow may act to push tracer northwards. Therefore, an overturning circulation (e.g. into and out of Frederick Henry Bay) in a well-mixed water column may retain tracer in the region for longer. Again, these age distributions are dependent on the size of the region initially chosen.
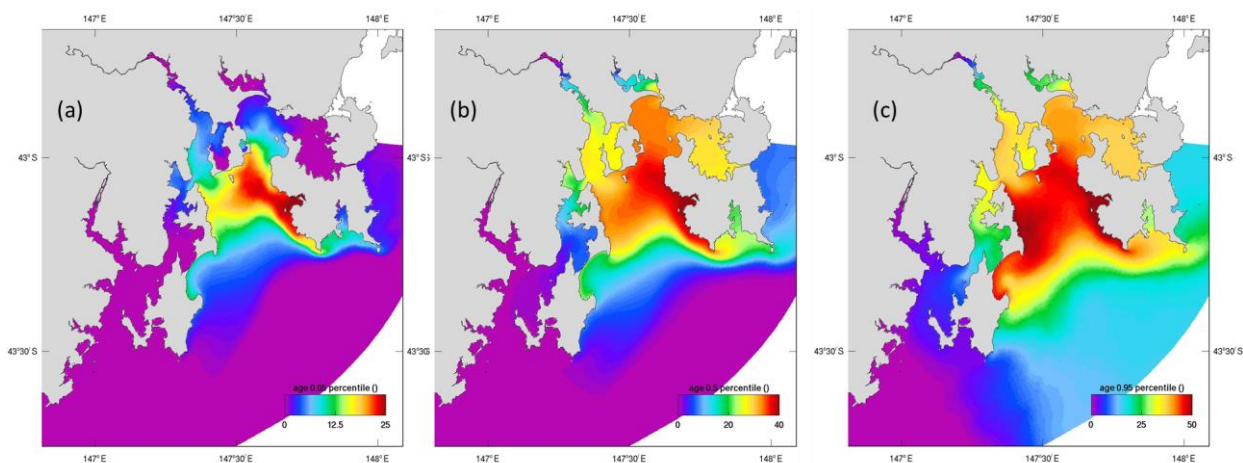

Figure 4.32. (a) 5th percentile, (b) median and (c) 95th percentile surface distribution of tracer age.

4.3.7   Particles

Particles may be released from specific sites and tracked in a Lagrangian manner throughout the domain. These particles are neutrally buoyant and not associated with settling or decay attributes, hence move in a passive manner guided by the flow. Particles were released from Storm Bay sites (SB261, SB117, SB190, SB055, Figure 4.26) at a constant rate, and became distributed throughout the domain over time. Eventually, the particles exit through the boundaries of a given region (e.g. greater Storm Bay region 0, Figure 4.30), and the average time it takes for the particles to exit the region is indicative of the residence time of that region.

For the Storm Bay lease sites, particles were released in the top 1 m of the water column at a rate of 10 particles / hour. The average time that 913798 particles spent in region 0 (greater Storm Bay) was 4.4 days from Dec 2015 to Aug 2018. Snapshots of particle distributions were consistent with the mean flow, age, and passive tracer percentiles presented in the previous analyses, i.e. particles were largely confined to northern Storm Bay, with some particles finding their way into the Derwent Estuary, northern D'Entrecasteaux Channel, Frederick Henry and Norfolk Bays and Pittwater. Particles exit Storm Bay around the tip of Tasman Peninsula. Once more, the same issues regarding forcing and region boundaries apply for this metric as for the age tracer. Additionally, the mean time may be biased by the tidal forcing, where particles may quickly exit the region on one phase of the tide, but re-enter on the other.

4.4   Sediment model

The sediment transport model adds a multilayer sediment bed to the hydrodynamic model grid and simulates sinking, deposition and resuspension of multiple size-classes of suspended sediment (Margvelashvili et al., 2008). The model solves advection-diffusion equations of the mass conservation of suspended and bottom sediments and is particularly suitable for representing fine sediment dynamics, including resuspension and transport of biogeochemical particles. Sediment particles settle on the seabed due to the gravity force and resuspend into the water column whenever the bottom shear stresses, exerted by waves and currents, exceed the critical shear stress of erosion. The resuspension and deposition fluxes are parameterised with the Ariathurai and Krone (1976) formula. Estimates of the bottom shear stress, required by this formula, are derived through the Grant and Madsen boundary layer model (Madsen, 1994). Bottom roughness is scaled by ripple dimensions (Grant and Madsen, 1982) which are considered the model input parameters and must be specified through observations or calibration study. Apart from the resuspension and deposition processes, sediment fluxes across the benthic and pelagic layers are also driven by bioturbation processes.

Sediments in benthic layers undergo vertical mixing due to bioturbation, represented by local diffusion. The corresponding diffusion coefficient is scaled with the sediment depth so that the bioturbation of sediments ceases to operate at the bottom of the biologically active layer. The resistance of sediments to resuspension increases with the sediment depth and there is no direct exchange of particles in horizontal directions within the benthic sediments.

The numerical grid for sediment variables in the water column coincides with the numerical grid for the hydrodynamic model (Figure 4.33). Within the bottom sediments, the model utilises a time-varying sediment-thickness-adapted grid, with the top active sediment layer having constant thickness, and the thickness of deeper layers varying with time to accommodate the deposited sediment. In the benthic layer (except hard substrate), 1m of the top sediments is resolved into 12 layers; over the hard substrate (e.g. reefs) the initial thickness of sediments is set to 1 cm. Horizontal resolution within sediments follows the resolution of the water column grid.

The sediment transport model is driven by waves, currents, and turbulent diffusion simulated by the hydrodynamic and wave models. The sediment transport model runs in a stand-alone mode (i.e. hydrodynamic / wave variables are simulated upfront to provide input to the sediment model). The simulation time-step is larger than that of the hydrodynamic model and there is no feedback from the sediment processes to the hydrodynamics, i.e. the impact of sediments on flow, density, waves, and turbulence are not simulated. This decoupling of the sediment and hydrodynamic / wave models provides substantial benefits in computational efficiency.

The model simulates resuspension, deposition, and transport of only fine-sediments (carbonate and non-carbonate mud and lighter, clay-sized particles) initialised in the benthic layer and delivered from catchments during the simulation period. Heavier particles (gravel and sand, which during the resuspension event tend to accumulate within a thin near-bottom layer typically not resolved by the 3D model grid), were kept immobilised within the benthic layers. Recently the formulation of the sediment transport model has been refined to include the presence of hard substrate (e.g. rocky reefs) in benthic layers.
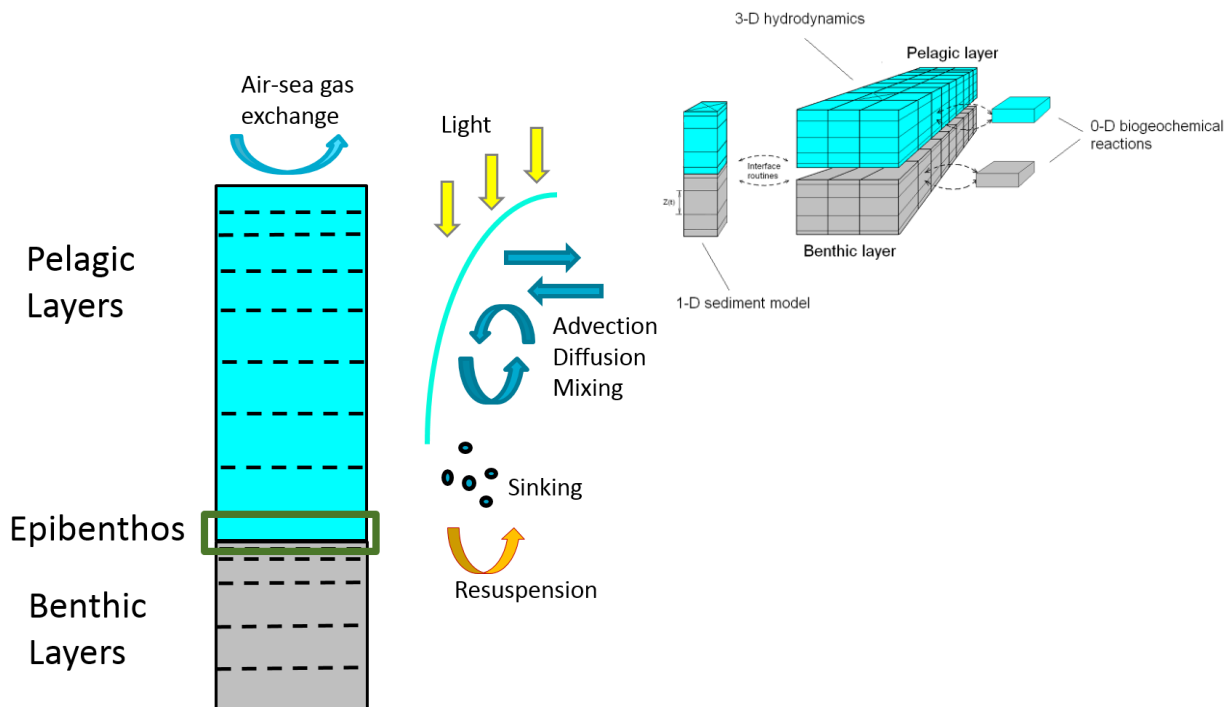
Figure 4.33 Schematic diagram showing the structural implementation of sediment and biogeochemical model processes within the hydrodynamic transport model grid.

4.4.1 Initial conditions

In shallow coastal waters typical time for the suspended sediment to adjust to the hydrodynamic forcing can be relatively short (hours and days). Hence, to initialise the sediment transport model, the initial concentration of suspended sediment was set to zero throughout the model domain. In benthic layers the model was initialised with the observed spatial distribution of gravel, sand and mud acquired from both the Geoscience Australia MARine Sediment (MARS) database and from the Derwent Estuary field programs (Green et al 2003). As illustrated in Figure 4.34, MARS samples represent predominantly open coastal waters, samples from the local field programs are allocated predominantly inside the Derwent estuary. To support the development of the optical model each sediment class (i.e. mud, sand, gravel) was delineated further into carbonate and non-carbonate fractions (Figure 4.35a,b,c). For samples with only a bulk fractionation of the carbonate and non-carbonate classes, an assumption was made of the proportional allocation of carbonates to each sediment class. For example, in a sediment sample with 20% of bulk carbonates, we assumed these carbonates to comprise of 20% gravel carbonates, 20% sand carbonates, and 20% mud carbonates. No data was available about the carbonate fractionation inside the Derwent estuary so for these samples we assumed all benthic sediments to be 100 % non-carbonate.

Over the hard substrate (e.g. rocky reef Figure 4.36), the initial thickness of sediments in Storm Bay was set to about 1 cm. The rest of the region was initialised with the 100 cm of benthic sediments; the porosity in this layer was defined as a function of the concentration of benthic sediment components.

To reconcile the initial distribution of sediments with the hydrodynamic forcing and boundary conditions, a pilot sediment transport model was run for about one year; all subsequent simulations were hot-started from the sediment distributions established after this one-year run.
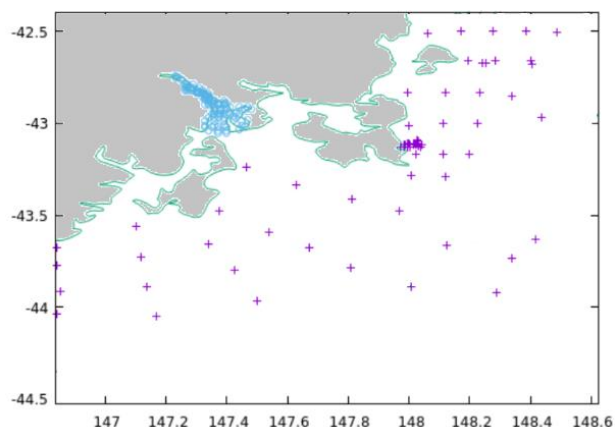
Figure 4.34 Benthic sediment sampling sites (crosse indicate MARS data, circles are DEP programs)
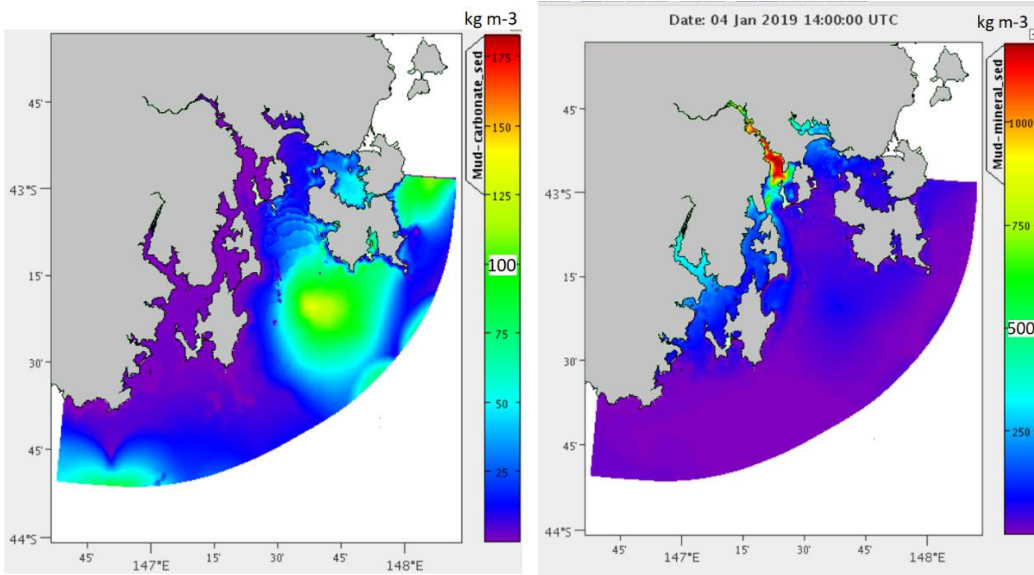
Figure 4.35a Initial distribution of carbonate and non-carbonate mud in benthic sediments.
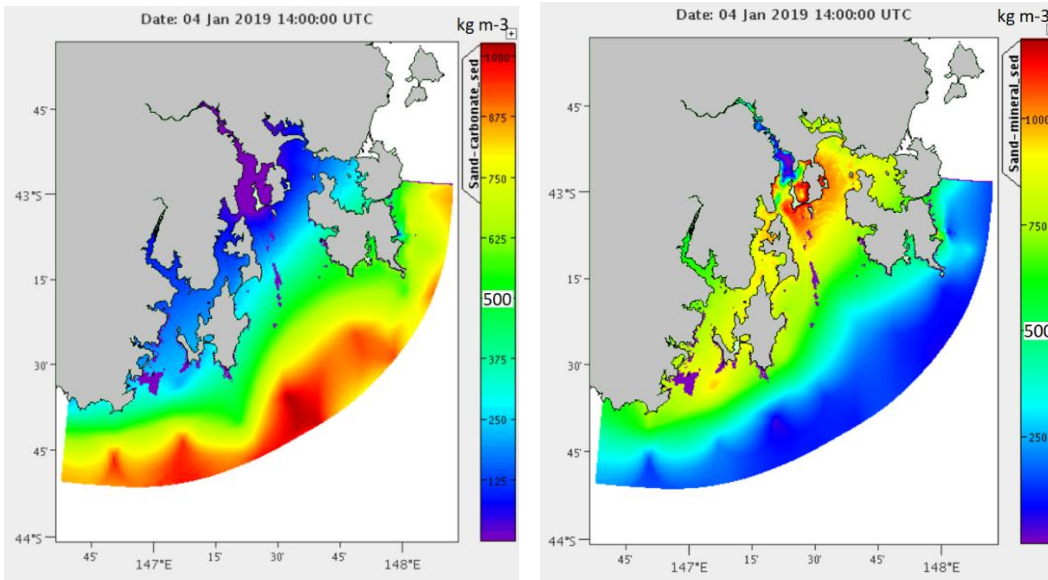
Figure 4.35b Initial distribution of carbonate and non-carbonate sand in benthic sediments.
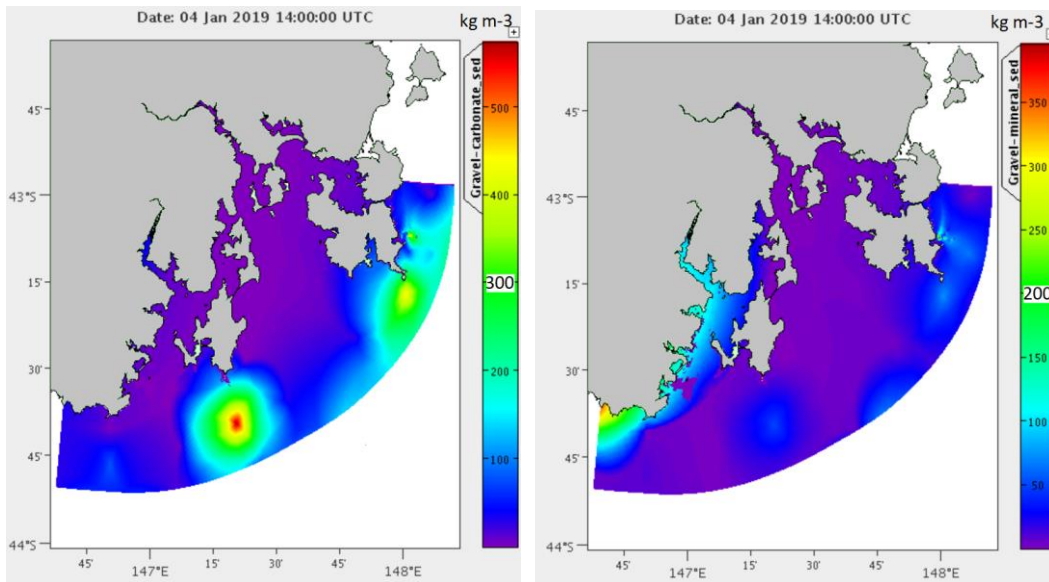
Figure 4.35c Initial distribution of carbonate and non-carbonate gravel in benthic sediments.
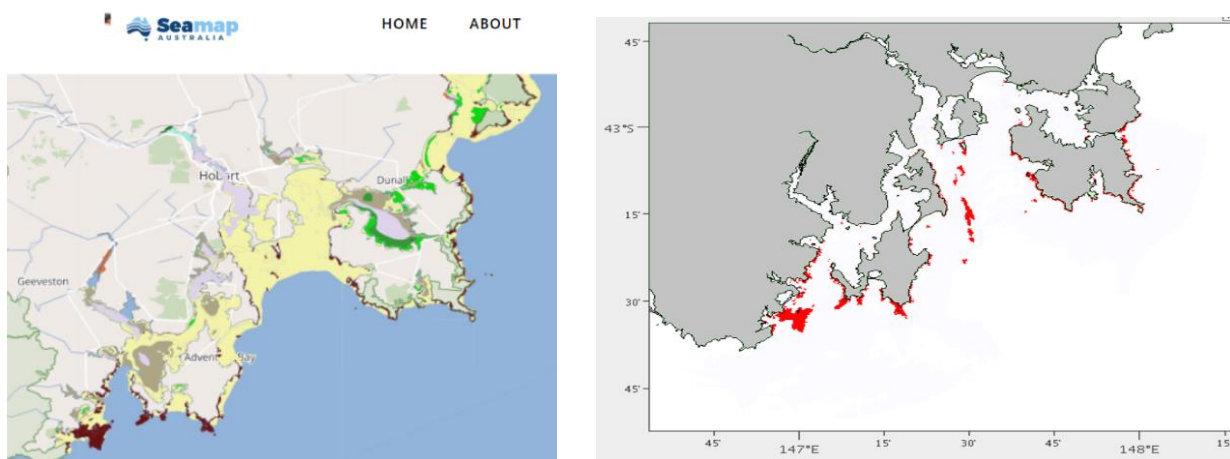

Figure 4.36 Reef rocks according to Seamap Australia DB (left plot, brown), and reef rocks in the model (right plot, red).

4.4.2 Boundary conditions

At the ocean boundary, sediment concentration was set to zero for the incoming flow, and a free flow boundary condition was used when currents move sediments outside the study area into the ocean.

At the river boundaries when DEP monthly data was available, the sediment concentration was specified according to this data. Otherwise, at the river boundaries the concentration of the suspended sediment was set to 4 mg L^{-1} (consistent with the DEP monthly field data at New Norfolk site). According to this specification, sediment loads from catchments for river boundaries are scaled linearly by the river flow - the higher the river flow, the higher the catchment load (i.e. the product of the river flow and the suspended sediment concentration). Catchment sediments

are subdivided into two fractions of particles each fraction having the boundary concentration of 2 mg L^{-1} and the settling velocity corresponding to the settling velocity of either silt or clay sized particles.

4.4.3   Hydrodynamic and wave forcing

The sediment transport model is driven by both waves and currents. In earlier applications of the sediment transport model around Australia currents were typically available from the SHOC hydrodynamic model and waves were provisioned by BoM AUSWAVE model. This configuration worked well for large-scale applications (e.g. eReefs model in the Great Barrier Reef region), however, in Storm Bay the resolution of the AUSWAVE model (about 0.1 degree) is too coarse to provide an accurate description of waves in this region. AUSWAVE does not resolve estuarine and river channels and cannot capture sheltering effects induced by topographic and coastal features, particularly around islands and coastal embayments.

To provide an adequate description of the wave fields in Storm Bay, an open-source public-domain third generation near-shore wave model (Simulating WAves Nearshore - SWAN) has been implemented in the study region in offline mode. The model runs on a 4D curvilinear numerical grid encompassing 2 spatial dimensions, directional angle, and frequency domain. The spatial component of this grid is represented by a curvilinear numerical grid which coincides with the 2D numerical grid for the Storm Bay hydrodynamic model and resolves relatively small-scale coastal features (unresolved by BoM AUSWAVEs). Default SWAN settings were used to specify directional angles and frequency bins. The model was driven by ACCESS-R and ACCESS-VT winds at the surface and global Wave Watch 3 (WW3) model at the open ocean boundary (a very coarse 0.5 degree resolution) (Puri et. al., 2012). Neither hydrodynamic currents nor changing surface elevation has been included into the SWAN model formulation at this stage. Despite missing these forcing components, the model shows a reasonable agreement with measurements (Figures 4.37 and 4.38). Wave fields were simulated from 2015 to mid-2020 and three-hourly snapshots of these data were stored on disk to provide input for the subsequent simulations by the sediment transport model.

To ascertain the impact of the refined wave model on sediment transport, two sediment resuspension simulation were completed using either the fine-resolution SWAN model or AUSWAVEs. Results from these simulations show close agreement in suspended sediment concentrations in the open waters of Storm Bay and significant discrepancies between the simulations in constrained coastal areas, inside lagoons and in river channels – all areas which are unresolved by AUSWAVEs (see Appendix A2 for more details).
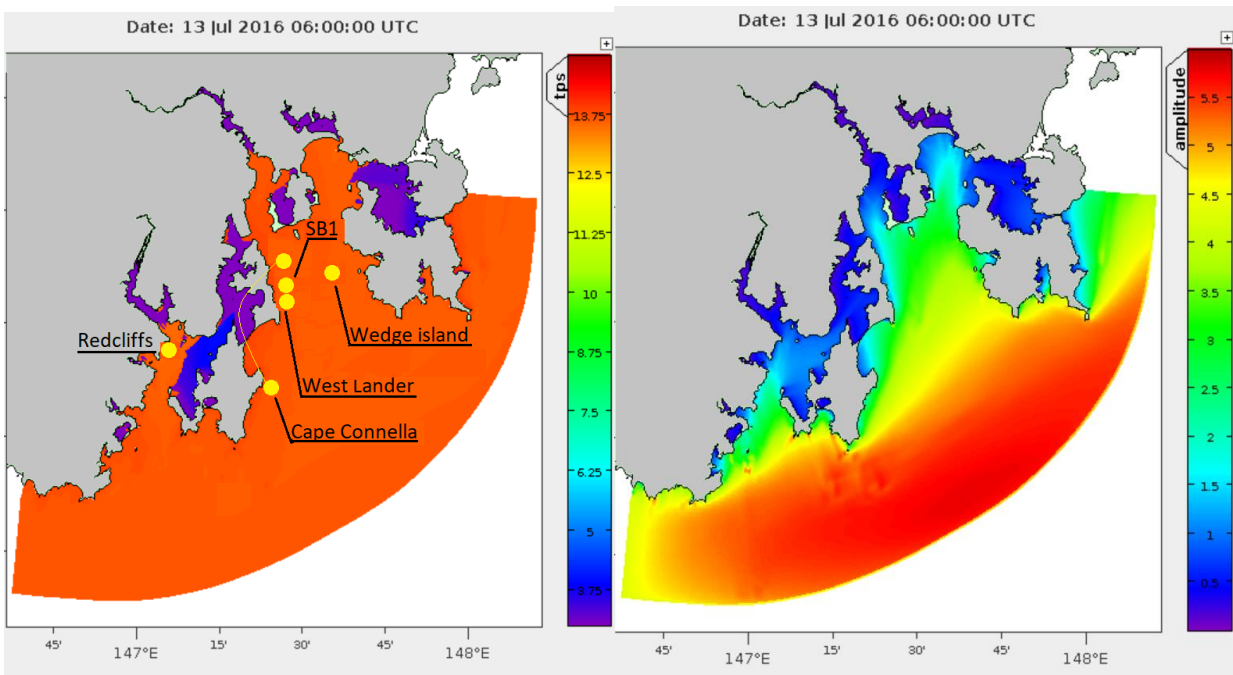
Figure 4.37 Wave model validation sites overlaying the SWAN simulated peak wave period (left plot). A snapshot of SWAN simulated significant wave height (right plot).
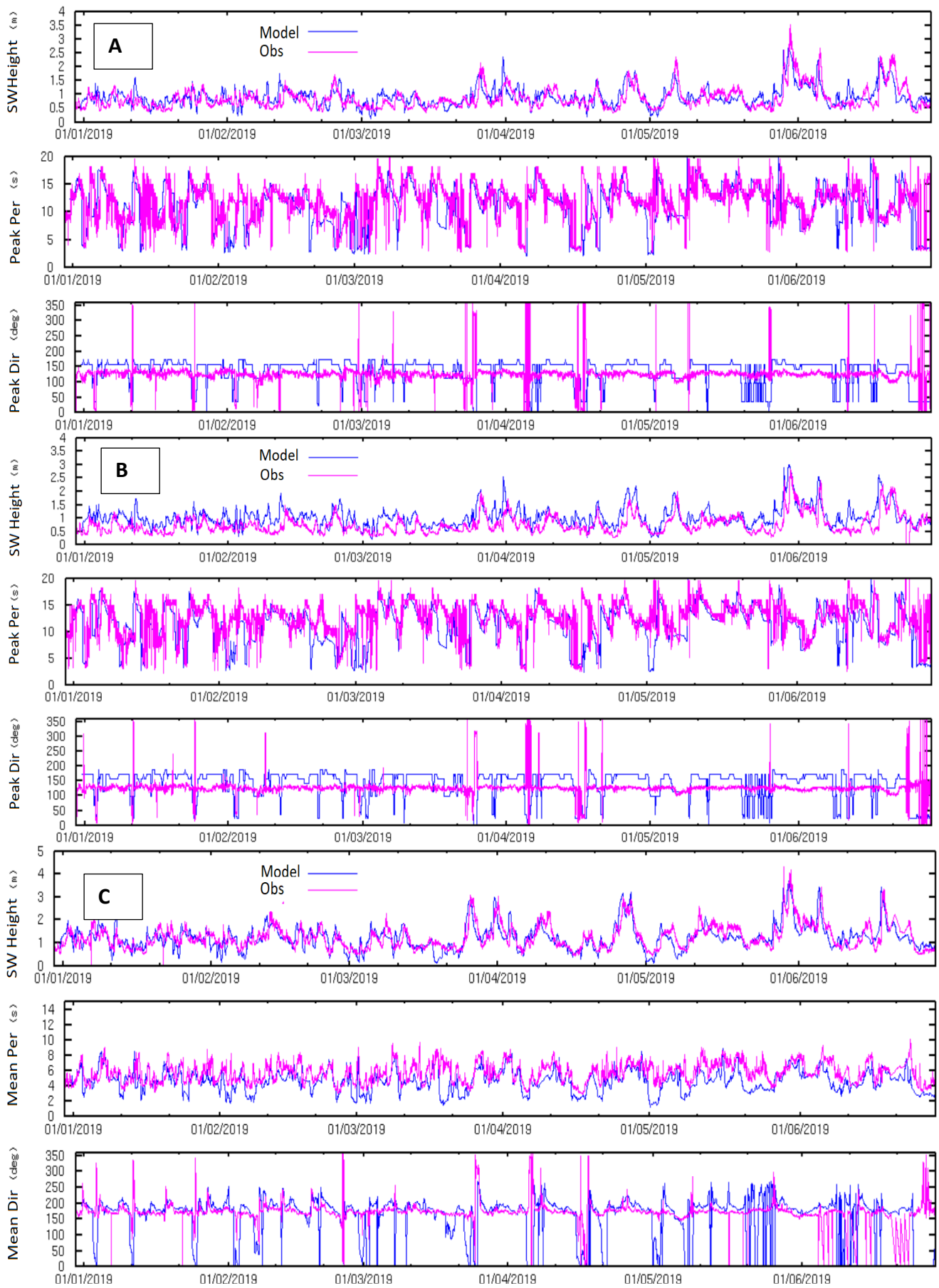
Figure 4.38 Fine resolution wave model vs observations at (A) SB1, (B) Cape Cornella and (C) Wedge Island.

4.4.4   Observations for sediment model calibration

One of the key challenges facing the development of the sediment transport model in Storm Bay is the task of constraining the model uncertainty with observations. The model is based on semi-empirical site-specific relationships which must be fine-tuned to fit the model to observations. This task is particularly challenging in Tasmanian region because of the scale and variability of the heterogeneous coastal and shelf environments. The problem is further exacerbated by typically poor quality of observations. Field-samples are scattered in space and time and represent single-point data rather than variables integrated over the grid-cell area. Time series of turbidity tend to provide good temporal coverage of the signal at specific locations but give poor spatial coverage of the domain. Remote sensing products offer higher resolution of the surface layer but may not have sufficient coverage in time and in depth. Different sets of data have their own uncertainty which often are not known upfront and, in some cases, might be comparable to or even exceed the uncertainty of the model.

Over the course of this project several deployments of benthic landers have been carried out in Storm Bay in 2019-2020. The duration of every deployment was several months. The landers were equipped with a number of sensors including an ADCP profiler measuring velocities and acoustic backscatter at 300 or 600 kHz. Three out of 4 landers had also turbidity sensors located about 1 m above the seabed. According to literature (Sirabahenda, 2019), a linear regression often provides a reasonable approximation of the scaling relationship between turbidity and suspended sediment concentration in coastal waters. This relationship, however, varies across the regions (e.g. sediments in the upper reaches of the estuary and sediments in the open coastal waters may have different chemical and physical/optical properties because of the different origin of these sediments).

To evaluate the scaling relationship between turbidity and suspended sediment concentration in Storm Bay (i.e. at the deployment sites), a few samples of TSS collected at the deployment sites were augmented with a relatively large number of monthly data collected by the Derwent Estuary Program (DEP) in the lower Derwent at G2, E, and B3 sites (location map in Figure 4.39). The selection of these sites was based on their proximity to Storm Bay; the water depth at these locations was also comparable to the depth at the deployment sites. Figure 4.40 top-left image shows a scatter plot between turbidity and total suspended sediment concentration for all samples collected at these sites over the course of several years (2014-2017). The top-right and the bottom-left plots in this Figure separate these data into the samples collected near the sea-surface and samples collected near the seabed. According to these data, no obvious relationship between TSS and turbidity can be inferred from the surface samples. The visual inspection of the bottom samples suggests at least 2 tendencies for the suspended sediment to scale with TSS – some samples are close to 1:10 line and other points tend to allocate along the 1:2 line. The scaling relationship between suspended sediments and turbidity of 1:10 is rather extreme, as a typical scaling for many coastal applications is close to 1:1 rather than 1:10. Based on this observation, we assumed that the 2 highest values (circled by the red ellipse and contributing heavily to 1:10 scaling relationship) were outliers from the general conditions found. By excluding these outliers, the scaling relationship was more robust (Figure 4.40 bottom-right plot) with Storm Bay TSS concentration (mg/L) found to be about twice the observed turbidity (NTU).

$$1.0 \text{ TSS (g/L)} = 2.02 \text{ Turbidity (NTU)} \qquad\qquad (1)$$

Apart from the lander deployments carried out by CSIRO, a number of other records of surface turbidity in the study region (these records were often coincident with wave buoy measurements) were made available to the project. Some of these data were processed and analysed during this study but they were not used to calibrate the sediment transport model. The reasons for this decision are as follows:

1. Concentrations of suspended sediment in surface layers are typically low. Optical properties in these layers are likely to be dominated by biological cycling of organic material rather than benthic sediment resuspension.

2. The scaling relationship between sediment and turbidity was established for sediments close to the seabed and is inappropriate for surface measurements.

3. The quality of the turbidity records taken by different institutions and companies using various instruments and measurement procedures was not always consistent.

Given all these considerations, only the near bottom data collected from the CSIRO benthic moorings were used to calibrate the model. The calibration procedure involved manual tuning of the model parameters to best fit the measurements. The list of varying parameters comprised bottom roughness, diffusion coefficient, critical shear stress of resuspension, and bottom boundary layer formulation.
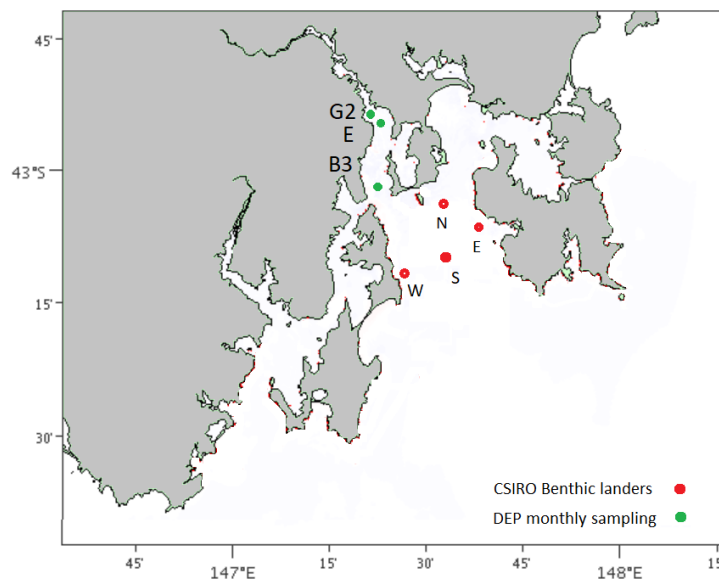
Figure 4.39 Location map for DEP sites and CSIRO landers underpinning calibration of the sediment transport model
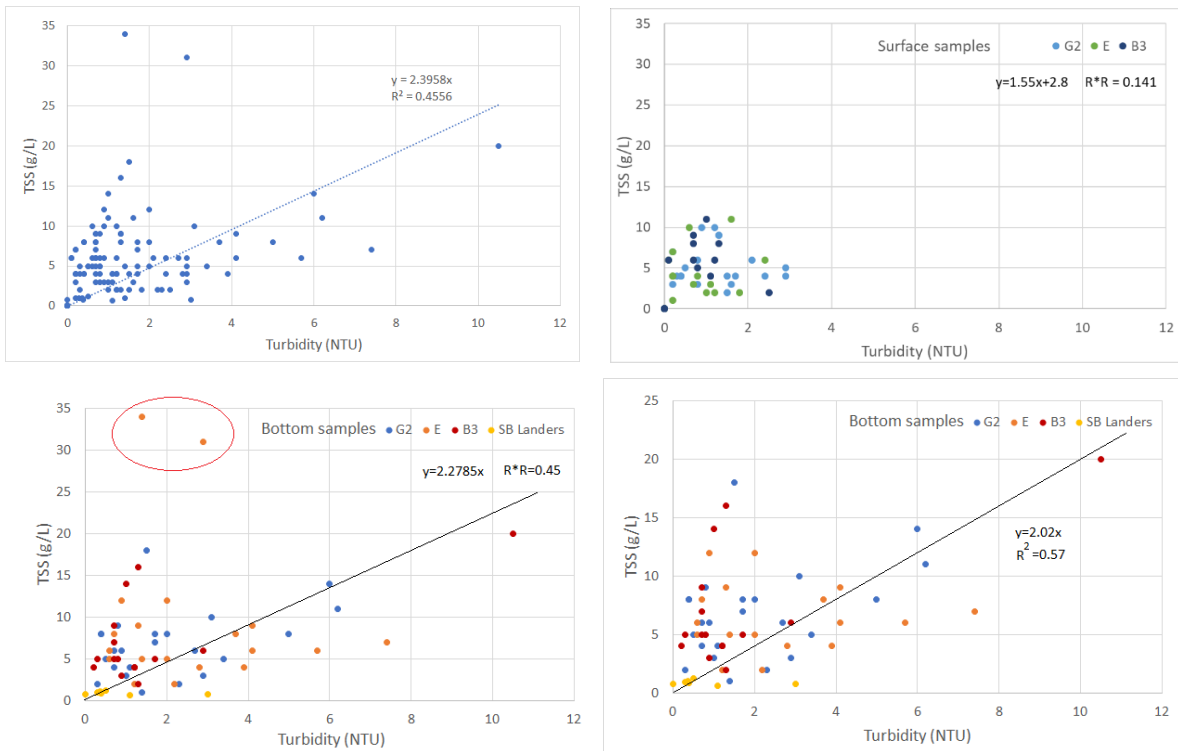
Figure 4.40. TSS vs turbidity in the lower Derwent and Storm Bay (top-left plot). Top-right and bottom-left plots show the same data as the top-left except that colour-coded by the site location and split into surface and bottom samples. Data courtesy of the DEP ambient monitoring program (2014 – 2019) and CSIRO west and south lander deployment.

Observation sites

This section provides an overview of the turbidity and ADCP-backscatter records collected at 4 CSIRO deployment sites (see location map in Figure 4.39). Data collected at these sites have been used in this project to calibrate the sediment transport model.

Turbidity was measured at about 1 m height above the seabed at 3 out of the 4 deployment sites (western, southern, and northern moorings). The corresponding records comprise 5 sample bursts taken every 15 min over the course of several months. As illustrated in Figure 4.41, the raw data is contaminated with a significant noise likely associated with turbulent eddies in the bottom boundary layer (having characteristic spatial scales of metres and time scales of seconds and minutes). To reduce the noise level at these scales, the raw data was passed through a low pass filter with a 1 hour cut off period (red line in Figure 4.41). All records of turbidity and acoustic backscatter shown in the rest of this section were passed through this 1h low pass filter.

West lander site

In Figure 4.42 turbidity measured at the west lander site was plotted alongside the simulated bottom shear velocity at that site. According to this plot, turbidity levels at this site were relatively low in January and February 2019 and they were much higher for the rest of the deployment period (Mar, April, May). Nothing remarkable happens with the bottom shear stress over that period to explain such low levels of turbidity in January-February.
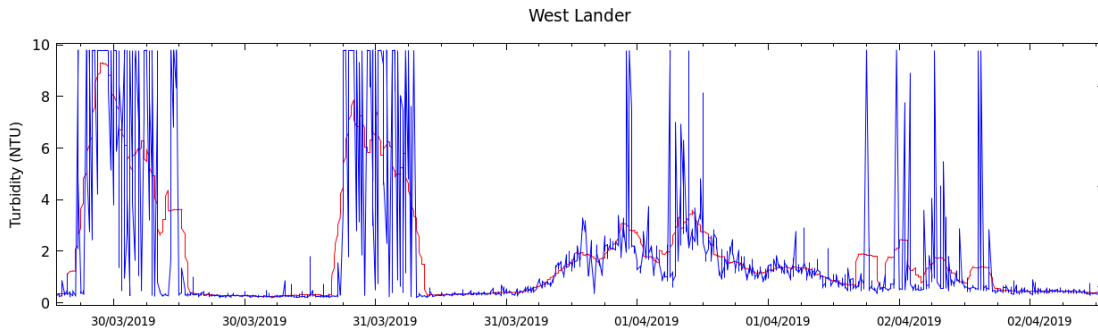
Figure 4.41 Hourly mean (red) vs raw turbidity records at the west lander site
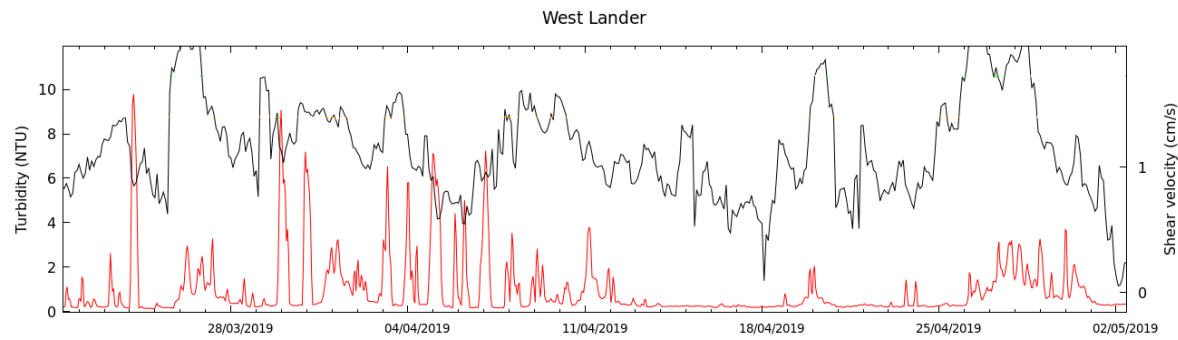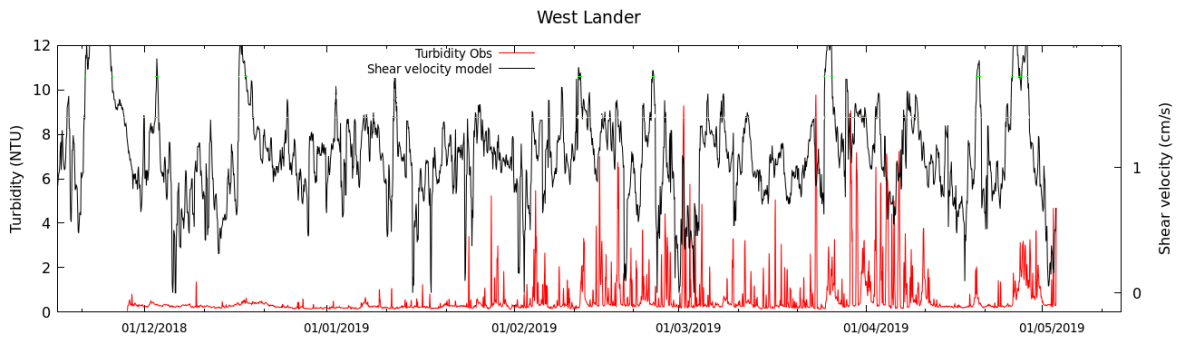
Figure 4.42 Observed Turbidity vs simulated bottom shear stress at the west lander site. The bottom plot is a zoom into a subset of the top plot.
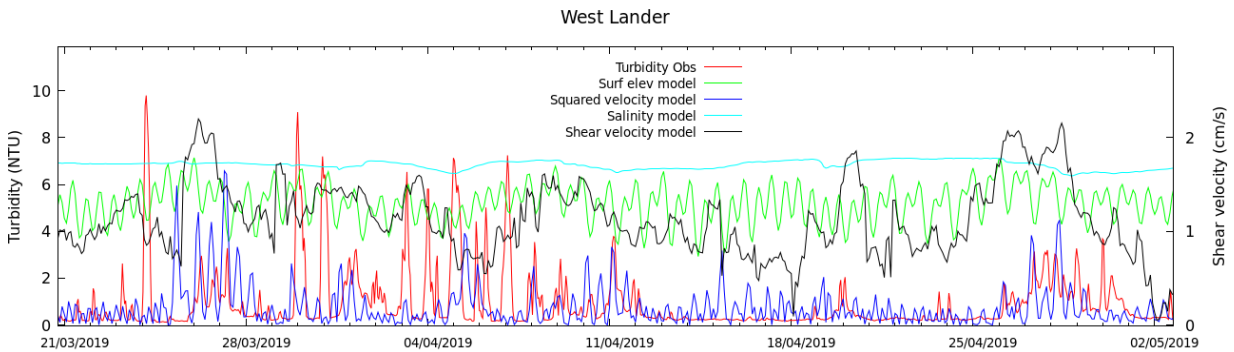
Figure 4.43 Observed turbidity vs simulated salinity, surface elevation, bottom shear velocity, and squared velocity of currents at the west lander site.

A feature prominent in these records is a number of turbidity peaks with a characteristic time scale of several hours (up to 10 hours). A qualitative visual inspection does not suggest any significant correlation between these peaks and the bottom shear velocity (Figure 4.42, bottom plot). Similarly, there is no clear relationship between these turbidity spikes and simulated salinity, surface elevation, or squared velocity of currents - a proxy to the kinetic energy (Figure 4.43). The only significant correlation these data show, is the correlation between elevated turbidity and the kinetic energy of currents during extreme weather events lasting for several consecutive days.

Each mooring in Storm Bay was equipped with a bottom mounted, upward looking ADCP profiler (300 or 600 kHz). Records of the acoustic backscatter delivered by these instruments provide further insight into the suspended sediment levels in the region. Unlike turbidity sensors taking measurements at about 1 m above the seabed, the first near bottom record of the ADCP profiler starts at a about 1.5 – 2 metres above the seabed (depending on the blanking distance of a particular device).

Comparison of the optical and acoustic backscatter at the west lander site indicates similarities as well as a considerable difference between these records (Figure 4.44). Both optical and acoustic data tend to register elevated backscatter during extreme weather events. Unlike optical data, however, the ADCP backscatter does not suggest any persistent anomalies in the suspended sediment levels in January-February 2019 (Figure 4.44, top plot). Furthermore, high-frequency spikes (characteristic time of about 10 hours and less) are much less pronounced in the acoustic readings (Figure 4.44 bottom plot). These discrepancies between optical and acoustic data could be attributed to both differences in sensitivies of the acoustic and optical measurements and also to the varying locations of the optical and acoustic sensors.
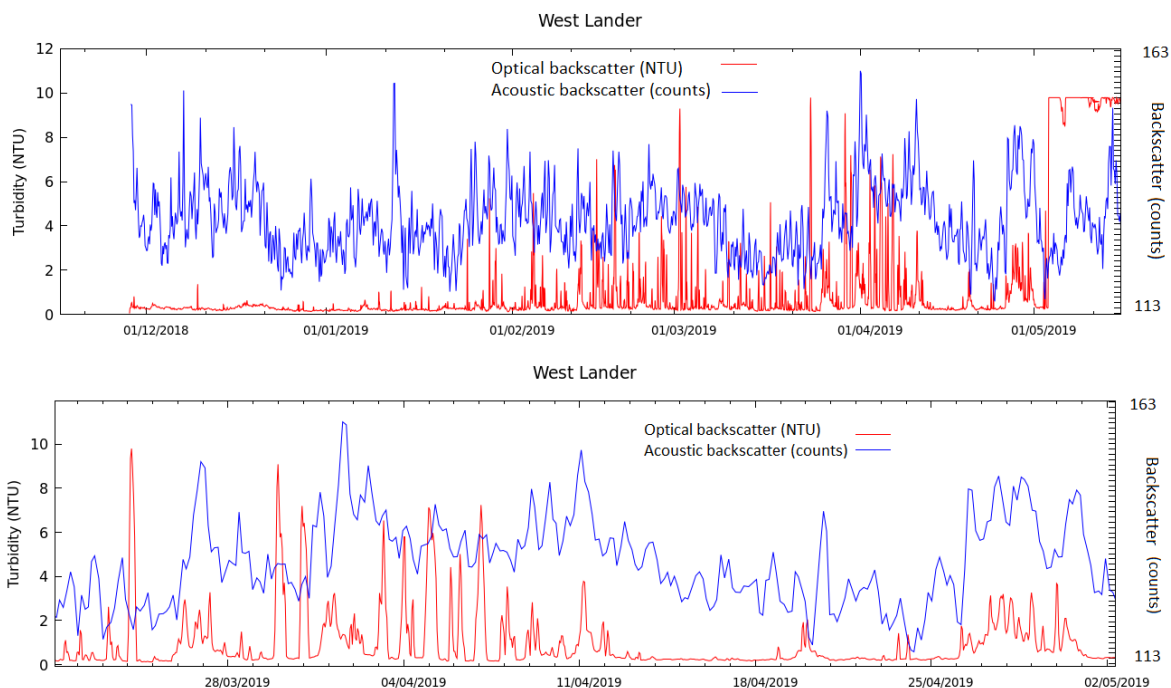
Figure 4.44 Measured turbidity vs ADCP backscatter at the west lander site [the bottom plot is a zoom into a subset of the top plot].

Based on this analysis (of the optical and acoustic data combined with the model predictions) we speculate that the most reliable, deterministic feature (present in both optical and acoustic

records) are periods of elevated turbidity lasting for several consecutive days and likely triggered by extreme weather events. Hence, the calibration strategy is to tune the model parameters to reproduce the timing and the magnitude of such extreme resuspension events.
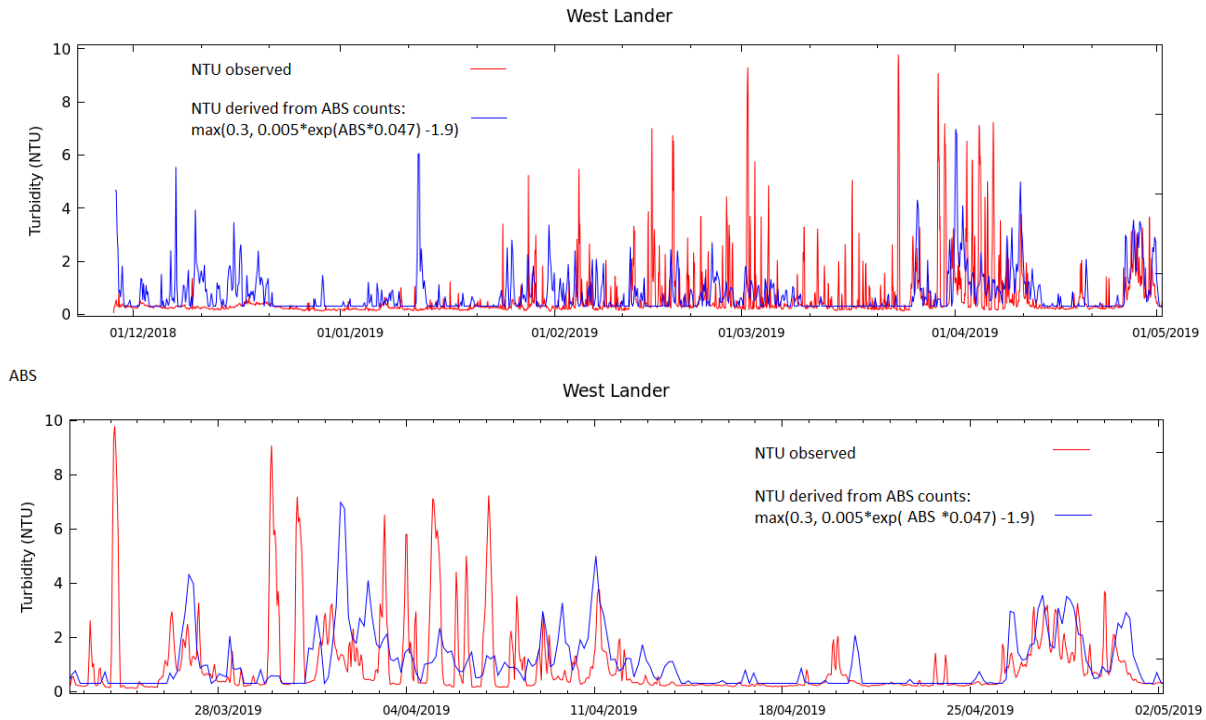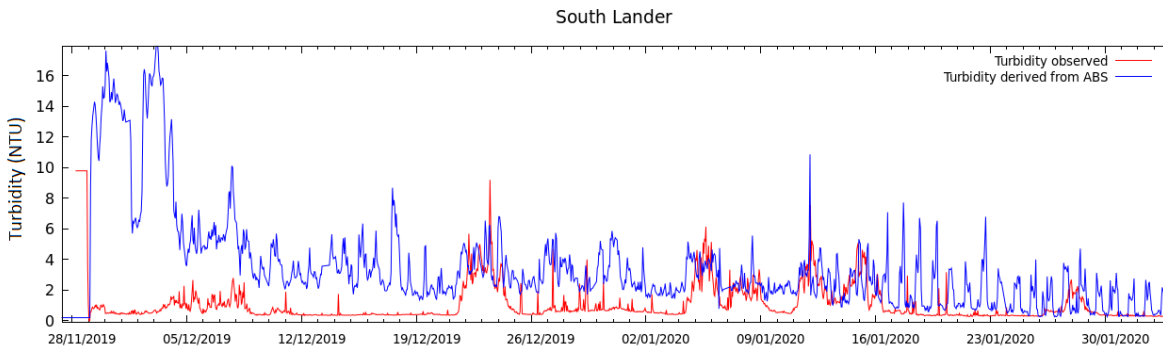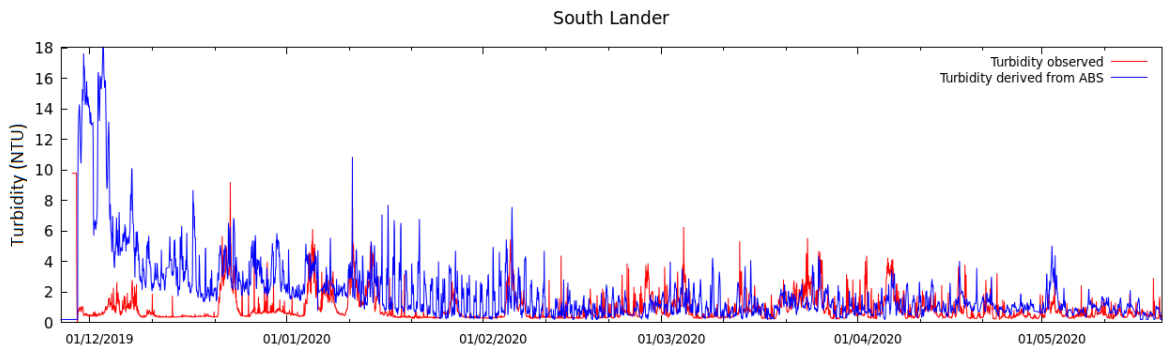

Figure 4.45 Measured turbidity vs turbidity derived from ADCP acoustic backscatter at the West lander site [the bottom plot is a zoom into a subset of the top plot].

Figure 4.45 illustrates a scaling relationship between the optical and acoustic backscatter inferred from the records collected at the west-lander site (300kHz ADCP):

$$\text{Turbidity (NTU)} = \max(0.3,\ 0.005 * \exp(ABS * 0.047) - C) \qquad\qquad (2)$$

Here ABS is an acoustic backscatter in counts, C is a constant within 0 to 2.0 range. This scaling has been established through the manual tuning of the parameters in (2) by matching acoustic and optical records during extreme resuspension events. The functional form of this relationship is consistent with the sonic equation (Gartner 2004; Deines, 1999).

According to Figure 4.45, turbidity derived from acoustic backscatter using the relationship (2) in general is consistent with the observed turbidity during extreme events. Note that spurious peaks in the observed turbidity are gone when the turbidity is derived from the ADCP backscatter using the scaling relationship (2) (see Figure 4.45 bottom plot).

A relationship similar to (2) has been derived from the data collected at the north lander site ADCP operating at 600 kHz:

Turbidity (NTU) = max (0.3, 2.5*0.005*exp(ABS*0.047) - C)   (3)

East lander site

No turbidity has been measured directly at the east lander site. Instead, to estimate turbidity levels at this location, the scaling relationship (3) has been applied to the ADCP backscatter data collected at that site (Figure 4.46).
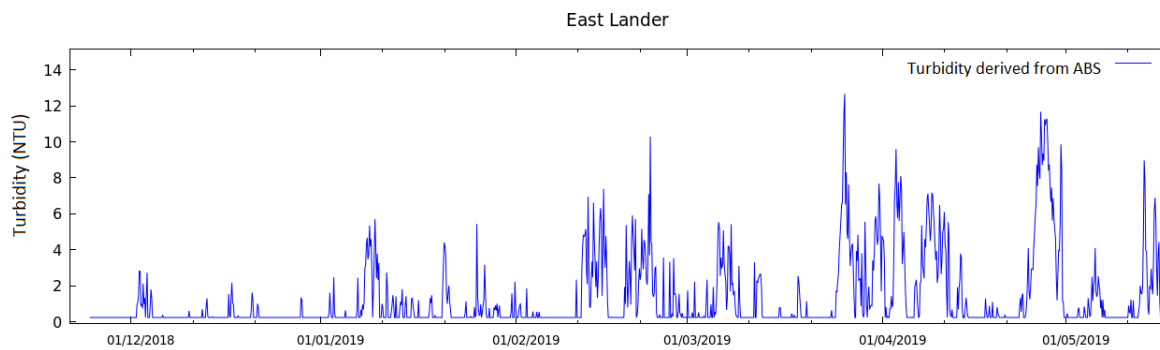
Figure 4.46 Turbidity derived from the ADCP backscatter at the east lander site.

North and south lander sites

Figures 4.47 and 4.48 show observed turbidity and turbidity derived from the ADCP backscatter at the north and south deployment sites, respectively. Unlike the western site, the ADCP based turbidity at these sites looks much noisier compared to the direct observation of turbidity. Both north and south landers show a tendency for the ADCP derived turbidity to decline gradually over the first 2 months of the deployment. Observations of the turbidity do not show such gradual changes in optical properties. Both observed and inferred turbidity tend to pick up extreme resuspension events.

Figure 4.47 Measured turbidity vs turbidity derived from ADCP backscatter at the South lander site [the bottom plot is a zoom into a subset of the top plot].
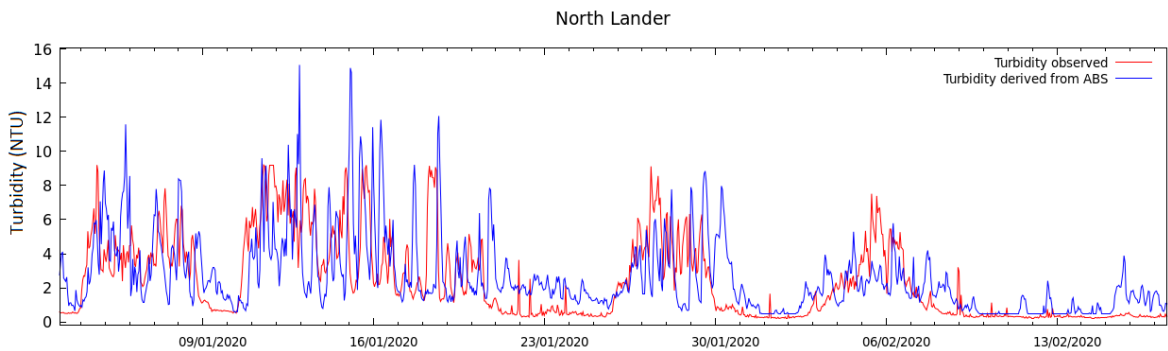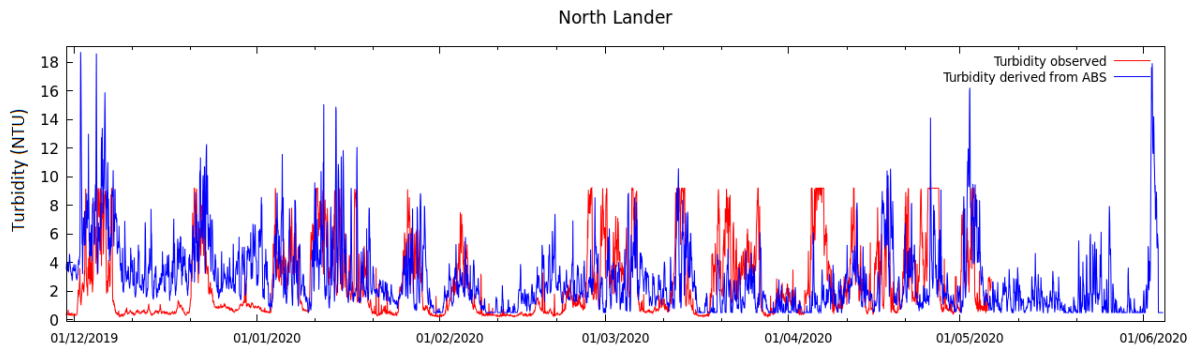
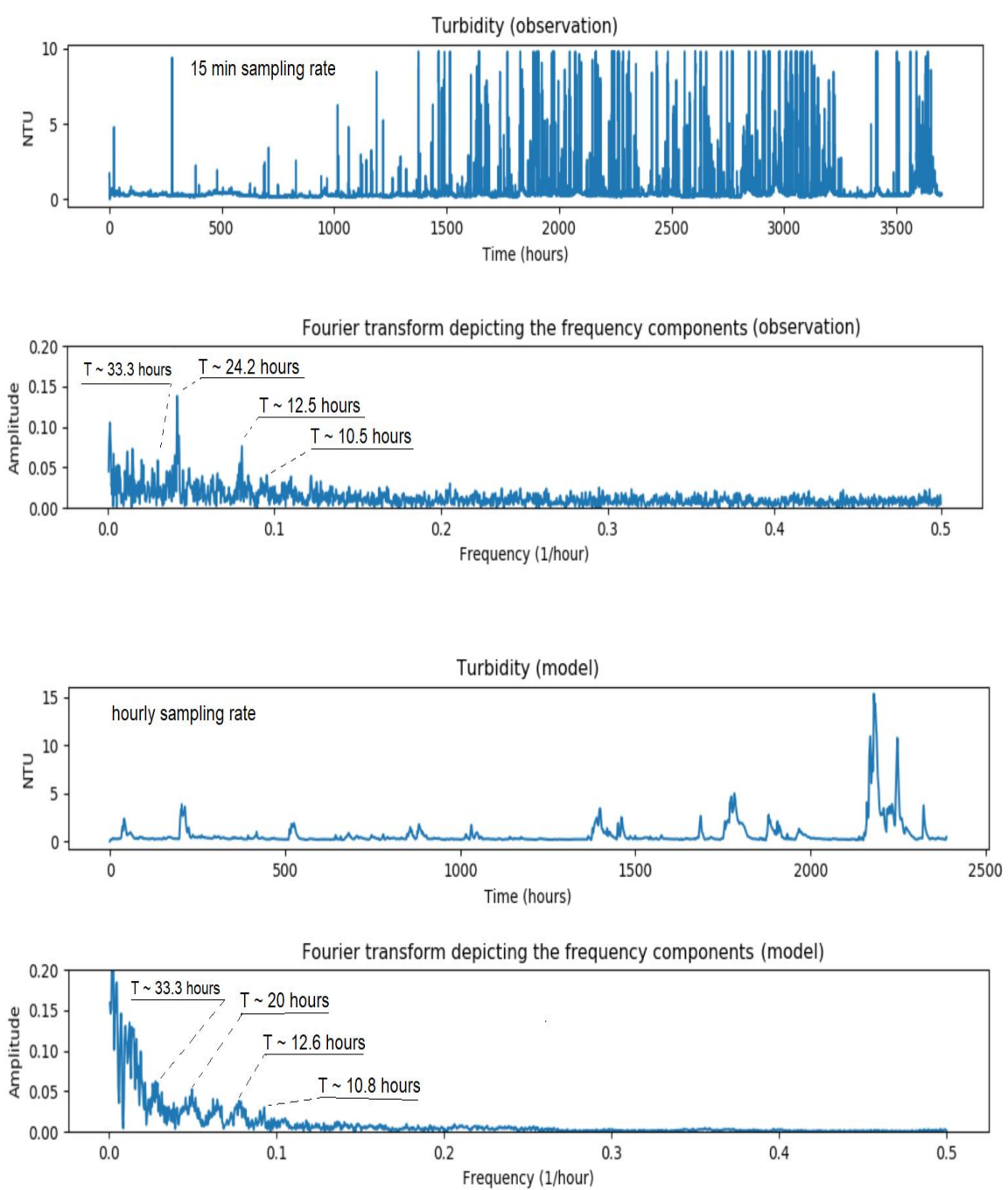**Figure 4.48 Measured turbidity vs turbidity derived from ADCP backscatter at the North lander site [the bottom plot is a zoom into a subset of the top plot].**

4.4.5   Sediment model calibration against observations

Figures 4.49-4.54 illustrate the quality of the calibrated model by depicting simulated suspended sediment concentrations next to the records of TSS derived from measurements. The scaling relationship (1) was used to derive TSS from the turbidity records. In the case of ADCP backscatter, the signal was first converted from ADCP backscatter counts to turbidity via (2) or (3) (depending on the ADCP frequency), and then from the turbidity to TSS using the relationship (1).

At the west-lander site because of the low signal to noise ratio the model is tested against both TSS derived from the turbidity records (Figure 4.49) and TSS derived from the ADCP backscatter signal (Figure 4.50). According to these data, the model tends to reproduce elevated concentrations of suspended sediment for major resuspension events but grossly underestimates the sediment concentration in early April 2019. Note that from 3 to 10 April 2019, TSS derived from turbidity shows isolated peaks of suspended sediment concentration, whilst acoustic backscatter suggests elevated but relatively homogeneous distributions of suspended sediment. Similarly, TSS derived from turbidity suggests low concentrations of suspended sediment in January-February 2019, while TSS derived from ADCP backscatter indicates a vigorous resuspension of sediments over the same period. These inconsistences suggest significant uncertainty of TSS inferred from observations (and are likely attributed to both the stochastic nature of the suspended sediment fields and observational errors).

Spectral decomposition of the turbidity record at the West lander site (Figure 4.50b , second plot from the top) shows a relatively high-energy spectral components at low-frequencies (periods exceeding 10 hours). The plot highlights distinct semidiurnal and diurnal tidal components in this part of the spectrum and illustrates several harmonics likely associated with the relatively long-term turbidity events (time periods exceeding diurnal tide period). For the high-frequency components (oscillations having less than 10 hours period) the spectral energy is relatively low and irregular across the whole domain. Likely stochastic nature of such high-frequency oscillations places them outside the scope of this modelling study based on the relatively low-resolution deterministic models.

The spectrum for the simulated turbidity (Figure 4.50b, bottom plot) when tested against observations (Figure 4.50b, second plot from the top) indicates that the model underestimates amplitudes for the diurnal and semidiurnal oscillations of the turbidity and overestimates amplitudes in the lower-frequency part of the spectrum (turbidity events lasting longer than the diurnal period). The period of the simulated semidiurnal signal is consistent with observations. The period of the simulated diurnal variability of the turbidity is below the measurements by about 4.5 hours. Both model and observations suggest low-energy oscillations of the turbidity at the time scales less than 10 hours.

No turbidity was measured at the eastern deployment site. Hence, the model was tested against TSS derived from the ADCP backscatter using the relationship established for the 600 kHz ADCP (3). As illustrated in Figure 4.51, the model is consistent with observations.

At the northern and eastern sites, the model was tested against TSS derived from turbidity records (rather than ADCP backscatter, which is much noisier at these sites, Figures 4.47 and 4.48). According to Figures 4.52 and 4.53, both sites show a reasonable agreement between model and observations.

Comparison of the model with the monthly near-bottom samples of TSS at the DEP B3 and E sites (Figure 4.54) indicates that the model mean is within the standard deviation of the observed data. The model tends to underestimate mean concentrations at these sites. Simulated TSS show much smaller variability at the E site compared to data. Note also significant uncertainty is likely to be associated with these field data because of the limited number of samples and the error-prone nature of the near bottom sampling in a relatively deep water (about 25 m) with strong currents.
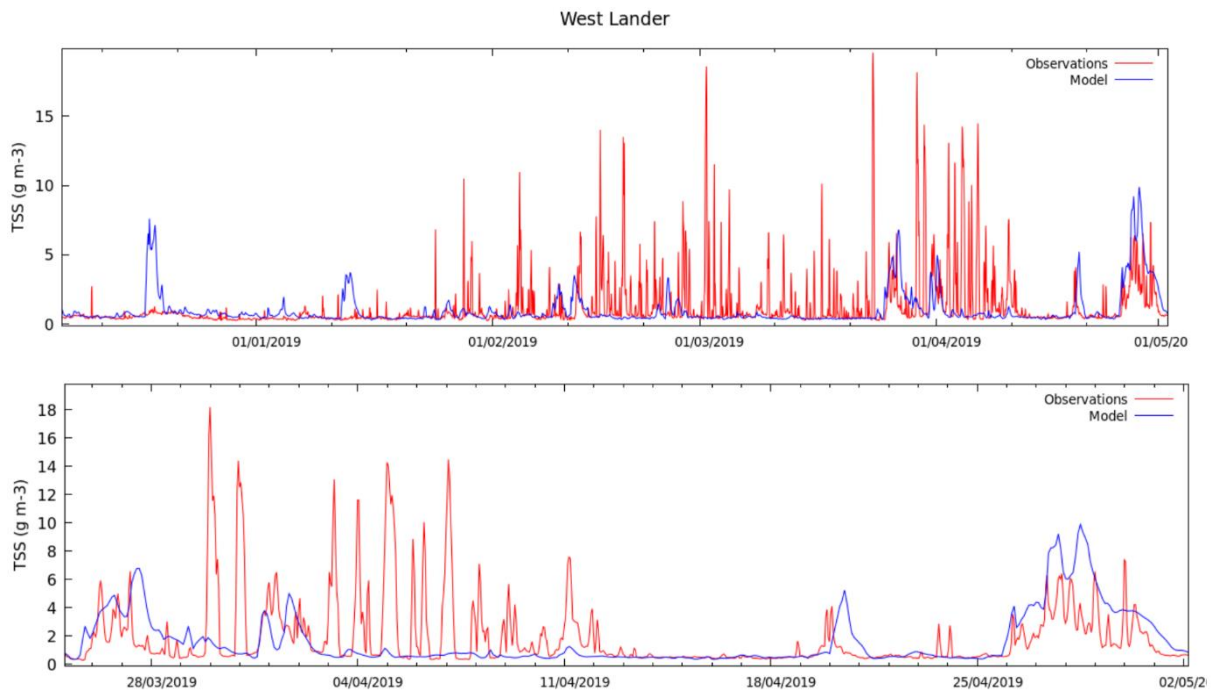
Figure 4.49 Simulated TSS vs TSS derived from the turbidity records at the west lander site [the bottom plot is a zoom into a subset of the top plot].
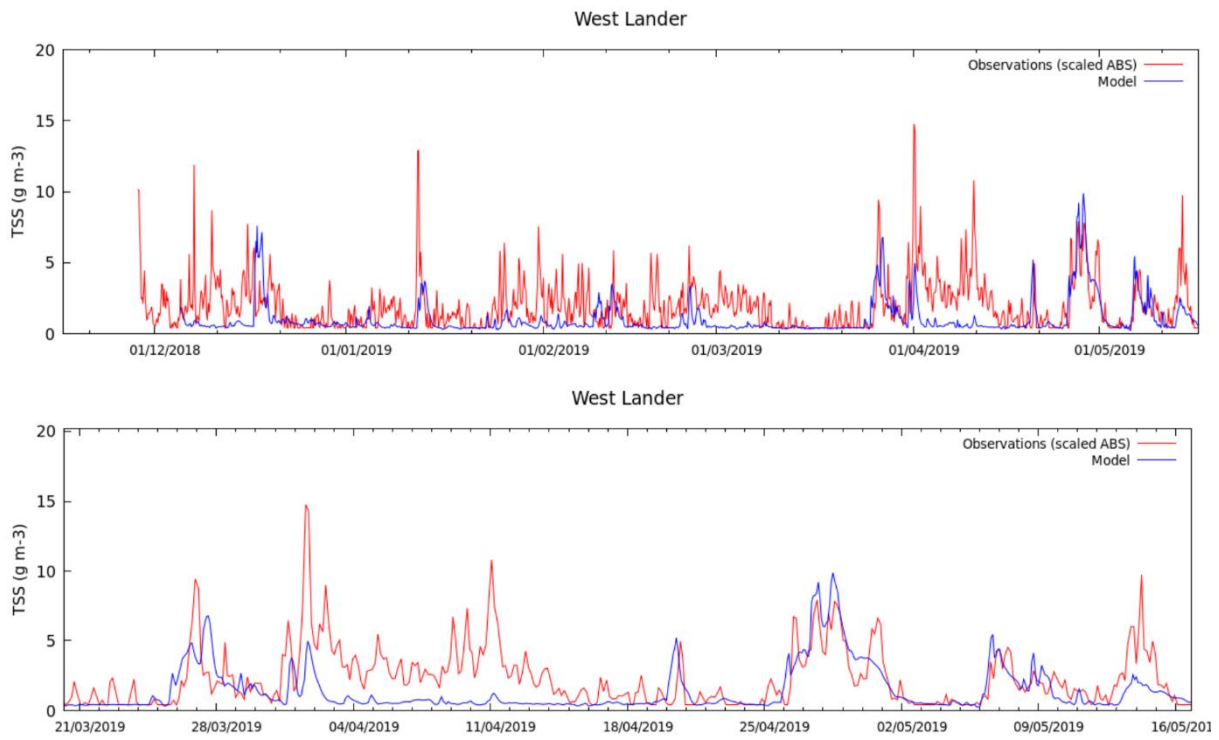
Figure 4.50 Simulated TSS vs TSS derived from ADCP backscatter records at the west lander site [the bottom plot is a zoom into a subset of the top plot].

Figure 4.50b Spectral decomposition of the observed (top 2 plots) and simulated (bottom 2 plots) turbidity at West lander site.
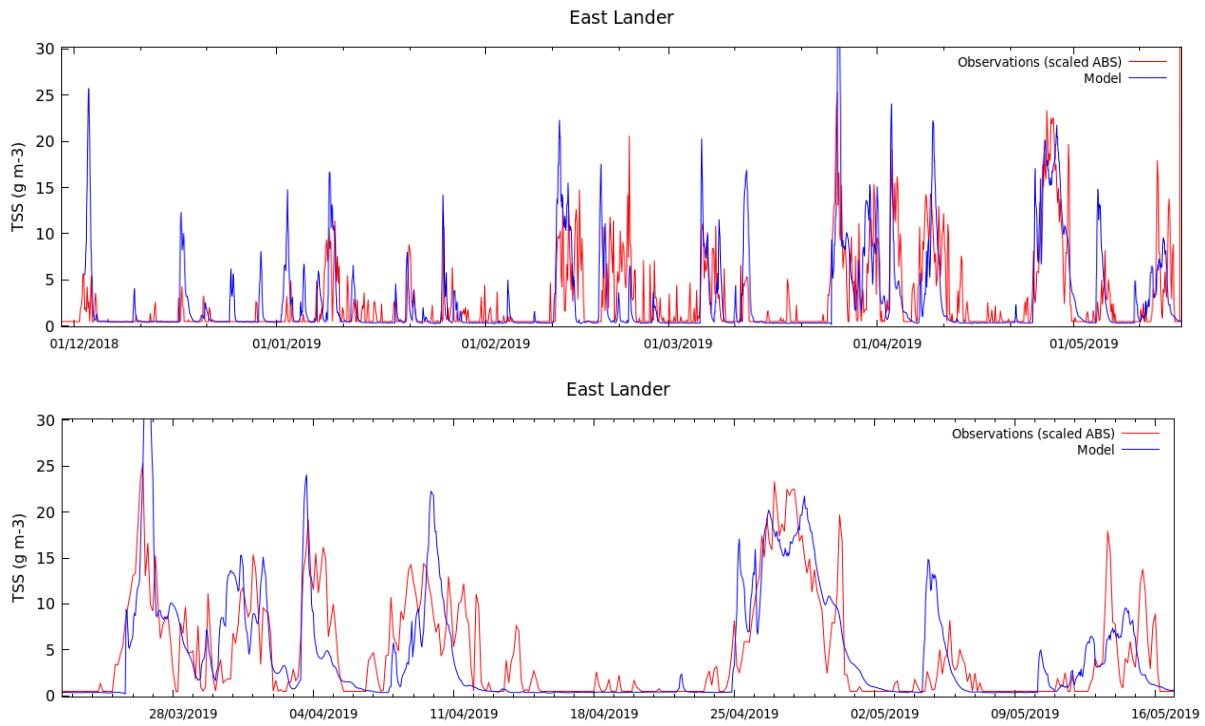
Figure 4.51 Simulated TSS vs TSS derived from ADCP backscatter at the east lander site [the bottom plot is a zoom into a subset of the top plot].
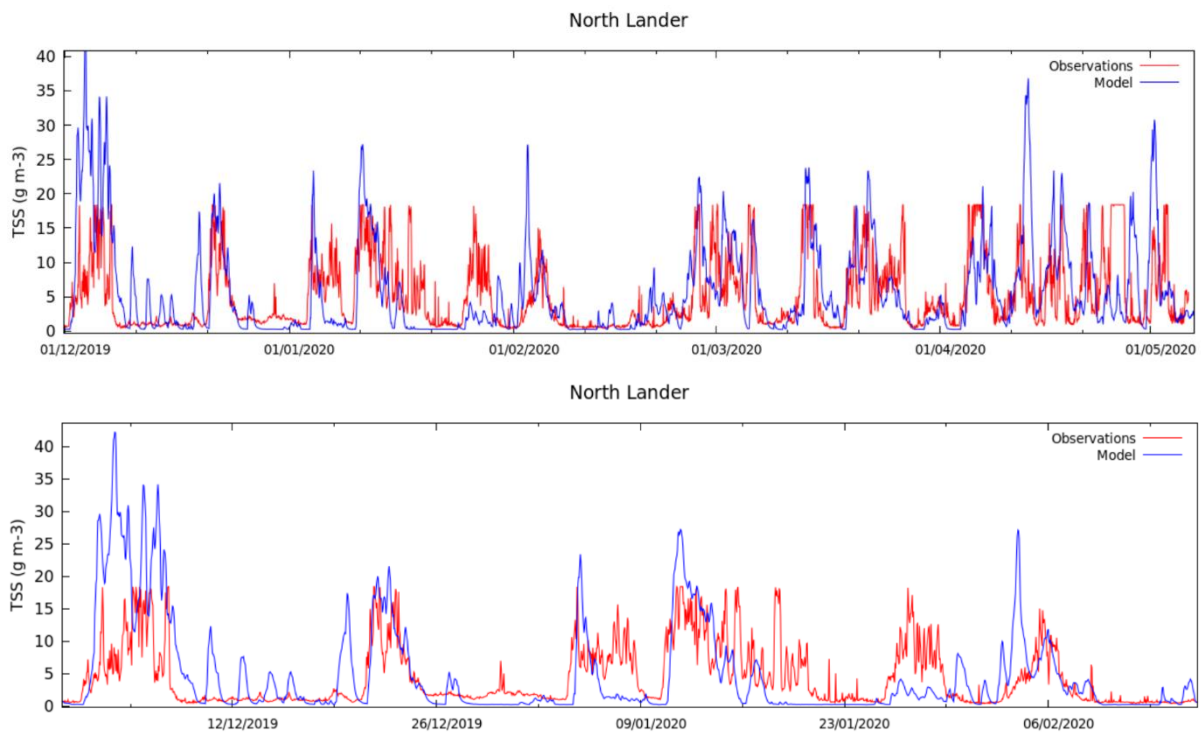
Figure 4.52 Simulated TSS vs TSS derived from turbidity records at the north lander site [the bottom plot is a zoom into a subset of the top plot].
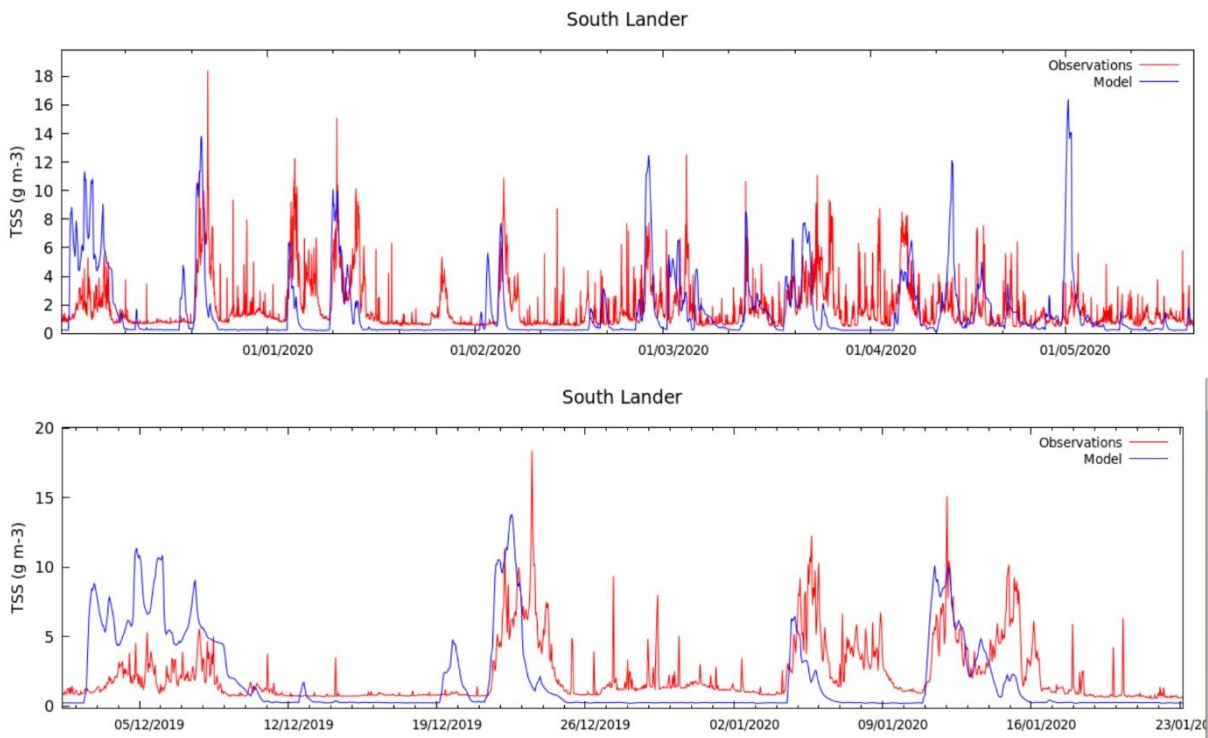
Figure 4.53 Simulated TSS vs TSS derived from turbidity records at the south lander site [the bottom plot is a zoom into a subset of the top plot].
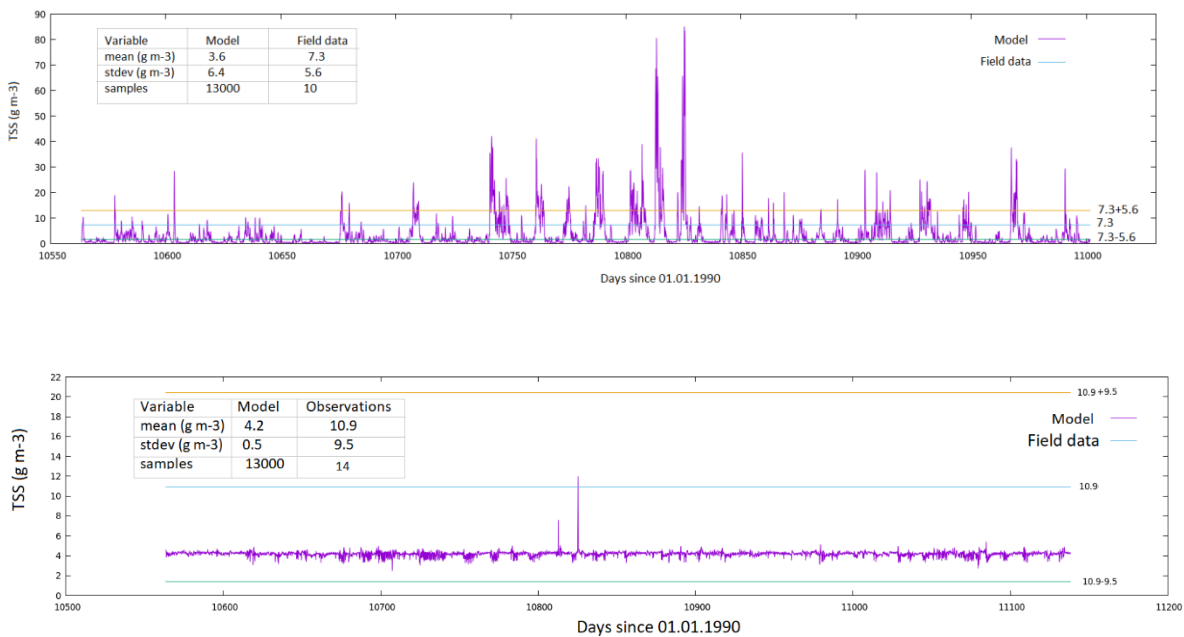
Figure 4.54 Model vs monthly near bottom samples taken at B3 (top plot) and E (bottom plot) DEP sites (location map in Figure 4.39).

4.4.6   Sediment model simulated data

The distribution of the bottom shear velocity in the Storm Bay region calculated over the course of several years (2015-2019) for the winter and summer seasons is shown in Figure 4.55. The 5th, 50th, and 95th percentiles can be interpreted here as representing distributions typical for the low, intermediate, and high-energy environments (e.g. extreme weather events). As expected, the highest shear stresses tend to develop along the coastline exposed to ocean waves. Inside estuarine channels and coastal embayments, on the other hand, the bottom shear stress is relatively small. In winter months storms and ocean-swell tend to enhance the bottom stress, particularly in Storm Bay and in coastal regions open to the ocean swell. The model also suggests the 95th percentile of the bottom friction inside estuarine channels in winter is lower than that in the summer season.

Simulated sediment mobility (expressed as the probability for the benthic sediments to resuspend) in the winter season is shown in Figure 4.56. The critical bottom shear stress of resuspension is set to 0.15, 0.2, and 0.35 N m^{-2} for the top, intermediate, and deep level sediments, respectively (1.22, 1.41, and 1.87 cm s^{-1} in shear velocity units). According to this data, sediments in shallow coastal waters open to the ocean swell tend to have the highest mobility rate, consistent with the distribution of the bottom shear stress shown in Figure 4.55. The lowest probability of resuspension is found in sediments located within the estuarine channels, inside coastal embayments and behind land features sheltering them from the oceanic swell.

The simulated erosion map (Figure 4.57, left plot) indicates an irregular patchy distribution of sediment deposits. Broad-scale features (kilometres and more) shown on this map are plausible, but the fine structure is not credible since it correlates with the thickness of the numerical grid layers near the seabed (shown in the middle plot) and, hence, is influenced by the structure of the numerical grid.

According to the model, over the simulated period the highest levels of suspended sediment concentration tend to develop in the upper reaches of the estuaries, inside Fredrick Henry Bay, and in shallow coastal regions of Storm Bay (Figure 4.58). To assess the impact of catchment derived sediments on the suspended sediment concentration, an idealised scenario with no input of sediments from catchments was simulated and compared to the calibration model run (Figure 4.59). According to this analysis, for the simulation period (2015-2019) catchment loads result in an increase in the 95th percentile of the surface suspended sediment concentration inside the Derwent and the Huon Estuaries, in the northern part of the Storm Bay, in North-West Bay and in the southern part of the D'Entrecasteaux Channel.
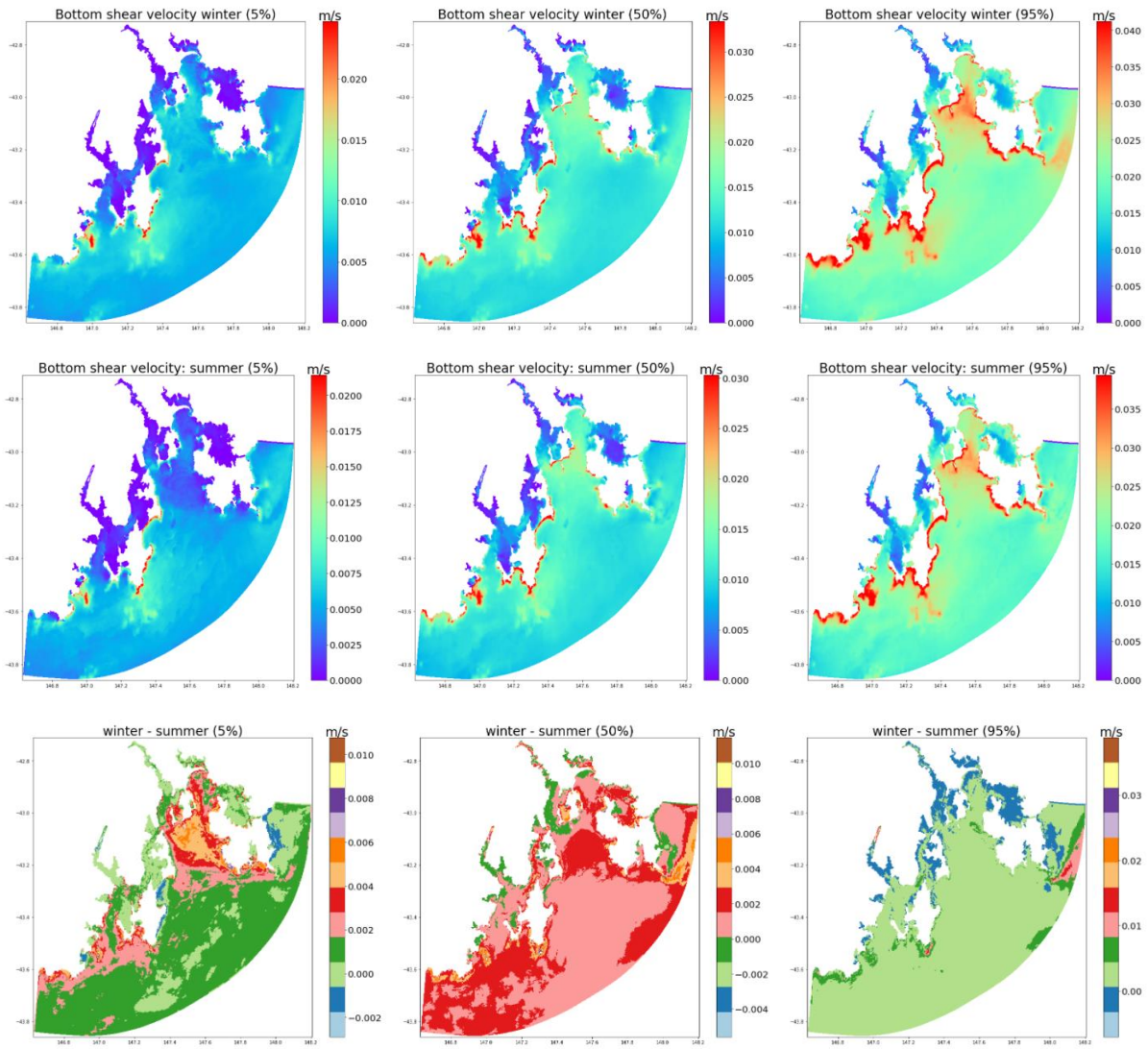
Figure 4.55 Simulated 5th, 50th, and 95th percentile of the bottom shear velocity over the winter and summer seasons (top and middle plots, respectively). Bottom plots show difference between the winter and summer seasons. [Note that the scale varies between plots to ensure spatial details in each figure are clearly shown].
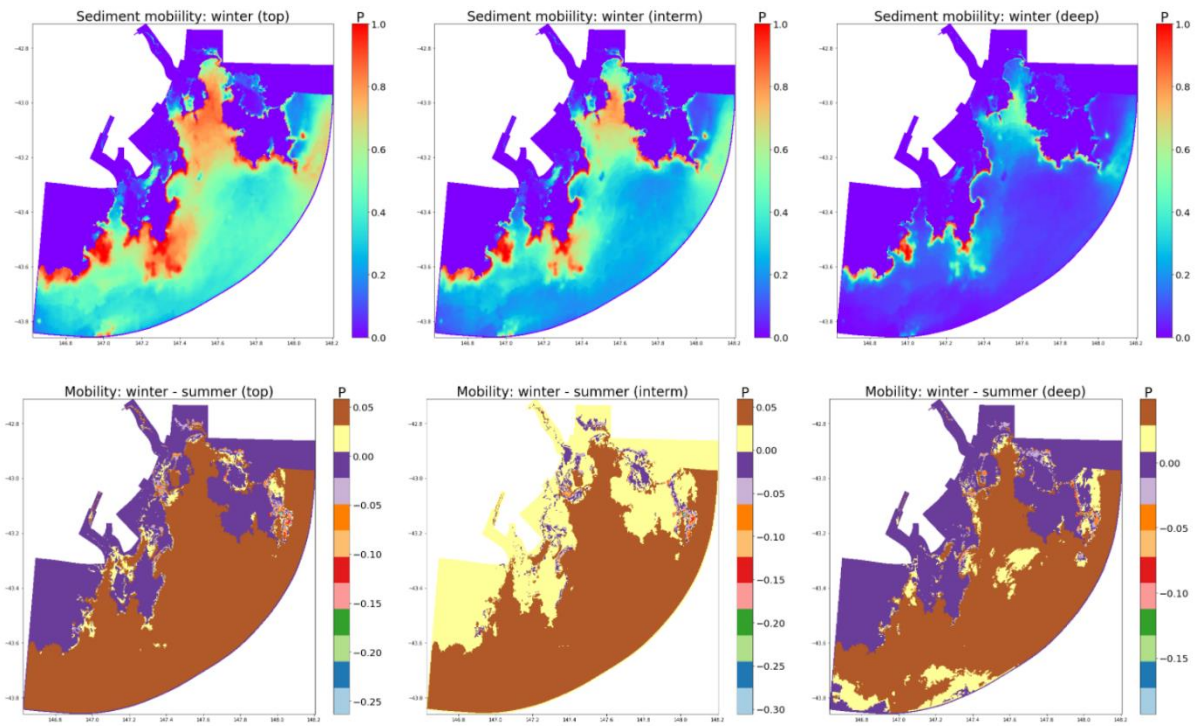
Figure 4.56 Simulated sediment mobility in winter season for the top, intermediate, and deep level sediments (top plots) and the difference of the mobility simulated for the winter and summer seasons (bottom plots). The critical bottom shear stress of resuspension is set to 0.15, 0.2, and 0.35 N m^{-2} for the top, intermediate, and deep level sediments, respectively (or 1.22, 1.41, and 1.87 cm s^{-1} in shear velocity units).
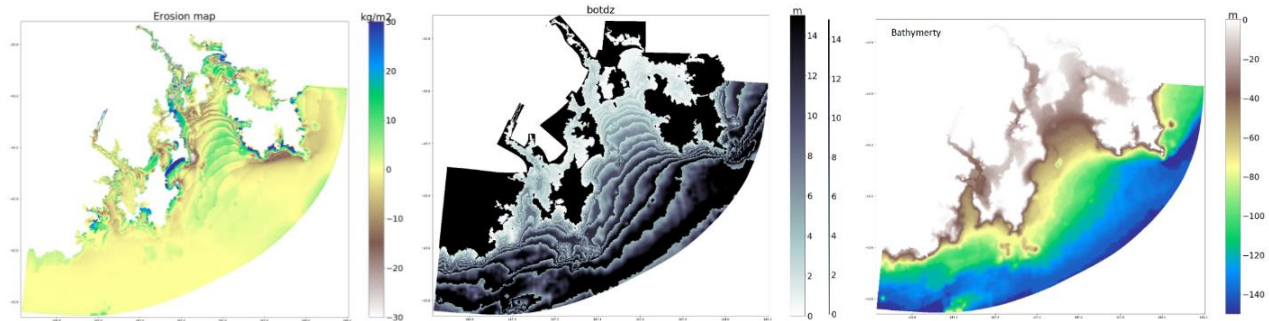
Figure 4.57 Erosion map in kg m^{-2} (left plot), the thickness of the numerical grid layers near the seabed in m (middle plot), and the bathymetry map in m (right plot).
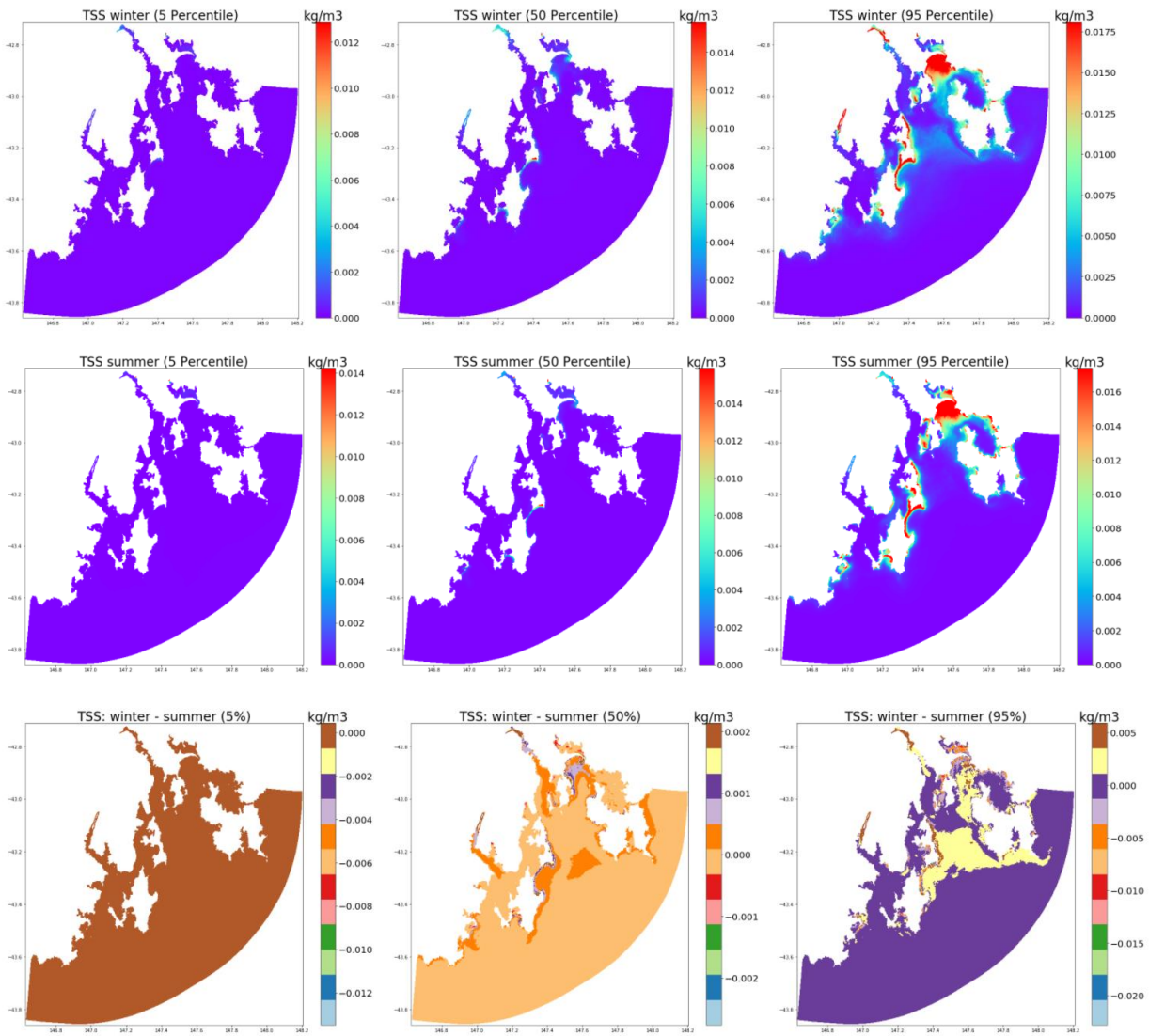
Figure 4.58 Simulated 5ᵗʰ, 50ᵗʰ, and 95ᵗʰ percentile of the suspended sediment concentration over the winter and summer seasons (top and middle plots, respectively). Bottom plots show difference between the winter and summer seasons for each percentile pair.
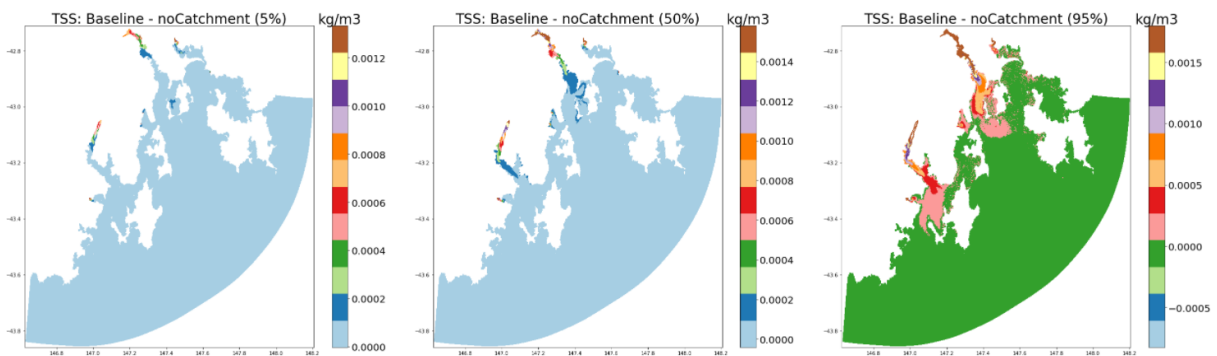
Figure 4.59 Difference between percentiles of the surface suspended sediment concentration calculated for the calibration run (identified as 'Baseline') and the scenario with no input of sediments from catchments.

4.4.7 Near real time wave and sediment models

The Near Real Time (NRT) wave and sediment transport models in Storm Bay have been implemented within the Cronicle framework (Figure 4.8) for automated operation.

The parameters of the NRT sediment transport model coincide with the parameters of the hindcast calibrated model (presented earlier in this section of the report). The implementation of the NRT wave model has improved (compared to the hindcast model) through the more accurate specification of the open boundary conditions (using Auswaves data with about 10km grid resolution instead of the Wavewatch 3 data with about 50km resolution grid). As illustrated below (Figure 4.60) both NRT and hindcast wave-models are close to observations.
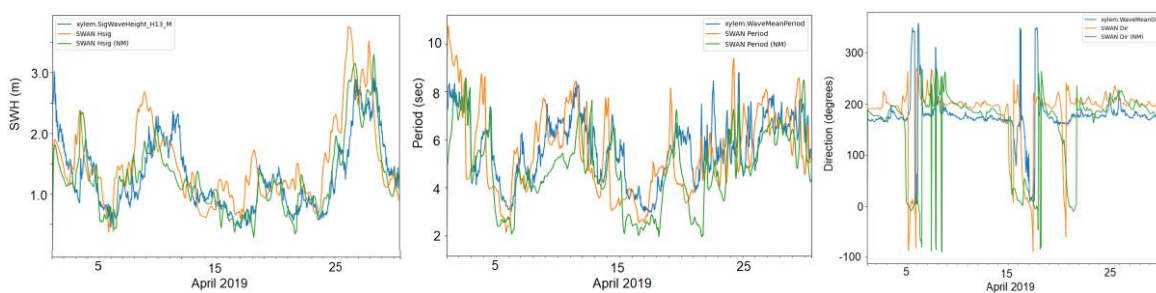
Figure 4.60 Significant wave height (left), period (centre), and wave direction (right), according to observations (blue), hindcast model (green), and NRT model (yellow). Wedge Island site (site map in Figure 4.37).

4.5   Biogeochemical model

The CSIRO Environmental Modelling Suite (EMS) includes a biogeochemical model that in this project is linked via a hydrodynamic transport model to a high resolution 3D hydrodynamic model SHOC (Herzfeld 2006) and a multilayer sediment model (MECOSED, Margvelashvili 2008). Biogeochemical dissolved tracers for carbon, nitrogen, phosphorous and oxygen are advected and diffused in an identical fashion to physical tracers such as temperature and salinity and ecological particulate tracers sink and are resuspended by the same formulation as sediment particles. At each ecological time step, non-conservative ecological rate processes such as growth, nutrient uptake, grazing, and mortality are integrated within the ecological module which returns updated tracer concentrations to the hydrodynamic transport model via an interface routine.

The ecological model is integrated on the same model grid as the hydrodynamic model with the water column is organised in 3 'zones': pelagic, epibenthic and sediment. The Storm Bay model pelagic zone has 35 layers in the vertical with 0.5 m resolution at the surface and 20 m resolution at the bottom. The epibenthic zone overlaps with the lowest pelagic layer and shares the same dissolved and suspended particulate material fields. The sediment is modelled in multiple layers with a thin layer of easily resuspendable material overlying thicker layers of consolidated sediment.

Dissolved nutrients are advected and diffused throughout the model domain in an identical fashion to temperature and salinity while particulate substances sink and are resuspended in the same way as sediment particles. For each layer and grid location the time evolution of each model substance (Y) is the sum of conservative advection, diffusion and sinking processes (ωY) and non-conservative biogeochemical rate processes (βY):

$$\partial Y/\partial t = -\varphi Y + \beta Y \tag{1}$$

where $\varphi Y = (\mathbf{u}\Delta Y + \Delta_H A_H \Delta Y) - (\partial/\partial z)K_z(\partial Y/\partial z) + (\partial \mathbf{w_s} Y/\partial z)$

and $\Delta = (\partial/\partial x) + (\partial/\partial y) + (\partial/\partial z)$; $\Delta_H = (\partial/\partial x) + (\partial/\partial y)$

[Here $\mathbf{u}$ is the velocity vector; A_H and K_z are the horizontal and vertical diffusion coefficients and $\mathbf{w_s}$ is the settling velocity.]

Non-conservative biogeochemical processes are organized into pelagic processes of phytoplankton and zooplankton growth and mortality, detritus remineralisation and fluxes of dissolved oxygen, nitrogen and phosphorus; epibenthic processes of growth and mortality of macroalgae, and sediment based processes of phytoplankton mortality, microphytobenthos growth, detrital remineralisation and fluxes of dissolved substances.

The biogeochemical model (Figure 4.61) includes four groups of microalgae (small and large phytoplankton, dinoflagellates and microphytobenthos) and macrophytes (epiphytic algae, kelp and seagrass) which grow at a group specific rates determined by size, access to dissolved nutrients (nitrogen and phosphate) and photosynthetically active radiation (PAR) (Baird et al., 2020, CSIRO Coastal Environmental Modelling Team 2018). Autotrophs are assumed to take up ammonium and nitrate with equal preference, and phosphate and dissolved inorganic carbon are taken up by phytoplankton at the Redfield ratio (106C:16N:1P) and by macrophytes at the Atkinson ratio (550C:30N:1P). Ambient PAR is calculated from incident surface mean PAR

attenuated by seawater, coloured dissolved organic substances (estimated from an inverse linear relationship with salinity), and organic and inorganic particles. Chlorophyll is calculated from a dynamic carbon to chlorophyll ratio (Baird et al 2013).

Micro- and meso-zooplankton graze on small and large phytoplankton respectively, at rates determined by swimming speed and particle encounter rate (Baird et al., 2020, CSIRO Coastal Environmental Modelling Team 2018). Half of grazed material is released as dissolved and particulate carbon, nitrogen, and phosphate, with the remainder forming detritus. Additional detritus accumulates by mortality. Detritus and dissolved organic substances are remineralised into inorganic carbon, nitrogen and phosphate with labile detritus transformed most rapidly (days), refractory detritus slower (months) and dissolved organic material transformed over the longest timescales (years). The evolution (by photosynthesis) and utilization (by respiration and remineralisation) of dissolved oxygen is also included in the model, and depending on prevailing concentrations facilitates or inhibits the oxidation of ammonia to nitrate and its subsequent denitrification to dinitrogen gas which is then lost from the system. Further details of the biogeochemical model, including model equations and parameter values previously used in temperate Australian waters, may be found in (Wild-Allen et al., 2013; Wild-Allen & Andrewartha 2016).
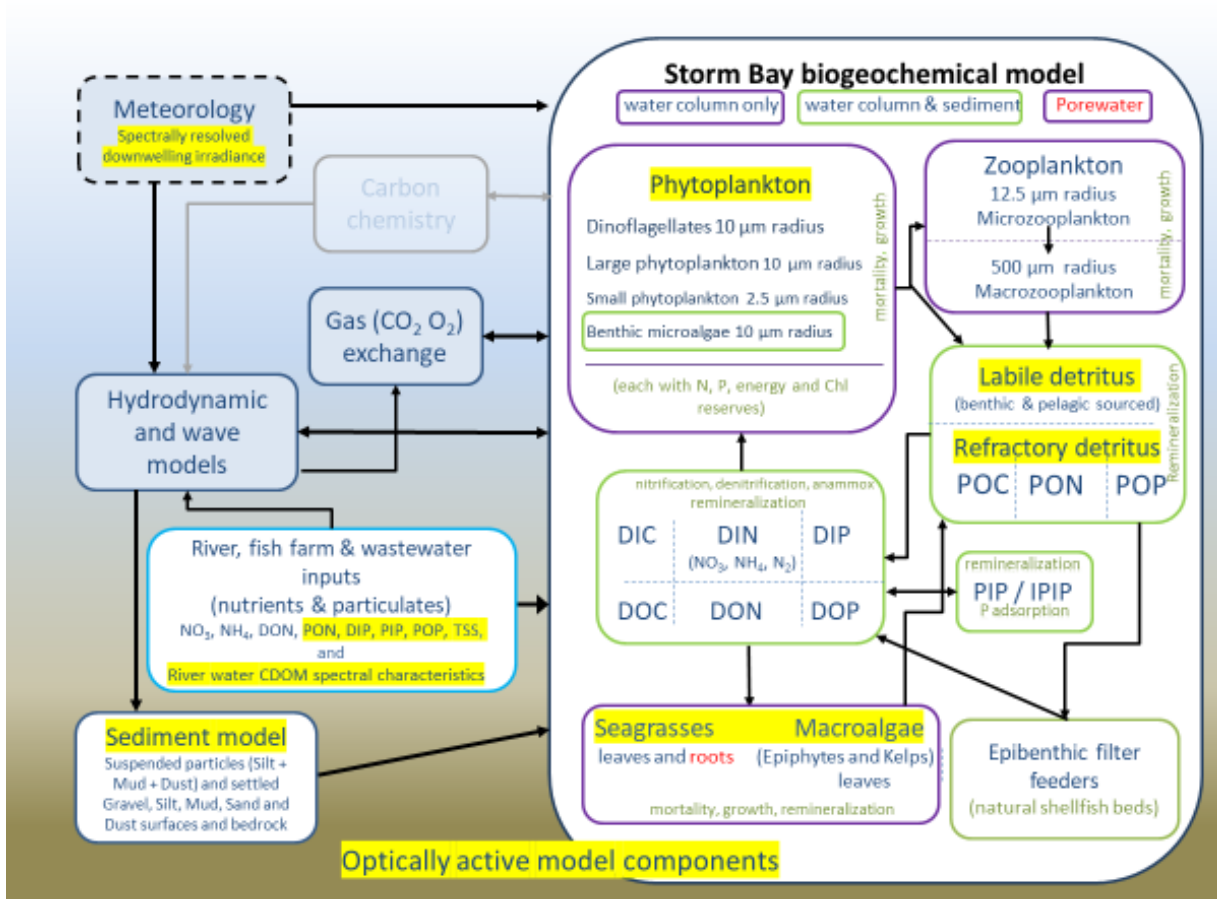
Figure 4.61 Schematic diagram of the CSIRO EMS biogeochemical model components and links.

4.5.1   Optical Model

The optical model attenuates incident sea surface spectral irradiance throughout the water column (Figure 4.62). Optically active dissolved and particulate substances (shown in yellow in Figure 4.61) absorb and scatter light according to their optical properties and concentration. In addition to the computation of scalar spectrally-resolved light for accurate resolution of photosynthesis in each model layer, sea leaving radiance is also calculated for model comparison with remotely sensed sea surface colour. By combining the sea leaving radiance in the red, green, and blue wavelengths a true colour image can be generated directly from the model output for comparison with satellite products. Whilst satellite images of the region are often covered in cloud, the model provides a synthesis hypothesis of conditions beneath the clouds 365 days a year.
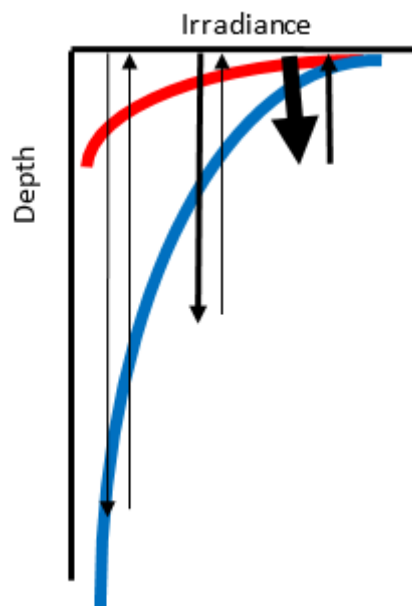
Figure 4.62 In situ spectrally resolved light is calculated by the attenuation of spectrally resolved incident irradiation by optically active dissolved and particulate substances. Remote-sensing reflectance is calculated from the optical-depth weighted reflectance and bottom reflectance.

A full description of the optical model equations and parameter derivations is given in Baird et al. (2016). The optical model was originally designed for simulation of optical properties in the tropical waters of the Great Barrier Reef in northeast Australia; to accurately reproduce optical conditions in Storm Bay the following adaptations have been made:

1. *CDOM absorption.* Chromophoric Dissolved Organic Matter (CDOM), from marine and terrestrial sources, absorbs light strongly at short wavelengths (<500 nm), and exponentially less so at longer wavelengths. CDOM absorption in river runoff is particularly strong in Tasmanian waters, and also variable between rivers. To account for this variability, we track three colours of CDOM (pale, amber and dark) from the freshwater inputs (Figure 4.63), with different absorption intensities and hues. For example, Huon River contains primarily dark waters, and northern rivers pale. The hues of CDOM from each river add together at a location to determine the absorption at that point and use data collected in Tasmanian waters (Figure 4.64) Cherukuru et al., 2014 & 2016, and Nechad et al., 2015. Following comparison of simulated and observed OC3M chlorophyll, pale CDOM with attenuation of 0.01 m^{-1} was

added to the ocean boundary to better represent the spectral attenuation of coastal ocean water.

2. *Suspended sediments*. The optical properties (mass-specific absorption and scattering coefficients) of suspended particles use data from Cherukuru et al., 2014 and Stramski et al., 2007 for sediment characteristics that most closely match the characteristics of local particles (Figure 4.65).

3. *Phytoplankton absorption.* The mass-specific absorption coefficients for suspended microalgae have been calculated using the following equivalent spherical radii and pigments: small phytoplankton (r = 2.5 μm, pig = chlorophyll-a, zeaxanthin, echinenone carotene, phycoerythrin, phycocyanin) and large phytoplankton, microphytobenthos and dinoflagellates (r = 10 μm, pig = chlorophyll-a, fucoxanthin).

4. *Diagnostic variables.* New simulated satellite products have been developed in particular simulated normalised fluorescence line height (anomaly at 678 nm), which is a useful satellite proxy for chlorophyll independent of CDOM concentration (Roesler & Barnard 2013).
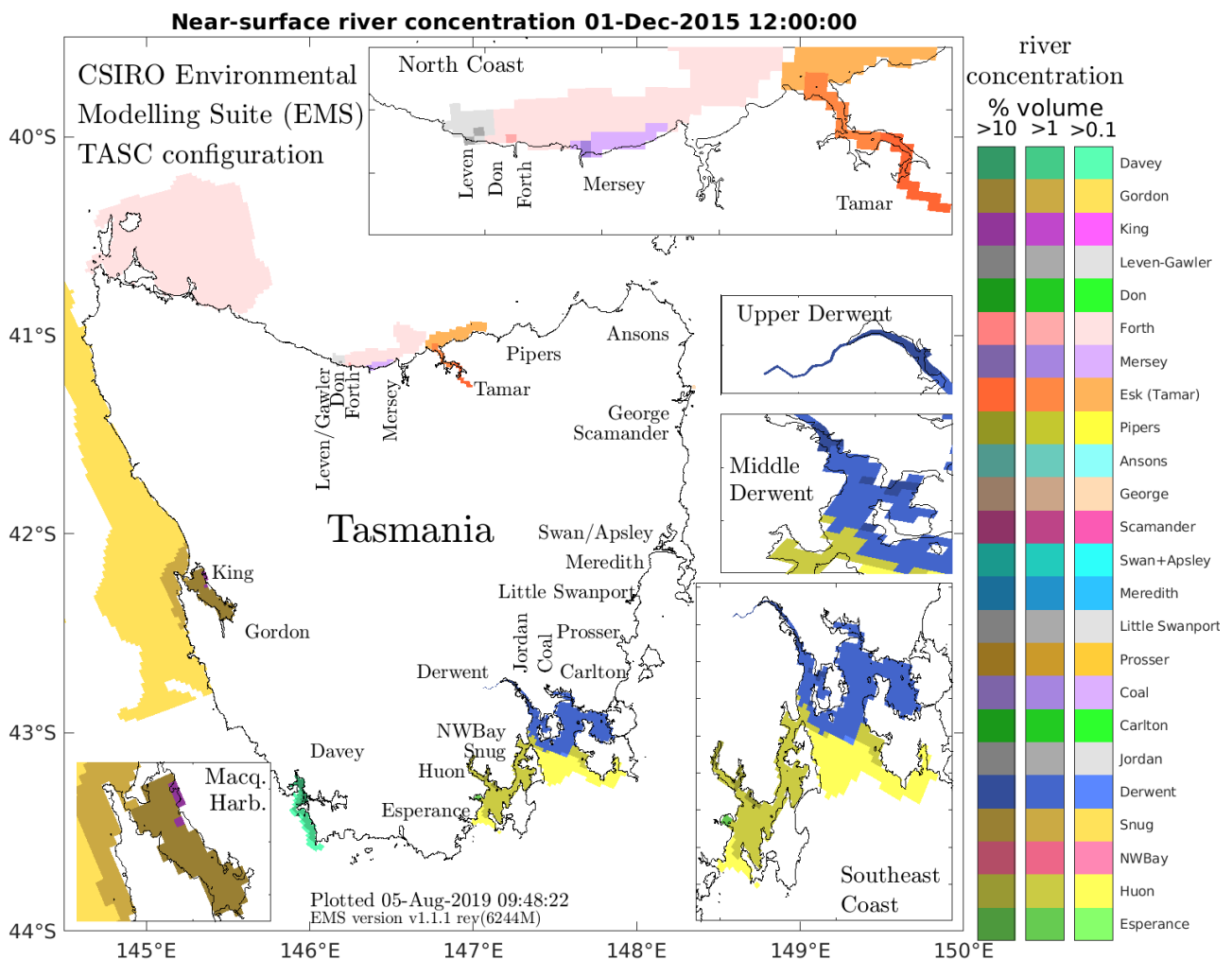
Figure 4.63 River tracers used to track the influence of river water optical properties through the model domain.
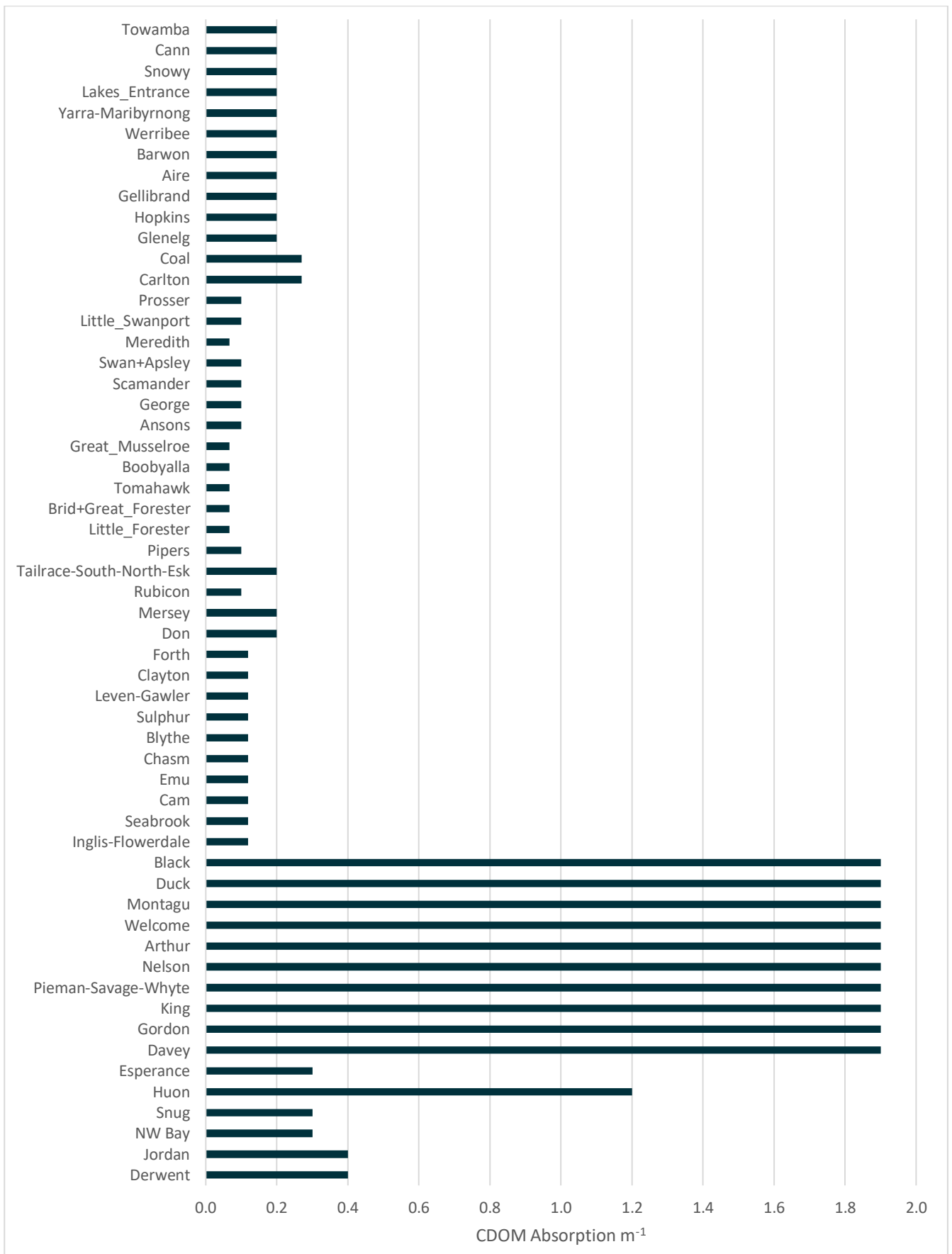
Figure 4.64 Absorption by coloured dissolved organic material for rivers in southeast Australia (estimated from Cherukuru et al., 2014).
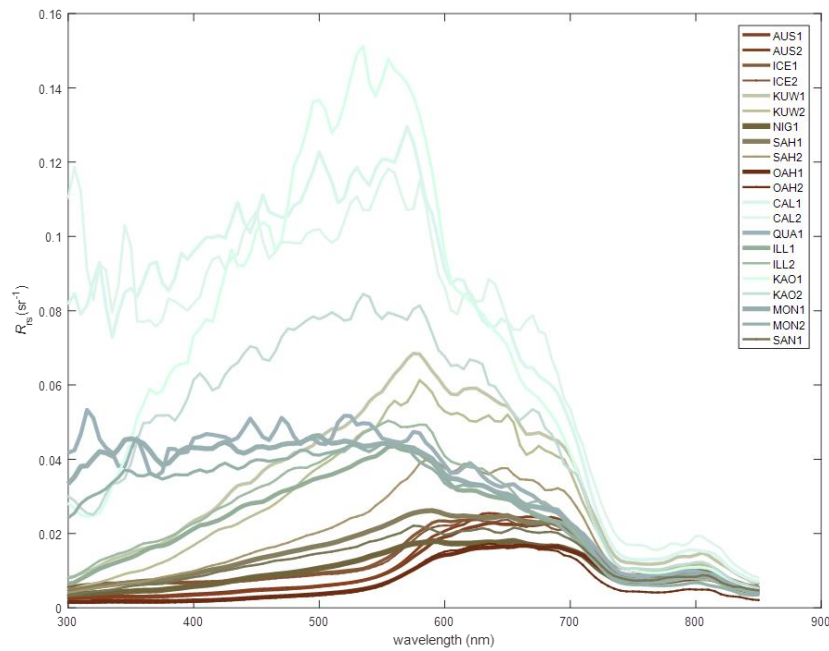
Figure 4.65 Variations in the optical properties of terrigenous mineral-rich particulate matter suspended in sea water (from Stramski et al., 2007).

4.5.2   Biogeochemical model configuration

The full list of model processes explicitly included in the biogeochemical and optical model are shown in Table 4.6. Parameter values have where possible been sourced from literature reporting local observations in Tasmania or otherwise found from model parameter data libraries (Robson et al., 2018) or modelling studies in Australian temperate waters (Wild-Allen et al., 2013; Wild-Allen & Andrewartha 2016). During the biogeochemical model calibration and validation process poorly known parameter values have been adjusted within observed ranges to optimise the model fit to available observations. A summary of biogeochemical model parameter values is provided in Appendix A4.

The hydrodynamic model has been calibrated and generated transport model files for the period Dec 2014 - Dec 2020. The biogeochemical model was run for Dec 2014 – June 2020 and then transitioned to run in near real time. For the ongoing operation of the near real time biogeochemical model estimates for wastewater discharge, fish farms and other industry load inputs were made based on the annual cycle of values determined for 2020. River loads of biogeochemical model substances were estimated from average concentrations scaled against near real time river flow.

The biogeochemical transport model is currently optimised over 28 window partitions and running at around 52 model days per day (52:1) on the CSIRO high performance compute infrastructure.

Table 4.6 Biogeochemical processes implemented in the Storm Bay model.

Pelagic	Epibenthic	Sediment
Remineralization	Macroalgae_spectral_grow(b)	Remineralisation
Microphytobenthos_spectral_grow	Macroalgae_mortality(b)	Light_spectral(HPLC)
Phytoplankton_spectral_grow(small)	Macroalgae_spectral_grow(g)	Microphytobenthos_spectral_grow
Phytoplankton_spectral_grow(large)	Macroalgae_mortality(g)	Carbon_chemistry
Dinoflagellate_spectral_grow	Seagrass_spectral_grow(Z)	Microphytobenthos_spectral_mortality
Phytoplankton_spectral_mortality(small)	Seagrass_spectral_mortality_proto	Phytoplankton_spectral_mortality(small)
Phytoplankton_spectral_mortality(large)	Filter_feeder	Phytoplankton_spectral_mortality(large)
Dinoflagellate_spectral_mortality	Mass_balance	Dinoflagellate_spectral_mortality
Zooplankton_mortality(small)	Light_spectral_uq	Zooplankton_mortality(small)
Zooplankton_mortality(large)	Diffusion	Zooplankton_mortality(large)
Zooplankton_large_carnivore_spectral_grow	Diffusion_heat	Nitrification_denitrification_anammox
Zooplankton_small_spectral_grow		P_adsorption
Nitrification_denitrification_anammox		Mass_balance
P_adsorption		
Carbon_chemistry		
Gas_exchange(Carbon, Oxygen)		
Mass_balance		
Light_spectral		

Initial condition

The initial biogeochemical model condition incorporates the hydrodynamic and sediment initial conditions as well as initial conditions for the biogeochemical parameters. A year-long pilot simulation was run, (informed by the values provided in Appendix A4), to determine a spatially and self-consistent initial condition for all biogeochemical model water column and sediment tracer concentrations. Atmospheric carbon dioxide concentrations were forced with data from the Cape Grim Baseline Air Pollution Station.

Ecologically, a significant area within the TASSE model domain contains rocky reef or rock outcrops. To represent this ecological habitat within the model an additional sediment type of hard rock (see sediment model section) was added to the sediment model types of gravel, dust, sand, mud. The thickness of this new substrate is a 1 cm layer with close to 0 concentration of sediments on top of the reef and the porosity of this layer is set close to 1. Seagrass was initialised from the pilot simulation (that demonstrated viable areas for seagrass meadow formation), modified to omit seagrass from known rocky reef areas and Ralphs Bay (Figure 4.66).
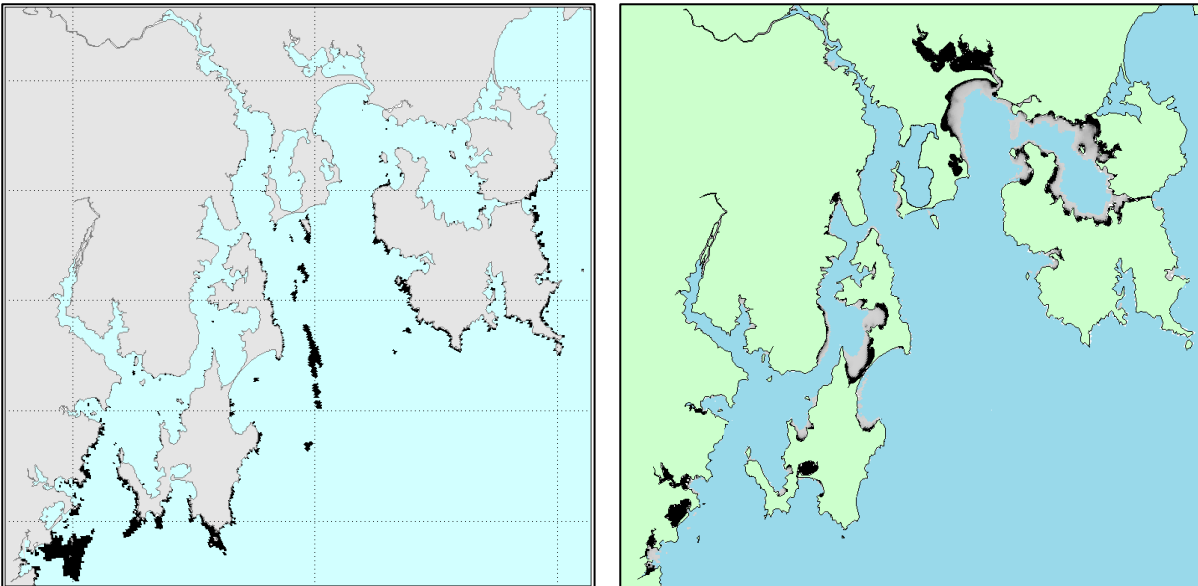
Figure 4.66 Initial condition for rocky reefs (left) and seagrass (right) [after 1 year of simulation with seagrass removed in Ralphs Bay and from rocky reefs].

Model forcing

Marine boundary

Ocean fluxes of sediment and biogeochemical tracers into Storm Bay are determined from the regional (SETAS) model hydrodynamic forcing as an upstream condition. For nitrogen, high resolution observations in the region (Figure 4.67) from moorings and gliders (optical nitrate sensors calibrated against laboratory sample analysis) have been correlated with temperature, depth, longitude and time of year (Figure 4.68; 222,934 observations, cubic relationship, R2 of 0.82). Similarly, high resolution observations of oxygen from sensors on gliders and moorings (Figure 4.69) have been calibrated against laboratory bottle samples and correlated with temperature, depth, longitude and time of year (Figure 4.70; 908,010 observations, cubic relationship, R2 of 0.87). Using these relationships, nitrate and oxygen concentrations entering the model are estimated from the hydrodynamic conditions along the model boundary; phosphate concentrations are scaled according to the molar Redfield ratio of 16N:1P appropriate for oceanic conditions with the minimum DIP concentration set to 2 mg m^{-3} (Figure 4.71a, b & c).
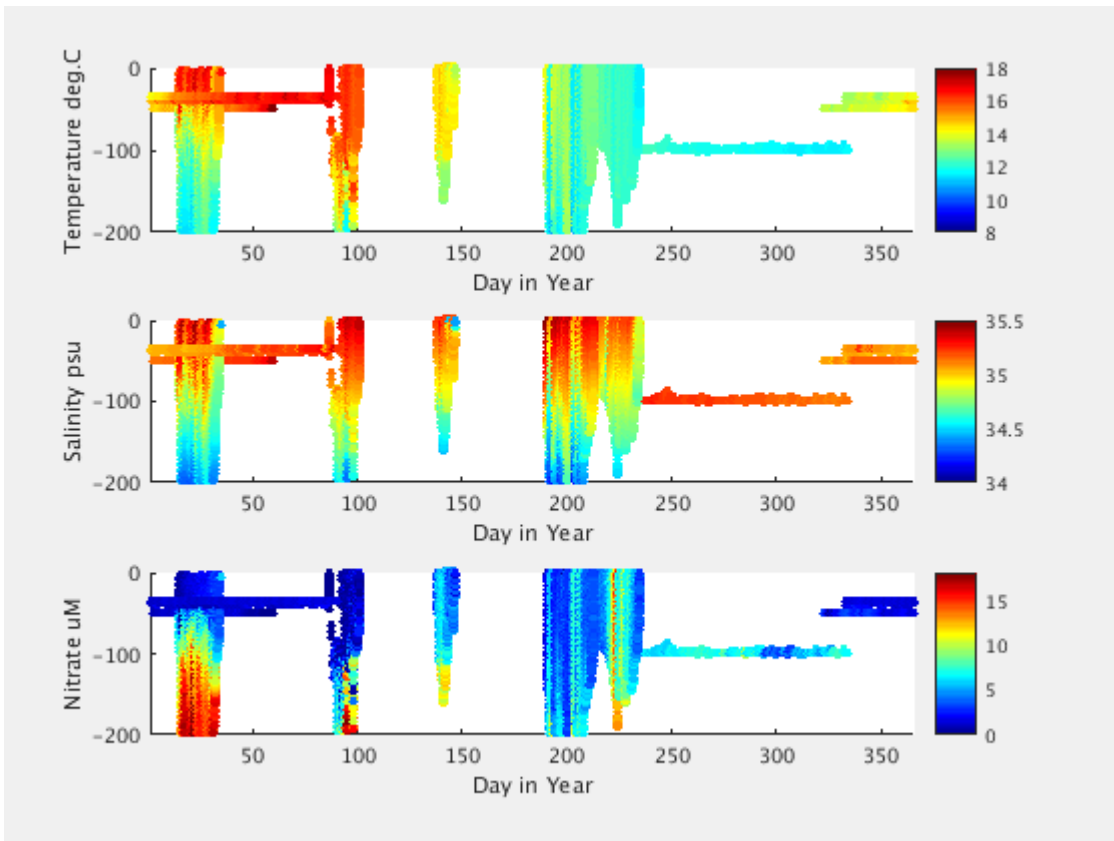
Figure 4.67 Climatology of temperature, salinity, and calibrated optical nitrate observations in outer Storm Bay from recent glider and mooring observations.
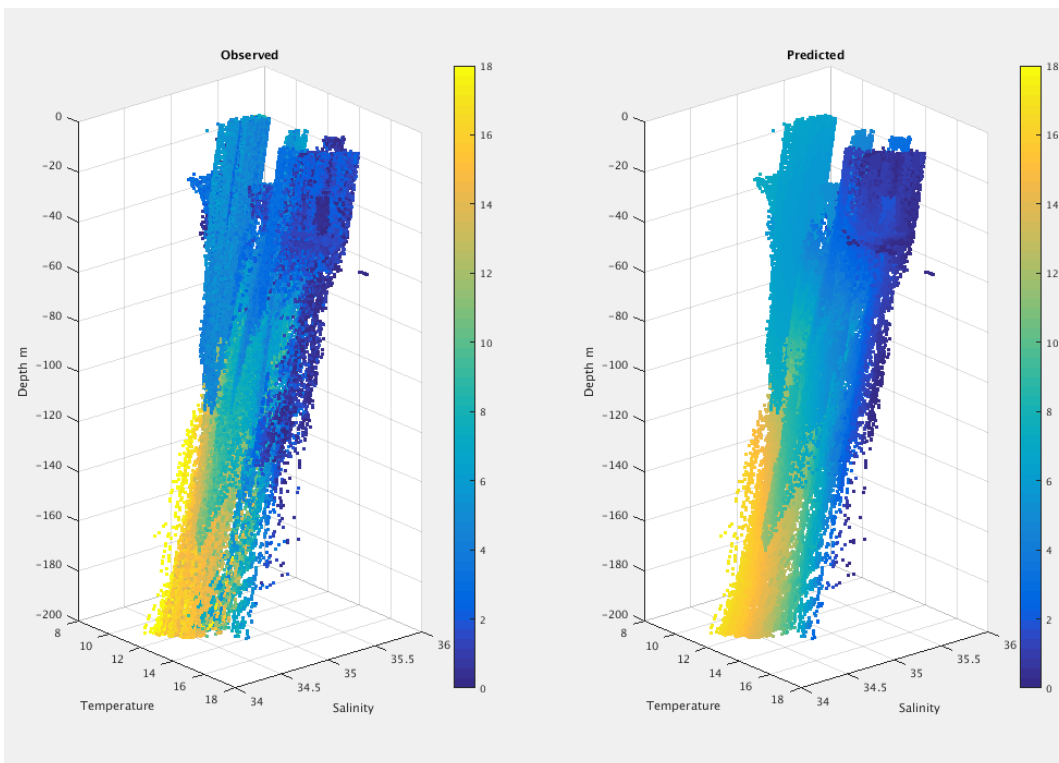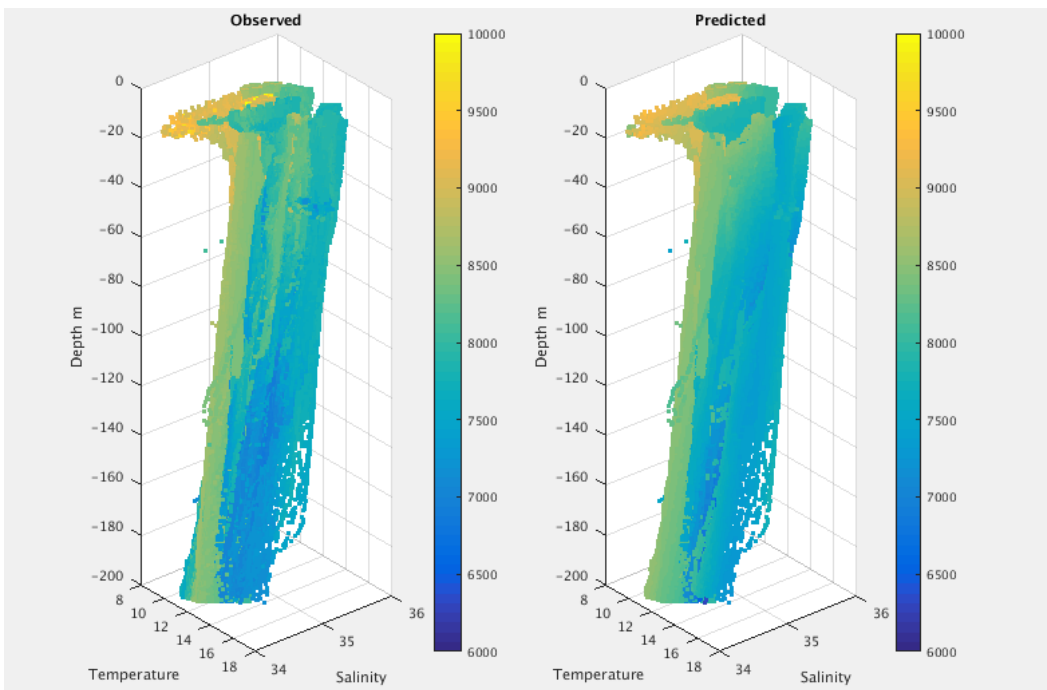

Figure 4.68 Observed (left) and predicted (right) nitrate concentration (µM N) from temperature, depth, longitude, and time of year.
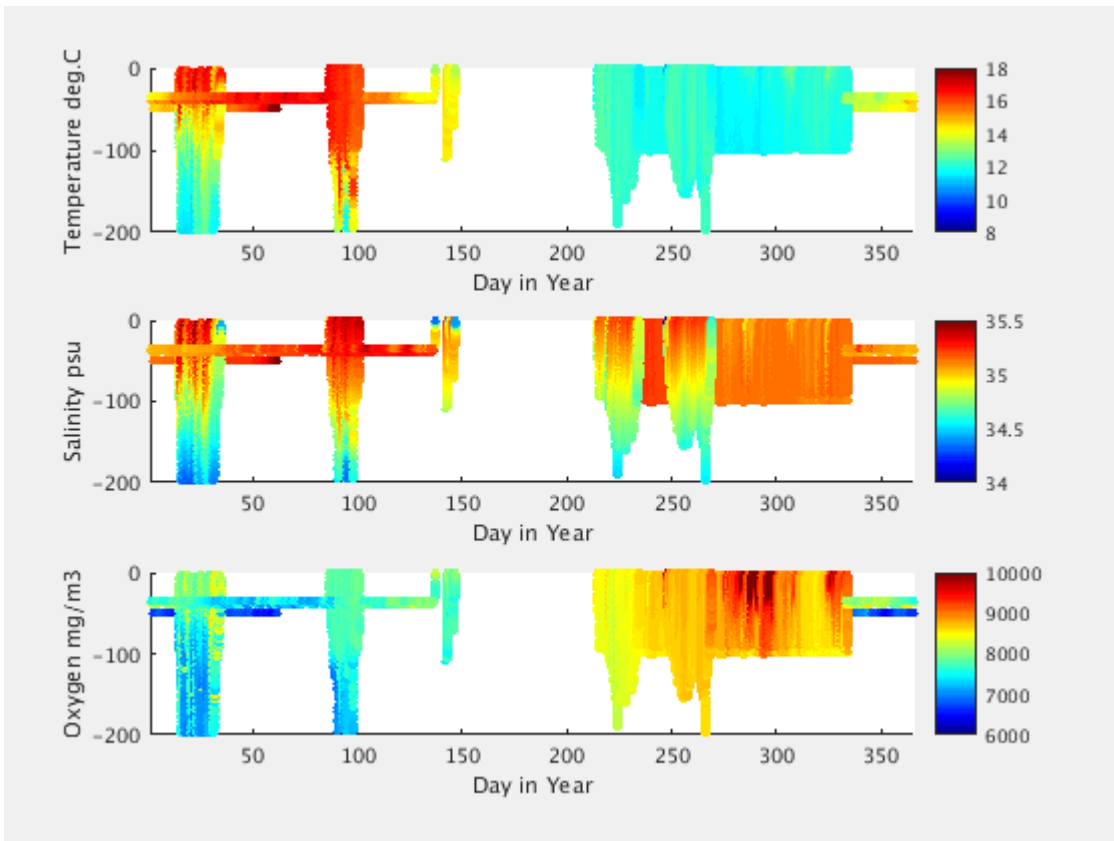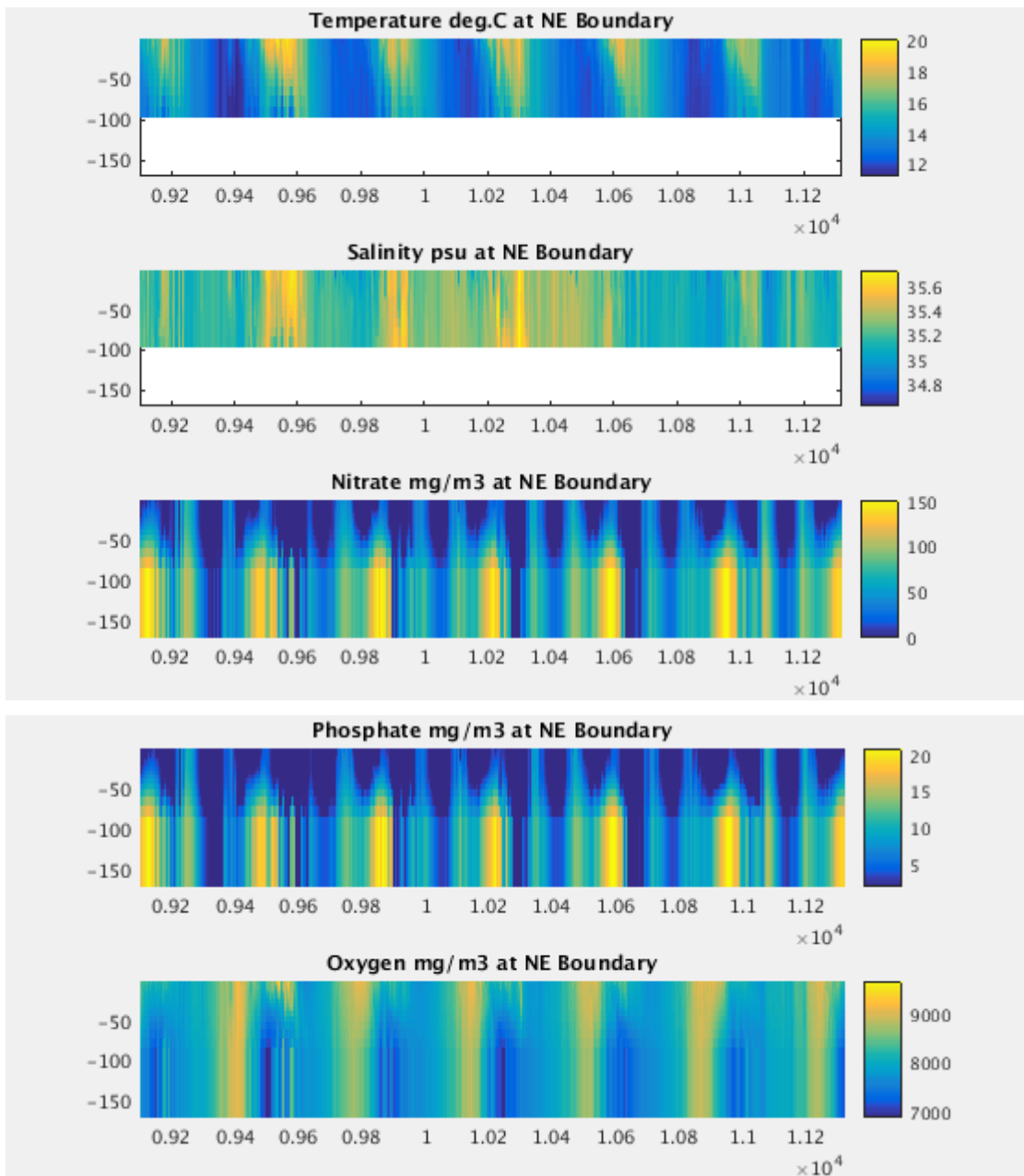
Figure 4.69 Climatology of temperature, salinity, and calibrated oxygen observations in outer Storm Bay from recent glider and mooring observations.

Figure 4.70 Observed (left) and predicted (right) oxygen (mg O m^{-3}) concentration from temperature, depth, longitude, and time of year.

Figure 4.71a Example depth resolved ocean boundary forcing on the northeast TASSE model boundary for 2015-2020.
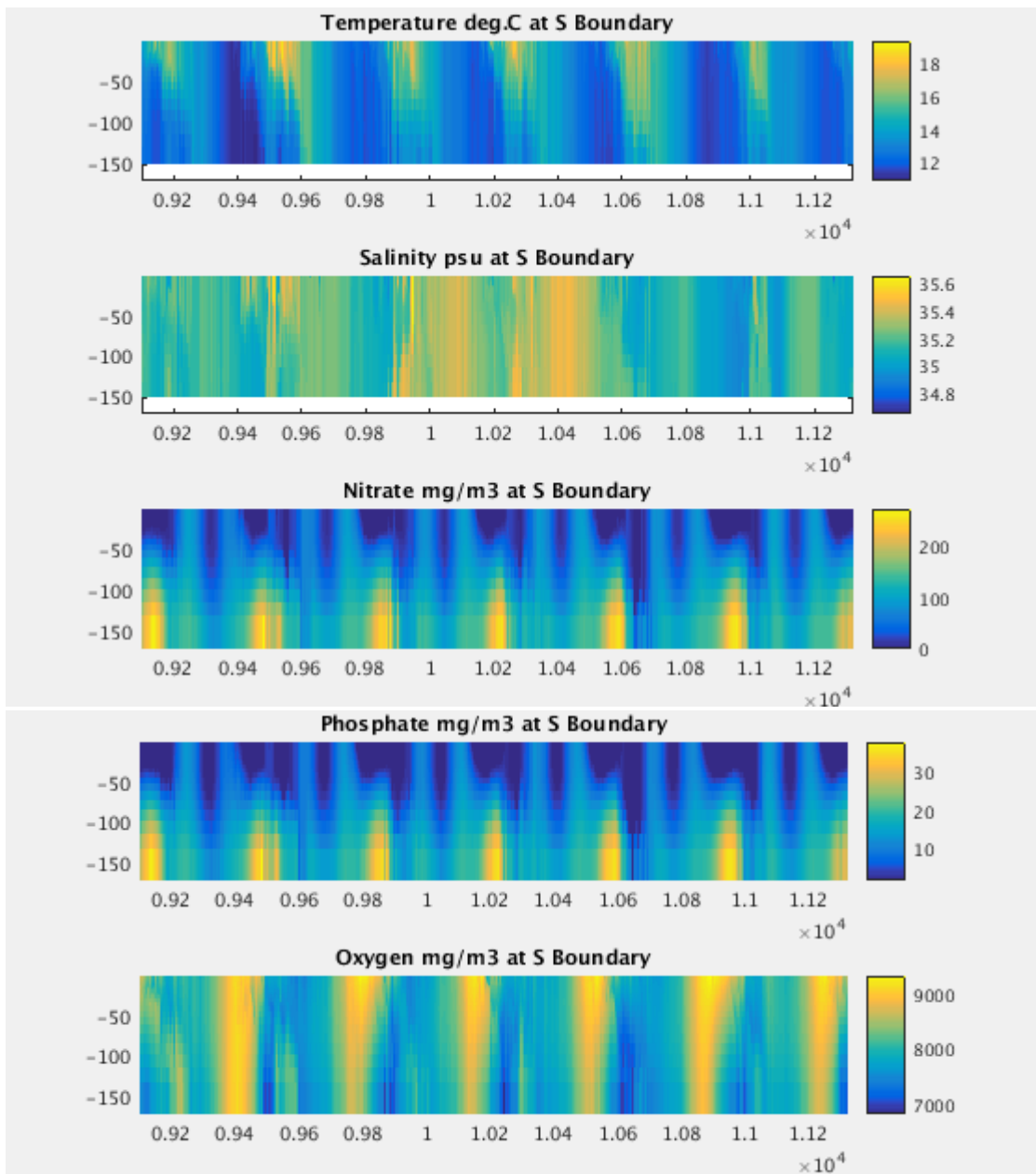
Figure 4.71b Example depth resolved ocean boundary forcing on the southern TASSE model boundary for 2015-2020.
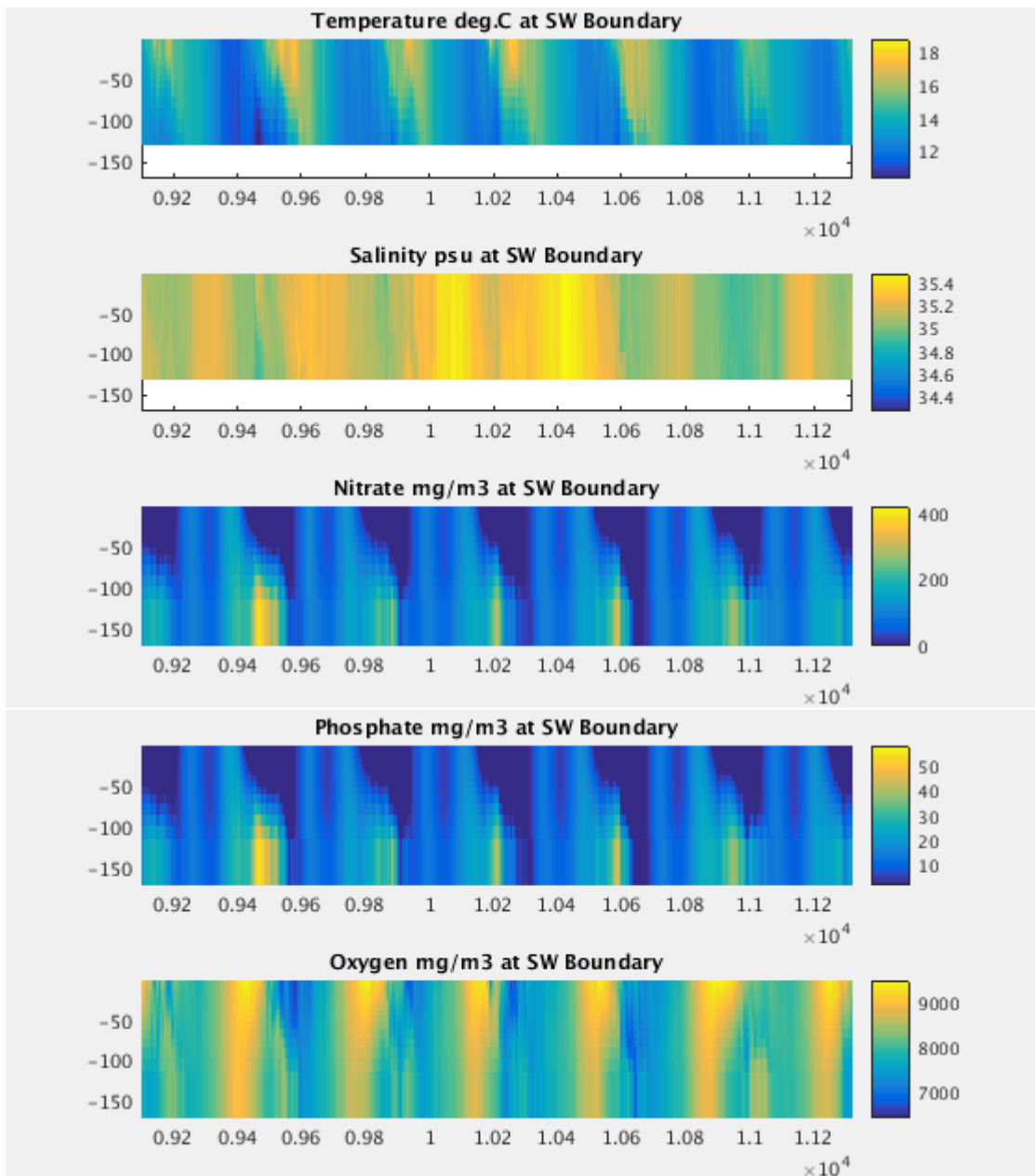
Figure 4.71c Example depth resolved ocean boundary forcing on the southwest TASSE model boundary for 2015-2020.

Plankton concentrations along the model boundary were determined from remotely sensed ocean surface chlorophyll (OC3M algorithm) attributed to small, large and dinoflagellate phytoplankton chlorophyll according to the concentrations required to simulate the observed OC3M; concentrations were generalised to the surface 30m of the water column (Figure 4.72a & 4.72b) which would be the upper part of the ocean surface mixed layer with access to elevated PAR to support plankton growth. Whilst the actual vertical distribution of plankton at the model boundary on a given day is unknown our assumption provides a plausible concentration for incoming water, consistent with ocean colour observations. Vertical distributions of nutrients (scaled against the density structure) and light (attenuated by optically active substances) will quickly determine whether the plankton grow or decline in specific layers, resulting in a realistic vertical distribution within a few spatial cells of the ocean boundary.

There is considerable interannual variability in the observed timing and patchiness of offshore phytoplankton blooms. Elevated coastal concentrations reported inshore in winter include the influence of CDOM from seasonal peak river flow. Zooplankton concentrations were scaled against phytoplankton concentrations assuming coupled seasonal variation in biomass. Oceanic concentrations of other biogeochemical model tracers were estimated from sparse observations and/or literature values.
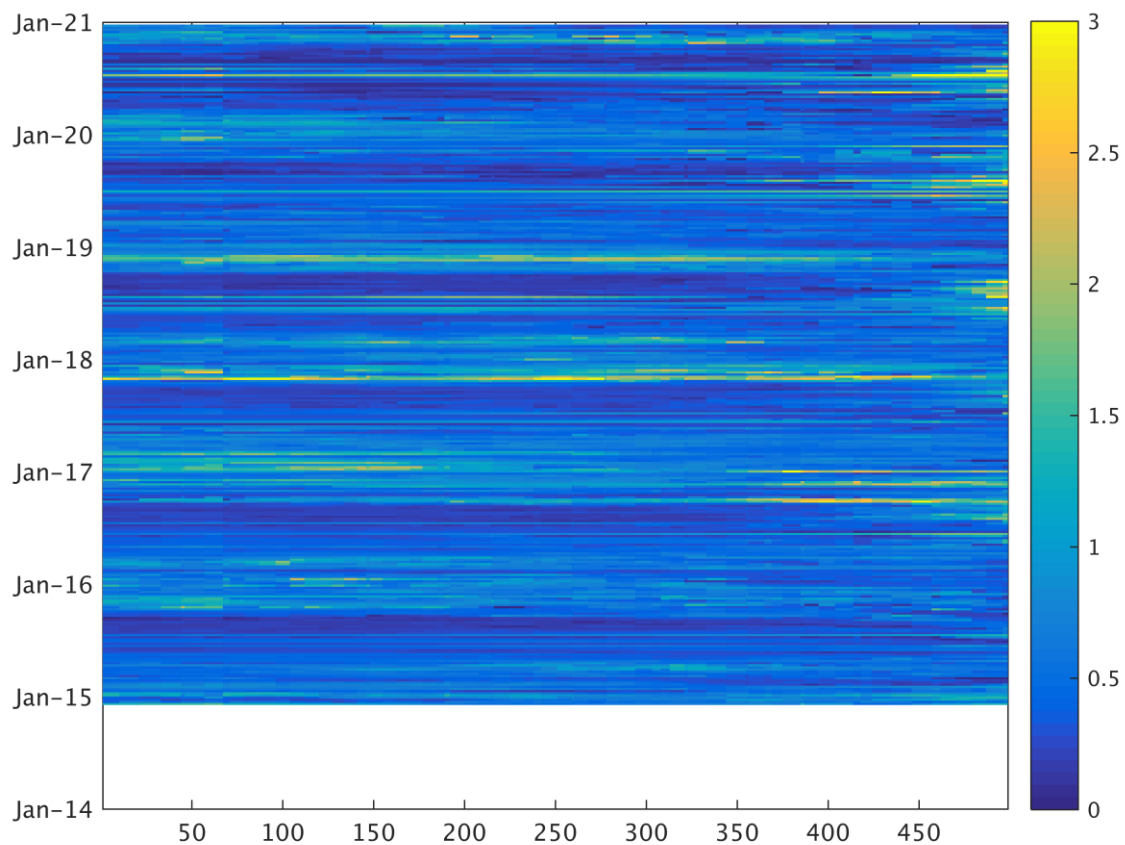

Figure 4.72a Remotely sensed OC3M chlorophyll concentration along the model ocean boundary from west (left) to east (right) for 2015 – 2020.
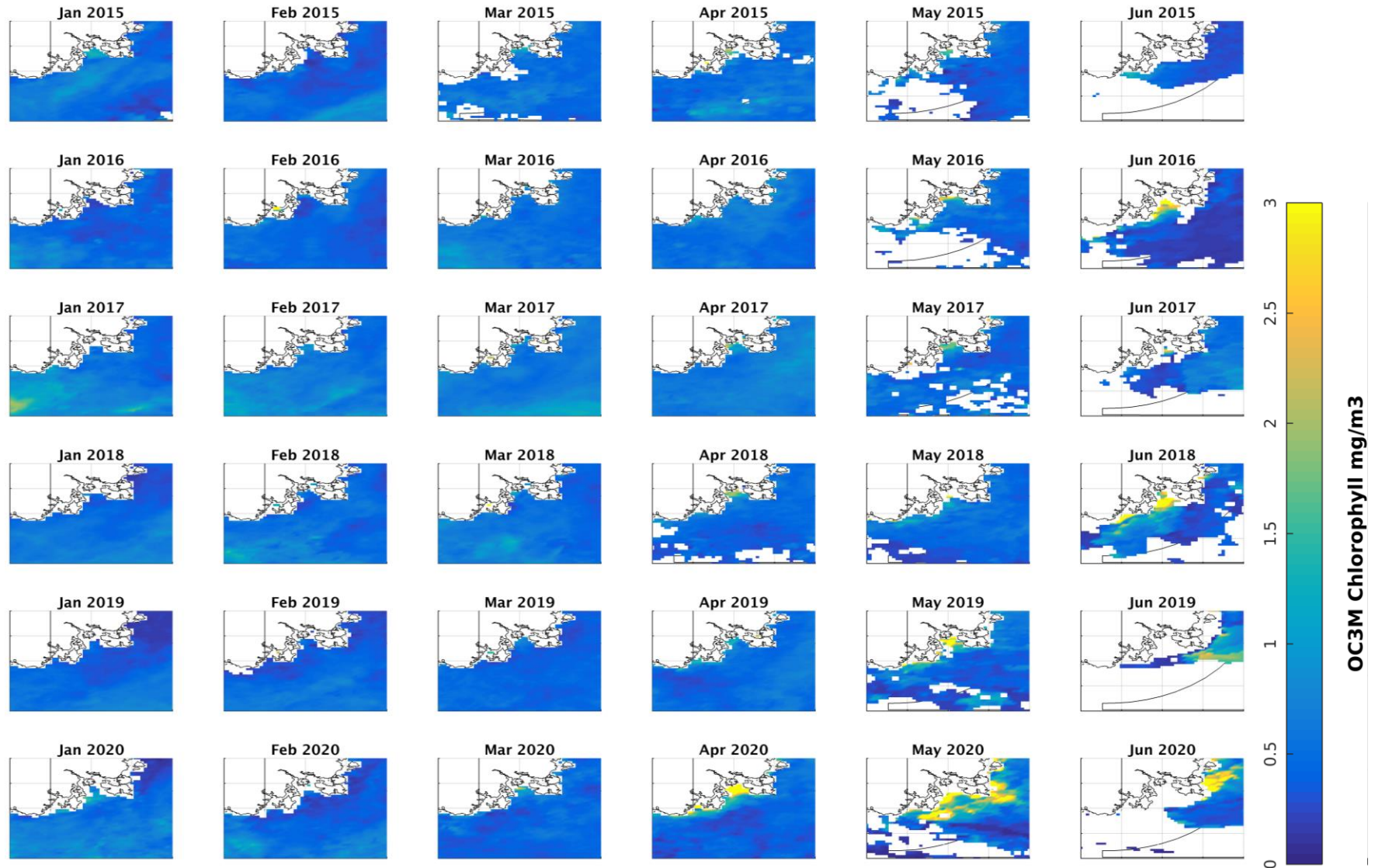
Figure 4.72b Monthly mean surface chlorophyll from remote sensing (merged level 3 product from Europe http://www.globcolour.info/ - access valid Nov 2022) 2015 - 2020.
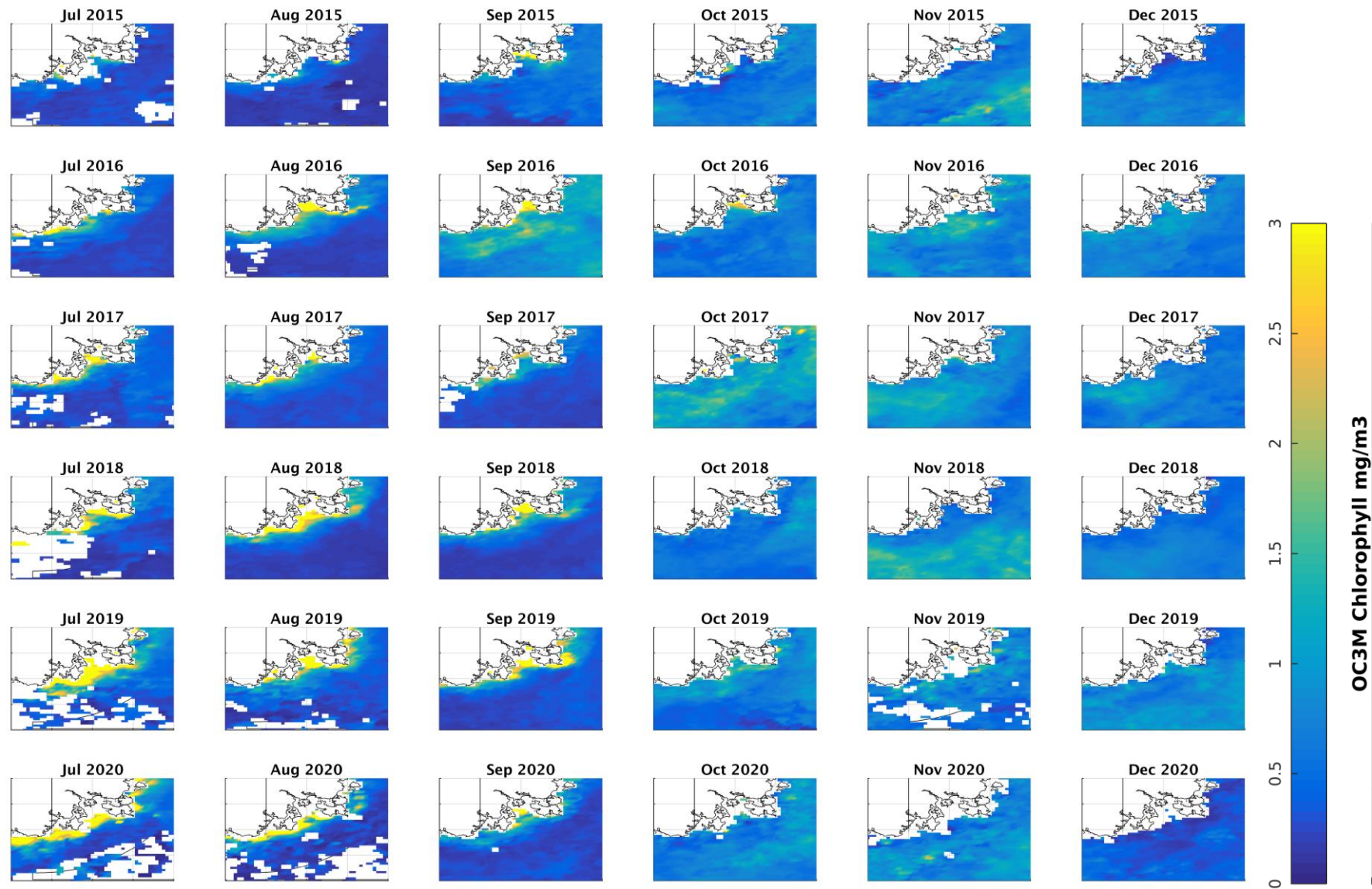
Figure 4.72b (continued) Monthly mean surface chlorophyll from remote sensing (merged level 3 product from Europe http://www.globcolour.info/ - access valid Nov 2022) for 2015 - 2020.

River loads

Data to characterise river nutrient and sediment loads into the Storm Bay region have been sourced primarily from the EPA, the Derwent Estuary Program, and historical studies. Observations for most river systems and biogeochemical model tracers are sparse (and in some cases > 10 years old) and have been scaled against flow to provide a dynamic estimate of river load. Estimated river loads from 8 gauged rivers which discharge into southeast Tasmania is shown in Figure 4.73; these rivers are the Derwent, Huon, Jordon, Northwest Bay, Snug, Esperance, Coal and Carlton. Note that all tracers should be considered indicative of actual conditions (in the absence of in situ observations) at river and ocean boundaries and model results close to these boundaries should be treated with caution due to the potential for small inconsistencies between tracers confounding results.
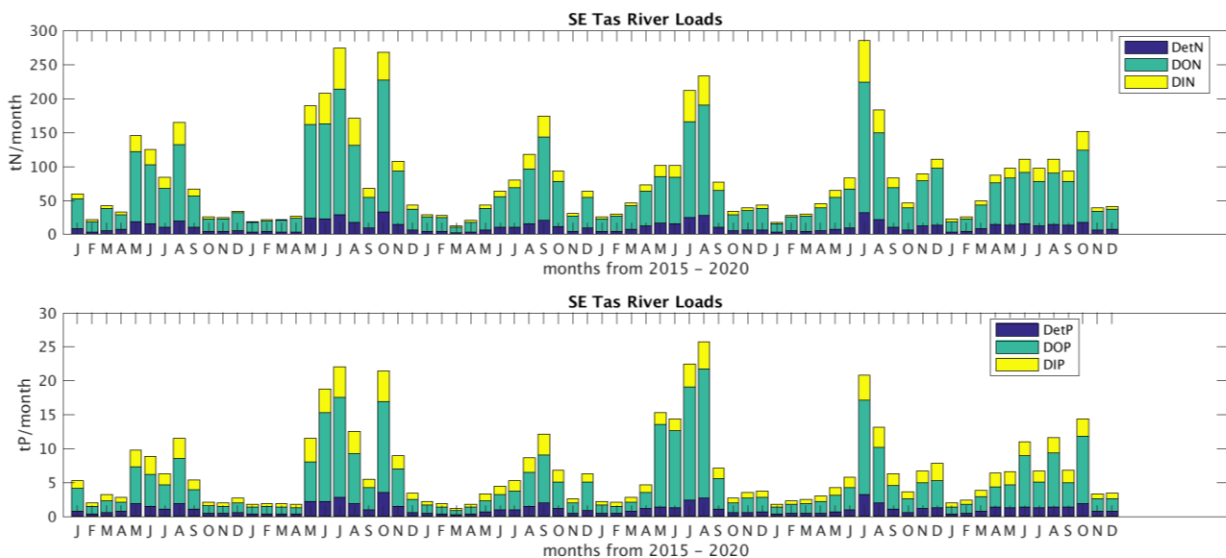
Figure 4.73 Estimate of cumulative nitrogen and phosphorous river loads for 2015 – 2020 from 8 gauged rivers in southeast Tasmania; these rivers are the Derwent, Huon, Jordon, Northwest Bay, Snug, Esperance, Coal and Carlton.

Anthropogenic loads

Anthropogenic nutrient and biogeochemical loads from Wastewater Treatment Plants (WWTP) and fish farms throughout the region have been sourced from TasWater and the Department of Natural Resources and Environment Tasmania, Marine Farming Branch, respectively. In the model, the lease specific monthly mean fish farm nutrient or WWTP load is assumed to be immediately dispersed throughout the model grid cell(s) in which the farm or WWTP is located. Fish farm loads are dispersed uniformly throughout the lease area between 0.5 and 10 m depth (across 17 model layers between 0 – 10.4 m deep); WWTP loads are dispersed at 15 m for all deep sites and -0.5 to -1.5m for all shallow sites unless the specific outfall pipe depth is known. The outfall locations of 25 WWTP and 2 industry discharge points (Norske & Nystar) and their estimated cumulative nutrient load are shown in Figures 4.74 & 4.75.
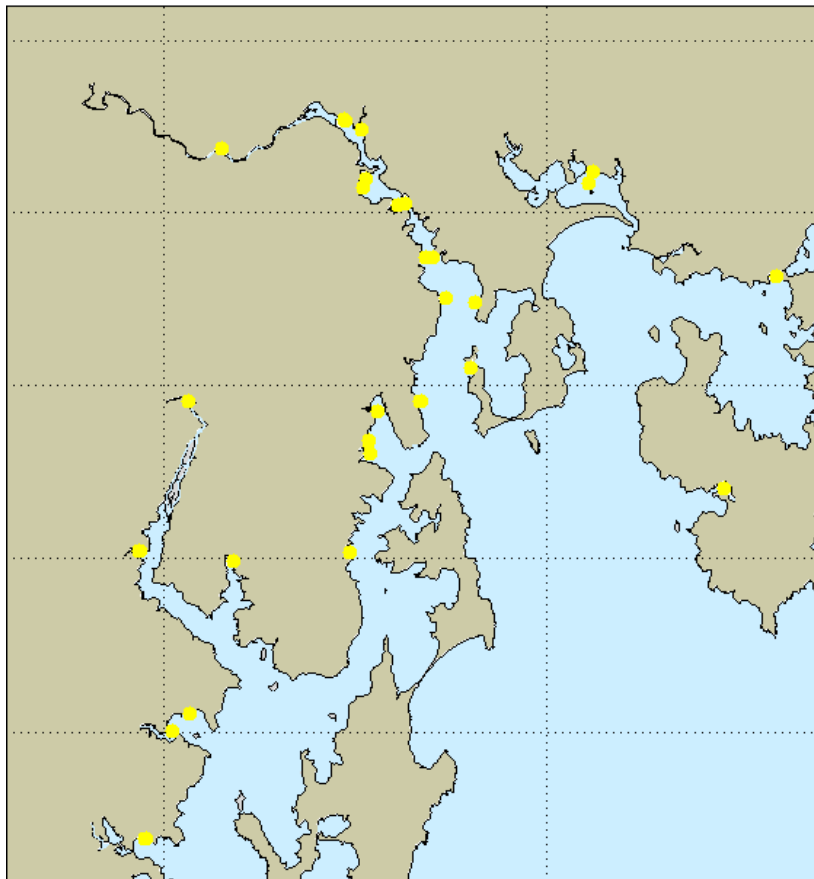
Figure 4.74 Wastewater treatment plants included in the Storm Bay model.
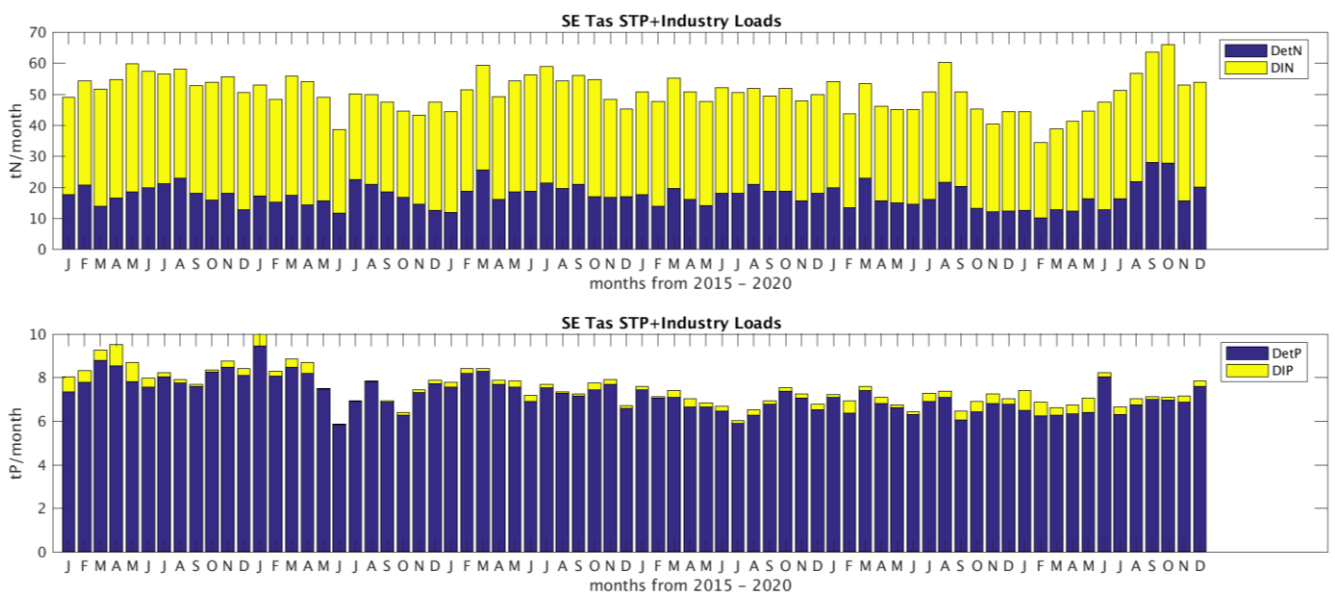

Figure 4.75 Estimate of cumulative nitrogen and phosphorous loads for 2015 – 2020 from 25 sewerage treatment plants and 2 industry outfalls (Norske and Nystar) in southeast Tasmania.
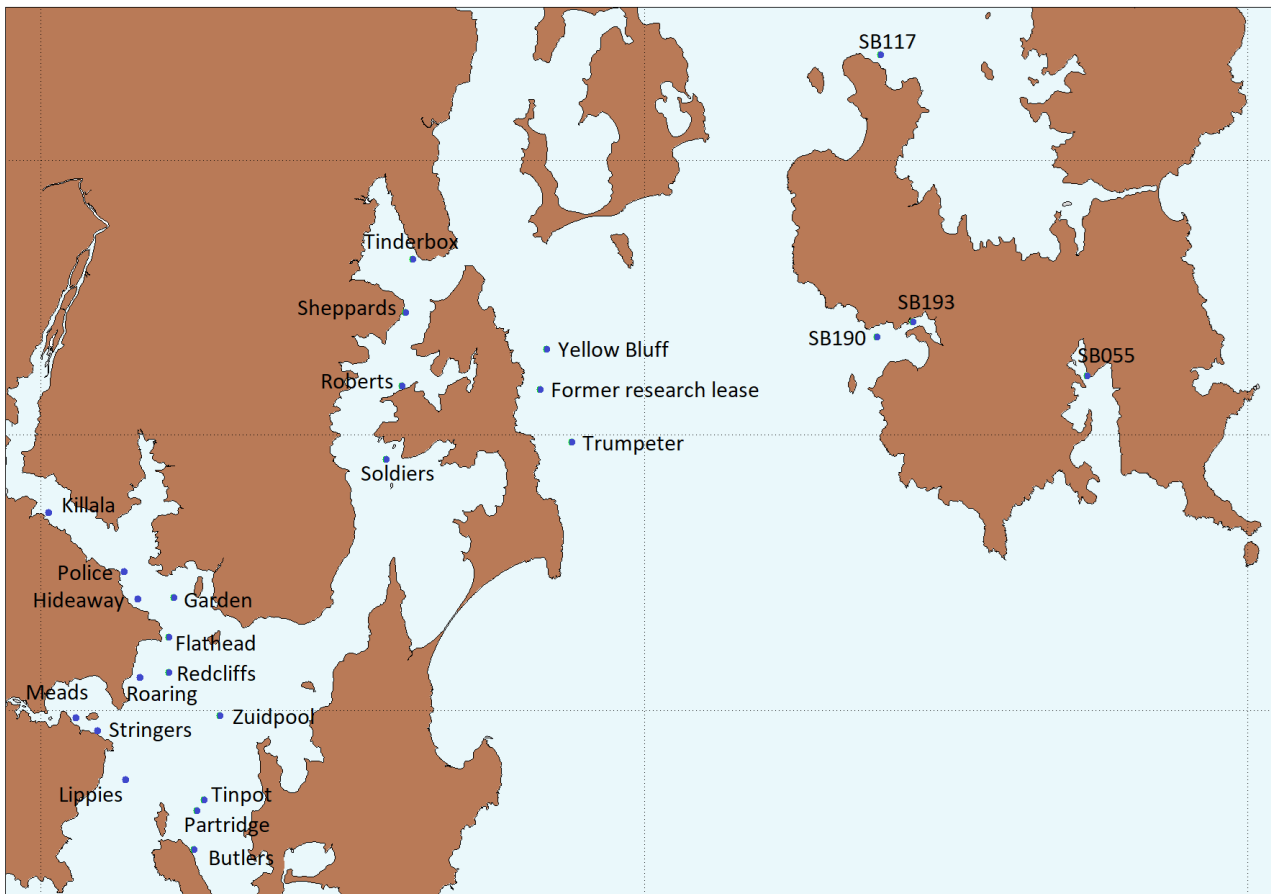
Figure 4.76 Lease location centre points for fish farms in southeast Tasmania. Note that loads are distributed throughout the entire lease area (typically across multiple grid cells according to the lease shape), for each farm site.
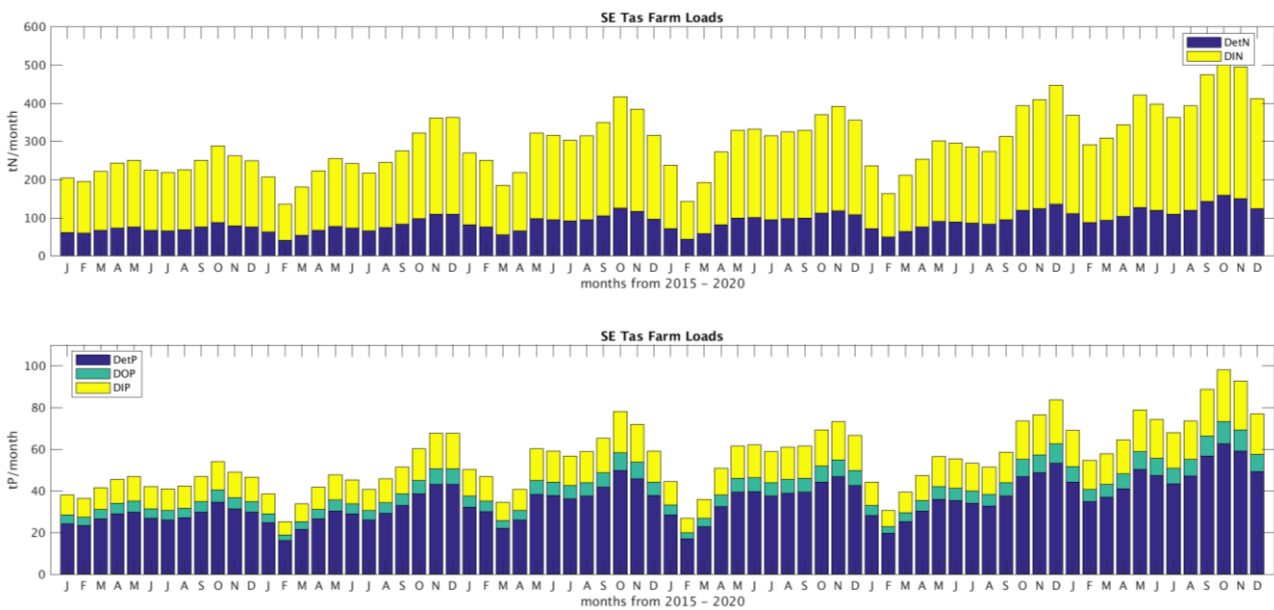

Figure 4.77 Estimated cumulative nitrogen and phosphorous loads for 2015 – 2020 from 25 fish farm leases in southeast Tasmania.

The lease locations of 25 fish farms in the Huon, D'Entrecasteaux Channel and Storm Bay area and their estimated cumulative load are shown in Figures 4.76 & 4.77.

Allocation of salmon feed in the model

CSIRO received feed data in tonnes or kgs per month for the period December 2014 to March 2021 from the EPA for 25 fish farm lease areas. Feed data were converted into estimated dissolved and particulate nutrient loads based on assumptions and literature cited in Bushman et al., 2007, Wild-Allen et al., 2010, and Wang et al., 2012 as:

Feed content relevant to model

- 7.2 % total nitrogen
- 1.2 % total phosphorus
- 4.0 % water

Feed loss

- 3 % of the feed is lost into the water column through messy eating, as dust or as excess pellets
- Nitrogen in the lost feed is partitioned as 15 % nitrate and 85 % particulate nitrogen
- Phosphorus is partitioned as 15% DIP and 85% particulate phosphorous.
- Particulate N and P waste is partitioned between the model pools of 'labile detritus' (which has a fixed N:P ratio), and refractory detrital P. All the particulate waste nitrogen and sufficient particulate waste phosphorous to match the P:N Redfield ratio becomes model 'labile detritus'; remaining excess particulate waste P is assigned to model 'refractory P'.

Excretion

- 45% of nitrogen in the feed is excreted as ammonia/urea. The remaining faecal nitrogen is excreted as particulate nitrogen (62 % - 45 % = 17 %)
- 70% of phosphorous in the feed is excreted, partitioned as 18% DIP, 44% particulate and 8% dissolved organic phosphorus
- Particulate N and P waste is partitioned between the model pools of 'labile detritus' (which has a fixed N:P ratio), and refractory detrital P. All the particulate waste nitrogen and sufficient particulate waste phosphorous to match the P:N Redfield ratio becomes model 'labile detritus'; remaining excess particulate waste P is assigned to model 'refractory P'.

For the hindcast biogeochemical model simulation from 2015 - 2020 we have sourced the best available data for river loads, wastewater discharge locations, fish farms and other industry loads.

For the ongoing operation of the near real time biogeochemical model estimates for wastewater discharge, fish farms and other industry load inputs were made based on the annual cycle of values determined for 2020. River loads of biogeochemical model substances were estimated from average concentrations scaled against near real time river flow.
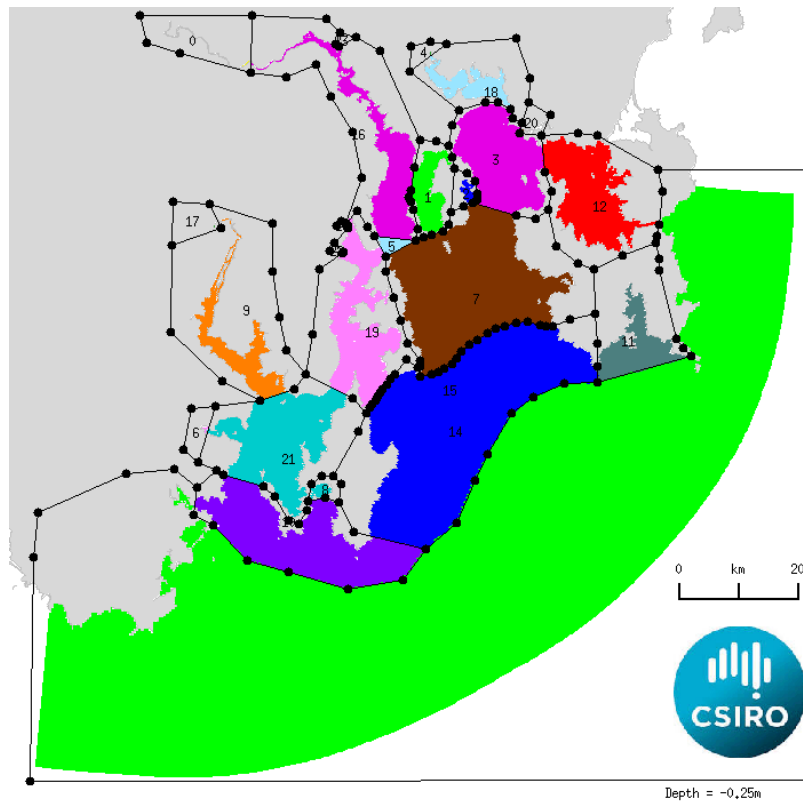
Figure 4.78 The Storm Bay model area was divided into a number of sub regions based on bathymetry and coastal morphology for model analysis.

4.5.3   Biogeochemical model evaluation

The purpose of the Storm Bay biogeochemical model is to simulate the water quality in Storm Bay suitable for assessing future salmon farm expansion and to characterise the primary sources of nutrients into Storm Bay from ocean currents, sediment resuspension, river and anthropogenic inputs. To evaluate whether the model is fit for this purpose we consider 5 specific assessment criteria (Rykeil 1996, Hipsey et al., 2020):

1.   The hydrodynamic model reproduces the 3D circulation and observed spatial and temporal variability in temperature and salinity, including water column stratification and mixing.

2.   The sediment model reproduces the observed spatial and temporal variability in suspended sediment concentration, resuspension and deposition.

3.   The model conserves heat, momentum and mass of carbon, nitrogen and phosphorous during advection, diffusion, deposition, resuspension and biogeochemical cycling.

4.   The biogeochemical model reproduces the observed spatial and temporal variability in water quality, specifically chlorophyll, nitrogen, phosphorous, dissolved oxygen and optical transparency.

5. The biogeochemical model is qualitatively consistent with current understanding of denitrification flux, sediment composition, nutrient limitation, benthic reef and macrophyte distribution.

The first 2 assessment criteria have been successfully addressed by the hydrodynamic and sediment modelling teams (this report section 4.2 and 4.4 respectively) and the 3rd assessment criteria has been achieved during the successful execution of simulations, as any violations in conservation would have caused the simulation to abort. In this section we assess criteria 4 and 5.

To evaluate the accuracy of the biogeochemical model, simulated properties were compared with observed properties and statistical metrics were computed to quantify model skill, similar to the evaluation of the hydrodynamic and sediment model described earlier. Where possible, observations obtained across multiple parameters, time and space scales were used to evaluate model performance, these included daily remotely sensed chlorophyll (out with coastal effects and cloud cover), continuous glider data from transects within the model domain, monthly in situ monitoring data and benthic lander sensor data.

Model skill was evaluated by statistical comparison of observations with model output for the equivalent water property, location and time. We consider bias, the root mean square error (RMSE), the mean absolute error (MAE) and the modified Willmott index or 'd2' (Willmott et al., 1985). The Willmott index uses the sum of absolute values.

Model bias assesses whether the simulated variables are under- or over-predicting observed values. The RMSE is a measure of the absolute magnitude of the "error" calculated by averaging the square of the deviation over the time-series. An RMSE or MAE of 0 indicates a perfect fit.

The Willmott index of agreement is designed to quantify errors that are unevenly distributed in time or space and reduce the influence of errors during periods of large observed mean or variance. The Willmott index is the ratio of the mean absolute error and the mean absolute deviation about the observed mean and varies between 0 and 1. A value of 1 indicates a perfect match (x = y), and 0 indicates no agreement.

$$\text{Willmott} = 1 - [\ \sum |\ x - y\ |\ )\ /\ [\ \sum |\ x - \bar{y}\ |\ ) + (|\ y - \bar{y}\ |\ )]$$

where x and y are vectors or arrays of time series data (x =observed, y = modelled).

A Willmott index above 0.7 is regularly obtained for high resolution models with high spatial and temporal observations for physical parameters such as salinity and temperature; model reproduction of observed biogeochemical properties is considered to be fit for purpose when the Willmott index is above 0.40 [the lower threshold accounts for inherent uncertainties in observation method (e.g. chlorophyll HPLC vs fluorescence, Skerratt et al., 2019), sample representality (e.g. 1 litre vs 200 m^3), variability in sensor calibration (particularly for fluorescence, dissolved oxygen and turbidity) and representation of the observed substance in the model.

Other skill metrics e.g. RMSE, MAE and bias show complementary information with low values (tending to zero) indicating good to very good model skill.

Remotely sensed OC3M chlorophyll

Daily merged OC3M chlorophyll observations were compared with simulated OC3M calculated by the spectral optical model. Simulated OC3M is derived from the model predicted sea leaving

radiance at equivalent wavelengths to those measured by the satellite and therefore includes the optical effects of simulated chlorophyll, CDOM, sediments and bottom reflection (in shallow water), in the same way as they are included in the remotely sensed observation. The remotely sensed data was available as a daily merged data product from multiple satellites on a 1km spatially resolved grid from the European Service for Ocean Colour (https://globcolour.info - access valid Nov 2022).
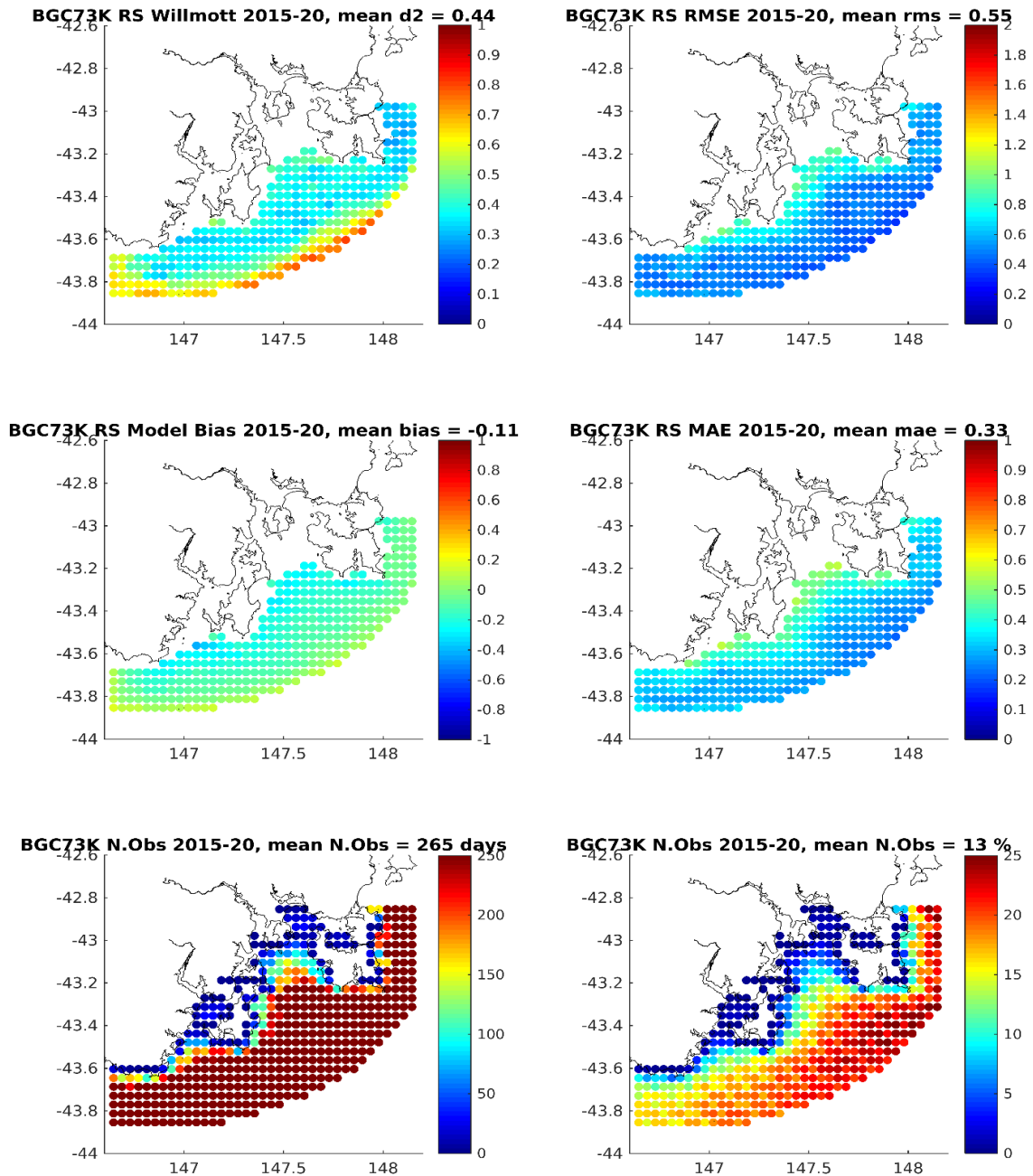

Figure 4.79 Summary of pixel based model vs remotely sensed OC3M chlorophyll assessment using merged daily observations (https://globcolour.info - access valid Nov 2022) from 2015-2020. Willmott skill score and root mean square error (top), model bias and mean absolute error (middle) and mean number of observations and percent clear days (bottom).

Data coverage was good in offshore waters, but poorer inshore due to cloud cover and coastal effects (Figure 4.79 lower panel). In pixels where observations exceeded 10% of days (i.e. > 3 days per month) the time series of observations and spatially equivalent simulated OC3M were compared with statistical metrics summarised in Figure 4.79 & 4.80. Model skill in reproducing the observed OC3M chlorophyll increased from inshore to offshore waters with increasing Willmott skill, and decreasing RMSE and MAE in offshore waters; model bias was very small throughout the assessed region. The spatial patterns in model skill closely match the distribution and density of observations, and confirm that the optical environment in outer Storm Bay and on the shelf is well simulated. In the most inshore waters analysed (including south of Bruny Island and in inner Storm Bay) the model skill is slightly poorer. Notwithstanding the sparse number of observations in inshore waters, and the possibility that these observations could be compromised by adjacent cloud or coastal effects, the poorer skill statistics suggests that the model may be underestimating some optical influence in these areas. Any spatial or temporal mismatch in the simulated CDOM rich river plumes from the Derwent and Huon rivers, plus any rivers unresolved by the model (particularly minor ungauged rivers in the southwest), likely contribute to the slightly poorer statistical match of simulated and observed OC3M chlorophyll in inshore waters.
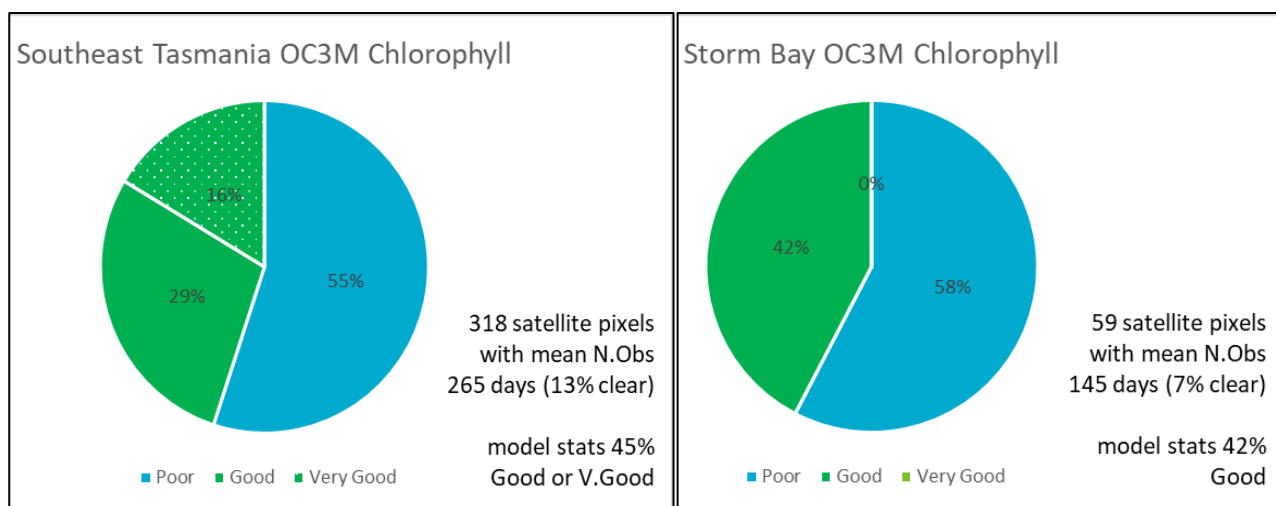

Figure 4.80 Summary of statistical analysis of observed and simulated OC3M Chlorophyll for the whole of Southeast Tasmania (left) and the subregion (Figure 4.78) of outer Storm Bay (right) [Willmott skill score good > 0.40; very good >0.60].

Monthly mean simulated OC3M chlorophyll for 2015-20 are shown in Figure 4.81 and may be compared to observations (which are shown in Figure 4.72b). Inshore waters show high concentrations of simulated OC3M chlorophyll due in part to the strong influence of CDOM, particularly in winter in the Huon, D'Entrecasteaux Channel and Derwent estuaries; in the shallow waters of Fredrick Henry Bay sediment resuspension and bottom reflectance also contribute to the OC3M chlorophyll signal. Seasonal and interannual variation in OC3M chlorophyll are well reproduced by the model with peak concentrations simulated throughout the region in spring and summer months.

Time series plots for Storm Bay, South Bruny and Offshore subregions of the model (Figure 4.82) also show elevated concentration of OC3M chlorophyll in inshore waters, particularly in winter

due to the influence of CDOM rich river discharge. In offshore waters, peak OC3M chlorophyll concentrations are smaller (<2 mg Chl m-3) and generally occur in spring in both observations and model. Simulated peak concentrations in OC3M are often smaller than observed, possibly due to under representation of the optical contribution of river TSS and/or CDOM in inshore waters (river contributions of TSS and CDOM are both estimated from literature values scaled against flow), or poor simulation of phytoplankton cell sizes and/or patch distribution in offshore waters during peak OC3M events.
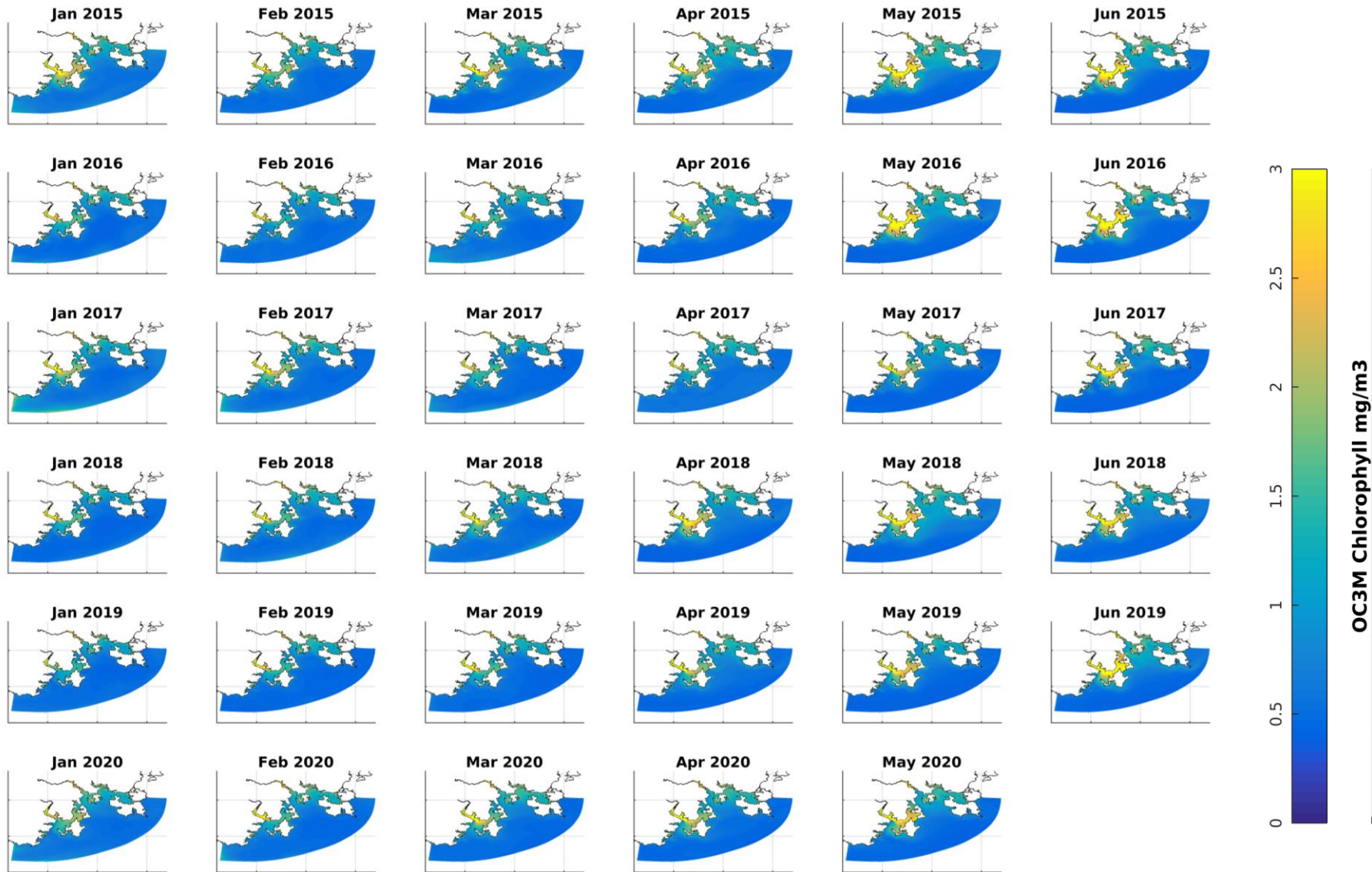
Figure 4.81 Monthly mean simulated OC3M chlorophyll for 2015-20.
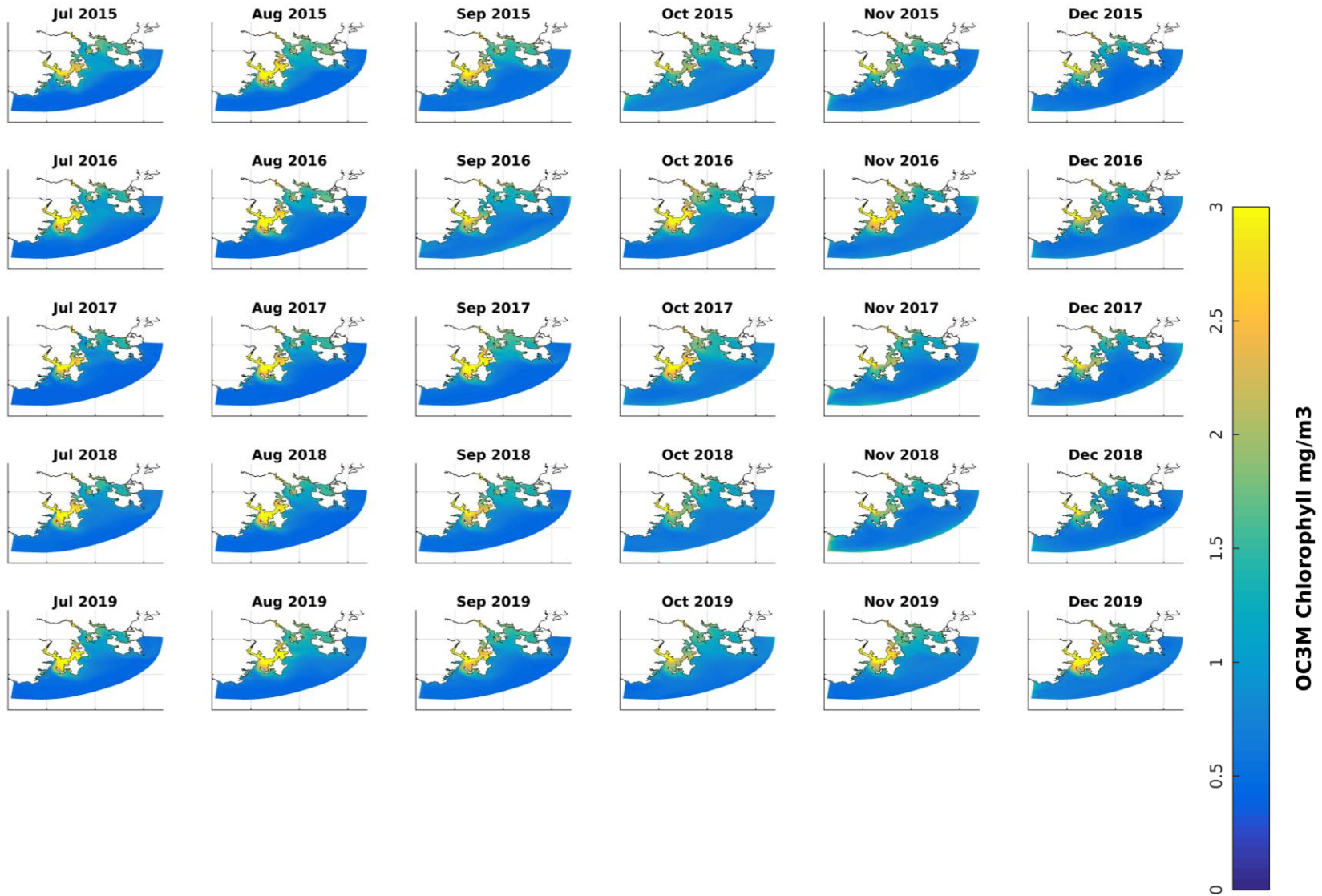
Figure 4.81 (continued) Monthly mean simulated OC3M chlorophyll for 2015-19.
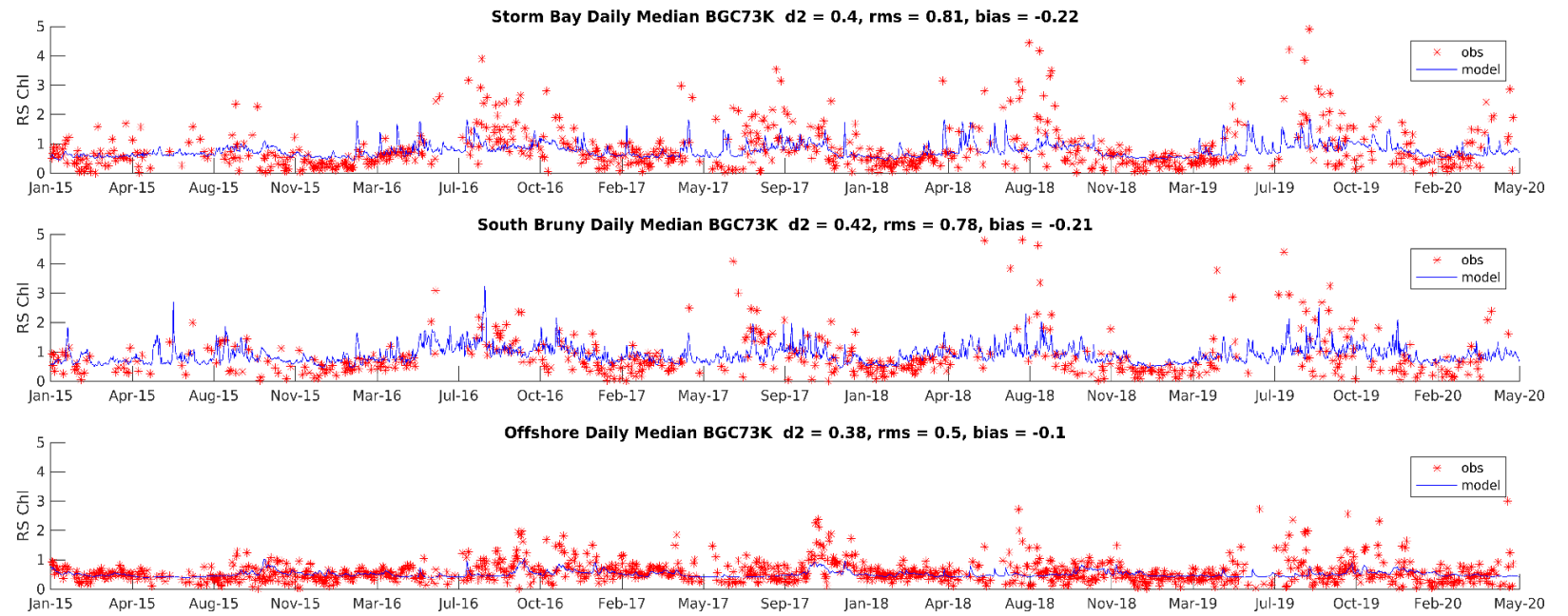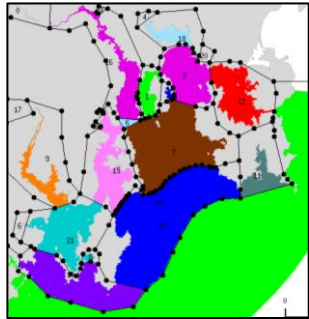
Figure 4.82 Time series of observed and simulated OC3M chlorophyll for outer Storm Bay (inset dark blue area), South Bruny Island (inset purple area) and Offshore (inset bright green area) subregions of the model.

Glider transects

Simulated temperature, salinity, oxygen, chlorophyll, spectral irradiance and nitrate were compared against glider observations for 14 glider missions in Storm Bay from 2015-2020. Model and observations were matched in time and space along the undulating path of the glider through the model domain (as described in section 4.2.3). Example comparisons for the May 2017 and August 2019 missions are shown in Figures 4.83, & 4.84; equivalent plots for the other glider missions are provided in Appendix A5. Summary statistics for all water properties and each glider mission are shown in Table 4.7.

In general the model reproduced the spatial and temporal distribution of observed water properties very well for all glider missions [notwithstanding double penalty errors associated with any spatial or temporal offset in simulated gradients in water properties and/or water mass fronts, as discussed in section 4.4.3]. Glider missions crossing Storm Bay captured the transition from inshore waters, which were fresher at the surface and often higher in chlorophyll to offshore waters, which were generally low in chlorophyll. Gradients in observed dissolved oxygen were well reproduced by the model, however there was often an offset in the magnitude of oxygen concentration, possibly due to bias in the sensor response (oxygen sensors often drift in calibration and samples were unavailable to confirm sensor accuracy). Nitrate concentrations were also well reproduced by the model and the seasonal contrasts in water mass characteristics associated with Zeehan and EAC current influence were well described by missions to the east and west of Storm Bay. Glider observations of spectral irradiance were well reproduced by the model, despite the potential for transient clouds to impact the magnitude of observations (clouds are included in the model, albeit at a relatively coarse scale).

Over 14 glider missions, sampling an average of 7 model substances, 91% of the observations verses model statistical analysis showed good or very good model skill (Willmott skill score > 0.40 or >0.60 respectively) (Figure 4.85).
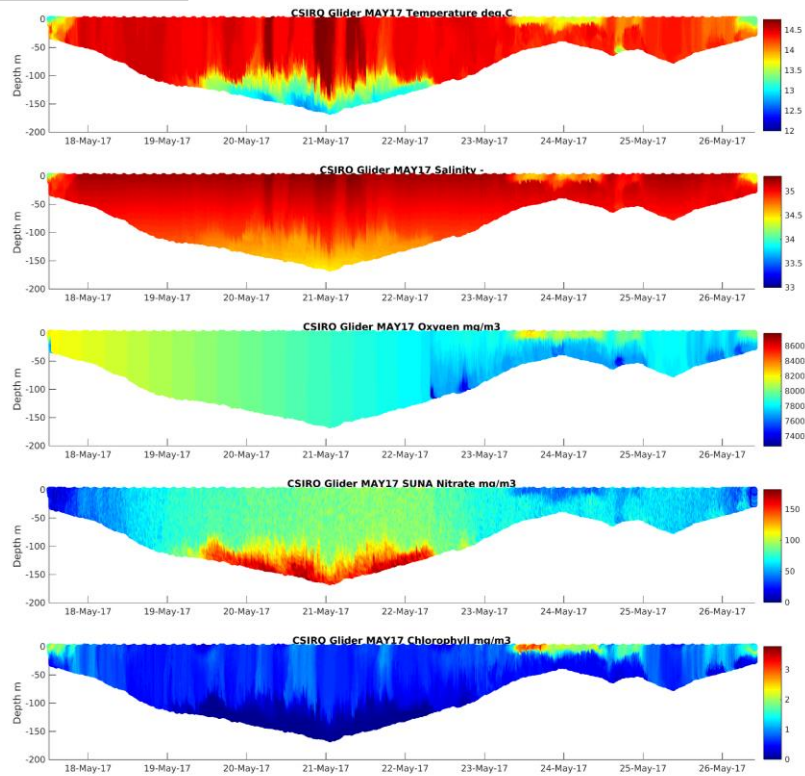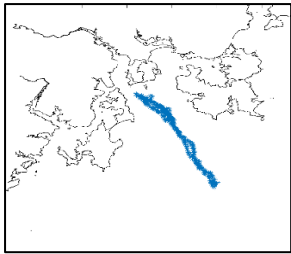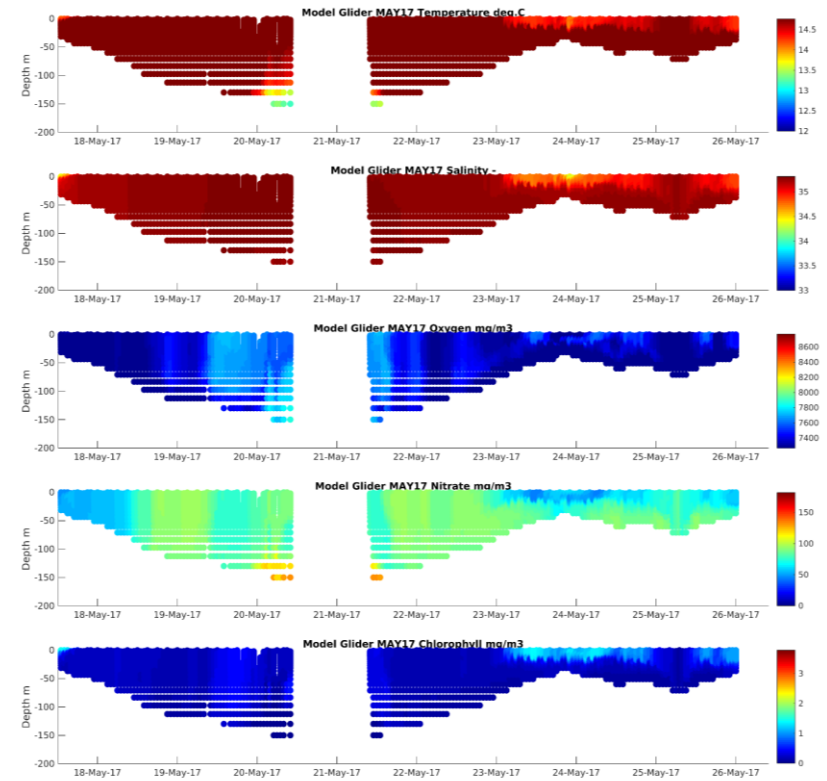
Figure 4.83 Vertical distribution of observed glider (left) and equivalent model (right) water properties from the CSIRO glider deployment in May 2017 (glider path shown top left; gap in the model timeseries when glider travelled beyond the model domain).
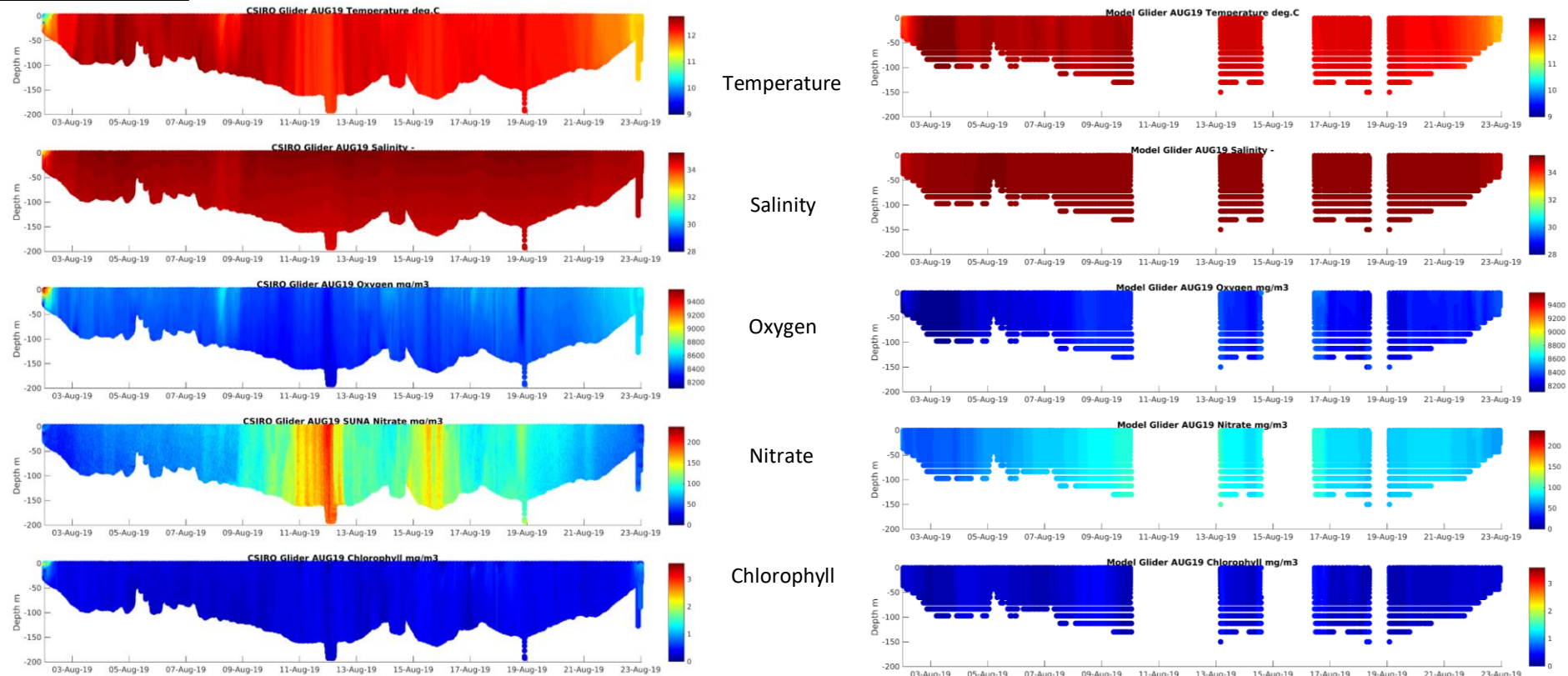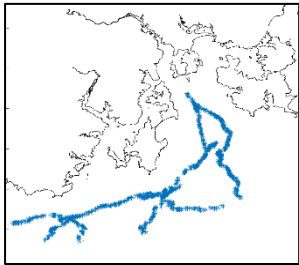
Figure 4.84 Vertical distribution of observed glider (left) and equivalent model (right) water properties from the CSIRO glider deployment in August 2019 (glider path shown top left; gaps in the model timeseries when glider travelled beyond the model domain).

Table 4.7 Summary statistics for all IMOS glider missions in Storm Bay 2015-2020 computed from timeseries of matched glider and modelled water properties [yellow/green Willmott score > 0.4 (good), dark green Willmott score > 0.6 (very good), red Willmott score < 0.3 (poor); blue model bias low, red model bias high].

| Willmott Skill	Chl-a mg/m3	Oxygen mg/m3	Ed 440 W/m2/nm	Ed 490 W/m2/nm	Ed 550 W/m2/nm	Ed 670 W/m2/nm	Nitrate mg/m3	Temp deg.C	Salinity PSU
Feb-15	0.60	0.73	0.85	0.86	0.89	0.88		0.81	0.69
Apr-15	0.60	0.34	0.87	0.86	0.88	0.86		0.57	0.47
Jun-15	0.50	0.17	0.84	0.85	0.89	0.90		0.95	0.93
Aug-15	0.55	0.33	0.92	0.90	0.93	0.91		0.70	0.88
Oct-15	0.46	0.45	0.85	0.85	0.89	0.92		0.80	0.75
Apr-16	0.62	0.40	0.81	0.79	0.80	0.87		0.57	0.55
Sep-16	0.77	0.41	0.92	0.93	0.91	0.80		0.63	0.96
Feb-17	0.66	0.86	0.91	0.91	0.92	0.93		0.68	0.71
Mar-17	0.70	0.57	0.88	0.90	0.91	0.87		0.84	0.64
May-17	0.71	0.33					0.74	0.53	0.58
Sep-18	0.48	0.13					0.10	0.83	0.50
Apr-19	0.55	0.78					0.63	0.89	0.31
Aug-19	0.33	0.16					0.85	0.85	0.63
Jan-20	0.57	0.55					0.72	0.90	0.56
Normalised Bias									
Feb-15	-0.35	0.03	-0.47	-0.43	-0.32	-0.35		-0.06	-0.01
Apr-15	-0.44	0.01	-0.35	-0.33	-0.23	-0.44		-0.02	0.00
Jun-15	-0.58	-0.08	-0.40	-0.34	-0.18	-0.46		0.01	0.00
Aug-15	-0.47	-0.05	-0.25	-0.26	-0.13	-0.39		-0.02	0.00
Oct-15	0.56	0.01	-0.32	-0.34	-0.22	-0.31		-0.02	0.00
Apr-16	-0.42	0.00	-0.36	-0.32	-0.26	-0.22		-0.03	-0.01
Sep-16	-0.06	0.09	-0.28	-0.26	-0.31	-0.55		0.00	0.00
Feb-17	-0.44	-0.02	-0.12	-0.18	-0.13	-0.25		-0.06	0.00
Mar-17	-0.29	0.15	-0.39	-0.35	-0.30	-0.40		-0.03	0.00
May-17	-0.51	-0.07					0.12	0.04	0.00
Sep-18	-0.20	0.04					5.11	0.00	0.01
Apr-19	-0.69	0.01					0.57	0.01	0.00
Aug-19	-0.23	-0.03					0.02	0.01	0.00
Jan-20	0.08	0.03					-0.67	0.02	0.00
Mean									
Willmott	0.58	0.44	0.87	0.87	0.89	0.88	0.61	0.75	0.65
Correlation	0.44	0.19	0.79	0.79	0.82	0.85	0.66	0.71	0.61
Normalised Bias	-0.38	0.01	-0.35	-0.33	-0.23	-0.39	0.12	-0.01	0.00
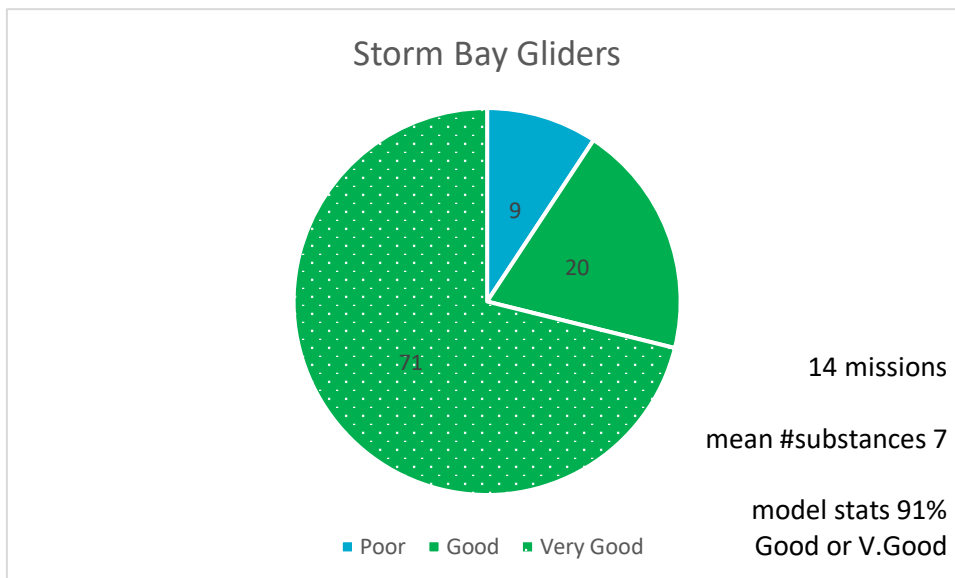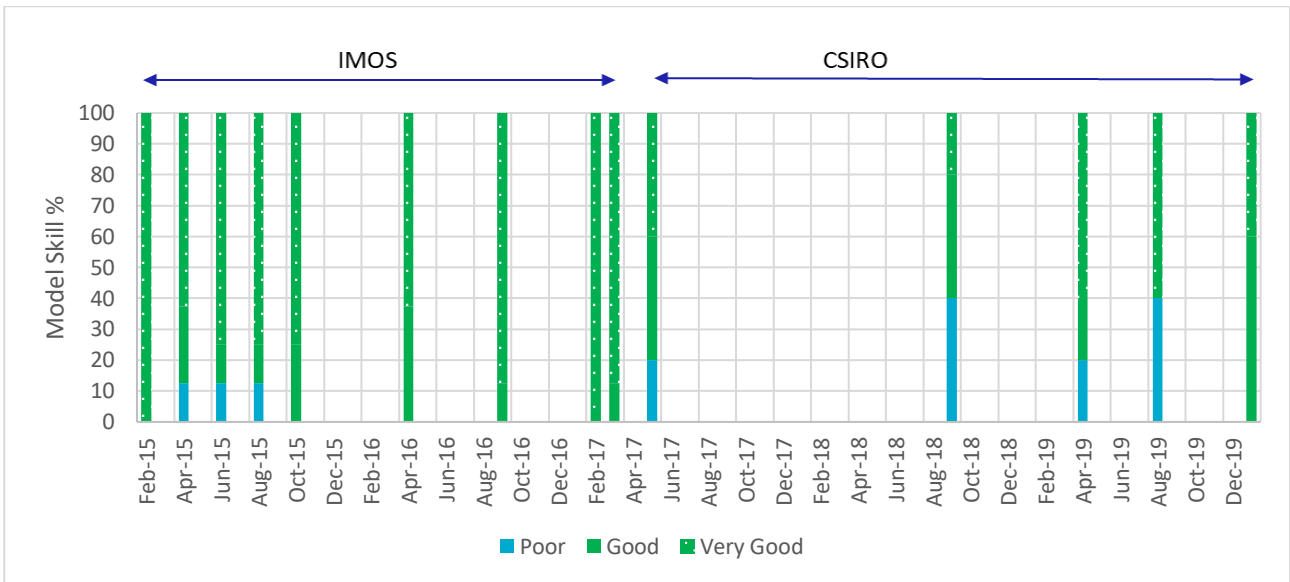
Figure 4.85 Summary of statistical analysis for glider observations compared to equivalent model output for all Storm Bay glider missions and substances [Willmott skill score good > 0.40; very good >0.60].

In situ monitoring data

In situ data collected in at sites throughout southeast Tasmania for environmental monitoring purposes (Figure 4.86) were made available by the EPA, IMAS, the BEMP and the DEP. Substances measured at each station vary as does the temporal resolution (see Table 4.8); for the period 2015 -2020 in situ observations at Storm Bay stations were relatively sparse, however the adjacent estuaries and side bays were well sampled at approximately monthly intervals.
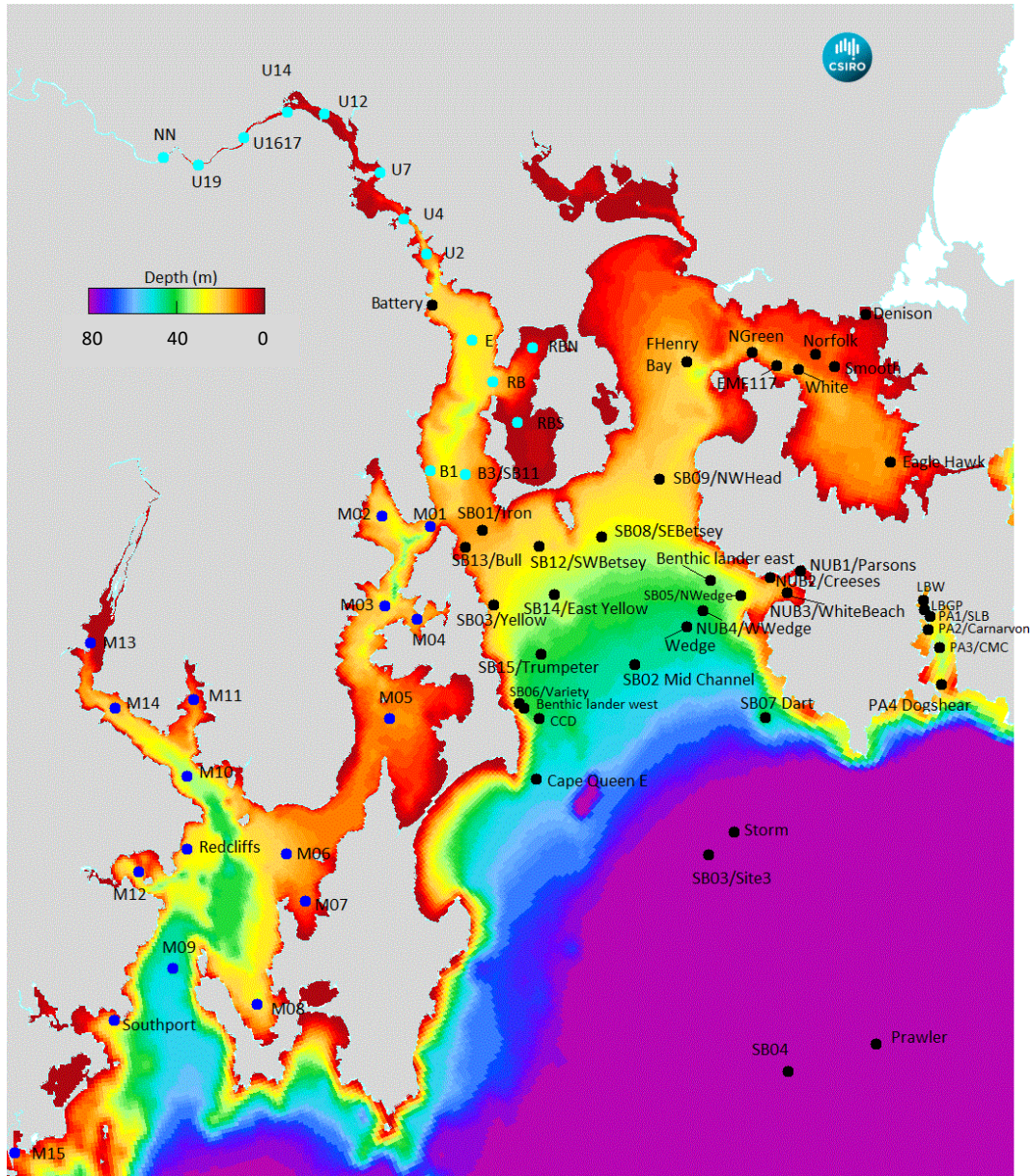
Figure 4.86 Sites locations for field observations: ● EPA/IMAS/BEMP Aquenal ● DEP sites; ● Additional EPA/IMAS sites including eastern bays

Table 4.8 In situ biogeochemical observations made available to the project for model skill assessment.

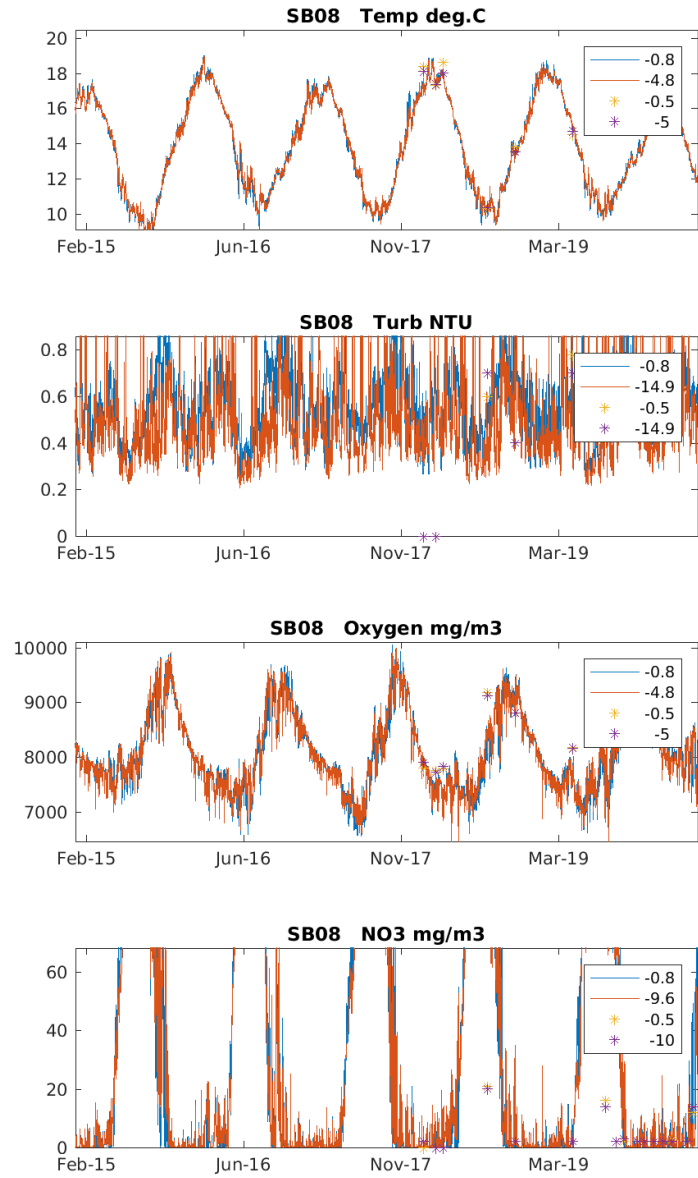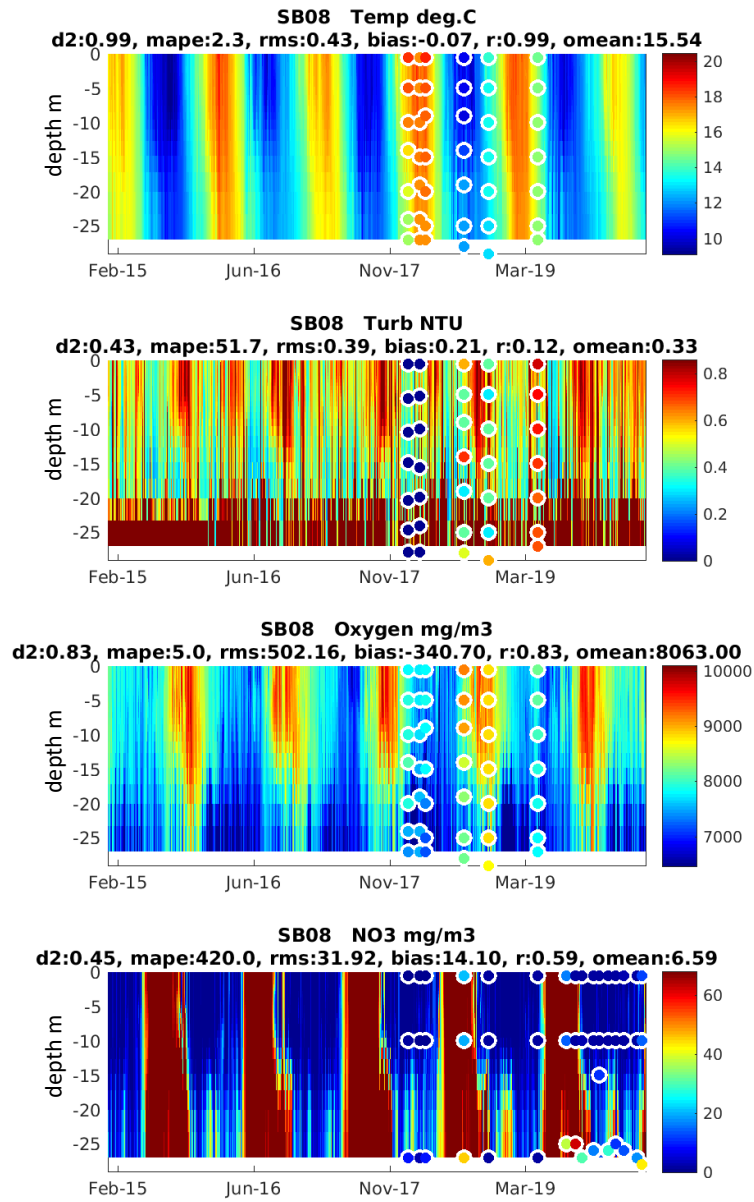|	EPA-SB	IMAS-SB	BEMP_HEDC Huon Estuary	BEMP_SER Rivers in Channel	BEMP_TPNB Port Arthur Nubeena	EPA_NB	Derwent (DEP)
Program Code / **Program Location**	**Storm Bay**	**Storm Bay**	**D' Entrecasteaux**	**and Huon**	**Storm Bay**	**Norfolk Bay**	**Derwent Estuary**
Sample frequency **Site names and number used in report (total =95)**	Monthly samples 27 Sites SB_1-11 (2018-2021) no samples in SB from April 2015 to 2018	Monthly samples 9 sites SB_1- 9 (2009 until April 2021) no samples in SB from April 2015 to 2018	Monthly samples 15 Sites: M1-M15 continuous	Monthly samples 3 sites Snug, Huon, Esperance Rivers	1-2 monthly samples 9 sites: PA1-9, NUB1-4, TPNB5 (Storm Bay)	Monthly samples 9 sites: NB1-8 and NB 10	Monthly samples 16 sites (7 used for model validation E, B1-3, RB, RBN, RBS. NN used for BGC river forcing)
Nutrients and BGC observations							
Ammonia as N	Ammonia as N	Ammonia as N	Ammonia as N	Ammonia as N	Ammonia as N	Ammonia as N	Ammonia as N
Nitrate as N	Nitrate as N	Nitrate as N	Nitrate as N	Nitrate as N	Nitrate as N	Nitrate as N	Nitrate as N
NOx: Nitrite and Nitrate as N	NOx	NOx	NOx	NOx	NOx	NOx	NOx
Total Kjeldahl (N)	TKN	TKN	TKN	X	TKN	TKN	X
Nitrogen (Total) as N	TN	TN	TN	TN	TN	TN	TN
Phosphorus Dissolved Reactive as P	DIP	DIP	DIP	DIP	DIP	DIP	DIP
Phosphorus (Total) as P	TP	TP	TP	TP	TP	TP	TP
Chl pigment extracted or Chl collected at discrete depths	X	Chl at discrete depths	Chl pigment extracted	X	X	X	Chl at discrete depths
Chlorophyll a (Int_AST) depth integrated (12 m Lund tube)	Chl a ext Lund tube	X	Chl a ext Lund tube	X	Chl a ext Lund tube	Chl a ext Lund tube	X
Turbidity	Turbidity	X	Turbidity	Turbidity	Turbidity	Turbidity	X
Dissolved Oxygen mg/L	DO mg/L	DO mg/L	DO mg/L	DO mg/L	DO mg/L	DO mg/L	DO mg/L
Dissolved Oxygen % Saturation	DO % Saturation	X	DO % Saturation	DO % Saturation	DO % Saturation	DO % Saturation	DO % Saturation
Salinity	Salinity	Salinity	Salinity	Salinity	Salinity	Salinity	Salinity
Water Temperature	Water Temperature	Water Temperature	Water Temperature	Water Temperature	Water Temperature	Water Temperature	Water Temperature
Conductivity	Conductivity	Conductivity	Conductivity	Conductivity	Conductivity	Conductivity	Conductivity
Pigments	X	X	pigments (major)	X	X	X	X
Silica	X	Silica	Silica	X	X	X	X
Pesticides	X	X	X	Pesticides	X	X	X
Microscopic speciation	Phytoplankton	X	Phytoplankton	X	Phytoplankton	Phytoplankton	X
Non purgable organic carbon	NPOC	X	X	X	X	NPOC	X
Secchi depth (only done for DEP)	X	X	X	X	X	X	Secchi depth
TSS (only done for DEP)	X	X	X	X	X	X	TSS

Figure 4.87 Comparison of modelled (continuous data) and observed (discrete samples) water quality parameters at station SB08 with statistical analysis [at selected depths (right)].
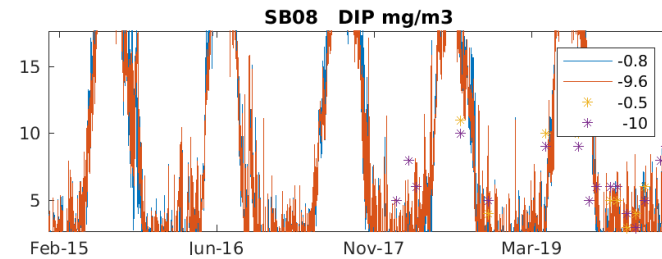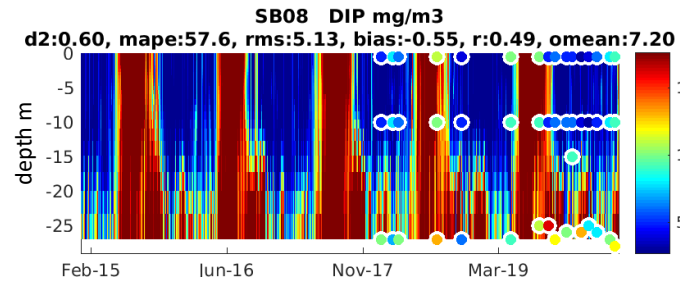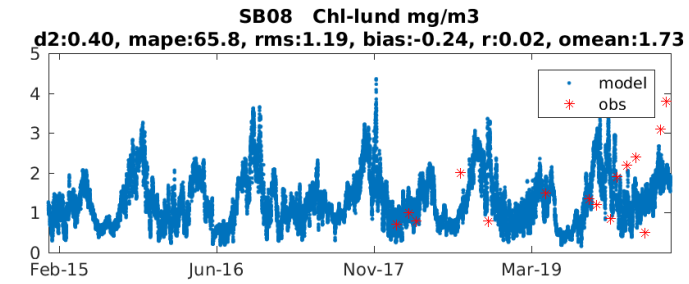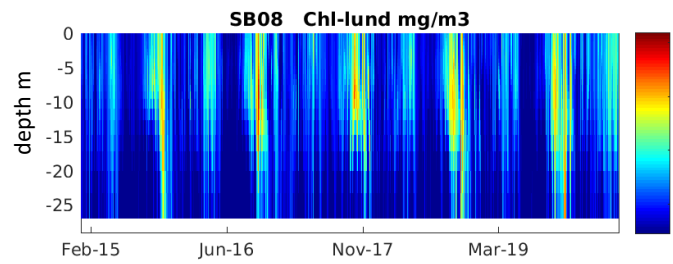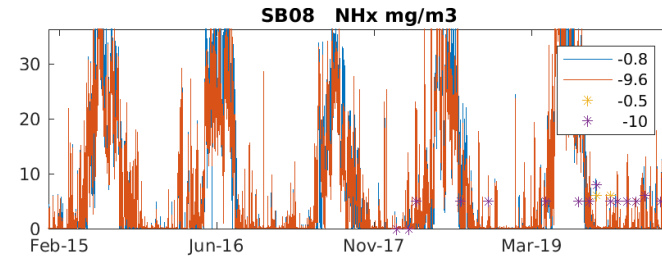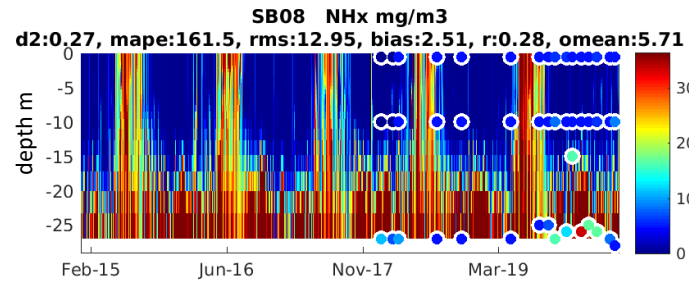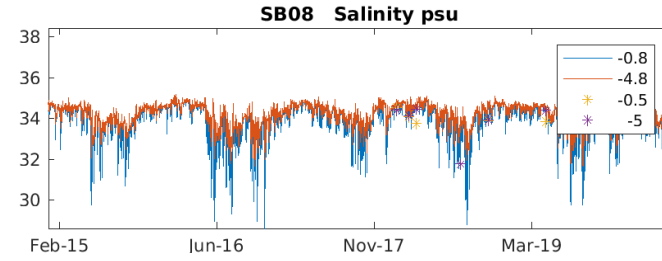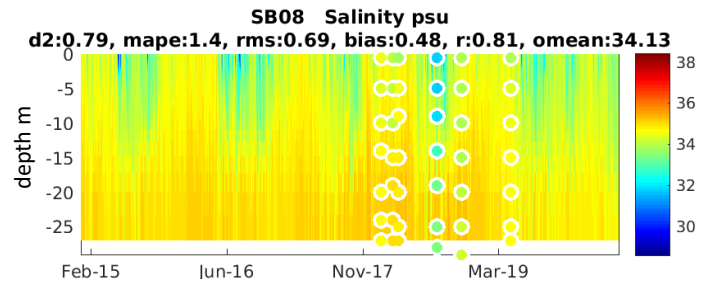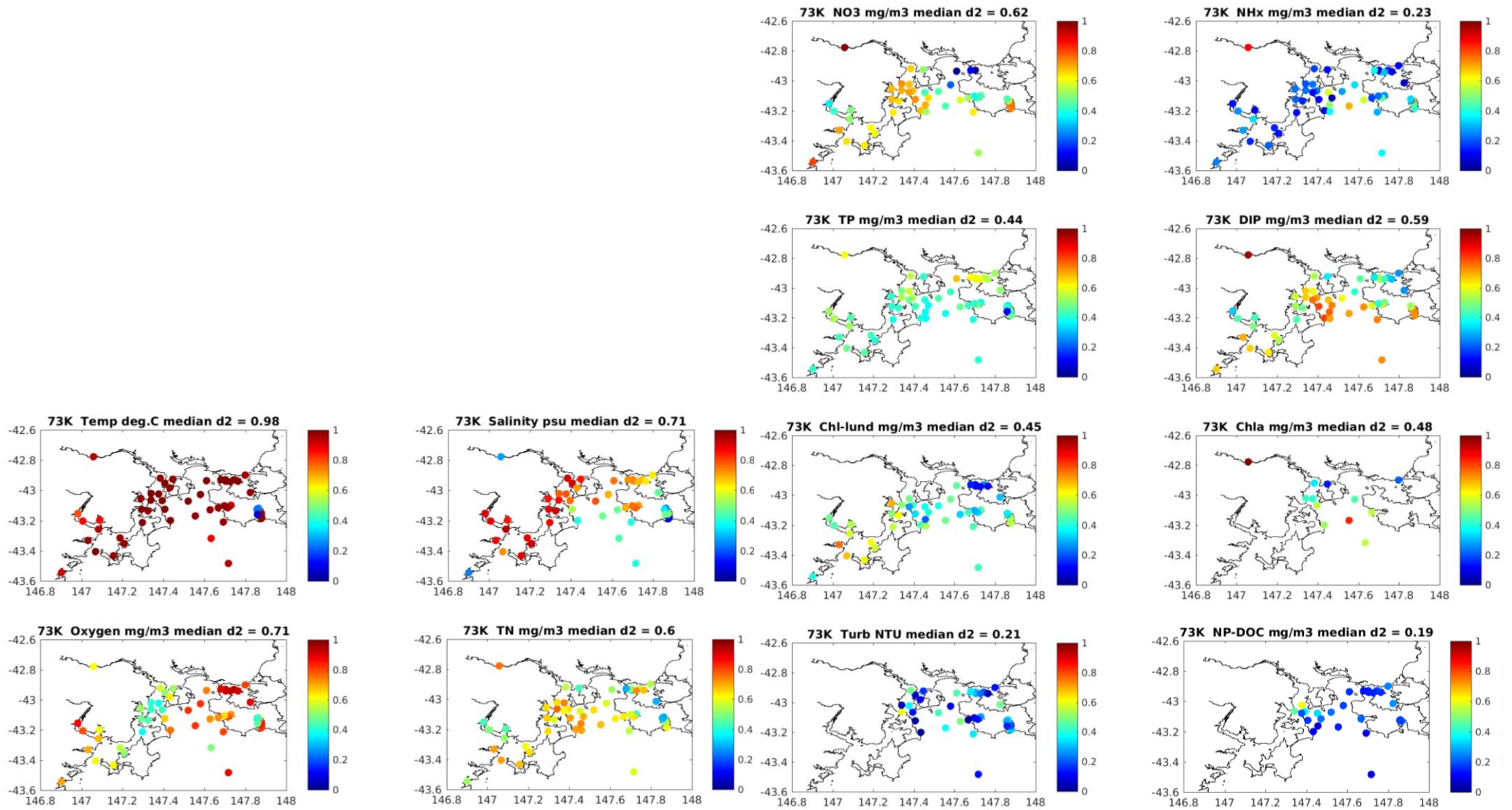
Figure 4.87 Comparison of modelled (continuous data) and observed (discrete samples) water quality parameters at station SB08 with statistical analysis [at selected depths (right)].

Figure 4.88a Spatial distribution of Willmott skill (d2) for model run 73K vs observations at stations throughout the region from 2015 to (May) 2020.
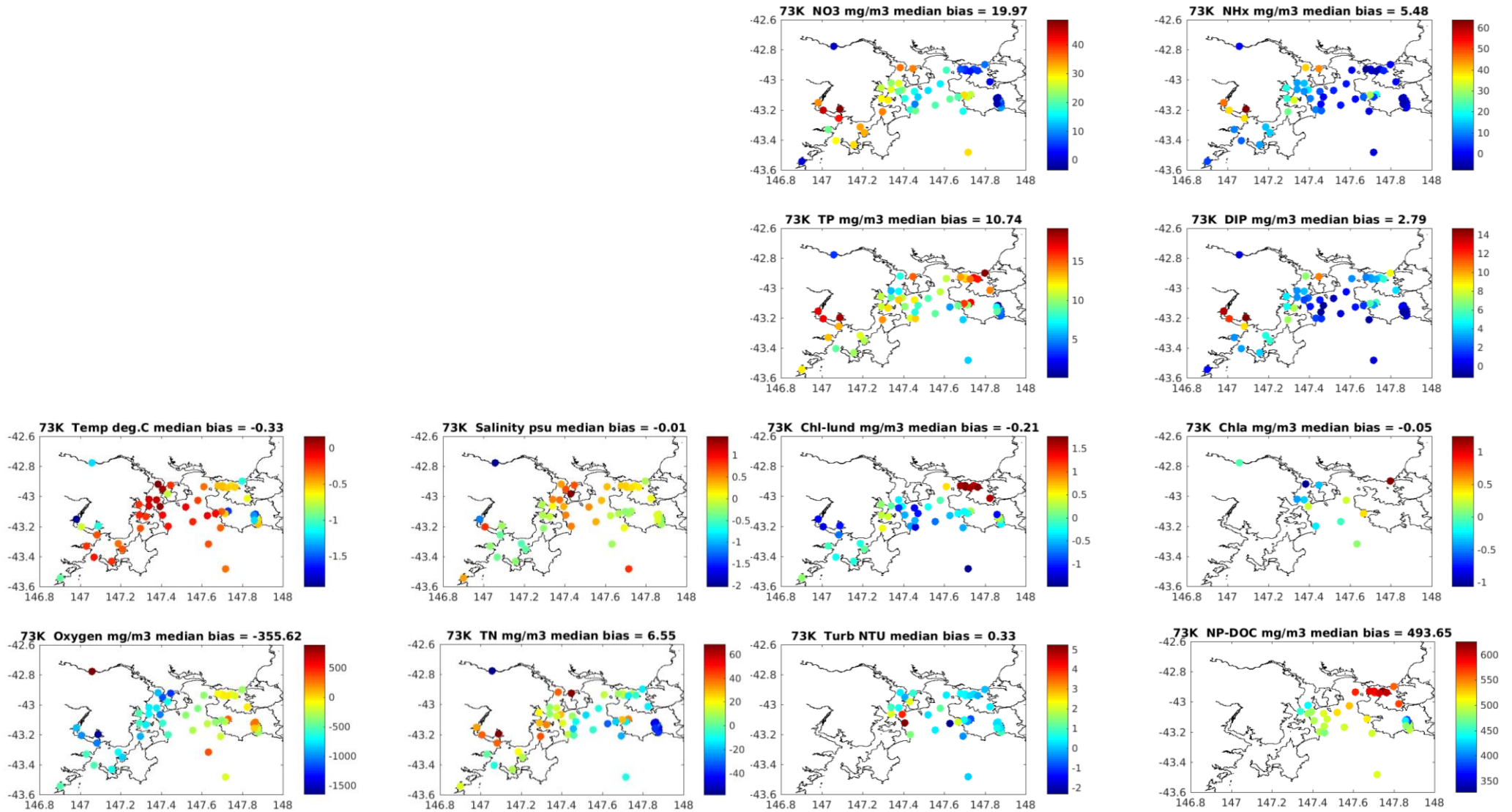
Figure 4.88b Spatial distribution of model bias c.f. observations for model run 73K at stations throughout the region from 2015 to (May) 2020.

Table 4.9a Summary statistics for timeseries comparison of observed and simulated water quality at stations throughout the region from 2015 to (May) 2020 [Willmott & Correlation > 0.4 are coloured green, < 0.3 are red, model bias low is blue, model bias high is orange].

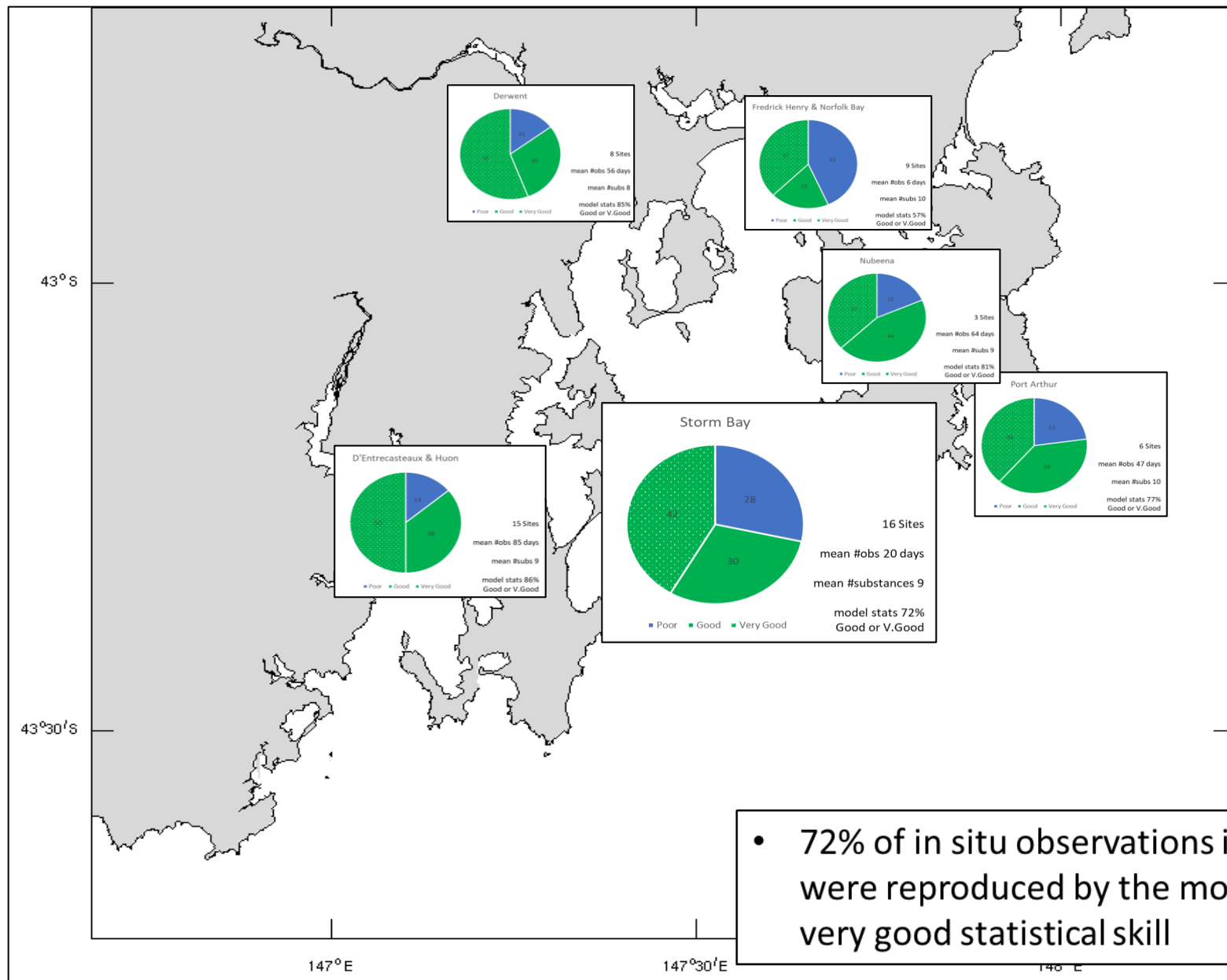| BGC73K		Mean Willmott	Mean Correlation	Median Normalised Bias	N. Obs	N.Days	N.Substances
Storm Bay	SB01_Iron	0.57	0.52	0.20	1259	42	11
	SB03_Yellow	0.55	0.43	0.09	377	16	10
	SB08_SEBetsy	0.56	0.51	0.00	395	16	10
	SB09_NWHead	0.51	0.45	0.11	413	16	11
	SB05_NWedge	0.54	0.46	0.20	1550	58	11
	NUB4_SWedge	0.61	0.49	0.00	1552	63	9
	SB02_Mid	0.60	0.49	0.01	453	15	11
	SB06_Variety	0.54	0.39	0.04	464	16	11
	SB04_CQE	0.53	0.27	-0.02	473	16	10
	SB03_site3	0.59	0.92	0.02	54	2	4
	SB07_Dart	0.53	0.33	-0.02	523	14	10
	SB11_Evariety	0.54	0.51	0.50	167	10	7
	SB12	0.48	0.52	0.45	167	10	7
	SB13	0.45	0.43	0.45	167	10	7
	SB14	0.45	0.42	-0.03	167	10	7
	SB15	0.48	0.32	0.03	167	10	7
Fredrick Henry & Norfolk Bay	FHenryB	0.53	0.51	0.21	210	6	10
	Ngreen	0.46	0.35	0.23	192	6	10
	EMF117	0.51	0.37	0.24	492	6	10
	NB2_EMF117N	0.46	0.41	0.24	438	6	10
	White	0.55	0.43	0.27	210	6	10
	Norfolk	0.52	0.50	0.34	126	6	10
	Smooth	0.49	0.43	0.48	192	6	10
	Denison	0.48	0.40	0.32	84	6	10
	Eaglehawk	0.45	0.40	0.20	174	6	10
Nubeena	NUB2_Creeses	0.52	0.50	0.10	1406	64	9
	NUB3_WhiteB	0.60	0.53	-0.01	1396	64	9
	NUB1	0.53	0.48	0.12	1386	64	9
Port Arthur	PA4_Dog	0.60	0.50	-0.03	1629	65	10
	PA3_CMC	0.64	0.51	-0.02	1663	65	10
	PA2_Carnarvon	0.64	0.51	-0.01	1611	65	10
	PA1_SLB	0.61	0.57	0.00	1490	65	10
	LBGP	0.44	0.29	0.06	273	13	10
	PA6	0.45	0.06	-0.07	179	9	10
Derwent	SB11_B3	0.61	0.58	0.13	1275	26	10
	B3	0.60	0.55	0.05	2833	64	9
	B1	0.59	0.51	0.02	2974	64	9
	RB	0.80	0.75	0.00	2120	54	3
	RBS	0.77	0.77	-0.06	677	54	3
	RBN	0.48	0.39	0.25	1925	64	9
	E	0.59	0.51	0.14	2919	63	9
	NN	0.78	0.83	-0.03	1892	60	9
D'Entrecasteaux	M15	0.55	0.41	0.06	1613	83	9
	M09	0.63	0.56	-0.01	1613	83	9
	M08	0.63	0.58	0.04	1613	83	9
	M07	0.59	0.52	0.04	1612	83	9
	M06	0.61	0.56	0.07	1613	83	9
	M12	0.68	0.65	0.00	1613	83	9
	M10	0.61	0.59	0.14	1613	83	9
	M11	0.53	0.51	0.24	1613	83	9
	M14	0.57	0.55	0.15	1613	83	9
	M13	0.53	0.42	0.12	1613	83	9
	M05	0.56	0.53	0.42	1613	83	9
	M03	0.60	0.55	0.26	1613	83	9
	M04	0.58	0.57	0.30	1613	83	9
	M02	0.62	0.61	0.14	1613	83	9
	M01	0.61	0.58	0.15	2503	109	10

Table 4.9b Summary statistics for each observed substance from timeseries comparison of observed and simulated water quality at stations throughout the region from 2015 to (May) 2020 [Willmott & Correlation > 0.4 are coloured green, < 0.3 are red, model bias low is blue, model bias high is orange].

	Mean Willmott	Mean Correlation	Median Normalised Bias	N. Obs	N.days	N.Sites
Temp deg.C	0.96	0.96	-0.02	12423	2421	55
Salinity psu	0.68	0.63	0.00	12330	2412	55
Oxygen mg/m3	0.69	0.62	-0.05	10695	2325	55
All Chl-a mg/m3	0.44	0.20	-0.13	2578	2419	63
NO3 mg/m3	0.56	0.66	1.79	5419	2462	57
NH4 mg/m3	0.27	0.21	0.96	5419	2458	57
TN mg/m3	0.59	0.40	0.03	5419	2462	57
DIP mg/m3	0.58	0.58	0.43	5419	2462	57
TP mg/m3	0.47	0.34	0.36	5419	2462	57
DOC mg/m3	0.21	0.17	1.56	928	313	34

For each substance, the timeseries of data from each station was compared with the equivalent model variable (and nearest grid location) with quantitative statistical analysis. Example figures for Storm Bay station SB08 are shown in Figure 4.87; equivalent analysis for all other stations is provided in Appendix A6. Note that as our analysis targeted exact match-ups in time and space between model and observation it would score poorly during periods when the simulated hydrodynamics was slightly offset in space or time (known as the double penalty issue and discussed in the hydrodynamic model assessment section 4.2.2).

Summary plots of model skill are provided in Figure 4.88 & 4.89 and Table 4.9. In general the model reproduces the observed seasonal and interannual variation in water quality for most variables at most stations very well, noting that observed sample collection is biased to fair weather days and seasons.

Reviewing the summary statistics by substance we note that model is performing well for most substances, however mean skill for simulated nitrate and ammonia across all sites is bias high. On inspection of the dissolved inorganic nitrogen dynamics at sites in Storm Bay (Figure 4.88a & b), we find acceptable model skill albeit with bias of around +1µM [bias is around +2µM in the Huon and Derwent Estuaries and the D'Entrecasteaux Channel].

Figure 4.89 Summary of model skill in reproducing observed in-situ monitoring data for sub-regions of the model.

Benthic lander data

Continuous water property observations from 4 Storm Bay benthic lander deployments (detailed in Section 5.2) that sampled the evolution of bottom water properties over 2 x 6 month periods in 2018-19 and 2019-20 were compared with equivalent model output.

Statistical analysis showed generally good agreement between simulated and observed temperature, oxygen and nitrate (Table 4.10). There appeared to be significant sensor drift in the observed salinity records, however stochastic variability associated with mixing, water mass and estuarine outflow appeared to be well captured, particularly at the Eastern and Northern lander sites (Figure 4.90 & 4.91). Similar variability in the observed oxygen was also fairly well reproduced by the model, and the model bias observed in 2018-19 was reduced in 2019-20. Continuous sensing of nitrate by UV spectrophotometer was problematic with the sensors reporting low variability in 2018-19 and failing in 2019-20. The model skill in reproducing the sensor and lab nitrate samples was relatively good with low bias, and there was little evidence to suggest that observed or simulated resuspension events contributed significant amounts of nitrate to bottom waters.

The simulation of sediment resuspension and observed turbidity and backscatter has been presented in Section 4.4.5. Observed variability in chlorophyll and CDOM was largely due to local resuspension of microphytobenthos, chlorophyll degradation products and humic substances and was not well simulated by the model [noting that the model formulation does not fully resolve chlorophyll degradation and CDOM production from organic matter].

Table 4.10 Statistical analysis of observed water properties at benthic lander sites vs equivalent model output [Willmott & Correlation > 0.4 are coloured green, < 0.2 are red, model bias low is blue, model bias high is orange].

Willmott Skill Score	West 38 m	East 39 m	North 29 m	South 48 m
Temp °C	0.96	0.97	0.84	0.78
Salinity psu	0.19	0.18	0.07	0.19
Oxygen mg/m3	0.47	0.34	0.49	0.71
Chl-a mg/m3	0.26	0.53	0.21	0.14
NO3 mg/m3	0.41	0.12	0.88	0.89
Turbidity NTU	0.33			0.41
CDOM ppb		0.16	0.05	
Backscatter		0.18	0.4	

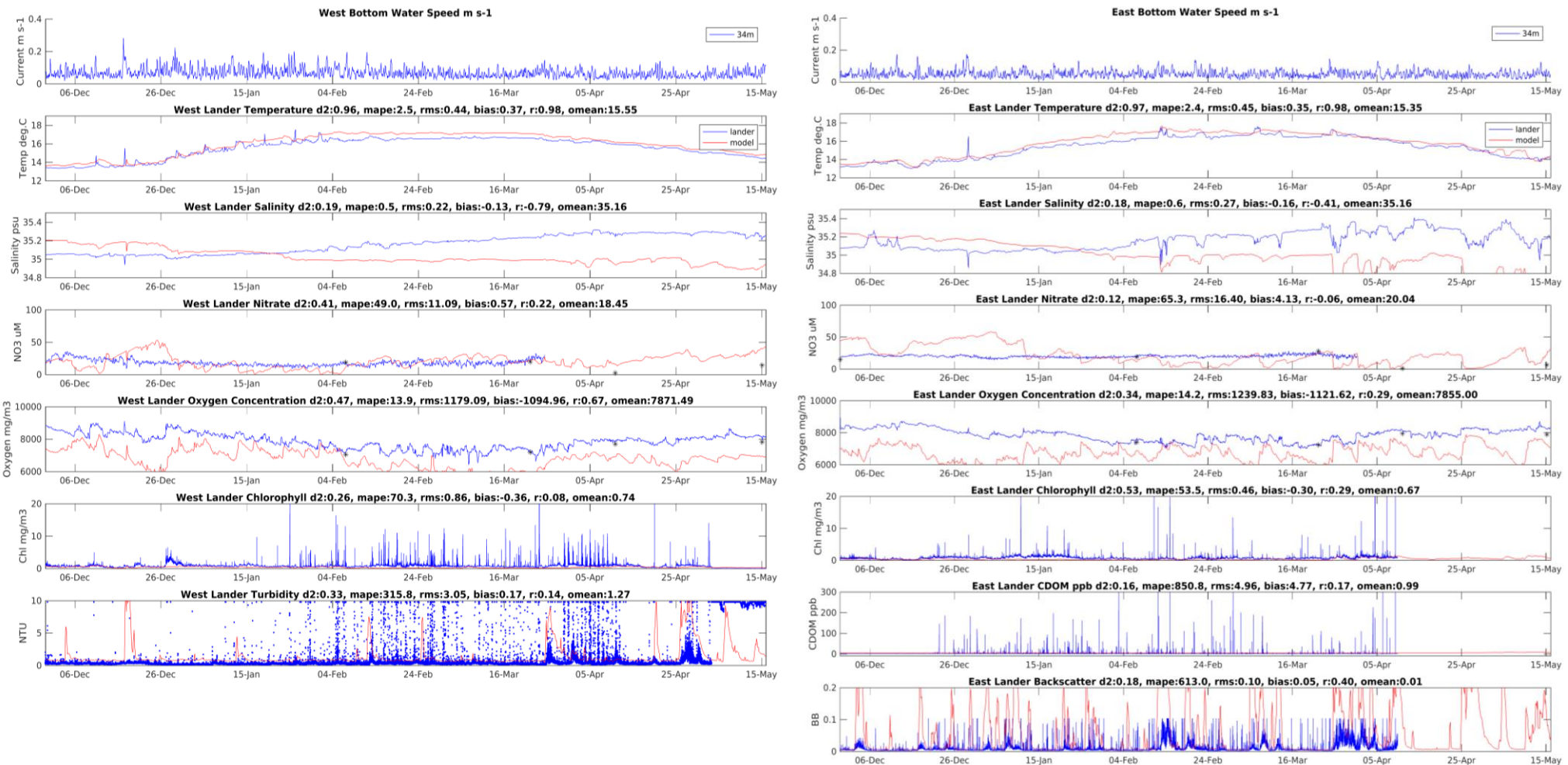| Normalised bias	West 38 m	East 39 m	North 29 m	South 48 m
Temp °C	0.02	0.02	0.01	0.00
Salinity psu	0.00	0.00	0.02	0.06
Oxygen mg/m3	-0.14	-0.14	-0.01	0.00
Chl-a mg/m3	-0.49	-0.45	-0.12	-0.17
NO3 mg/m3	0.03	0.21	-0.20	-0.12
Turbidity NTU	0.13			0.65
CDOM ppb		4.82	1.48	
Backscatter		5.00	1.67	

Figure 4.90 Model (red) vs observed (blue) water properties at the West (left) and East (right) lander sites in Storm Bay in 2018-19.
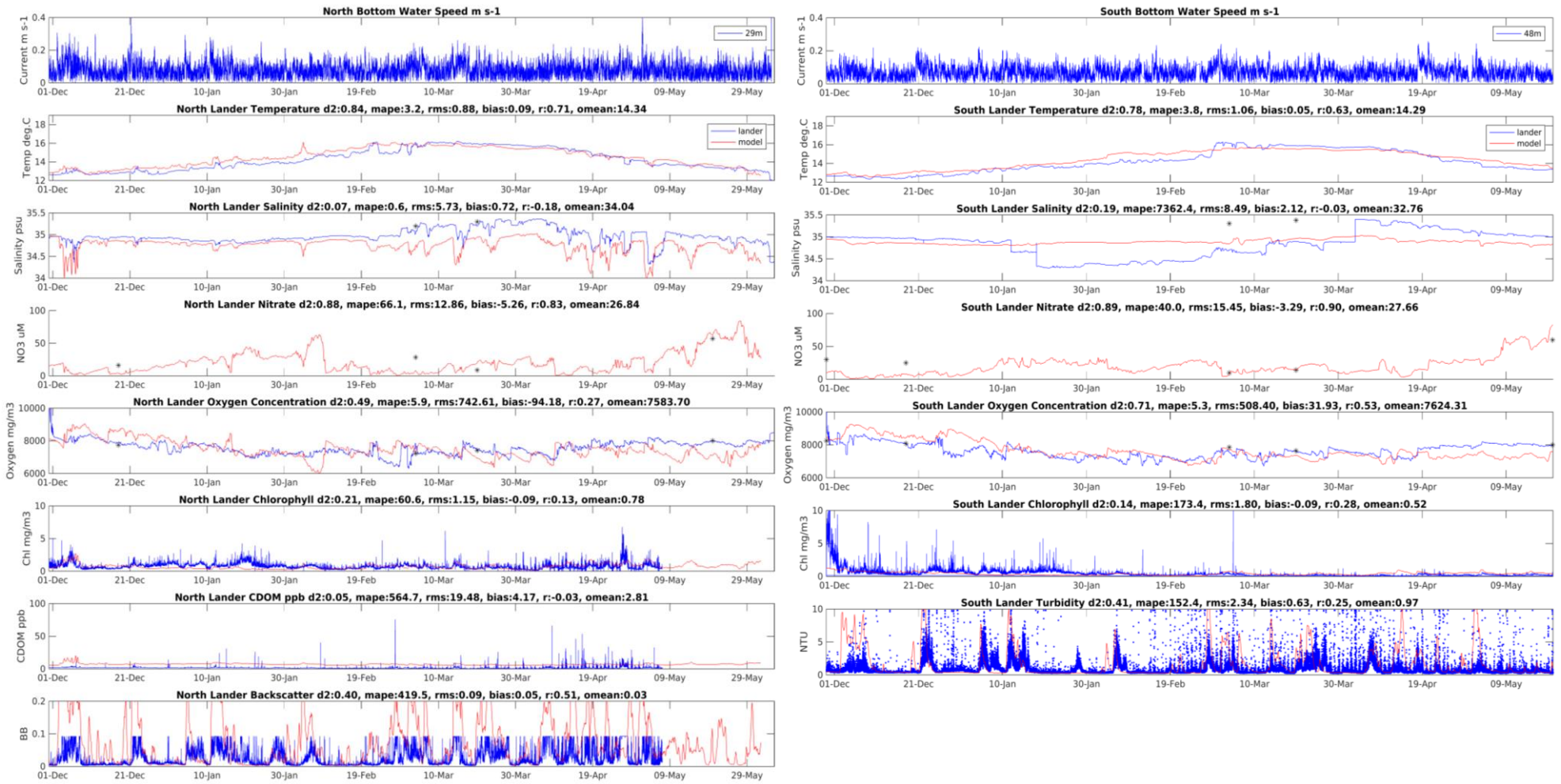
Figure 4.91 Model (red) vs observed (blue) water properties at the North (left) and South (right) lander sites in Storm Bay in 2019-20.

Denitrification

Microbial denitrification is an important ecosystem process whereby dissolved nitrate and ammonia are transformed by microbial activity to N_2 gas which is then lost from the aquatic system to the atmosphere. In the model we simulate denitrification as a function of nitrate, ammonia and dissolved oxygen concentration to emulate reduction and denitrification of nitrate and direct oxidation of ammonia. We hypothesise that some denitrification occurs in the water column but most denitrification occurs in the sediment which has a rich community of microbes.

Due to the complex analytical method, few measurements of denitrification have been made in southeast Tasmania. To evaluate the model performance in simulating denitrification we compare our current model results with previously published values for the Huon and Derwent Estuaries, and the D'Entrecasteaux Channel (Wild-Allen et al., 2010; Wild-Allen et al., 2013; Wild-Allen & Andrewartha 2016). In these studies simulated denitrification rates were shown to be consistent with sparse observations in southeast Tasmania and in similar water bodies.

Notwithstanding the evolution in model and process resolution, and any change in organic matter loading to the region, estimates of annual denitrification from sub regions of the current Storm Bay biogeochemical model compare well to literature values for the same waterways (Figure 4.92). The simulated denitrification fluxes in Storm Bay (Figure 4.93) are a hypothesis of system dynamics consistent with our understanding of these fluxes in adjacent waterways.
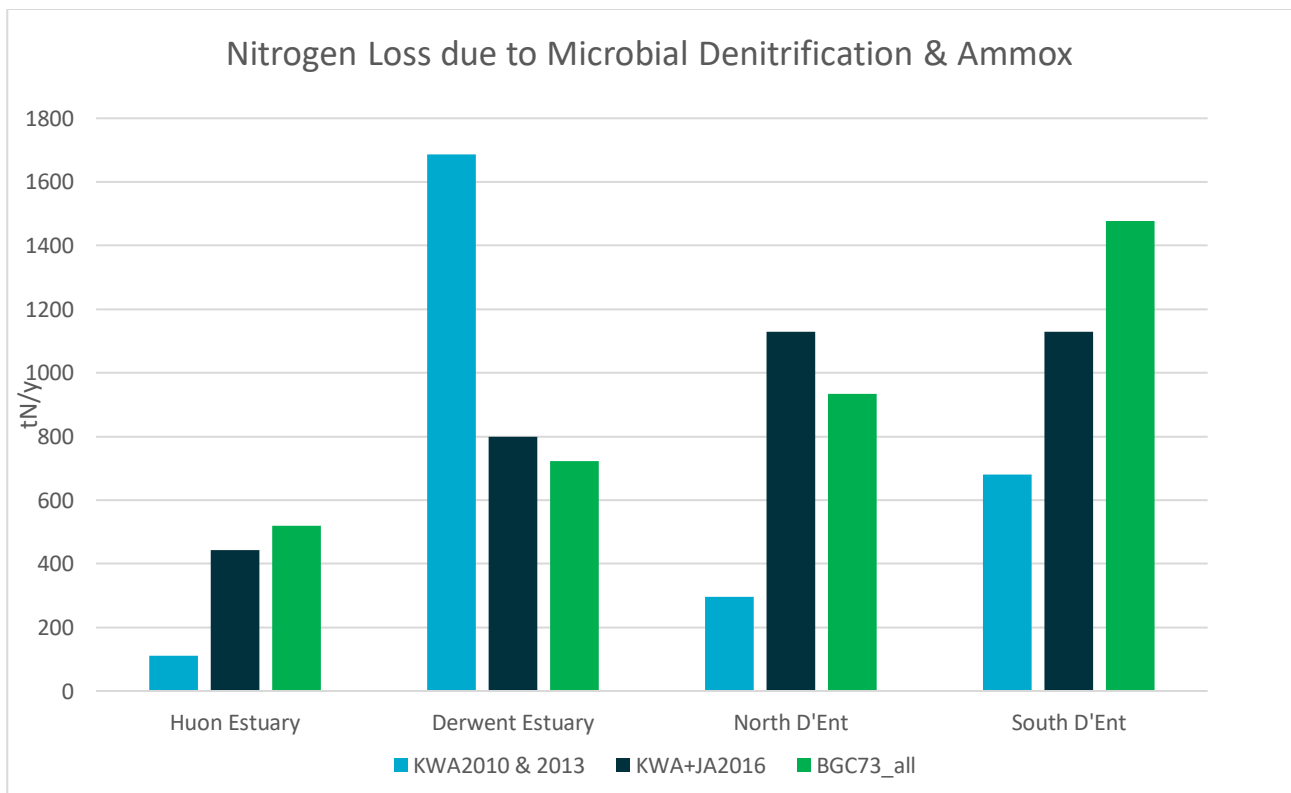
Figure 4.92 Comparison of modelled (green) and published (blue & black) estimates of annual denitrification for the Huon and Derwent Estuaries and the D'Entrecasteaux Channel.
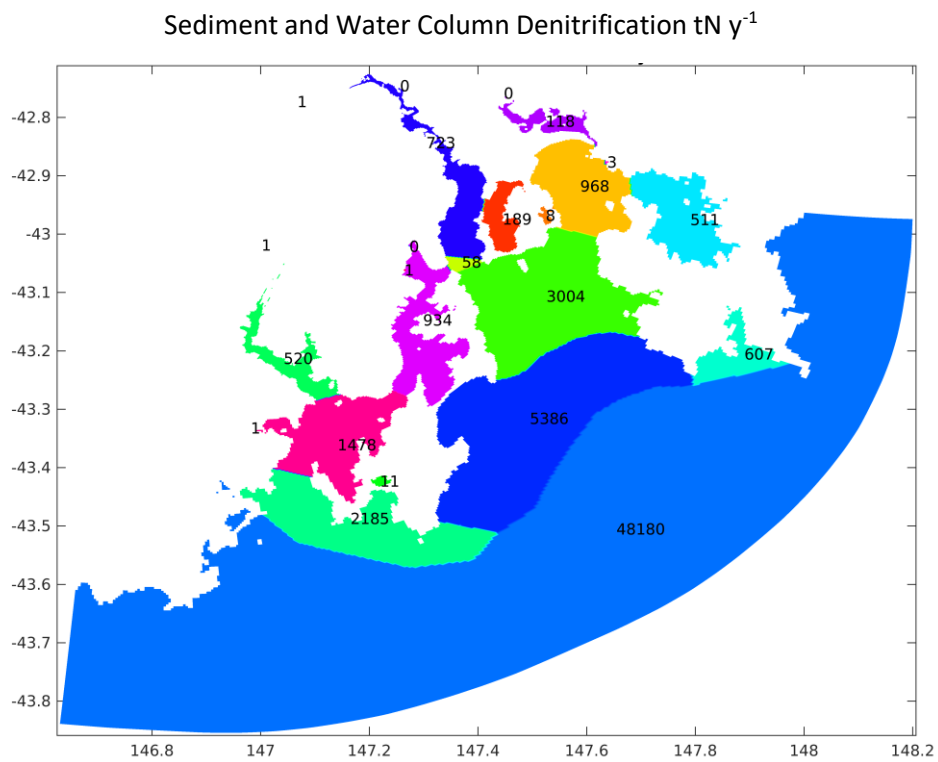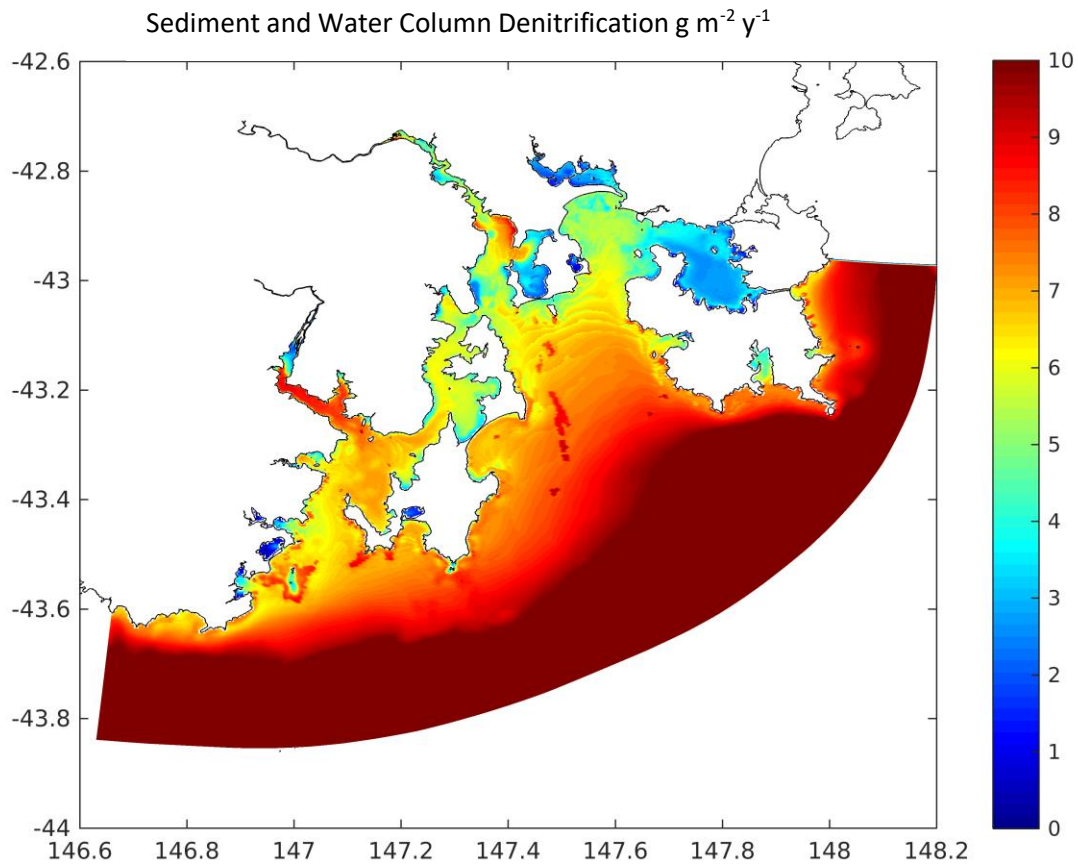
Figure 4.93 Simulated spatially resolved mean total denitrification flux (top) and annual mean total denitrification by sub regions (bottom), for 2015-2019 [sub-region colours are only for differentiation].

Sediment organic matter

To evaluate whether sediment processes were sufficiently resolved, simulated profiles of sediment organic matter content were calculated from modelled pools of organic matter and detritus, (relative to inorganic sediment). Simulated fractions of sediment organic matter were persistent in deep sediment layers and were within observed ranges for the region (see section 5.2).

Over multiple years of simulation, surface sediment organic matter declined, particularly in areas exposed to wave resuspension and in areas of sandy sediments; this included much of Storm Bay (Figure 4.94). In other sheltered areas and in deeper water (where organic matter supply exceeded loss due to resuspension and remineralisation), surface sediment organic matter accumulated (Figure 4.95).

Whilst there is an opportunity for further analysis of local spatial sediment variability (and comparison against more detailed IMAS sampling) the broadscale patterns demonstrated by the model throughout the region appear realistic.
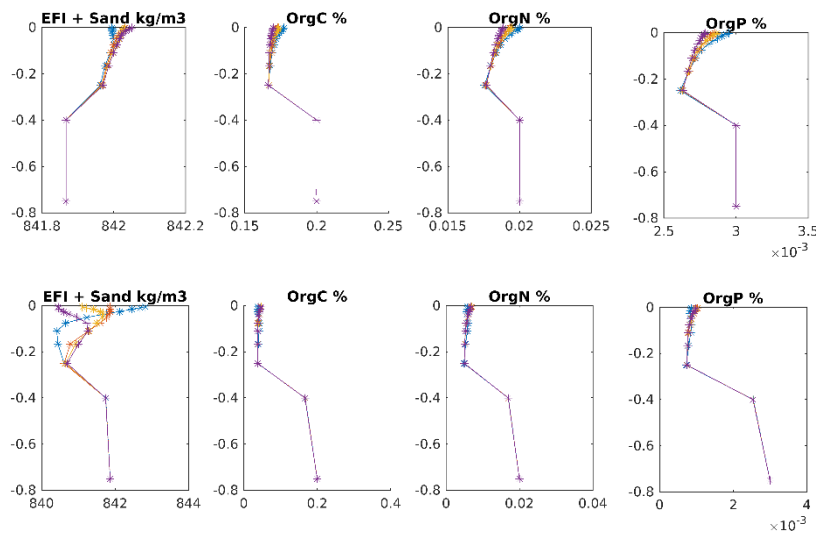
Figure 4.94 Simulated sediment profiles at stations in Storm Bay in Dec 2015 (upper panel) and Dec 2019 (lower panel).
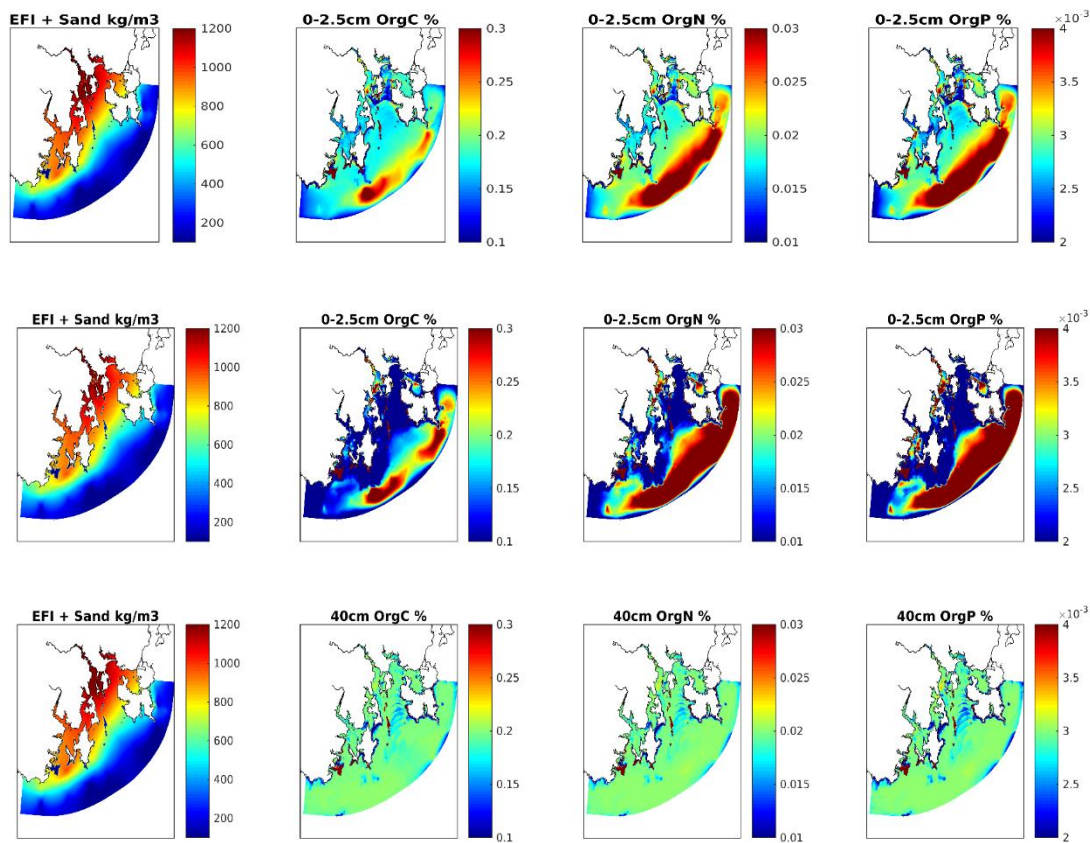
Figure 4.95 Simulated spatial distribution of inorganic sediment and % organic matter in Dec 2015 (upper panel) and Dec 2019 (middle and lower panel).

Potential nutrient limitation

To ensure that the model simulated a realistic phytoplankton and macrophyte response to the addition of anthropogenic nitrogen and phosphorous loads, nutrient fields were evaluated to determine potential limitation. The Redfield molar ratio of N:P is approximately 16:1 for ocean conditions; when less than 16 moles of N are available for each P, then the system is considered potentially nitrogen limited. Other studies in southeast Tasmania have found no evidence of P limitation for autotrophic growth (e.g. the CSIRO Atlas for Regional Seas database of nutrients (Condie & Dunn 2006)).

Analysis of model nutrient fields shows the molar ratio of N:P varies spatially, with depth and with season due to nutrient uptake and growth by phytoplankton and macrophytes in shallow water (Figures 4.96 & 4.97). Assimilation of nitrogen exceeds supply to surface waters in summer months resulting in potential N limitation over large areas down to 50m depth (Figure 4.97). In the Derwent and Huon Estuaries high CDOM and turbidity limit available light for photosynthetic growth and nutrients remain in excess throughout the year.

In the analysis of model results there was no evidence of P limitation for autotrophic growth, and there was no systematic decline in inorganic nutrient availability over the 2015-2020 model run.
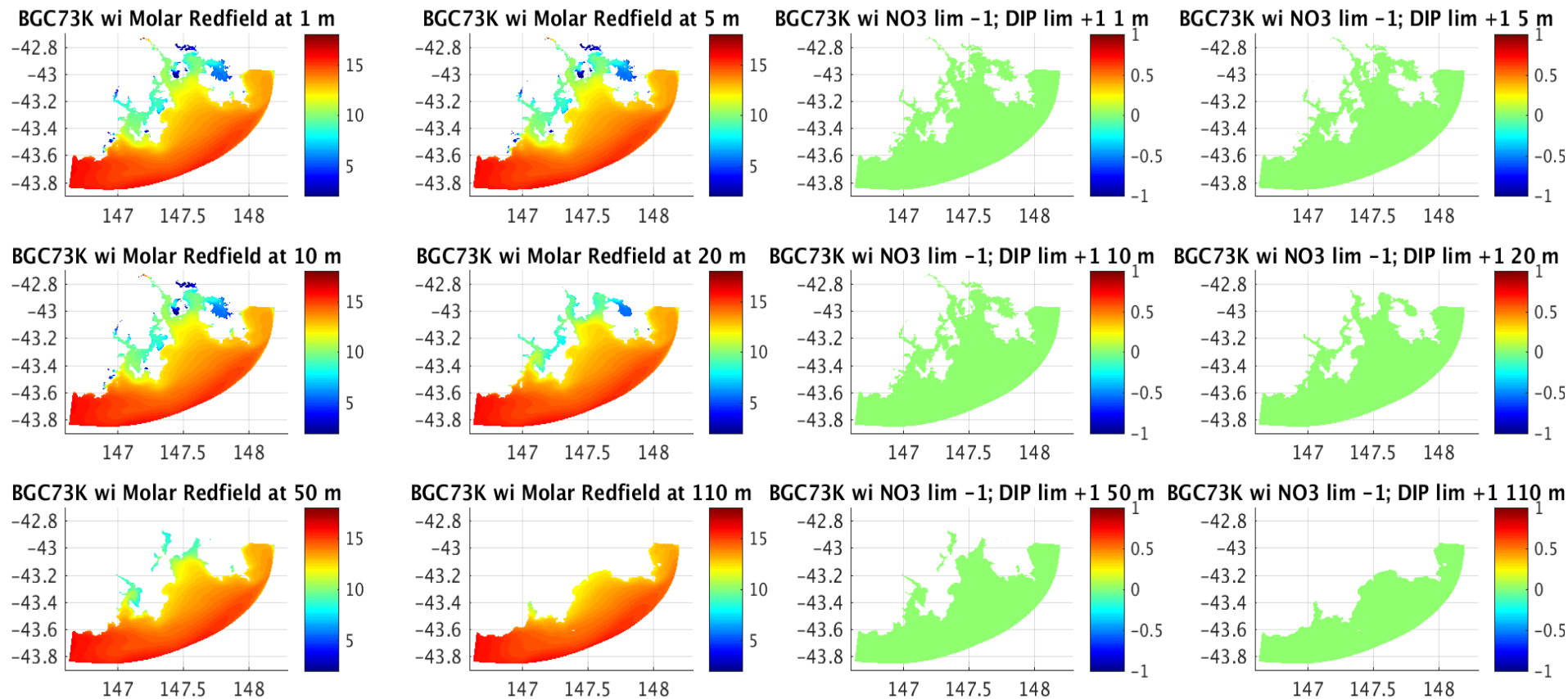
Figure 4.96 Mean winter molar ratio of dissolved inorganic nitrogen to phosphorous (left) and potential nutrient limitation (right) [N limitation (blue), P limitation (red)] at various depths for the period 2015 - 2019.
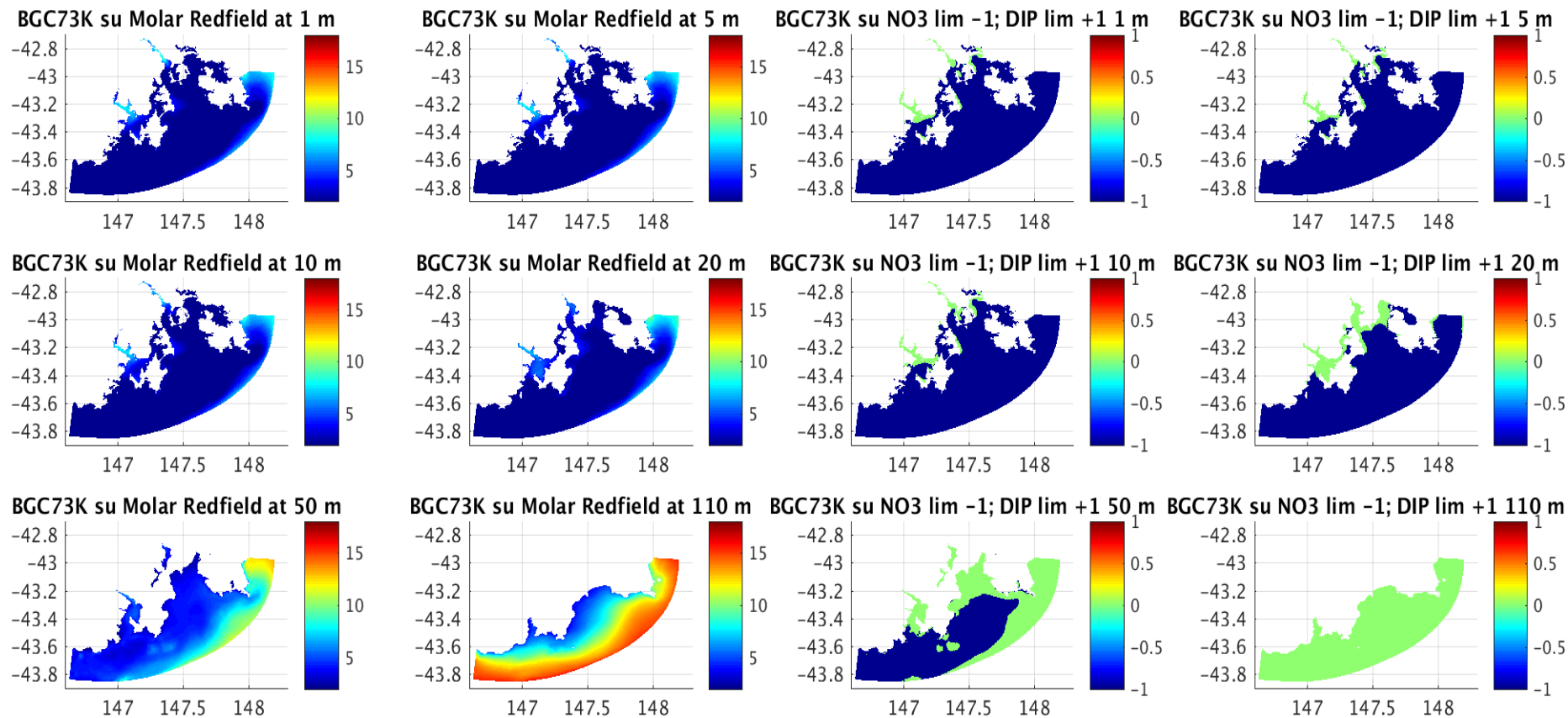
Figure 4.97 Mean summer molar ratio of dissolved inorganic nitrogen to phosphorous (left) and potential nutrient limitation (right) [N limitation (blue), P limitation (red)] at various depths for the period 2015 - 2019.

Epibenthos distributions

The Storm Bay biogeochemical model includes nominal distributions of epibenthic macrophytes and filter feeders. These are important components in the biogeochemical cycling of carbon, nitrogen, phosphorous and oxygen, particularly for the accurate simulation of bottom waters and benthic pelagic exchange. Epibenthic distributions generally evolve over much longer timescales than plankton dynamics in the water column. Spatial distributions of epibenthic variables simulated in Dec 2019 are shown in Figure 4.98. Simulated distributions of biomass broadly align with known distributions and offer the opportunity for further research and analysis to address specific research questions.
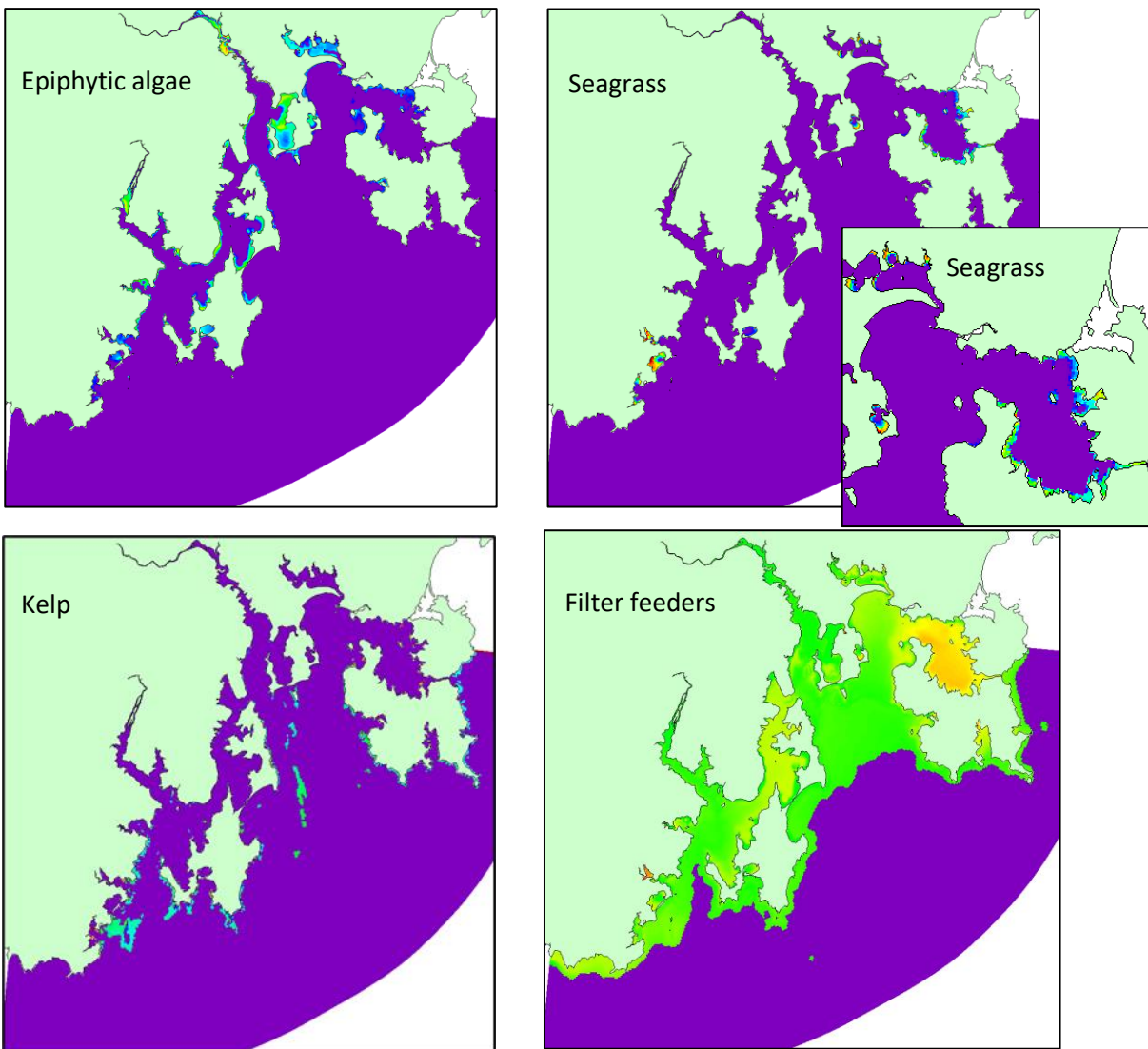
Figure 4.98 **Spatial distributions of epiphytic macroalgae, seagrass, kelp and filter feeders in Dec 2019 [uncalibrated nitrogen biomass shown for each component with range from low (purple) to high (orange)].**

Summary of model evaluation

The seasonal and interannual variability in a broad range of water quality variables in Storm Bay observed by satellites, gliders, in situ monitoring and benthic landers was generally well reproduced by the biogeochemical model over the period 2019-2020.

Model evaluation against remotely sensed OC3M chlorophyll demonstrated that the model was able to reproduce the observed seasonal and interannual dynamics of OC3M chlorophyll in offshore waters in Storm Bay. Observed spikes in OC3M were not well simulated possibly due to poor representation of the optical contribution of river TSS, CDOM, phytoplankton cell size or patch distribution. Due to cloud and coastal effects there was insufficient remotely sensed data to evaluate the model performance in inshore waters; glider, in situ monitoring data and continuous sensor data were used to evaluate the model in inshore waters.

Glider observations of the spatial and temporal distribution of water properties were generally very well reproduced by the model [notwithstanding double penalty errors associated with any spatial or temporal offset in simulated gradients in water properties and/or water mass fronts]. Over 14 glider missions, sampling an average of 7 model substances, 91% of the observations verses model statistical analysis showed good or very good model skill.

Comparison of the model against in situ observation showed that in general the model reproduced the observed seasonal and interannual variation in water quality for most variables at most stations very well, noting that observed sample collection is bias to fair weather days and seasons and our analysis would score poorly in the case of any spatial or temporal offset in simulated gradients in water properties. Statistical analysis showed the 72% of in situ water quality timeseries observations in Storm Bay were reproduced by the model with good or very good statistical skill, although there was a bias of around +1µM for dissolved inorganic nitrogen in Storm Bay.

Model evaluation against continuous sensor data collected during 4 benthic lander deployments showed good agreement between simulated and observed temperature, oxygen and nitrate. Stochastic variability associated with mixing, water mass and estuarine outflow appeared to be well captured for most water properties. There was little evidence to suggest that observed or simulated resuspension events contributed significant amounts of nitrate to bottom waters.

From further analysis, model results were also found to be consistent with current understanding of denitrification flux, surface sediment composition, potential nutrient limitation and the spatial distribution of macrophytes. We therefore have confidence that the Storm Bay model is able to provide a realistic representation of the biogeochemical dynamics in Storm Bay.

We conclude that the model is fit for the purpose: to simulate the water quality in Storm Bay for assessing future salmon farm expansion and to characterise the primary sources of nutrients into Storm Bay from ocean currents, sediment resuspension, river and anthropogenic inputs.

4.5.4 Biogeochemical model hindcast analysis

A summary of key findings from the biogeochemical model hindcast simulation from 2015-2020 for water quality variables (temperature, salinity, chlorophyll, dissolved inorganic nitrogen, dissolved oxygen, light penetration), are included in this section; further details including results for phosphorous, all monthly means, 10th and 90th percentile distributions for surface and bottom waters are included in Appendix A7.

Interannual variability

Simulated interannual variation in water quality in southeast Tasmania is primarily driven by variability in atmospheric, ocean and river forcing. Monthly mean surface temperature and salinity (Figure 4.99) show similar patterns from year to year with highest variation in inshore waters due to the influence of coastal discharge. Conditions in a given month can vary by a few degrees or several PSU from year to year and peak seasonality may be a few weeks earlier or later in any specific year (Figure 4.99).
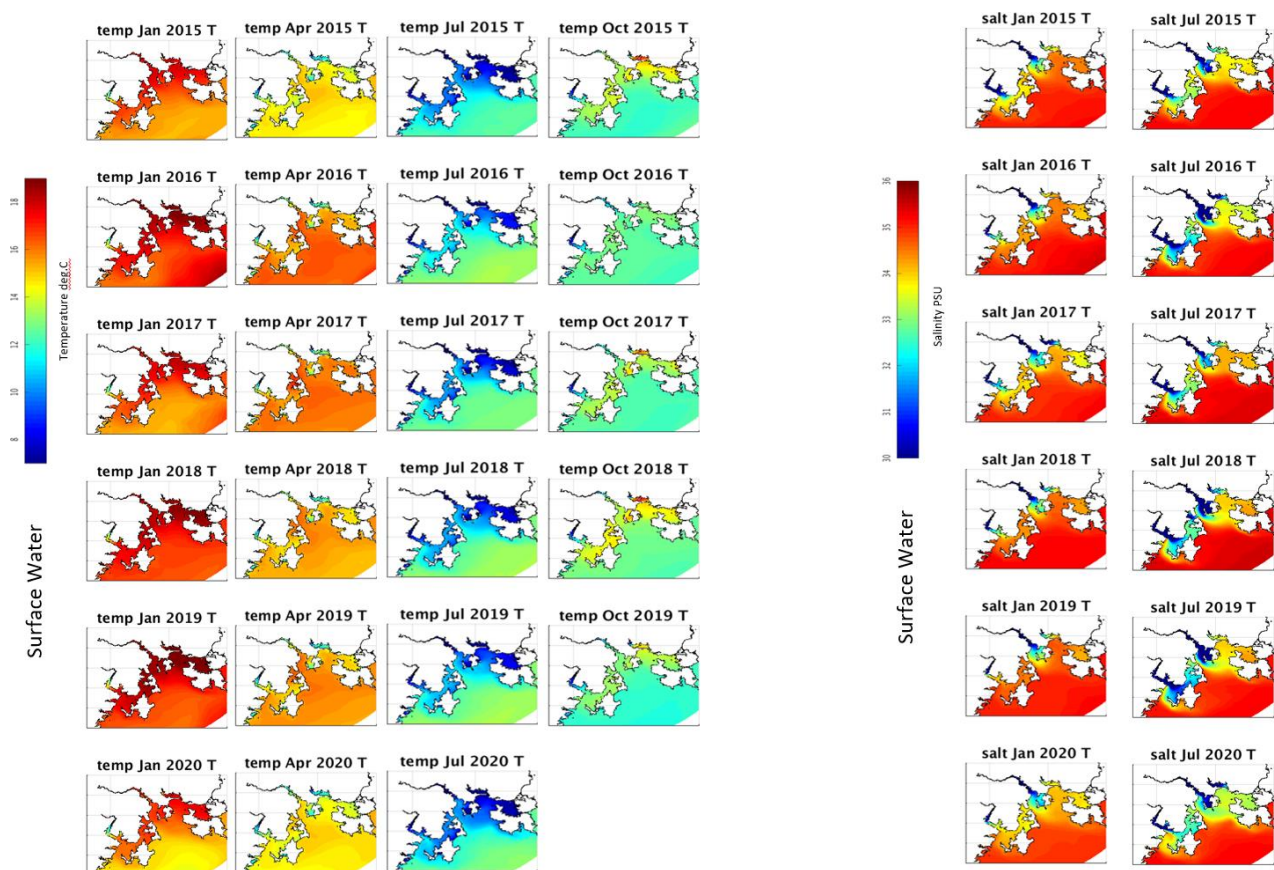
Figure 4.99 Simulated monthly mean surface temperature (left) in summer, autumn, winter and spring (Jan, Apr, Jul, Oct) and surface salinity (right) in summer and winter (Jan, Jul).

Storm Bay is influenced by coastal freshwater discharge with more extensive plumes in years and months with high river flow. There is also interannual variability in ocean currents, and the volume, depth, and frontal location of seasonal water mass intrusions into Storm Bay. This

seasonal and interannual variability in hydrodynamic forcing fundamentally drives the variation in water quality in Storm Bay.

Modelled chlorophyll distributions show seasonal and interannual variation throughout southeast Tasmania (Figure 4.100) with similar spatial patterns in each year. Chlorophyll concentrations are highest in inshore waters and bays where there is ready access to nutrients and phytoplankton can remain in the euphotic layer, due either to shallow water and/or stratification limiting vertical mixing beyond the euphotic layer (often defined as depth of 1% surface light – e.g. Sigman & Hain 2012). Monthly mean depth averaged (0-12 m) chlorophyll is generally seasonally low in winter and high in spring, although the magnitude and area of bloom events varies from year to year. Note that in addition to interannual variation in hydrodynamic forcing and the delivery of water mass associated nutrient and biogeochemical loads to the region, any variation in the timing and discharge of anthropogenic nutrient loads will also contribute to resulting interannual variability in simulated chlorophyll.
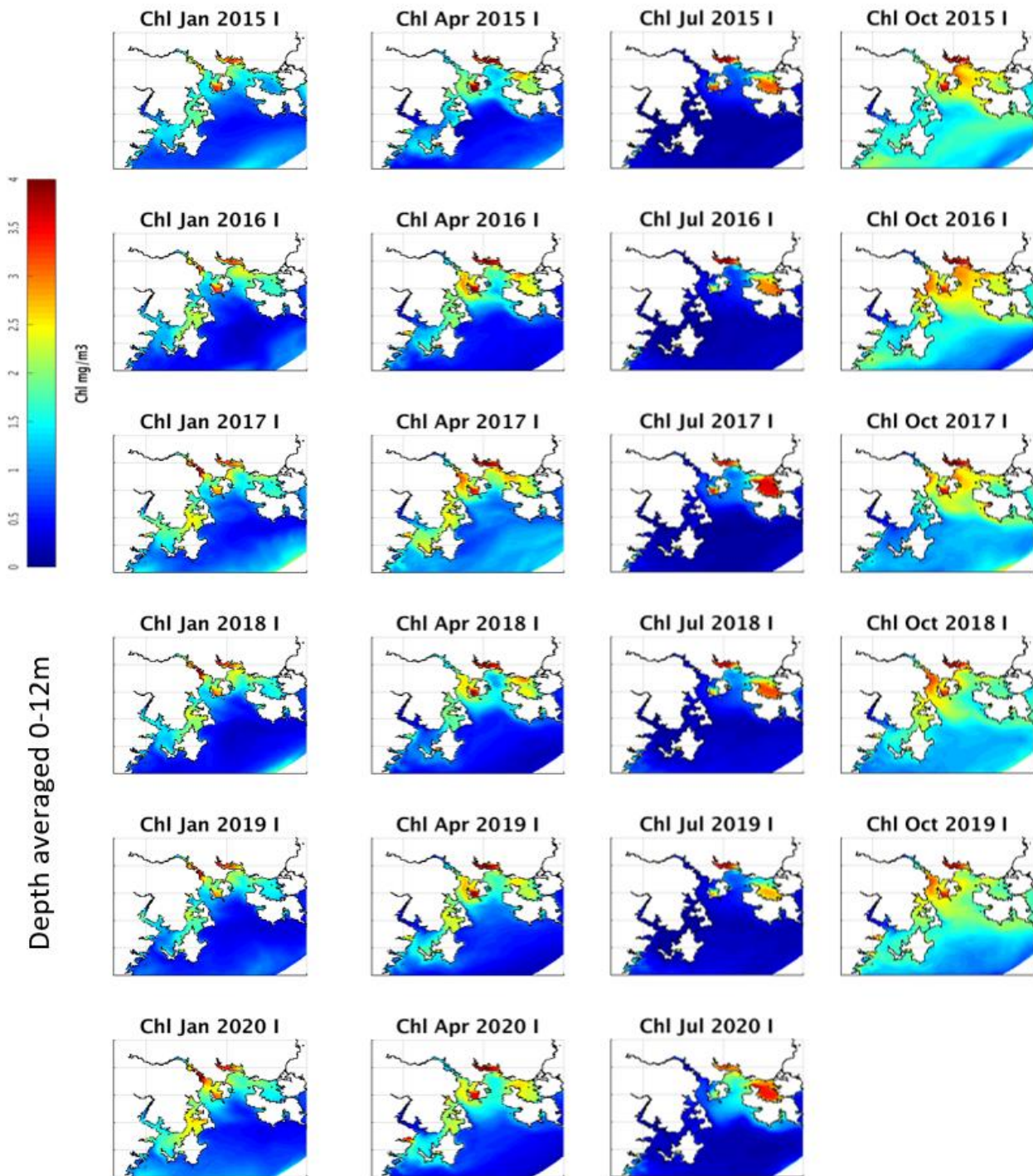
Figure 4.100 Simulated monthly mean depth averaged (0-12 m) chlorophyll in summer, autumn, winter and spring (Jan, Apr, Jul, Oct).
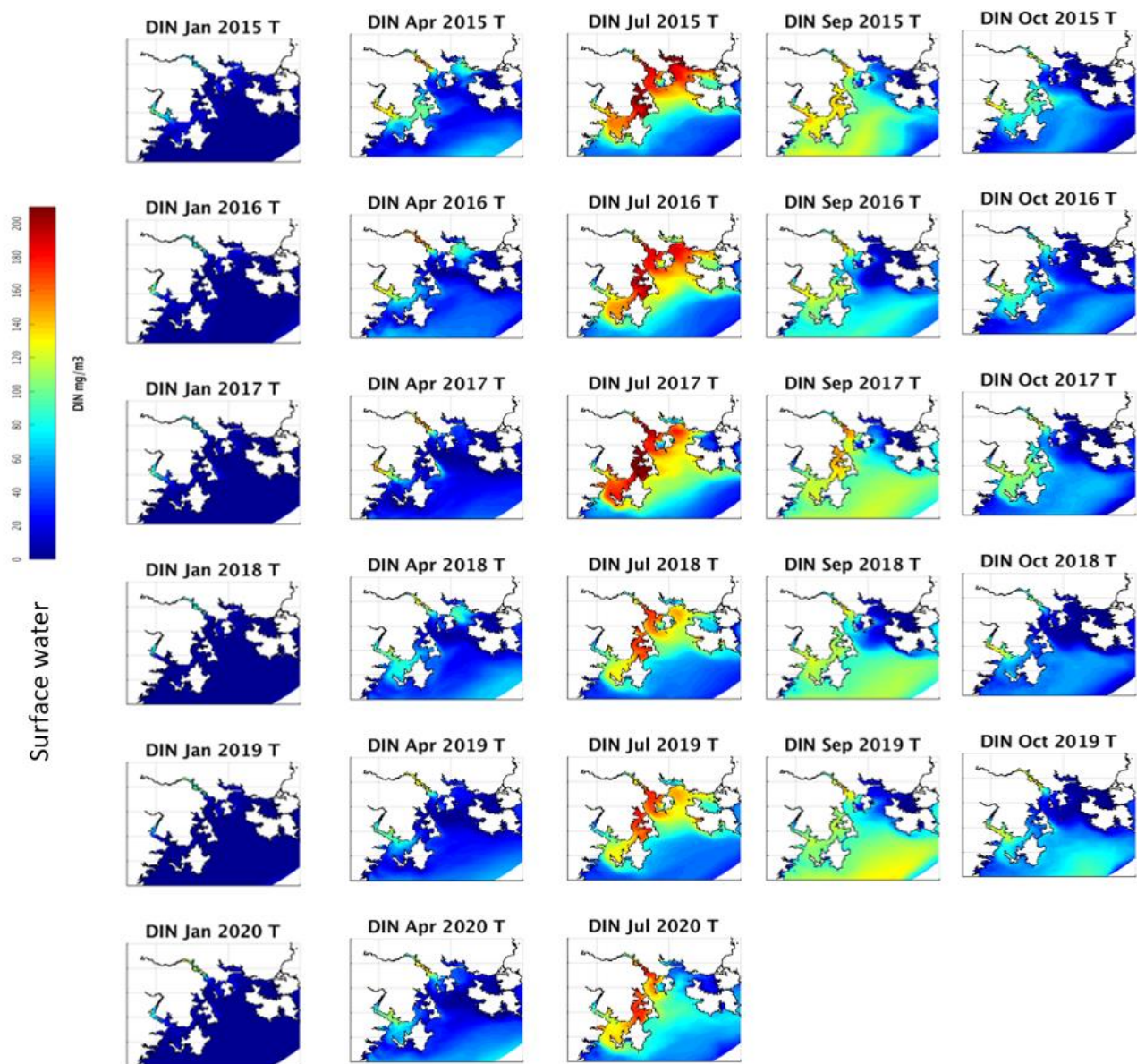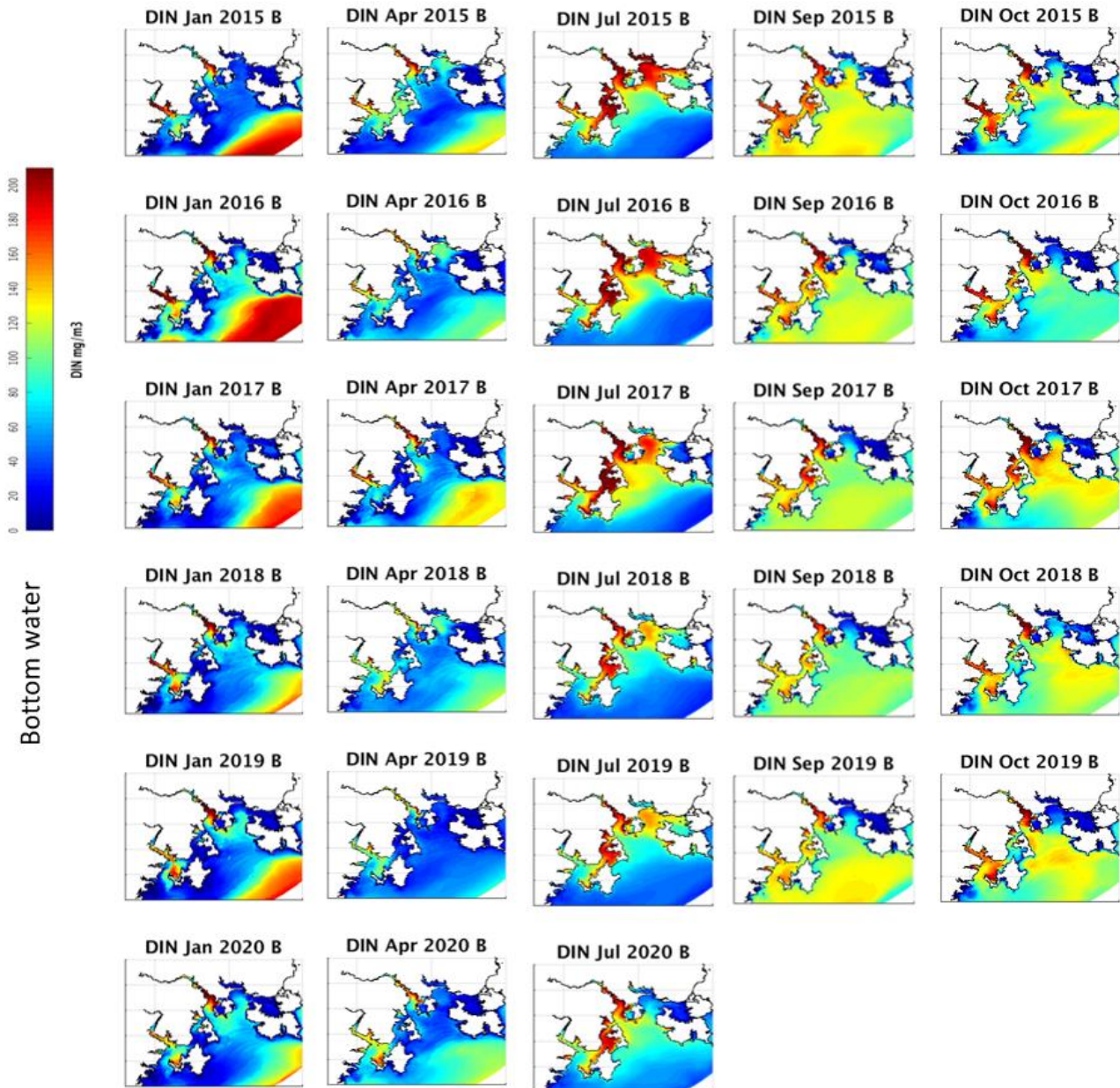
Figure 4.101 Simulated monthly mean surface dissolved inorganic nitrogen in summer, autumn, winter late winter and spring (Jan, Apr, Jul, Sep, Oct).

Low concentrations of dissolved inorganic nitrogen (DIN) can limit phytoplankton growth in southeast Tasmanian waters. Seasonal and interannual variation in simulated surface DIN (Figure 4.101) shows similar spatial and temporal patterns in each year with highest concentrations found in inshore waters and estuaries. Surface DIN is generally depleted in summer months whilst concentrations peak in winter months when lower levels of light, lower temperatures and higher vertical mixing limit phytoplankton uptake and growth. Simulations suggest that in early winter elevated DIN in inshore and estuarine waters results from coastal runoff and anthropogenic loads; in late winter, as the Zeehan Current declines, nutrient rich subantarctic ocean water moves into the region. Interannual variability in surface DIN dynamics results from the timing and magnitude of river and anthropogenic nutrient loads and the influence of the Zeehan Current in modulating the incursion of subantarctic water.

Simulated seasonal and interannual variability in inshore bottom water DIN (Figure 4.102) is similar to the variability seen in surface waters, however a much greater influence of oceanic

water masses is simulated in offshore regions. In addition to the late winter influx of subantarctic water as the Zeehan Current declines, high concentrations of DIN are simulated in offshore waters in summer underneath the East Australia Current eddies. Depending on the timing and intensity of the East Australian Current eddies, more or less DIN may be driven into Storm Bay and the adjacent waterways; there is strong interannual variability in this mechanism.

Figure 4.102 Simulated monthly mean bottom water dissolved inorganic nitrogen in summer, autumn, winter late winter and spring (Jan, Apr, Jul, Sep, Oct).

Modelled monthly mean bottom water oxygen saturation (Figure 4.103) shows the southeast Tasmanian region is generally well oxygenated. Oxygen saturation in the estuaries is lower than in well flushed open waters, due in part to persistent salinity stratification restricting the vertical transport of atmospheric oxygen through the water column. In offshore waters interannual variation in oxygen saturation is largely associated with the influx of deep subantarctic water

under the East Australia Current in summer and autumn; this water has lower oxygen. In addition to hydrodynamic factors, algal blooms and the degradation of organic matter contributes to the seasonal and interannual variation in bottom water saturation.
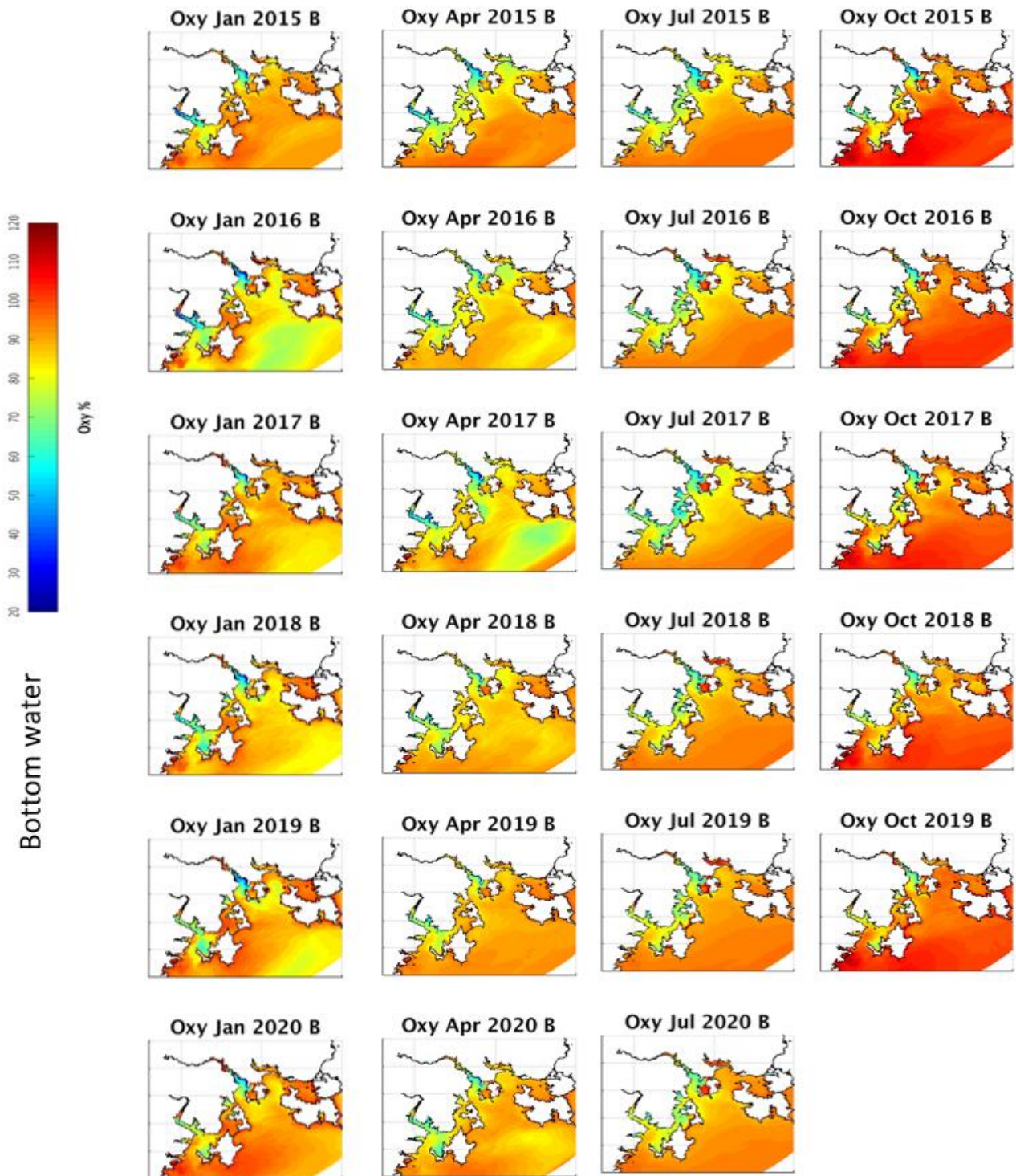
Figure 4.103 Simulated monthly mean bottom water dissolved oxygen saturation in summer, autumn, winter and spring (Jan, Apr, Jul, Oct).

Seasonal variation in water quality in Storm Bay

The seasonal cycle in water properties (averaged for each month for 2015-2019) is shown for a transect across Storm Bay (Figure 4.104). Additional spatial and transect plots for all model substances and months are included in Appendix A7. The transect plots show the transition from summer stratification across the whole bay to winter conditions which are well mixed offshore and stratified due to peak freshwater discharge in inshore waters. Chlorophyll is found in the top 20 m with higher concentrations inshore and a peak spring bloom concentrations in October.

The vertical distribution of DIN across Storm Bay clearly shows the seasonal influence of subantarctic water (under the EAC) in summer and autumn, coastal discharge in winter and subantarctic water influx (as the Zeehan Current weakens) in late winter and early spring. Transects of oxygen saturation across Storm Bay show a slight decline in saturation with depth during periods of stratification and during influx of deep ocean water in summer.

Box and whisker plots were prepared from model output in all grid cells in the Storm Bay region over 2015-2019 (Figure 4.105); these figures encompass the total spatial and temporal variability in Storm Bay for this period. In Storm Bay surface DIN concentrations peak in winter and tend to zero in summer months. Bottom water DIN concentrations vary throughout the year with influx from subantarctic water (under the EAC) augmenting concentrations in summer and autumn, and also in late winter and spring (as the Zeehan Current weakens). Chlorophyll concentrations in Storm Bay peak with an October spring bloom and there is a weaker autumn bloom in April. Regional bottom water oxygen saturation remains >80% with only slight variation over the year.

To evaluate the impact of seasonally changing turbidity on epibenthic seagrass and seaweeds the area of Storm Bay which received greater than 1% surface light (often thought of as the minimum amount of light required to support photosynthetic growth – e.g. Sigman & Hain 2012) was calculated for each month (Figure 4.105). The area with greater than 1% surface light was greatest in summer months and lower from autumn through to spring. In summer months there was reduced river influx of suspended solids and CDOM, resuspension of bottom sediments would also have been reduced c.f. during stormy winter weather, and chlorophyll concentrations were quite low, constrained by very low surface DIN concentrations; these condition resulted in low turbidity and a large area of Storm Bay where greater than 1% surface light reached the seabed. In other seasons elevated chlorophyll concentrations, greater river CDOM and suspended solids, and more resuspension would have increased water column turbidity and reduced the area where greater than 1% surface light reached the seabed.
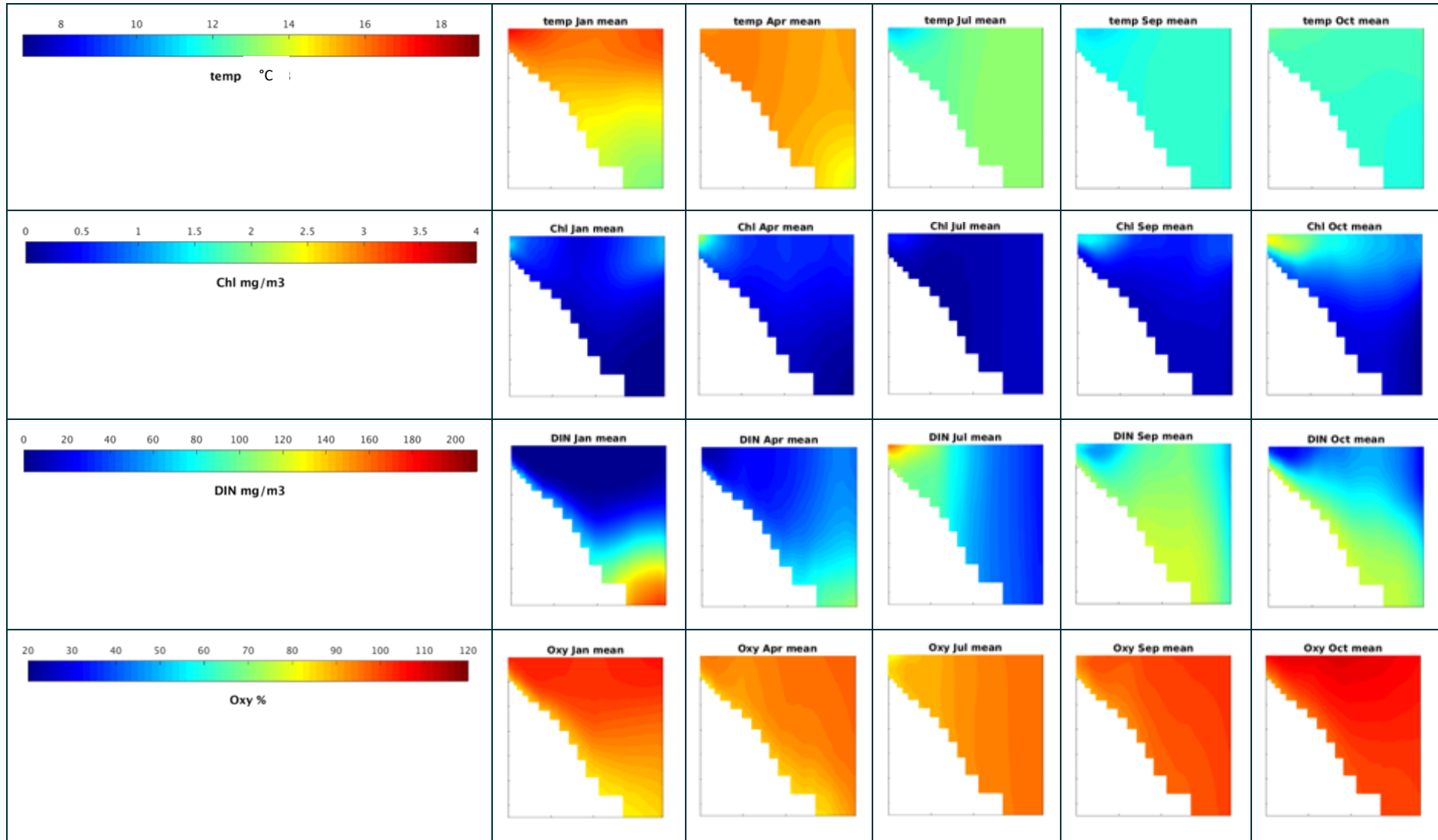
Figure 4.104 Mean water quality (temperature, chlorophyll, dissolved inorganic nitrogen, oxygen saturation) for 2015-2019 along a 70km long transect crossing Storm Bay from inshore (left) to offshore (right) in summer, autumn, winter late winter and spring (Jan, Apr, Jul, Sep, Oct) [vertical scale is 0 – 120 m depth].
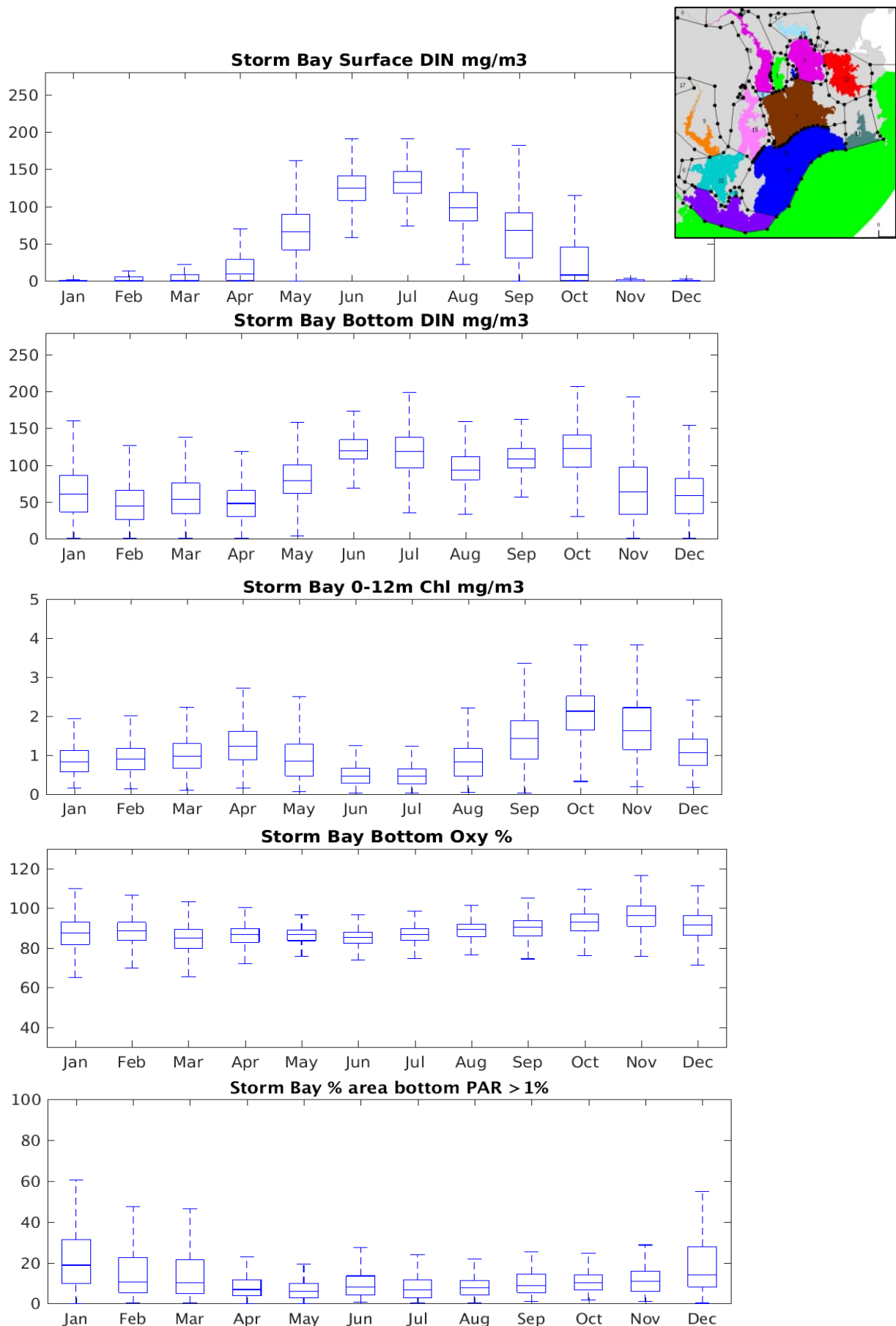
Figure 4.105 Seasonal variation in water quality in Storm Bay. Box plot shows mean, 25th and 75th percentiles and range for all Storm Bay model cells (brown region in inset map) over 2015-2019; for light transmission the % area of Storm Bay where bottom PAR exceeds 1% surface light is shown.

Nutrient budget in Storm Bay

A nitrogen mass balance budget was calculated for Storm Bay by summing all the simulated nitrogen variables in the model for each flux term. Modelled total nitrogen includes nitrate, ammonia, dissolved organic nitrogen, phytoplankton nitrogen (small, large, dinoflagellate, microphytobenthos), zooplankton nitrogen (small, large), and detrital nitrogen (pelagic labile, benthic labile, refractory). To check accuracy of the budget calculation, the total mass of nitrogen in the model at the start and end of each year was reconciled against the flux terms. Total mass of nitrogen in the model included total pelagic sediment and epibenthic nitrogen (seagrass, epibenthic algae, kelp, filter feeders).

Nitrogen fluxes across marine sections spanning mid-Storm Bay (Ocean), the entrance to Fredrick Henry Bay (F-H Bay) and the entrance to the Derwent and D'Entrecasteaux Channels (delineating the Storm Bay sub-region shown in brown in Figure 4.78), were calculated by summing the total depth integrated flux for each nitrogen model variable across the section every 25 hours (to minimise aliasing due to tidal flow); total influx and outflow were then summed as positive and negative contributions to Storm Bay. Fish farm load was calculated by summing all Storm Bay farm nitrogen loads to the system and denitrification was calculated by summing all pelagic and sediment denitrification terms for the Storm Bay area. The model also included a very small atmospheric nitrogen load, which was a constant in all years.

	Ocean	F-H Bay	Derwent + D'Ent	Ocean	F-H Bay	Derwent + D'Ent	fish farm	denit	atmos
2015	7361	4385	8884	-16880	-2987	-5126	438	-2833	46
2016	11484	3742	6706	-14288	-3234	-6373	636	-3027	46
2017	9752	2927	6361	-12272	-3079	-4690	935	-3196	46
2018	10251	3151	5432	-11374	-2706	-4882	734	-3090	46
2019	8524	3004	7243	-11676	-2601	-4295	1076	-3198	46

Figure 4.106 Annual nitrogen budget for Storm Bay for 2015 – 2019 [fluxes through ocean, Fredrick Henry Bay and Derwent-D'Entrecasteaux Channel sections; input from Storm Bay fish farms; loss by denitrification; input from atmospheric deposition].

The numerical error in the annual calculated nitrogen budget was less than 0.8% for all years except 2015, when the reconciliation of fluxes and biomass in the model showed a loss of mass of ~2.6%. This may be due to stronger gradients of change in the sediment during the first year of simulation due to the time required for the sediment to reach quasi-equilibrium. As the numerical error is smaller in later years of simulation, it is possible that there were some inaccuracies in the calculation of fluxes during the first year of simulation; average summary figures are therefore based on the period 2016-2019.

The nitrogen budget in Storm Bay shows considerable interannual variability in flux terms across the marine sections, particularly across the Ocean and Derwent-D'Entrecasteaux Channel sections (Figure 4.106). This is largely due to interannual variations in the influx of ocean water masses and estuarine outflow into the region. For the period 2015 – 2019 fish farm contribution of nitrogen to the region slowly increased and there was also a smaller but gradual increase in denitrification.
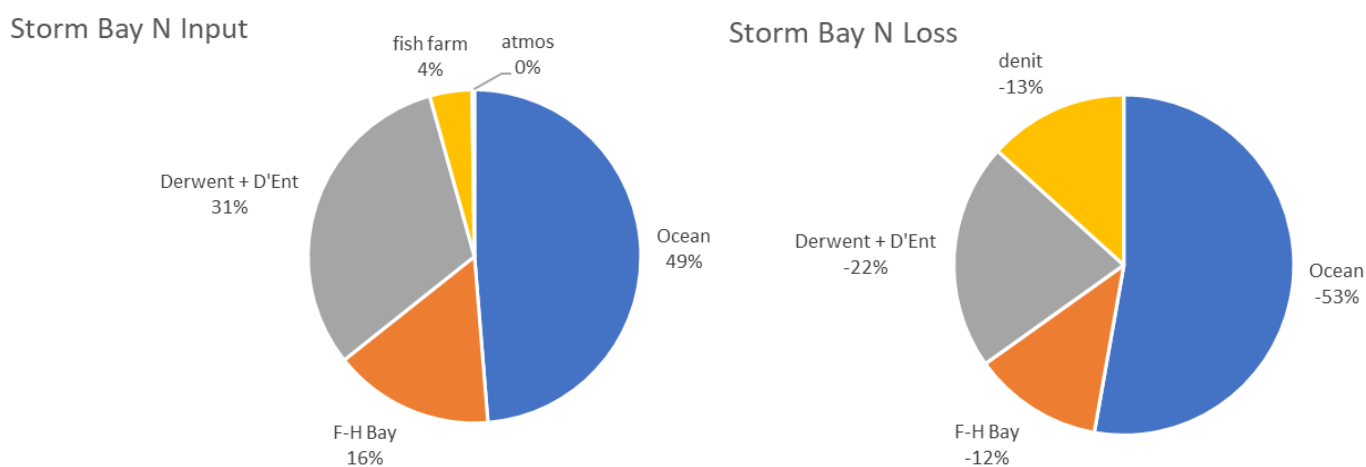
Figure 4.107 Mean annual input and loss terms in the Storm Bay nitrogen budget for 2016-2019 [fluxes through ocean, Fredrick Henry Bay and Derwent-D'Entrecasteaux Channel sections; input from Storm Bay fish farms; loss by denitrification; input from atmospheric deposition].

Summary plots for proportional loads and losses to Storm Bay are shown in Figure 4.107. Ocean input to Storm Bay accounts for 49% of the total nitrogen load, followed by fluxes from the Derwent and D'Entrecasteaux Channel systems (which includes some of the river, sewerage and fish farm nitrogen discharged in these systems). Fish farm nitrogen contributed on average 4% of the total load to Storm Bay and for completeness, atmospheric input was 0.2%. Most nitrogen is lost from Storm Bay by transport to the ocean (53%) and transport into the Derwent and D'Entrecasteaux Channel system (22%). Denitrification accounts for 13% of the total loss of nitrogen from Storm Bay.

A summary schematic shows the net fluxes of nitrogen into (+ve) and out of (-ve) Storm Bay for the period 2016-2019 (Figure 4.108). During this period the Storm Bay region was not in steady state and in all years there was a net export or erosion of total nitrogen from the Storm Bay area into other regions.
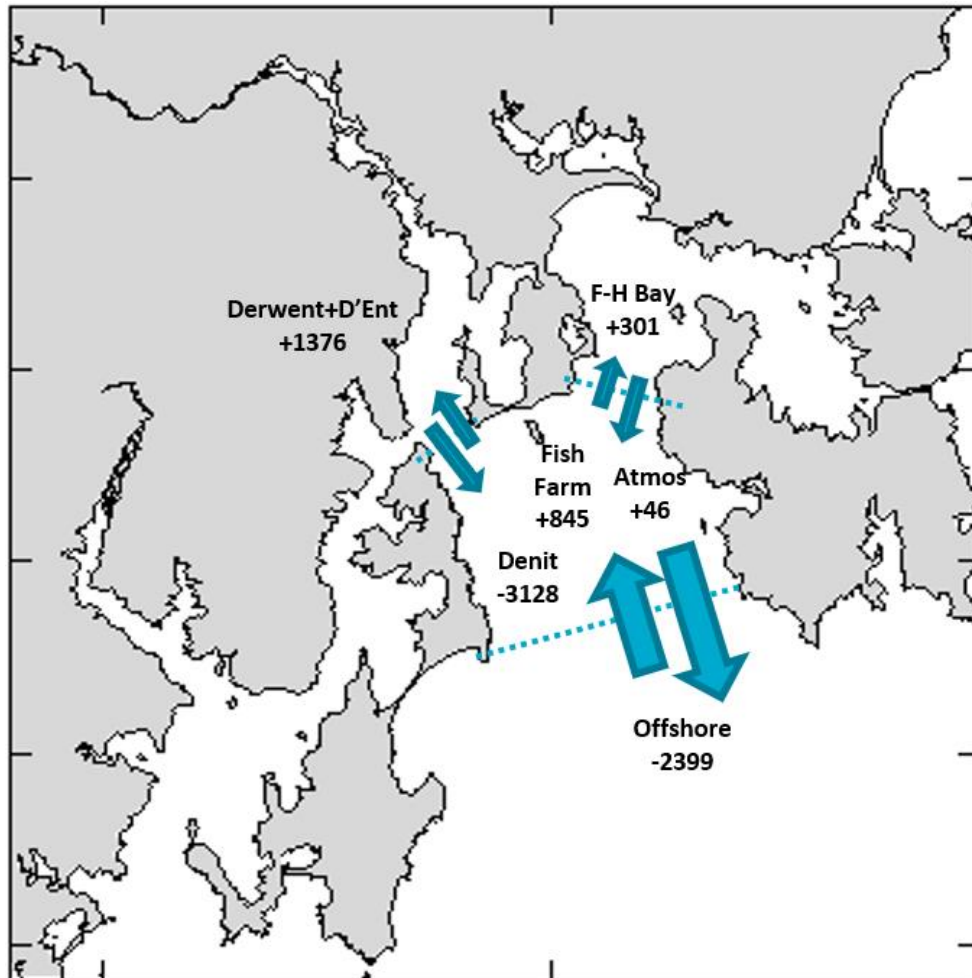
Figure 4.108 Summary of mean annual net fluxes of nitrogen (tN/y) into (+ve) and out of (-ve) Storm Bay for the period 2016-2019 [fluxes through ocean, Fredrick Henry Bay and Derwent-D'Entrecasteaux Channel sections; input from Storm Bay fish farms; loss by denitrification; input from atmospheric deposition].

4.6   Storm Bay Scenario Simulations

The Storm Bay model has been used to explore the impact of a number of alternative management scenarios on water quality in Storm Bay. Specific objectives for the scenario simulations were:

1. To quantify the impact of natural and historical anthropogenic nutrient supply on water quality (e.g. chlorophyll, nutrients, light penetration & dissolved oxygen concentration).
2. To predict plausible future impacts of anthropogenic nutrient supply on water quality under various management scenarios.
3. Inform the MAREE desktop emulator being developed in the FRDC Storm Bay Decision Support Tools project (alongside a number of other bespoke simulations).

4.6.1   Scenario selection and parameterisation

The EPA, NRE Marine Farming Branch, FRDC and researchers at CSIRO and IMAS all provided input and discussed a number of relevant scenarios with the 5 highest priority scenarios listed in Table 4.11. Each model run covered a 5 year period, Jan 2015 – Dec 2019 with actual meteorology, ocean and river forcing,

so as to encompass recent seasonal and interannual variability in ocean circulation, river flow and weather conditions.

Table 4.11 Summary of model runs and scenarios to characterise current, historical and projected water quality in Storm Bay under various management regimes.

	Scenario	River Load	STP + Ind. load	Farm Load	Purpose	Analysis
1	2015-20 Hindcast Simulation [Tasse77K]	2015-2020	2015-20	2015-20	Calibration run	Monthly mean [or 90 percentile] (of 5 years) WQ & interannual variability [Chl, DIN, DIP, bottom water Oxygen, light penetration] Nitrogen budget for Storm Bay
2	Pre-Development (near Pristine) [Tasse78K]	2015-2020	none	none	Quantify impact of anthropogenic loads on WQ in Storm Bay	Monthly mean anomaly cf #3 [or 90 percentile] (of 5 years) WQ & interannual variability [Chl, DIN, DIP, bottom water Oxygen, light penetration] Nitrogen budget for Storm Bay
3	Pre-Storm Bay Development (c.2013) [Tasse82K]	2015-2020	2015 load repeated each year	2013 loads repeated each year (farms in Huon, D'Ent & Nubeena)	Quantify impact of anthropogenic load (circa 2013) on WQ in Storm Bay	Monthly mean [or 90 percentile] (of 5 years) WQ & interannual variability [Chl, DIN, DIP, bottom water Oxygen, light penetration] Nitrogen budget for Storm Bay
4	Post-Storm Bay development: 2020+2ktN in SB [Tasse80K]	2015-2020	2020 load repeated each year	2020 loads in Huon & D'Ent plus 2275tN in SB, repeated each year	Predict plausible future impacts of anthropogenic loads on WQ in Storm Bay	Monthly mean anomaly cf #3 [or 90 percentile] (of 5 years) WQ & interannual variability [Chl, DIN, DIP, bottom water Oxygen, light penetration] Nitrogen budget for Storm Bay
4.5	Post-Storm Bay development: 2020+3ktN in SB [Tasse87K]	2015-2020	2020 load repeated each year	2020 loads in Huon & D'Ent plus 3286tN in SB, repeated each year	Predict plausible future impacts of anthropogenic loads on WQ in Storm Bay	Monthly mean anomaly cf #3 [or 90 percentile] (of 5 years) WQ & interannual variability [Chl, DIN, DIP, bottom water Oxygen, light penetration] Nitrogen budget for Storm Bay
5	Post-Storm Bay development: 2020+4.5ktN in SB [Tasse81K]	2015-2020	2020 load repeated each year	2020 loads in Huon & D'Ent plus 4550tN in SB, repeated each year	Predict plausible future impacts of anthropogenic loads on WQ in Storm Bay	Monthly mean anomaly cf #3 [or 90 percentile] (of 5 years) WQ & interannual variability [Chl, DIN, DIP, bottom water Oxygen, light penetration] Nitrogen budget for Storm Bay

The naming convention for each Post-Storm Bay development scenario clarifies the adjacent waterway fish farm load (2020 load) plus the additional total fish farm nitrogen load discharged in Storm Bay as approximately 2ktN, 3ktN and 4.5ktN for scenarios #4, #4.5 and #5 respectively.

Fish farm waste in all scenarios conmprises of dissolved nitrogen, dissolved phosphorous, labile particulate nitrogen, labile particulate phosphorous and labile particulate carbon. Discharge amounts were calculated from fish feed data (provided by EPA) for hindcast periods and from future waste load projections (provided by EPA) for Post-Storm Bay development scenarios. For the Post-Storm Bay development scenarios, salmon farm waste was distributed across leases in Storm Bay according to Table 4.12 [for completeness details of the dissolved fraction are resolved in Table 4.13, and the particulate fraction in Table 4.14]. For Tassal the N and P load in Nubeena was determined from 2020 feed data; the remaining scenario allocation for Tassal was equally assigned to SB277, SB278, SB279, SB280. For Petuna the allocation was wholly assigned to SB282. For HAC the scenario allocation was equally divided between SB281 and SB261 lease location (noting that the HAC SB261 lease is actually 4 'patches' in the model) (Table 4.15, Figure 4.109).

Table 4.12: Scenario loads of total (dissolved + particulate) nitrogen allocated to each salmon company for leases in Storm Bay (including Nubeena).

Storm Bay Leases	#2 Pre-Development tN/y	#3 Pre-SB (c.2013) tN/y	#4 2020+2ktN in SB tN/y	#4.5 2020+3ktN in SB tN/y	#5 2020+4.5ktN in SB tN/y
Tassal (incl. Nubeena)	0	121	669	986	1337
HAC	0	0	1148	1643	2295
Petuna	0	0	459	657	918
All	**0**	**121**	**2275**	**3286**	**4550**

Table 4.13 Scenario loads of dissolved inorganic nitrogen allocated to each salmon company for leases in Storm Bay (including Nubeena).

Storm Bay Leases	#2 Pre-Development tN/y	#3 Pre-SB (c.2013) tN/y	#4 2020+2ktN in SB tN/y	#4.5 2020+3ktN in SB tN/y	#5 2020+4.5ktN in SB tN/y
Tassal (incl. Nubeena)	0	84	467	689	934
HAC	0	0	802	1147	1603
Petuna	0	0	321	459	641
All	**0**	**84**	**1589**	**2295**	**3178**

Table 4.14 Scenario loads of particulate nitrogen allocated to each salmon company for leases in Storm Bay (including Nubeena).

Storm Bay Leases	#2 Pre-Development tN/y	#3 Pre-SB (c.2013) tN/y	#4 2020+2ktN in SB tN/y	#4.5 2020+3ktN in SB tN/y	#5 2020+4.5ktN in SB tN/y
Tassal (incl. Nubeena)	0	36	202	297	403
HAC	0	0	346	495	692
Petuna	0	0	138	198	277
All	**0**	**36**	**686**	**991**	**1372**

Table 4.15: Storm Bay Lease locations used in the scenario simulations

Leases	Name	Latitude	Longitude
Tassal (incl. Nubeena)	SB277	147.6230	-43.1344
	SB278	147.6128	-43.1424
	SB279	147.6414	-43.1324
	SB280	147.6397	-43.1409
	SB190	147.6953	-43.1101
HAC	SB261	147.4436	-43.1846
	SB281	147.4268	-43.1212
Petuna	SB282	147.5517	-43.1099
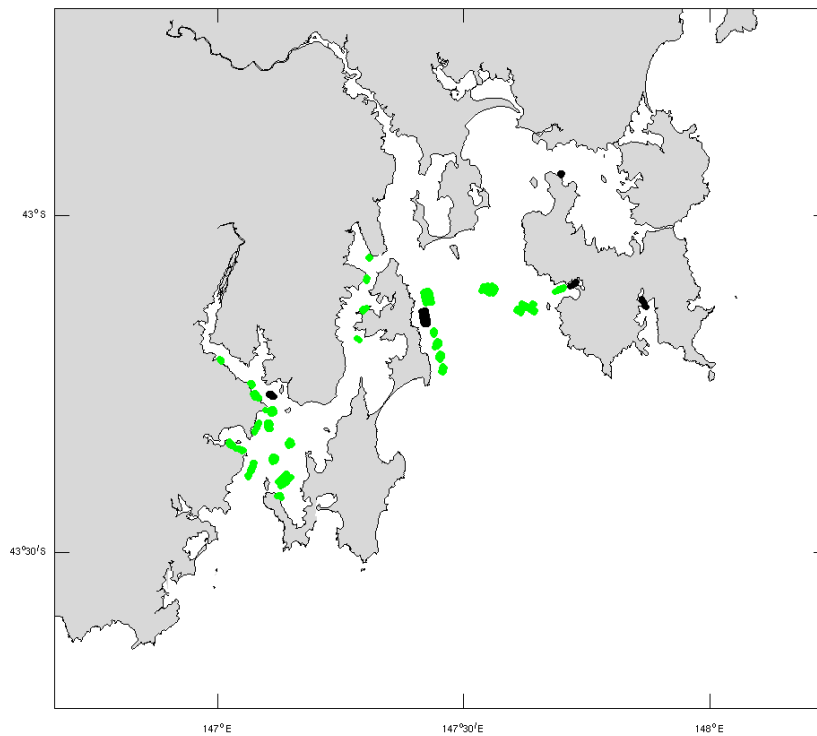
Figure 4.109: Fish Farm lease locations used in the Post-Storm Bay scenario simulations comprising active fish farms in 2020 plus future lease sites in Storm Bay (green); empty sites are shown in black.

For the Post-Storm Bay scenarios the temporal discharge at Storm Bay leases was scaled over an annual cycle following the pattern in production at HAC leases in 2020; using this scaling, waste load in November was roughly double the load in January and the total annual discharge matched the details in Tables 4.12. In addition to the prescribed Storm Bay salmon farm loads the Post-Storm Bay scenario simulations also included STP and Industry point source discharge for 2020 and salmon farm loads at sites throughout the Huon Estuary and D'Entrecasteaux Channel for 2020 (Figure 4.110).

For each scenario, the model simulation ran for the period Jan 2015 – Dec 2019 with actual meteorology, ocean and river forcing. For each scenario annual cycles of prescribed STP, Industry and fish farm loads were repeated identically for each year of the simulation.

The Storm Bay biogeochemical model runs at ~52:1 (52 days simulated in 1 day real time), with each 5 year model run requiring ~35 days of uninterrupted compute time on the NCI in Canberra. Each model scenario simulation generated ~1.5TB of model output, requiring dedicated storage and efficient analysis scripts to provide the interpretation of results. To rapidliy identify differences between simulations, anomalies

between scenarios were calculated relative to the *#3 Pre-Storm Bay (c.2013)* scenario as detailed in Table 4.16.

Scenario STP, Industry & Fish Farm Loads

Total N load tN/y

	Pre-Development	Pre-SB (c.2013)	2020+2ktN in SB	2020+3ktN in SB	2020+4.5ktN in SB
Storm Bay	0	0	2018	3029	4293
Nubeena	0	121	257	257	257
D'Ent	0	1430	2947	2947	2947
Huon	0	456	313	313	313
STP+Ind	0	657	594	594	594

Scenario STP, Industry & Fish Farm Loads

Total P load tP/y

	Pre-Development	Pre-SB (c.2013)	2020+2ktN in SB	2020+3ktN in SB	2020+4.5ktN in SB
Storm Bay	0	0	378	567	803
Nubeena	0	23	48	48	48
D'Ent	0	268	551	551	551
Huon	0	85	59	59	59
STP+Ind	0	102	86	86	86

Figure 4.110 Annual anthropogenic total nitrogen (top) and phosporous (bottom) load from STP+Industry (green) and fish farms in sub-regions of the model (other colours) for each scenario simulation. Note that all Post-Storm Bay scenarios had identical 2020 STP+Industry loads and 2020 fish farm loads in Nubeena, D'Entrecasteaux and Huon.

Table 4.16 Calculation of anomalies between model simulations to rapidly identify differences in water quality resulting from each scenario.

Hindcast simulation #1 – Pre-SB (c.2013) #3	=	Progressive impact of recent anthropogenic loads on WQ since circa 2013
Pre-development #2 – Pre-SB (c.2013) #3	=	Impact of anthropogenic loads surrounding Storm Bay (circa 2013) on WQ
Post-development: 2020+2ktN in SB #4 – Pre-SB (c.2013) #3	=	Impact of 2020 STP, Industry, Fish Farms, +2ktN load in SB, on WQ since 2013
Post-development: 2020+3ktN in SB #4.5 – Pre-SB (c.2013) #3	=	Impact of 2020 STP, Industry, Fish Farms, +3ktN load in SB, on WQ since 2013
Post-development: 2020+4.5ktN in SB #5 – Pre-SB (c.2013) #3	=	Impact of 2020 STP, Industry, Fish Farms, +4.5ktN load in SB, on WQ since 2013

4.6.2 Scenario results and analysis

To summarise the key water quality impacts of varying fish farm loads in Storm Bay a selection of anomaly plots and analysis are presented; additional plots and analysis including 10th and 90th percentile distributions are provided in Appendix A8.

Spatial variation in water quality with changing farm load

The difference in water quality between the *#3 Pre-SB (c.2013)* scenario and all other model scenarios was evaluated and shows systematic changes in water properties with increasing anthropogenic nutrient load.

Mean monthly surface dissolved inorganic nitrogen increased in all seasons with increased nutrient load (Figure 4.111a and Figure 4.111b). Storm Bay and the south D'Entrecasteaux Channel showed the greatest increase in surface DIN (>20%, > 14 mg m^{-3}), due to increases in farm loads between 2013 – 2020 plus the addition of future loads in Storm Bay. In the Huon estuary surface DIN decreased due to a reduction in the number of active fish farms in this area since 2013 and in future projections. The *#2 Pre-Development* scenario showed a reduction in surface DIN in the Derwent, Huon and D'Entrecasteaux Channel relative to the *#3 Pre-SB (c.2013)* scenario which included 2015 sewerage, industry and 2013 fish farm nutrient loads. Note that the increase in Derwent surface DIN in the Post-Storm Bay scenarios *#4, #4.5* and *#5* is mostly due to changes in fish farm load as there was a net reduction in sewerage and industry load between 2015 and 2020.
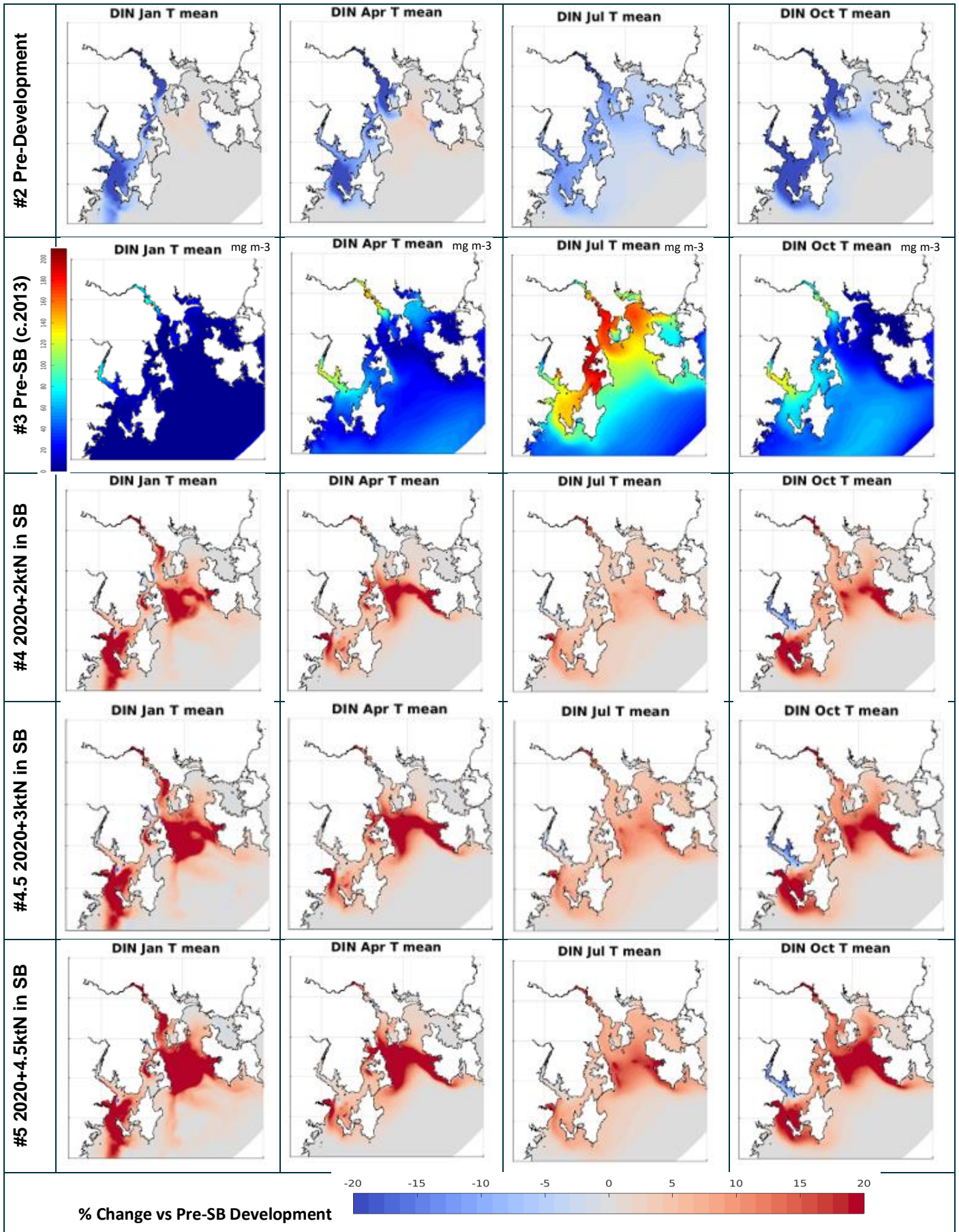
Figure 4.111a Percent change in simulated monthly mean surface dissolved inorganic nitrogen for each scenario relative to #3 Pre-SB (c.2013) in summer, autumn, winter and spring (Jan, Apr, Jul, Oct).
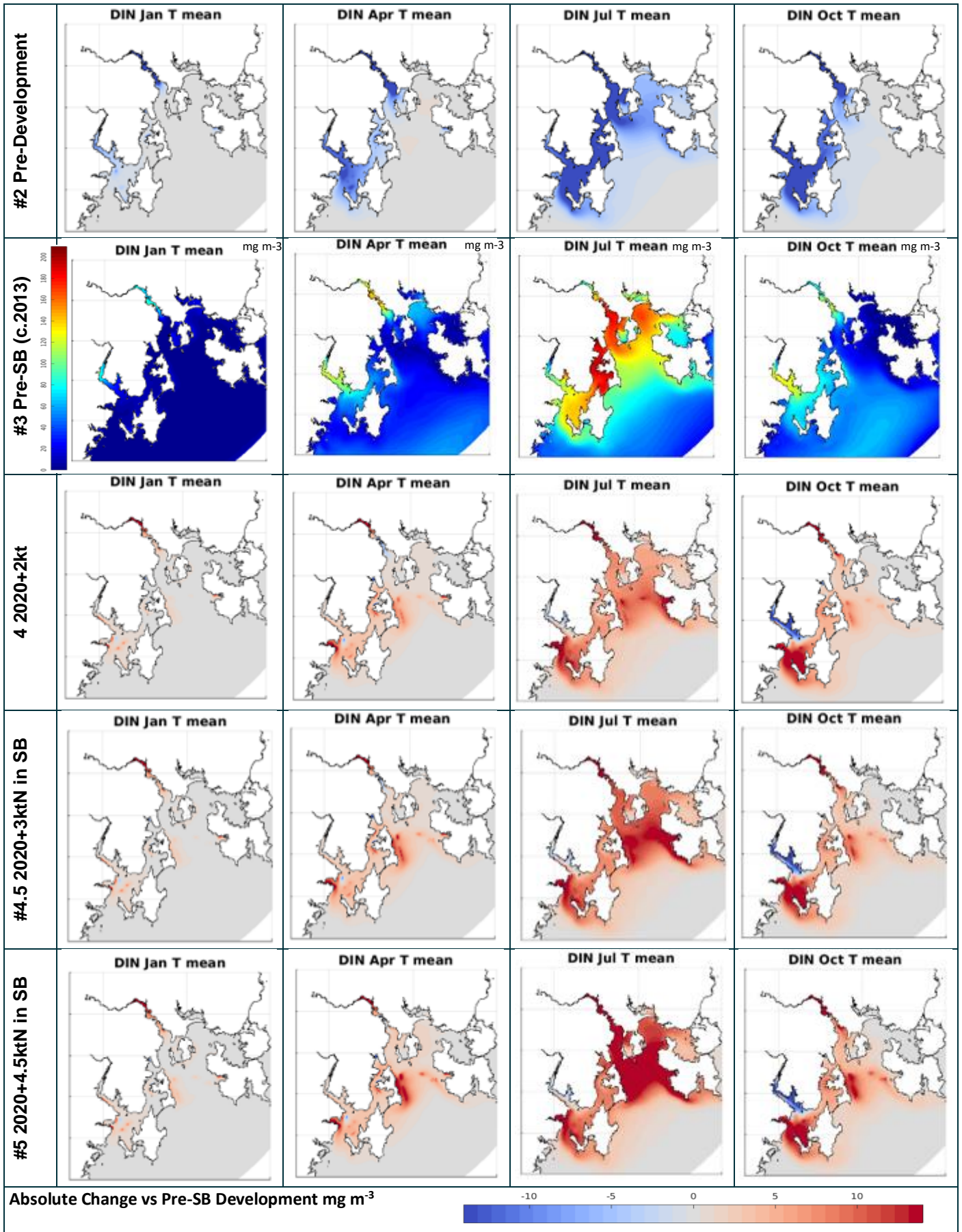
Figure 4.111b Absolute change in simulated monthly mean surface dissolved inorganic nitrogen for each scenario relative to #3 Pre-SB (c.2013) in summer, autumn, winter and spring (Jan, Apr, Jul, Oct).
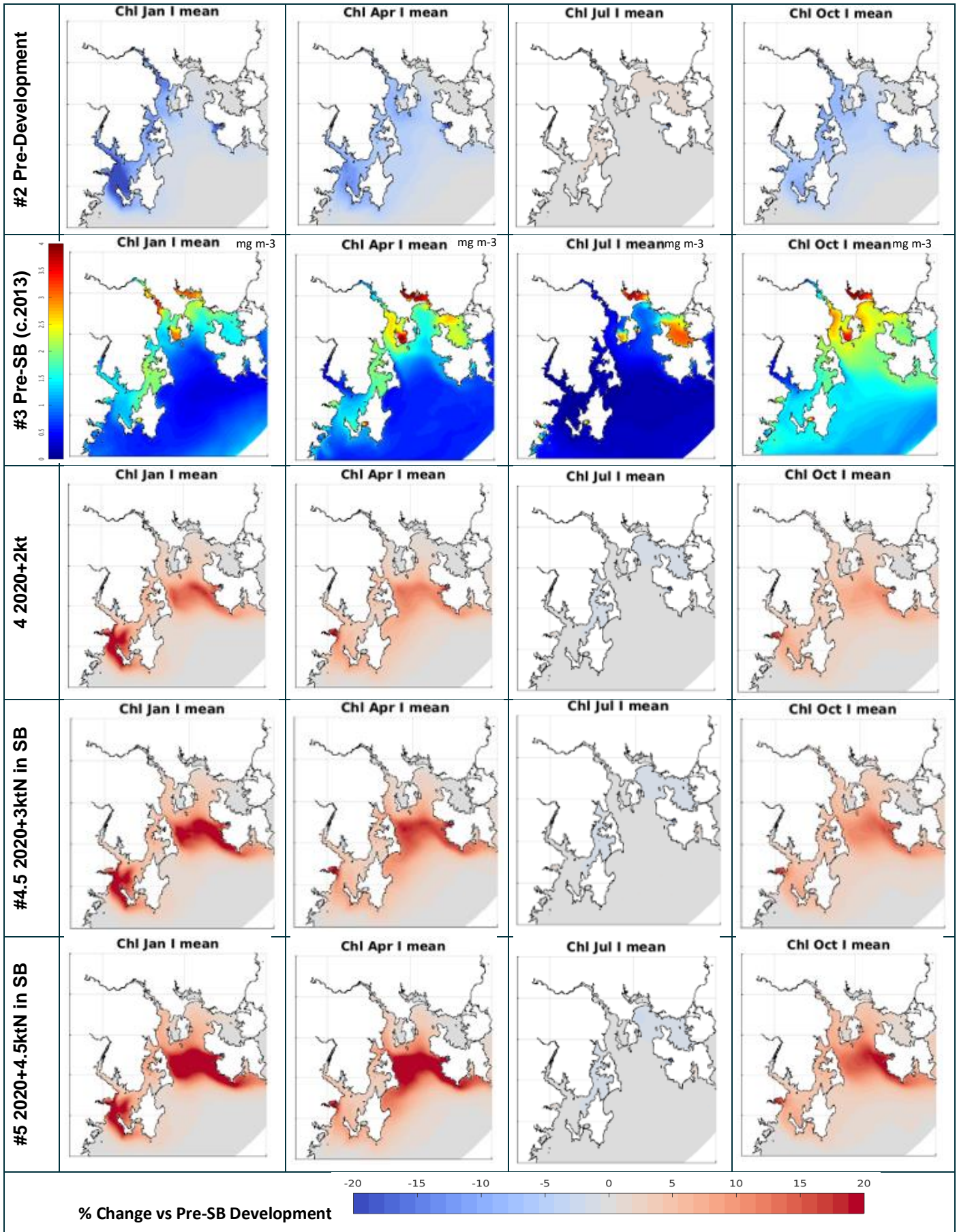
Figure 4.112a Percent change in simulated monthly mean depth averaged chlorophyll (0-12 m) for each scenario relative to #3 Pre-SB (c.2013) in summer, autumn, winter and spring (Jan, Apr, Jul, Oct).
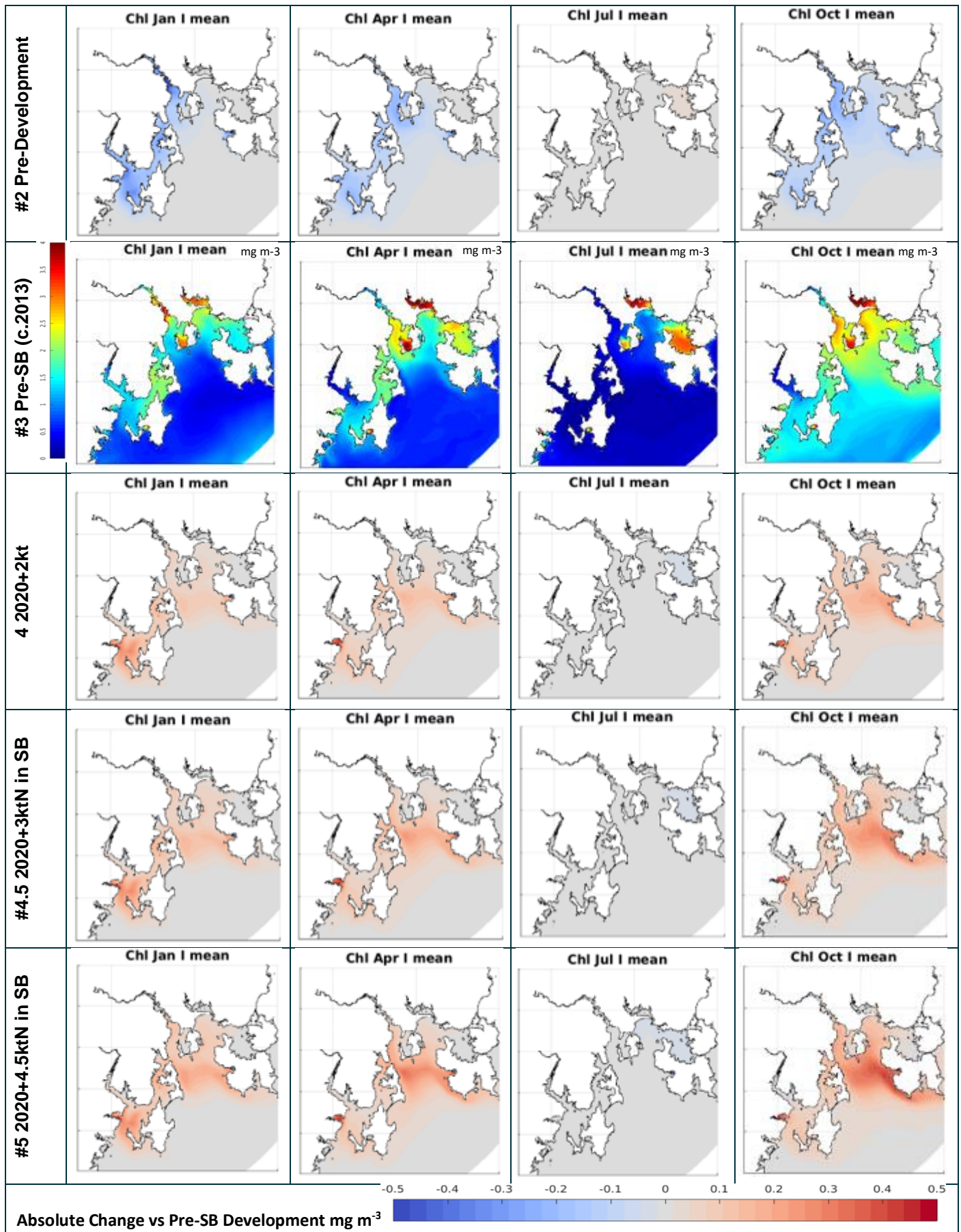
Figure 4.112b Absolute change in simulated monthly mean depth averaged chlorophyll (0-12 m) for each scenario relative to #3 Pre-SB (c.2013) in summer, autumn, winter and spring (Jan, Apr, Jul, Oct).
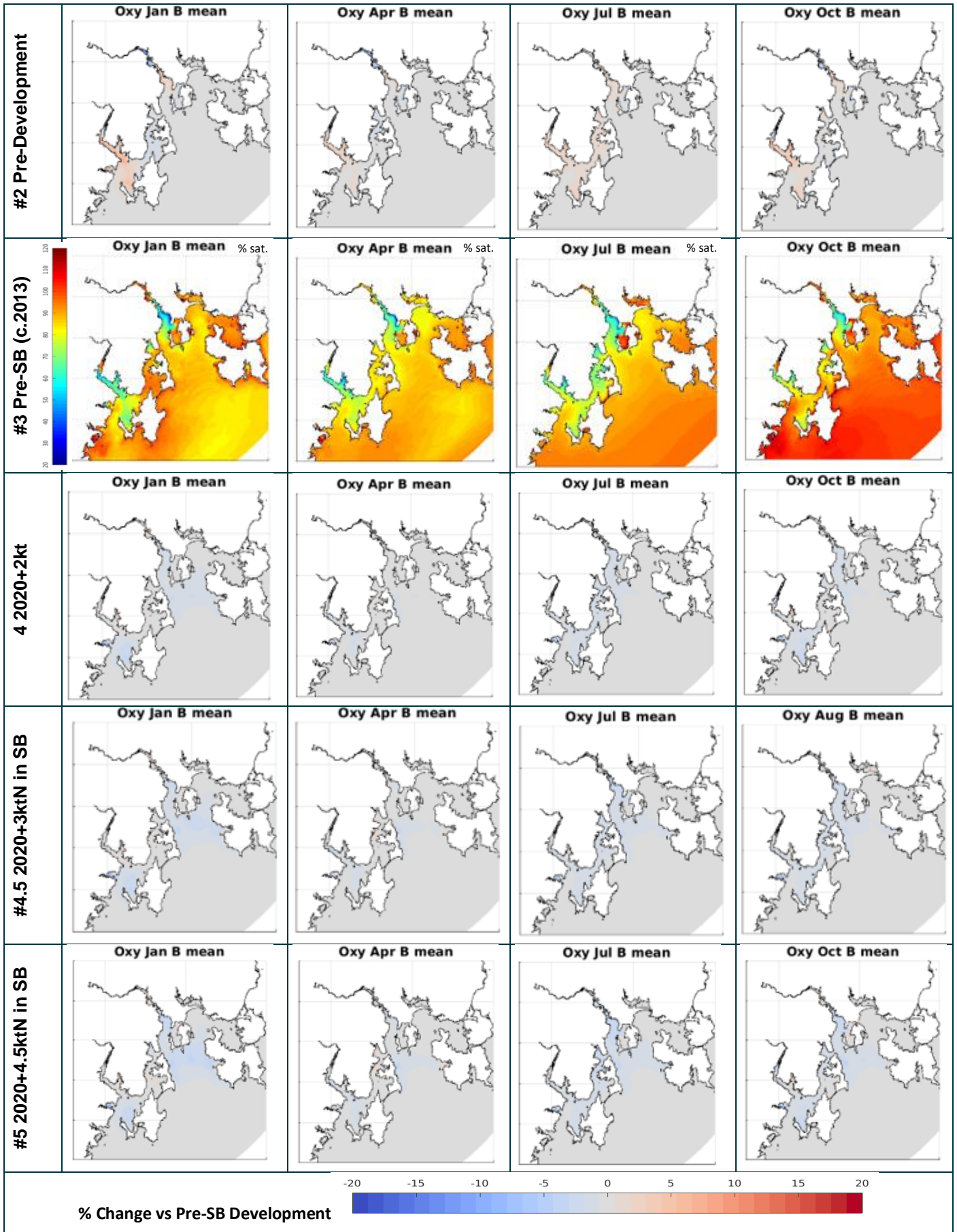
Figure 4.113a Percent change in simulated monthly mean bottom water oxygen saturation for each scenario relative to #3 Pre-SB (c.2013) in summer, autumn, winter and spring (Jan, Apr, Jul, Oct).
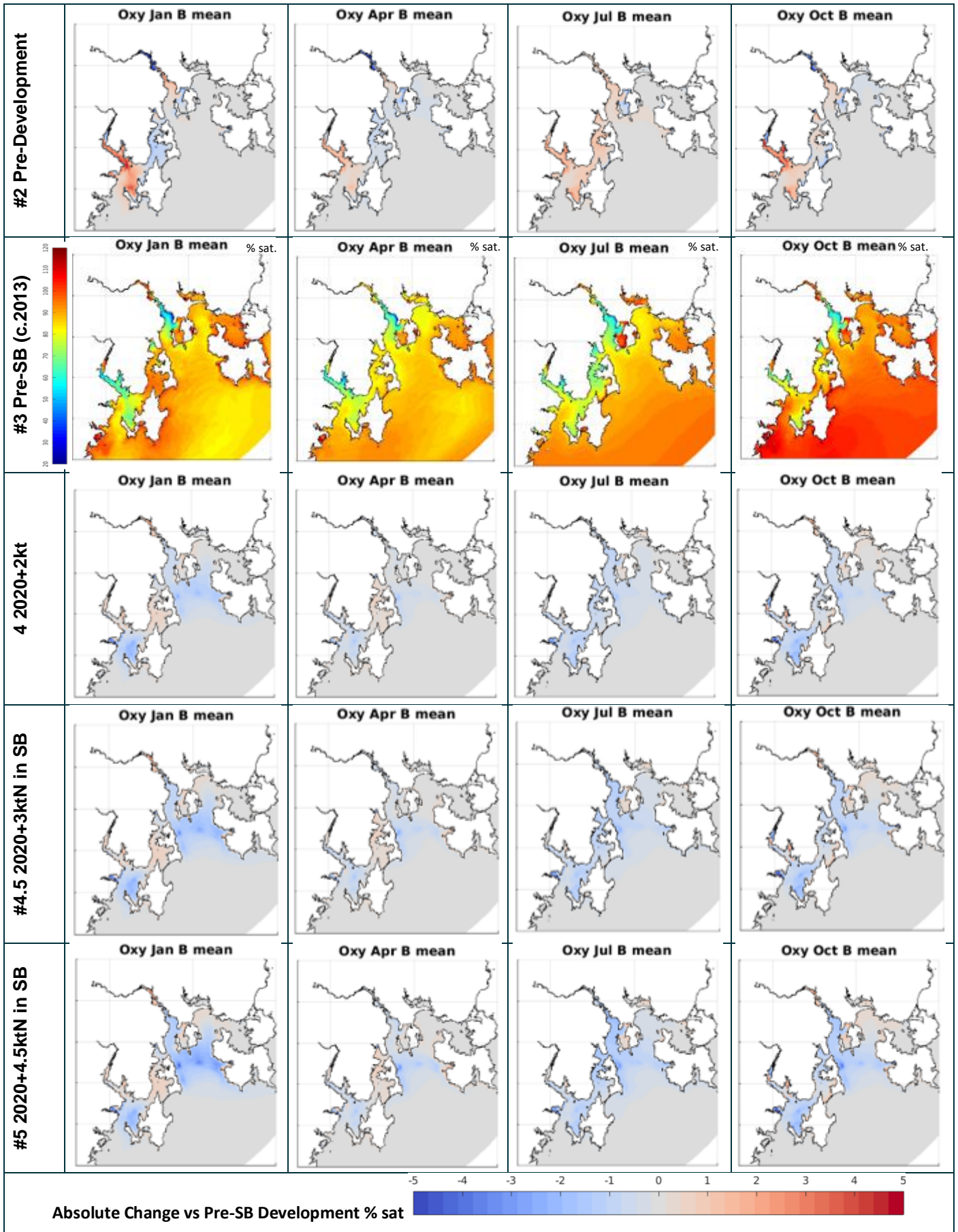
Figure 4.113b Absolute change in simulated monthly mean bottom water oxygen saturation for each scenario relative to #3 Pre-SB (c.2013) in summer, autumn, winter and spring (Jan, Apr, Jul, Oct).
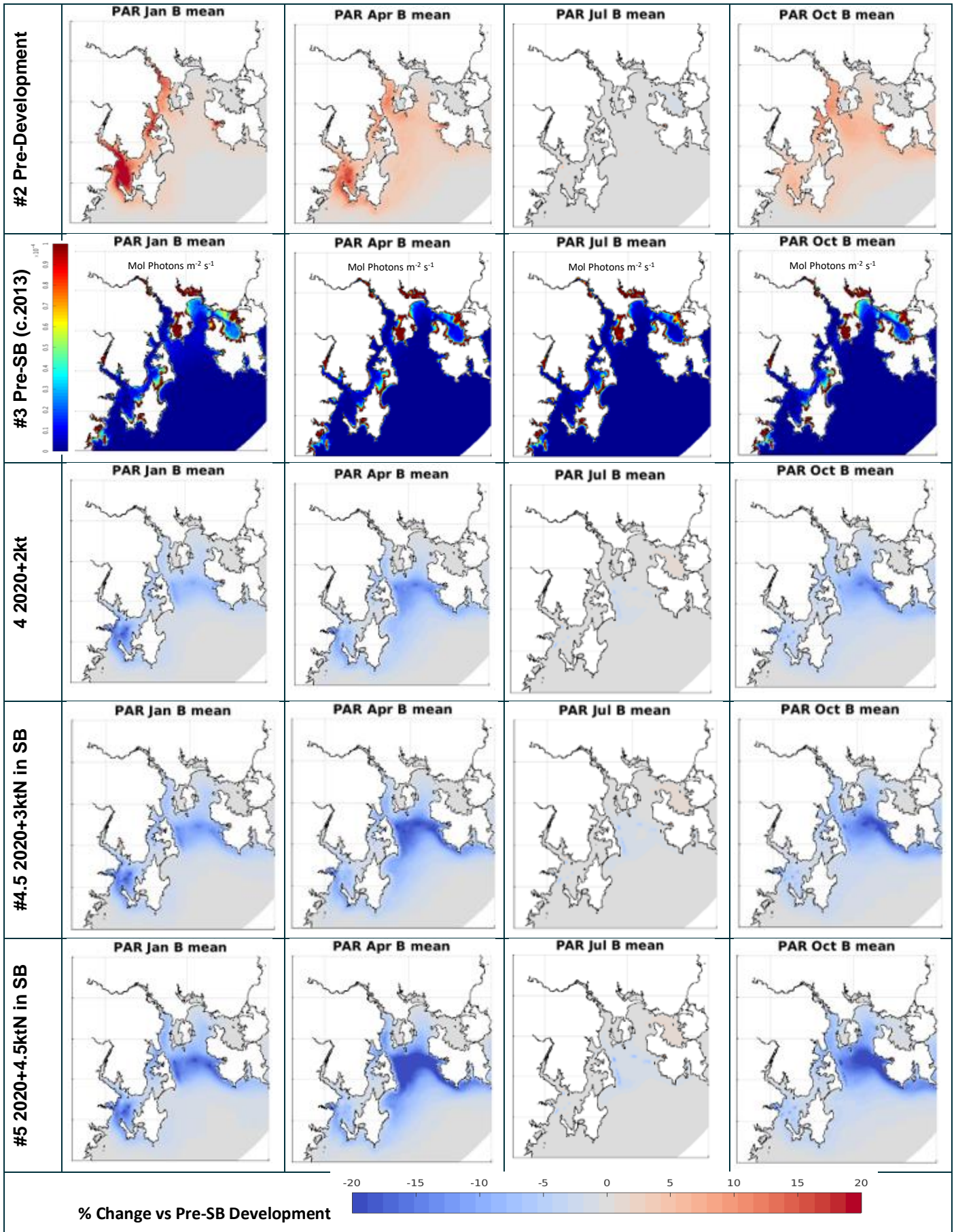
Figure 4.114a Percent change in simulated monthly mean bottom PAR for each scenario relative to #3 Pre-SB (c.2013) in summer, autumn, winter and spring (Jan, Apr, Jul, Oct).
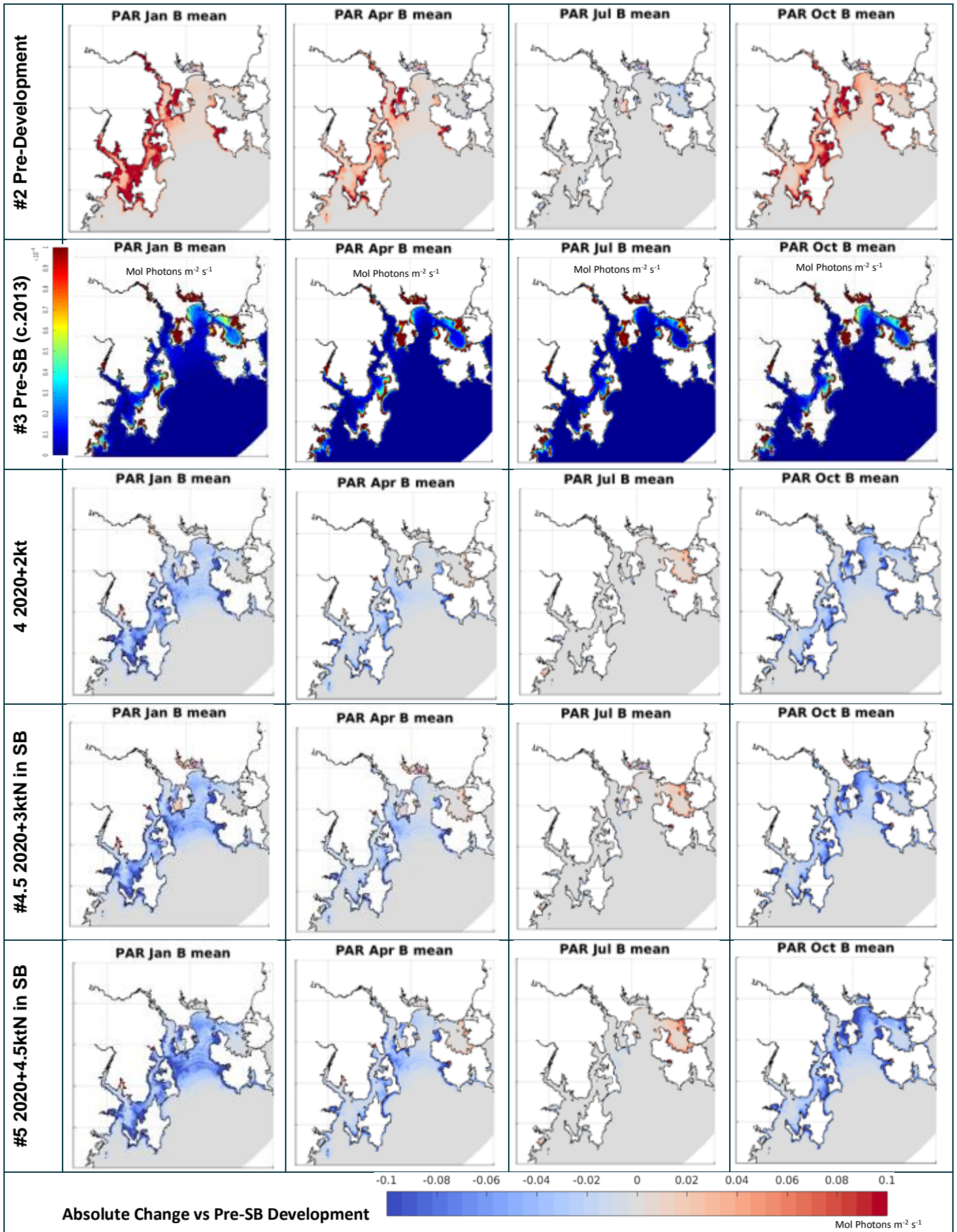
Figure 4.114b Absolute change in simulated monthly mean bottom PAR for each scenario relative to #3 Pre-SB (c.2013) in summer, autumn, winter and spring (Jan, Apr, Jul, Oct).

Simulated mean monthly depth averaged (0-12 m) chlorophyll showed a systematic increase in spring, summer and autumn with increasing nutrient load (Figure 4.112a and Figure 4.112b). Chlorophyll concentrations were >20 % (>0.5 mg m^{-3}) higher in parts of Storm Bay and the southern D'Entrecasteaux Channel in scenario *#5 2020+4.5ktN in SB* compared with *#3 Pre-SB (c.2013)*. In *#2 Pre-Development* scenario there was a decrease in chlorophyll concentration particularly in the southern D'Entrecasteaux Channel, but also more generally throughout the Huon and Derwent estuaries and in Storm Bay. In winter there was little change in chlorophyll concentration despite the increase in available surface DIN shown in Figures 4.111a & 4.111b; this was likely due to seasonally low levels of PAR and low water temperatures limiting phytoplankton growth.

Bottom water oxygen saturation simulated by the model showed a small systematic decline with increasing nutrient load (Figure 4.113a and Figure 4.113b). There was a small (<5% saturation) reduction in bottom water oxygen saturation in Storm Bay and inshore waters in the Post-Storm Bay scenarios *#4, #4.5* and *#5*, with greatest reductions localised at lease sites in Storm Bay. In the #2 Pre-Development scenario the reduction in nutrient loads resulted in a small increase (<5% saturation) in bottom water oxygen saturation in the Huon Estuary, the southern D'Entrecasteaux Channel and the Derwent Estuary.

Changes to the amount of light reaching the seabed are important to epibenthos, so difference plots for bottom PAR for each scenario are included in Figure 4.114a and Figure 4.114b [note that in deep water the amount of light reaching the seabed is very small and % change will therefore also be a very small absolute value]. There was a systematic decline in the amount of light reaching the seabed with increasing nutrient load to the system due to light attenuation by increased phytoplankton biomass. The absolute reduction in bottom light was greatest in the *#5 2020+4.5ktN in SB* scenario in spring and summer. Conversely bottom light availability increased in the *#2 Pre-Development scenario* linked to the reduction in nutrients, chlorophyll and associated suspended organic matter.

Seasonal variation in water quality in Storm Bay with changing farm load

To investigate any scenario impacts on the seasonal cycle of water quality in Storm Bay, monthly means for all grid cells in the Storm Bay region (brown area in Figure 4.115 inset) for each scenario were plotted adjacent to *#3 Pre-SB (c.2013)* (shown in black).

With increased nutrient loading, DIN and chlorophyll concentrations in Storm Bay increased, and bottom water oxygen saturation and the area of Storm Bay where bottom PAR exceeded 1% surface light declined. For all scenarios surface DIN concentrations in Storm Bay tended to zero in summer, suggesting that the system remained nitrogen limited at this time. With increasing nutrient load, chlorophyll concentrations increased in summer, autumn and spring utilising all the additional surface DIN in summer and fraction of the additional surface DIN in autumn and spring; in winter there was no change in chlorophyll due to seasonally low light levels and cool temperatures limiting phytoplankton growth.

Changes in Storm Bay bottom water oxygen saturation with increasing nutrient load were very small and consistent throughout the year. With increasing nutrient load, the decline in area of Storm Bay where bottom PAR exceeded 1% surface light was most pronounced in summer months.

In Figure 4.115 the box plots show the mean, the 25th to 75th percentile of the data and the range. It is clear from these plots that the spatial (all data in Storm Bay) and temporal (interannual) variation within Storm Bay in any given month exceeds the small but systematic changes in monthly mean due to nutrient enrichment. This suggests that it may be difficult to distinguish changes in water quality due to increased fish farms from natural variability.
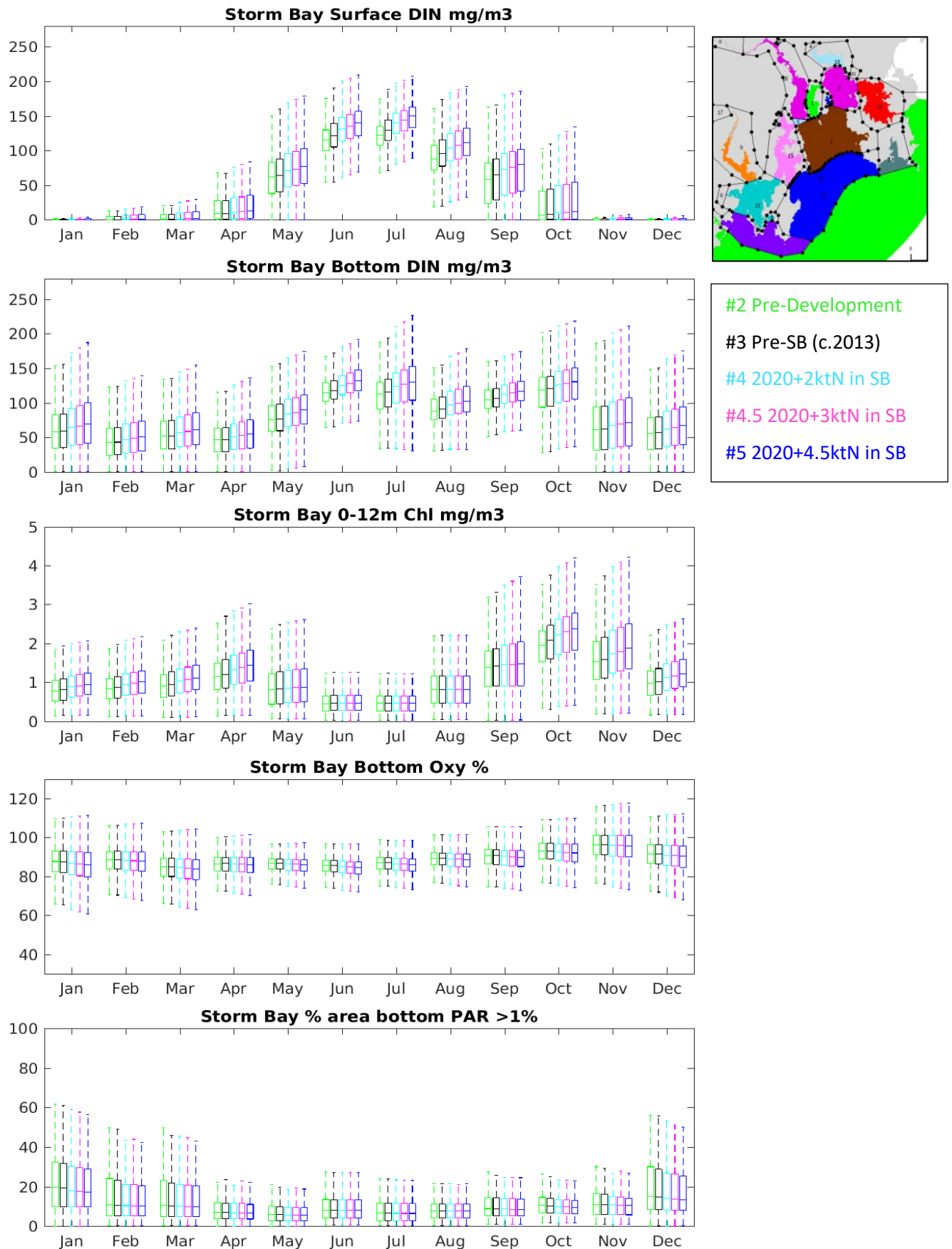
Figure 4.115 Seasonal variation in water quality in Storm Bay for each model scenario. Box plot shows mean, 25th and 75th percentiles and range for all Storm Bay model cells (brown region in inset map) over 2015-2019; for light transmission the % area of Storm Bay where bottom PAR exceeds 1% surface light is shown.

To summarise the systematic changes in water quality in Storm Bay for each scenario, the mean change was calculated for each modelled substance (Table 4.17). The largest relative change was for surface DIN (the sum of ammonia + nitrate) which increased by between 12% (4 mg m^{-3}) to 25% (7.7 mg m^{-3}) in the Post-Storm Bay development scenarios *#4, #4.5* and *#5*. With increasing nutrient load in *#5 2020+4.5ktN in SB* scenario, chlorophyll increased by 10% (0.12 mg m^{-3}), bottom oxygen declined 1% (76.1 mg m^{-3}) and the area of Storm Bay where bottom PAR exceeded 1% surface light declined by 5% (3768.7 m^2).

Table 4.17 Annual mean values for #3 Pre-SB (c.2013) for all model grid cells in Storm Bay from 2015 – 2019; coloured values are absolute difference vs. #3 Pre-SB (c.2013) for matched bar colours in Figure 4.115; negative values denote a reduction.

Storm Bay Surface	Pre-SB Development (c.2013)		S1 Pre-Development	2020+2ktN in SB	2020+3ktN in SB	2020+4.5ktN in SB	
NO3	36.5	mg/m3	-2.0	2.5	3.5	4.7	mg/m3
NH4	8.2	mg/m3	-0.8	1.4	2.1	3.0	mg/m3
DIP	9.1	mg/m3	-0.3	0.3	0.5	0.7	mg/m3
Chl	1.0	mg/m3	-0.04	0.06	0.09	0.12	mg/m3
Oxy_sat	97.5	%	-0.3	0.2	0.3	0.4	%
Oxygen	8131.2	mg/m3	-24.1	12.3	17.3	23.5	mg/m3
PAR	12.4	% area > 1%	0.24	-0.43	-0.60	-0.78	% area > 1%
DIN	44.7	mg/m3	-2.8	4.0	5.6	7.7	mg/m3

Storm Bay Bottom	Pre-SB Development		S1 Pre-Development	2020+2ktN in SB	2020+3ktN in SB	2020+4.5ktN in SB	
NO3	46.5	mg/m3	-1.0	2.2	3.0	4.0	mg/m3
NH4	33.4	mg/m3	-0.8	3.4	4.8	6.5	mg/m3
DIP	14.3	mg/m3	-0.2	0.8	1.1	1.5	mg/m3
Chl	1.1	mg/m3	-0.04	0.07	0.10	0.13	mg/m3
Oxy_sat	88.4	%	0.0	-0.5	-0.7	-0.9	%
Oxygen	7360.1	mg/m3	2.1	-38.8	-55.8	-76.1	mg/m3
PAR	1.0	% surface light	0.03	-0.02	-0.03	-0.04	% surface light
DIN	79.9	mg/m3	-1.8	5.6	7.8	10.6	mg/m3

Nutrient budget in Storm Bay with changing farm load

To understand the fate of increasing nutrient load to Storm Bay the total nitrogen budget was calculated for each scenario (Figure 4.116). With increasing nutrient load the ocean influx of nitrogen to Storm Bay declined and the export increased. Export of nitrogen from Storm Bay to Fredrick Henry Bay and the Derwent plus D'Entrecasteaux Channel also increased and some of this loss was returned back into Storm Bay in slightly elevated influx from both of these waterways. There was little change in denitrification between scenarios.

For all scenarios there was a net export or erosion of total nitrogen from the Storm Bay area into other regions. As nutrient load increased in the Post-Storm Bay development scenarios, the net erosion of total nitrogen from Storm Bay declined and more nitrogen was retained in Storm Bay. Relative to *#3 Pre-SB (c.2013)* there was between 7% and 14% more nitrogen retained in Storm Bay in the Post-Storm Bay development scenarios *#4, #4.5* and *#5* during the simulation period.
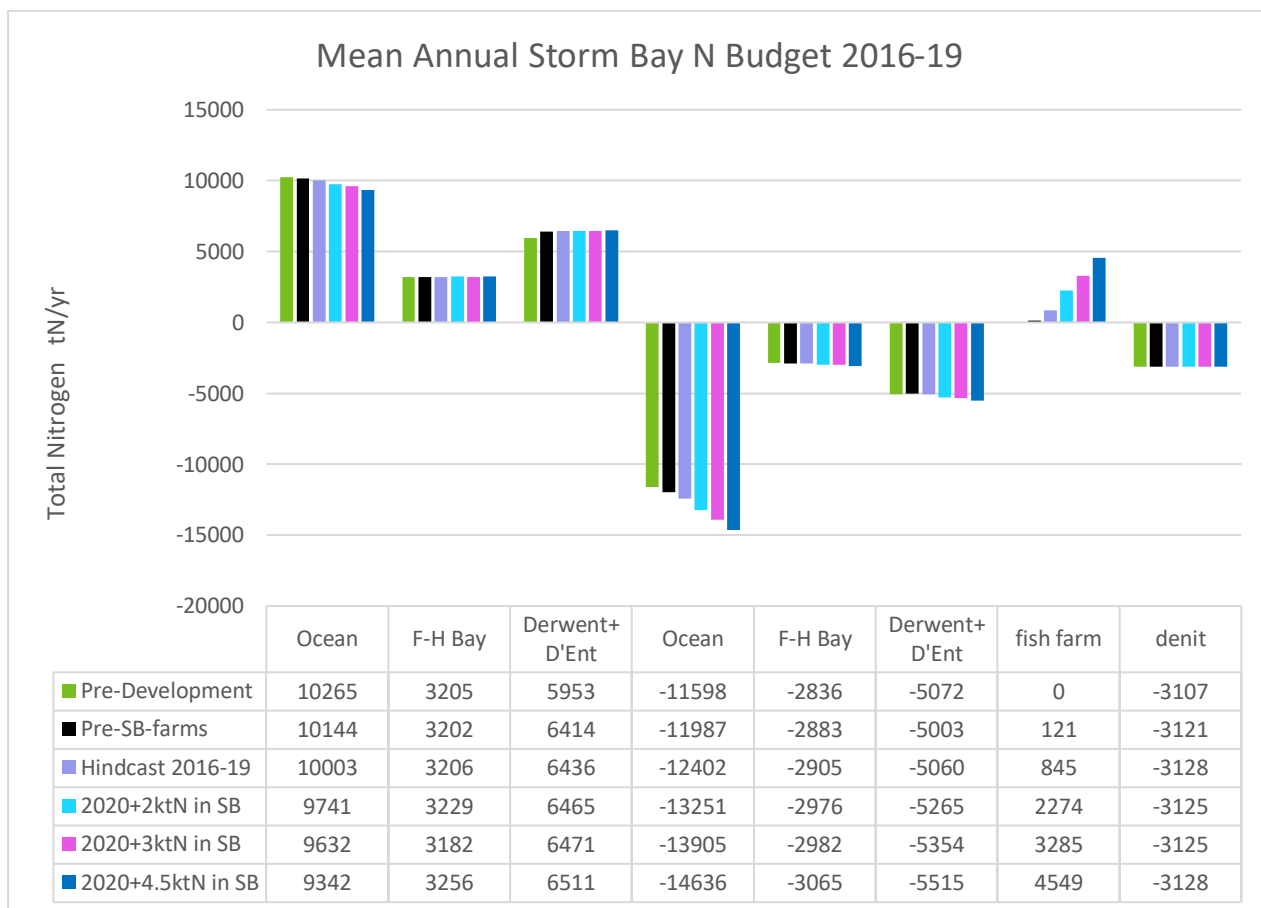
Figure 4.116 Mean annual Storm Bay nitrogen budget for each scenario 2016-2019 [plus 46tN/y atmospheric deposition].

Annual mean chlorophyll in Storm Bay with changing farm load

In previous studies (e.g. Wild-Allen, et al 2010) annual mean near surface chlorophyll concentration has been used as a classification metric for trophic status of a system. This classification was based on Smith (1998) who found:

- oligotrophic conditions when annual mean chlorophyll < 1 mg m^{-3}

- mesotrophic conditions when annual mean chlorophyll was 1–3 mg m^{-3}

- eutrophic conditions when annual mean chlorophyll > 3 mg m^{-3}.

Daily model output from Jan 2015 – Dec 2019 was used to calculate a 5 year annual mean chlorophyll distribution for each scenario (Figure 4.117). In all scenarios, coastal waters throughout the model domain were mostly < 3 mg m^{-3} for annual mean chlorophyll concentration with small areas of higher concentration only found in a few shallow bays where favourable light, nutrients and mixing supported higher phytoplankton biomass. Most of Storm Bay is classified as oligotrophic with some mesotrophic areas in the north and off Nubeena.

With increasing fish farm nutrient load the Post-Storm Bay scenarios showed an increase in the area classified as mesotrophic in Storm Bay (Figure 4.118). For the Pre-Development *2* scenario 31% of Storm Bay was classified as mesotrophic; for the Post-Storm Bay development scenarios #4, #4.5 and #5, the simulated mesotrophic area increased to 40%, 42% and 45% of Storm Bay respectively.

# 2 Pre-Development	#3 Pre-SB (c.2013)	# 4 2020+2ktN in SB	#4.5 2020+3ktN in SB	# 5 2020+4.5ktN in SB
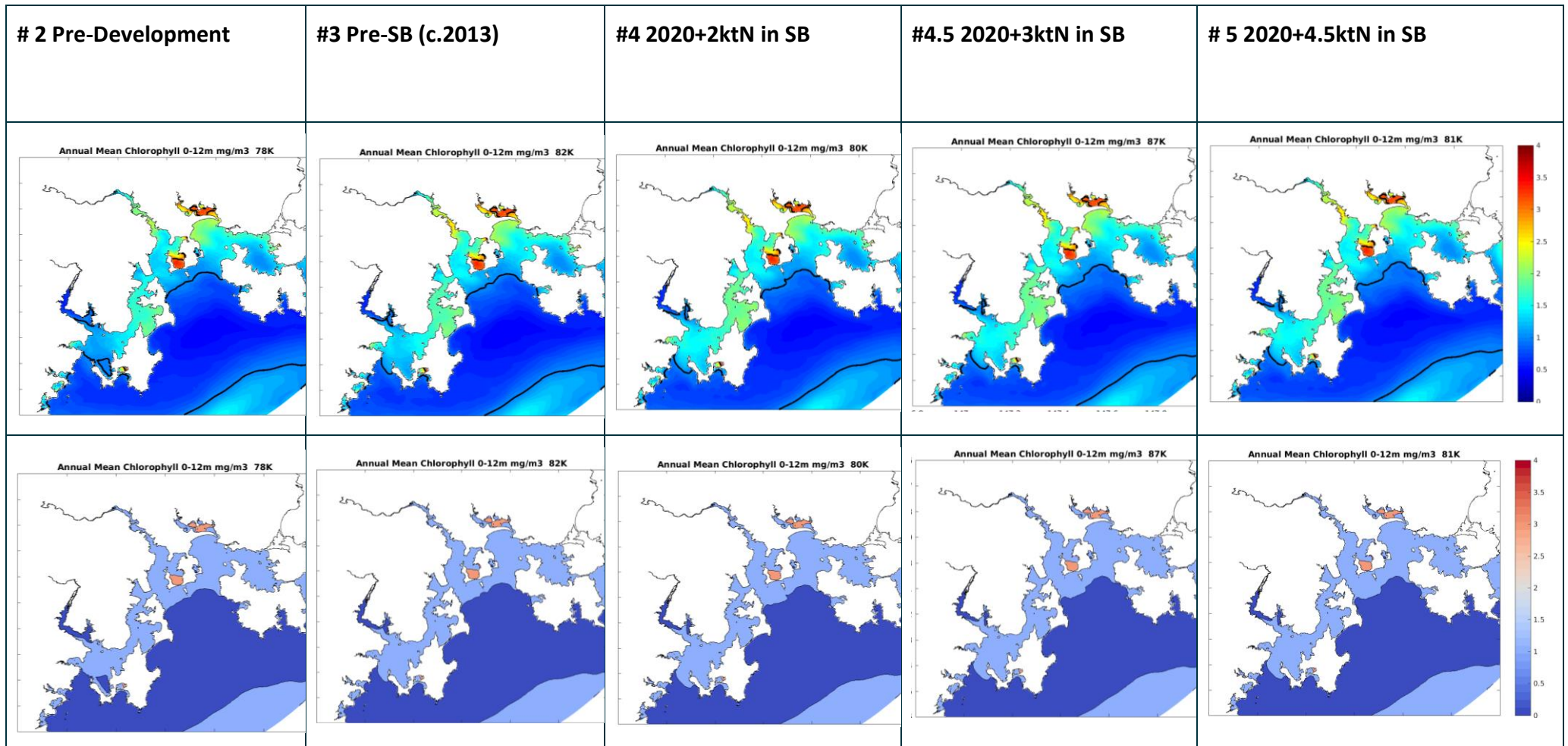
Figure 4.117 Annual mean chlorophyll concentration in the top 12 m of the water column for each model scenario [contour lines are at 1mg m^{-3} and 3mg m^{-3}; lower row of images has simplified colour scheme for oligotrophic (dark blue), mesotrophic (light blue) and eutrophic (light red) classification].

Storm Bay Trophic Status

	Pre Development	Pre-SB Development	2020+2ktN in SB	2020+3ktN in SB	2020+4.5ktN in SB
Eutrophic	0	0	0	0	0
Mesotrophic	31	34	40	42	45
Oligotrophic	69	66	60	58	55
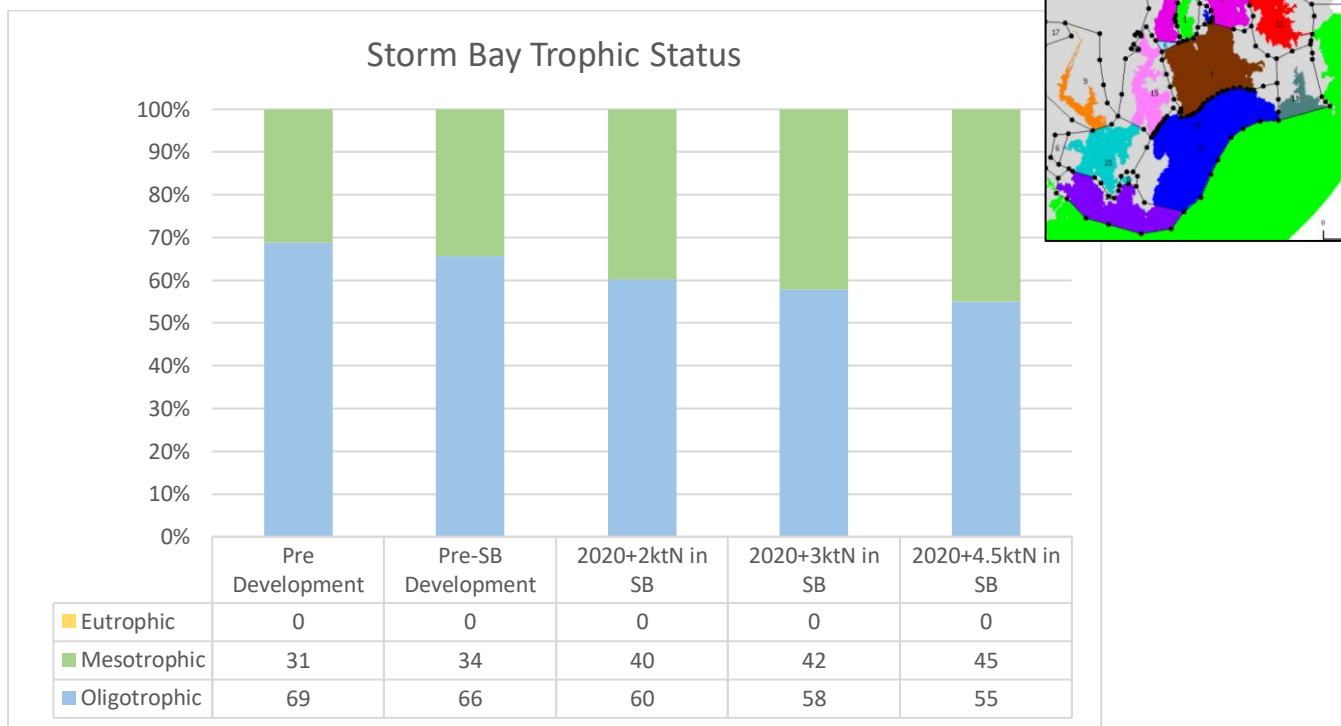
Figure 4.118 Area of oligotrophic (<1 mg m^{-3}) and mesotrophic (1–3m mg^{-3}) annual mean chlorophyll classification (after Smith 1998) in Storm Bay (brown region in inset figure) for each model scenario.

Storm Bay monitoring sites with changing farm load

The seasonal variation in water quality at specific monitoring sites in Storm Bay (Figure 4.119) was analysed for each scenario (e.g. Figures 4.120 – 4.123; Appendix A8). Daily model output from Jan 2015 – Dec 2019 were used to calculate monthly means and show the range of variability at the site over the 5 year model run. In this preliminary analysis we have not subtracted any bias in model results c.f. observations, although relative changes shown are consistent between scenarios.

Default Guideline Values determined for the Bruny Bioregion and corresponding OSRA segment (EPA 2021) for each site location (and each available substance), have been added to the figures for comparison (Figures 4.120 – 4.123). It should be noted that the DGV's have been calculated from a comparatively small set of temporal samples at monitoring site locations within each OSRA segment and are therefore biased by sampling regime and seasonal weather (e.g. may not include data for rough winter conditions). DGV's may therefore be fit for the purpose of comparison with similarly collected water samples, but are likely not fit for the purpose of comparison with model output with high temporal resolution in all seasons. A more considered analysis could use the metrics employed in the generation of the DGV's to derive a 'model specific DGV' and use this to inform analysis of model output with high temporal resolution.

Given the potential offset in model results due to bias c.f. observations, and the mis-match in temporal resolution of model data and data used to generate the DGV's, any conclusions drawn re model deviation from DGV's may be indicative of general trends, but should be treated with caution.
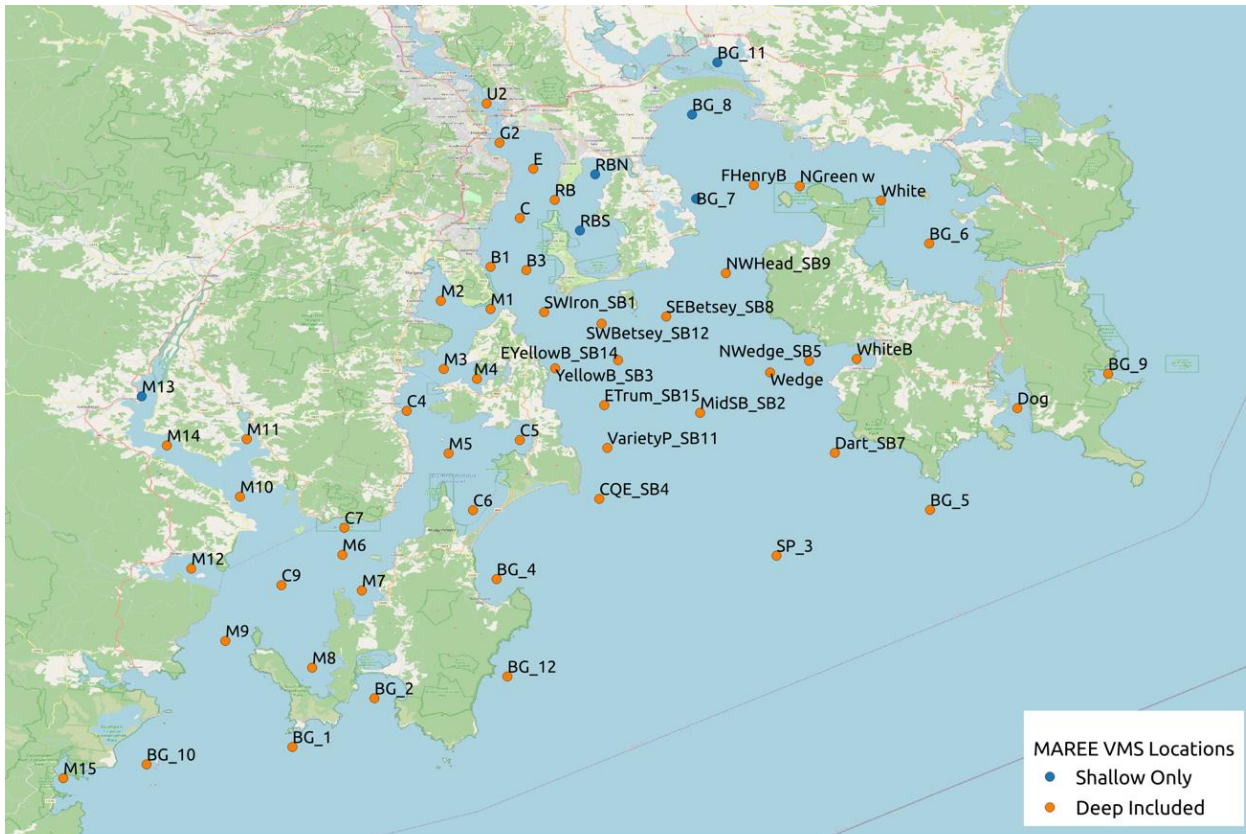
Figure 4.119 Virtual monitoring site locations where model data was saved for preliminary analysis [these data were also used for 'training' the MAREE decision support tool].

At all monitoring stations comparison of scenarios showed a general increase in nutrients and chlorophyll, and a decrease in secchi depth and bottom water dissolved oxygen, as scenario nutrient load progressively increased (Figures 4.120 – 4.123). The box plots in these figures show the mean, the 25th to 75th percentile of the data and the range. It is clear from these plots that the temporal (interannual) variation within a given month at each station exceeds the small but systematic changes in monthly mean due to nutrient enrichment. This shows that it will be difficult to distinguish changes in water quality due to increased fish farms from natural variability at monitoring sites using monitoring data alone.
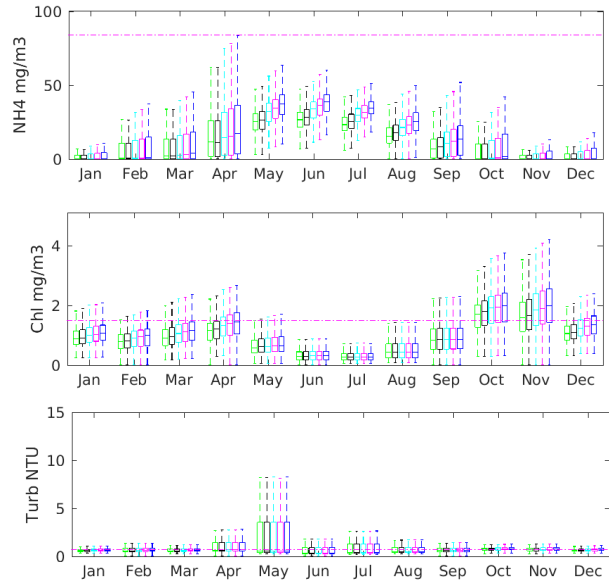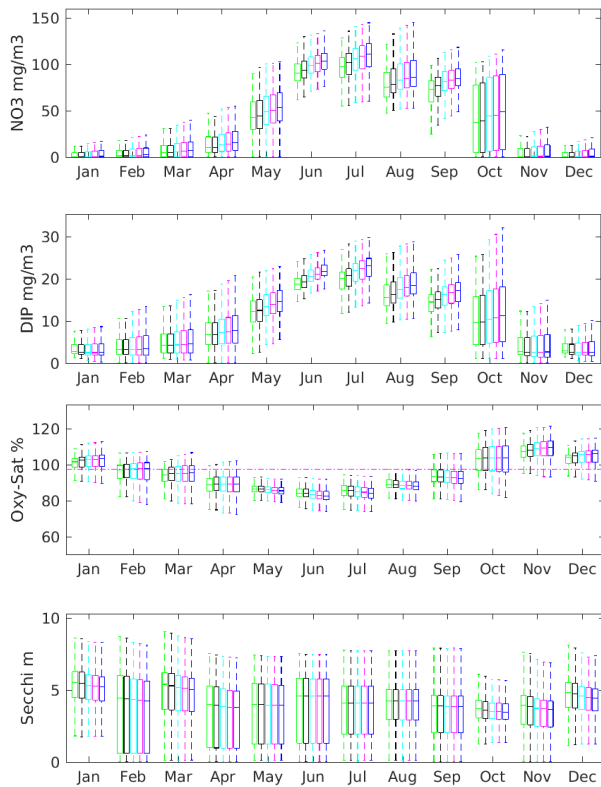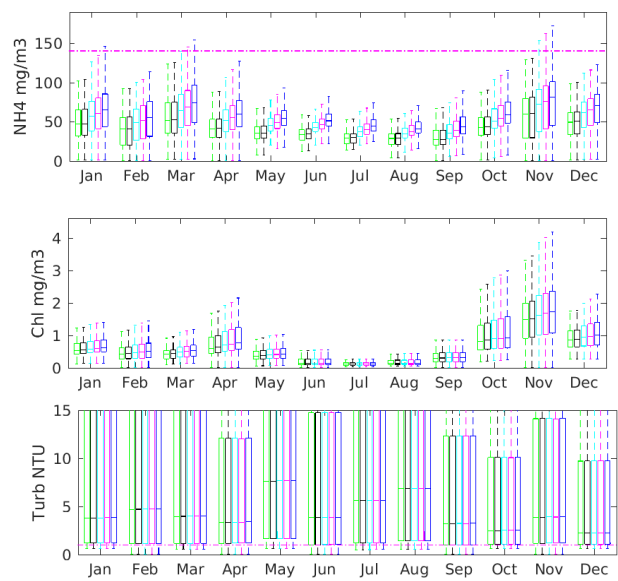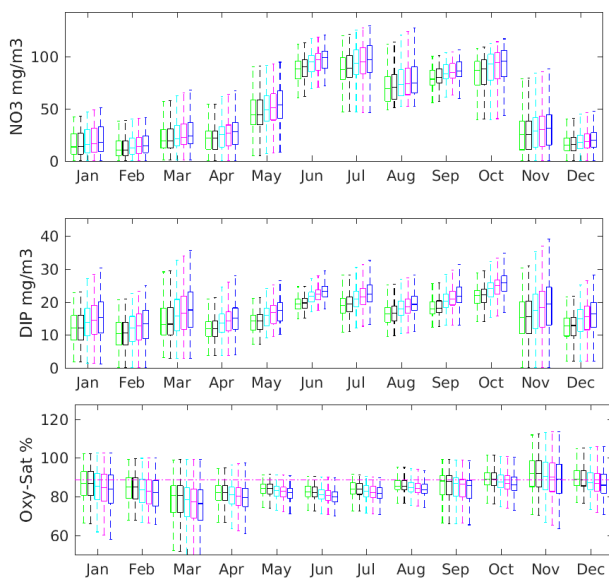
Figure 4.120 Seasonal variation in water quality at monitoring site Yellow Bluff SB03 in Storm Bay for each model scenario. Box plots shows mean, 25th and 75th percentiles and range over 2015-2019 in surface waters (top panel) and bottom* waters (bottom panel). [*depth averaged chlorophyll 0-12m]. DGVs for Bruny Bioregion OSRA segment 93 are plotted as pink line.
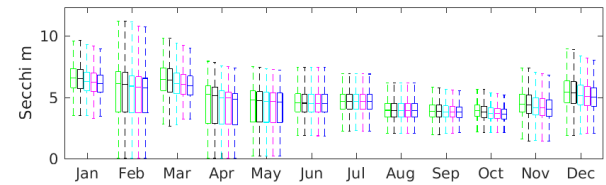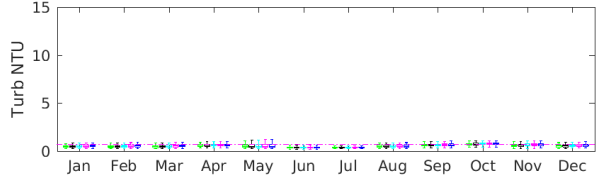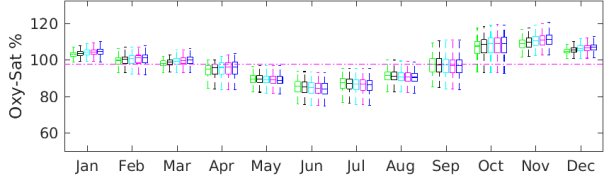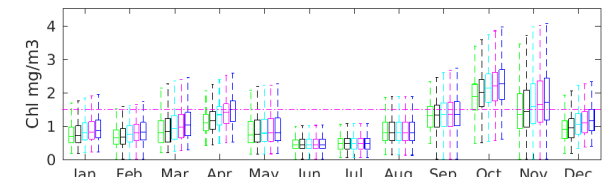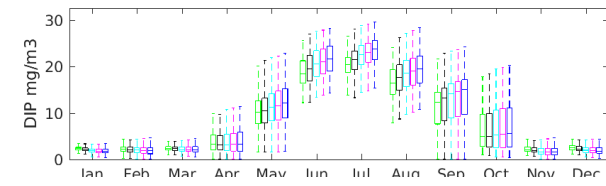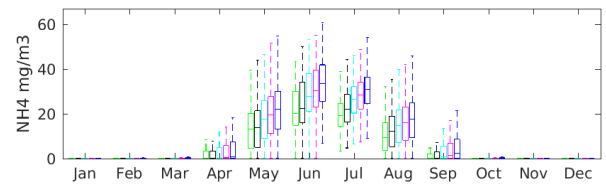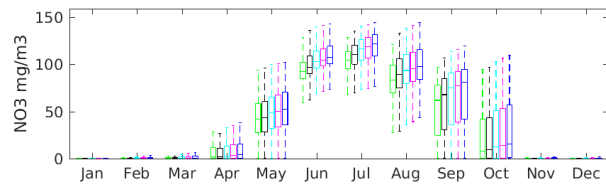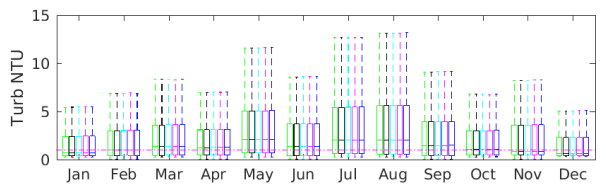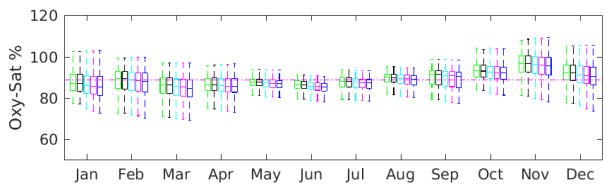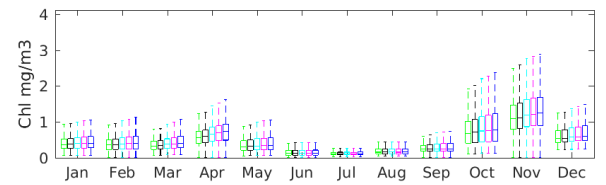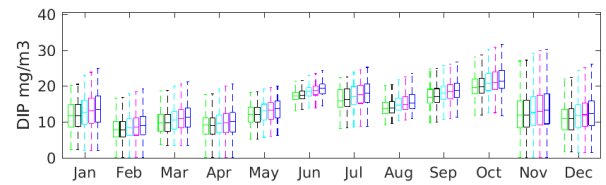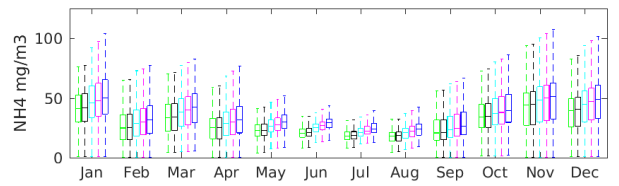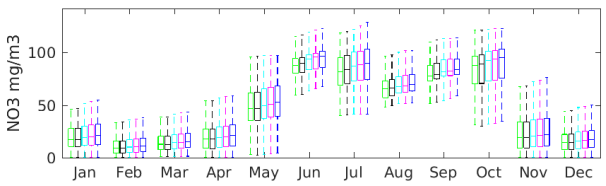
Figure 4.121 Seasonal variation in water quality at monitoring site Yellow Bluff SB03 in Storm Bay for each model scenario. Box plots shows mean, 25th and 75th percentiles and range over 2015-2019 in surface waters (top panel) and bottom* waters (bottom panel). [*depth averaged chlorophyll 0-12m]. DGVs for Bruny Bioregion OSRA segment are plotted as pink line.
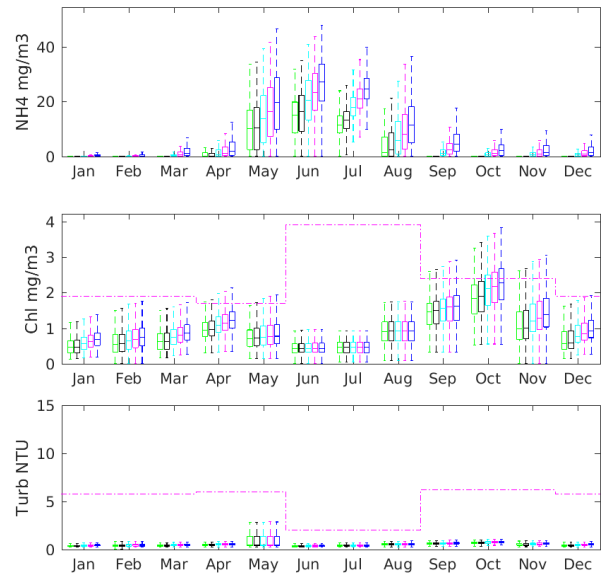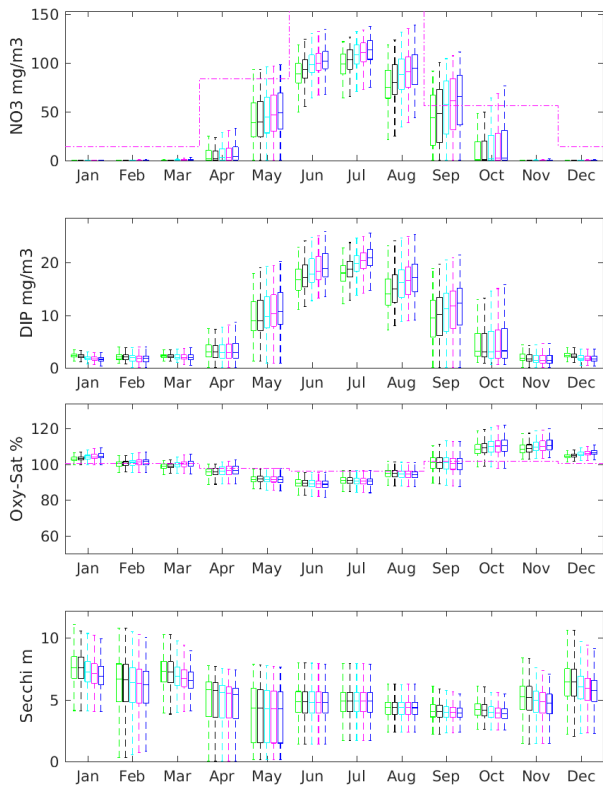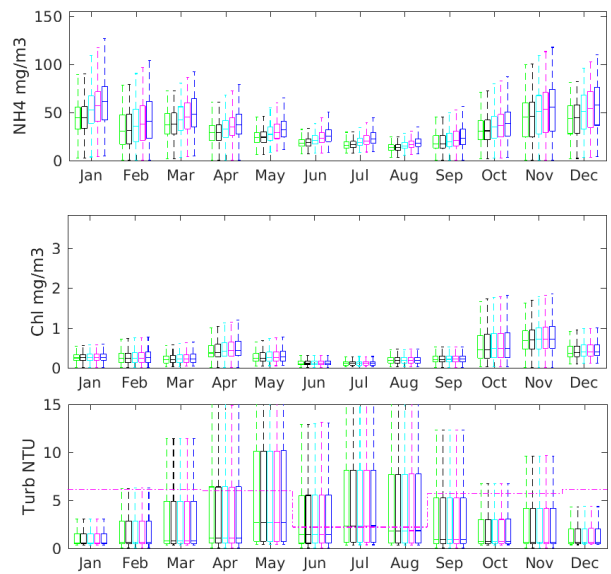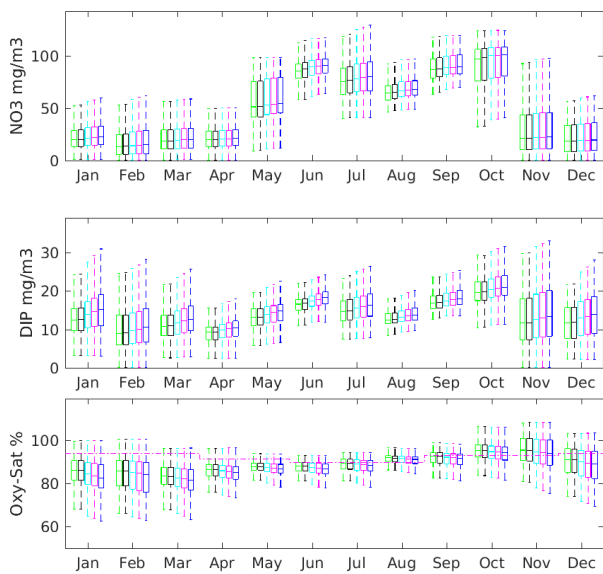
Figure 4.122 Seasonal variation in water quality at monitoring site Yellow Bluff SB03 in Storm Bay for each model scenario. Box plots shows mean, 25th and 75th percentiles and range over 2015-2019 in surface waters (top panel) and bottom* waters (bottom panel). [*depth averaged chlorophyll 0-12m]. DGVs for Bruny Bioregion OSRA segment 80 are plotted as pink line.
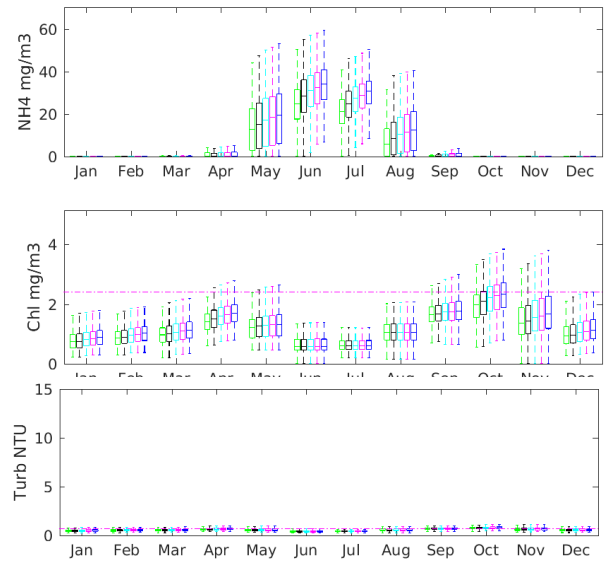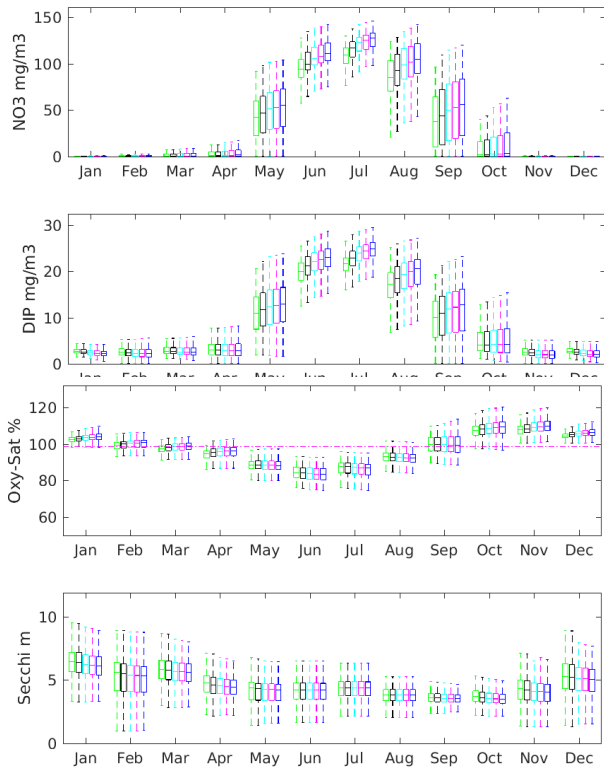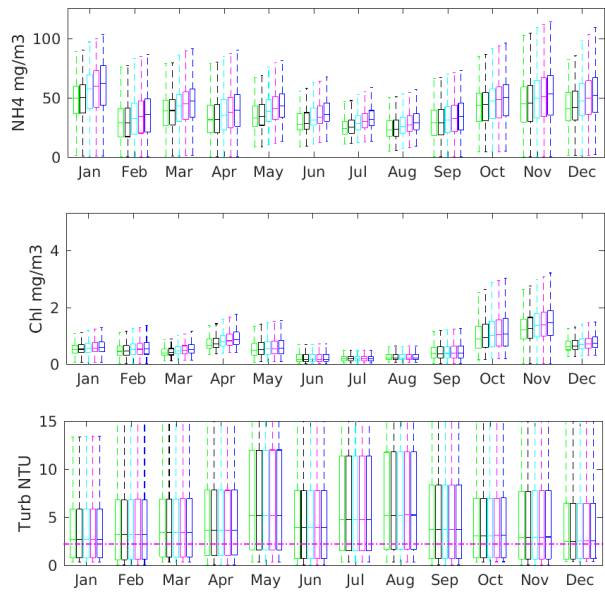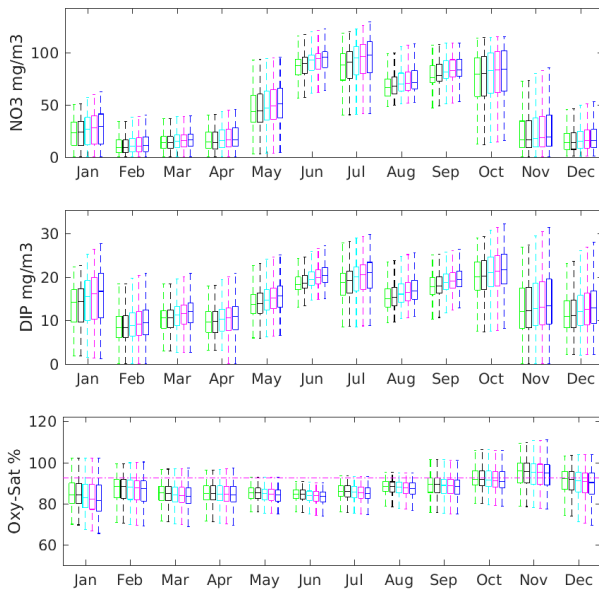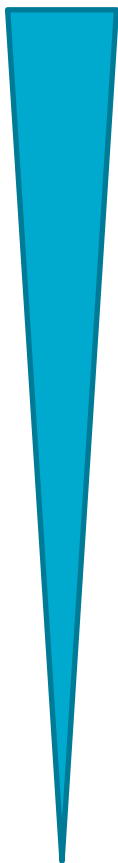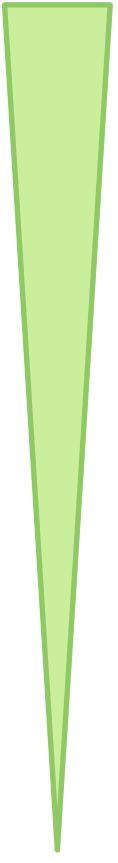
Figure 4.123 Seasonal variation in water quality at monitoring site Yellow Bluff SB03 in Storm Bay for each model scenario. Box plots shows mean, 25th and 75th percentiles and range over 2015-2019 in surface waters (top panel) and bottom* waters (bottom panel). [*depth averaged chlorophyll 0-12m]. DGVs for Bruny Bioregion OSRA segment 81 are plotted as pink line.

To identify monitoring sites that may be 'hotspots' of change across multiple variables we performed a preliminary rapid ranking of sites similar to Wild-Allen et al (2010). An unweighted mean was calculated from percent increase in surface and bottom water nutrients and turbidity, depth integrated chlorophyll and percent decrease in secchi depth and bottom water oxygen. For the *#5 2020+4.5ktN in SB* scenario this analysis suggests that the greatest water quality impacts would be observed at Wedge, VarietyP_SB11 and EYellowB_SB14, which are all close to farm leases; conversely the least water quality impacts would occur at offshore monitoring sites SP_3, BG_12 and BG_5 (Table 4.18). Similar analysis for the Pre-development scenario demonstrated that should all salmon farms be removed from the region, greatest improvement in water quality at Storm Bay monitoring sites is anticipated at WhiteB, NWedge_SB5 and SWIron_SB1.

Table 4.18 Preliminary rapid ranking analysis of Storm Bay monitoring site sensitivity to simulated changes in water quality for each scenario [note that an increase in nutrients, chlorophyll, turbidity and a decrease in secchi depth and bottom water dissolved oxygen were assumed to be negative impacts on water quality].

	#5 2020+4.5ktN in SB	#4.5 2020+3ktN in SB	#4 2020+2ktN in SB			#2 Pre_devopment
Greatest **negative** change in WQ				Greatest **positive** change in WQ		Whiteb
	Wedge	Wedge	Wedge			NWedge_SB5
	VarietyP_SB11	Whiteb	Whiteb			SWIron_SB1
	EYellowB_SB14	VarietyP_SB11	VarietyP_SB11			SWBetsey_SB12
	ETRUM_SB15	ETRUM_SB15	YellowB_SB3			SEBetsey_SB8
	Whiteb	YellowB_SB3	ETRUM_SB15			EYellowB_SB14
	YellowB_SB3	EYellowB_SB14	NWedge_SB5			NWHead_SB9
	NWedge_SB5	NWedge_SB5	EYellowB_SB14			YellowB_SB3
	SWBetsey_SB12	SWBetsey_SB12	SWBetsey_SB12			Wedge
	SEBetsey_SB8	SEBetsey_SB8	SEBetsey_SB8			ETRUM_SB15
	SWIron_SB1	SWIron_SB1	SWIron_SB1			BG_12
	MidSB_SB2	MidSB_SB2	MidSB_SB2			VarietyP_SB11
	Dart_SB7	CQE_SB4	CQE_SB4			MidSB_SB2
	CQE_SB4	Dart_SB7	Dart_SB7			Dart_SB7
	NWHead_SB9	NWHead_SB9	NWHead_SB9			CQE_SB4
	BG_4	BG_4	BG_4			BG_4
	BG_5	BG_5	BG_12			BG_5
	BG_12	BG_12	BG_5			
Least negative change in WQ	SP_3	SP_3	SP_3	Least positive change in WQ		SP_3

Further analysis of model output is recommended to investigate whether the spatial array of stations is sufficient or includes any redundancy. Similarly, the high temporal resolution of model output is available to explore the temporal sampling strategy and identify whether some stations would benefit from the deployment of continuous water quality sensors. An 'observing system simulation experiment' could also be completed (and repeated for each scenario) to provide insight into the overall effectiveness of the monitoring program in fulfilling its objectives, and a cost-benefit analysis might identify priority upgrades to the monitoring program design that could also reduce cost.

Summary of scenario results and recommendations

Model scenario simulations show that progressive increases in fish farm nutrient loads in southeast Tasmania result in corresponding increases in DIN and chlorophyll concentration and declines in bottom water oxygen and light. Changes in water quality are not distributed evenly throughout the region but are mostly localised to the waterway in which discharge occurred. In Storm Bay increased nutrient loads enhanced chlorophyll concentrations in summer, autumn and spring; nearly all the additional surface DIN was utilised in summer and some of the additional surface DIN was utilised in autumn and spring. With increased nutrient load additional phytoplankton and associated organic matter increased water column turbidity and reduced the amount of light reaching the seabed, with greatest impacts in spring and summer.

Analysis has shown relative (percent) and absolute change in simulated water quality variables, including changes in annual mean chlorophyll as a proxy for trophic state (Smith 1998). In Storm Bay the model scenario simulations suggest a reduction in oligotrophic area and an increase in mesotrophic area from 34% in the Pre-Storm Bay development scenario to 40%, 42% and 45% of Storm Bay area in the *#4 2020+2ktN in SB*, *#4.5 2020+3ktN in SB* and *#5 2020+4.5ktN in SB* scenarios; no areas of Storm Bay became eutrophic in any of the simulations.

Preliminary analysis of change in water quality at monitoring program sites in Storm Bay found that most sites showed some change with increasing farm loads, with the greatest change observed at sites close to farm lease locations. Interannual variability in water quality at sites in Storm Bay is high, and the range of variability in a given month exceeds the small but systematic changes in water quality in the nutrient enrichment scenarios. It will therefore be difficult to distinguish changes in water quality due to increased fish farms from natural variability using monitoring data alone. The use of continuous sensing systems, model output and ongoing scenario simulations with- and with-out anthropogenic loads could help to distinguish natural variability from fish farm induced change in water quality.
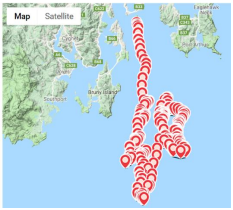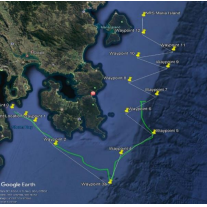
Our nutrient budget analysis to date has focused specifically on Storm Bay. We recommend extending this analysis to encompass the whole Derwent, D'Entrecasteaux Channel, Huon Estuary and the broader Fredrick Henry Bay; this would allow discrimination of regional river, sewerage and industry discharge, fish farm inputs and ocean contributions to better contextualise the relative contributions of each nutrient source to the whole connected system.

5 High priority observations

5.1 Glider deployments

To investigate the influence of boundary currents on Storm Bay, and specifically the potential delivery of nutrients from these currents into the bay a number of glider missions have been deployed. To date the project has achieved 6 glider deployments, 3 to characterise the Zeehan Current (peak flow along the west coast of Tasmania in winter), and 3 to characterise the East Australia Current (peak flow along the east coast of Tasmania in summer) (Table 5.1). Unfortunately, during the final glider deployment in January 2021, the platform was damaged and lost in a significant storm.

Table 5.1 Summary of glider deployments achieved to date.

Target	Start	End	Duration	
Outer Storm Bay, Shelf & Zeehan Current	4 Sep 2018	27 Sep 2018	23 days	
Southeast Storm Bay, Shelf & East Australia Current	27 Mar 2019	10 Apr 2019	14 days	
Southwest Shelf & Zeehan Current	2 Aug 2019	23 Aug 2019	21 days	
Outer Storm Bay, Shelf & East Australia Current	14 Jan 2020	5 Feb 2020	21 days	

Zeehan Current, Southwest Shelf & Outer Storm Bay	8 Jul 2020	31 Jul 2020	23 days	
Southeast Storm Bay	15 Jan 2021	17 Jan 2021	3 days Glider lost 🙁	

5.1.1   Zeehan Current Characterisation

Glider missions in September 2018, August 2019 and July 2020 have characterised the water properties of the Zeehan Current (ZC) which extends down the west coast and around the south coast of Tasmania in winter (Figure 5.1).

From these observations we can confirm that the ZC is a warm surface current that flows along the shelf. In 2018 and 2019 ZC water appeared to around 100m and in 2020 to 150m depth which was the whole water column (Figures 5.2 – 5.4). ZC water was observed to have low nitrate concentration in all years with elevated concentrations of nitrate only observed on the oceanic offshore side of the current (Figure 5.5). Inshore, Storm Bay waters in winter were cooler and fresher, modified by Derwent and Huon river outflows, and inshore nitrate concentrations were also low.

Chlorophyll concentrations were elevated in inshore waters, particularly at the surface which may in part be due to the influence of CDOM contributing to the fluorometer signal. In offshore waters surface chlorophyll was lower in concentration with distinct diel variation. The daily variation was likely due to active phytoplankton photosynthesis during daylight hours which limits the amount of available chlorophyll pigment reaction centres to return a fluorescence response to the light activated sensor. This process is known as fluorescence quenching and results in an underestimation of chlorophyll pigments in actively photosynthesising phytoplankton populations; more accurate fluorescence estimates of chlorophyll concentration are made in darkness.

Water mass analysis (Figure 5.6) shows warmer high salinity offshore surface waters influenced by the ZC are low in phytoplankton chlorophyll, whilst cooler lower salinity inshore waters have higher phytoplankton chlorophyll content. Warm saline offshore surface waters influenced by the ZC are low in nitrate content and the inshore cooler and fresher waters are also low in nitrate content.
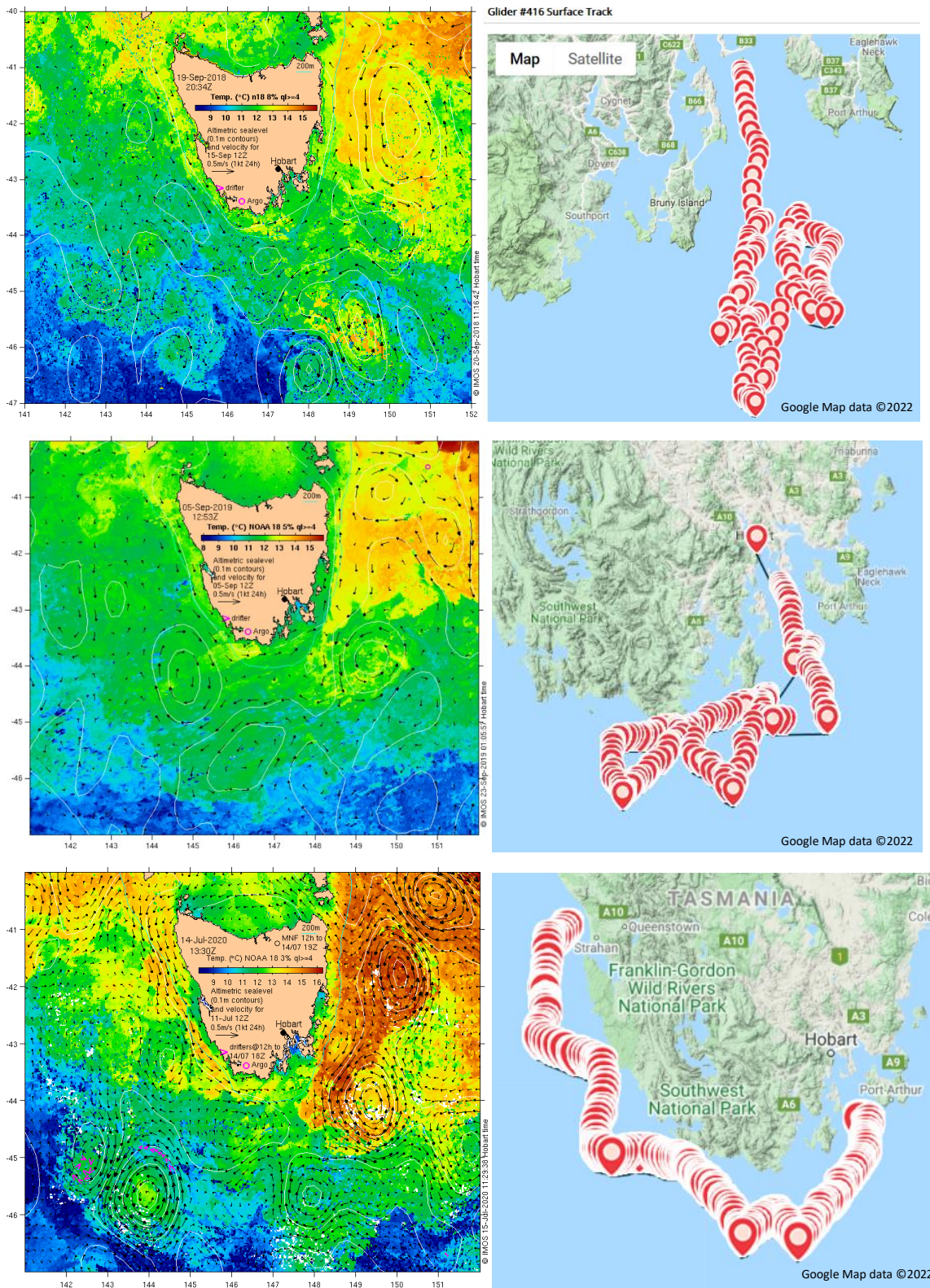
Figure 5.1 Sea surface temperature with surface currents derived from altimetry (right) and glider track (left) in Sep 2018 (top), Aug 2019 (middle) and Jul 2020 (bottom) (IMOS Ocean Current data http://oceancurrent.imos.org.au/ - access valid Nov 2022).
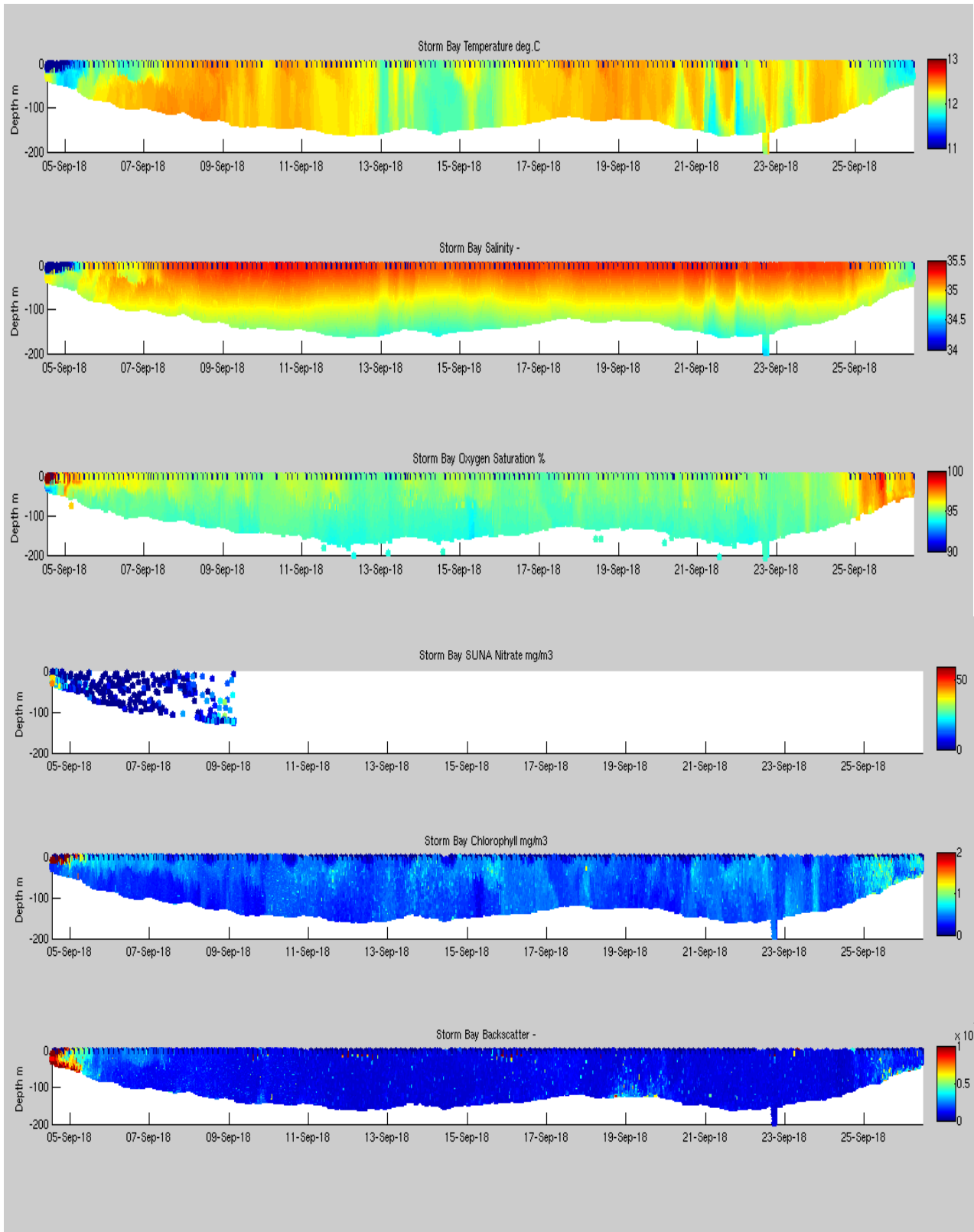
Figure 5.2 Temporal evolution of glider observations in Sep 2018, from top to bottom: temperature, salinity, oxygen saturation, calibrated nitrate, chlorophyll, and backscatter.
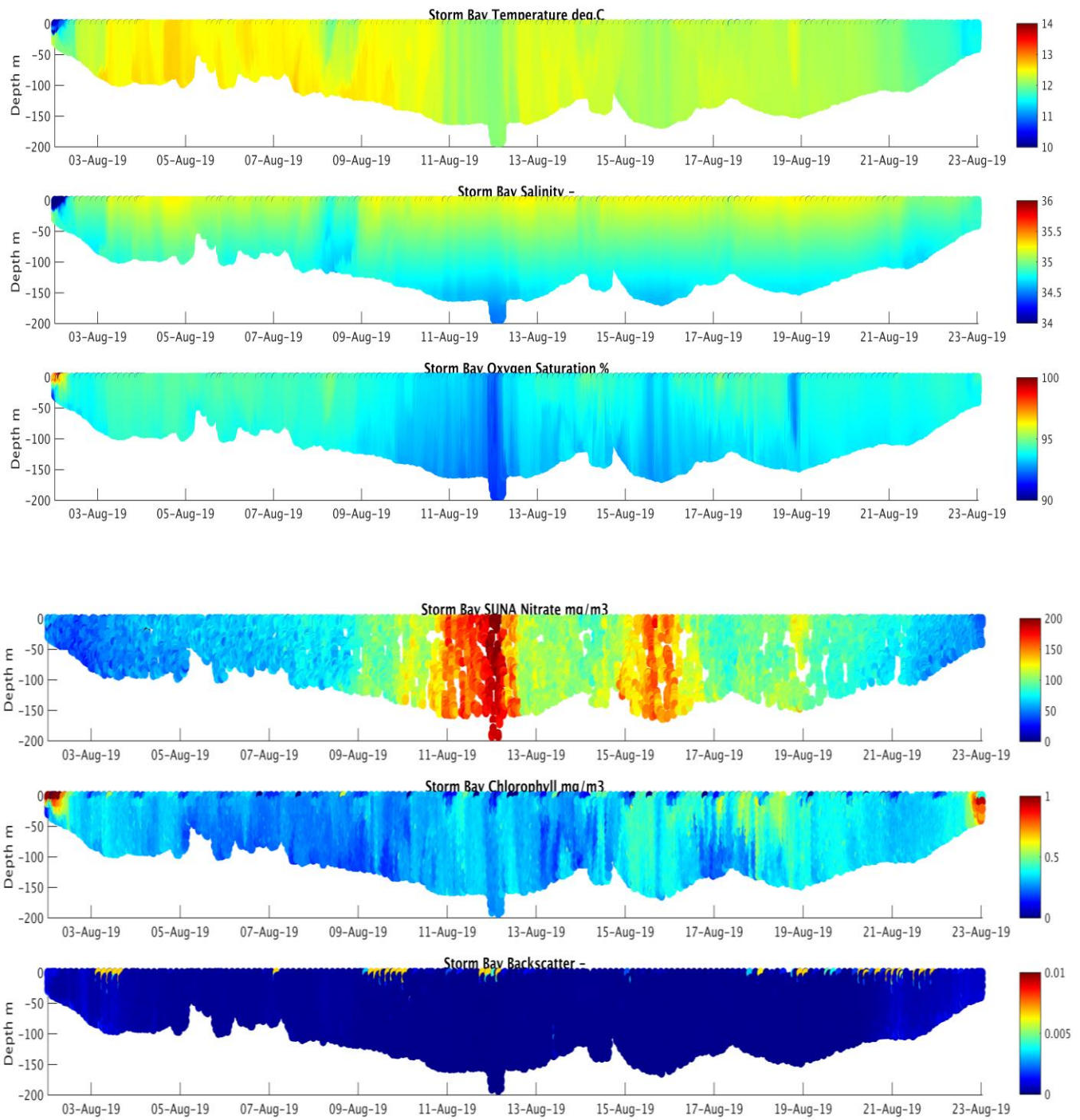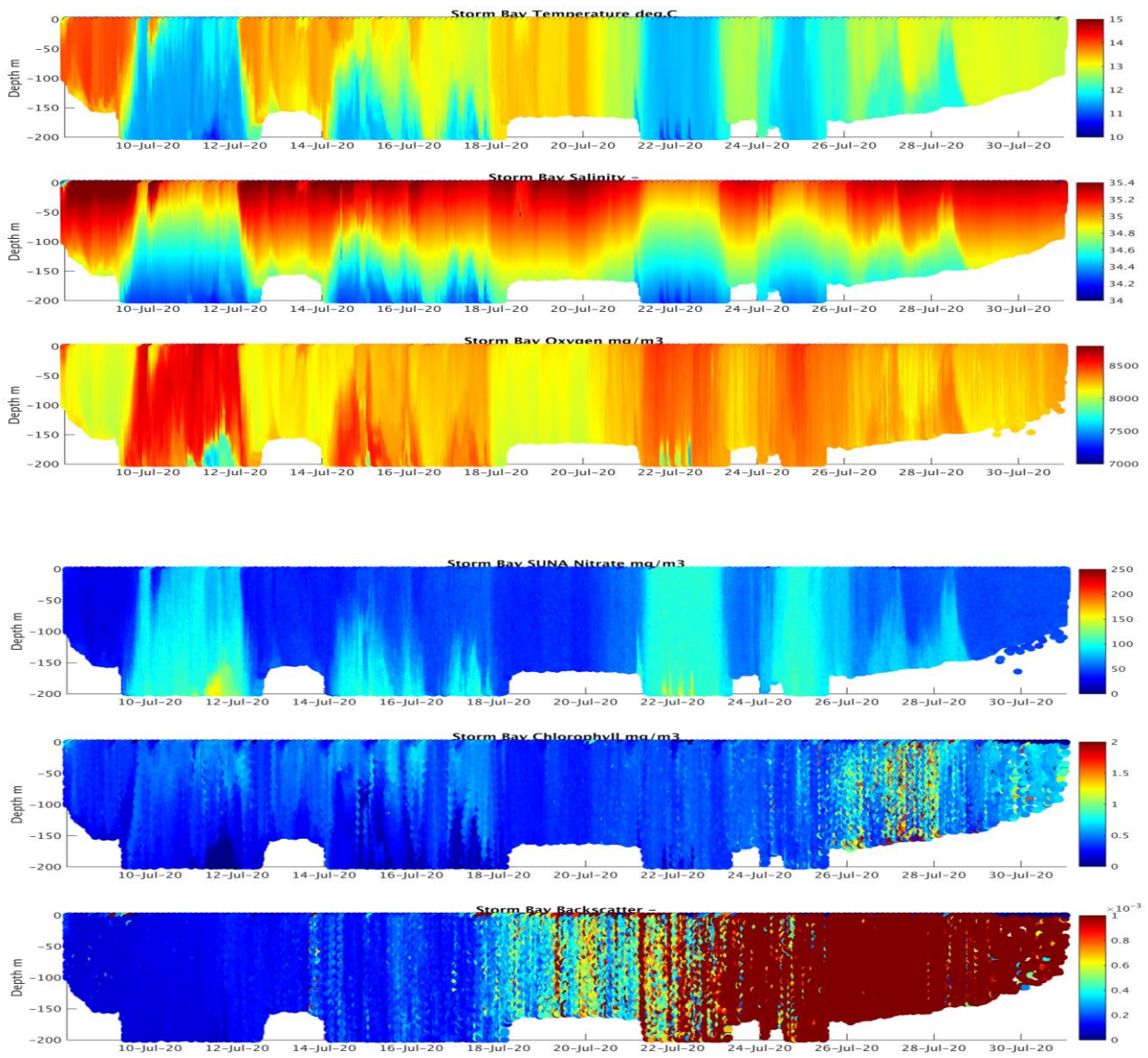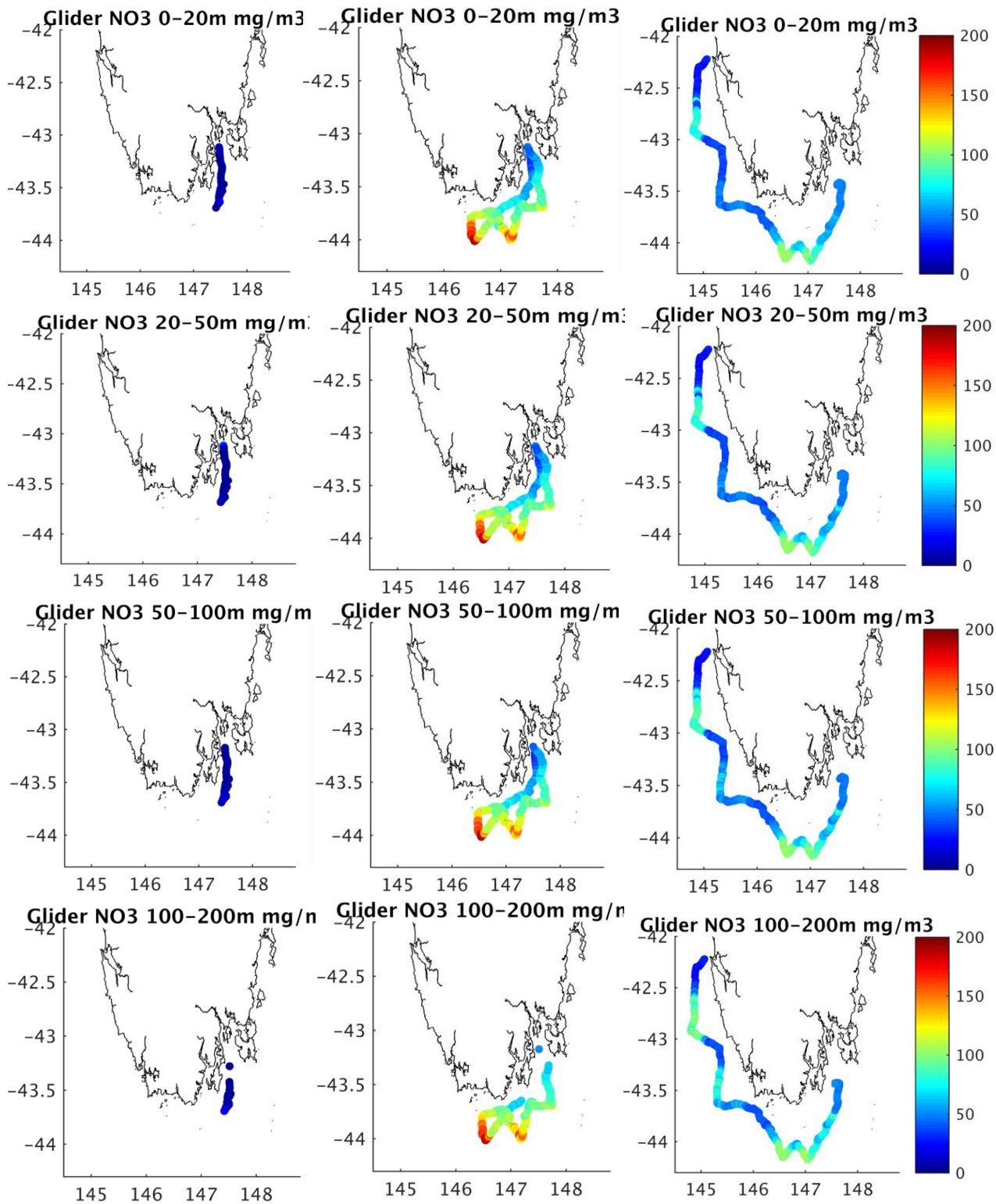
Figure 5.3 Temporal evolution of glider observations in Aug 2019, from top to bottom: temperature, salinity, oxygen saturation, calibrated nitrate, chlorophyll, and backscatter.

Figure 5.4 Temporal evolution of glider observations in July 2020, from top to bottom: temperature, salinity, oxygen concentration, calibrated nitrate, chlorophyll, and backscatter.

Figure 5.5 Spatial plots of nitrate observed along the glider track at increasing depth intervals (from top to bottom) in September 2018 (left column), August 2019 (middle column) and July 2020 (right column).
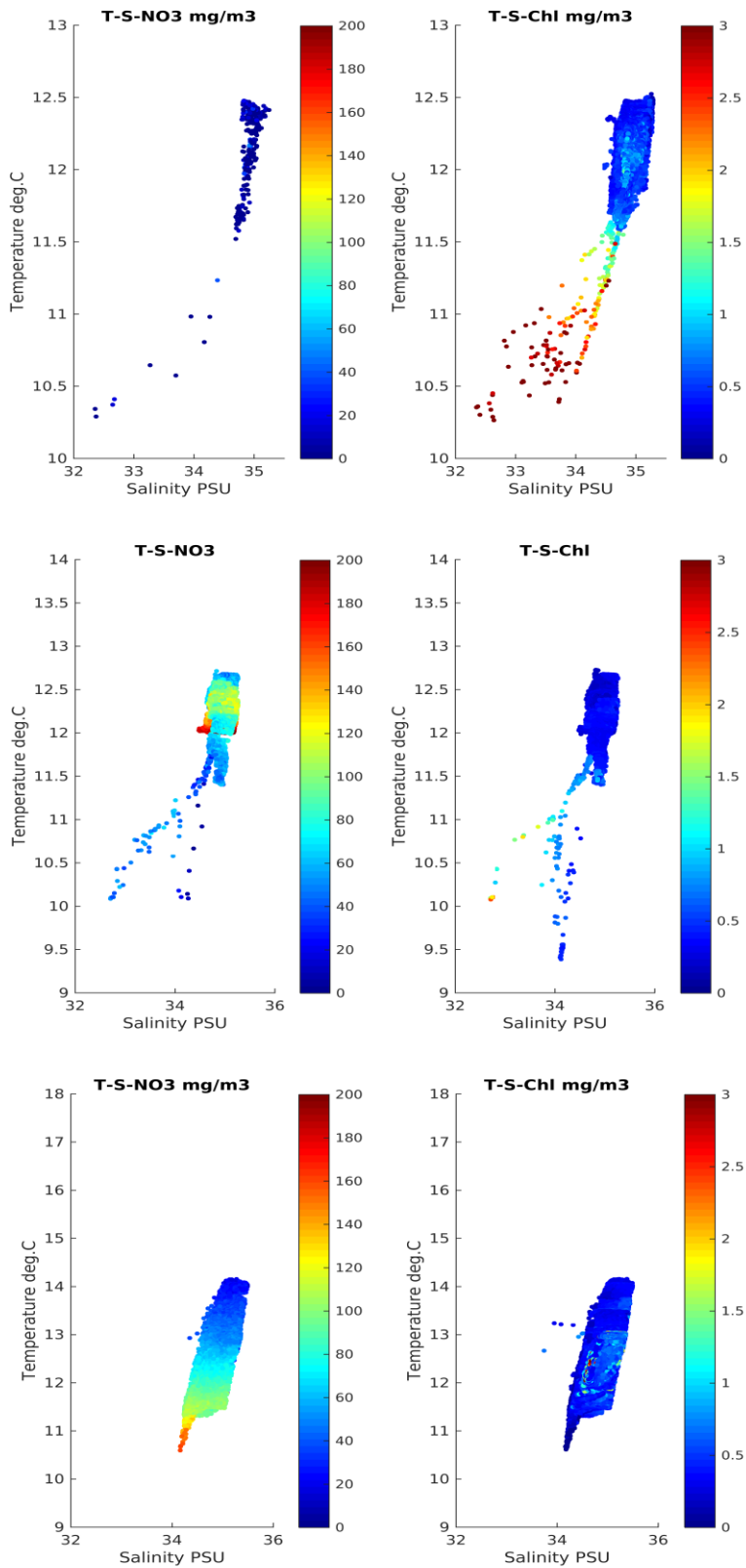
Figure 5.6 Water mass analysis of the glider observations coloured by nitrate (left) and chlorophyll (right) concentration in Sep 2018 (upper pair), Aug 2019 (middle pair) and Jul 2020 (lower pair).

5.1.2   East Australia Current Characterisation

Glider missions in April 2019, February 2020 and January 2021 have characterised the water properties of the East Australia Current (EAC) off southeast Tasmania in summer. The EAC extends down the east coast and south of Tasmania as a train of distinctive cyclonic and anticyclonic mesoscale eddies (Figure 5.7).
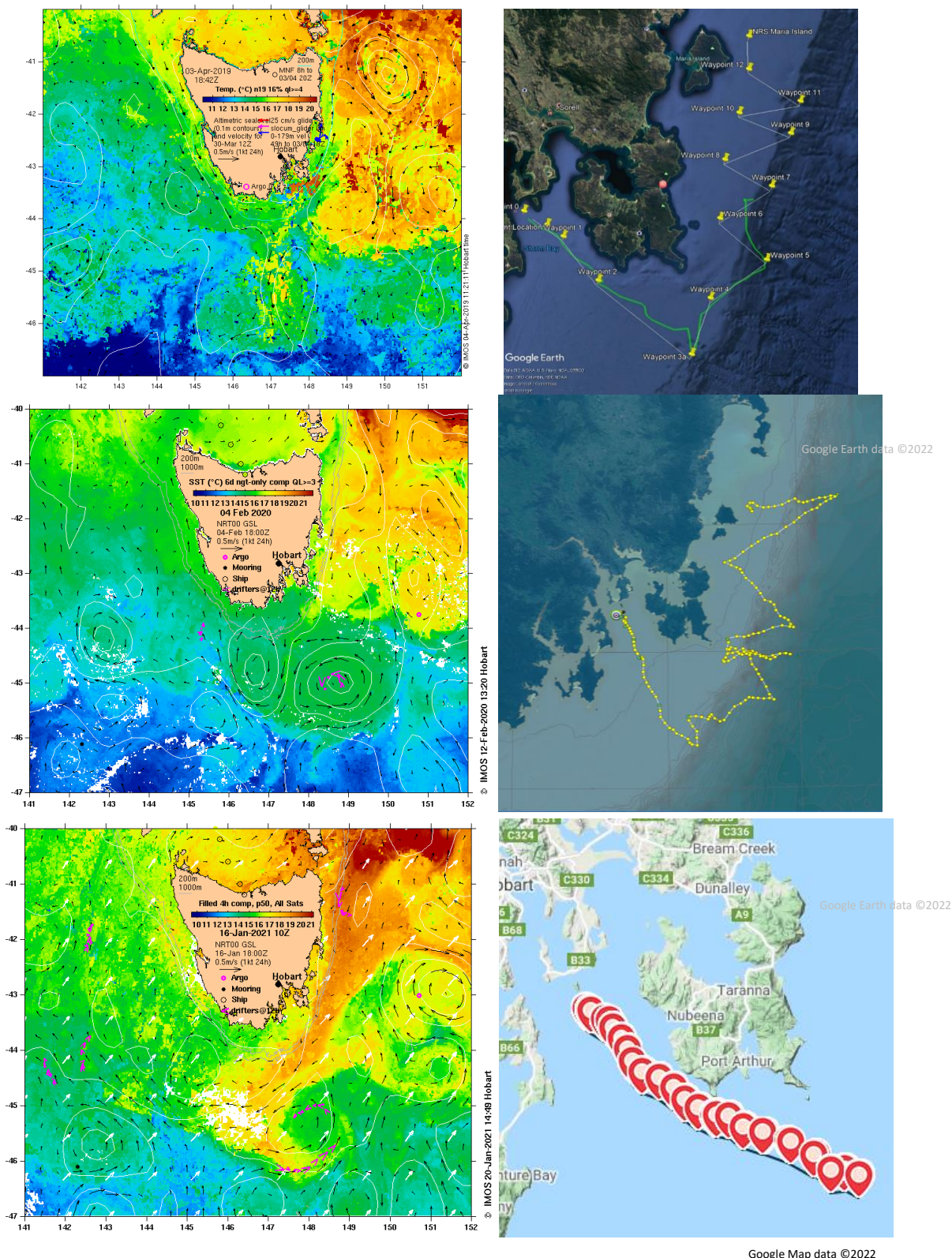
Figure 5.7 Sea surface temperature and currents derived from altimetry (left) and glider track (right) to sample the East Australia Current entering Storm Bay in April 2019 (top), Feb 2020 (middle) and Jan 2021 (bottom) (IMOS Ocean Current data http://oceancurrent.imos.org.au/ - access valid Nov 2022).

Observations characterise the EAC current influence to the southeast of Storm Bay as a shallow warm and saline surface current that is around 50m deep (Figures 5.8 – 5.10). Surface nitrate concentrations were low but increased at depth, below the influence of the current. Inshore waters in Storm Bay were slightly fresher due to the influence of the Derwent and Huon river systems. Chlorophyll concentrations in offshore waters in Feb 2020 were greatest between 30 – 50 m depth, where phytoplankton would have had access to both light and nitrogen from greater depths. In surface waters diel variations in chlorophyll concentration were observed likely due to fluorescence quenching by actively photosynthesising cells during daylight hours. Fluorescence measurement of chlorophyll is more accurate at night.

Data from the IMOS Maria Island NRS in March/April 2019 shows a community dominated by diatoms, with low numbers of dinoflagellates. Small (< 25 µm) diameter ciliates (heterotrophic grazers) are often in high numbers at this time of year. In January 2020, diatoms were still the most abundant group, with a lower diversity of dinoflagellates, and ciliates almost completely absent. January 2021 showed much lower diatom and dinoflagellate abundances overall, with flagellate (< 5 µm numerically dominant)
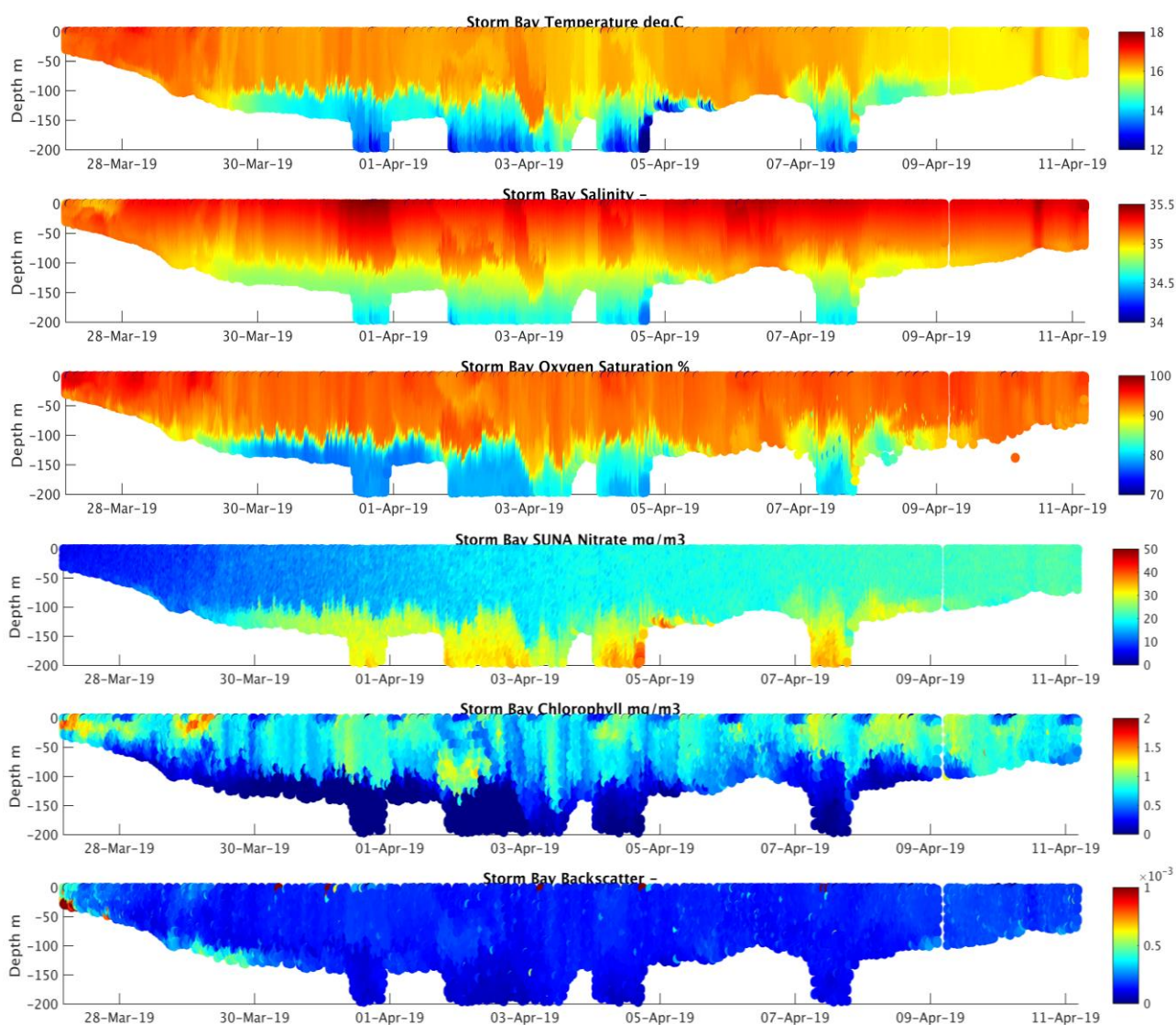
Figure 5.8: Evolution of temperature salinity, oxygen saturation, chlorophyll, nitrate, and backscatter during the April 2019 glider deployment that commenced in Storm Bay (plot left) and was completed off Maria Island (plot right).
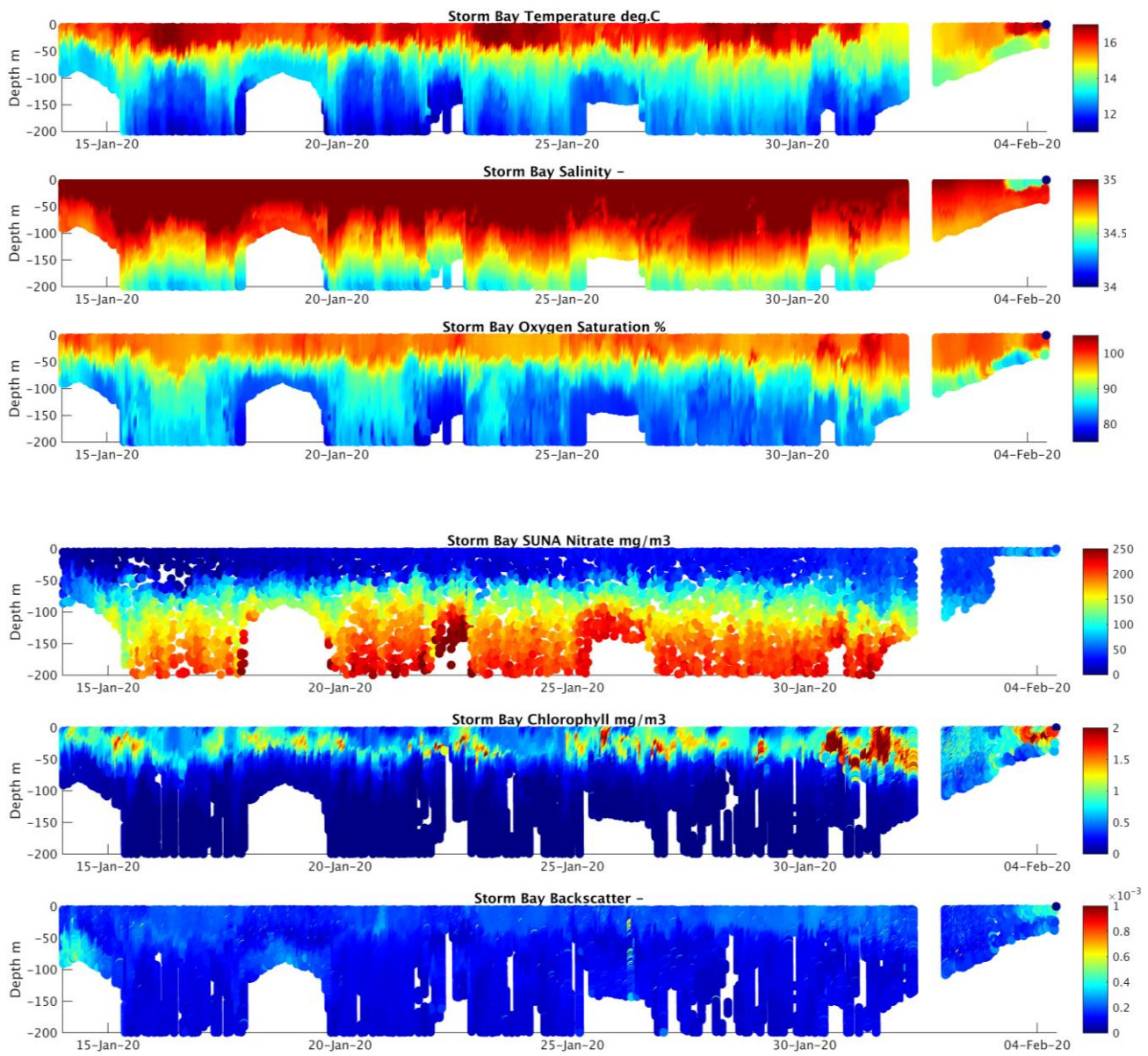
Figure 5.9: Evolution of temperature salinity, oxygen saturation, chlorophyll, nitrate, and backscatter during the February 2020 glider deployment that commenced at Maria Island (plot left) and ended in Storm Bay (plot right).
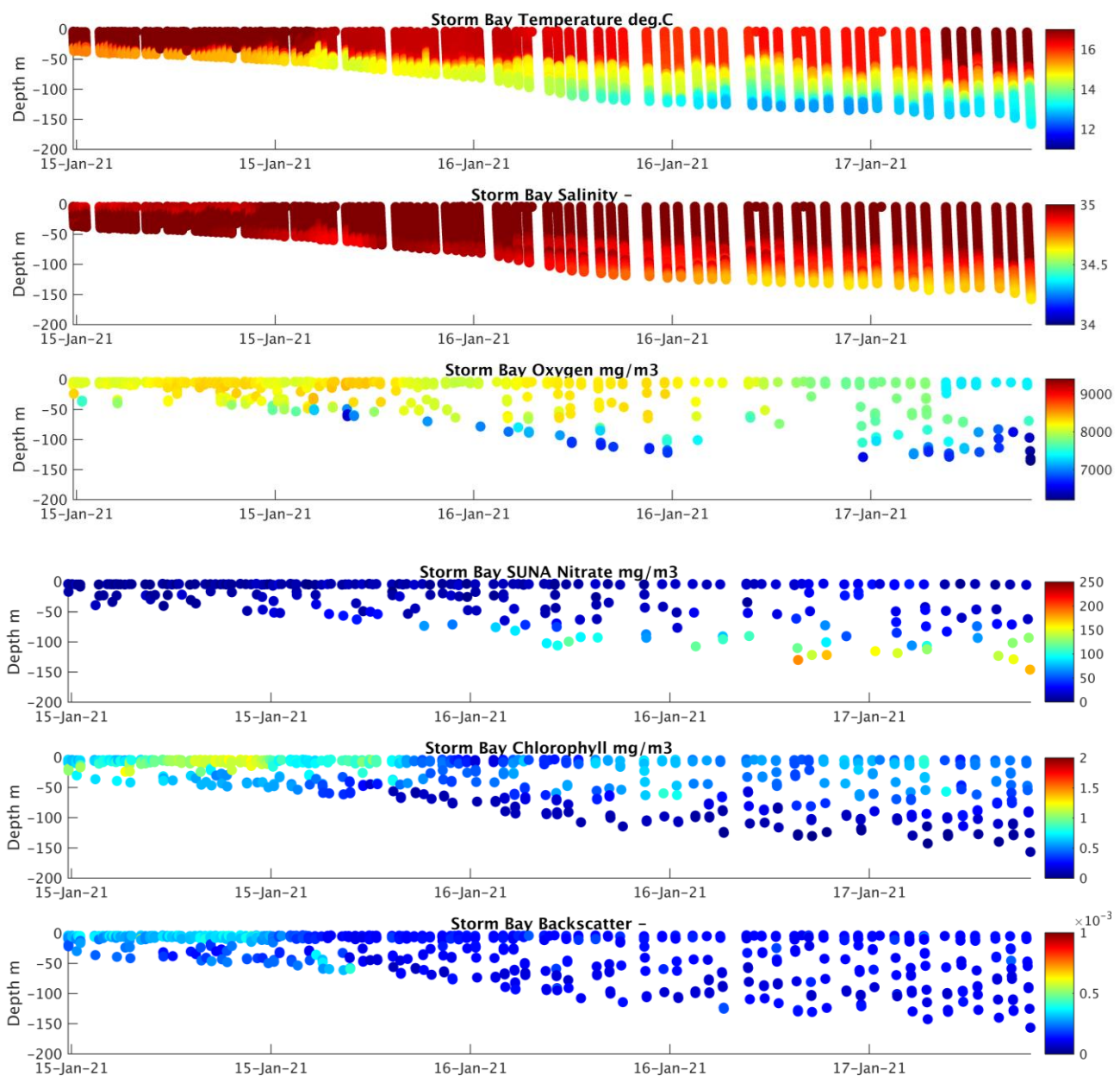
Figure 5.10 Evolution of temperature salinity, oxygen concentration, chlorophyll, nitrate, and backscatter during the January 2021 glider deployment that commenced in Storm Bay (plot left) and ended off the Tasman peninsular (plot right). Data shown was downloaded via satellite link prior to loss of the glider.

Water mass analysis of the glider deployments shows the warm salty EAC water to be low in nitrate concentration, whilst the cool fresh deep water has high nitrate content (Figure 5.11); chlorophyll concentrations were greater in the warmer surface waters and also the inshore Storm Bay waters.
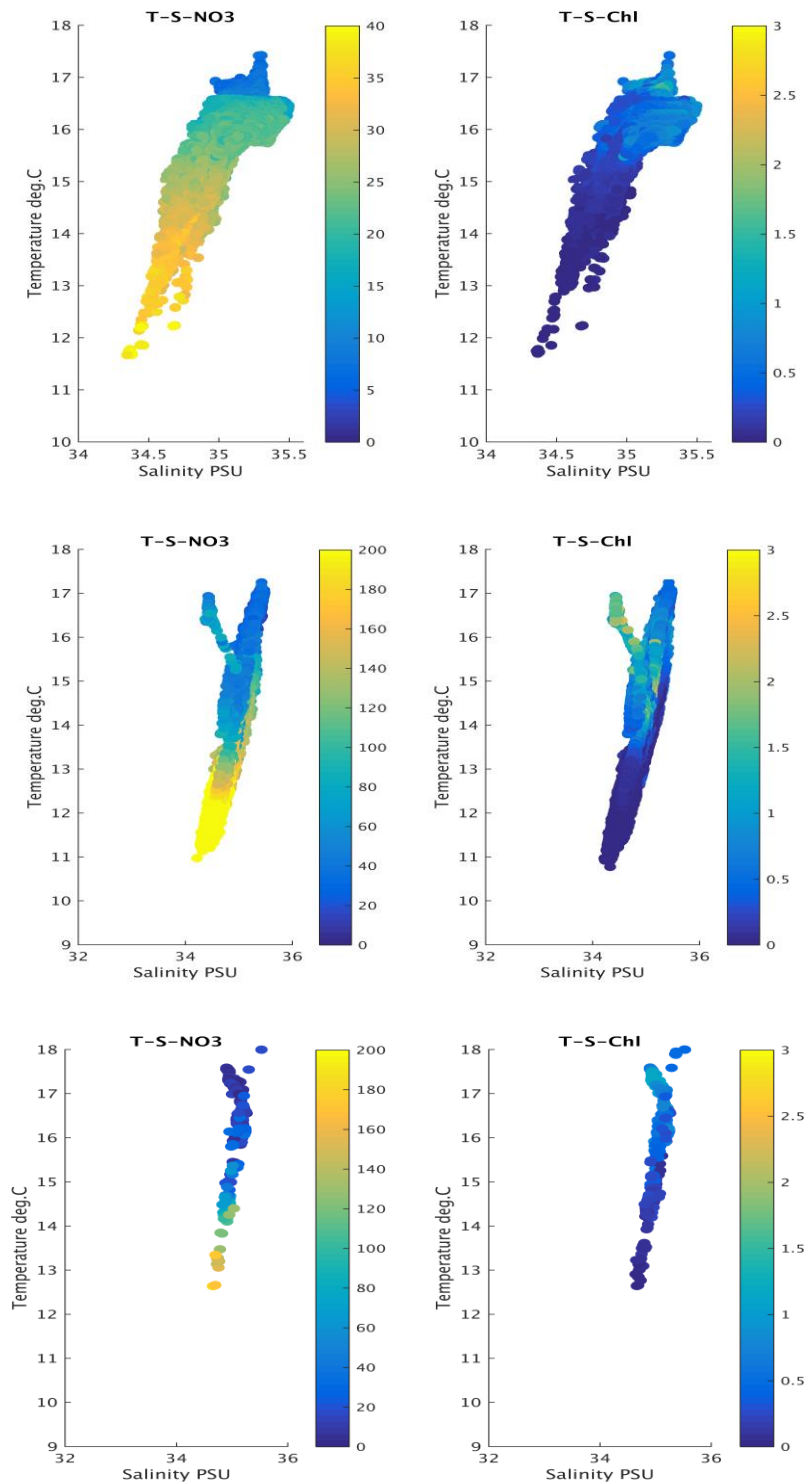
Figure 5.11 Water mass characteristics and associated nitrogen (left) and chlorophyll (right) in April 2019 (upper pair), February 2020 (middle pair) and January 2021 (lower pair).

Spatial plots of nitrate concentration (Figure 5.12) show elevated concentrations of nitrate at depths generally greater than 50 m which is below the surface layers of EAC water. In February 2020 elevated nutrient concentrations were also observed inshore in Storm Bay and at depths between 20 – 50 m off the East Coast.
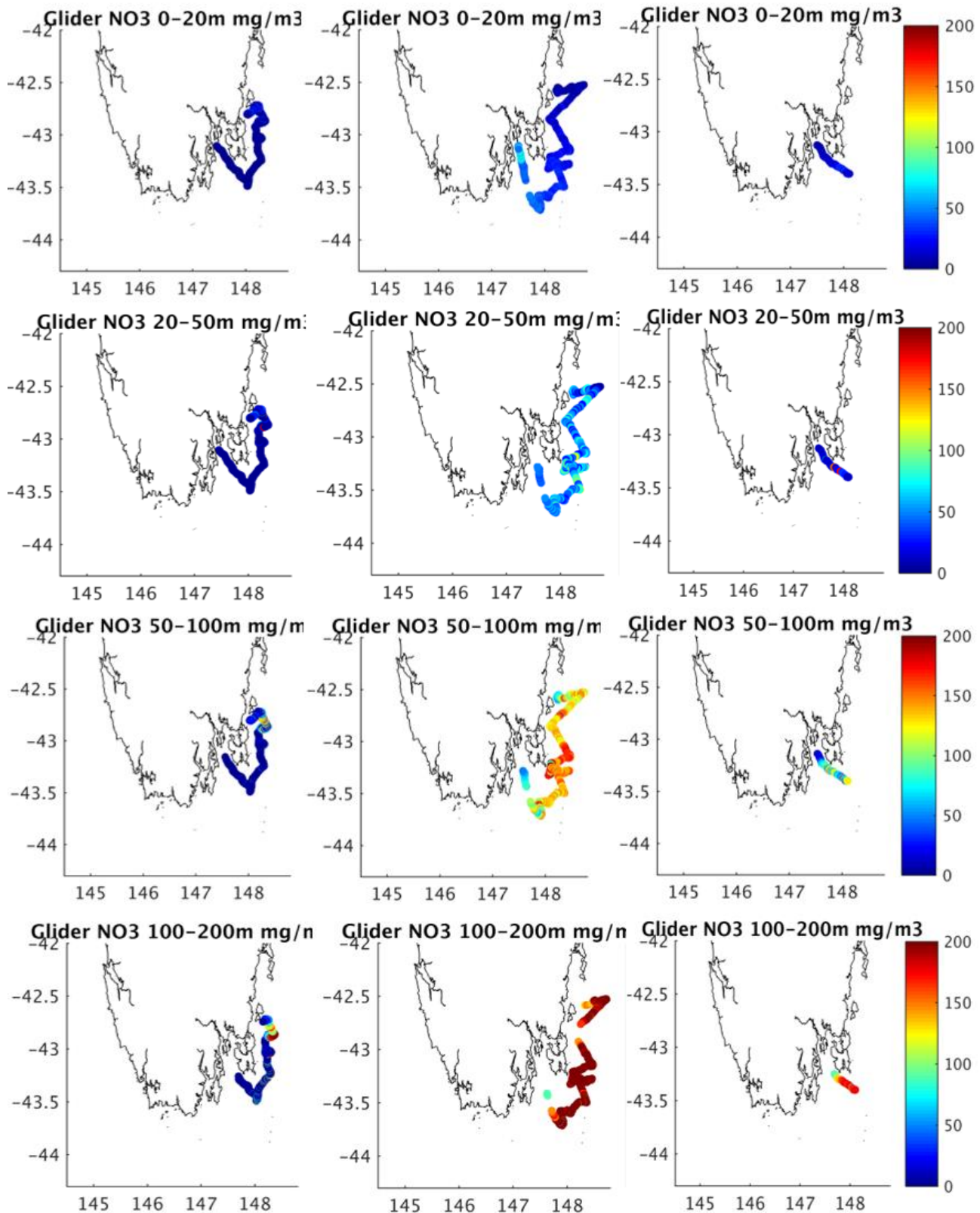
Figure 5.12 Spatial plots of nitrate observed along the glider track at increasing depth intervals (from top to bottom) in April 2019 (left column), February 2020 (middle column) and January 2021 (right column).

IMOS glider deployments Tasmanian East Coast February-April 2019

Of additional interest to the project were 2 IMOS glider deployments on the east coast of Tasmania between February – April 2019 and coincident with our April 2019 glider deployment. The IMOS gliders

were deployed off Binalong Bay and sampled the Tasmanian shelf and East Australia Current along the east coast (Figure 5.13). The IMOS gliders recorded temperature, pressure, salinity, dissolved oxygen, and chlorophyll and characterised the EAC on the East Coast as a shallow warm saline current to approximately 50m depth.
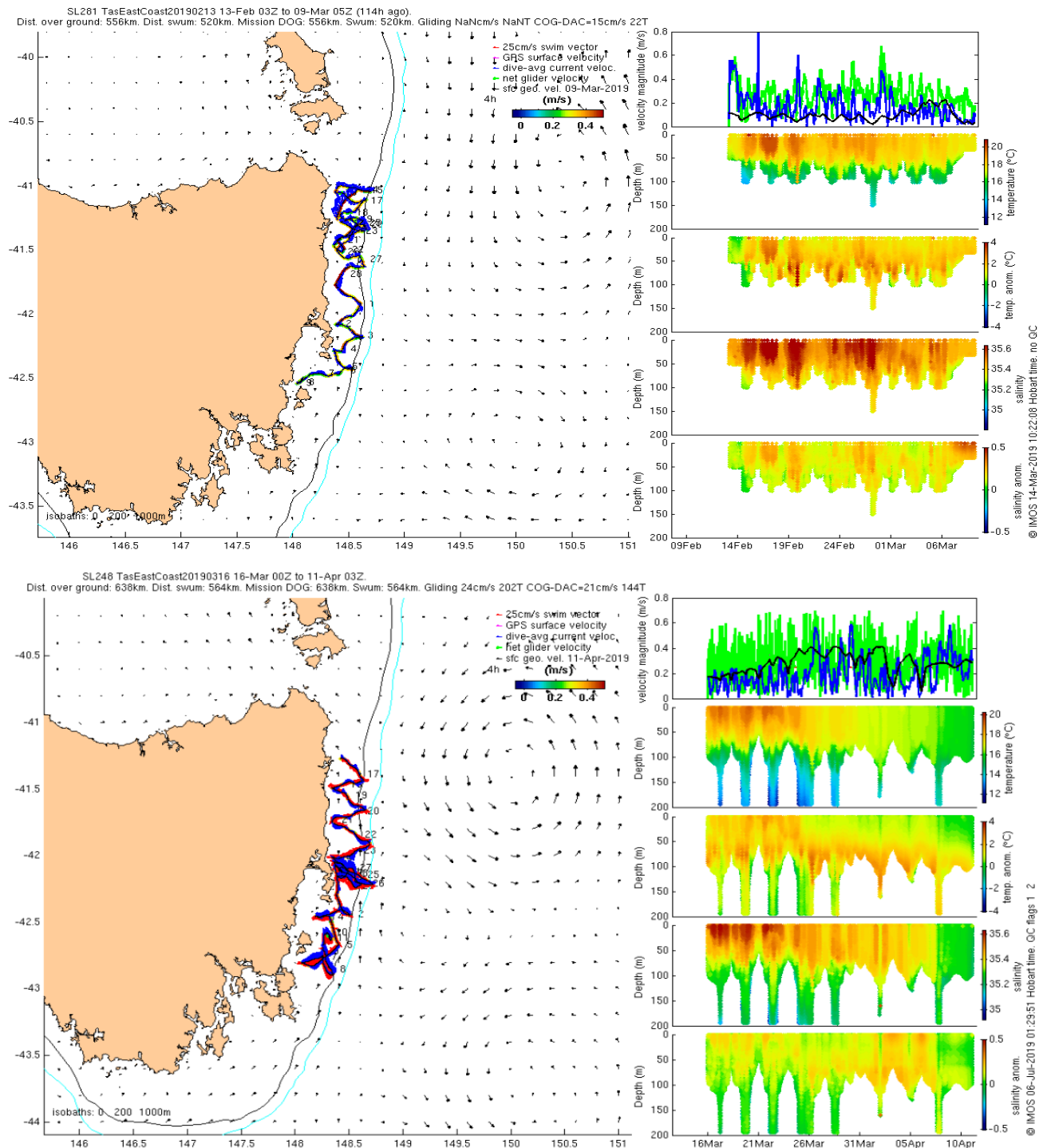
Figure 5.13 IMOS Glider tracks (left) and raw data profiles (right) for velocity, temperature, temperature anomaly, salinity, and salinity anomaly.

5.2   Benthic landers and process studies

Benthic lander frames were designed and built to accommodate CTD, ADCP, chlorophyll, turbidity, and oxygen sensors, ISUS nitrate sensor, battery packs, and the acoustically activated retrieval system (Figure 5.14). Minor modifications to brackets and fittings allowed last minute optimisation of sensor placement and the addition of a LISST-x25 to the eastern lander to measure the average particle size of suspended sediment for accurate sediment model parameterisation of resuspension (a key process impacting nutrient cycling in Storm Bay).

The motivation for lander deployment was to record long term continuous data to characterise seasonal water mass intrusions, and local current and wave induced resuspension. In addition, a field campaign was run simultaneously to obtain samples from each site as close to monthly as weather would permit. The primary aim of this data was to provide some ground-truthing for the remotely deployed instrumentation but also allowed some characterisation of how the water column was changing.
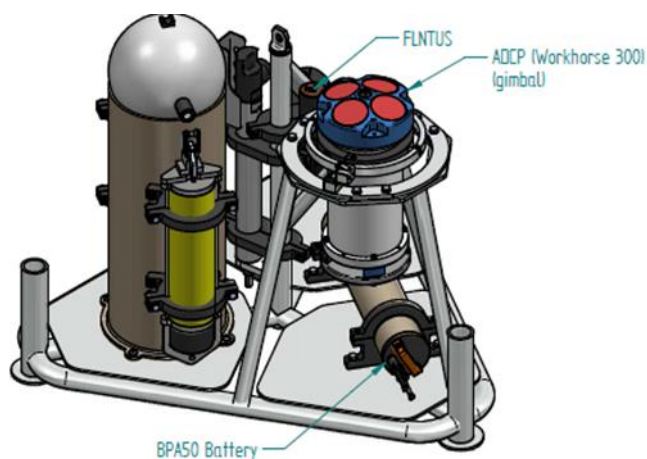

Figure 5.14: Benthic lander frame design

5.2.1   2018-19 Deployments

Two benthic landers were successfully deployed on opposite sides of Storm Bay from the MV *Soul Commitment* on 29th Nov 2018 (Table 5.2; Figure 5.15) and recovered on the 16th May 2019.

Table 5.2 Benthic lander positions at the time of deployment

Site	Latitude (degrees)	Longitude (degrees)	Water depth (m)
West	-43.20342	147.43860	38
East	-43.20332	147.43863	38.5

At both sites the seabed was gently sloping and appeared to consist of soft sediment as determined from the echo sounder. CTD casts, oxygen, plankton, and nutrient samples were taken from surface and bottom waters throughout the deployment to verify in situ sensor performance. Underwater video confirmed the landers were resting on a sandy bottom and sediment samples were obtained for characterisation.
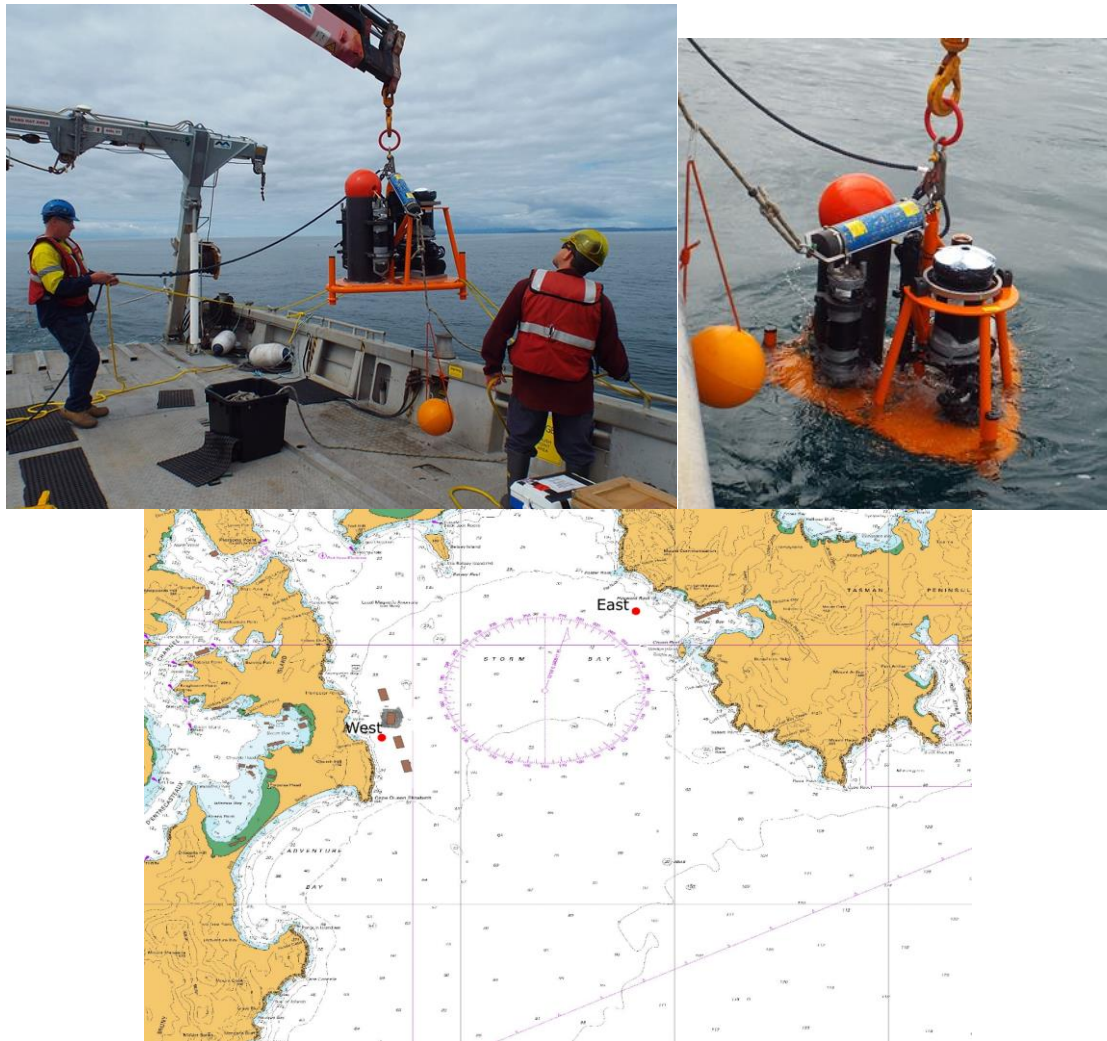
Figure 5.15 **Benthic lander deployment from MV Soul Commitment, November 2018. Red dots show lander locations and brown rectangles indicate marine lease areas according to ListMap.**

Monthly sampling

The water column at both sites showed a typical warming during the summer months along with some stratification, though this seems to be stronger in the west (Figure 5.16). Both sites were impacted by a storm during April 2019 which appears to have fully mixed the water column. Nutrient samples were analysed by the method in Rees et al., (2019) and as expected, bottom water nutrient concentrations were generally greater than those in surface waters (Figure 5.17), though there does appear to be elevated levels of ammonium in surface waters at both sites during February. The reasons for this are unclear at this stage.
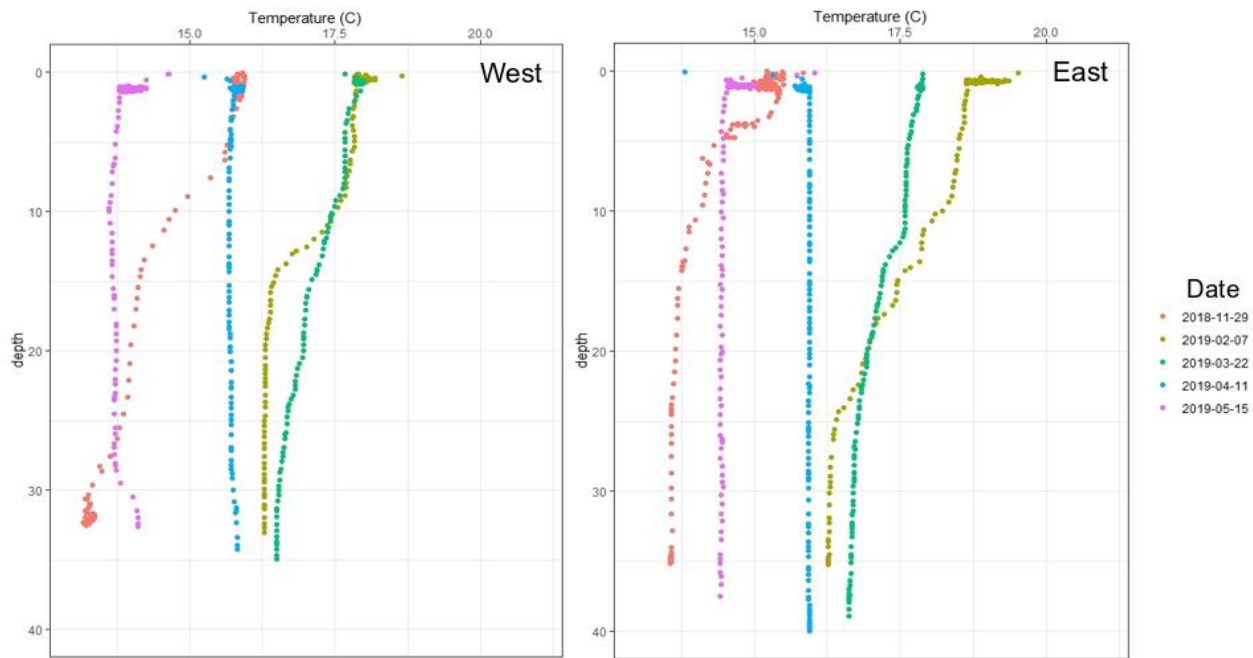
Figure 5.16 Monthly CTD casts at Lander sites

Water column chlorophyll concentrations were generally highest in surface waters during February and March at both sites, again as would be expected, however, during April 2019 concentrations were similar in surface and bottom waters due to the water column mixing that occurred as a result of recent strong winds (Figure 5.18).

Comparing the pigment analyses of the four sampling trips (Figure 5.19), the most striking differences were that both cryptophytes (as indicated by the presence of alloxanthin) and dinoflagellates (peridinin) were present in all samples at both sites and both depths for April and May, compared to the February and March samples when they did not appear to be part of the phytoplankton community composition. The April samples, again at both sites and both depths, were dominated by diatoms (fucoxanthin) more so than the other three months sampled. In general, all samples contain prasinophytes (prasinoxanthin, chl-b), haptophytes (hex-fuco) and small numbers of cyanobacteria (zeaxanthin) and chrysophytes (but-fuco). It is likely that numbers of cyanobacteria and chrysophytes were relatively small, as while zeaxanthin and but-fuco are diagnostic pigments for these groups, they can also be accessory pigments in prasinophytes and haptophytes, respectively.
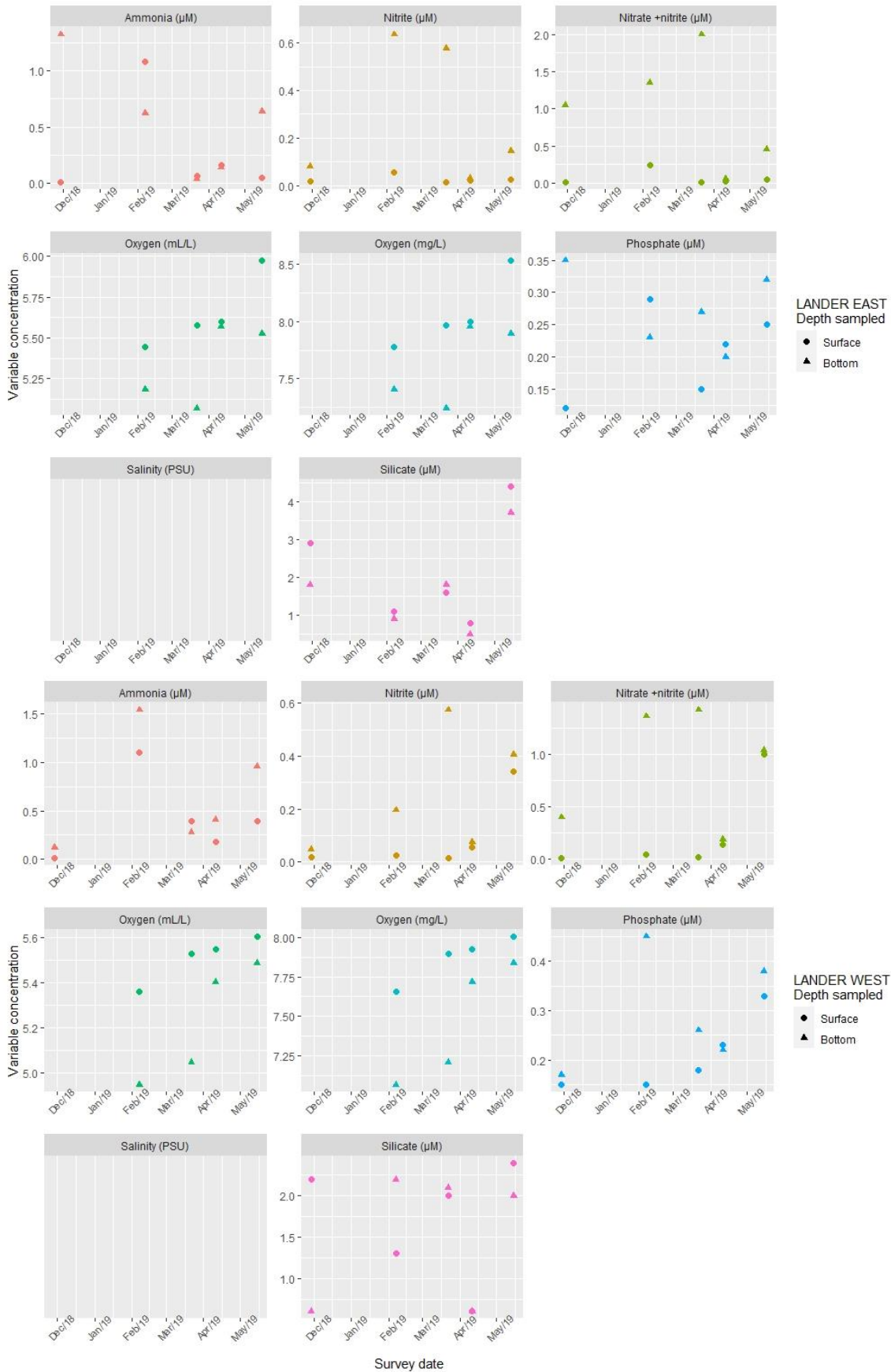
Figure 5.17: Monthly water column nutrient and oxygen concentrations measured at the two lander sites (East and West) sampled December 2018 to May 2019.
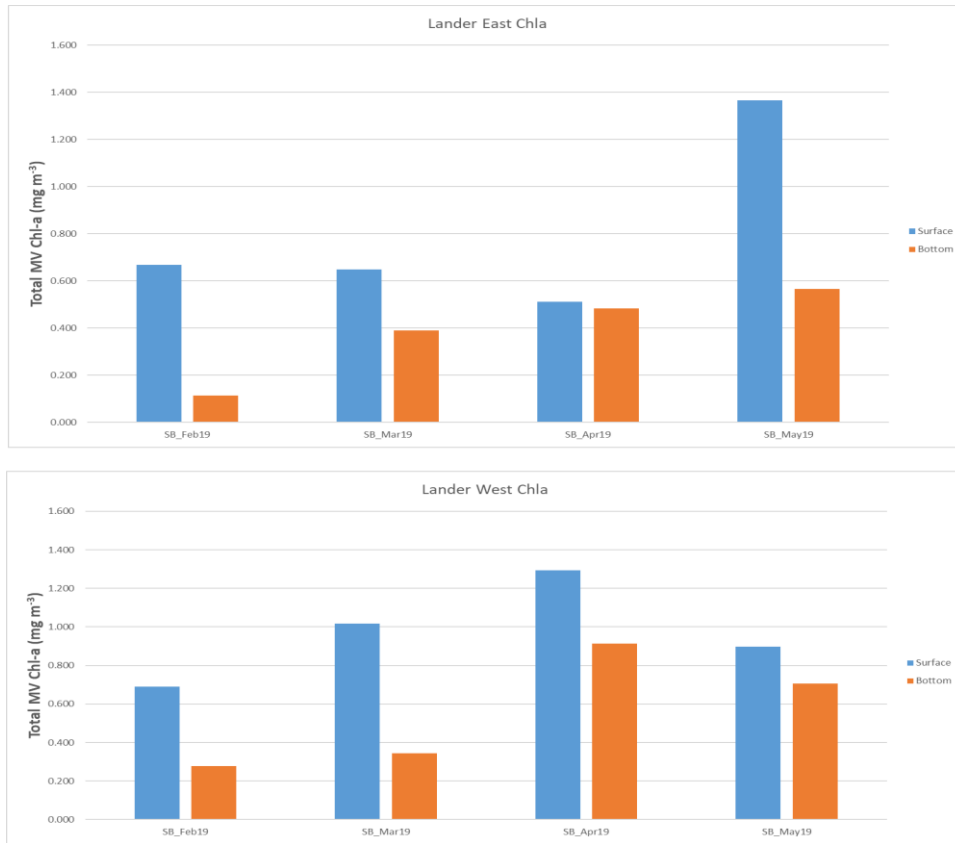
Figure 5.18: Monthly chlorophyll-a concentration at the two lander sites for surface (blue) and bottom (orange) samples (East and West) sampled December 2018 to May 2019.
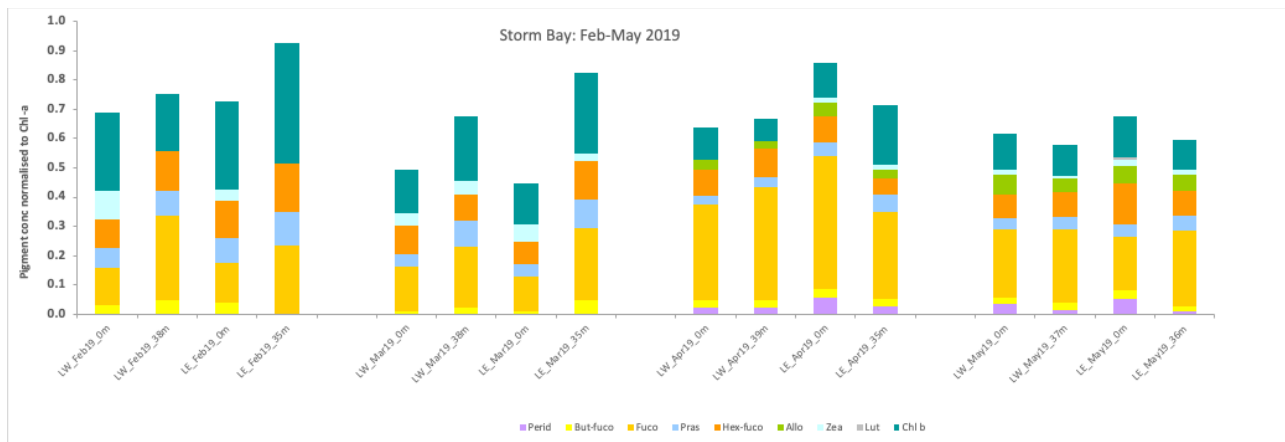

Figure 5.19 Monthly pigment composition of surface and bottom water samples collected at the lander sites. LW = Lander west and LE = lander east

The phytoplankton community composition was similar at both depths sampled (Figure 5.20), with a diatom-rich community and low numbers of the bioluminescent dinoflagellate *Noctiluca scintillans*. More normal distributions appear to have resumed by May, although the eastern site had a spike in chlorophyll in surface waters, which may be due to material transported from elsewhere. Phytoplankton community composition was similar in surface waters at both sites in May 2019, with an increase in the diversity of dinoflagellate species, including the HAB species *Gymnodinium catenatum,* which is otherwise very rarely observed at these sites. Oxygen levels show surface waters have higher concentration than bottom waters,

with the exception of the April sampling when a recent storm resulted in a fully mixed water column at both the west and east sites.

In general, the phytoplankton community composition analysis at both sites revealed a rich diatom-dominated assemblage typical of southeast Tasmanian coastal environments in spring 2018, transitioning to a less diverse composition in mid-late summer 2019. Small heterotrophic ciliates were more abundant in the late stages of summer, while dinoflagellate species were more prominent moving into autumn (Figure 5.20). These data suggest that the model formulation with functional groups which characterise small phytoplankton, large phytoplankton, dinoflagellates and microphytobenthos is sufficient to represent the broad population dynamics of the species present.
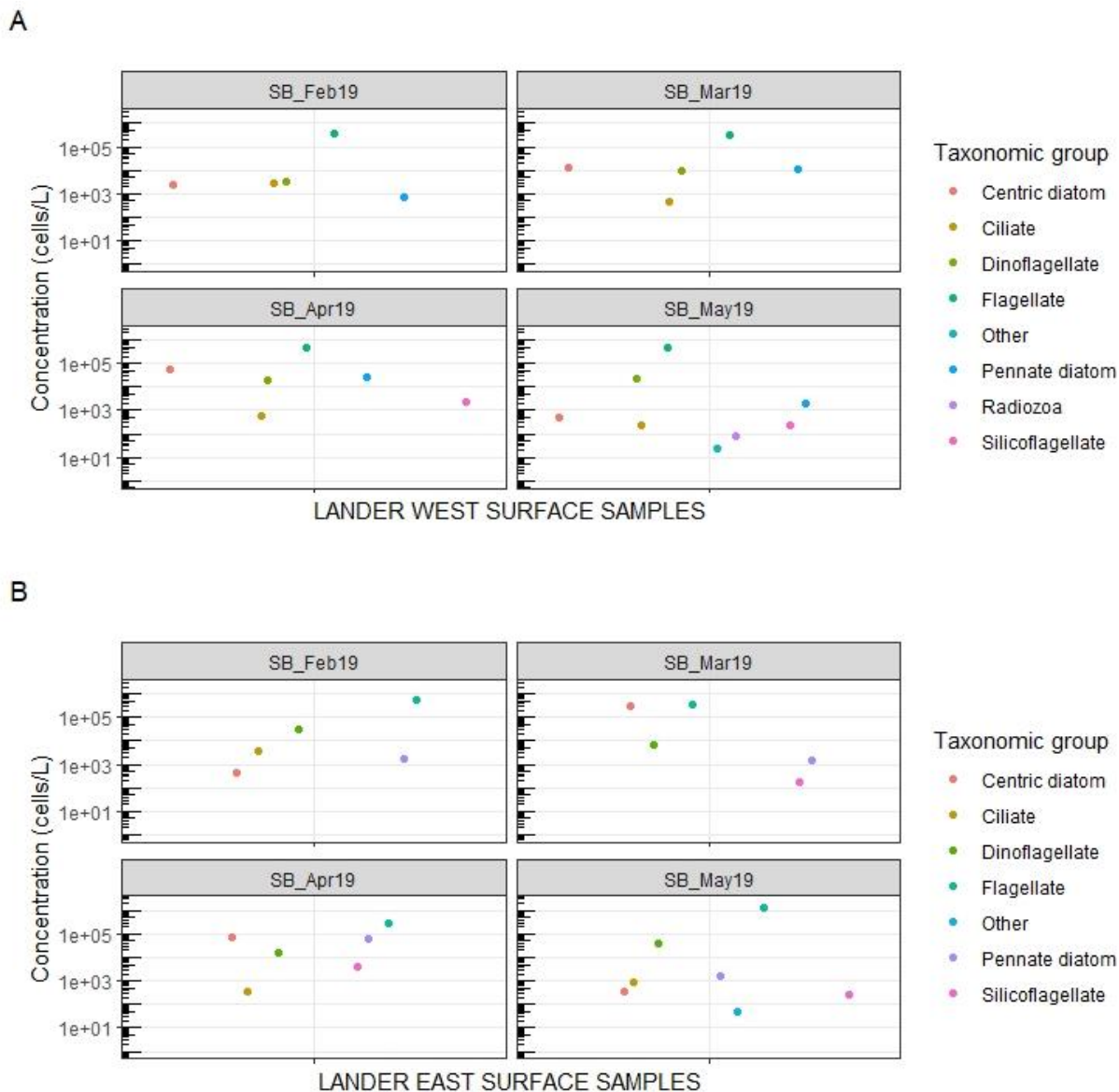

Figure 5.20 Monthly phytoplankton community composition summarised as major taxonomic groups for surface samples from the two lander sites (East and West) sampled December 2018 to May 2019.

Benthic Lander data

Western Site

Bottom water nitrate measurements made by the lander at the western site appear to show 3-4 periods when nutrient was being released from the sediment (Figure 5.21). Comparison of these periods with the turbidity data indicates that these events were not always accompanied by an increase in turbidity and similarly, an increase in turbidity did not always appear to directly result in nutrient release.
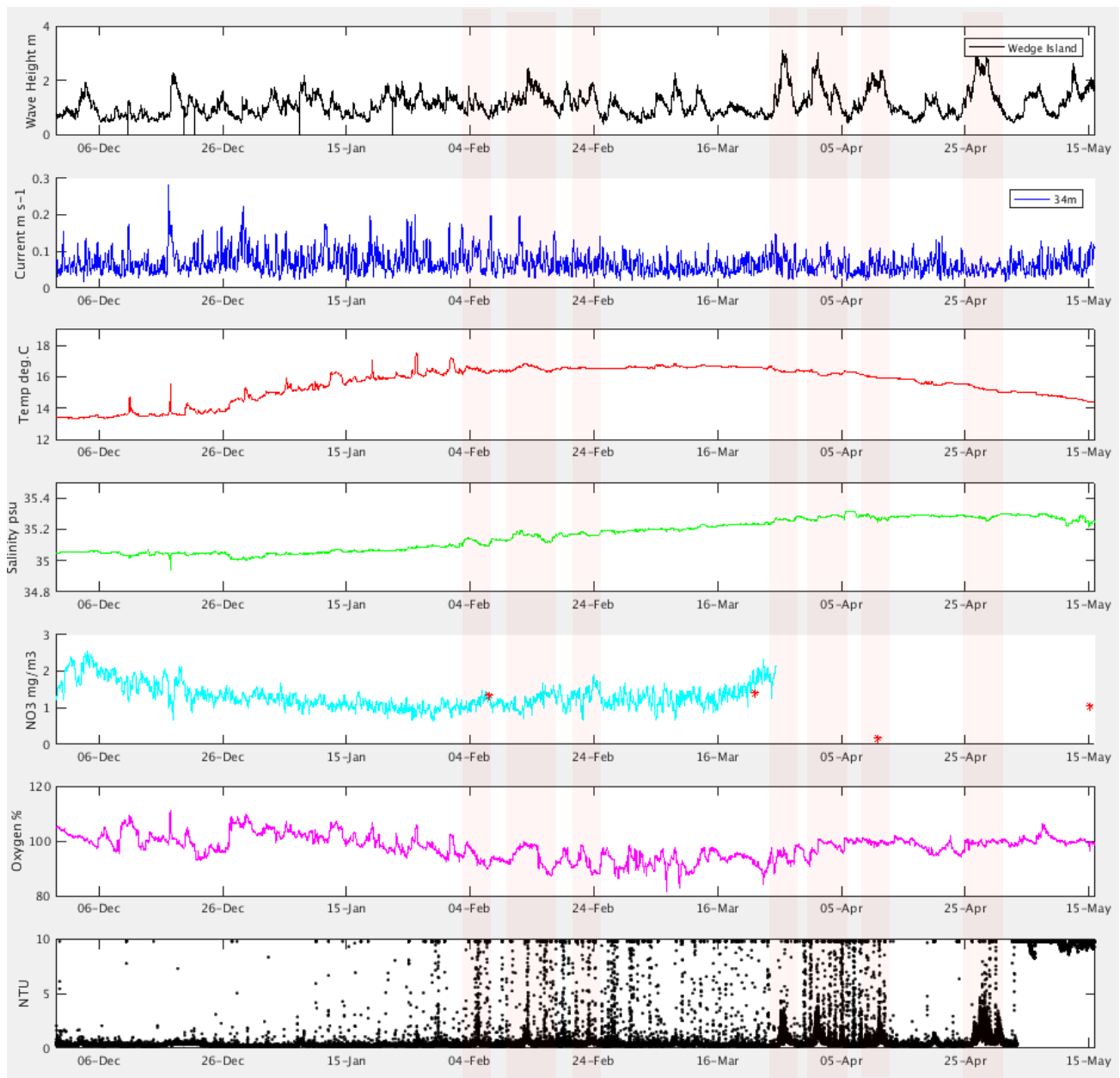

Figure 5.21 Time series of wave height (at Tassal Wedge Island wave buoy) and water properties measured over the six-month lander deployment period at the western site. Pink shading highlights times when significant re-suspension appears to have occurred. Red dots in the nitrate plot show concentrations measured during the monthly surveys.
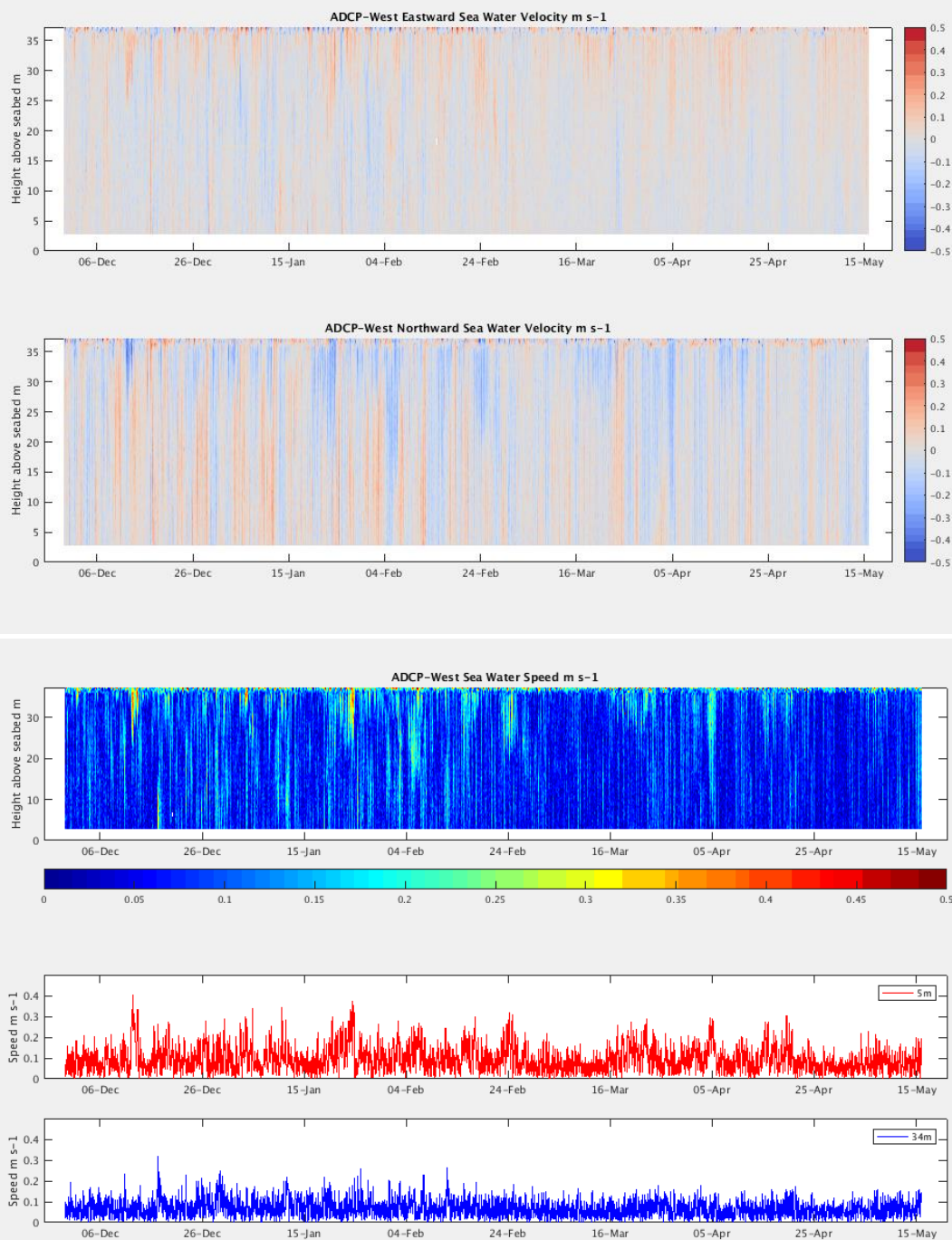
Figure 5.22 Timeseries of ADCP velocity profiles (upper panel) at the western lander site with calculated current speed profile, and surface and bottom current speed timeseries (lower panel).

Results suggest that at times, nutrient increase maybe driven by bottom water movement (Figure 5.22) which could be bringing nutrients with it or have sufficient velocity to induce irrigation of the sediment but not cause re-suspension, bearing in mind the sediments are quite coarse. In addition, whether a resuspension event directly results in nutrient release will depend on accumulation and processing of organic matter and how long the sediment has been undisturbed to allow for anoxia to establish and a build-up of nutrients in the pore water.

Eastern site

At the eastern site in Storm Bay there appears to have been several periods of nutrient release into bottom waters and these, along with bottom water back-scatter (suspended sediment), appear to be strongly related to periods when the significant wave height, as measured at the Tassal wave rider buoy (close to the study site) exceeded 2 m (Figure 5.23). However, as with the data from the western site, while increased re-suspension of sediment appears to be directly related to wave activity, there isn't always a release of nutrients associated with these events (and vice versa) suggesting that history of sediment resuspension/deposition and advection of water past the lander site (Figure 5.24) also contribute to the bottom nutrient concentration.
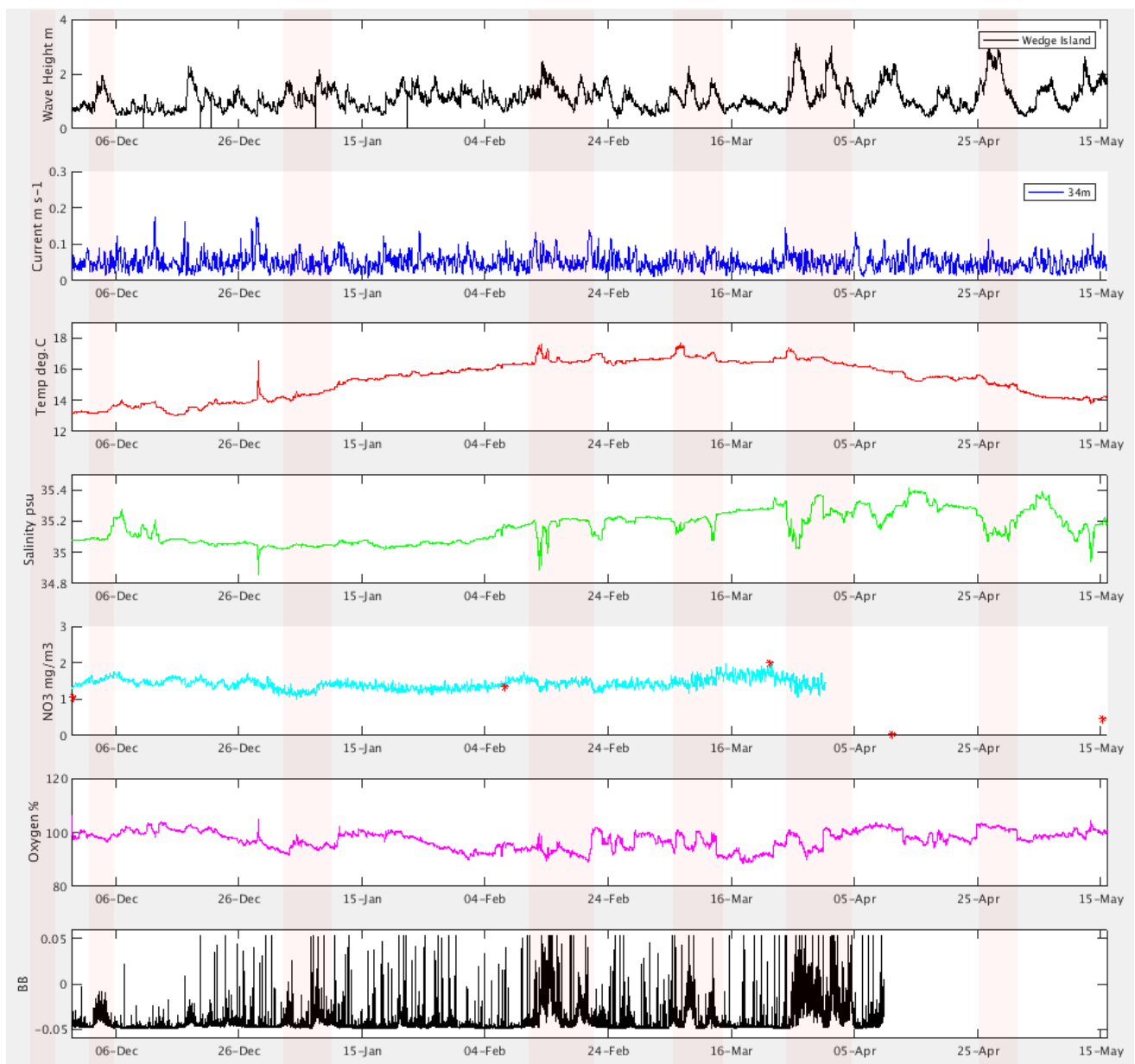

Figure 5.23 Time series of wave height (at Tassal Wedge Island wave buoy) and water properties measured over the six-month lander deployment period at the eastern site. Pink shading highlights times when significant re-suspension appears to have occurred. Red dots in the nitrate plot show concentrations measured during the monthly surveys.
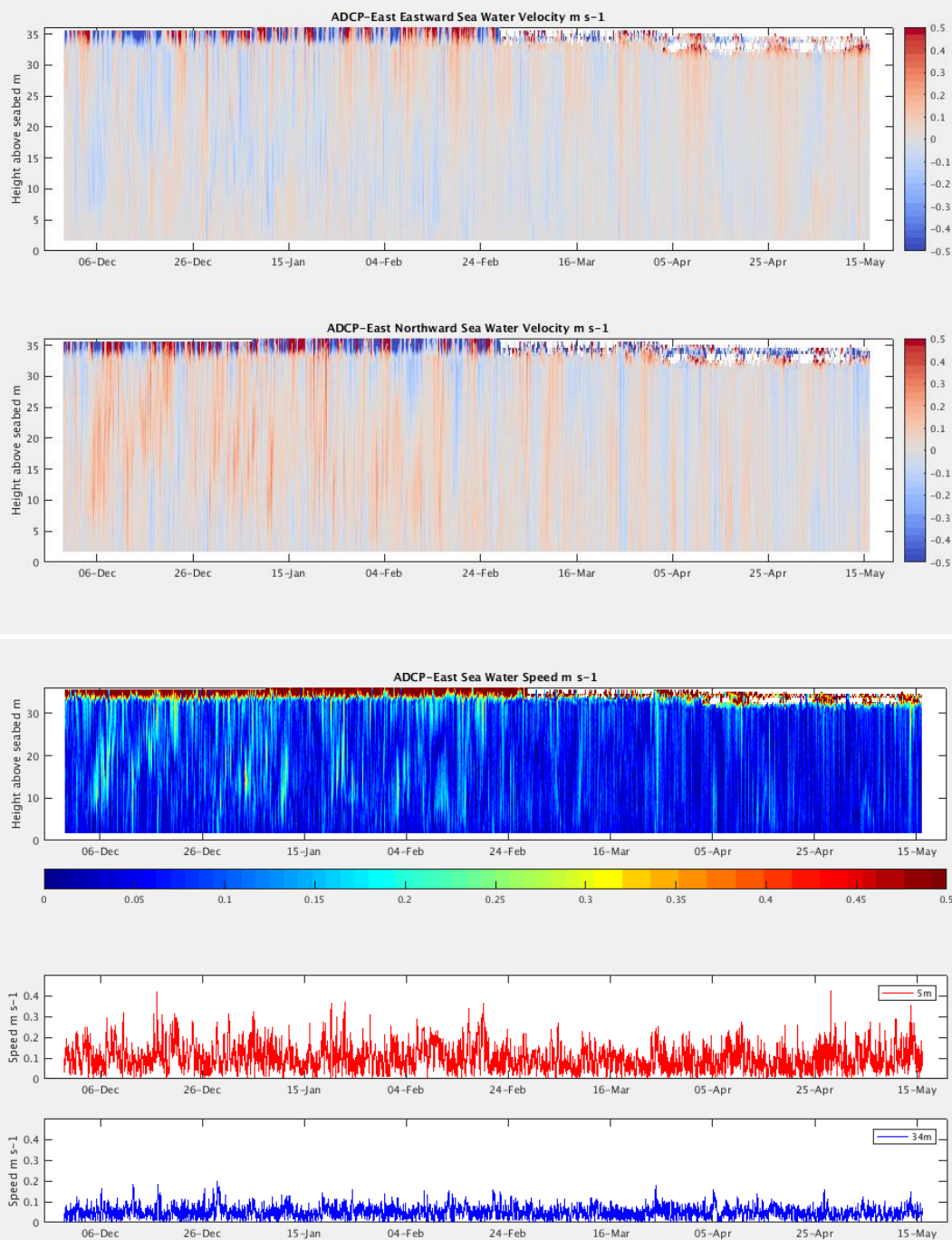
Figure 5.24 Timeseries of ADCP velocity profiles (upper panel) at the eastern lander site with calculated current speed profile, and surface and bottom current speed timeseries (lower panel).

5.2.2 2019-2020 Deployment

The benthic landers were redeployed in new locations in November 2019 (Table 5.3; Figure 5.25), in a north-south configuration and were again sampled monthly for water column parameters.

Table 5.3 Benthic lander (North and South) positions at the time of deployment

Site	Latitude (degrees)	Longitude (degrees)	Water depth (m)

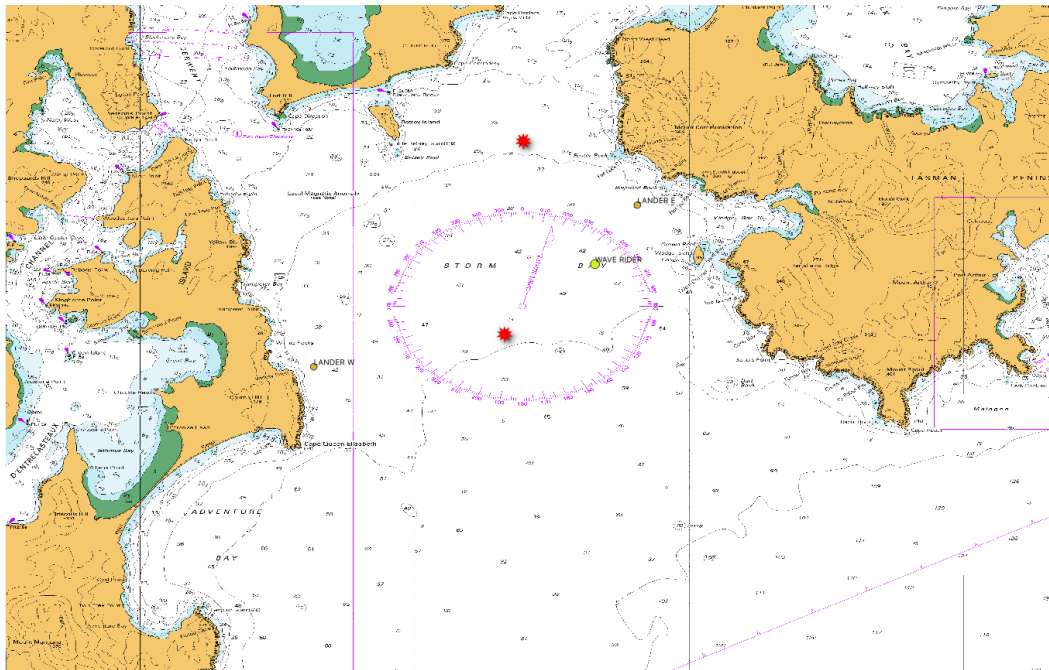| North | 43° 3.998' S | 147° 33.772' | 29 |
| South | 43° 10.212' | 147° 33.273' E | 48 |

Figure 5.25 Benthic lander deployment, November 2019. Red dots show lander locations

Monthly sampling

As with the 2018-19 deployment, the 2019-20 study sites exhibited quite strong stratification during the late autumn/early summer months (Figure 5.26) which was particularly prevalent at the shallower northern site. Again, storms in late summer/early spring resulted in the water column becoming fully mixed.

Nutrient data from the monthly sampling from December 2019 to May 2020 are shown in Figure 5.27. As with the previous deployments, nutrients are typically higher in bottom waters and depleted in surface waters. The exception is silicate which across both deployments tends to be higher in surface waters. Oxygen levels are consistently highest in surface waters.

Total chlorophyll concentrations were reasonably consistent in surface and bottom waters during the sampling period, with the exception of March 2020 when there appears to have been significantly elevated concentrations in surface waters at both sites (Figure 5.28). Pigment analyses (Figure 5.29) suggest that at the time of all three samplings, diatoms (fucoxanthin) were dominating the phytoplankton community at both the surface and deeper depths. In almost all the samples, there were prasinophytes (prasinoxanthin, chl-b), haptophytes (hex-fuco) and chrysophytes (but-fuco). Interestingly, cryptophytes (as indicated by the presence of alloxanthin and crocoxanthin) and cyanobacteria (zeaxanthin) are present in the December and 20-March-2020 (Mar20B) samples but were absent at the time of the February sampling. This suggests there was some temporary change in the water body/nutrient regime between December and the end of March which influenced their presence.

Phytoplankton community composition (summarised as major taxonomic groups) are shown in Figure 5.30. Community diversity at both sites is typically diatom-rich, with overall diversity increasing over the monitoring period. Diversity was richer at the northern site, consistent with observations from long-term monitoring in Storm Bay which showed that diversity (and abundance) decrease with distance (and increasing water depth) from the Derwent Estuary (Swadling et al., 2017). The model formulation with functional groups which characterise small phytoplankton, large phytoplankton, dinoflagellates and microphytobenthos is sufficient to represent the broad population dynamics of the species present.
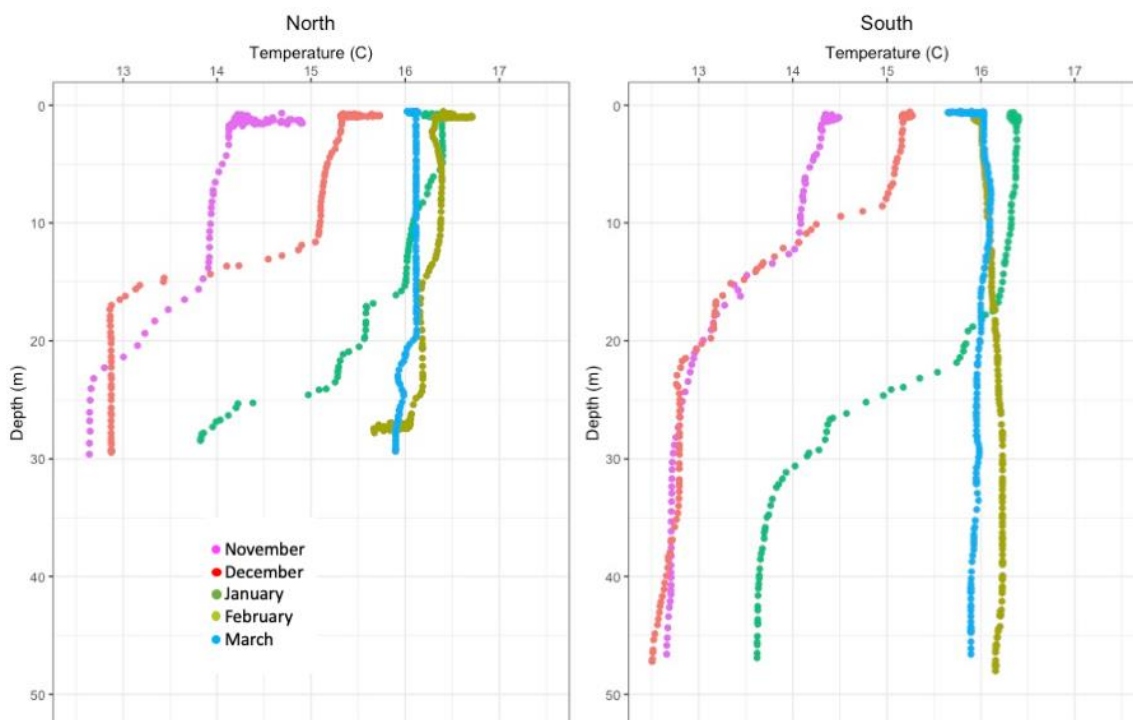

Figure 5.26 Monthly CTD profiles collected during benthic lander deployment at the northern and southern locations.
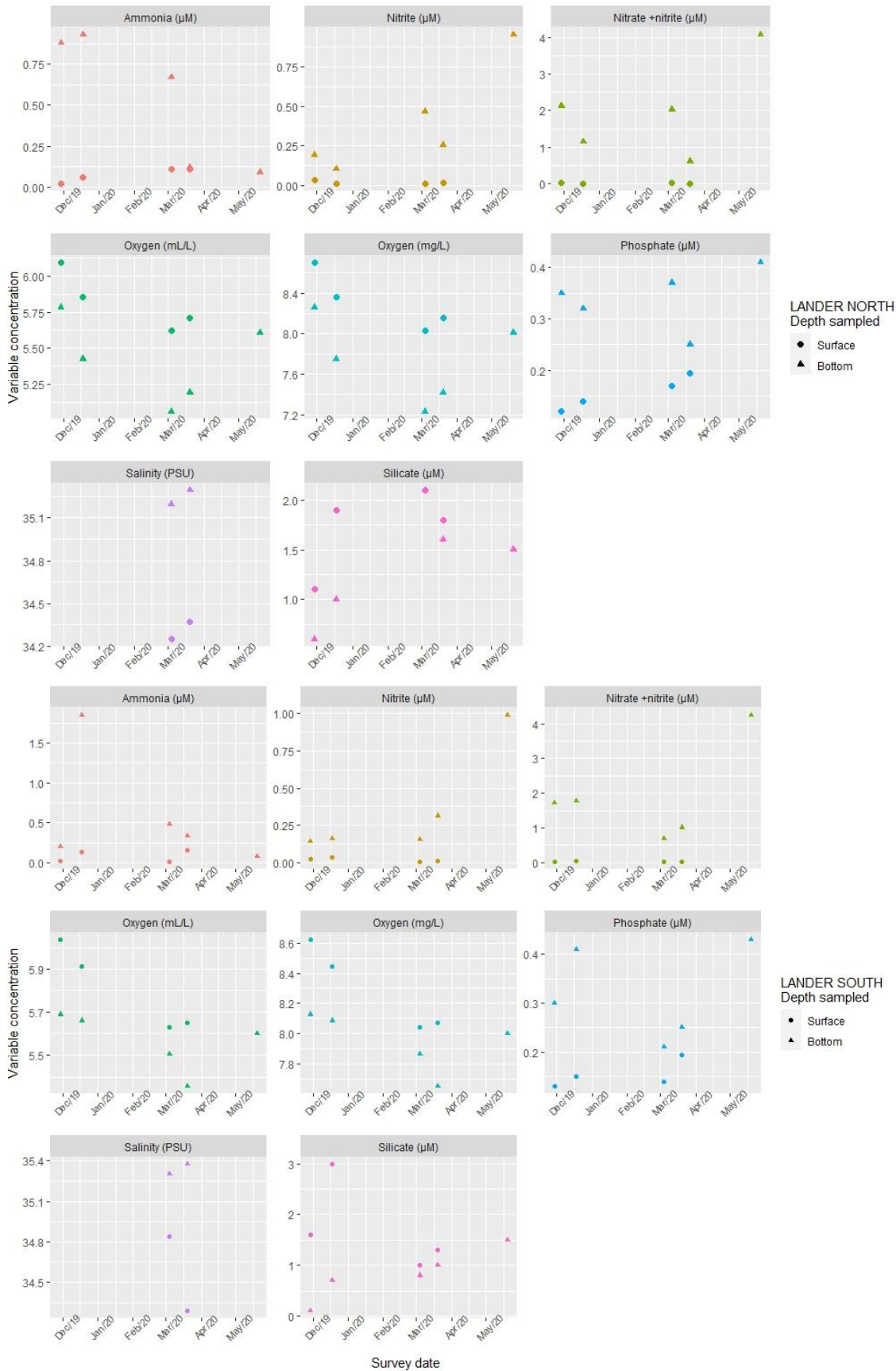
Figure 5.27 Monthly water column nutrient and oxygen concentrations measured at the two lander sites (North and South) sampled December 2019 to May 2020.
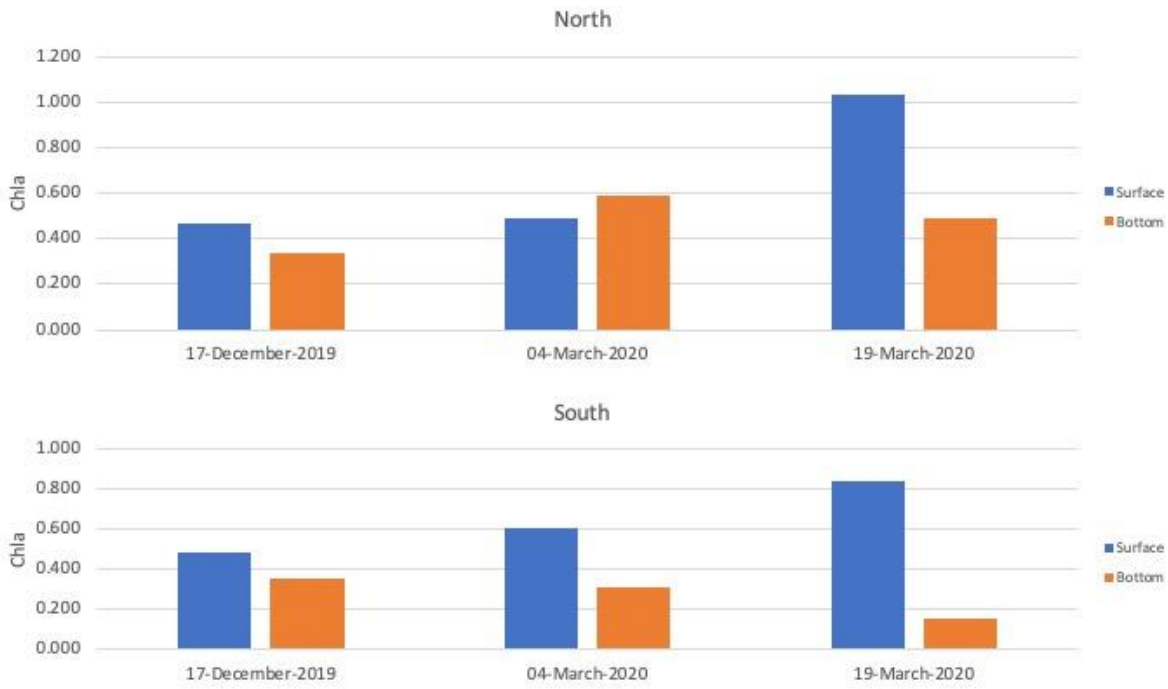
Figure 5.28 Water column total chlorophyll-a (mgm^{-3}) measured at the lander sites in surface (blue) and bottom (orange) water.
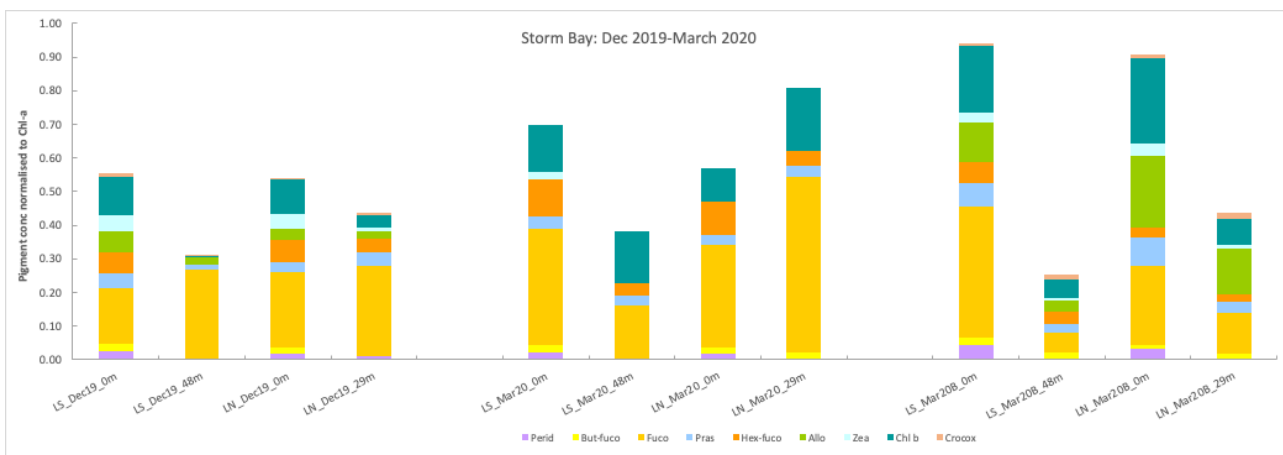

Figure 5.29: Water column phytoplankton pigment composition for samples collected in surface and bottom waters at the lander sites. LS = Lander south and LN = Lander north.
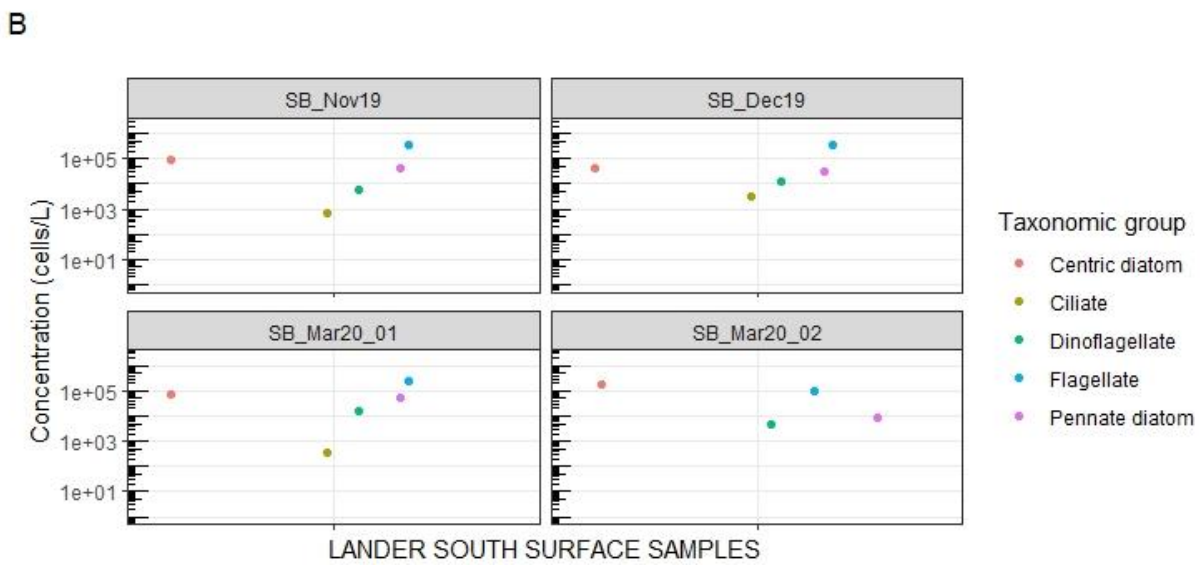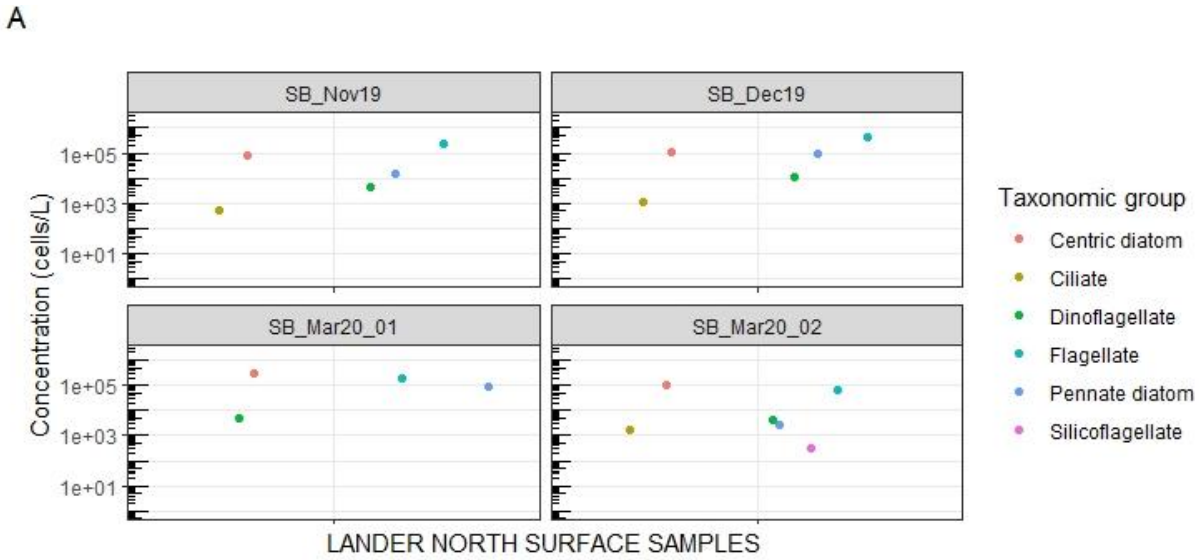
Figure 5.30 Monthly phytoplankton community composition summarised as major taxonomic groups for surface samples from the two lander sites (north and south) sampled November 2019 to March 2020. Note two sampling events in March 2020.

Total suspended solids in bottom waters were reasonably consistent across both sites (Figure 5.31) except for a large increase at the north lander at the beginning of March. The relative contribution of organic vs inorganic components was approximately even at the south lander during the sampling period, but inorganic components tended to dominate at the north lander site (Figure 5.32). This may well reflect the different depths and susceptibility to resuspension and/or that north lander was much closer to the influence from riverine inputs.
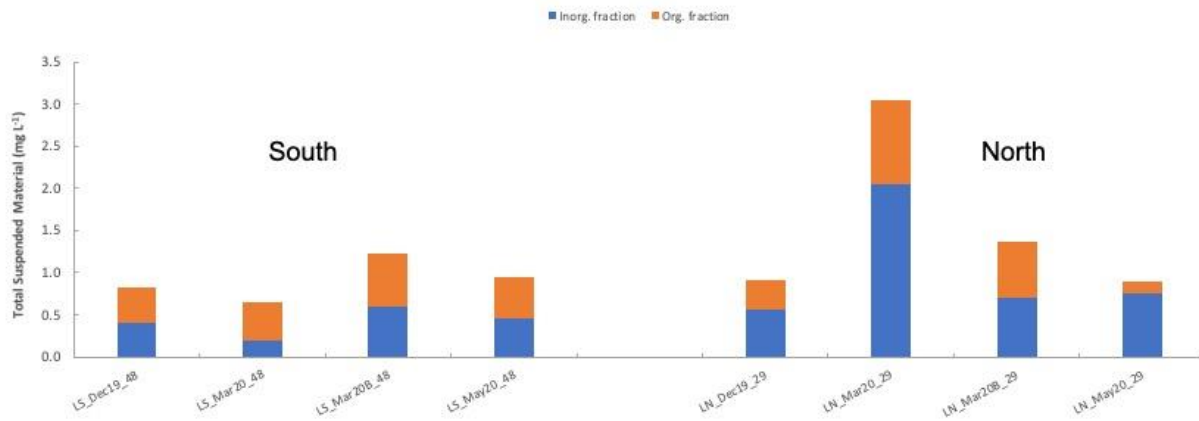
Figure 5.31 Water column Total Suspended Solids (TSS; mgL^{-1}) measured in bottom waters at the lander sites during 2019-20. Organic and inorganic fractions are shown in orange and blue respectively.
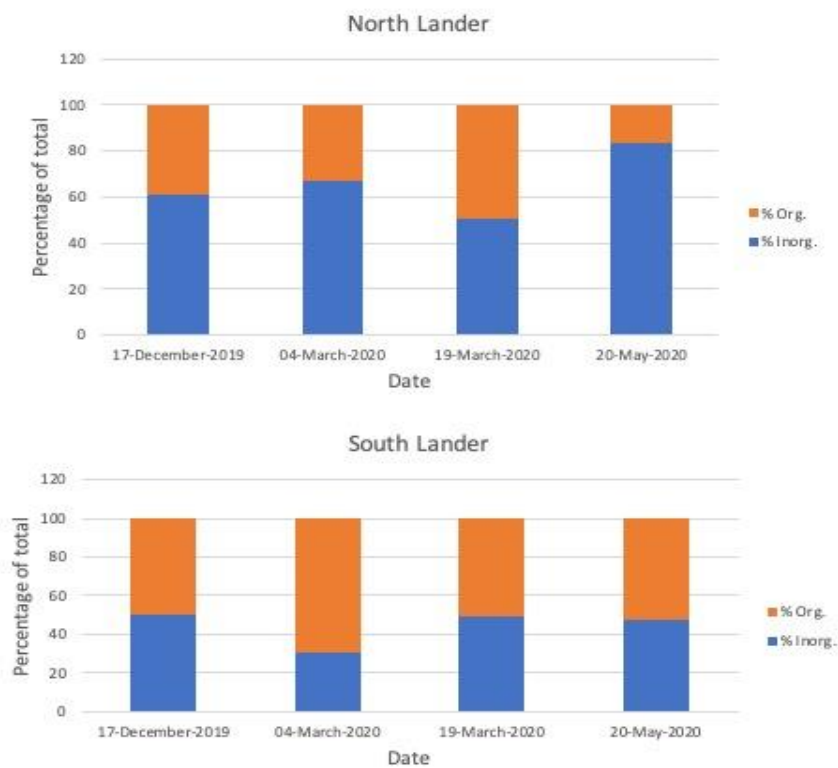

Figure 5.32 Percentage contribution of organic (orange) and inorganic (blue) components in TSS sampled at the lander sites

Total sediment nitrogen averaged around 0.01 % (w/w) and organic carbon 0.3 % (w/w) across the lander sites which is typical of sandy sediments (Figure 5.33; Table 5.4). High C:N ratios suggest a degree of influence from terrestrial material at all sites though caution is required in interpreting this data as such low concentrations can lead to relatively large heterogeneity within sediments. However, more negative δ^{13}C values for the carbon isotopes support this conclusion.
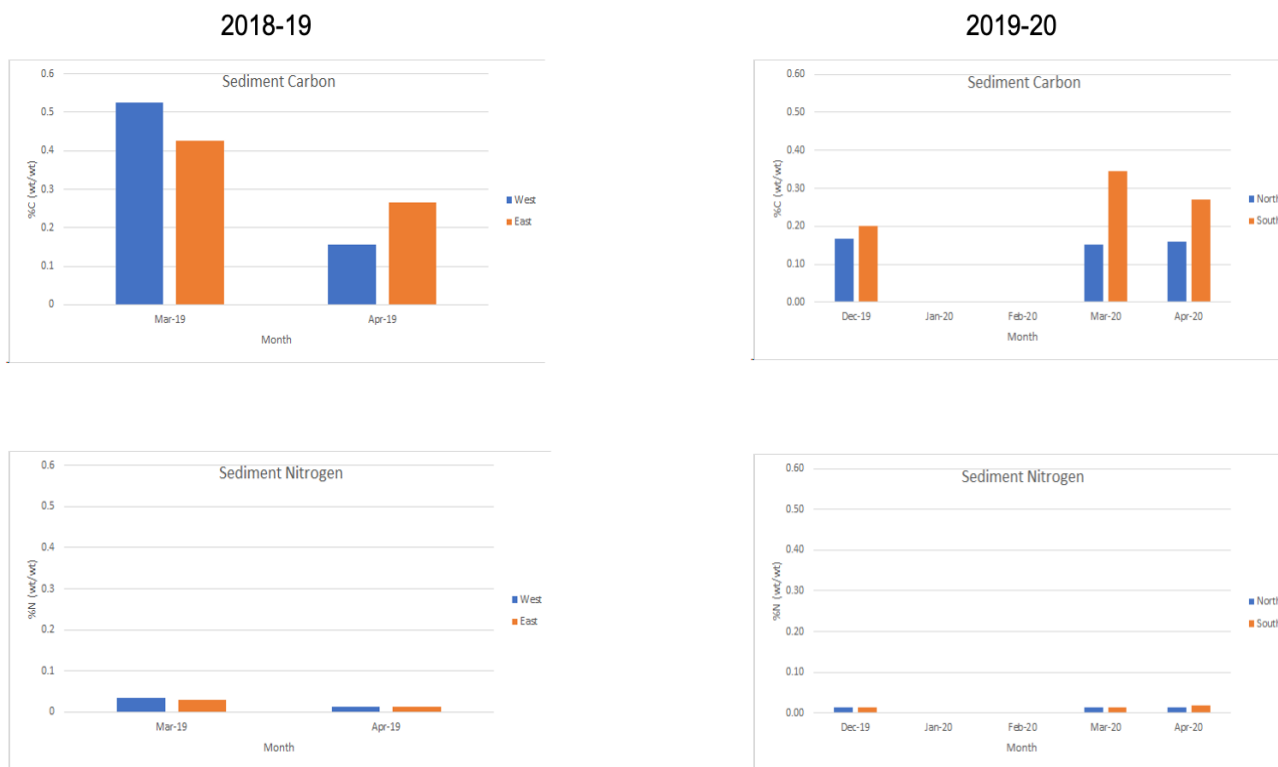
| 2018-19 | 2019-20 |

Figure 5.33 Sediment organic carbon and total nitrogen content (µg/g; w/w) at the lander sites for 2018-19 and 2019-20

Table 5.4 Percent (w/w), C:N (w/w) and stable isotope values for sedimentary organic carbon and total nitrogen at lander sites during 2018-19 and 2019-20.

2018-19

		%N	δ 15N	%C	δ 13C	C:N
Mar-19	West	0.03	9.5	0.53	-20.9	15.3
	East	0.03	10.5	0.43	-16.8	13.9
Apr-19	West	0.01	6.4	0.16	-21.5	11.9
	East	0.01	6.4	0.27	-19.0	23.0

2019-20

		%N	δ 15N	%C	δ 13C	C:N
Dec-19	North	0.01	8.3	0.17	-22.2	13.0
	South	0.01	7.9	0.20	-23.4	15.3
Mar-20	North	0.01	8.1	0.15	-23.2	10.1
	South	0.01	8.3	0.35	-14.9	24.3
Apr-20	North	0.01	8.4	0.16	-23.1	11.6
	South	0.02	8.2	0.27	-20.7	14.6

Benthic Lander data

Retrieval of the two benthic landers for the 2019-20 survey period was significantly delayed. Firstly, the COVID-19 restrictions put in place during March 2020 resulted in an inability to attempt retrieval until May 20th. The southern lander was able to be retrieved after several attempts to release the float. Unfortunately, the float on the northern lander failed to release. This was eventually recovered using a grapple hook on 4th June. Both landers suffered from extensive growth and apparent instrument failure during the deployment.

All sensor data collected at the norther lander site are shown in Figures 5.34a and 5.34b, and at the southern lander site in Figures 4.35a and 4.35b. In general, bottom water temperature and dissolved oxygen (Figure 5.36) were broadly similar across both sites with slightly more variability being observed at the northern site. A comparison of backscatter (northern lander) and turbidity (southern lander) shows that some resuspension events occurred simultaneously at both sites but as would be expected, the shallower northern site had longer/more frequent events (Figure 5.37). Data recorded at both landers were in relative agreement with fluctuations measured by TSS analyses of bottom water collected during the sampling program (Figure 5.37 and 5.37b), though direct conversion of turbidity/ADCP backscatter to TSS would require significantly more calibration samples, the lander data importantly provides a continuous record of relative bottom water turbidity.
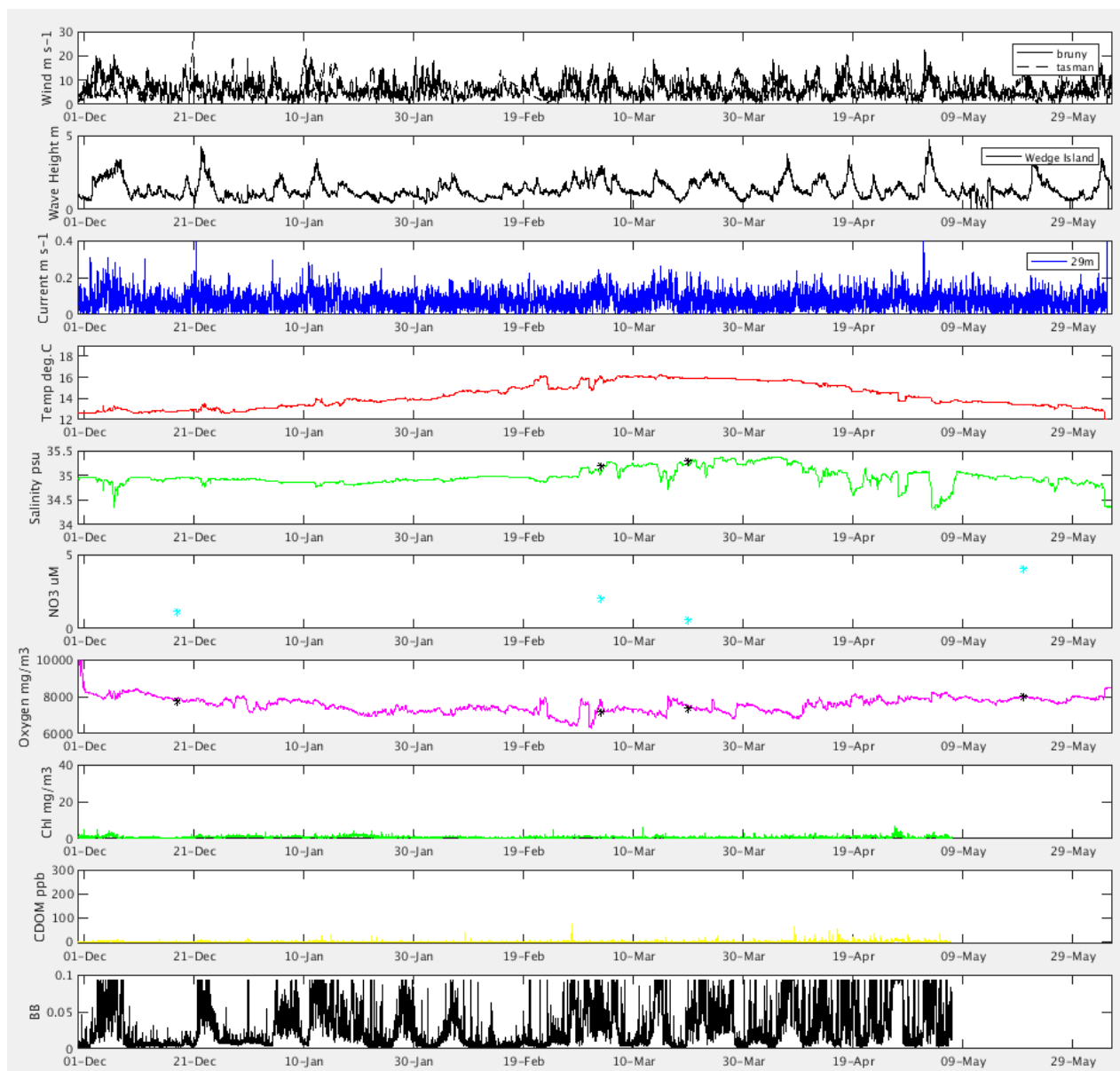

Figure 5.34a Time series of wind speed (at BOM Bruny & Tasman Island sites), wave height (at Tassal Wedge Island wave buoy) and water properties measured over the six-month lander deployment period at the Northern Lander site. Blue markers in the nitrate plot show concentrations measured during surveys.

Figure 5.34b Timeseries of ADCP velocity profiles (upper panel) at the northern lander site with calculated current speed profile, and surface and bottom current speed timeseries (lower panel).
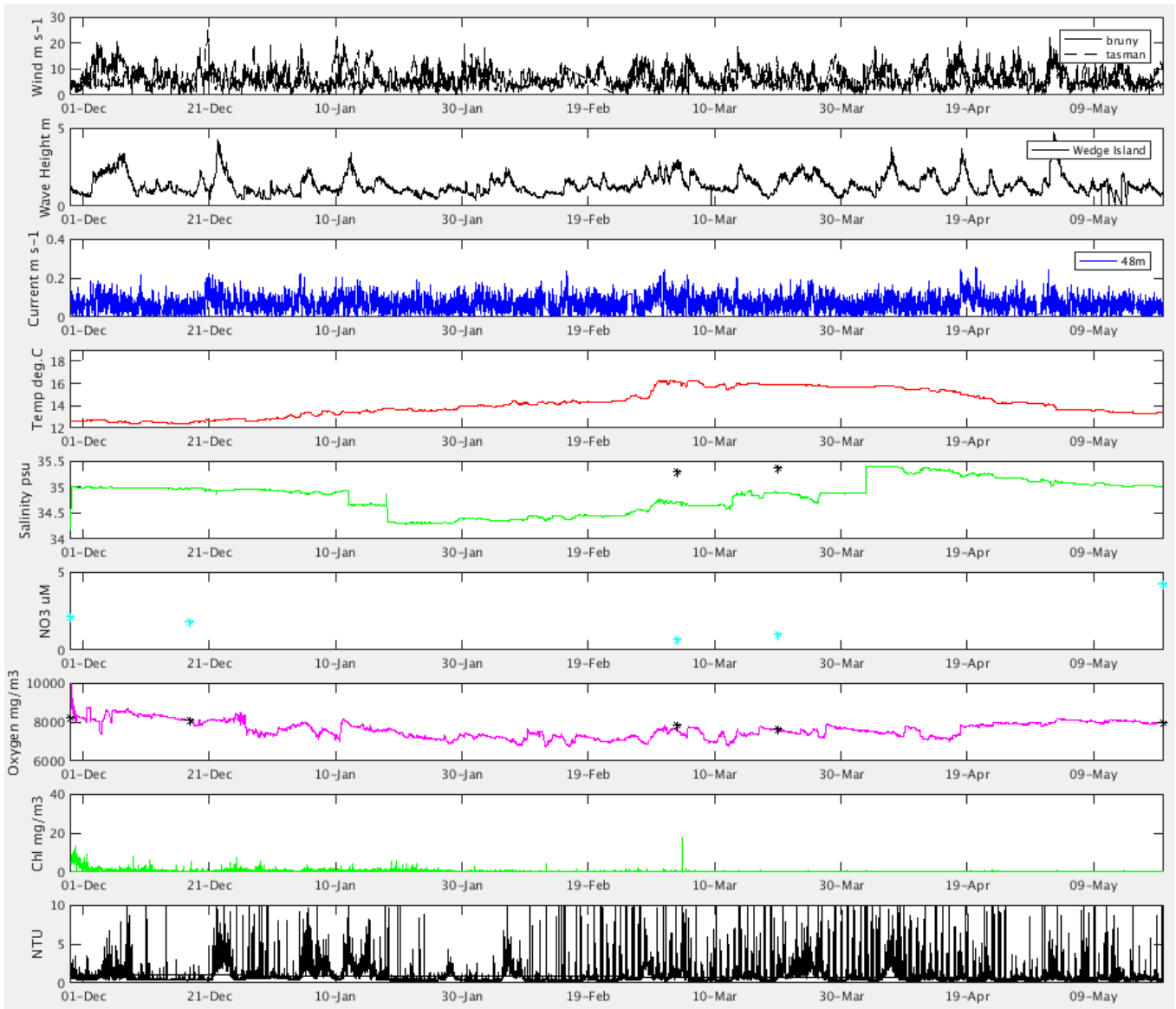
Figure 5.35a Time series of wind speed (at BOM Bruny & Tasman Island sites), wave height (at Tassal Wedge Island wave buoy) and water properties measured over the six-month lander deployment period at the Southern Lander site. Blue markers in the nitrate plot show concentrations measured during surveys.
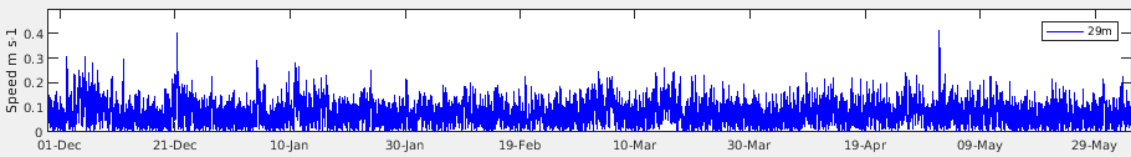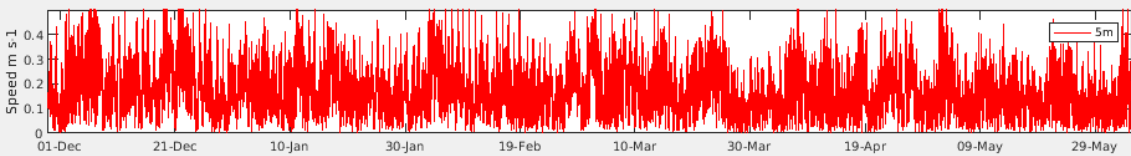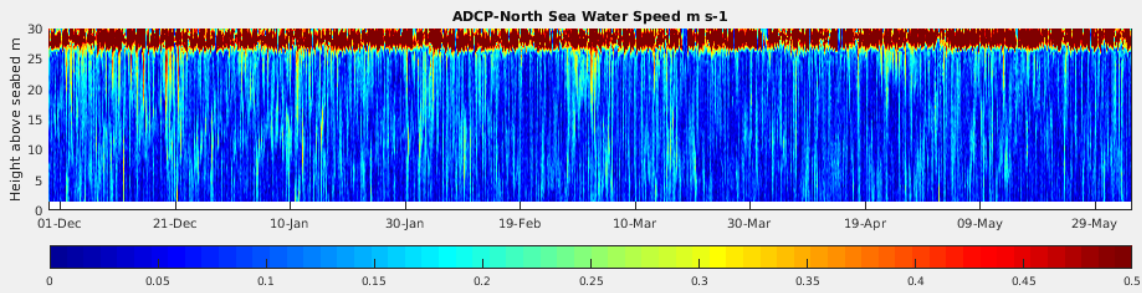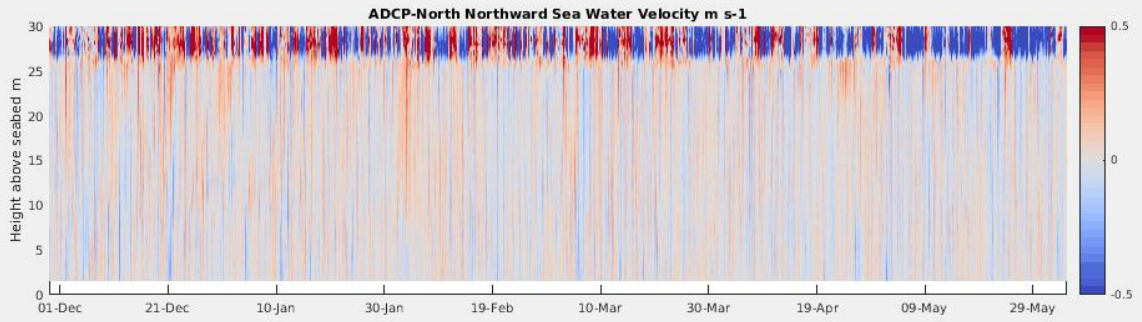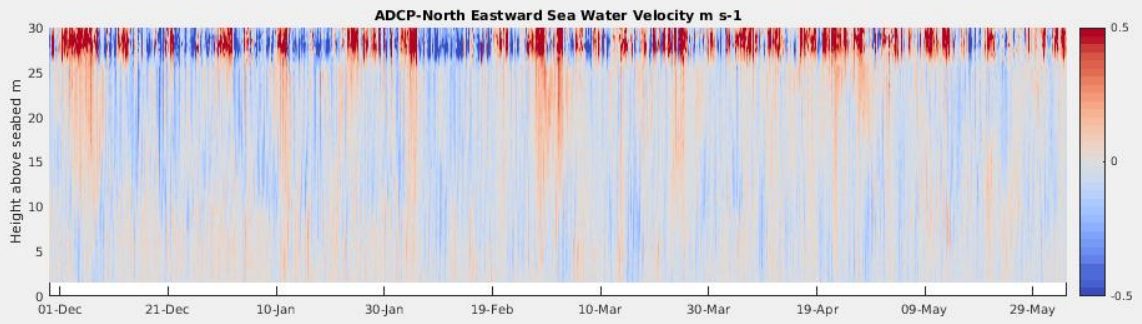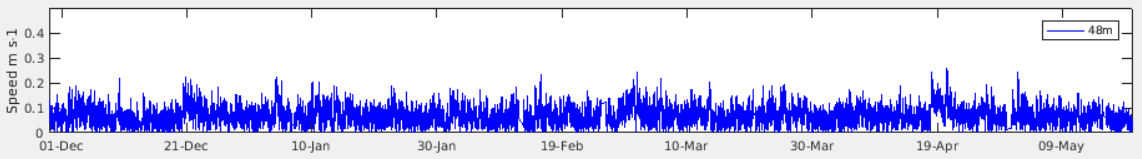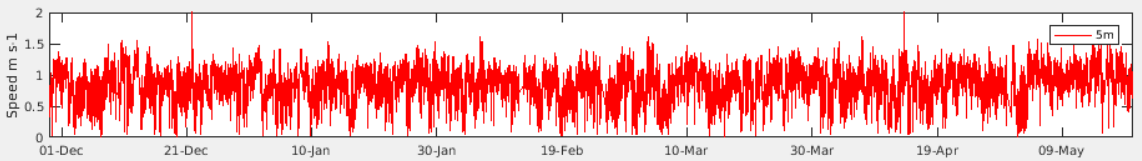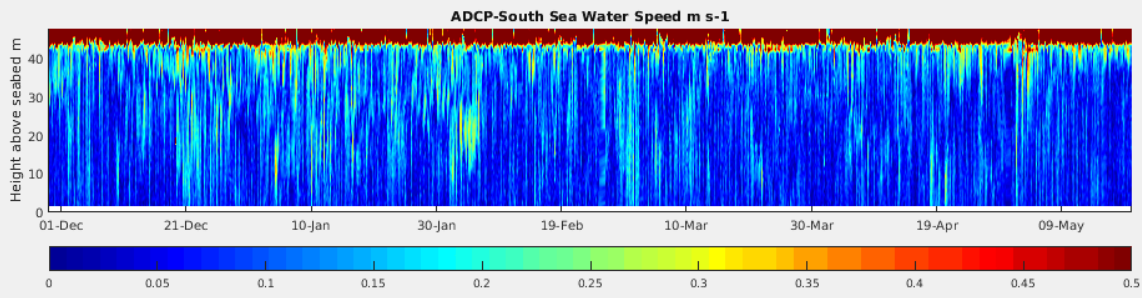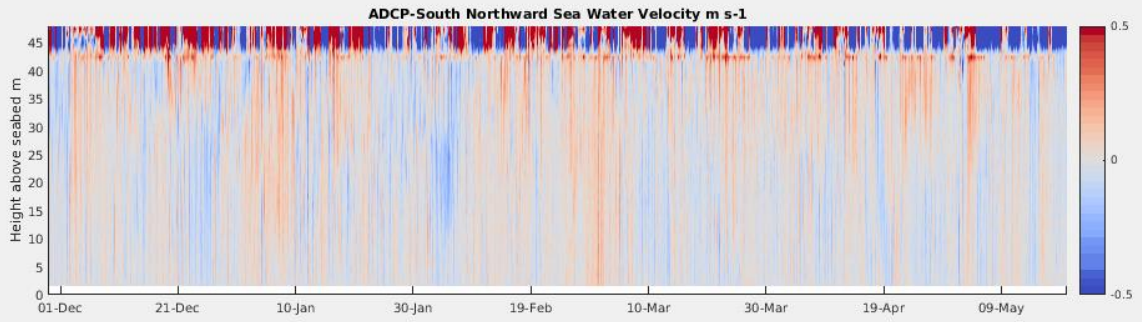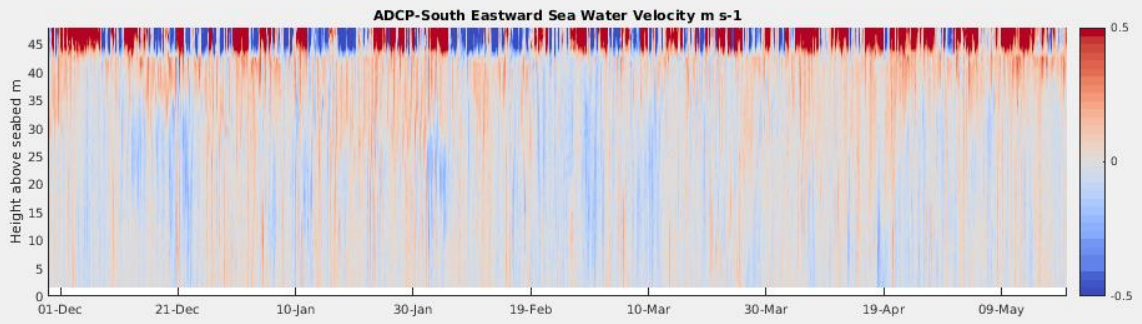
Figure 5.35b Timeseries of ADCP velocity profiles (upper panel) at the southern lander site with calculated current speed profile, and surface and bottom current speed timeseries (lower panel).
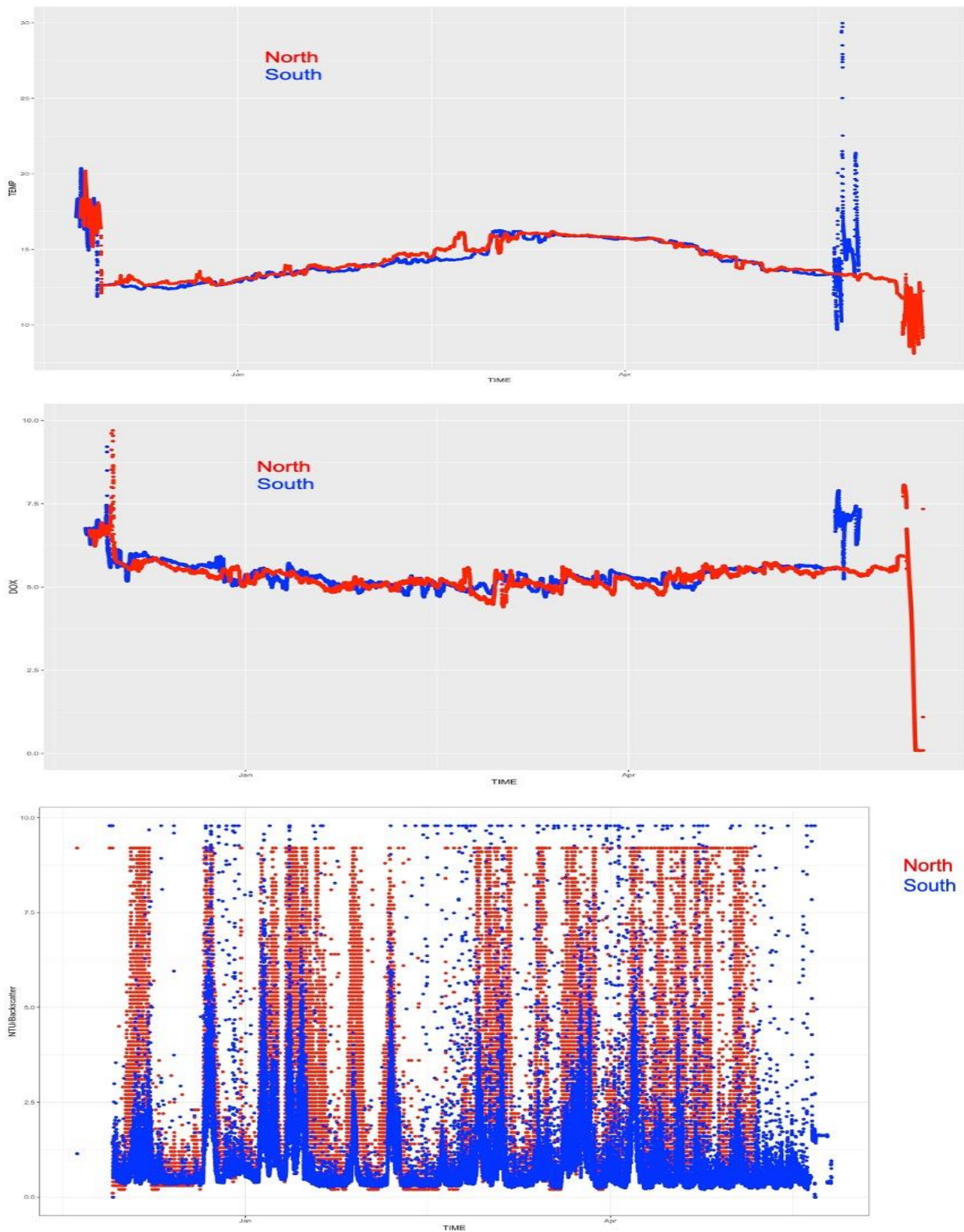
Figure 5.36 Bottom water temperature, oxygen and turbidity measured in-situ by the benthic landers at the northern and southern locations. Note: due to instrument failure on the northern lander turbidity is represented by ADCP backscatter thus the magnitude of events are not directly comparable.
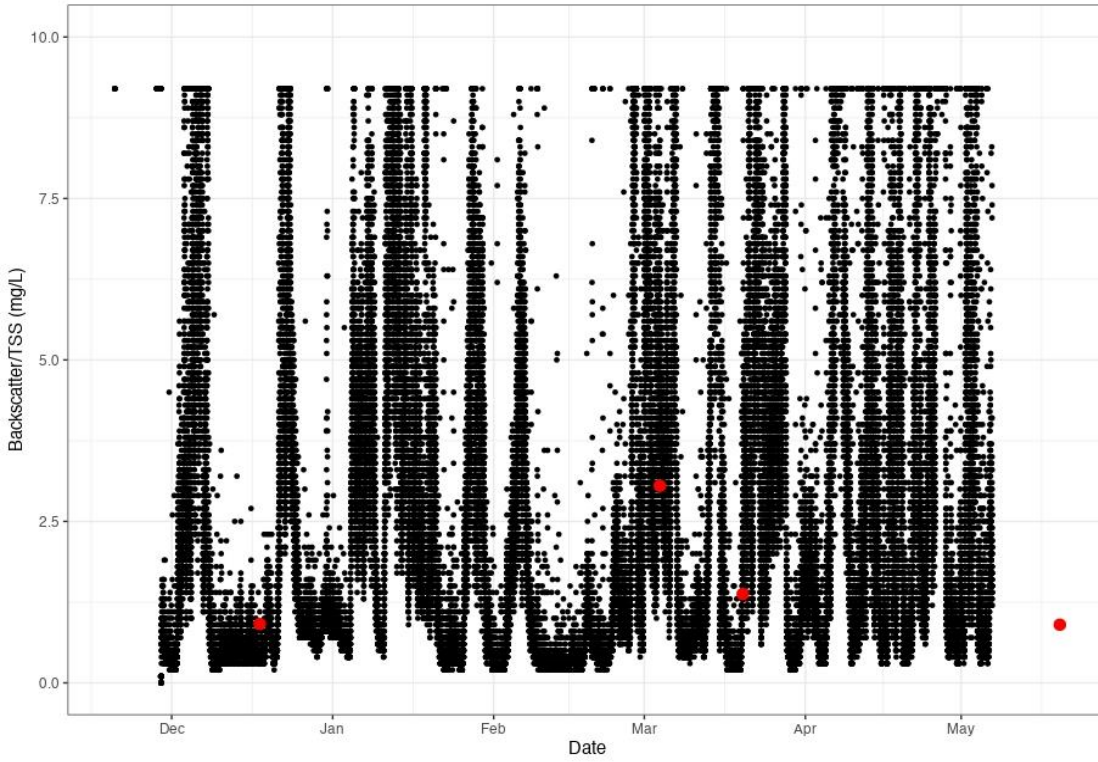
Figure 5.37a ADCP Backscatter measured at the northern lander with spot TSS measurements (red dots) from monthly samples.
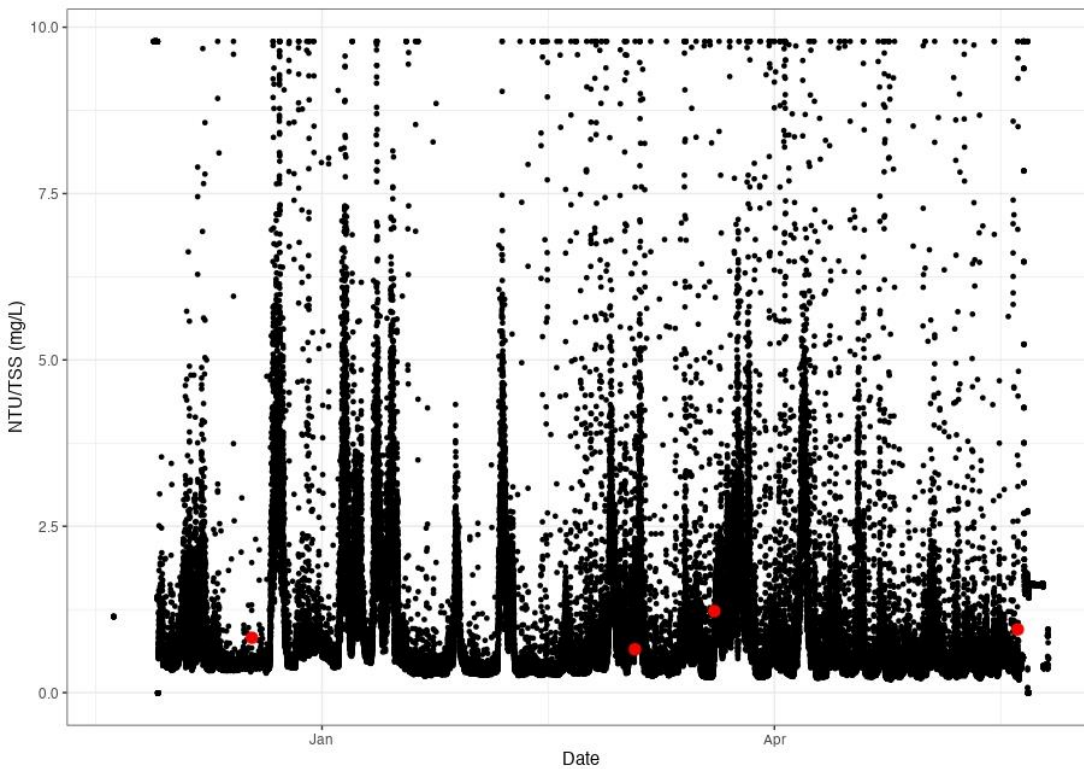
Figure 5.37b Turbidity measured at the southern lander with spot TSS measurements (red dots) from monthly samples.

5.2.3   2021 Deployment

Hydrodynamic modelling indicated the possibility that during periods of significant EAC extension, there is the potential for cold bottom water to intrude into Storm Bay and that this could influence the nutrient regime of the bay. To investigate this, a benthic lander was deployed at a site 43° 13.225' S, 147° 39.60' E (Figure 5.38). The original science plan was to utilise repeated "fly pasts" by an autonomous glider to identify likely intrusions and then mobilise a field survey to confirm. Unfortunately the glider was lost due to rough weather only a few days after deployment, so an alternative plan utilising satellite imagery (Figure 5.39) and the hydrodynamic model was employed, as predictors of conditions likely to result in an intrusion. Once such conditions became apparent, a transect survey was undertaken in April 2021. A series of 18 equally spaced stations for CTD casts and nutrient samples, phytoplankton and pigments were planned; however, uncomfortably large swell conditions meant that only a subset of stations could be sampled in the time available. Sampling commenced at the most southerly station (Stn 1, see Figure 5.38) and proceeded north. Water depths sampled ranged from ~90m to 50m in the most inshore station.
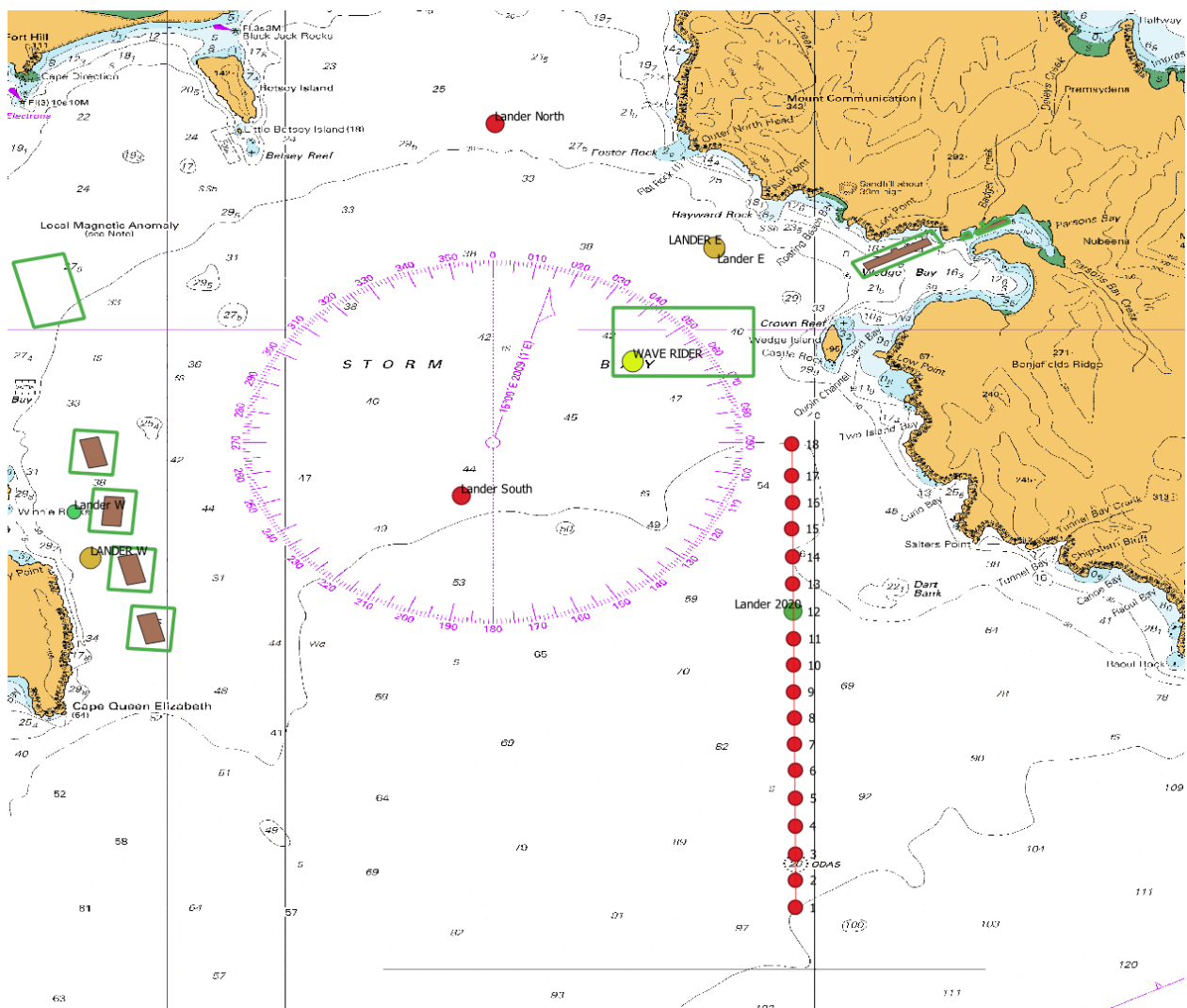
Figure 5.38 Sampling locations for the transect survey conducted 7th April 2021. Station 12 coincides with the location of the lander deployed in January 2021.
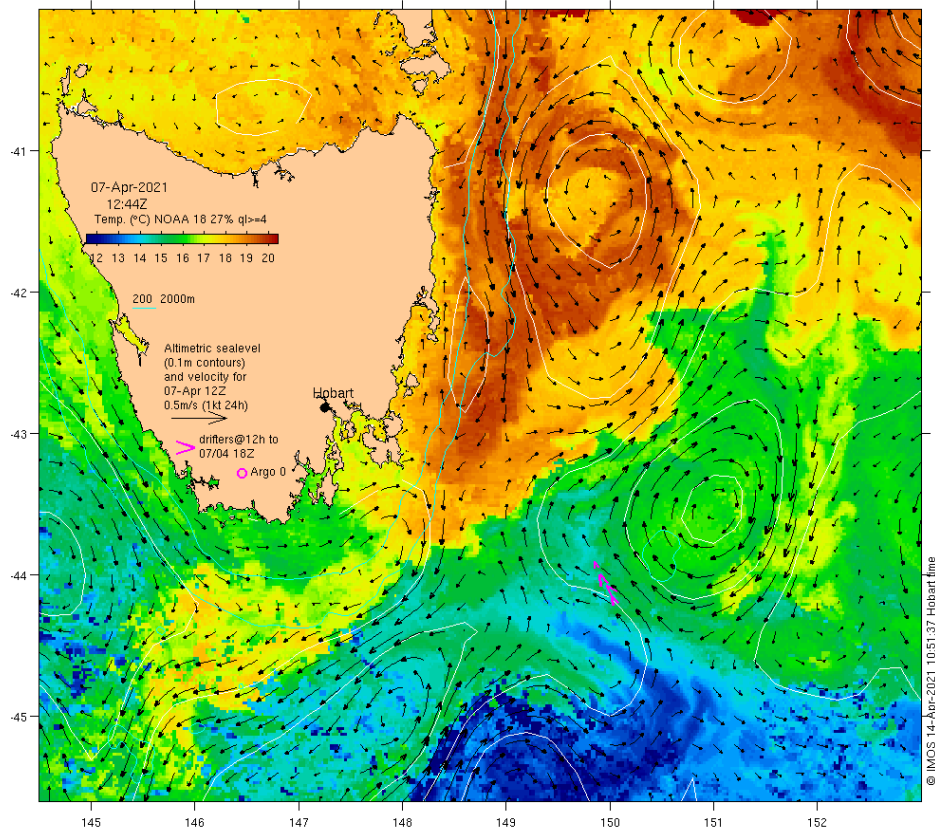
Figure 5.39 Ocean currents and sea surface temperature around Tasmania on 7th April 2021 (IMOS).

CTD profiles

Temperature profiles from the CTD casts undertaken as part of the field survey are presented in Figure 5.40a. The southern-most, deeper sites appear to show a small enhanced decrease in temperature just above the bottom and this extends into the bay where the water depth is greater than ~75 m. This slight decrease in temperature is also associated with a small increase in the recorded dissolved oxygen within the same CTD casts (Figure 5.40b). Both these observations are consistent with what we might expect in the presence of a bottom water intrusion.

Figure 5.40a CTD temperature profiles at selected transect stations sampled in April 2021. From South to North, stations presented are 1, 3, 5, 7, 9, 12, 13, 15 and 18, see map Figure 5.38 for CTD locations.
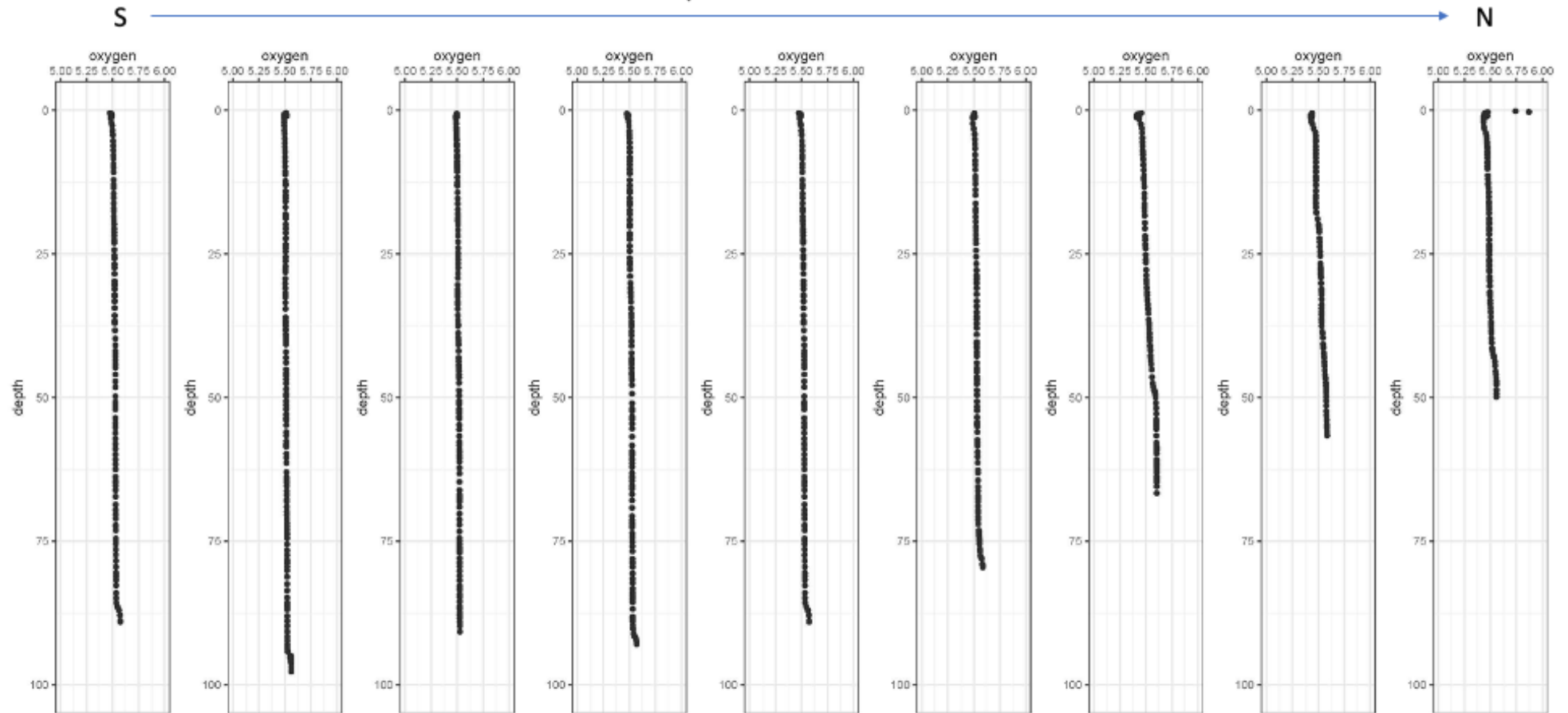
Figure 5.40b CTD dissolved oxygen profiles at selected transect stations sampled in April 2021. From South to North, stations presented are 1, 3, 5, 7, 9, 12, 13, 15 and 18, see map Figure 5.38 for CTD locations.

Nutrient profiles

Nutrient samples for nitrate and nitrite, and phosphate showed a strong trend of near surface depletion, increasing concentration with depth, with highest concentrations in the deepest sample (Figure 5.41). This trend was also observed for silicate, with the exception of Station 12, where higher concentrations penetrated further up the water column. Nitrite concentrations were depleted in surface waters, but concentrations tended to be similar in the 3 deeper samples. Ammonia patterns were variable, and no consistent trend was observed.
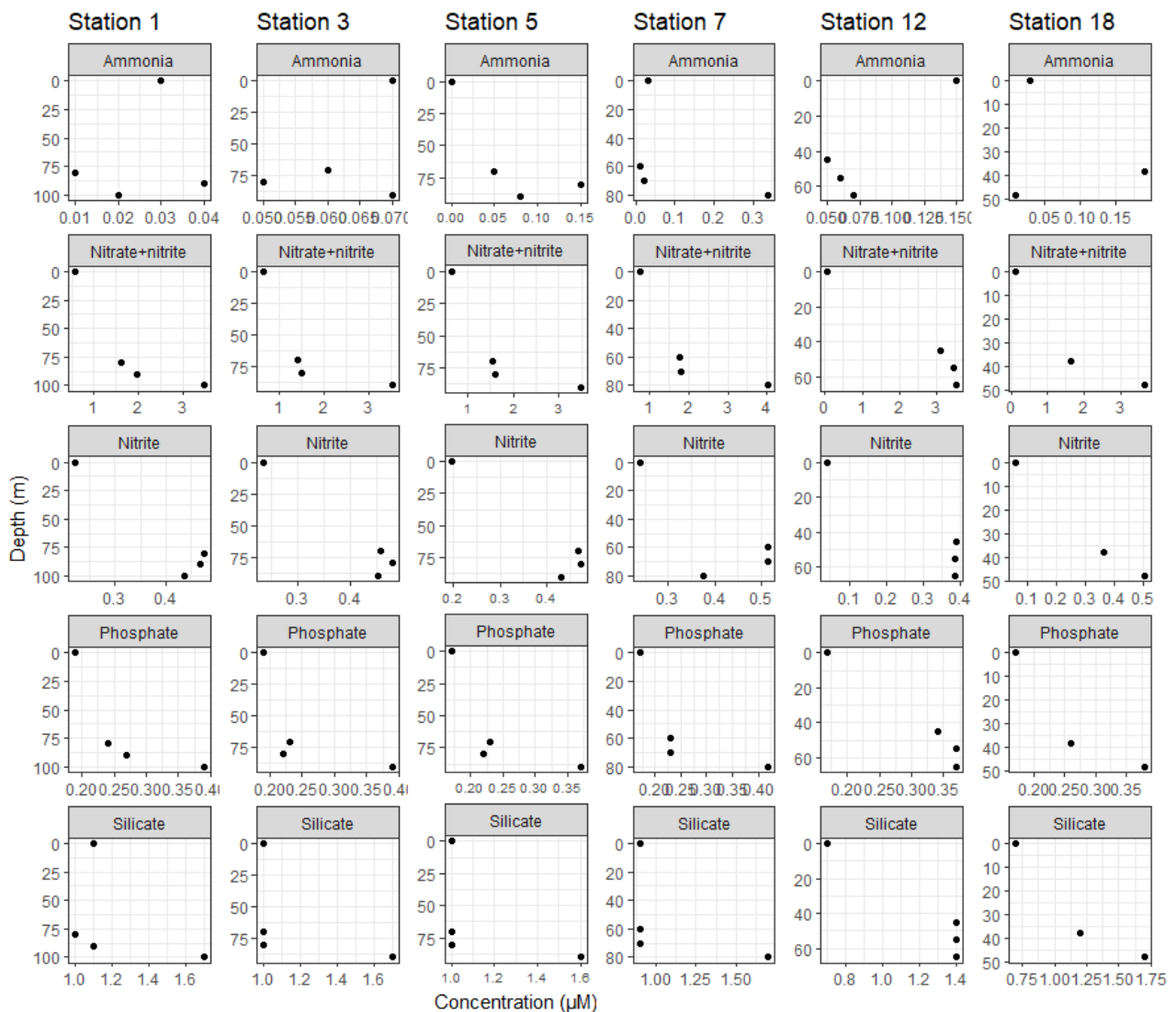
Figure 5.41 Nutrient profiles from 6 stations sampled during the transect survey on April 7, 2021. Samples were collected at the surface, 20 m from the bottom, 10 m from the bottom and bottom of the water column. See Figure 5.38 for station locations, Station 12 corresponds to the lander site.

Benthic lander data

Preliminary analysis of lander and field data (Figure 5.42) shows elevated nutrients at depth and during short periods when cooler water with reduced salinity and oxygen passed the lander site. Optical backscatter at the lander also shows episodic sediment resuspension during a January

storm event, and likely during similar wave events later in the timeseries (unfortunately the Wedge Island wave buoy was out of service after January).
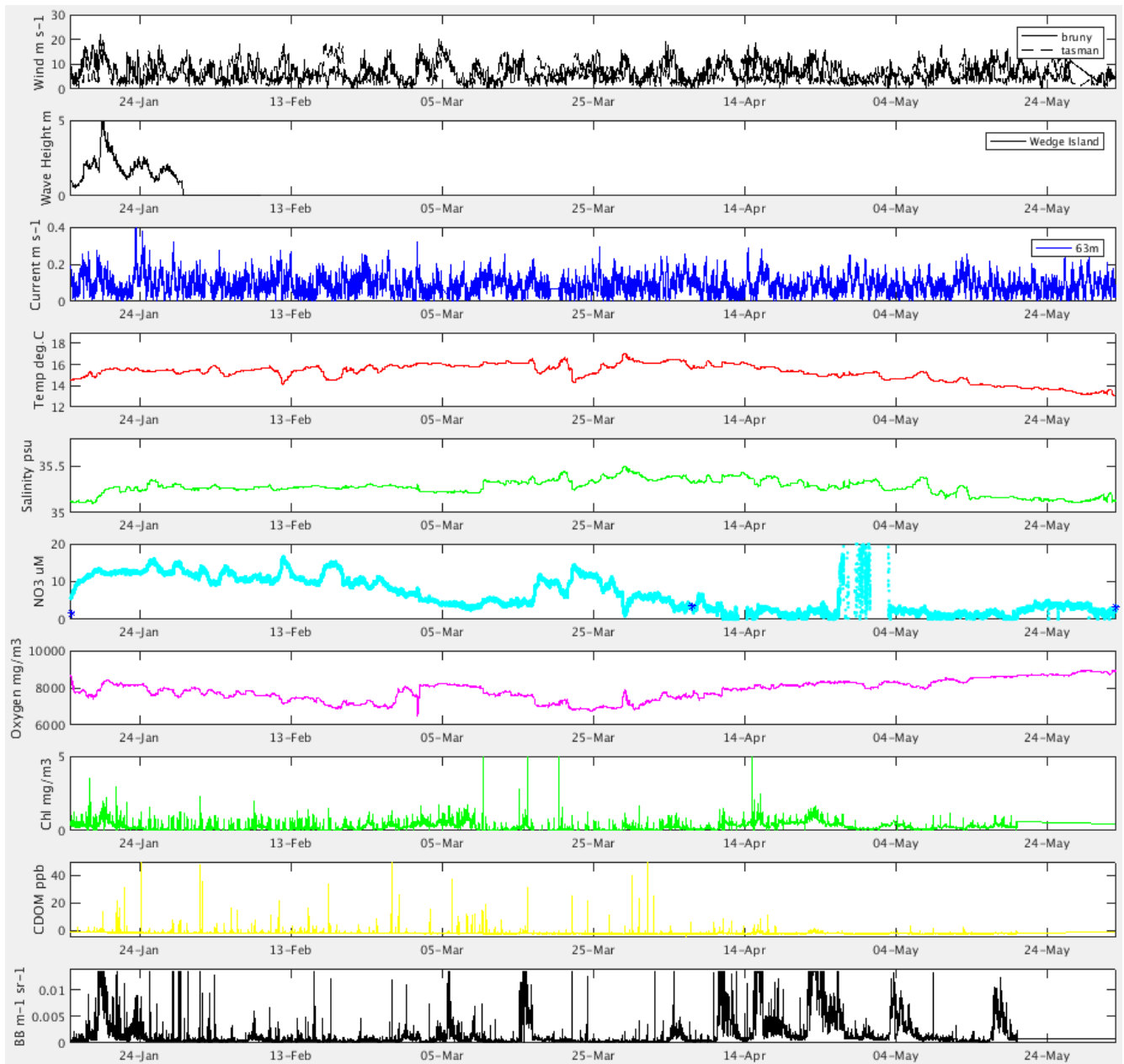
Figure 5.42 Time series of wind speed (at BOM Bruny & Tasman Island sites), wave height (at Tassal Wedge Island wave buoy) and water properties measured over the six-month lander deployment period at the Tasman site. Blue markers in the nitrate plot show concentrations measured during surveys.
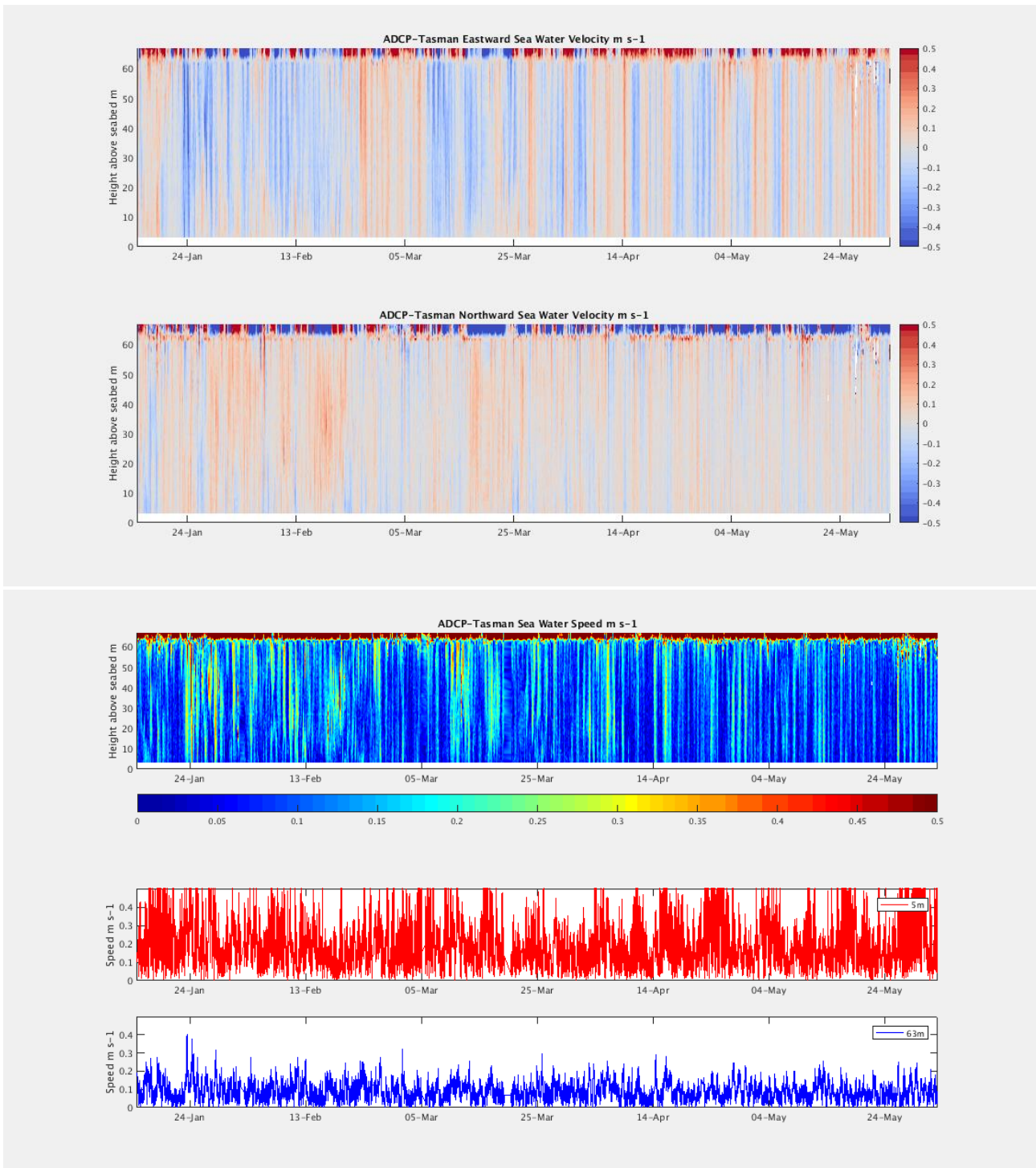
Figure 5.43 Timeseries of ADCP velocity profiles (upper panel) at the Tasman lander site with calculated current speed profile, and surface and bottom current speed timeseries (lower panel).

5.2.4 Genomics data from lander deployments

Surface water, bottom water and sediment samples were collected at the lander sites at 4 dates for genomics analysis: on the 11/04/2019 (East and West landers); on the 18/12/2019, 04/03/2020 and 20/03/2020 (South and North landers). Two litre water samples were filtered onto 0.2µm Sterivex filters. Five gram sediment samples from the top 2cm of the sediment were homogenized. The bacterial communities from these samples have been analysed via tag sequencing of the bacterial 16S rRNA gene.

The motivation for the genomic work was to create a baseline dataset of the microbiota in the surface sediments and in the surface and bottom water masses and to use this to put the results of the resuspension experiment (section 5.2.5) in context.

Water and sediment samples harboured very different bacterial communities as shown by statistical analyses (Figure 5.44). Sediment samples were dominated by gammaproteobacteria and planctomycetota, followed by alphaproteobacteria, actinobacteria and acidobacteria. Water samples were dominated by alphaproteobacteria, gammaproteobacteria and bacteroidota. Water samples also contained on average approximately 10% chloroplast 16S rRNA derived from eukaryotic phytoplankton (Figure 5.45).

Sediment samples contained a number of sediment specific major bacterial taxa: planctomycetota, acidobacteria, the NB1-j phylum, myxococcota, chloroflexi, nitrospirota, desulfobacterota and gemmatimonadota (Figure 5.45).

Figure 5.44 Non-metric multidimensional scaling plot illustrating the strong difference between the water and sediment bacterial communities at Storm Bay. Sfc=surface water samples. BTM=bottom water samples. Sediment=sediment samples.
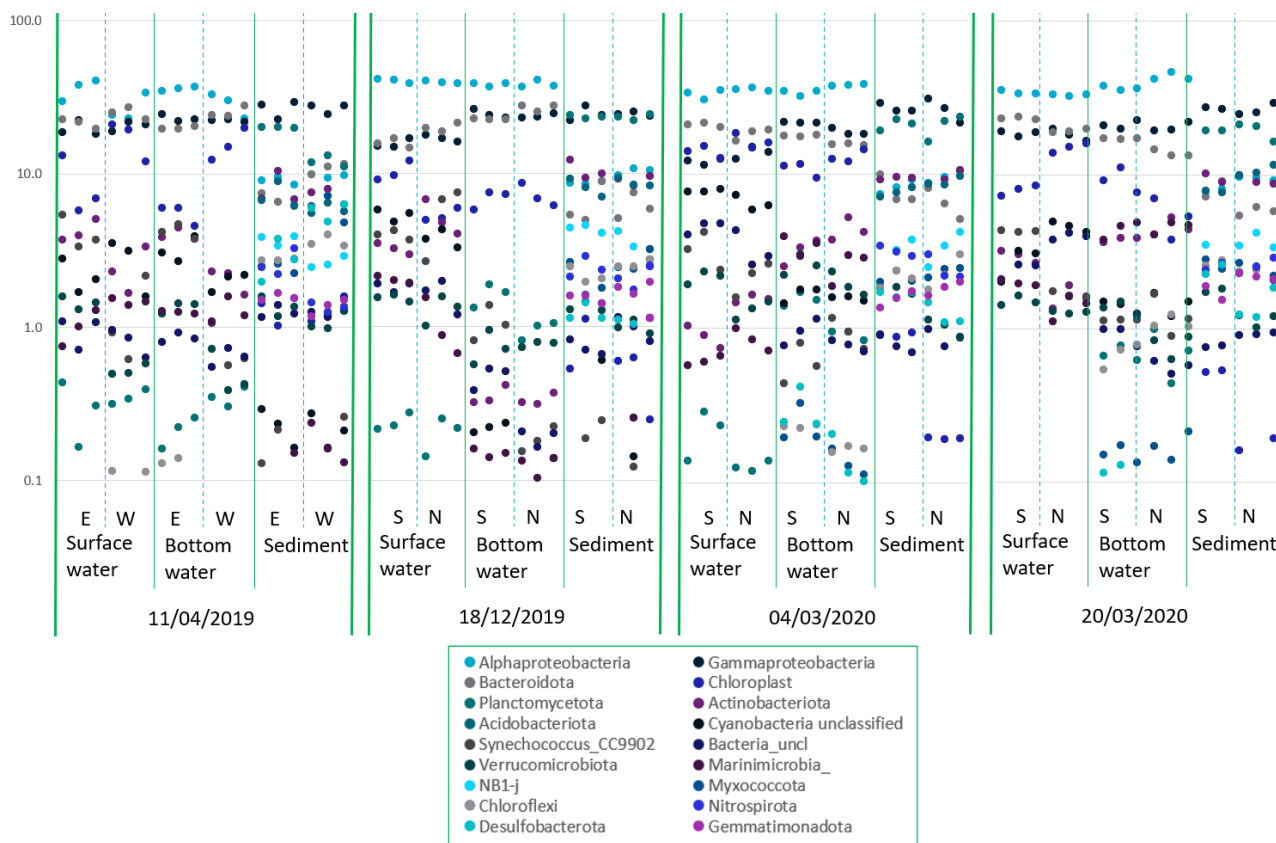
Figure 5.45 Monthly bacterial community composition summarised as major taxonomic groups for surface and bottom water samples and sediment samples from the lander sites. Numbers show relative abundances of the major taxa as percentage values. E=East Lander. W=West Lander. S=South Lander. N=North Lander.

The bacterial communities in the surface and bottom water samples were also different (Figure 5.45, Figure 5.46). This difference was strong for all the samples collected at the South and North lander locations across the three dates, while slightly less clear for the 11/04/2019 samples, collected at the East and West lander locations. Chemical observations showed a similar picture with the lowest level of difference between surface and bottom water samples observed on the 11/04/2019.

Surface water samples had a higher percentage of cyanobacteria (8% vs 3%) and slightly more eukaryote phytoplankton (12% vs 9%) than bottom water samples. Bottom water samples contained more of the bacterial taxa that were major components of the sediment community (in particular planktomycetota, acidobacteria, chloroflexi, desulfobacterota, myxococcota).
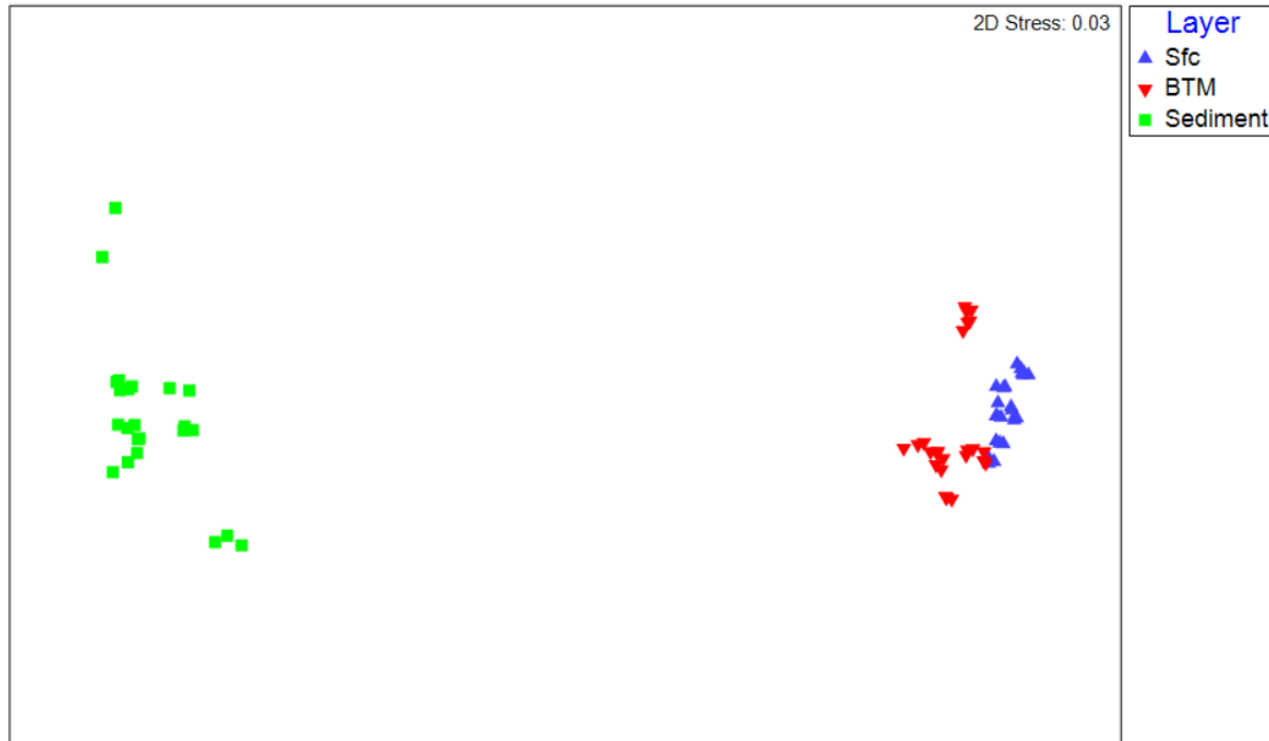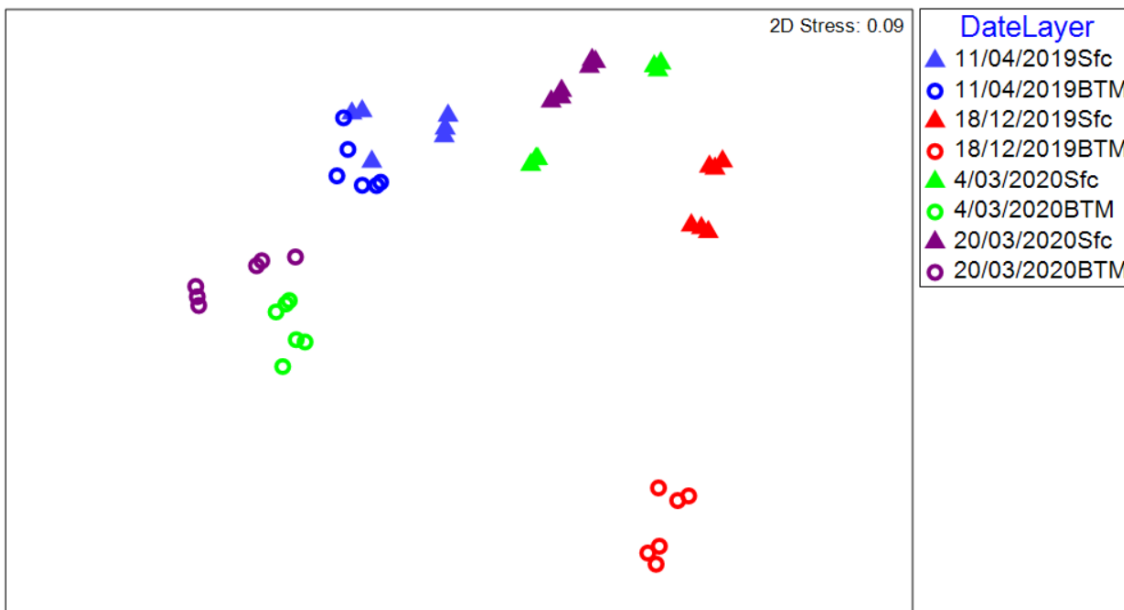
Figure 5.46. Non-metric multidimensional scaling plot illustrating the differences between the surface and bottom water bacterial communities at the different sampling dates at Storm Bay. Sfc = surface. BTM=bottom.

5.2.5   Resuspension Process Study

To compliment the lander deployments a controlled laboratory resuspension flume experiment has been completed by visiting Frohlich Fellow Prof Gary Fones (Uni Portsmouth, UK) and CSIRO post-doc Kristen Karsh (Figure 5.47). This study characterises sediment porewater nutrient conditions and resuspension of solutes, sediments and microbial responses for samples collected in the Storm Bay region [Conningham, Ralphs Bay north, Derwent Estuary mouth (B3) and Trumpeter Bay gradient from fallowed lease].

Results show an increase in SPM with increasing velocity followed by a decrease in SPM when the impeller was switched off at the end of the experiment (Figure 5.48). In contrast to our expectation that during resuspension nutrients would be released from the sediment and increase the water column concentration, the converse was true. In almost all cases nutrient concentrations in overlying water decreased with increasing resuspension! A possible explanation for this unexpected result is that the resuspended sediment microbial community was released from oxygen limitation in the sediment and responded very rapidly with the consumption of resuspended organic material and nutrients.

Figure 5.47 Sediment resuspension annular flume (left), oxygen microelectrode (centre), gel sampler for sampling porewater nutrient gradients (right).
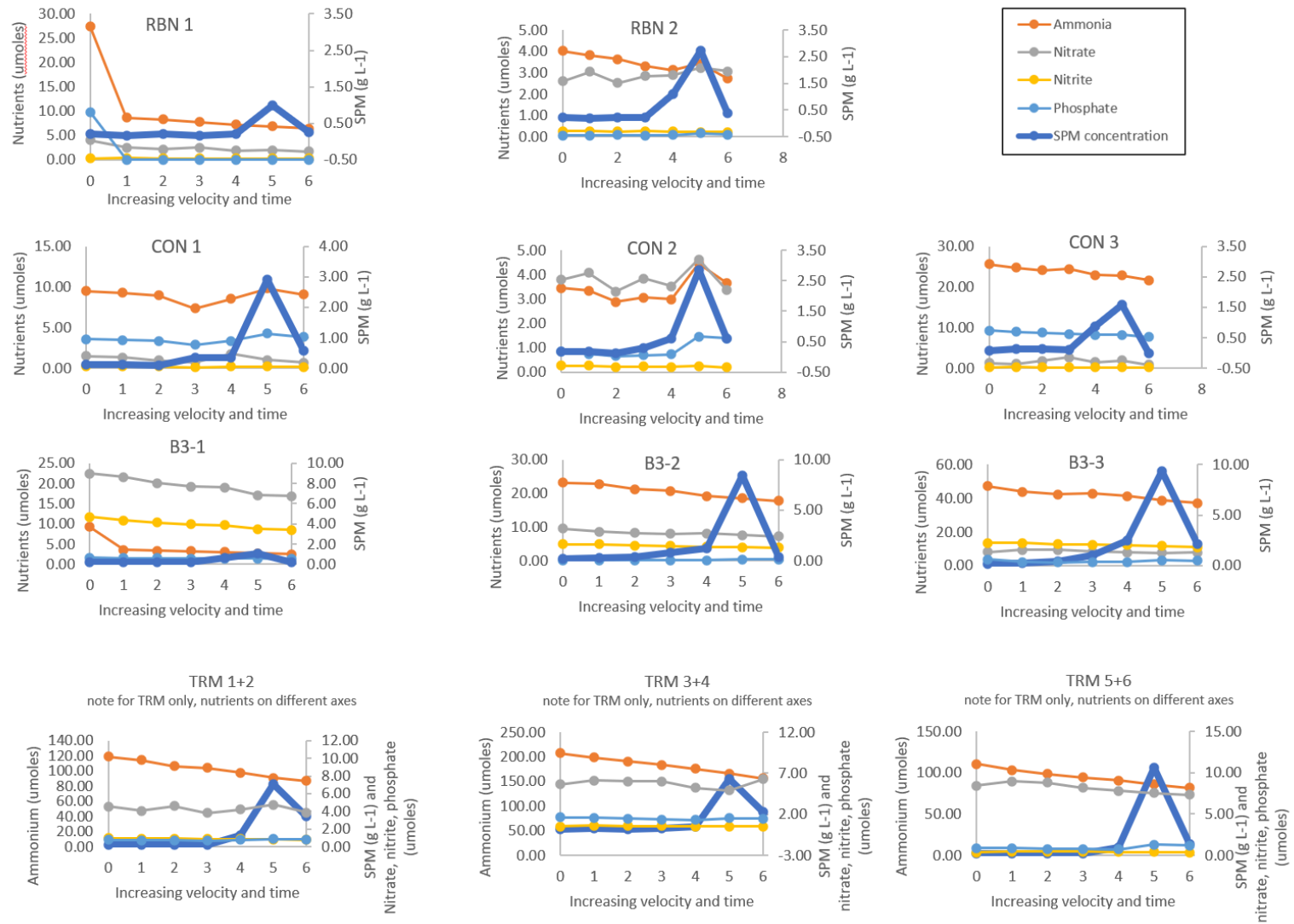
Figure 5.48 Results from the sediment resuspension process study showing changes in nutrient and suspended sediment concentration with increasing current velocity. Sediments were collected from sites Conningham (CON), Ralphs Bay north (RBN), Derwent Estuary mouth (B3) and Trumpeter Bay gradient (TRM).

Microbial Analysis

To characterise the microbial response to resuspension, transcriptomic analysis via small subunit rRNA transcript tag sequencing was carried out. For each experiment, we analysed the top 2 cm sediment (Sed1), water from before the start of the resuspension (T0), water at the maximum resuspension (T5) and 30 minutes after resuspension has been stopped (i.e., 30 minutes of settling time). Sequencing obtained broad community composition of the active community for the three biological kingdoms: Archaea, Bacteria and Eukaryotes.

The different sites and the replicate crates from the sites showed a wide variation in the dissolved nutrient concentrations measured (ammonia, nitrate, nitrite, phosphate). Similarly, the microbial communities were very different between sites and within replicates from each site.

The initial assumption that resuspension would result in an increase in dissolved nutrients was not observed for the nutrients measured, i.e. ammonia, nitrate, nitrite or phosphate. Interestingly, in most cases both the total of the dissolved inorganic nitrogen compounds and the individual components (ammonia, nitrate, nitrite) decreased during resuspension, with only a few exceptions.

Material from RBN (RBN1 and RBN2) showed a much lower change in water column microbial (both bacteria and archaea) activity due to resuspension compared to the other sites. Ralphs Bay is very shallow and is probably subject to frequent resuspension. Samples from site B3 are the closest geographically and most similar to the lander sites described in the previous chapter. The TRM samples, from a fallowed aquaculture site, represent the conditions expected at aquaculture sites; however, results should be interpreted with caution as the samples have been subject to extended laboratory incubations before the experiment, potentially changing the biogeochemistry and the biology of the samples.

Genomics results indicated significant and lasting increase in the activity of several bacterial and archaeal groups within the water column, following resuspension (while no eukaryote groups showed a similar response). The most notable bacterial response was by an uncultivated genus of the Desulfosarcinaceae family, called Sva0081. The activity of this genus, as reflected by its relative contribution to the total bacterial 16S rRNA pool, increased in every experiment, often by >10x, typically from 0.2-1% to 5-15% of the total bacterial activity. This genus is frequently found at high abundance in marine sediments and is associated with acetate and hydrogen metabolism, mostly under anaerobic conditions using sulphate as electron donor. There are results suggesting they may be able to oxidise acetate under aerobic conditions as well.

Other bacterial genera with significant and lasting increase in activity, across all or most of the samples included Thiogranum, Desulfatiglans, Desulfosarcina, Woeseia, Acidobacterial Subgroups 22 and 23, an uncultivated gammaproteobacterial genus called B2M28 and a genus within the Nitrosococceae family. Most of these genera are core members of the sediment microbiota and typically not found in the water column. They are often facultative anaerobes with the ability to switch to aerobic metabolism when exposed to aerobic conditions.

The most notable archaeal response was by the uncultivated genus SOKP01, belonging to the class Lokiarchaeia. The activity of this genus increased in most experiments, and often by over 100x, typically from 0.5% to 5% of the total archaeal activity.

Summary of Findings

The synthesis of results suggest that the bacterial and archaeal community resuspended together with the sediment introduces significant, lasting new biogeochemical activity into the water column. This new biogeochemical activity can be responsible for the uptake of ammonia observed in most of the experiments. It can also be responsible for the uptake and degradation of other nutrients, including organic carbon and nitrogen, released during sediment resuspension.

This experiment has highlighted some of the complex interactions between microbial fauna, dissolved oxygen and nutrients that occur during resuspension events. We recommend further investigation to confirm whether these laboratory findings apply in situ. Our results raise the possibility that resuspension events, due to the new biogeochemical activity of the resuspended sediment microbiota, may have a positive effect on the overall quality of the environment (both water and sediment) around aquaculture leases. Further research should 1) identify the specific activities (via shotgun metatranscriptomics and measuring organic carbon and nitrogen content) to confirm the above hypothesis, 2) measure if and by how much the positive effect of the new biogeochemical activity exceeds the negative effect of the nutrient release, 3) establish how these two conflicting effects and their cumulative end-effect changes with increasing organic load of the sediment and 4) evaluate (and if necessary, improve), the existing model process representation of benthic-pelagic fluxes.

5.3 Profiling mooring trials

The Australian Integrated Marine Observing System (IMOS) has deployed a number of profiling mooring systems in outer Storm Bay (Table 5.5) as part of a trial of new platform technology and these data have been made available to the project. In August 2019 a McLane profiling crawler (PRAWLER) mooring system loaned to the CSIRO Science Engineering & Technology Program from NOAA (Figure 5.49 – 5.51) was deployed south of Cape Raoul on the outer shelf of Storm Bay for 6 months. Following deployments elsewhere in Australia and refurbishment, the same PRAWLER system was redeployed in June 2021 alongside a WireWalker profiling mooring system on loan from AIMS.

Table 5.5 IMOS profiling mooring deployments in outer Storm Bay.

Date	Site	Latitude (degrees)	Longitude (degrees)	Water depth (m)	Parameters
Aug-Dec 2019	PRAWLER	-44.4618	147.8089	131	T,S,O,(N)
Jun-Sep 2021	WireWalker	-43.3708	147.7203	110	T,S,Chl,PAR
Jun-Sep 2021	PRAWLER	-43.3545	147.7070	110	T,S,O,Chl,BB,(N)
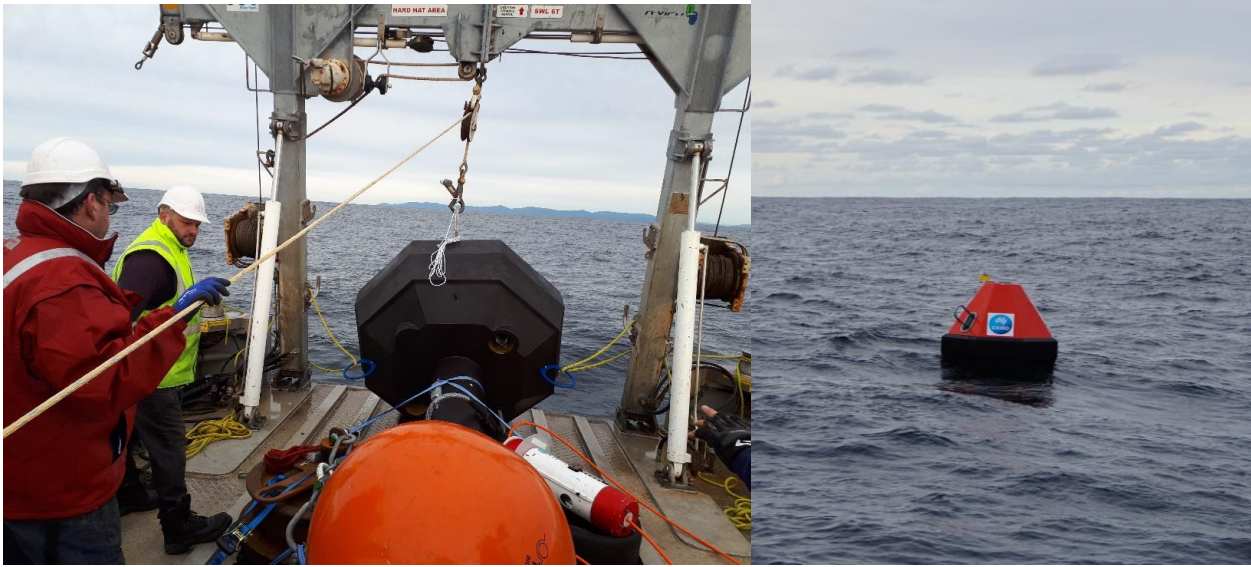
Figure 5.49 PRAWLER mooring ready for deployment (left) and successfully deployed (right).
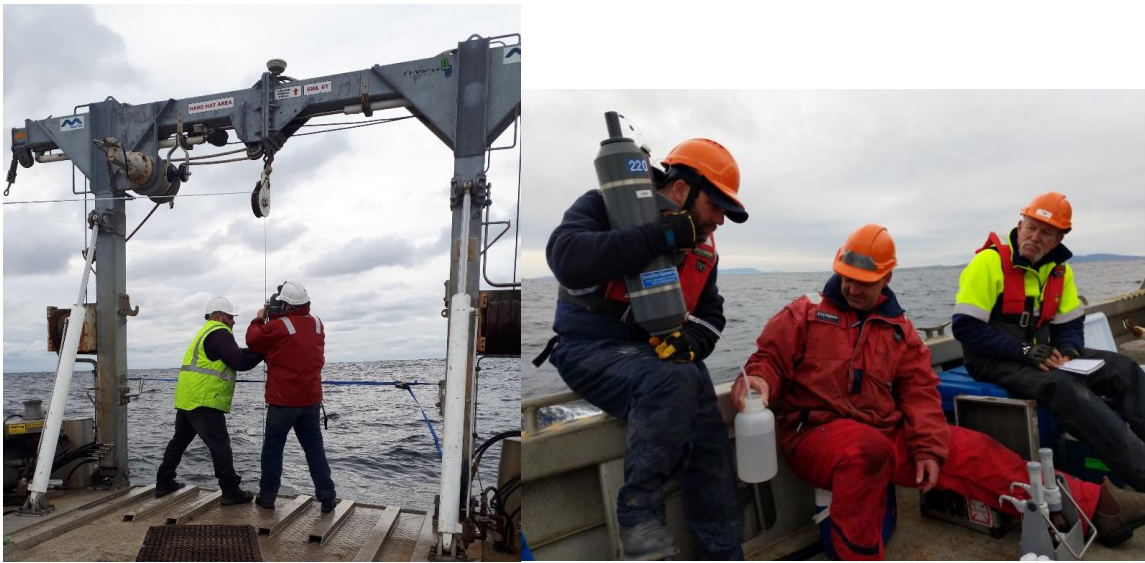
Figure 5.50 On deployment and recovery CTD casts and bottle samples were taken at 10, 20, 30, 50, 100 and 120 m for sensor verification.

August – December 2019 Deployment

In August 2019 a major storm with 11m significant wave height bounced the PRAWLER mooring along the bottom ~100m to the northeast of its original position, however all systems remained operational. Overall, the system worked well and delivered continuous data daily via satellite link to NOAA, and FTP to CSIRO, throughout the deployment. The PRAWLER profiling truck carried sensors for temperature, pressure, salinity and oxygen and returned data from the profiling unit in near real time via satellite telemetry; additional sensors stored data for temperature, salinity, oxygen and nitrate at 100m, and temperature at 120 m (Figure 5.52 & 5.53).
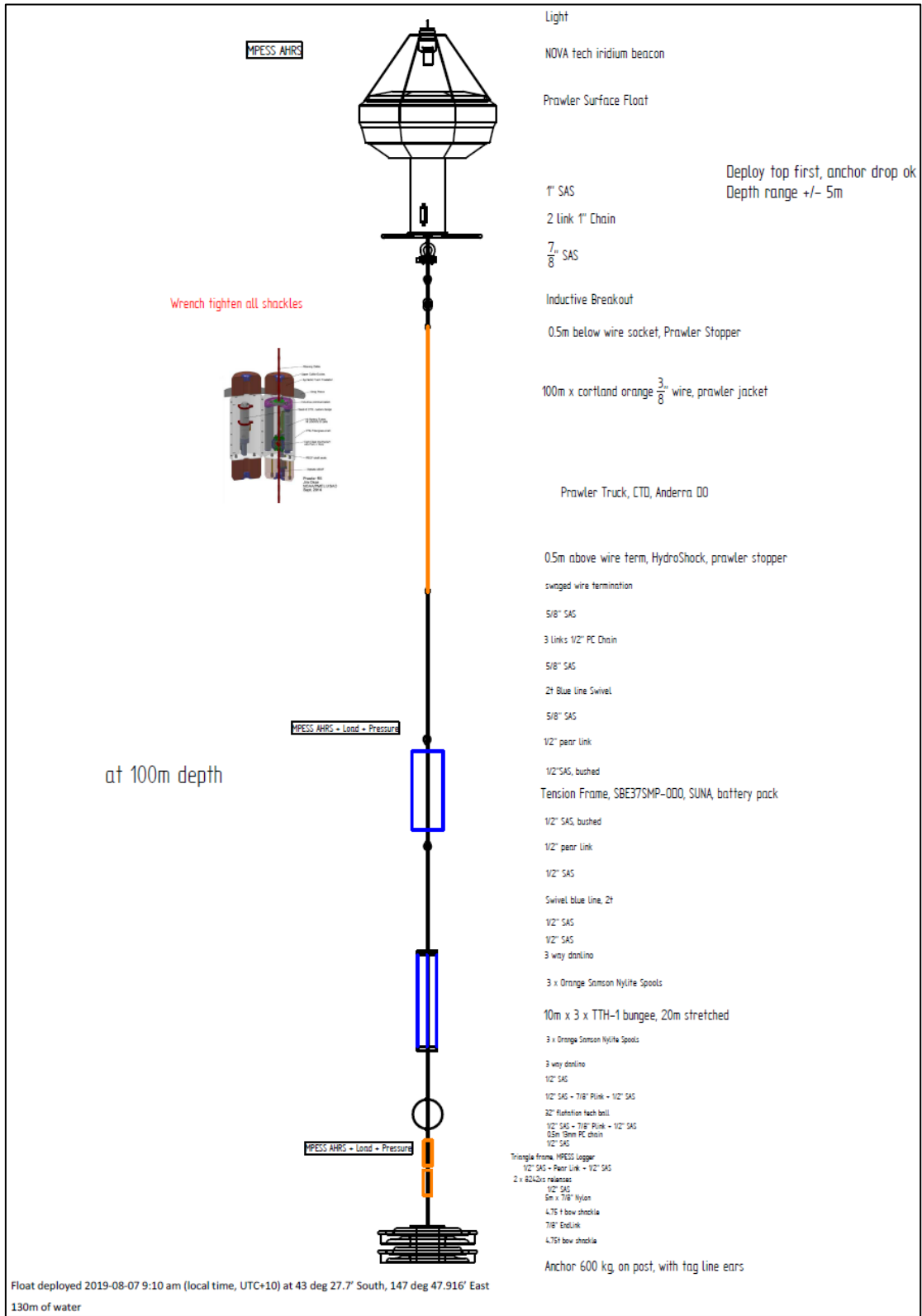
Figure 5.51 Mooring components including float, profiling section, anchor; delayed mode sensors were added at 100 m and 120 m.
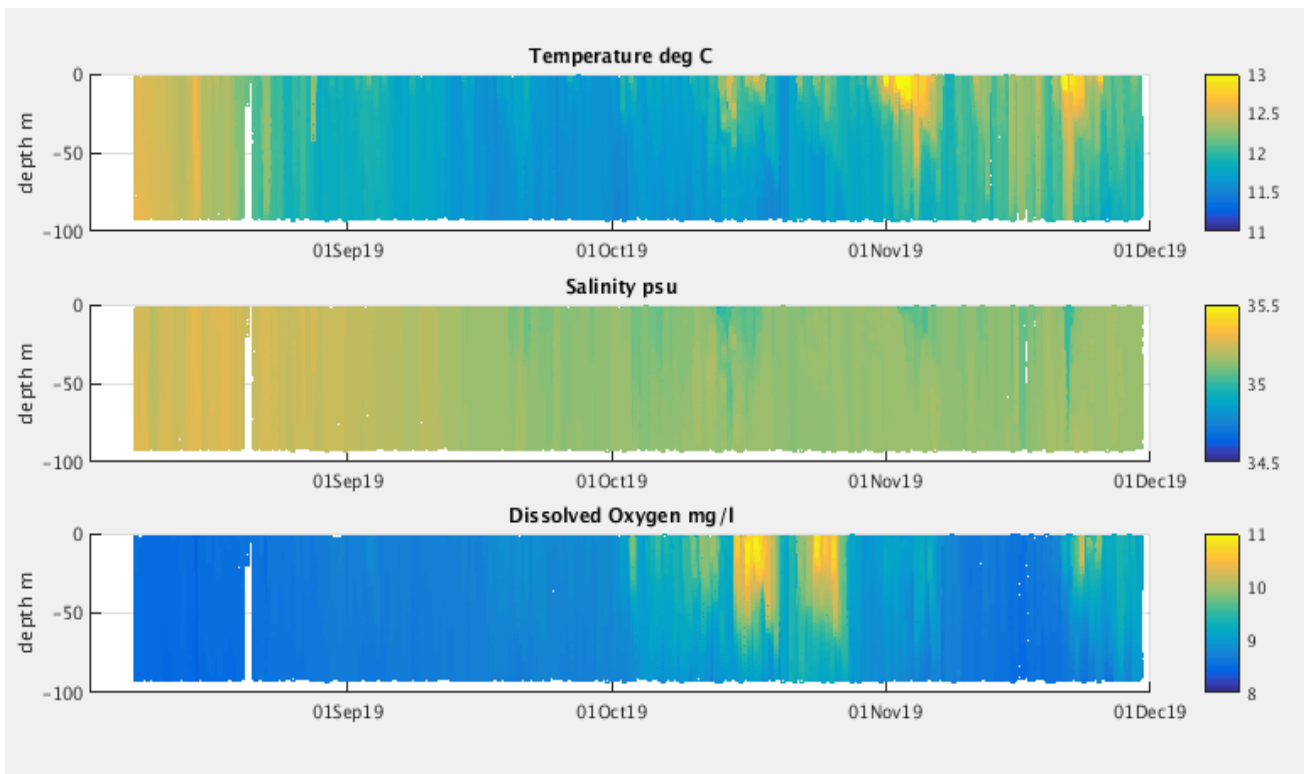
Figure 5.52 Data received in near real time from the PRAWLER profiling mooring.
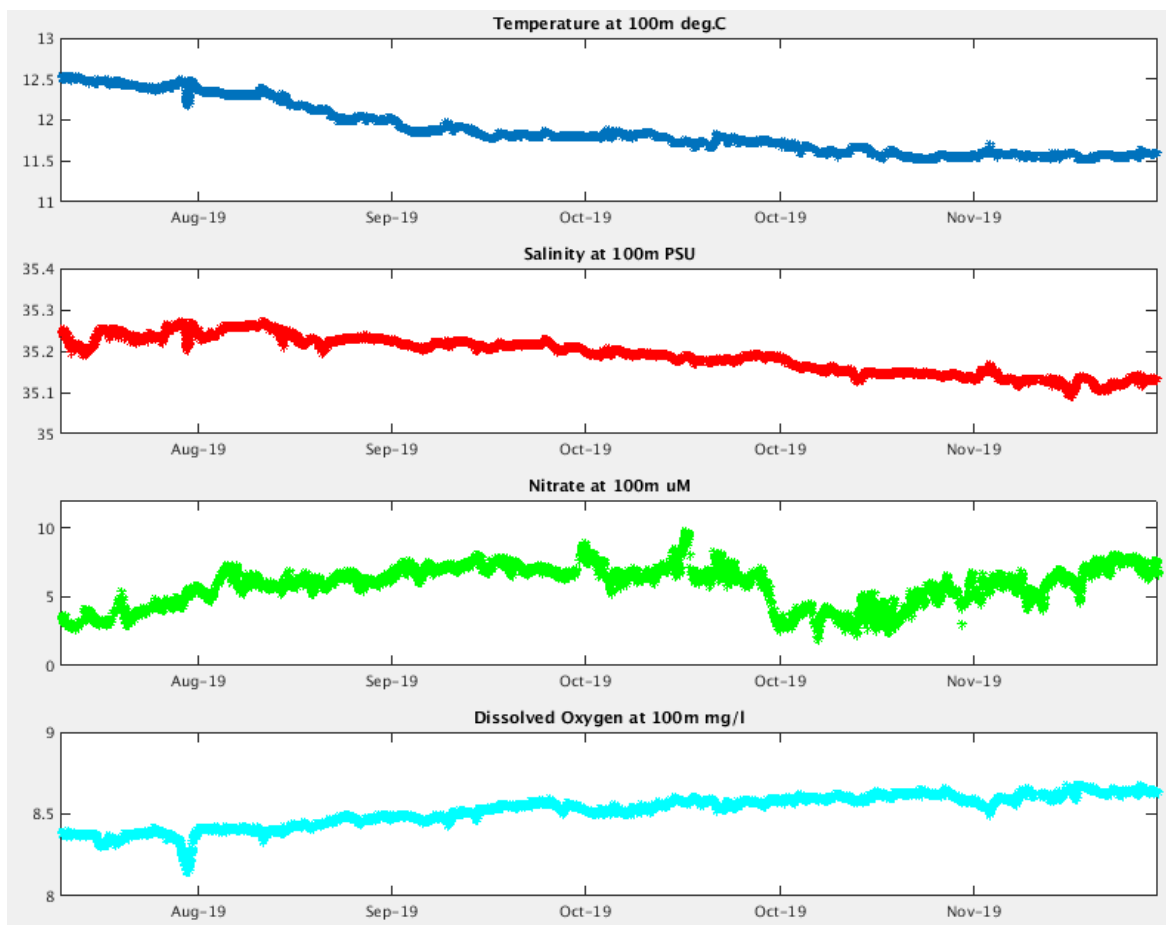
Figure 5.53 Time series of temperature, salinity, nitrate, and dissolved oxygen at 100m during the PRAWLER deployment; the mixing event in August is associated with the major storm.

June – September 2021 Deployment

A WireWalker profiling mooring system and a PRAWLER profiling mooring system (Figure 5.54) were deployed in outer Storm Bay from June – September 2021 as part of an IMOS technical trial. The WireWalker experienced difficulties with near real time communication of data, however the data was collected and stored by the unit during its deployment, with a full data set obtained on recovery. The PRAWLER delivered data in near real time from July through to September, after having some control issues on first deployment (Figures 5.55a & 5.55b). In addition to conductivity, temperature and depth data on both instruments, fluorescence, turbidity and PAR data was collected by the WireWalker, whilst the Prawler collected dissolved oxygen data. The profiling moorings, in 130m of water, were able to profile ~80m of the water column. The Prawler and WireWalker did 2461 and 6764 profiles of the water column, respectively, through this period.

The deployment of these moorings were also part of an engineering study into the effectiveness of these systems and the best methods for mooring design and configuration. This period provided valuable learnings in operational readiness of the systems, with problems discovered in both command and control, and communications, both being easily resolvable issues with more time spent using these new systems. The mooring designs used for this deployment, a taut mooring design with a bungee at the base of the mooring, has again proved effective, noting that profiling the full water column is a challenge with all mooring designs, and something that is still being assessed for best practice.
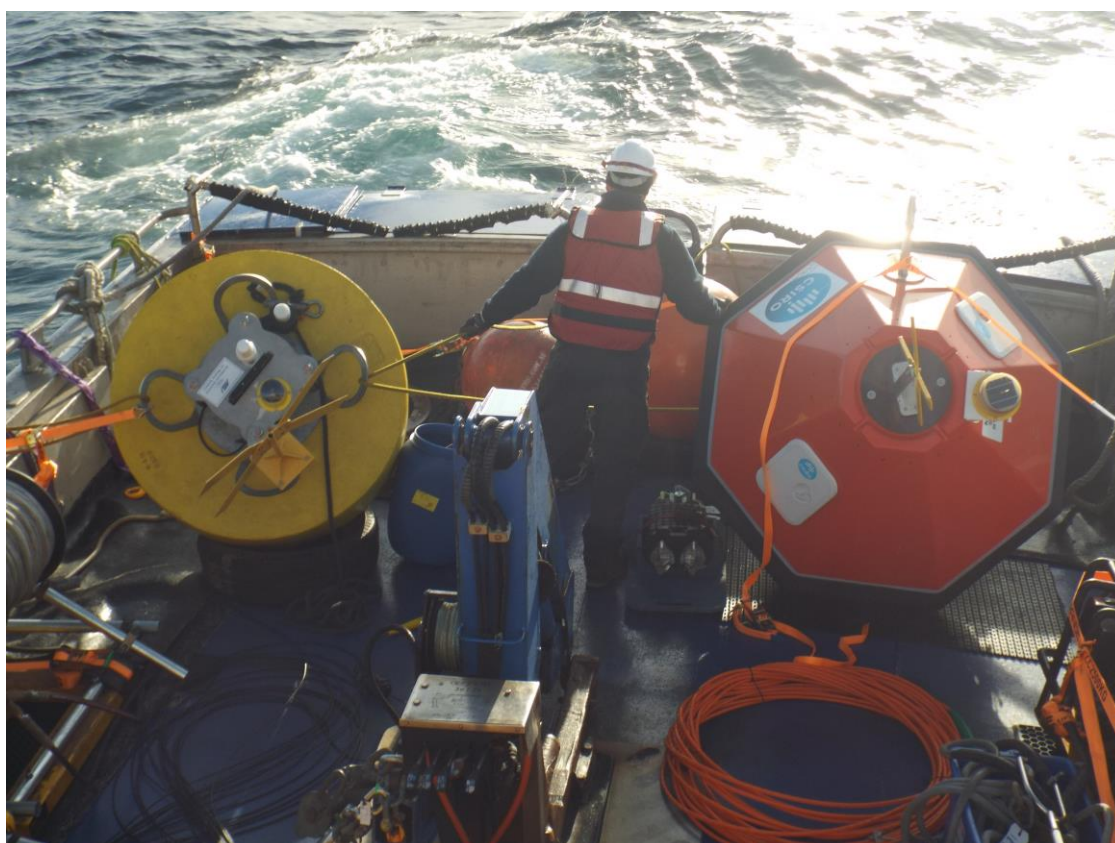
Figure 5.54 AIMS WireWalker (left) and CSIRO PRAWLER (right) profiling mooring systems en-route to deployment in June 2021.
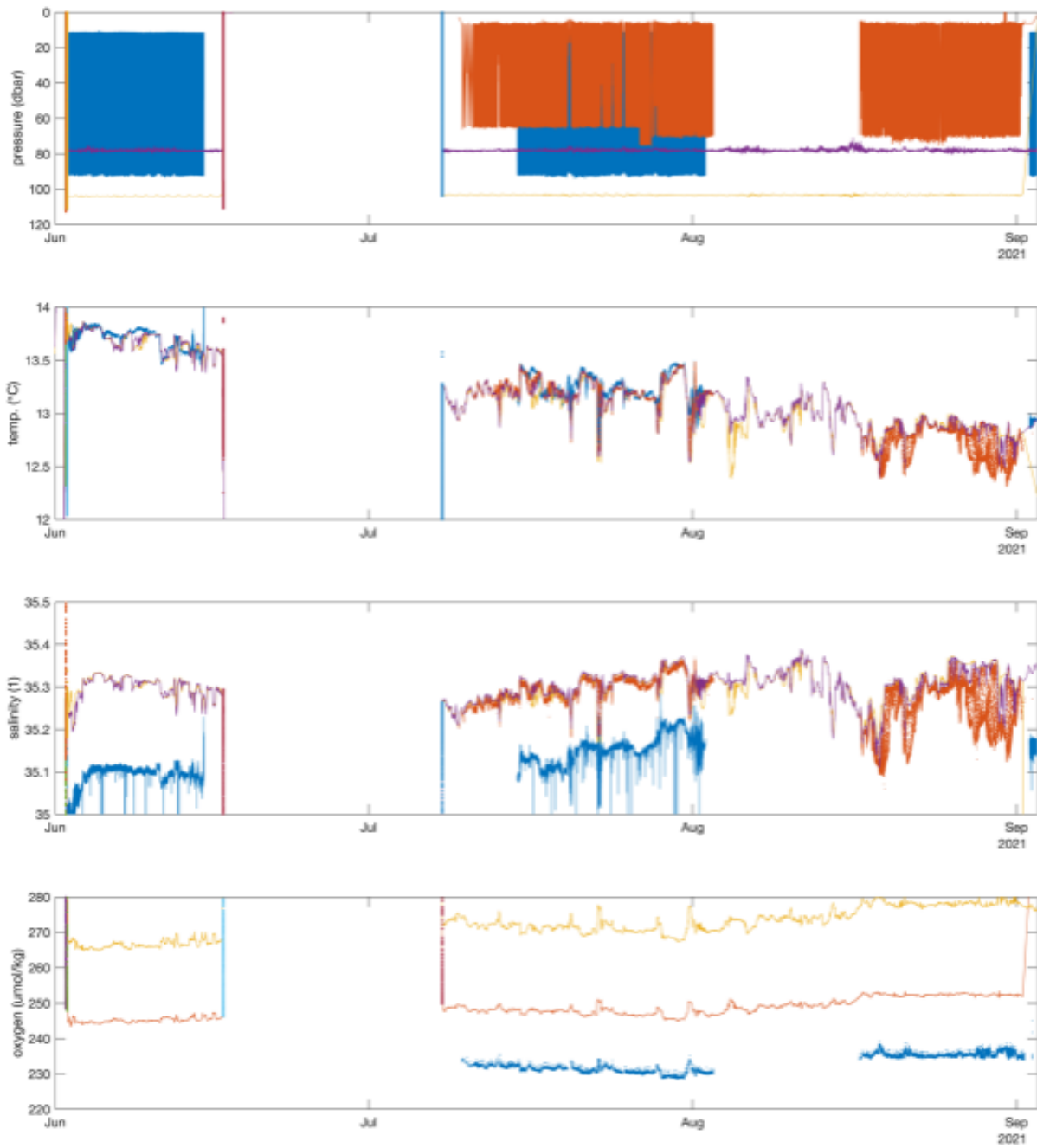
Figure 5.55a Example temperature, salinity and oxygen data from the WireWalker (blue in top plot) and PRAWLER (red purple and yellow) deployments in outer Storm Bay including data from fixed depth sensors at 80m and 90m.
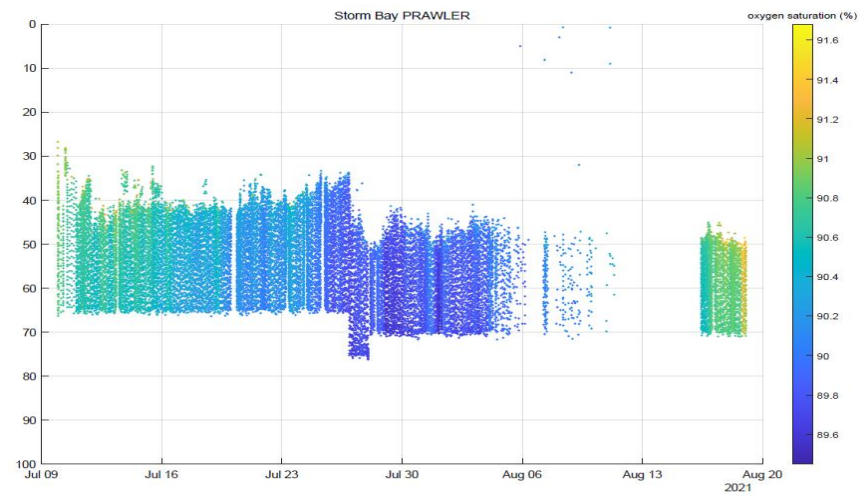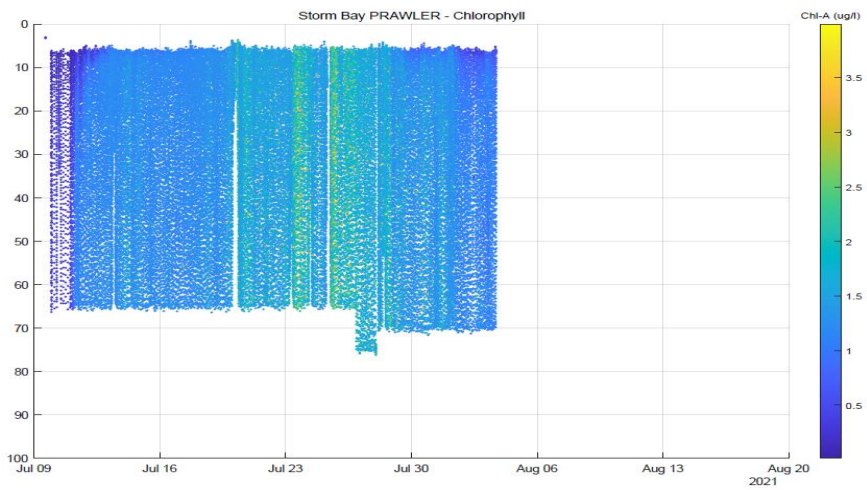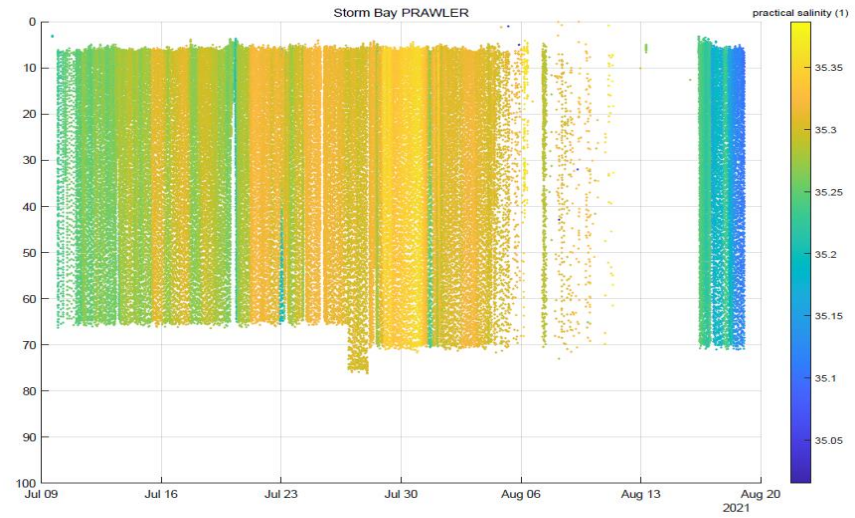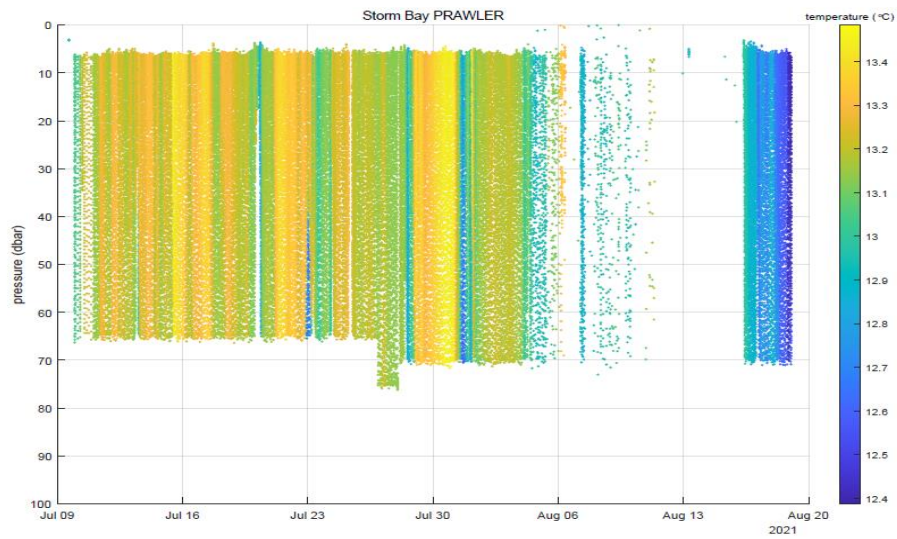
Figure 5.55b Profiling mooring data received in near real time from the PRAWLER deployment in outer Storm Bay Jun-Dec 2021 (temperature, salinity, chlorophyll, oxygen saturation).

5.4 RV Investigator Voyage

An opportunity arose to sample outer Storm Bay, the southern Tasmanian Shelf, and offshore waters south of Tasmania at part of the IN2020_V10 voyage departing and returning to Hobart in November 2020. Two berths and 48 hours of ship time were made available to the project, with Karen Wild-Allen and Ruth Eriksen electing to participate in the voyage. The RV Investigator (Marine National Facility) is a highly capable offshore oceanographic research vessel which allowed us to collect samples and deploy instrumentation to characterise water masses, nutrients and plankton distributions on the shelf immediately south of Storm Bay (in the vicinity of the model ocean boundary).

5.4.1   Voyage Sampling Plan

Within the constraints of the ship operations planned for IN2020_V10 6 CTD and rosette water bottle casts distributed as in Figure 5.56 were completed.

- 2 CTD at around 130m

- 2 CTD On the shelf break at around ~ 250m

- 2 CTD further offshore at around ~900-1000m

The CTD rosette was sampled for salinity, dissolved oxygen, nutrients, suspended particulate matter, chlorophyll, and pigments, CDOM, spectral absorption, phytoplankton species, isotopes, and inorganic carbon. These data were used to confirm the CTD sensor calibration and characterise the vertical distribution of nutrients, biogeochemical properties, and plankton.

In addition to the CTD casts, underway systems operated throughout the voyage and an undulating Triaxus tow was proposed along the red zig-zag track shown in Figure 5.56 to provide a continuous section of ocean properties (surface to 300m depth) to characterise the spatial distribution of water masses from the shelf break into Storm Bay, including any deep water nutrient rich water present.
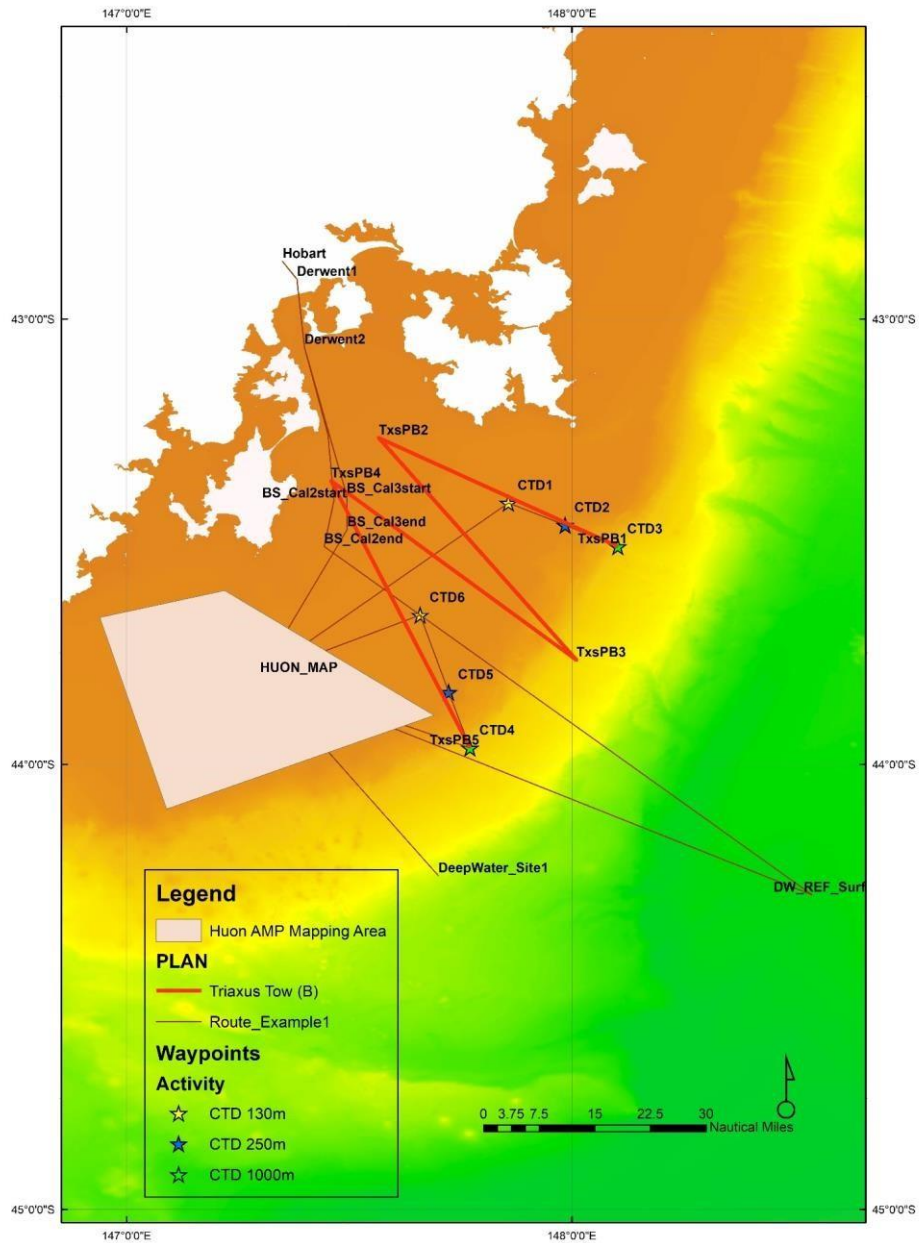
Figure 5.56 Voyage sampling plan for IN2020_V10, November 2020.

5.4.2   Oceanographic conditions

During the voyage, warm EAC water was present offshore along the east coast of Tasmania and extending to the south in a jet of 15°C surface water (Figure 5.57). South of this jet a number of quasi stationary cyclonic and anticyclonic eddies were also present and entrained a couple of drifting floats (shown as purple arrows). Inshore of the jet a slightly cooler water mass was present extending from the west coast, potentially drawing sub-Antarctic waters onto the shelf; Storm Bay and inshore waters were warm.

Clear days immediately prior to the voyage showed an extensive spring algal bloom on the Tasmanian shelf. On the 10th November the algal bloom was visible along the SE Tasmanian coast and south and west in the EAC extension (Figure 5.58).
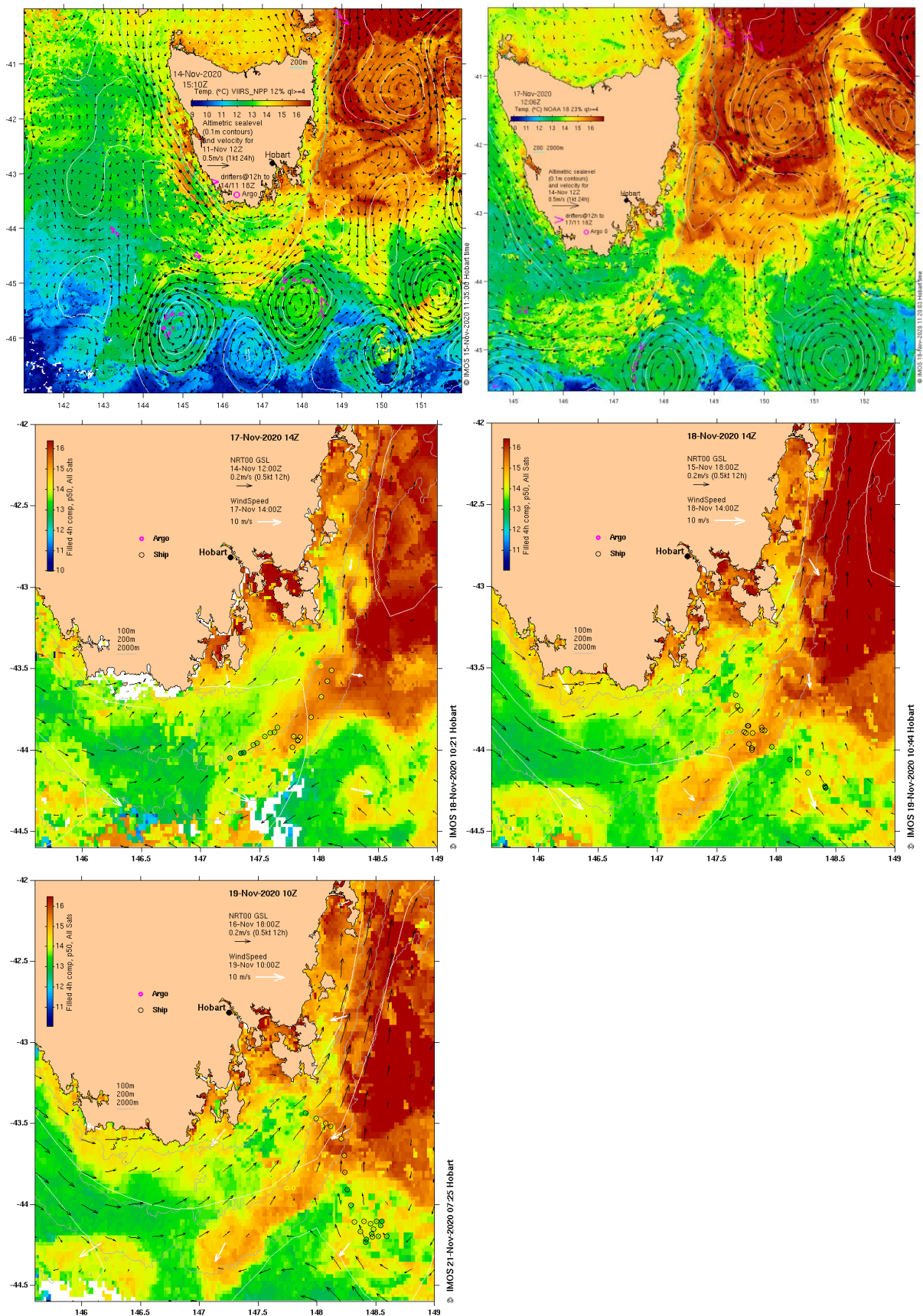
Figure 5.57 Ocean currents and sea surface temperature around Tasmania on 14th - 19th November 2020 (IMOS). In some images yellow & green dots mark the ships track.
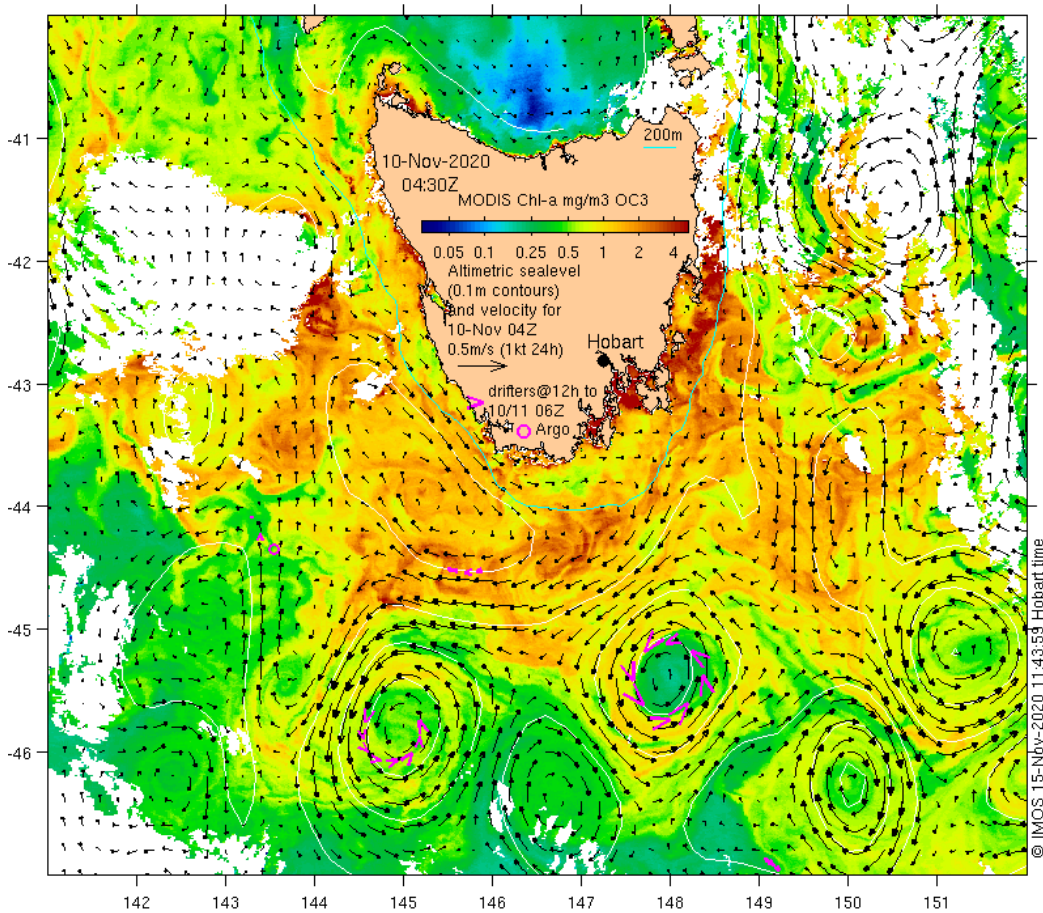
Figure 5.58 Modis OC3M sea surface chlorophyll (IMOS).

5.4.3 Underway Sensors

The underway sensors showed strong gradients in near surface temperature, salinity, fluorescence, and CO_2 throughout the voyage area (Figure 5.59). The filament of EAC water was clearly shown in the ship track as a warm and salty surface feature extending along the shelf edge. Greatest surface chlorophyll fluorescence was found inshore of the EAC water (which was comparatively depauperate in chlorophyll) and there was a biologically mediated drawdown of CO_2 in regions with high chlorophyll fluorescence. High resolution underway wet chemistry nutrient data were also collected along several voyage transects to characterise spatial patterns in surface waters and assist with the calibration of sensors on the Triaxus (Figure 5.60). These data show elevated nutrient concentrations in the far southeast ocean water outside of the EAC jet and also in the cooler water inshore of the EAC water. EAC water and inshore Storm Bay water was depauperate in nutrients with nitrogen being the nutrient in lowest supply relative to Redfield ratios for phytoplankton growth.
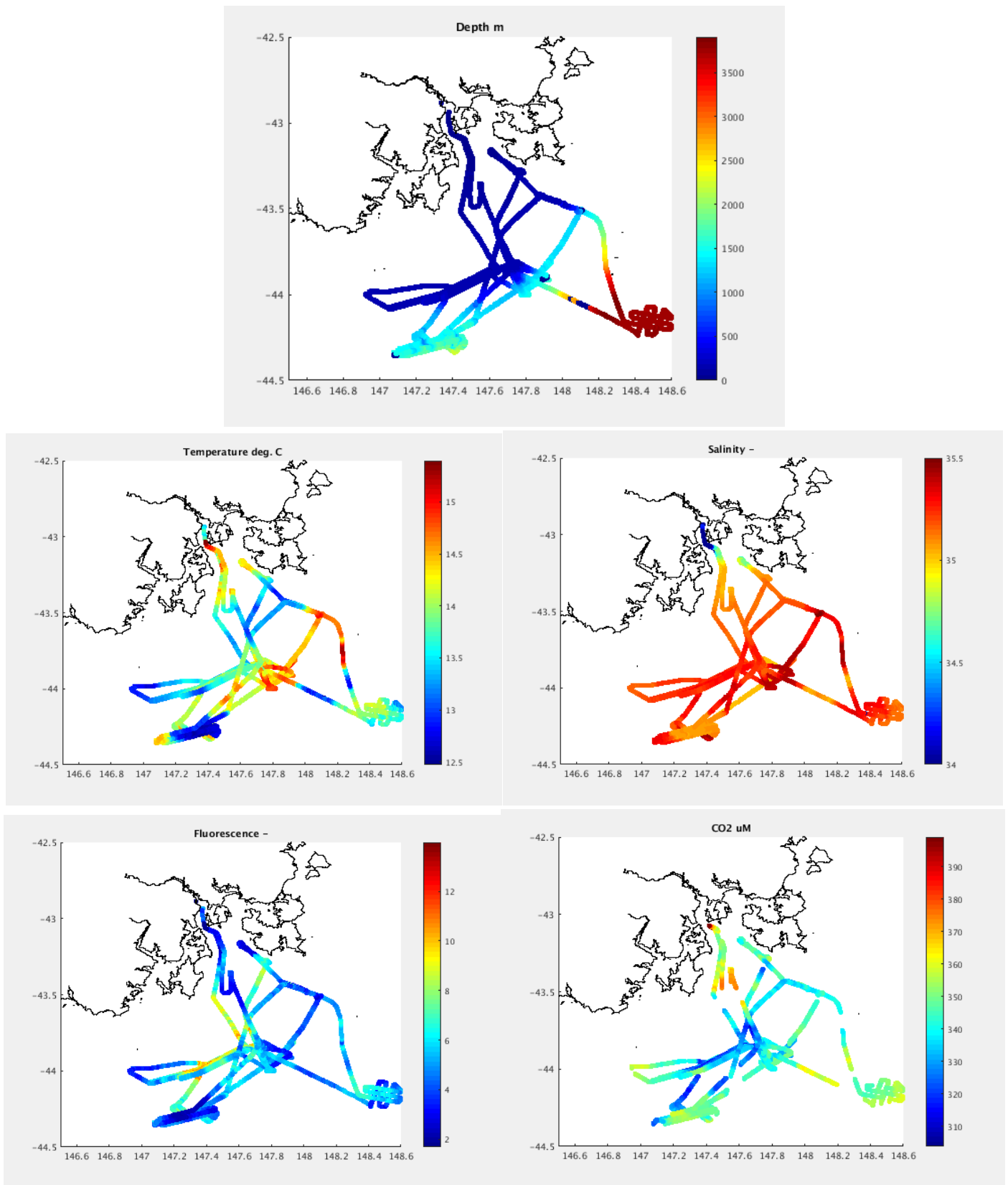
Figure 5.59 Underway observations of depth, temperature, salinity, fluorescence and pCO₂ during the voyage.
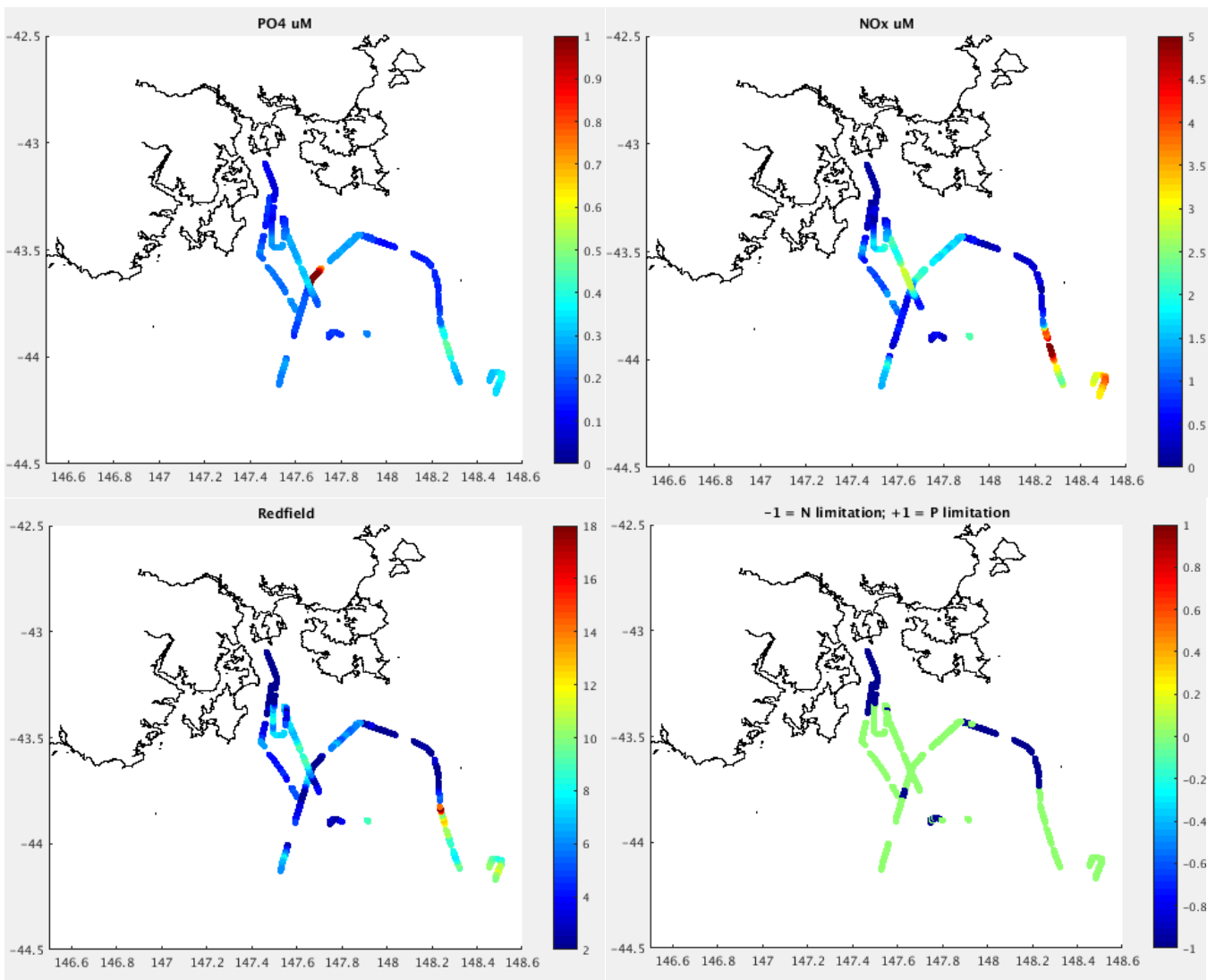
Figure 5.60 Underway observations of phosphate and nitrate, and calculated Redfield ratio (ratio of N:P) and potential for nutrient limitation of phytoplankton growth during the voyage.

5.4.4 CTD Data

Two transects of 3 CTD stations were achieved across the shelf to the southeast and southwest of Storm Bay. Water samples were collected for analysis of plankton pigments, phytoplankton species, CDOM, suspended solids, spectral absorption, and isotopic analysis (Figure 5.61). Nutrient samples were also taken and analysed by the methods described in Rees et al., (2019). At most stations a bottom layer of higher density water was observed with elevated concentrations of nitrate and phosphate (Figure 5.62 & 5.63); concentrations of ammonia and nitrite were greatest in surface waters. Redfield ratios were close to the global average of 16:1 (nitrate:phosphate, Figure 5.64)

Figure 5.61 Water sampling from the CTD rosette.

Eastern Storm Bay Shelf Transect 1
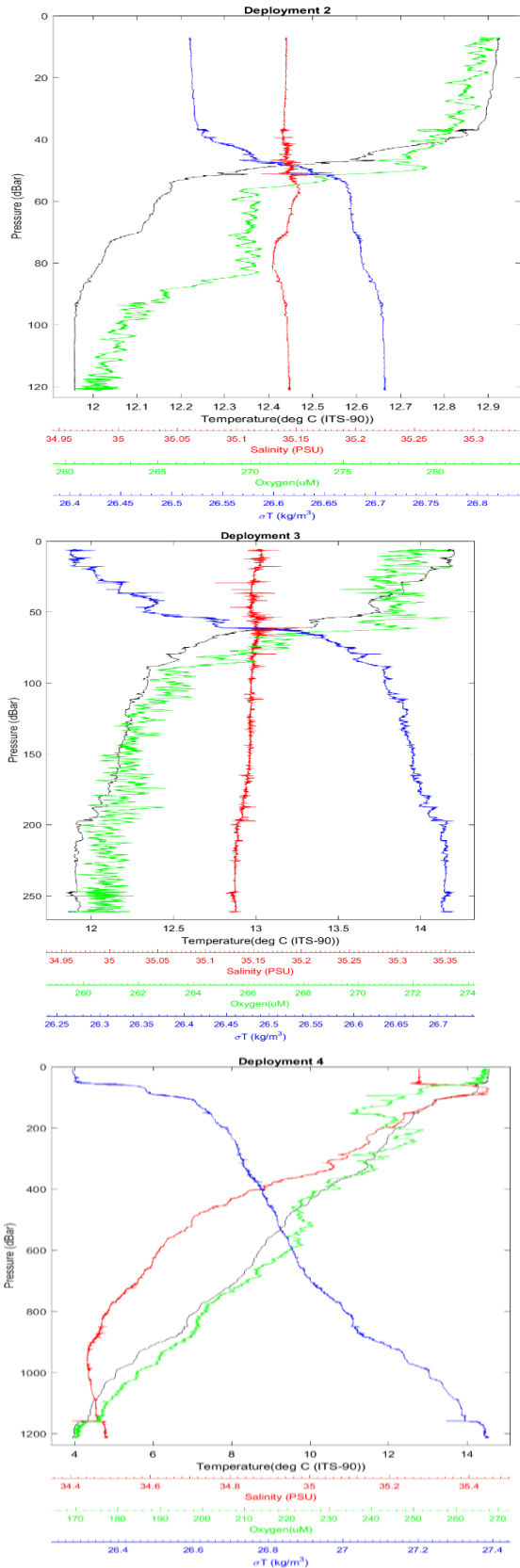
Western Storm Bay Shelf Transect 2
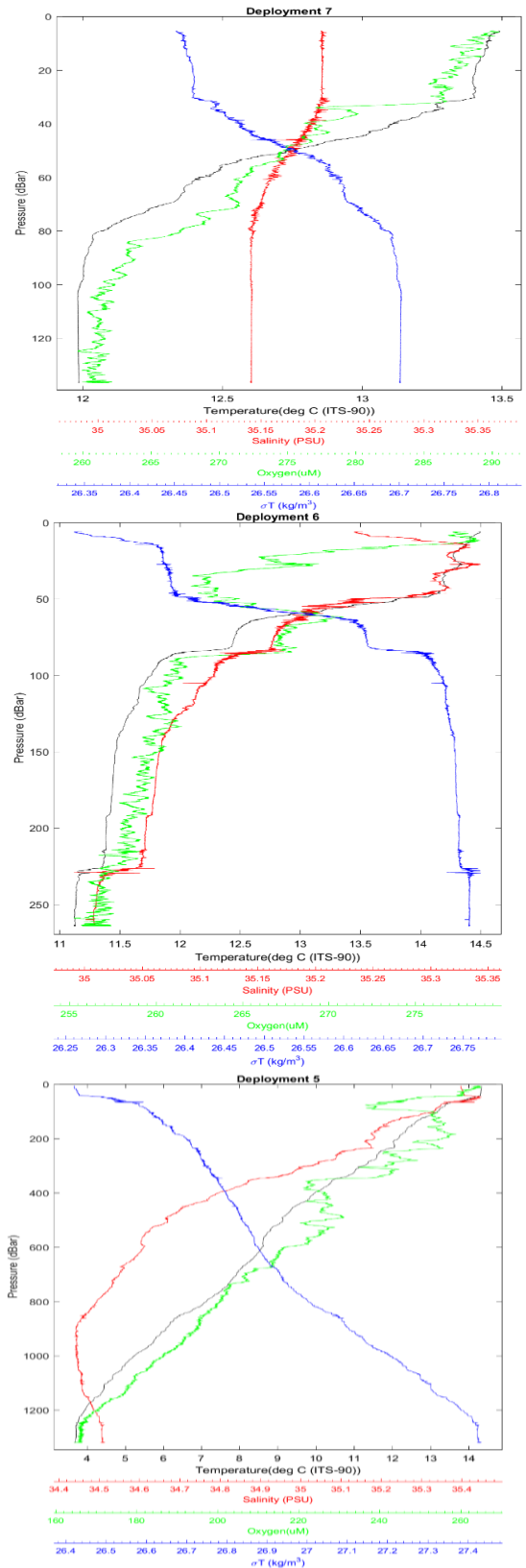
Figure 5.62 CTD profiles from Stations 1 to 6 arranged as inshore (top row), mid shelf (middle) and outer shelf (lower panel).
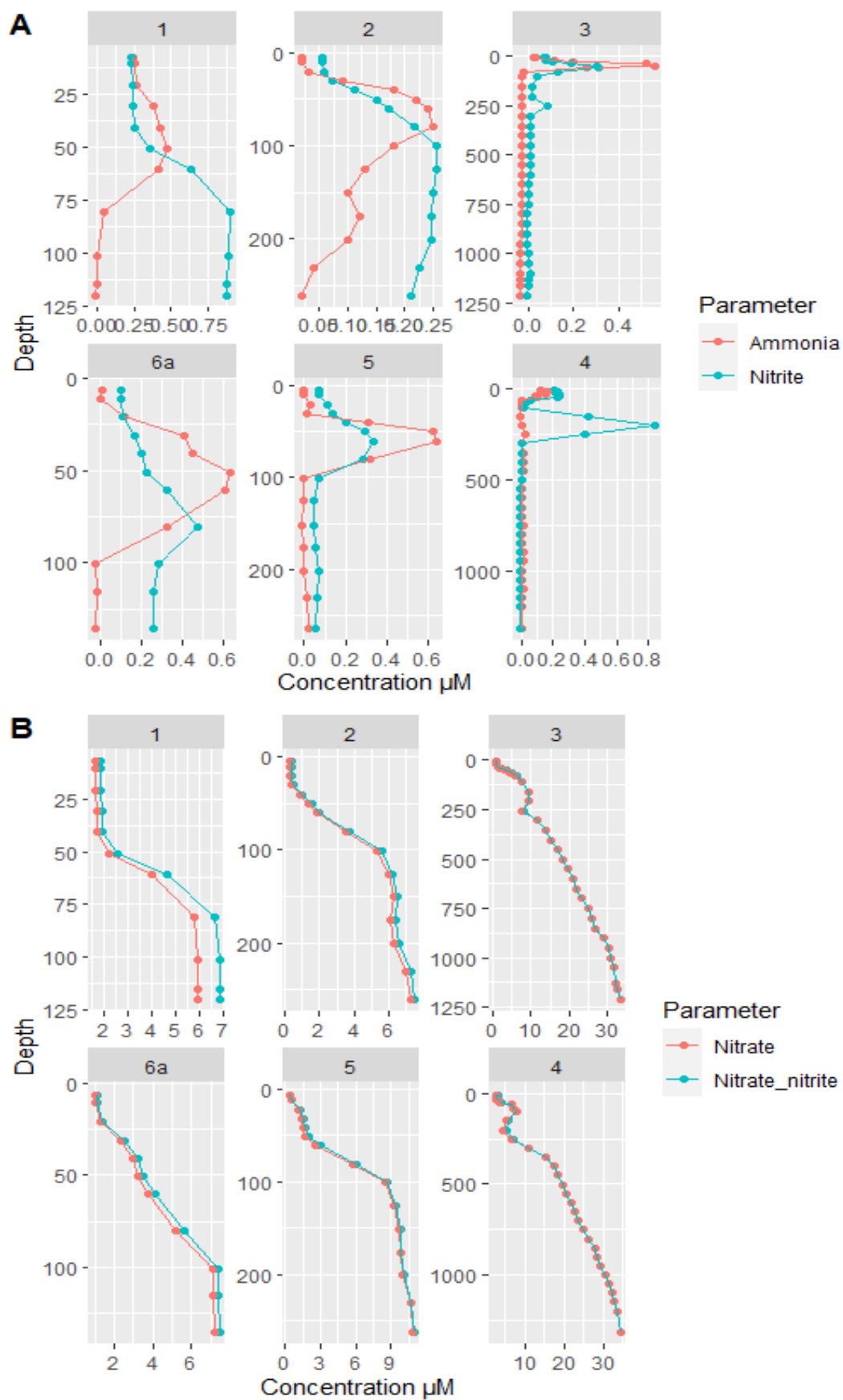
Figure 5.63 Nutrient profiles for Eastern Storm Bay (CTD stations 1,2,3) and Western Storm Bay (CTD stations 6a,5,4) from inshore (left) to offshore (right).
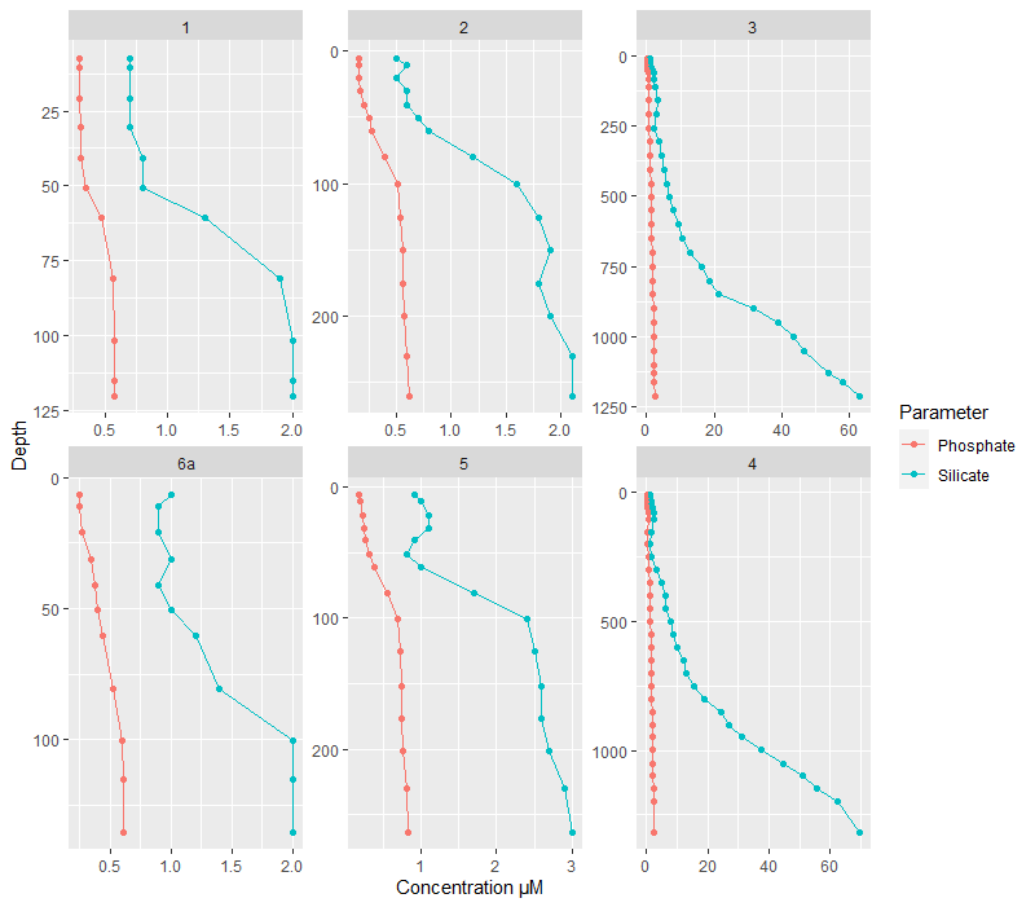
Figure 5.63 (continued) Nutrient profiles for Eastern Storm Bay (CTD stations 1,2,3) and Western Storm Bay (CTD stations 6a,5,4) from inshore (left) to offshore (right).
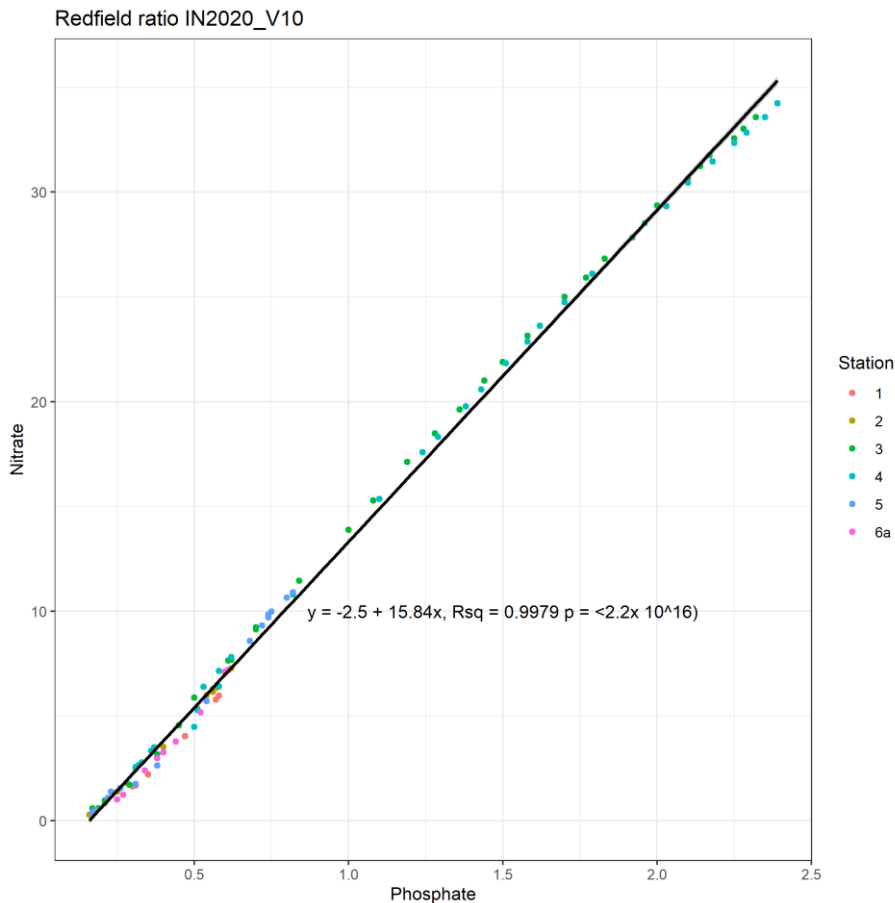
Figure 5.64 Redfield ratio for all CTD data from IN2021_V10. Highest concentrations are associated with deeper waters at the more offshore stations (Stations 3 and 4), see map Figure 5.56 for CTD locations.

Pigments were sampled from the surface, DCM (~20 m) and 40 m depth at all stations. Total chlorophyll-a values were consistent with concentrations observed in previous studies in late Spring (~2 mg.m-3), with lowest values typically at 40 m (Figure 5.65). Marker pigments were used to estimate algal community composition and concentration, including those species that are either not well preserved or too small to consistently identify with light microscopy. Selected marker pigments were normalised against the total chlorophyl a concentration (Figure 5.66), with the community composition within each site very similar. All CTD stations and depths sampled were characterised by diatoms (fucoxanthin), haptophytes (19-hexanoyloxyfucoxanthin), and chrysophytes (19-butanoyoxyfucoxanthin), as well as cryptophytes (alloxanthin and crocoxanthin) and prasinophytes (prasinoxanthin).

Dinoflagellates (peridinin) were not detected at Station 6 and in very small quantities at Station 1, consistent with light microscopy observations made on-board. In addition to prasinoxanthin, green algae associated pigments lutein, zeaxanthin (can also be found in cyanobacteria) and loroxanthin were also detected. Eustigmatophytes (vaucheriaxanthin) were present at all stations/depths, although Stations 4 and 5 40 m samples had barely detectable peaks.

Figure 5.65 Chlorophyll-a depth profiles from Eastern Transect 1 (CTD 1-3) and Western Transect 2 (CTD 4-6b) during IN2020_v10. Only 5, 20 and 40 m depths were sampled for pigments. See map Figure 5.56 for CTD locations.
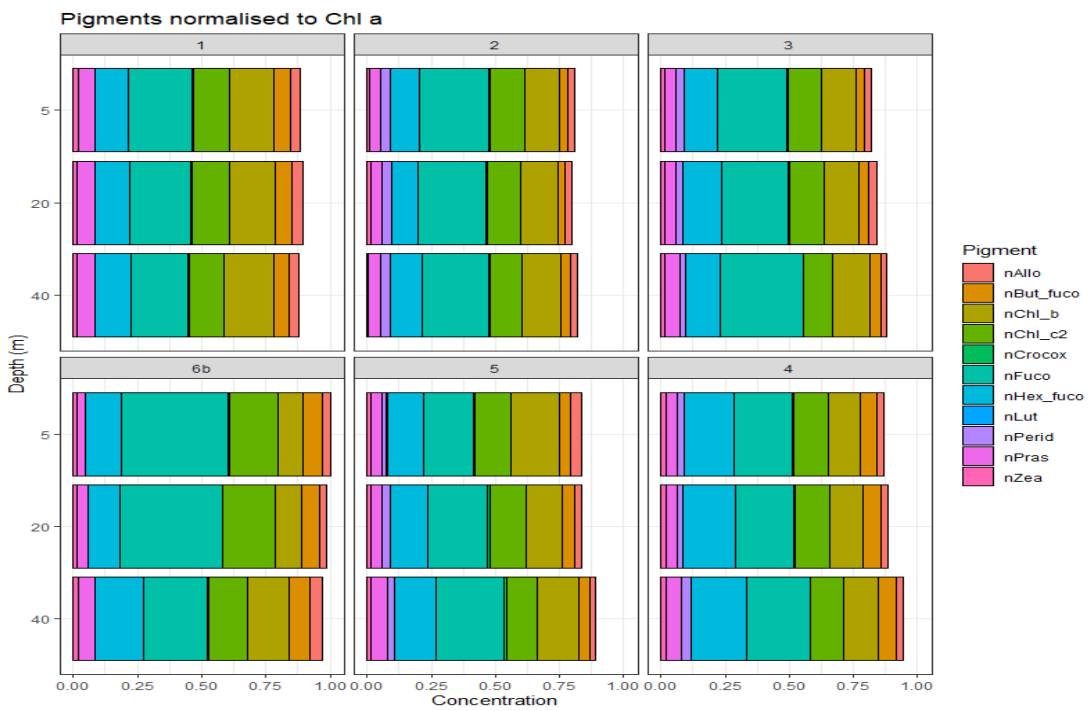
Figure 5.66 Dominant pigments normalised to Chlorophyll a from Eastern Transect 1 (CTD 1-3) and Western Transect 2 (CTD 4-6b) during IN2020_v10 from inshore (left) to offshore (right). Only 5, 20 and 40 m depths were sampled for pigments. See map Figure 5.56 for CTD locations.
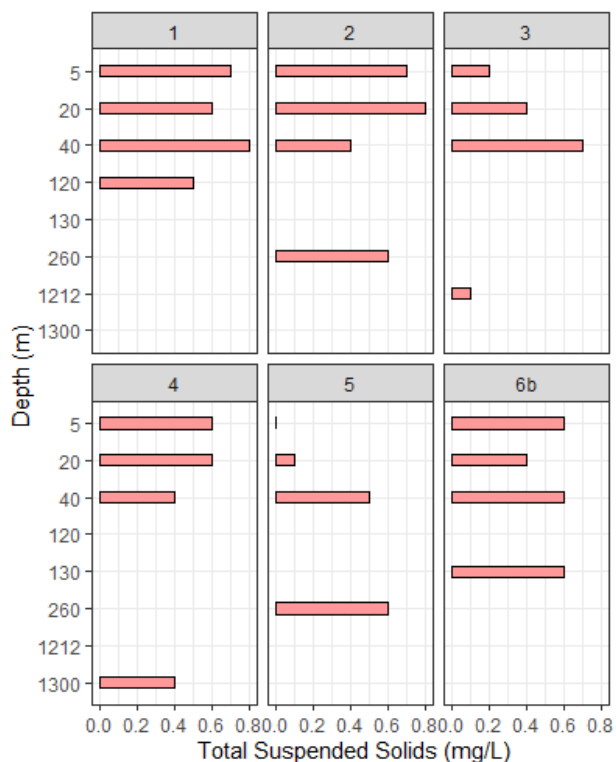
Figure 5.67 Total Suspended Solids depth profiles from Transect 1 (CTD 1-3) and Transect 2 (CTD 4-6b) during IN2020_v10. In addition to 5, 20 and 40 m depths the bottom water at each station was also sampled for TSS. See map. Figure 5.56 for CTD locations.
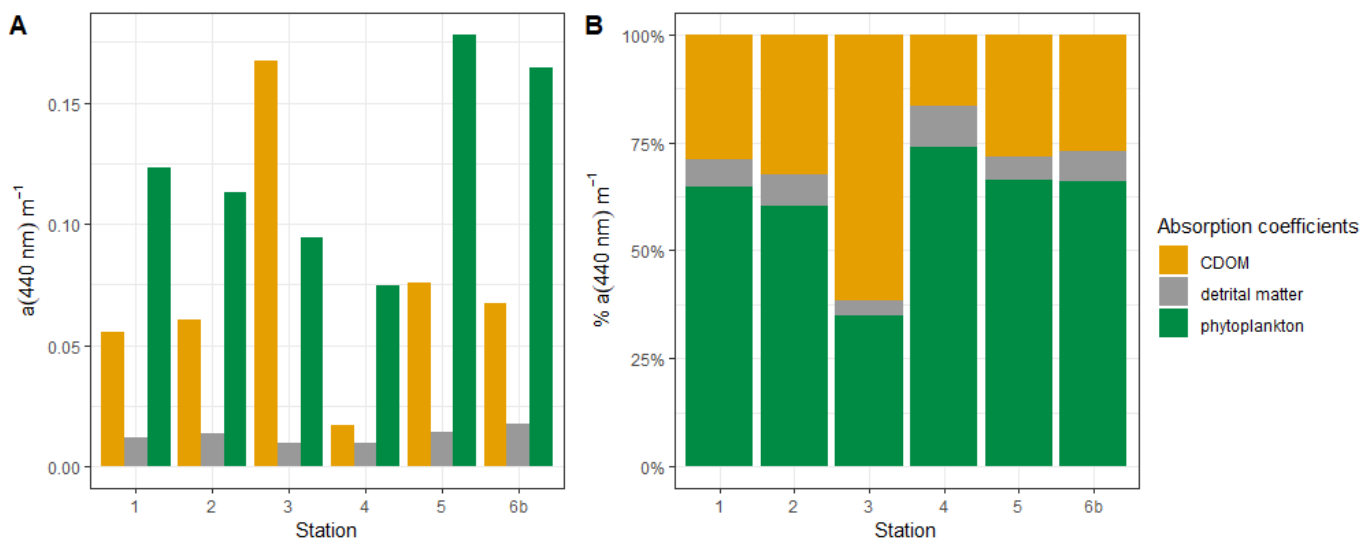
Figure 5.68 Absorption coefficients for Chromophoric Dissolved Organic matter (aCDOM), detrital matter and phytoplankton from Eastern Transect 1 (CTD 1-3) and Western Transect 2 (CTD 4-6b) during IN2020_v10 at A) 440 nm and B) as a proportion of total absorption at 440 nm. Only the 5 m depth was sampled for spectral absorption measurements. See map Figure 5.56 for CTD locations.
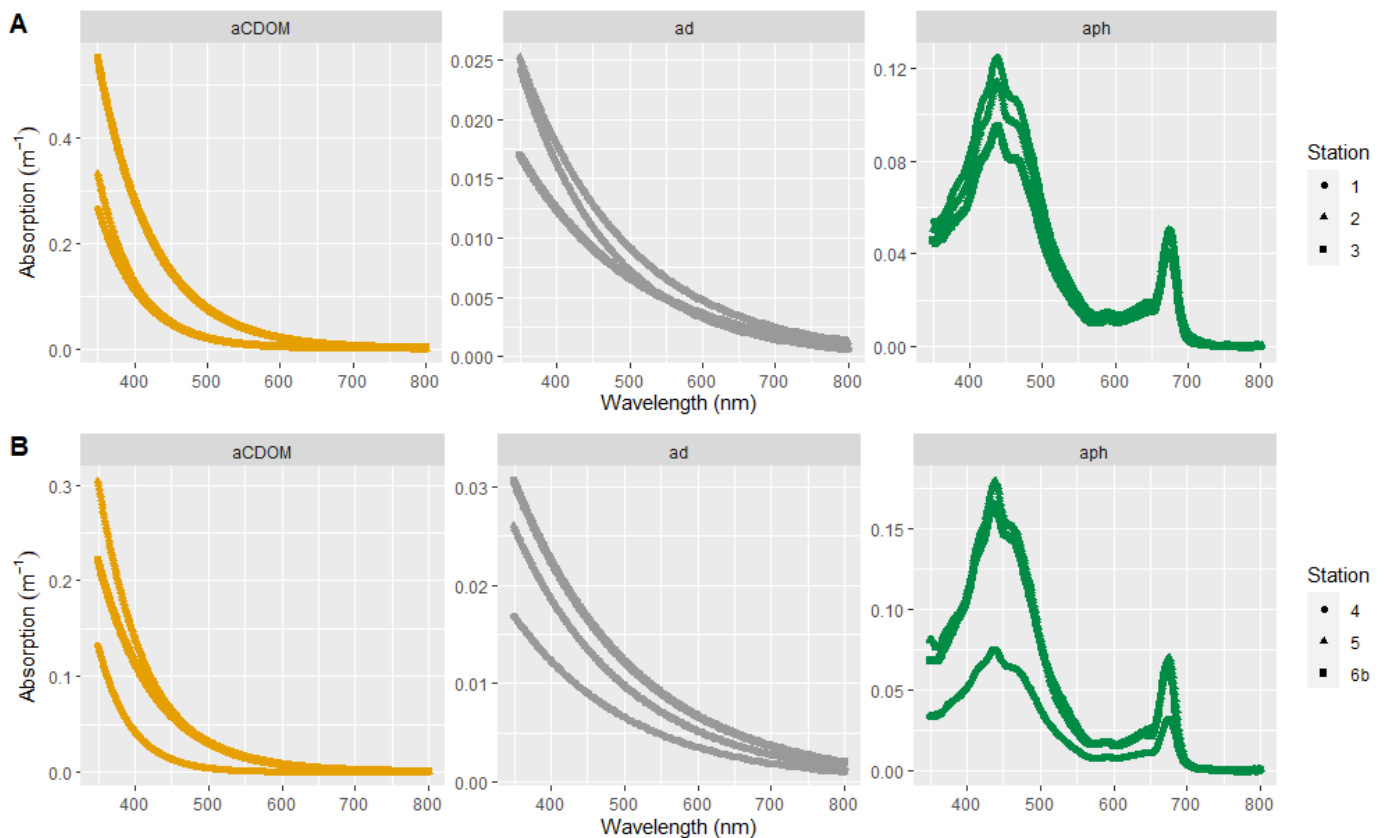
Figure 5.69 Absorption spectra for Chromophoric Dissolved Organic matter (aCDOM), detrital matter (ad) and phytoplankton (aph) from Eastern Transect 1 (CTD 1-3) and Western Transect 2 (CTD 4-6b) during IN2020_v10. Only the 5 m depth was sampled for spectral absorption measurements. See map Figure 5.56 for CTD locations.

The spectral properties of surface water samples collected at each of the 6 CTD stations was assessed by measuring a suite of optical properties. Surface waters in SE Tasmania are influenced by Chromophoric Dissolved Organic Matter (CDOM) from both terrestrial and marine sources, phytoplankton and detrital (or non-algal) matter and the total absorption of the sample is thus calculated as:

$$a(\lambda)=aph(\lambda)+ad(\lambda)+aCDOM(\lambda)+aw(\lambda)$$

where aph, ad, $aCDOM$ and aw are absorption coefficients (m^{-1}) due to phytoplankton, detrital or non-algal matter, CDOM and water respectively (Clementson et al 2004) at a specific wavelength λ.

CDOM is the proportion of dissolved organic matter that absorbs light and is thus characterised by its absorbance and fluorescence properties (Heller et al. 2016). CDOM absorbs light most strongly at shorter wavelengths in the blue region (< 500 nm, Figure 5.69), and is mostly attributed to traces of river runoff present at the time of sampling. Values of aCDOM at 440 nm (Figure 5.68) observed are very low (< 0.2 m^{-1}) and consistent with mean values for SE Tasmania observed by Cherukuru et al. (2014). The contribution of detrital matter (ad) was very low at all stations, with phytoplankton (aph) making up more than 50% of the total absorption at 440 nm for all stations except Station 3 on the shelf.
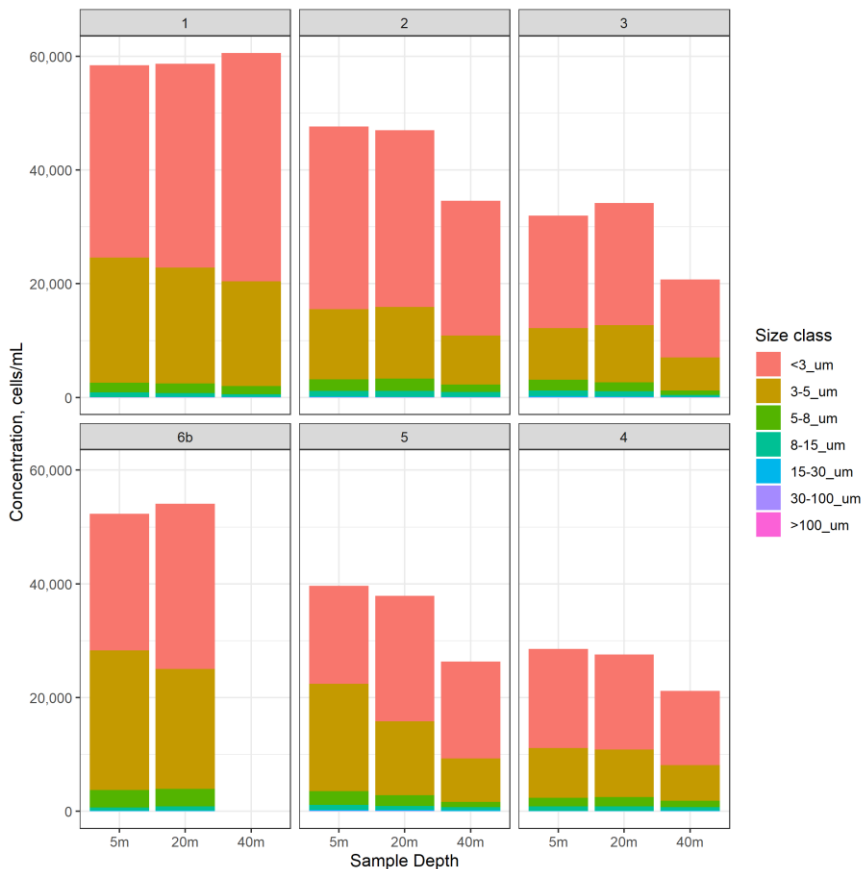
Figure 5.70 Size class distribution for eukaryotic cells determined by side-scatter length from Eastern Transect 1 (CTD 1-3) and Western Transect 2 (CTD 4-6b) during IN2020_v10 from inshore (left) to offshore (right). No sample for 40m depth, Station 6b, see map Figure 5.56 for CTD locations.

Flow cytometry samples collected from the CTD casts were analysed by side-scatter to estimate the size distribution (based on length) of the particles in the sample (see Figure 5.70). For both transects, the total number of cells/mL decreased with distance from the coast, and all samples were dominated by particles less than 5 µm in length. More detailed analysis of the picoplankton (phototrophic cells measured by the flow cytometer) community focused on the picocyanobacteria *Prochlorococcus* and *Synechococcus*, and picoeukaryotes which contribute to the <3 µm size fraction (Figure 5.71). The concentration of picoeukaryotes was almost invariant with depth at the stations closest to land, with a trend of decreasing abundance with distance from the coast and with depth at the more offshore stations. *Synechococcus* are widely distributed in marine systems, and were observed at all stations, abundances were similar in the 5 and 20m samples, with decreased abundances at 40m depth. *Synechococcus* typically have a strong seasonal cycle in SE Tasmania, with highest concentrations associated with the intrusion of EAC water in summer, and are almost completely absent in winter (Thompson et al, 2020). *Prochlorococcus* were only present in very low concentrations, and are considered a tropical species, also linked to transport southwards by the EAC. Concentrations were highest in the offshore stations.
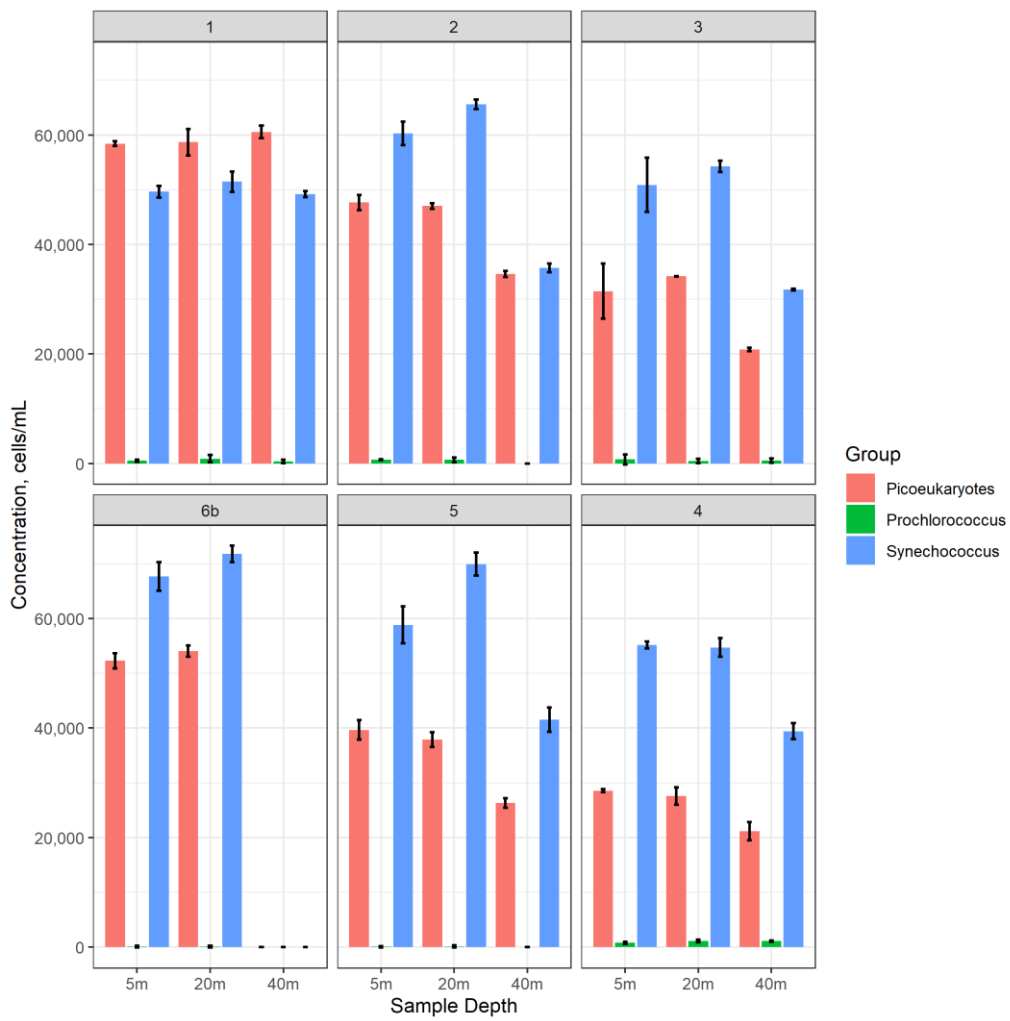
Figure 5.71a Picoplankton abundances determined by flow cytometry using autofluorescence from Eastern Transect 1 (CTD 1-3) and Western Transect 2 (CTD 4-6b) during IN2020_v10 from inshore (left) to offshore (right). No sample for 40m depth, Station 6b, see map Figure 5.56 for CTD locations.
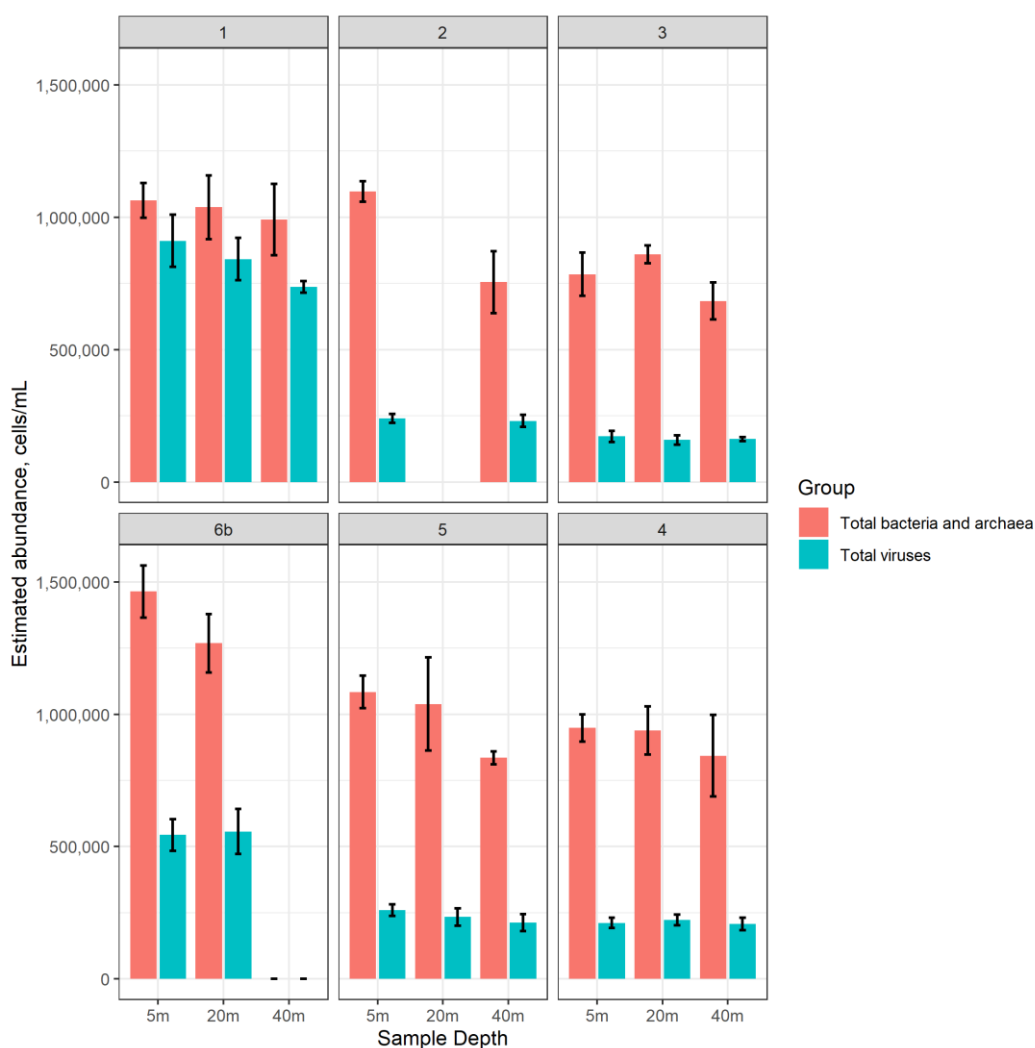
Figure 5.71b Total heterotrophic microbes determined by flow cytometry from Eastern Transect 1 (CTD 1-3) and Western Transect 2 (CTD 4-6b) during IN2020_v10 from inshore (left) to offshore (right). No sample for 40m depth, Station 6b, and no analysis for 20m depth, Station 2, see map Figure 5.56 for CTD locations.

The heterotrophic community was estimated from flow cytometry measurements of total viruses, and total bacteria and archaea (Figure 5.71b). The virus measurements are considered preliminary but initial data suggests total bacteria and archaea were more dominant than viruses, in all samples. Stations 1 had the highest total levels, with V1 and B+A2 categories (based on green fluorescence/side-scatter) being dominant in these samples, respectively. In general, abundances were highest at 5m and 20m, with 40m having lower levels of abundance. The pattern of overall decline in total abundances with distance off-shore observed in the eukaryotes was maintained.

5.4.5   Triaxus Underway Sections

Following 2 test deployments, and upgrades to the sensor payload a long transect tow was achieved which crossed the filament (including a mesoscale swirl) of EAC water extending southwest from the east of Tasmania (see SST images Figure 5.57). The transect commenced in open ocean water with high chlorophyll content and progressed through a cooler water mass flowing from the southwest with elevated nitrate content. At approximately 50km into the tow we entered warm salty water characteristic of the EAC and rotating in a cyclonic (clockwise)

swirl/eddy. This feature is well characterised by the sensors on the Triaxus (Figures 5.72 & 5.73), the ADCP (Figure 5.74 & 5.75) and continuous underway observations (including wet chemistry nutrient analysis). A further Triaxus transect was achieved from Station 5 towards Hobart on the final leg of the voyage. [Note that results shown are preliminary and will be revised when sensor calibration and data quality control are complete.]
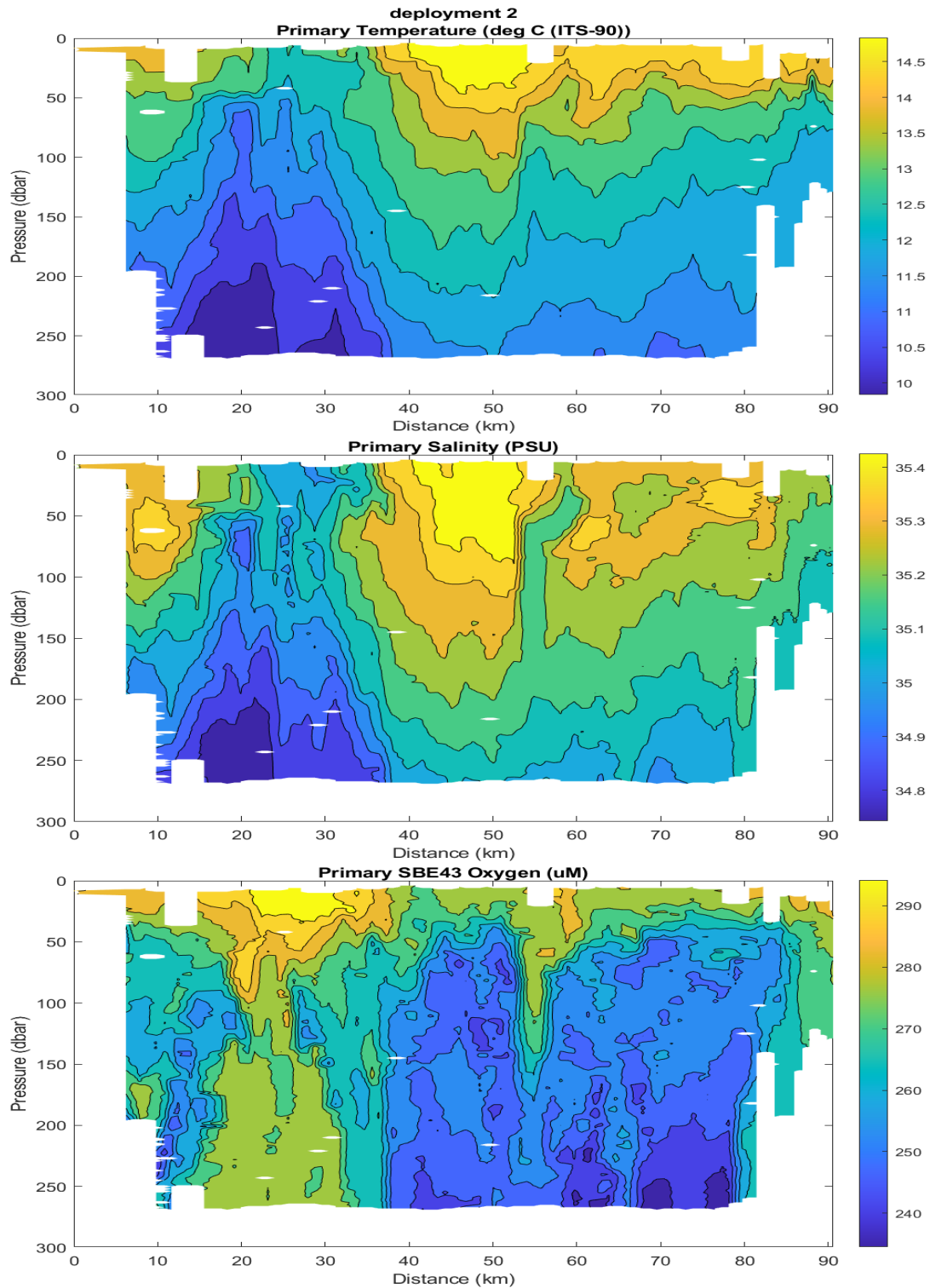
Figure 5.72 The evolution of temperature, salinity, and oxygen along Triaxus tow #2.
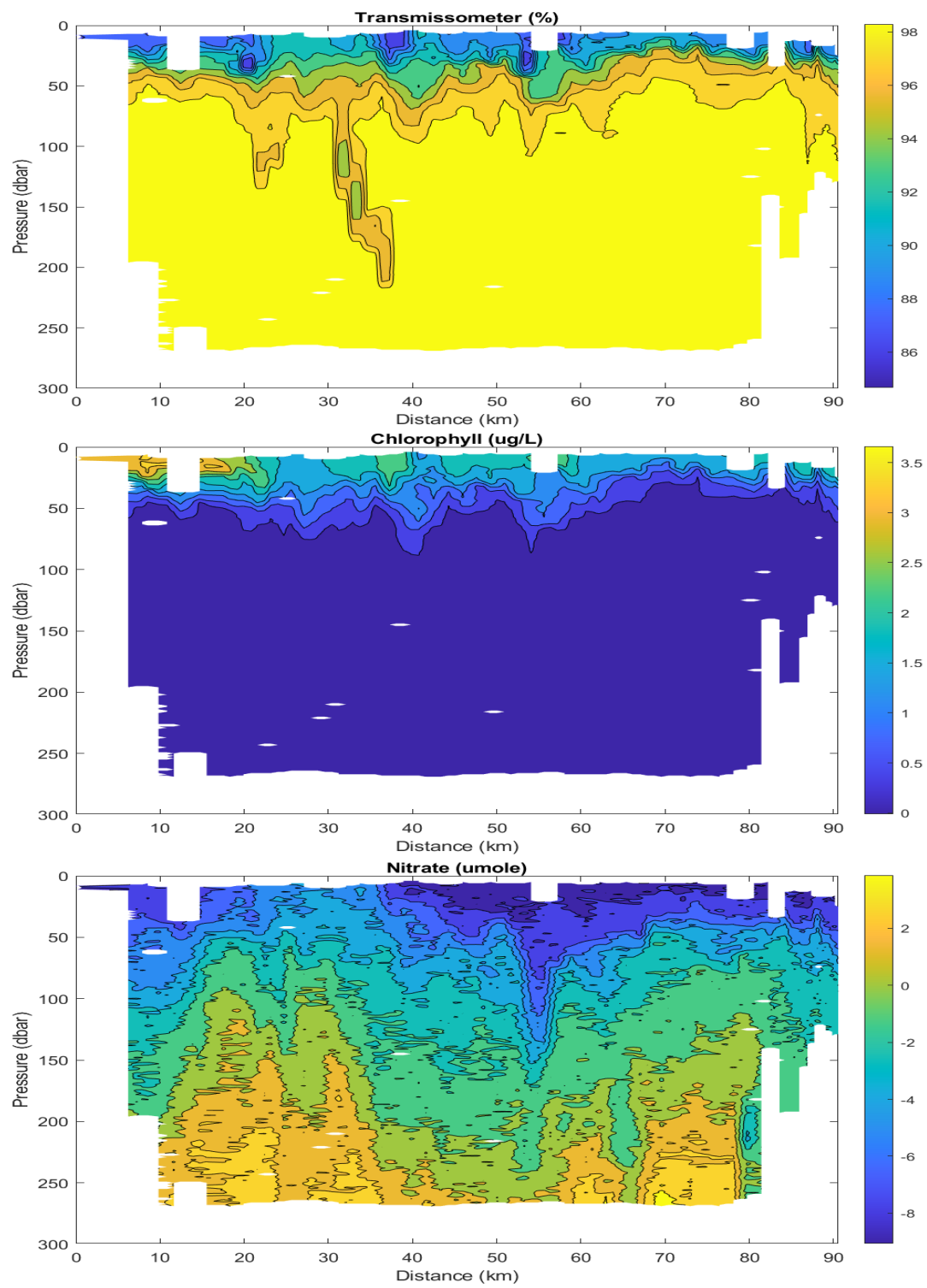
Figure 5.73 The evolution of transmission, chlorophyll, and nitrate along Triaxus tow #2 [uncalibrated data are shown from the SUNA UV nitrate sensor which had a negative bias].
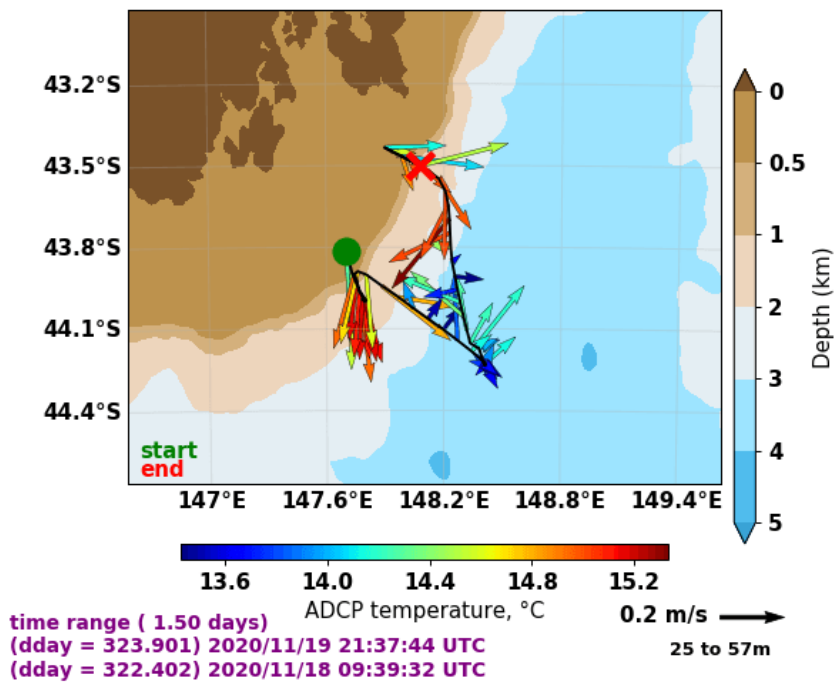
Figure 5.74 Surface currents on 20th November during the Triaxus tow shows the ships track crossing a cyclonic eddy south of the Tasman peninsular (centred near red X).
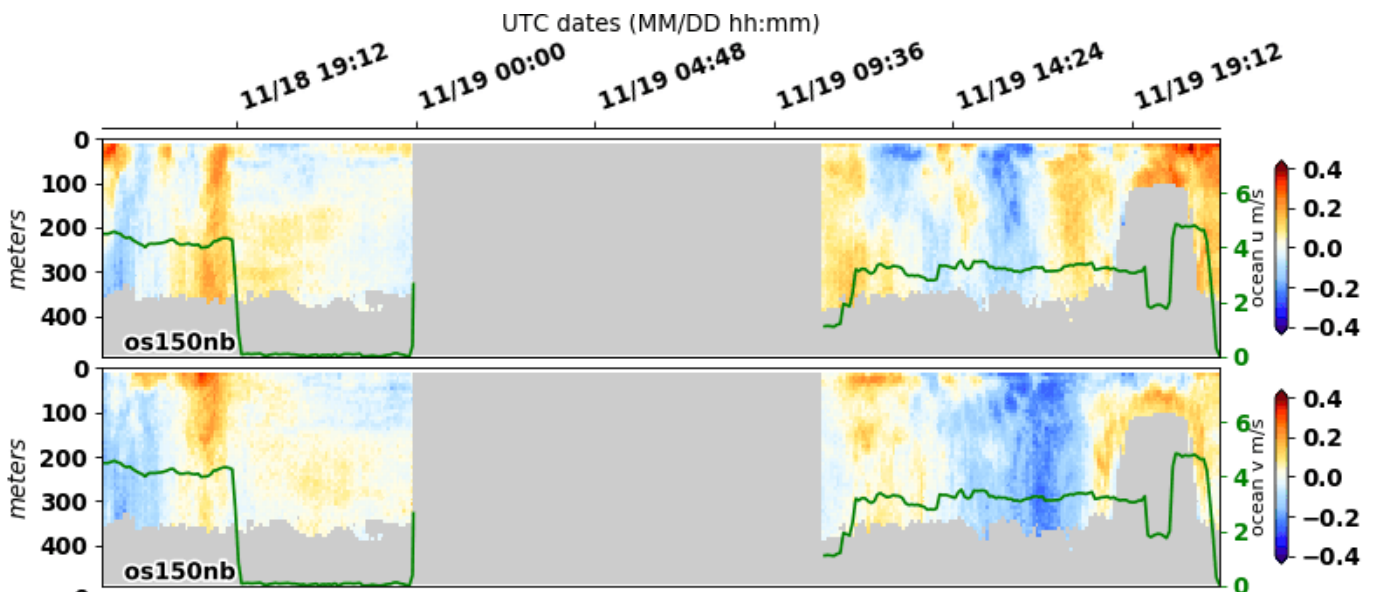
Figure 5.75 Profile of current velocity during the Triaxus tow (righthand part of plot) shows surface velocities extended to ~50m depth during the eddy transect with deeper velocities oriented to the north (as the bottom shoaled at the shelf edge).

5.4.6   Phytoplankton Observations

Phytoplankton samples were collected from 6 CTD casts and from the underway system. Samples from the CTD were preserved for post-voyage laboratory analysis, but the underway samples were examined live using a compound microscope fitted with epifluorescence filters to detect

chlorophyll-a autofluorescence (Figure 5.76). Phytoplankton samples from the underway system were concentrated by placing a 20 μm mesh net under the sample outlet for between 15 and 30 minutes.

Samples collected from inshore of the EAC water were highly diverse, with a mix of dinoflagellate species (predominantly *Tripos*, *Dinophysis*, *Gonyaulax* and *Protoperidinium*) and diatom species (*Skeletonema*, *Chaetoceros*, *Pseudo-nitzschia*, and *Guinardia*). The presence of large numbers of *Tripos fusus, T. furca* and *T. muelleri* suggested influence from Storm Bay as these species commonly bloom in the lower reaches of the Derwent.   Underway samples south of the EAC filament were comparatively sparse, with no dinoflagellate species observed. These samples consisted of only diatoms, predominantly barbed *Chaetoceros* species and *Corethron pennatum*, reminiscent of more southerly sub-Antarctic communities observed at the Southern Ocean Time Series (47S, 142 E). The preserved phytoplankton samples, pigment and flow cytometry samples collected from the CTD transects and underway system will add further definition to the phytoplankton communities present in the water masses identified by CTD, Triaxus and satellite data. Example pictures are shown in Figure 5.77.

Figure 5.76 Compound microscope fitted with epifluorescence filters for viewing live samples.
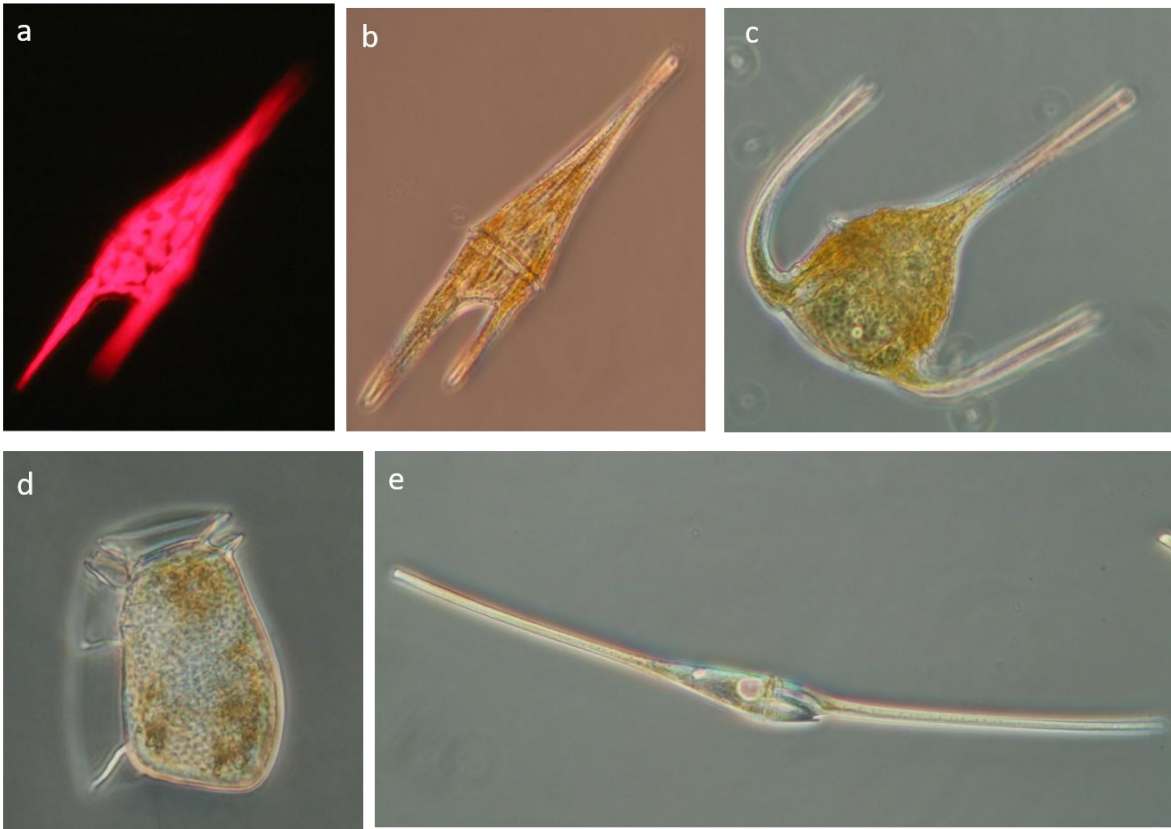
Figure 5.77 Dinoflagellate species observed inshore of the EAC water a) *Tripos furca* **b)** *Tripos furca* **c)** *Tripos muelleri* **d)** *Dinophysis truncata* **e)** *Tripos fusus***. Image a) shows chlorophyll-a autofluorescence for the cell shown in b).**

5.4.7 Testing of Underway pCO$_2$ Instrumentation

In addition to the water mass, nutrient and plankton sampling Craig Neill (CSIRO) installed two underway pCO$_2$ instruments in the underway seawater lab, (in addition to the one that is permanently there), to facilitate testing of new instrument designs and various CO$_2$ detectors (Figure 5.78). The RV Investigator's permanent pCO$_2$ system uses a Licor model LI-7000 non-dispersive infrared analyser (NDIR) as the CO$_2$ detector. Data collected by this suite of instrumentation will be made available to our project to inform the simulation of seawater carbon chemistry (including alkalinity and pH).
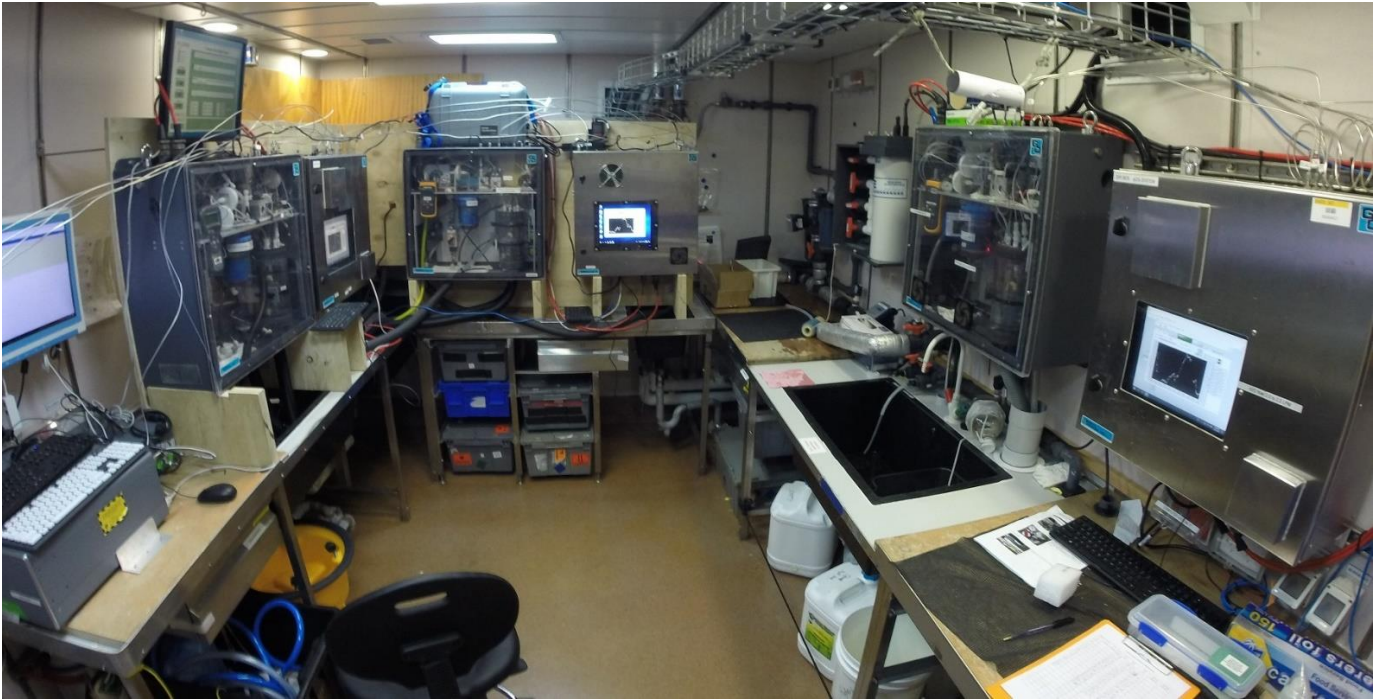
Figure 5.78 Underway seawater lab with three pCO$_2$ systems installed.

5.5 Near real time sensor deployments

In 2018 an opportunity arose for the strategic deployment of two CSIRO-owned near-real time (NRT) instruments in the study domain (led by Jack Beardsley). Two YSI EXO2 Multiparameter Sondes were installed to observe multiple parameters of interest, which were then used to routinely calibrate and validate the performance of the project's modelling systems. These systems remain deployed as part of the continual assessment and monitoring of the Derwent Estuary and upper D'Entrecasteaux Channel.

5.5.1 Hardware

Two identical NRT observation systems were built by Daniel Hugo (Data61/CSIRO). They were designed to be relatively compact and transportable, independently powered and highly versatile platforms to allow CSIRO to collect observations of multiple parameters in near-real time. Each system uses a YSI EXO2 Multiparameter Sonde fitted with an array of sensors (Figure 5.78).

- · Chlorophyll
- · Conductivity
- · Depth
- · Dissolved Oxygen
- · Dissolved Oxygen Saturation
- · ORP
- · pH
- · Phycoerythrin
- · Pressure
- · Salinity
- · Temperature
- · Turbidity

Figure 5.79 YSI EXO2 Multiparameter Sonde and list of parameters measured.

Each EXO2 unit was housed in a custom titanium frame (designed and built by CSIRO Engineering Services) to help protect each sonde from damage and external biofouling. A 20 kg weight was suspended 1 m below each sonde unit to ensure it remained stable throughout the water column, while also being connected to an above-surface (AS) unit (Figure 5.80). Each AS unit includes:

- · 1x WaterLog Storm3 data logger;
- · 1x 3G modem;
- · 1x 12Ah 12V battery and;
- · 2x 17W Solar Panels;
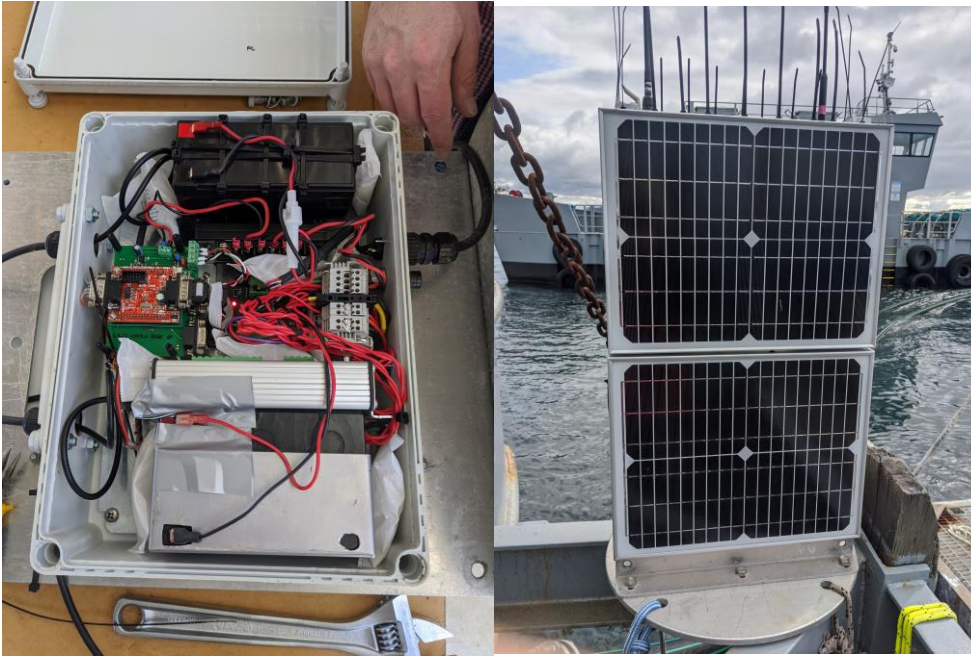
Figure 5.80 Above-surface unit internals (left) and outer housing (right).

5.5.2   Deployment Locations

Both NRT observation platforms have been providing near-continuous sampling since installation at sites in the Derwent Estuary and upper D'Entrecasteaux Channel. The instruments were specifically installed on the eastern end of the CSIRO Hobart Wharf and the Tassal Sheppards aquaculture lease respectively (Figure 5.81). These locations allow for strategic continuous sampling of water quality parameters in the Derwent Estuary and northern D'Entrecasteaux Channel, and fill geographic 'gaps' from other previously discussed observation sources.
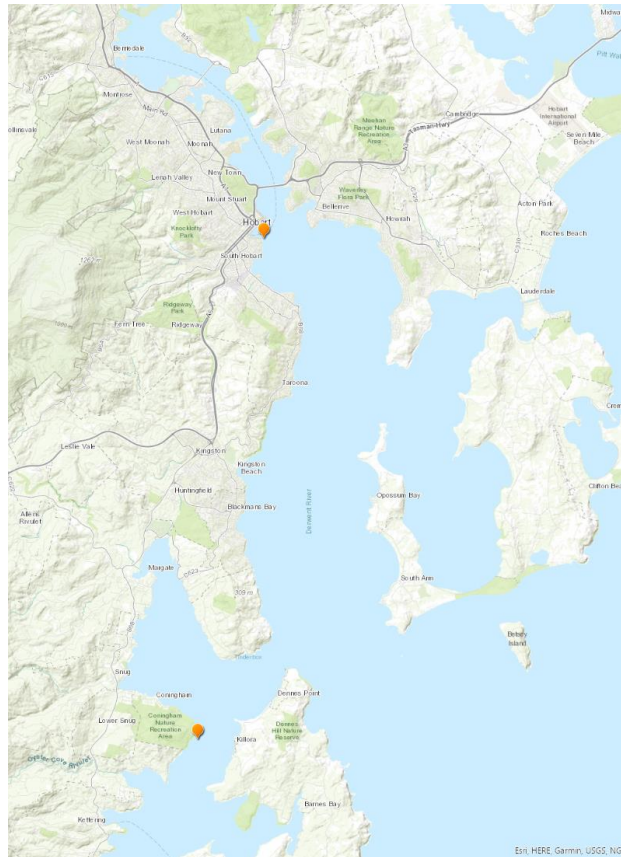
Figure 5.81 Hobart Wharf (North) and Sheppards Barge (South) NRT observation sites.

5.5.3 Fieldwork

Installation of the NRT instrument at the TASSAL Sheppards Lease was undertaken using the CSIRO vessel RV South Cape, while the CSIRO Hobart Wharf required manual installation only. Independent CTD casts and water sampling were also performed at each installation site for calibration and validation of the Sondes' performance (Figure 5.82). Each instrument was regularly surface cleaned (~4-6 weeks) to remove biofouling on the sensor heads and surrounds (we thank Tassal Sheppards staff for their assistance in this at the D'Entrecasteaux Channel site). This helped to ensure optimum instrument performance throughout the deployment window. Both instruments were also annually calibrated by YSI, resulting in small data gaps that were essential to maintaining reliable environmental monitoring.

Figure 5.82 Water sampling being undertaken by CSIRO staff aboard RV South Cape at the Sheppards Barge observation site.

5.5.4   Resulting Datasets

Each of the environmental variables listed in (Figure 5.79) are sampled every 15 minutes and simultaneously stored to the on-premises data logger + transmitted to the CSIRO/Data61 Senaps system via the respective on-board cellular modems. These results can be viewed, queried and plotted immediately by users of the CSIRO/Data61 Senaps Portal (Figure 5.83) for sensor QA/QC. Each Senaps data stream is automatically converted to observation inputs for routine model calibration and assessment, while also being simultaneously pushed to the EagleIO platform and Storm Bay Modelling and Information Dashboard for stakeholders to explore alongside the project's modelling output.

Figure 5.83 Example NRT data streams of temperature (blue/green) and salinity (pink/orange) for the CSIRO Hobart Wharf and Sheppards Barge sites between May 2021 and February 2022.

6   Accessing the Storm Bay Modelling & Information System

The Storm Bay Modelling & Information System has been developed to provide access to model outputs, decision support tools, and project reports. Components from the successful Macquarie Harbour and SIMA Austral (Chile) projects have been reimagined into a system specific for Storm Bay (Figure 6.1). The platform is designed to interface with the parallel FRDC project '2018-104 Next generation decision support tools to support sustainable aquaculture in Storm Bay' and a potential future Harmful Algal Bloom dashboards.

Stakeholder engagement and interaction is critical to the design of a successful interface; this commenced with a demonstration of the SIMA Austral Chile platform to stakeholders in February 2019 and a workshop to identify information of value to industry in July 2019. Additional meetings demonstrations and discussions have also been held with sub-sets of stakeholders throughout 2020-21.

The system can be accessed at: https://stormbaymodelling.csiro.au - access valid Nov 2022.
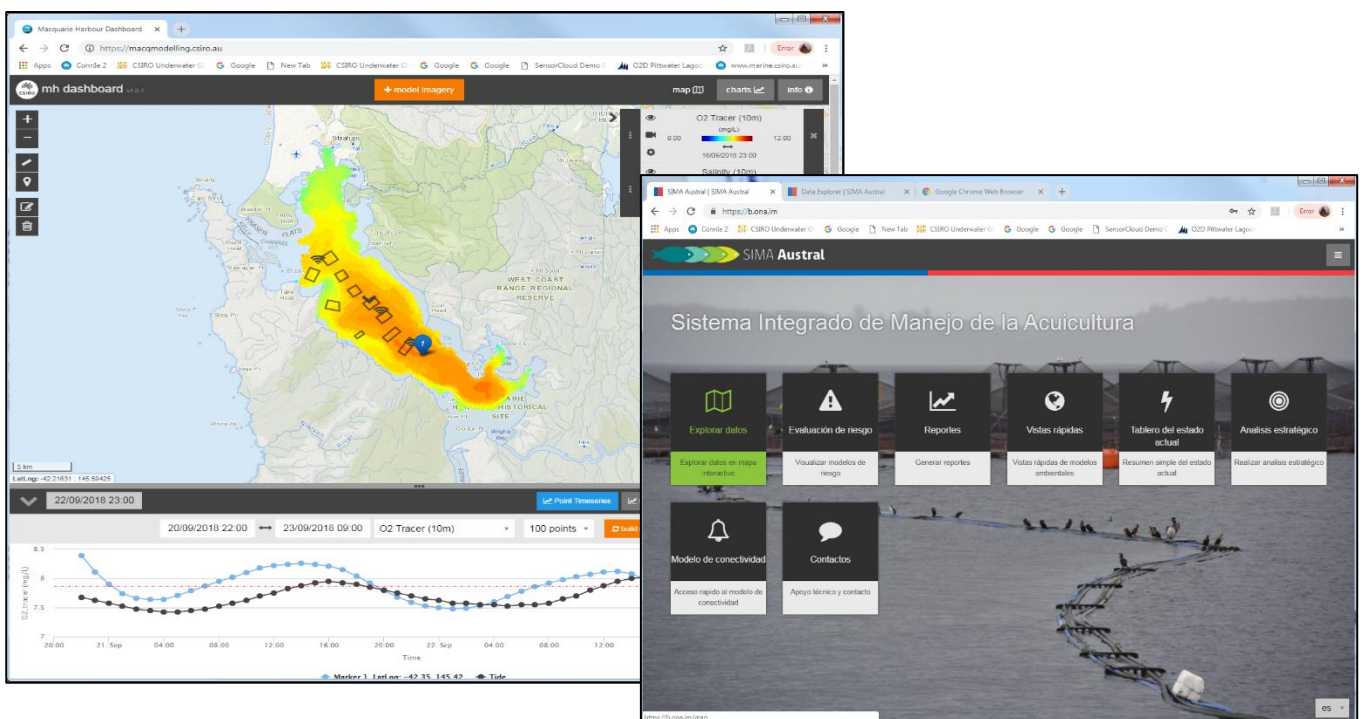
Figure 6.1: Example web-based visualisation systems to access model products, project reports and analysis in Macquarie Harbour (left) and SIMA Austral, Chile (right).

The Storm Bay Modelling & Information System home page (Figure 6.2) provides direct links to model outputs, tools, and reports from the project.
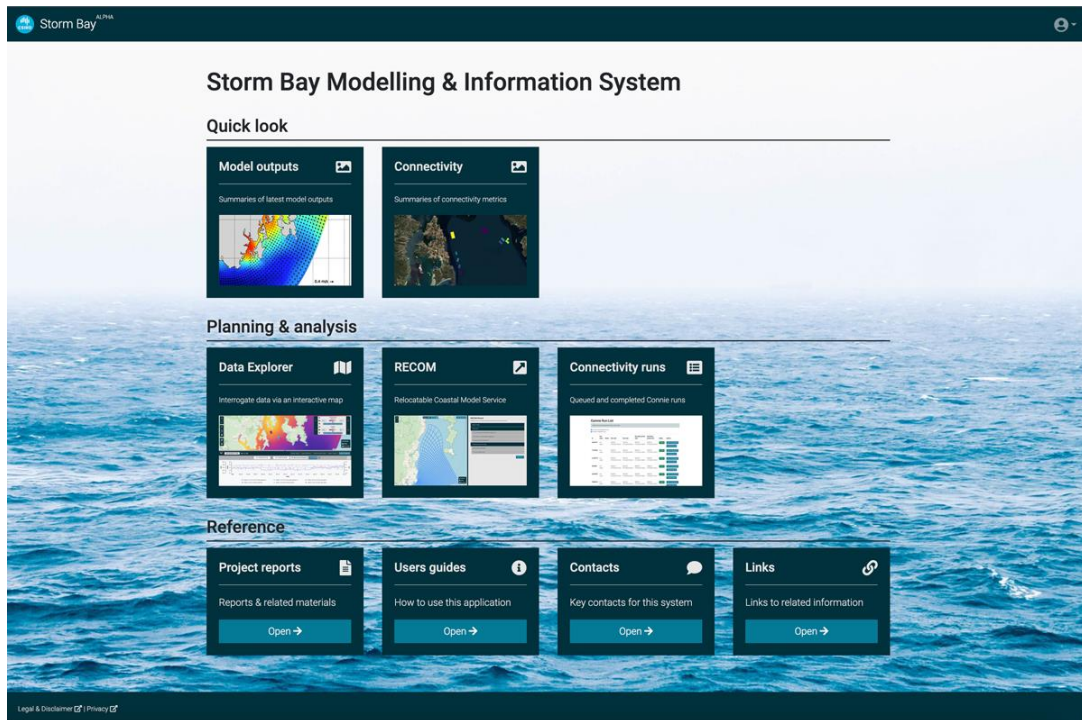
Figure 6.2: Homepage for the Storm Bay Information System (https://stormbaymodelling.csiro.au - access valid Nov 2022)

The **Data Explorer tool** (Figures 6.3 – 6.9) supports visualisation of various datatypes, such as model outputs, remote sensing products from NASA, observation data (e.g. CSIRO moorings), and connectivity model outputs. Single or multiple 'layers' of data can be loaded onto the map and interrogated to visualise time-series, depth profiles or transects of properties in specific locations of interest defined by the user.
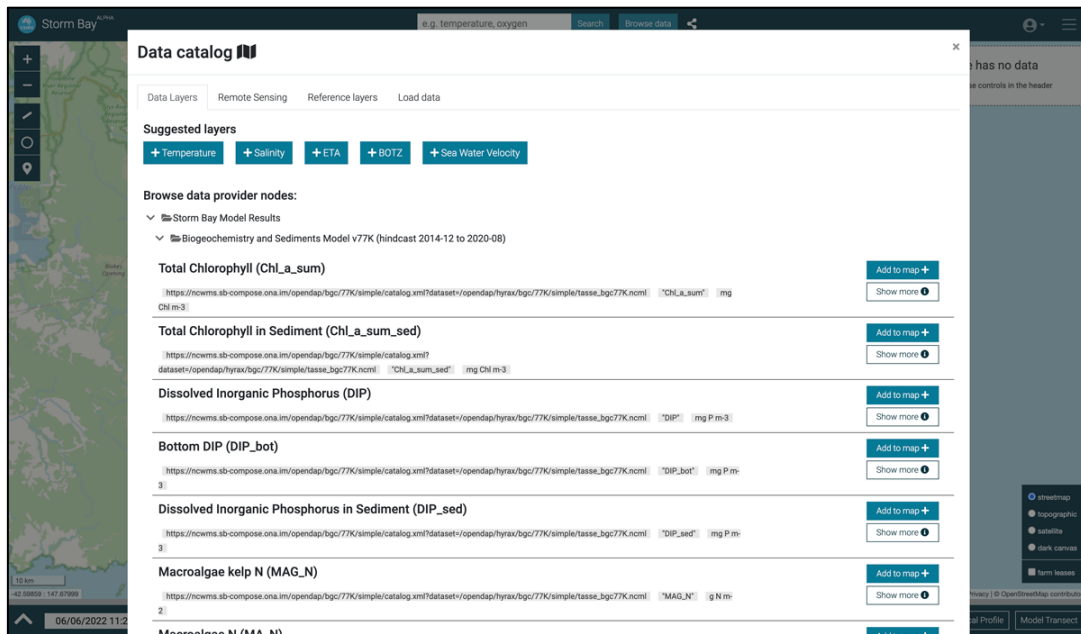
Figure 6.3: Browsing the data catalogue for model data.
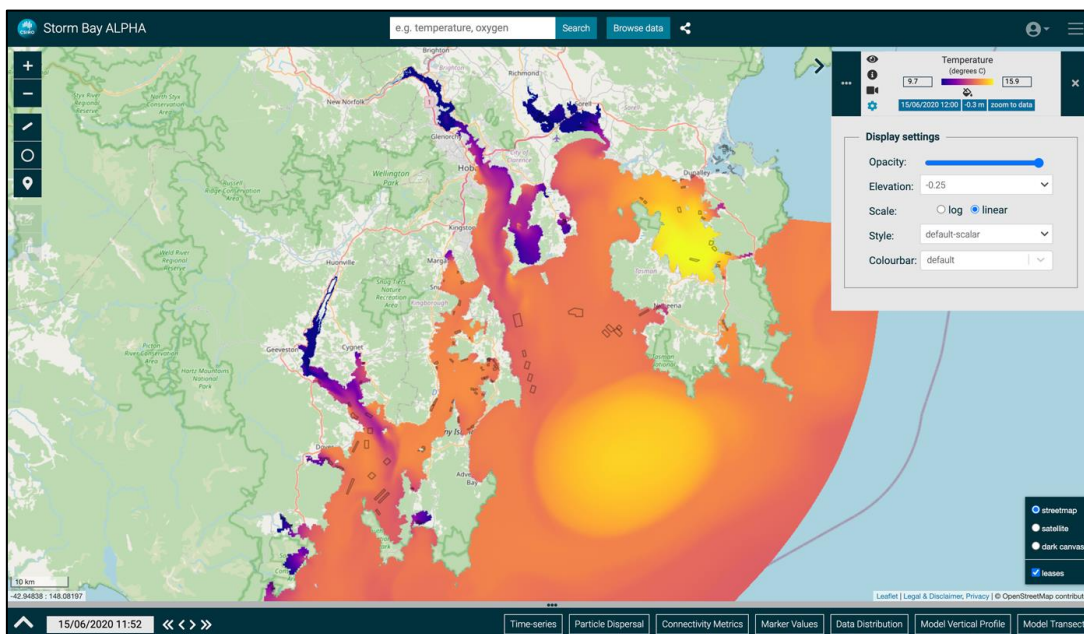
Figure 6.4: Example display of temperature data from the hydrodynamic model.

Add marker/s to map to view vertical profiles for one or more points/model variables (Figure 6.5).
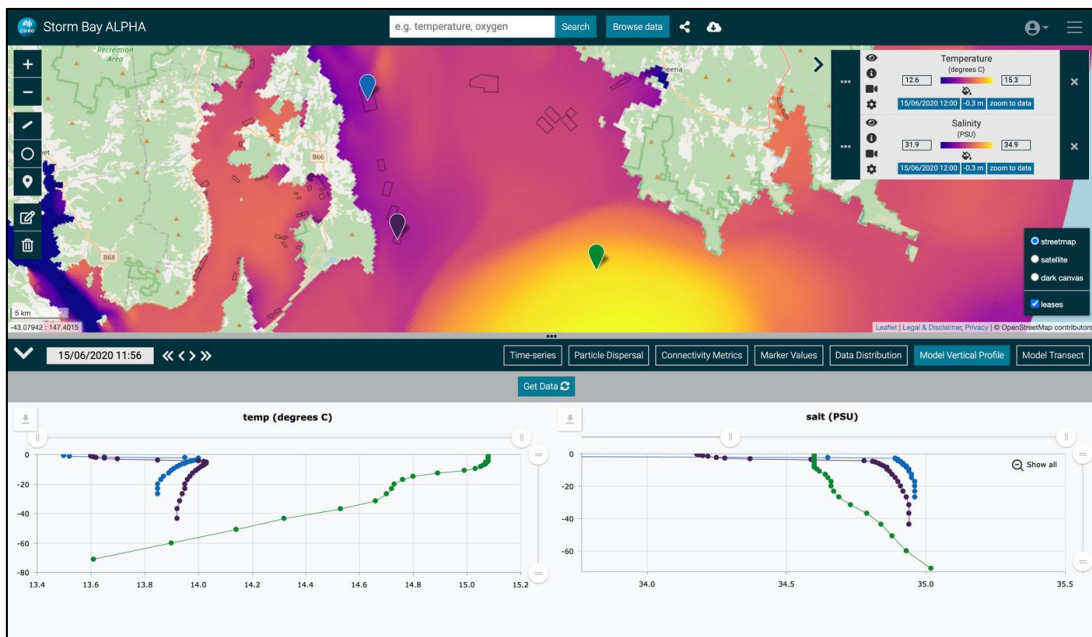
Figure 6.5: Vertical profiles of model temperature and salinity at three locations.

Draw a transect of interest to visualise model results along a path, for one or more model layers (Figure 6.6).
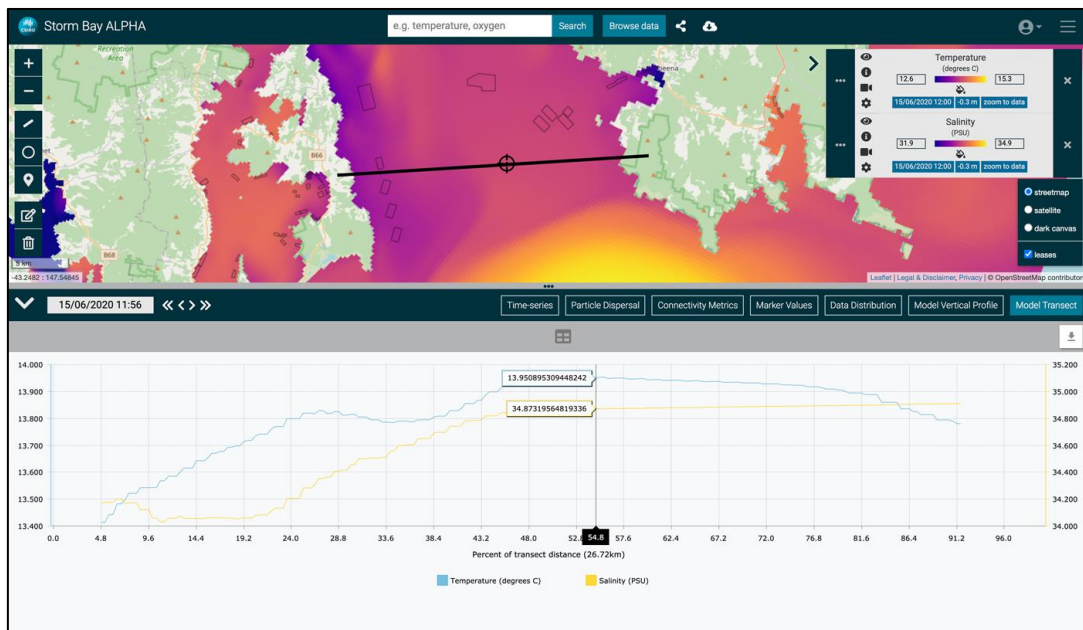
Figure 6.6: Transect of model temperature and salinity at -0.3m.

Add marker/s to a map to view the time-series for one or more points (Figure 6.7).
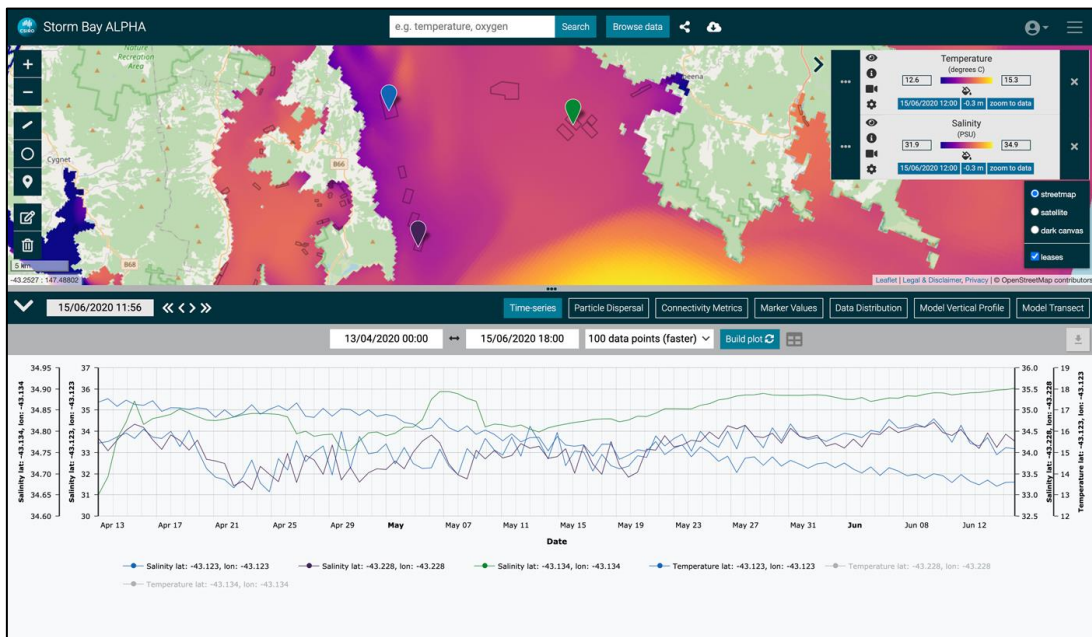
Figure 6.7: Time-series of model temperature and salinity at -0.3m for three locations.
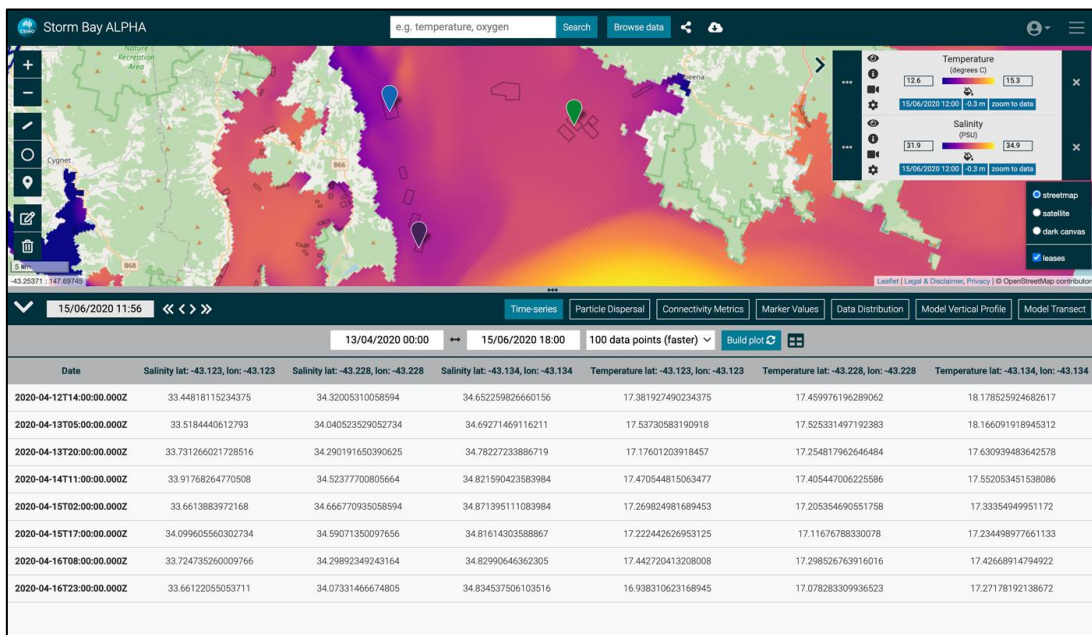
Figure 6.8: Time-series data viewed in a table; data export options include CSV, XLXS, PDF, etc. with support for annotation.

Integrated access to decision-support tools, such as particle dispersal simulations (Figure 6.9).
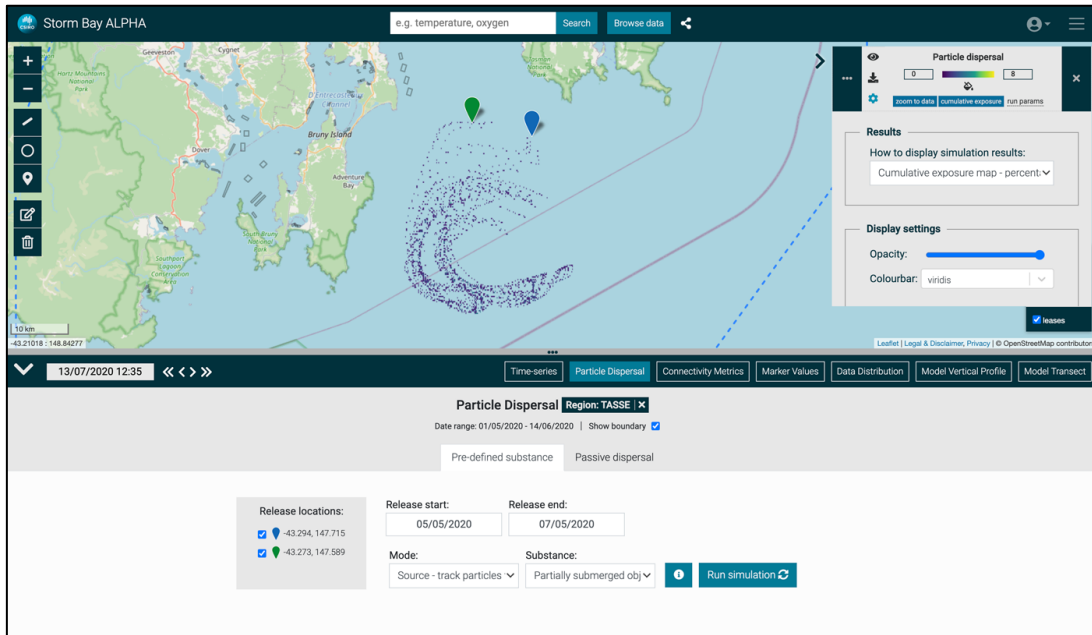
Figure 6.9: Particle dispersal simulation controls and an example visualisation of results.

The Model outputs page provides an at-a-glance overview of model results (Figure 6.10).
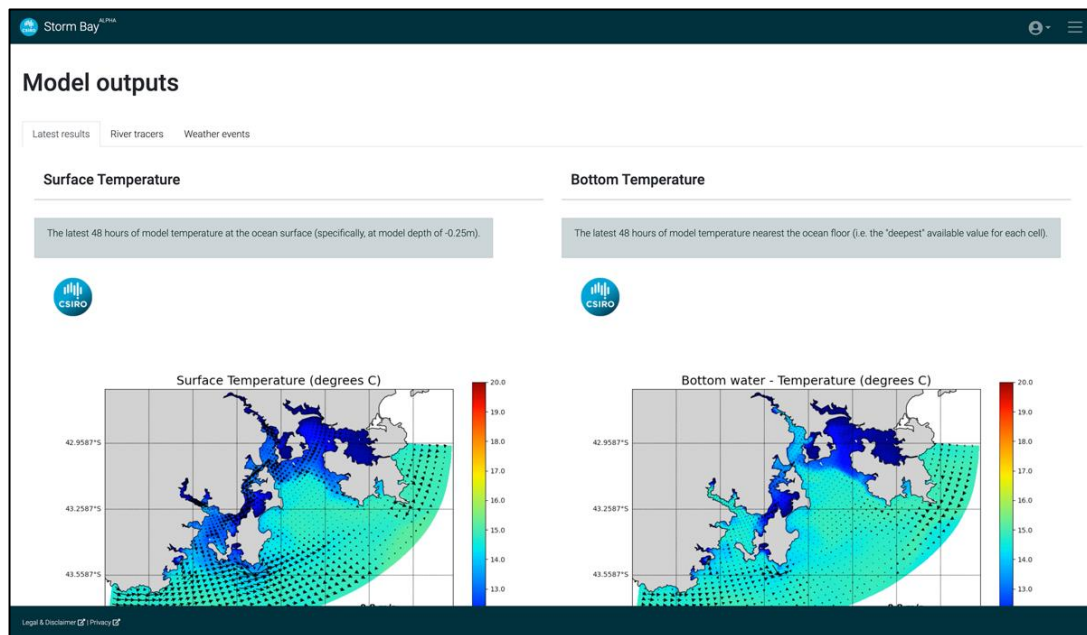
Figure 6.10: Example snapshots of latest model results, provided as animated MP4 movies.

The **Connectivity outputs** page similarly provides an at-a-glance overview for a variety of connectivity metrics (Figure 6.11).
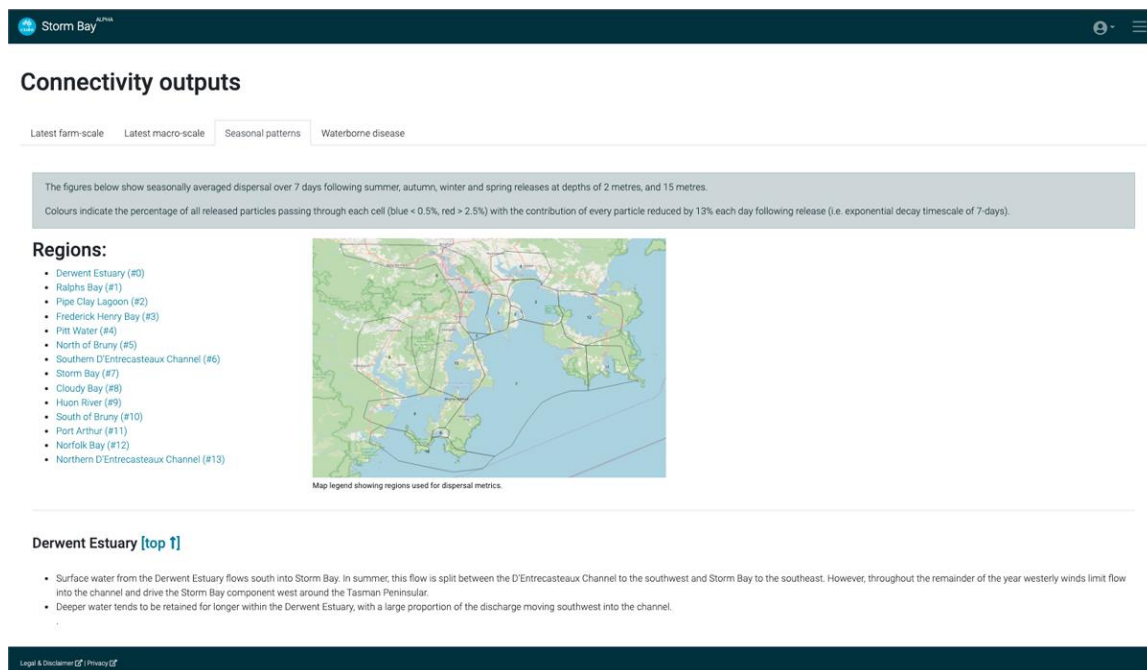
Figure 6.11: Summary of regional-scale seasonal connectivity patterns derived from TASSE hydrodynamic model.

The complimentary project: *Next generation decision support tools to support sustainable aquaculture in Storm Bay (FRDC project 2018-104)* will continue to generate additional layers of information for decision-makers, based on the outputs of this project:

- RECOM (Relocatable Coastal Model - https://recom.csiro.au – access valid Nov 2022) will integrate with hydrodynamic and biogeochemical outputs, extending the ability to perform fine-scale modelling in the Storm Bay region to identified expert users

- MAREE (Marine Ecological Emulator https://maree.csiro.au – access valid Nov 2022) will incorporate scenario outputs from the biogeochemical model into the emulator to provide rapid, ad-hoc assessments of nutrient load impacts

- CONNIE (Connectivity Modelling - https://connie.csiro.au – access valid Nov 2022) tool will leverage hydrodynamic model outputs to support enhanced particle tracking and connectivity modelling in the Storm Bay region

7   Project Communications

Project Publications

Langlais C, Herzfeld M, Griffin D, Wild-Allen K (2018) Assessment of the CSIRO Storm Bay Hydrodynamic Model Against Observations. FRDC 2017-215 Progress Report Work Package 1.1, CSIRO Oceans & Atmosphere, Hobart.

Langlais C, Schaeffer A, Legresy B, Herzfeld M, Wild-Allen K (2019) Summer Intrusions into Storm Bay. Australian Marine Science Association Conference, Poster Abstract, Perth, July 2019.

Langlais C, Schaeffer A, Legresy B, Herzfeld M, Wild-Allen K (2019) Summer Intrusions into Storm Bay. Australian Meteorological & Oceanography Society Annual Meeting, Poster Abstract, Darwin, June 2019.

Wild-Allen K, Andrewartha J, Beardsley J, Baird M, Eriksen R, Gregor R, Griffin D, Herzfeld M, Hughes D, Langlais C, Margvelashvili N, Martini A, Revill A, Rizwi F, Skerratt J, Schwanger C, Wild D. (2019) Storm Bay Biogeochemical Modelling and Information System. FRDC 2017-215 Technical Milestone Report March 2019. CSIRO Oceans & Atmosphere, Hobart.

Wild-Allen K, Gorton B (2019) Coastal Environmental Modelling in Storm Bay, Tasmania. CSIRO Information Sheet, June 2019.

Wild-Allen K, Andrewartha J, Beardsley J, Baird M, Eriksen R, Gregor R, Griffin D, Herzfeld M, Hughes D, Langlais C, Margvelashvili N, Martini A, Revill A, Rizwi F, Skerratt J, Schwanger C, Sherrin K, Frydman S, Wild D. (2019) Storm Bay Biogeochemical Modelling and Information System. FRDC 2017-215 Technical Milestone Report August 2019. CSIRO Oceans & Atmosphere, Hobart.

Wild-Allen K, Andrewartha J, Beardsley J, Baird M, Eriksen R, Gregor R, Griffin D, Herzfeld M, Hughes D, Langlais C, Margvelashvili N, Martini A, Revill A, Rizwi F, Skerratt J, Schwanger C, Sherrin K, Frydman S, Wild D. (2020) Storm Bay Biogeochemical Modelling and Information System. FRDC 2017-215 Technical Milestone Report August 2020. CSIRO Oceans & Atmosphere, Hobart.

Langlais C, Schaeffer A, Legresy B, Herzfeld M, Wild-Allen K (2021) Shelf break exchanges in South-East Tasmania and its impact on Storm Bay. Australian Meteorological & Oceanography Society online conference "Science for impact", Oral presentation 12 Feb 2021.

Wild-Allen K, Andrewartha J, Baird M, Beardsley J, Bodrossy L, Eriksen R, Gregor R, Griffin D, Herzfeld M, Hughes D, Langlais C, Margvelashvili N, Martini A, Revill A, Rizwi F, Skerratt J, Schwanger C, Sherrin K, Frydman S, Wild D. (2021) Storm Bay Biogeochemical Modelling and Information System. FRDC 2017-215 Technical Milestone Report February 2021. CSIRO Oceans & Atmosphere, Hobart.

Wild-Allen K (2021) Storm Bay biogeochemical modelling and information system: supporting sustainable aquaculture in Tasmania. CSIRO Information Sheet, June 2021.

Wild-Allen, K., Skerratt, J., Baird, M., Langlois, C. (2021) Quantifying the supply of nutrients to Storm Bay, southeast Tasmania, to evaluate the potential impact of expanding aquaculture on water quality. Abstract. Australian Marine Science Association Conference, July 2021.

Wild-Allen, K. (2021) Where the waters go – how rivers impact coastal water quality in southeast Tasmania. Abstract. Australian Water Association Conference, August 2021.

Wild-Allen K (2022) Storm Bay biogeochemical modelling and information system: supporting sustainable aquaculture in Tasmania. CSIRO Information Sheet v2, June 2022.

Wild-Allen, K., Skerratt, J., Baird, M., Langlois, C. (2022) Seasonal and interannual variation in nutrient supply to a coastal ecosystem with salmon aquaculture. Abstract. Australian Marine Science Association Conference, July 2022.

Wild-Allen, K., Skerratt, J., Baird, M., Langlois, C. (2022) Digital twin simulations distinguish anthropogenic nutrient impacts from natural variability in a complex coastal ecosystem with salmon aquaculture. Abstract. ECSA59 Conference, Estuarine Coastal Shelf Association, Spain, September 2022.

Meetings Attended

DATE	MEETING	TOPIC	TEAM MEMBERS
FEBRUARY 2019	Public Seminar and Stakeholder demonstration of SIMA platform	The SIMA Austral Project: integrated modelling, data services and decision support tools to improve the sustainability of salmon aquaculture in Chile	Karen Wild-Allen, Dan Wild, Farhan Rizwi
JUNE 2019	DPIPWE Marine Resources - Informal coffee room chat	Storm Bay field work & gliders	Andy Revill
JUNE 2019	Tasmanian Legislative Assembly (upper house)	Briefing on science being undertaken in Storm Bay to inform expansion of Salmon Farms	Karen Wild-Allen
JUNE 2019	'Our Waterway' The D'Entrecasteaux Channel and Huon Collaboration Mini Conference	Oral presentation 'Storm Bay Modelling and Information System'	Karen Wild-Allen & Jenny Skerratt
JULY 2019	Stakeholder dashboard workshop	Macquarie Harbour & Storm Bay project dashboards	Dan Wild, John Andrewartha, Karen Wild-Allen
JULY 2019	DPIPWE Salmon Biosecurity Working Group Presentation	Salmon Biosecurity	Karen Wild-Allen, Bec Gorton, Scott Condie
DECEMBER 2019	Storm Bay FRDC Steering Committee Meeting	Storm Bay expansion research program update meeting	Karen Wild-Allen
DECEMBER 2019	RECOM scenario meeting (UTAS)	Discussing draft locations for the demonstration RECOM model	Scott Condie, Bec Gorton
JANUARY 2020	Storm Bay Decision Support Tools (TASSAL)	Integration of modelling outputs, visualization, and decision support tools.	Bec Gorton, Dan Wild, Sven Dowideit
JANUARY 2020	RECOM scenario meeting (UTAS)	Discussing draft locations for the demonstration RECOM model	Scott Condie, Bec Gorton
JANUARY 2020	Storm Bay Decision Support Tools (EPA)	Integration of modelling outputs, visualization, and decision support tools.	Bec Gorton, Dan Wild

JANUARY 2020	Storm Bay Decision Support Tools (DPIPWE)	Integration of modelling outputs, visualization, and decision support tools.	Bec Gorton, Dan Wild, Sven Dowideit
JANUARY 2020	Storm Bay Decision Support Tools (HAC)	Integration of modelling outputs, visualization, and decision support tools.	Bec Gorton, Dan Wild
FEBRUARY 2020	Storm Bay Decision Support Tools	Integration of modelling outputs, visualization, and decision support tools.	Karen Wild-Allen, Farhan Rizwi, Dan Wild, Bec Gorton
APRIL 2020	Tasmanian Legislative Assembly (upper house)	Briefing on science being undertaken in Storm Bay to inform Salmon Inquiry	Karen Wild-Allen Alistair Hobday
APRIL 2020	Storm Bay Governance Committee	Update on project objectives and progress to date	Karen Wild-Allen
MAY 2020	Storm Bay Steering Committee	Update on project objectives and progress to date	Karen Wild-Allen
MAY 2020	Storm Bay Technical Advisory Group Meeting	Update on project objectives and progress to date	Karen Wild-Allen
JULY 2020	Storm Bay Decision Support Tools & IMAS Monitoring	Demonstration sub-regions for RECOM within Storm Bay	Karen Wild-Allen, Farhan Rizwi, Dan Wild, Bec Gorton
AUGUST 2020	Storm Bay Technical Advisory Group Meeting	Storm Bay expansion research program update meeting	Karen Wild-Allen
OCTOBER 2020	Storm Bay Decision Support Tools (TASSAL)	Integration of modelling outputs, visualization, and decision support tools.	Karen Wild-Allen, Bec Gorton, Scott Condie, Wendy Steel
OCTOBER 2020	Storm Bay Decision Support Tools (HAC)	Integration of modelling outputs, visualization, and decision support tools.	Karen Wild-Allen, Bec Gorton, Scott Condie, Farhan Rizwi, Dan Wild
OCTOBER 2020	Storm Bay Decision Support Tools (DPIPWE)	Integration of modelling outputs, visualization, and decision support tools.	Karen Wild-Allen, Bec Gorton, Scott Condie, Dan Wild
NOVEMBER 2020	Storm Bay Technical Advisory Group Meeting	Update on project objectives and progress to date	Karen Wild-Allen
NOVEMBER 2020	Storm Bay Governance Committee	Demonstration of 'Storm Bay Modelling and Information System'	Bec Gorton
DECEMBER 2020	International reviewers of BEMP	Modelling and observations to inform aquaculture management in Tasmania	Karen Wild-Allen
FEBRUARY 2021	Storm Bay Technical Advisory Group Meeting	Update on project objectives and progress to date	Karen Wild-Allen
FEBRUARY 2021	Australian Meteorological & Oceanography Society online conference	Oral presentation 'Shelf break exchanges in South-East Tasmania'.	Clothilde Langlais
APRIL 2021	Storm Bay Technical Advisory Group Meeting	Update on project objectives and progress to date	Karen Wild-Allen
JUNE 2021	Standing Committee on Agriculture and Water Resources	Inquiry into the Australian Aquaculture Sector	Karen Wild-Allen for CSIRO
JUNE 2021	FRDC & CSIRO media training	Preparation for Storm Bay Science Talks & media interviews	Karen Wild-Allen
JUNE 2021	FRDC Storm Bay Science Talks (incl. media interview with ABC)	Oral presentations of science achievements in project	Karen Wild-Allen, Mike Herzfeld, Mark Baird, Clothilde Langlais, Nugzar Margvelashvili, Dan Wild, Farhan Rizwi
JULY 2021	EPA & International reviewers of BEMP	Modelling and observations to inform aquaculture management in Storm Bay	Karen Wild-Allen

JULY 2021	Australian Marine Science Association Conference	Oral presentation 'Quantifying the supply of nutrients to Storm Bay'	Karen Wild-Allen
JULY 2021	Storm Bay Technical Advisory Group Meeting	Update on project objectives and progress to date	Karen Wild-Allen
AUGUST 2021	Beaker Street, TMAG Science Week	What happens to nutrients in coastal waters?	Karen Wild-Allen, Beth Fulton
AUGUST 2021	Australian Water Association Conference (incl. media interview with ABC)	Oral presentation 'Where the waters go – how rivers impact coastal water quality in southeast Tasmania'.	Karen Wild-Allen
SEPTEMBER 2021	EPA & DPIPWE Marine Farming	Definition of Storm Bay model scenarios	Karen Wild-Allen, Scott Condie
SEPTEMBER 2021	FRDC, CSIRO & UTAS	Salmonid Science Alliance meeting	
NOVEMBER 2021	Storm Bay Technical Advisory Group Meeting	Update on project objectives and progress to date	Karen Wild-Allen, Dan Wild
MARCH 2022	Storm Bay Technical Advisory Group Meeting	Update on project objectives and progress to date including Storm Bay model calibration	Karen Wild-Allen, Dan Wild
MARCH 2022	Storm Bay Steering Committee Meeting	Update on Storm Bay model calibration	Karen Wild-Allen
JUNE 2022	Storm Bay Technical Advisory Group Meeting	Update on project objectives and progress to date including model scenario results	Karen Wild-Allen, Dan Wild
JUNE 2022	Storm Bay Steering Committee Meeting	Update on model scenario results	Karen Wild-Allen
JUNE 2022	Environmental Open-House planning, communications & open house event. CSIRO & UTAS	Environmental Open-House	Karen Wild-Allen, Clothilde Langlais, Dan Wild, Jenny Skerratt, Ruth Eriksen, Scott Condie, Andrew Martini, Cassie Schwanger, Merinda McMahone

Project Websites

CSIRO Coastal Environmental Modelling Team - project summary

https://research.csiro.au/cem/projects/current-projects/storm-bay/ - access valid Nov 2022

Visualisation of recent glider mission:

http://www.marine.csiro.au/~bea195/glidervis/ - access valid Nov 2022

Storm Bay Modelling & Information System:

https://stormbaymodelling.csiro.au - access valid Nov 2022

8   References

Ariathurai, R., Krone, R. B., 1976. Finite element model for cohesive sediment transport. Journal of the Hydraulics Division, ASCE, 104, HY2, 323–328.

Bailey, J.E., Ollis, D.F., (1986) Biochemical engineering fundamentals. McGraw-Hill Book Company, New York, 984pp.

Baird, M. E., N. Cherukuru, E. Jones, N. Margvelashvili, M. Mongin, K. Oubelkheir, P. J. Ralph, F. Rizwi, B. J. Robson, T. Schroeder, J. Skerratt, A. D. L. Steven and K. A. Wild-Allen 2016. Remote-sensing reflectance and true colour produced by a coupled hydrodynamic, optical, sediment, biogeochemical model of the Great Barrier Reef, Australia: comparison with satellite data. Env. Model. Software 78: 79-96

Baird, M. E., Ralph, P. J., Rizwi, F., Wild-Allen, K. A., Steven, A. D. L., 2013. A dynamic model of the cellular carbon to chlorophyll ratio applied to a batch culture and a continental shelf ecosystem. Limnol. Oceanogr. 58, 1215-1226.

Baird, M. E., K. Wild-Allen, J. Parslow, M. Mongin, B. Robson, J. Skerratt, F. Rizwi, M. Soja-Woźniak, E. Jones, M. Herzfeld, N. Margvelashvili, J. Andrewartha, C. Langlais, M. Adams, N. Cherukuru, S. Hadley, P. Ralph, T. Schroeder, A. Steven, U. Rosebrock, L. Laiolo, M. Gustafsson, and D. Harrison (2020). CSIRO Environmental Modelling Suite (EMS): Scientific description of the optical and biogeochemical models (vB3p0). Geoscientific Model Development.13:4503-4553.

Blumberg, A.F., Herring, J. (1987) Circulation modelling using orthogonal curvilinear coordinates Nihoul, J.C.J. , Jamart , B.M. (Eds.), Three-Dimensional Models of Marine and Estuarine Dynamics, Elsevier

Buchanan, P.J., Swadling, K.M., Eriksen, R.S. et al. Rev Fish Biol Fisheries (2014) 24: 427. https://doi.org/10.1007/s11160-013-9312-z

Burchard, H., K., O. Peterson and T.P. Rippeth (1998) Comparing the performance of the Mellor Yamada and the k-? turbulence models. J. Geophys. Res., 103, 10,543 – 10,554.

Buschmann, A., Costa-Pierce, B.A., Cross, S., Iriarte, J.L.,.Olsen, Y., Reid, G. 2007. Nutrient impacts of farmed Atlantic Salmon (Salmo salar) on pelagic ecosystems and implications for carrying capacity. Report of the Technical Working Group (TWG) on Nutrients and Carrying Capacity of the Salmon Aquaculture Dialogue. https://www.researchgate.net/publication/282295533

Cherukuru, Nagur; Brando, Vittorio; Schroeder, Thomas; Clementson, Lesley; Dekker, Arnold. Influence of river discharge and ocean currents on coastal optical properties. Continental Shelf Research. 2014; 84:188–203. https://doi.org/10.1016/j.csr.2014.04.022

Cherukuru, Nagur; Davies, Peter; Brando, Vittorio; Anstee, Janet; Baird, Mark; Clementson, Lesley; et al. Physical oceanographic processes influence bio-optical properties in the Tasman Sea. Journal of Sea Research. 2016; 110:1-7. https://doi.org/10.1016/j.seares.2016.01.008

Clementson, L.A., Parslow, J.S., Turnbull, A.R., Bonham, P.I. 2004. Properties of light absorption in a highly coloured estuarine system in south-east Australia which is prone to blooms of the toxic

dinoflagellate Gymnodinium catenatum. Estuarine, Coastal and Shelf Science, 60 (1):101-112. https://doi.org/10.1016/j.ecss.2003.11.022.

Condie, S. A., and J. R. Dunn. 2006. Seasonal characteristics of the surface mixed layer in the Australasian region: implications for primary production regimes and biogeography. Marine and Freshwater Research 57:569-590.

CSIRO Coastal Environmental Modelling Team. 2018. CSIRO Environmental Modelling Suite: Scientific description of the optical, carbon chemistry and biogeochemical models. CSIRO Report, Hobart. [online access at https://research.csiro.au/cem/software/ems/].

Deines K.L. (1999) Backscatter estimation using Broadband acoustic Doppler current profilers. Proceedings of the IEEE Sixth Working Conference on Current Measurement (Cat. No.99CH36331). DOI: 10.1109/CCM.1999.755249

Duran, E.R., Phillips H.E, Furue R., Spence P., Bindoff N.L. (2020) Southern Australia Current System based on a gridded hydrography and a high-resolution model Progress in Oceanography, Volume 181, Article 102254

EPA (2021) Defaults Guideline Values for Aquativ Ecosystems, Oil Spill Response Atlas – Segment 80. EPA Tasmania, October 2021. www.epa.tas.gov.au.

EPA (2021) Defaults Guideline Values for Aquativ Ecosystems, Oil Spill Response Atlas – Segment 81. EPA Tasmania, October 2021. www.epa.tas.gov.au.

EPA (2021) Defaults Guideline Values for Aquativ Ecosystems, Oil Spill Response Atlas – Segment 93. EPA Tasmania, August 2021. www.epa.tas.gov.au.

Ebert, E. E. (2008) Fuzzy verification of high-resolution gridded forecasts: a review and proposed framework. Meteorol. Appl. 15, (51-64).

Egbert, G.D. and Erofeeva, S.Y. (2002) Efficient inverse modelling of barotropic ocean tides. Journal of Atmospheric and Oceanic Technology, 19(2), 183-204.

Grant, D., Madsen, O., 1982. Movable bed roughness in unsteady oscillatory flow. J. of Geophysical Research, V. 87, N C1, pp. 469-481.

Green G., Coughanowr C. (2003) State of the Derwent estuary 2003: a review of pollution sources, loads and environmental quality data from 1997-2003. Derwent Estuary Program, DPIWE, Tasmania.

Gartner J. (2004) Estimating suspended solids concentrations from backscatter intensity measured by acoustic Doppler current profiler in San Francisco Bay, California Marine Geology 211 (2004) 169 – 187.

Heller M.I., Wuttig K., Croot P.L. 2016. Identifying the Sources and Sinks of CDOM/FDOM across the Mauritanian Shelf and Their Potential Role in the Decomposition of Superoxide (O2-). Frontiers in Marine Science 3:132. https://www.frontiersin.org/article/10.3389/fmars.2016.00132

Herzfeld, M. (1997). The annual cycle of sea surface temperature in the Great Australian Bight. *Progress in Oceanography*, 39, *1-27*.

Herzfeld, M., 2006. An alternative coordinate system for solving finite difference ocean models. Ocean Modelling, 14, 174 – 196.

Herzfeld, M. (2015) Methods for freshwater riverine input into regional ocean models. Ocean Modelling, 90, 1-15.

Herzfeld, M., Andrewartha, J.R. (2012) A simple, stable and accurate Dirichlet open boundary condition for ocean model downscaling. Ocean Modelling, 43-44, 1-21.

Herzfeld, M., Engwirda, D., Rizwi, F. (2020) A coastal unstructured model using Voronoi meshes and C-grid staggering. Ocean Modelling, 148, 101599. https://doi.org/10.1016/j.ocemod.2020.101599

Hipsey, M.R., Gal, G., Arhonditsis, G.B., Carey, C.C., Elliott, J.A., Frassl, M.A., Janse, J. H., de Mora, L., Robson, B.J., June 2020. A system of metrics for the assessment and improvement of aquatic ecosystem models. Environ. Model. Software 128, 104697.

Horner-Devine, A.,R. D. Hetland, and D. MacDonald (2015), Transport and mixing in coastal river plumes, Annu. Rev. Fluid Mech., 47, 569– 594.

Jones, E.M., Oke, P.R., Rizwi, F., Murray, L.M. (2012), Assimilation of glider and mooring data into a coastal ocean model. Ocean Model., 47 , pp. 1-13.

Katarzyna, S., Tomczak, M. (1994) Subduction of central water near the Subtropical Front in the southern Tasman Sea. Deep Sea Res., 41, 1373-1386.

Kitaigorodskii, S.A., O.A. Kuznetsov and G.N. Panin (1973) Coefficients of drag, sensible heat and evaporation in the atmosphere over the surface of the sea. *Izv. Acad. Sci. USSR*

Kondo, J. (1975) Air-sea bulk transfer coefficients in diabatic conditions. Boundary-Layer Meteorology, 9, 91-112.

Langlais C, Herzfeld M, Griffin D, Wild-Allen K (2018) Assessment of the CSIRO Storm Bay Hydrodynamic Model Against Observations. FRDC 2017-215 Progress Report Work Package 1.1, CSIRO Oceans & Atmosphere, Hobart.

Large, W.G., and S. Pond (1981) Open ocean momentum flux measurements in moderate to strong winds, J. Phys. Oceanogr., 11, 324-336.

Leonard, B.P. (1991) The ULTIMATE conservative difference scheme applied to unsteady one-dimensional advection. Comp. Methods in Appl. Mech. and Eng., 19, 17 – 74.

Nechad, B; Ruddick, Kevin; Schroeder, Thomas; Oubelkheir, Kadija; Blondeau-Patissier, David; Cherukuru, Nagur; et al. CoastColour Round Robin datasets: a database to evaluate the performance of algorithms for the retrieval of water quality parameters in coastal waters. Earth Systems Science Data. 2015; 8:173–258. https://doi.org/10.5194/essdd-8-173-2015

Madsen, O.S., 1994. Spectral wave-current bottom boundary layer flows, in Coastal Engineering 1994 Proceedings, 24th International Conference Coastal Engineering Research Council/ASCE, pp. 384-398.

Margvelashvili, N. Y. (2009) Stretched Eulerian Coordinate Model of Coastal Sediment Transport. Computers and Geosciences. 35(6):1167-1176.

Margvelashvili, N., Saint-Cast, F., Condie, S., 2008. Numerical modelling of the suspended sediment transport in Torres Strait. Continental Shelf Research, 28, 2241-2256.

Margvelashvili, N., Andrewartha, J., Herzfeld, M., Robson, B. J., and Brando, V. E., (2013). Satellite data assimilation and estimation of a 3D coastal sediment transport model using error-subspace emulators: Environmental Modelling & Software, v. 40, p. 191-201.

Margvelashvili N., Andrewartha J., Baird M., Herzfeld M., Jones E., Mongin M., et al. (2018) Simulated fate of catchment-derived sediment on the Great Barrier Reef shelf. Marine Pollution Bulletin. 135:954-962.

Oke, P. R.; G. B. Brassington, D. A. Griffin, A. Schiller, 2008: The Bluelink ocean data assimilation system (BODAS), Ocean Modelling, 21(1-2), 46-70.

Oliver, E.C.J, Herzfeld, M., Holbrook , N.J., (2016) Modelling the shelf circulation off eastern Tasmania, Continental Shelf Research, 130, 14-33

Pilo, G. S., P. R. Oke, T. Rykova, R. Coleman, and K. Ridgway (2015), Do East Australian Current anticyclonic eddies leave the Tasman Sea?, J. Geophys. Res. Oceans, 120, 8099–8114, doi:10.1002/2015JC011026.

Puri, K., Dietachmayer, G., Steinle, P., Dix, M., Rikus, L., Logan, L., Naughton, M., Tingwell, C., Xiao, Y., Barras, V., Bermous, I., Bowen, R., Deschamps, L., Franklin, C., Fraser, J., Glowacki, T., Harris, B., Lee, J., Le, T., Roff, G., Sulaiman, A., Sims, H., Sun, X., Sun, Z., Zhu, H., Chattopadhyay, M., and Engel, C. (2012) Implementation of the initial ACCESS Numerical Weather Prediction system, Aust. Met. Oc. Journal, 63, 265-284.

Rees C, Pender L, Sherrin K, Schwanger C, Hughes P, Tibben S, Marouchos A, Rayner M. 2019. Methods for reproducible shipboard SFA nutrient measurement using RMNS and automated data processing. Limnol. Oceanogr.: Methods 17, 2019, 25–41

Ridgway, K. R. (2007), Seasonal circulation around Tasmania: An interface between eastern and western boundary dynamics, J. Geophys. Res., 112, C10016, doi:10.1029/2006JC003898.

Rintoul, S.R., Donguy, J.R., Roemmich, D.H. (1997) Seasonal variation of upper ocean thermal structure between Tasmania and Antarctica. Deep Sea Res., 44, 1185-1202.

Robson, B.J., Arhonditsis, G.B., Baird, M.E., Brebion, J., Edwards, K.F., Geoffroy, L., Hébert, M-P, van Dongen-Vogels, V., Jones, E.M., Kruk, C., Mongin, M., Shimoda, Y., Skerratt, J.H., Trevathan-Tackett, S., Wild-Allen, K., Kong, X., Steven, A. 2018. Towards evidence-based parameter priors for aquatic ecosystem modelling. Environmental Modelling & Software 100: 74-81

Roesler, CS, BarnardAH. 2013. Optical proxy for phytoplankton biomass in the absence of photophysiology: rethinking the absorption line height. Methods Oceanogr.,7(2013), pp.79-94,10.1016/j.mio.2013.12.003

Rykiel Jr., E.J., 1996. Testing ecological models: the meaning of validation. Ecol. Model. 90, 229–244.

Sigman, D. M. & Hain, M. P. (2012) The Biological Productivity of the Ocean. Nature Education Knowledge 3(10):21.

Simpson, J.J. and T.D. Dickey (1981) The relationship between downward irradiance and upper ocean structure. *Journal of Physical Oceanography*, 11, 309 - 323.

Sirabahenda Z., André St-Hilaire A., Courtenay S., and van den Heuvel M. (2019) Comparison of Acoustic to Optical Backscatter Continuous Measurements of Suspended Sediment Concentrations

and Their Characterization in an Agriculturally Impacted River Water 2019, 11, 981; doi:10.3390/w11050981

Skerratt, J., Mongin, M., Wild-Allen, K., Baird, M.E., Robson, B.J., Schaffelke, B., Soja-Woźniak, B., Margvelashvili, N., Davies, C.H., Richardson, A.J., Steven A.D.L. (2019) Simulated nutrient and plankton dynamics in the Great Barrier Reef (2011-2016). J. Mar. Syst., 192: 51-74.

Smagorinsky, J. (1963) General circulation experiments with the primitive equations, I. The basic experiment. Mon. Wea. Rev., 91, 99 – 164.

Smith, V.H., 1998. Cultural eutrophication of inland, estuarine and coastal waters. In: Pace, M.L., Groffman, P.M. (Eds.), Successes, Limitation and Frontiers in Ecosystem Science. Springer-Verlag, New York, pp. 7–49.

Stramma, L., Peterson, R.G., Tomczak, M. (1995) The South Pacific current. J. Phys. Oceanog., 25, 77-91.Stramski, D., M. Babin, S. B. Wozniak (2007) Variations in the optical properties of terrigenous mineral-rich particulate matter suspended in seawater. 52, 2418-2433.

Stramski, D., Babin, M. and Woźniak, S.B., 2007. Variations in the optical properties of terrigenous mineral-rich particulate matter suspended in seawater. *Limnology and Oceanography*, *52*(6), pp.2418-2433.

Swadling, K.M., Eriksen, R.S., Beard, J.M. and Crawford, C.M. Institute for Marine and Antarctic Studies, 2017, Salmon Sub-program: Marine currents, nutrients and plankton in the coastal waters of south eastern Tasmania and responses to changing weather patterns, Hobart, Tasmania, June. Final Report to FRDC, 86pp

Syzmanska, K., Tomczak, M. (1994) Subduction of central water near the subtropical front in the southern Tasman Sea. Deep Sea Research I, 41(9), 1373-1386. https://doi.org/10.1016/0967-0637(94)90103-1

Tartinville, B., Deleersnijder, E., Rancher, J. (1997) The water residence time in the Mururoa atoll lagoon: sensitivity analysis of a three-dimensional model. Coral Reefs, 16, 193 – 203.

Thomson P.G, Frampton D.M.F, Clementson L.A, Pattiaratchi C.B. Picophytoplankton: harbingers of change in our costal oceans. In Richardson A.J, Eriksen R, Moltmann T, Hodgson-Johnston I, Wallis J.R. (Eds). State and Trends of Australia's Ocean Report. doi: 10.26198/5e16a9dd49e7e

Volkman et al. (2009) A whole-of-ecosystem assessment of environmental issues for salmonid aquaculture. Aquafin CRC Project 4.2(2). http://frdc.com.au/Archived-Reports/FRDC%20Projects/2004-074-DLD.PDF

Wang, X., Olsen, L.M., Reitan, K.I., Olsen, Y. 2012. Discharge of nutrient wastes from salmon farms: environmental effects and potential for integrated multi-trophic aquaculture. Aquaculture Environment Interactions 2:267-283. Doi: 10.3354/aei00044

Wild-Allen, K. & Andrewartha, J. 2016. Connectivity between estuaries influences nutrient transport, cycling and water quality. Marine Chemistry 185:12-26. doi:10.1016/j.marchem.2016.05.011

Wild-Allen, K., Skerratt, J., Whitehead, J., Rizwi, F. and Parslow, J. 2013. Mechanisms driving estuarine water quality: a 3D biogeochemical model for informed management. Estuarine, Coastal & Shelf Science 135:33-45.

Willmott, C.J. (1981) On the validation of models. Phys. Geogr., 2, 184-194.

Zillman, J.W. (1972) A study of some aspects of the radiation and heat budgets of the southern hemisphere oceans. Bureua of meteorology, Meteorological study no. 26, Australian Govt. Pub. Service, Canberra.

9   Glossary

Abbreviation	
BEMP	Broadscale Environmental Monitoring Program
BGA	Blue-green algae sensor (senses phycoerythrin pigment, PE)
Bias	Bias refers to the tendency of a measurement process to over- or under-estimate the value of a population parameter
BoM	The Australian Bureau of Meteorology
CDOM	Chromophoric dissolved organic matter
Chl a	Chlorophyll-a
CTD	Conductivity Temperature Depth profiler
DEP	Derwent Estuary Program
DIN	Dissolved inorganic nitrogen (NH4 plus NOx)
DIP	Dissolved inorganic phosphorous
DO	Dissolved oxygen
DOC	Dissolved organic carbon
DON	Dissolved organic nitrogen
DPIPWE	Tasmanian government Department of Primary Industry, Parks, Water, and the Environment
EMS	Environmental modelling suite is the CSIRO hydrodynamic biogeochemical sediment wave optical model as a whole and in this study refers to the set up for TASSE Storm Bay model
EPA	Environment Protection Authority Tasmania
GHRSST	The group for high resolution sea surface temperature
HAC	Huon Aquaculture
IMOS	The Australian Integrated marine observing system
Kd(PAR)	Light attenuation coefficient
MAE	Mean absolute error
MAPE	Mean absolute percentage error
MODIS	Moderate Resolution Imaging Spectroradiometer
NH3	Ammonia
NOx	Nitrate plus nitrite
NRE	Department of Natural Resources and Environment Tasmania
NTU	Nephelometric Turbidity Unit
ORP	Oxidation-reduction potential
PRAWLER	McLane Labs Profiling Crawler
RMSE	Root mean square
SST	Sea surface temperature
TSS	Total suspended solids
WQ	Water quality

10 Appendices

The following appendices are provided in a 2nd document.

10.1 A.1 Data agreements

Data Owner	Data Variables	Conditions of Use	Is data directly (unmodified) available in model output? In reports?
BoM: meteorology	ACCESS Wind	Commercial agreement (negotiated for CSIRO by Ag & Food)	No, data is Interpolated in time & space
Hydro & NRE river flow	River flow	Hydro data use agreement. NRE Disclaimer and Use Conditions Whilst NRE has made every attempt to ensure the accuracy and reliability of the data provided, it is the responsibility of the data user to make their own decisions about the accuracy, currency, reliability and correctness of information provided. The Department of Natural Resources and Environment Tasmania, its employees and agents, and the Crown in the Right of the State of Tasmania do not accept any liability for any damage caused by, or economic loss arising from, reliance on this information. Data shown in these products includes real-time data from automated telemetry systems and has not been checked or quality controlled. The data displayed may be incorrect due to instrumentation failures. Data has quality codes associated with it. These codes indicate the level of accuracy that NRE has assigned to each Datum.	No & Yes
Raw data from NRE, Hydro, CSIRO, Geoscience Australia, Aus hydrographic office	Bathymetry	The model bathymetry is fit for the purpose of modelling Storm Bay. [probably not suitable for navigation, etc]	No, data is Interpolated in space
CSIRO/BoM: OceanMaps/Bran	Temperature, salinity, sea level, current velocities	Commercial agreement (negotiated for CSIRO by Ag & Food)	No & no
NRE & EPA: Monitoring and observations (Rivers loads gained from catchment reports)	Nutrient chlorophyll TSS secchi & other variables	<u>Provision of southern region broadscale environmental monitoring programs (BEMPs) water quality data</u> A. Reason for data transfer The BEMPs water quality data will be provided to you on the understanding that it will be used exclusively by CSIRO to hindcast/calibration of the biogeochemical model as well as envisaged near-real-time forecasting, including (but not limited to) use in the specific FRDC-funded Project entitled "2017-215: Storm Bay Biogeochemical Modelling & Information System: Supporting sustainable aquaculture expansion in Tasmania". B. Conditions of transfer	No and yes

		1. The data is provided for your use as defined in the 'reason for data transfer' above, and shall be held in strict confidence except as allowed for under the 'reason for data transfer'. The raw data is not to be transferred to other parties without prior permission from the EPA. 2. The dataset is not to be made publicly available without the approval of the data owners, noting that EPA is a custodian of the dataset but may not be the owner of the data itself. 3. This data is also provided to you on the basis that you understand and accept the following disclaimer: *As the EPA does not warrant that the data is free of errors or defects, the receiver of this data releases the EPA from all liability whether in contract or tort arising from any defects and errors in the data. No warranty condition undertaking or term expressed or implied statutory or otherwise as to the condition quality performance merchantability or fitness for purpose of the data is given or assumed by the EPA and all such warranties conditions undertakings and terms are hereby excluded, The receiver of the data agrees to indemnify the EPA against all loss, actions, proceedings, costs, claims, and damages caused or contributed to by any selling or trading in the data or outputs, any combination of the data, or any reliance by third parties on advice given by the receiver of the data derived in whole or part from information obtained by the receive*	
TasWater: STP loads as for NRE & EPA: above	average flow (ML/month) and ~ monthly values (mg-N/l) for NHx BOD5 NOx TN TP TSS	as for NRE & EPA: above	
Nystar: Industry load	Nutrient loads from outfall pipe (mg-N/l) NHx TN TP "TSS NFR non filterable residue	Not required except as bounded by the EPA agreement	Loads or concentrations are not available in model output, but they can be observed in the model if industry components are higher than the background marine waters. In reports they are available in summary plots
Norske Skog: Industry load	Nutrient loads from outfall pipe (mg-N/l) NHx NOx Dissolved Reactive P (aka model DIP) TSS Total N Total P	Not required except as bounded by the EPA agreement	As for Nystar
NRE: Fish farm loads	Salmon feed used at Tassal & HAC leases in SE Tas for 2014 - present	This dataset has been supplied to the Commonwealth Scientific and Industrial Research Organisation (CSIRO) as commercial in confidence (CIC), with the sensitivities of this dataset identified as significant and which has been identified by each entity providing the raw (source) data. This dataset has been supplied solely for use in Storm Bay Biogeochemical Modelling & Information System project. Access to this dataset	As for Nystar

		is to be restricted to the Storm Bay Biogeochemical Modelling & Information System project team, with the dataset to be stored by the CSIRO in a secure location (e.g. secure data server). This data is not to be provided to any other person or other organisation (i.e. any third party) without the prior written approval of the Director, Environment Protection Authority. Please ensure that all individuals having access to this dataset are made aware of the conditions under which the dataset has been supplied. Prior to the release of any publication or report to which this dataset has contributed, you are required to inform the Director, Environment Protection Authority accordingly and provide a draft of the report for review. Disclaimer: While the Department of Natural Resources and Environment Tasmania (NRE) believes the information supplied in this dataset to be reliable, error remains a possibility. Therefore, NRE does not guarantee the accuracy, completeness, timeliness, or correct sequencing of the information. The NRE shall not be responsible for any errors or omissions, or for the use of or results obtained from the use of this information.	
DEP: DEP monitoring data	Monthly monitoring data in Derwent Estuary	*Clearly acknowledge the Derwent Estuary Program as the data source and cite data use in your references as "Derwent Estuary Program"* [year] *", Ambient Water Quality monitoring data. Comma separated values datafile, Splashback.".* *Use the data only for the* CSIRO biogeochemical model in Storm Bay (TAASE); Nutrients from New Norfolk are used to force the model nutrients etc and all other sites are used to compare against the model results. There will be reports and presentations to *Fisheries* Research and Development Corporation fish farmers and public domain. There will be published papers in referred journals. *Hold the data in strict confidence and do not transfer or divulge the data or any part thereof (including interpretations) to other parties in any manner howsoever without the prior written consent of the Derwent Estuary Program.* *Provide the Derwent Estuary Program with copies of any resultant outputs. We recognise that some data requests come from consultants who are working for others. We provide this data on the proviso that your employer permits access to the resultant reports.*	No & yes
Tassal: monitoring data		Used data bound by the NRE EPA: above agreement	
HAC: monitoring data	Monthly water quality data at sites in Storm Bay & Norfolk Bay ADCP current profile data Wave Rider buoy data Profiling data at a number of leases	CSIRO is permitted to use the Data for the research project "Storm Bay Model & Information System" including publishing Data aggregates and statistical analysis in project publication and presentations. CSIRO must securely store all data made available to the project Use the data only for the purposes of advancing the project "Storm Bay Model & Information System" Provide draft figures & tables that include the Data to HAC for approval prior to publication or presentation (including project meetings & reports) Valid from 17/5/2019 to 17/5/2024	No & yes

CSIRO: Storm Bay Project data	Glider, & mooring data	Data collected within FRDC Storm Bay project available by request to steering committee. FRDC to be informed & acknowledged prior to publication	No & yes
IMOS: monitoring data	Storm Bay Gliders, John Church mooring, PRAWLER & WireWalker, OceanCurrents	Users of IMOS data are required to clearly acknowledge the source material by including the following statement: Data was sourced from Australia's Integrated Marine Observing System (IMOS) – IMOS is enabled by the National Collaborative Research Infrastructure Strategy (NCRIS). It is operated by a consortium of institutions as an unincorporated joint venture, with the University of Tasmania as Lead Agent.	No & yes
MNF data from IN2020_V10	underway data, CTD data, hydrochemistry, Triaxus data	The MNF complies with the Australian Government Public Data Policy by ensuring that Data acquired through the MNF is publicly available and accessible to the research community. The MNF must be acknowledged in all outputs derived from Data and/or Samples collected by, or with support from, the MNF. By accessing Data or collecting Samples with the support of the MNF, individuals acknowledge that: they will comply with the MNF Data and Samples Management Policy they will acknowledge the MNF in outputs with a statement adhering to the following form: "We acknowledge the use of the CSIRO Marine National Facility - grid.473585.8 - in undertaking this research." MNF has adopted a Global Research Identifier Database (GRID) persistent identifier to help to ensure the MNF is consistently referenced and described globally. GRID is a free, openly accessible database of research institution identifiers. Acknowledgment and citations should be in all forms of publication including presentations (where the acknowledgement should be on the closing slide), journals, books, reports and related research outputs.	No & yes
NASA's EOSDIS Global Imagery Browse Services.	Global remote sensing imagery	Falls under NASA's Open Data Policy, however, they "…ask that users who make use of GIBS in their clients or when referencing it in written or oral presentations to add the following acknowledgment: *We acknowledge the use of imagery provided by services from NASA's Global Imagery Browse Services (GIBS), part of NASA's Earth Observing System Data and Information System (EOSDIS).* For more details on policy, see: https://www.earthdata.nasa.gov/earth-science-data-systems-program/policies - access valid Nov 2022	No

10.2   A.2 Project datasets, storage and access

Project generated datasets

Dataset	Variables	Storage/Access	Status	Owner

Hydrodynamic model hindcast H1p5 (2014-12 to 2020-12)& NRT (2014-12 onwards)	Currents, T, S, Sea level	CSIRO Storm Bay Modelling & Information System	Available	CL
Sediment model hindcast (2018-01 to 2019-11) & NRT (2019-11 onwards)	Waves, Sediments	CSIRO Storm Bay Modelling & Information System	Available	NM
Biogeochemical model hindcast (2014-12 to 2020-08) & NRT (2020-08 onwards)	Oxygen, Chl, NO3, NH4, DIP, Turbidity, PAR	CSIRO Storm Bay Modelling & Information System	Available	KWA
Storm Bay scenario simulations (2015-01 to 2019-12)	Oxygen, Chl, NO3, NH4, DIP, Turbidity, PAR	CSIRO Storm Bay Modelling & Information System	Can be made available	KWA
Glider data from 6 missions	T, S, Oxygen, Chl, CDOM, NO3	CSIRO	Ready for repository	KWA
Benthic lander data from 5 deployments	Currents, T, S, Pressure, Chl, Oxygen, CDOM, NO3, Turbidity	CSIRO	Ready for repository	KWA
Storm Bay process study surveys	T,S, DO, chl a, nutrients, pigments, phytoplankton[3], TSS, sediment organic carbon and total N,	CSIRO AODN SRS Bio-optical database	Ready for repository	EB

---

[3] Phytoplankton will be available via Australian Ocean Data Network

Dataset	Variables	Storage	Status	Owner
	stable isotopes, genomics)			
CSIRO NRT sensor datasets (2018-12 to present)	T, S, Cond., Pressure, Chl, Oxygen, BGA-PE, pH, ORP, Turbidity	CSIRO Storm Bay Modelling & Information System	Available	Jack Beardsley

Other data sets of interest to the project

Dataset	Variables	Storage	Status	Owner
IMOS profiling mooring deployments	T, S, Oxygen, NO3, Chl	IMOS	Data sent to IMOS	PJ
Investigator voyage IN2020_V10	Currents, T, S, Pressure, Chl, Oxygen, NO3, Turbidity, Plankton[1]	CSIRO AODN SRS Bio-optical database	Data with MNF	MNF
Frohlich fellow resuspension study	Currents, Turbidity, Nutrients, Microbes	CSIRO	Ready for repository; should be deposited together with the in situ Storm Bay genomics data ('Storm Bay Process studies')	LB
Connectivity matrices (2015-01 onwards)	ISAV, POMV	CSIRO		Scott Condie
NASA Global Imagery Browse Services (2002-09 onwards)	MODIS True Colour, VIIRS True Colour, GHRSST, MODIS Chl	NASA	Available	NASA (EOSDIS)

10.3   A.3 Wave model comparison

To ascertain an impact of the refined wave model (SWAN) on the sediment transport, two scenarios with different wave forcing were simulated. The first scenario simulates sediment resuspension in Storm Bay enhanced by the fine-resolution SWAN model. Another scenario simulates sediment resuspension enhanced by the coarse-resolution BoM Auswaves model. Since Auswaves does not resolve river channels and fine-scale coastal features, wave fields predicted by Auswaves in open coastal waters have been interpolated inland (using interpolation routines built into the EMS modelling system). Figures A3.2 – A3.4 illustrate time series of the simulated wave

amplitude (half of the significant wave height), bottom shear velocity and suspended sediment concentration at a number of locations across the Storm Bay. Spatial snapshots of the same variables are shown in Figures A3.5 – A3.7. These data indicate a close agreement between scenarios based on fine-resolution SWAN and coarse-resolution Auswaves models in open waters of Storm Bay and significant discrepancies between these scenarios in constrained coastal areas and inside an inland lagoons and river channels - areas unresolved by Auswaves.
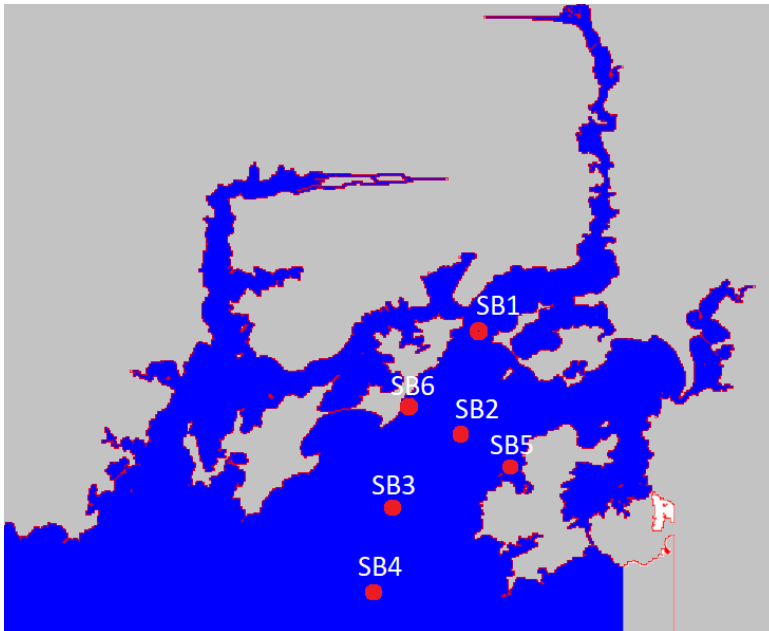
Figure A3.1 Location map for a Swan vs Auswaves evaluation experiment. The model grid is depicted in the index space.
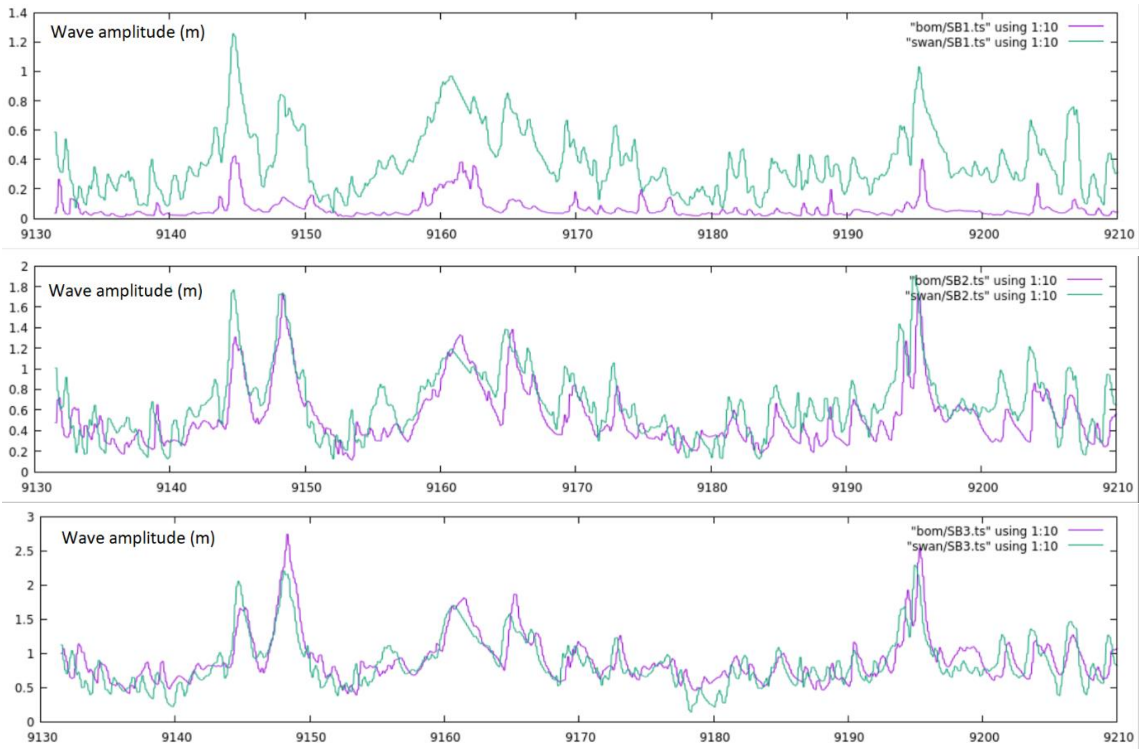
Figure A3.2a Wave amplitude predicted by Auswaves and Swan models at different locations in Storm Bay (see location map in Figure A3.1). Horizontal scale shows days since 01.01.1990.
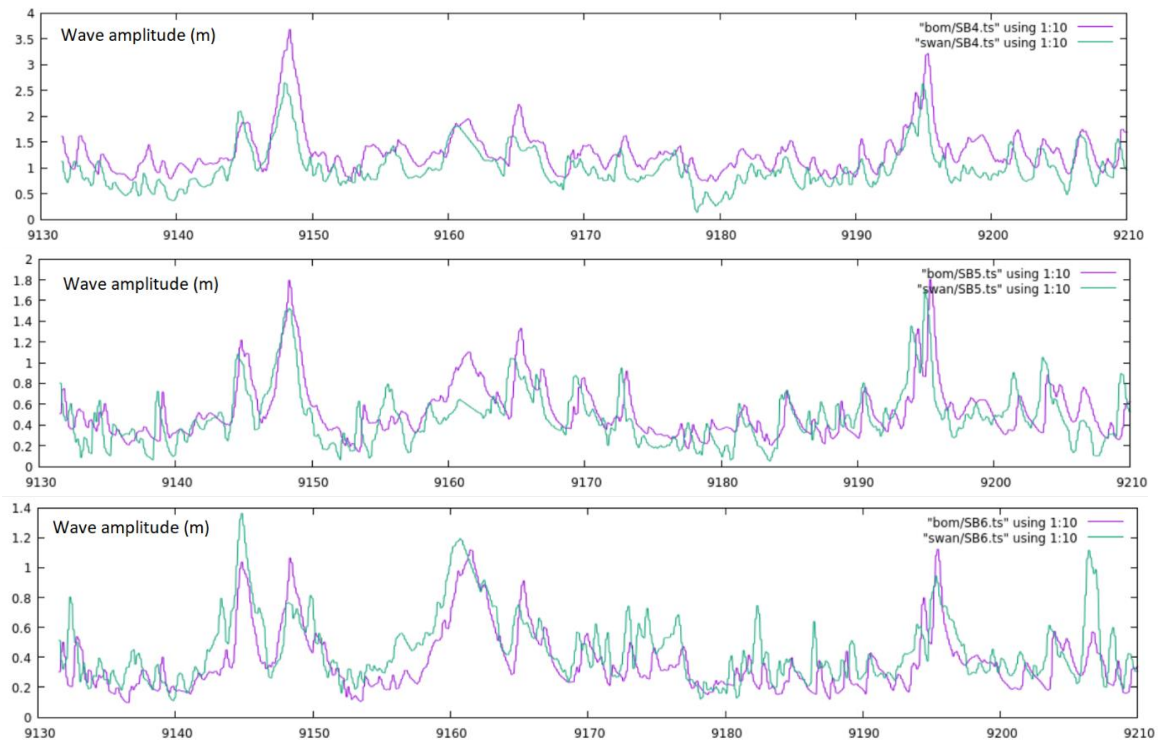
Figure A3.2b Wave amplitude predicted by Auswaves and Swan models at different locations in Storm Bay (location map in Figure A3.1) Horizontal scale shows days since 01.01.1990.
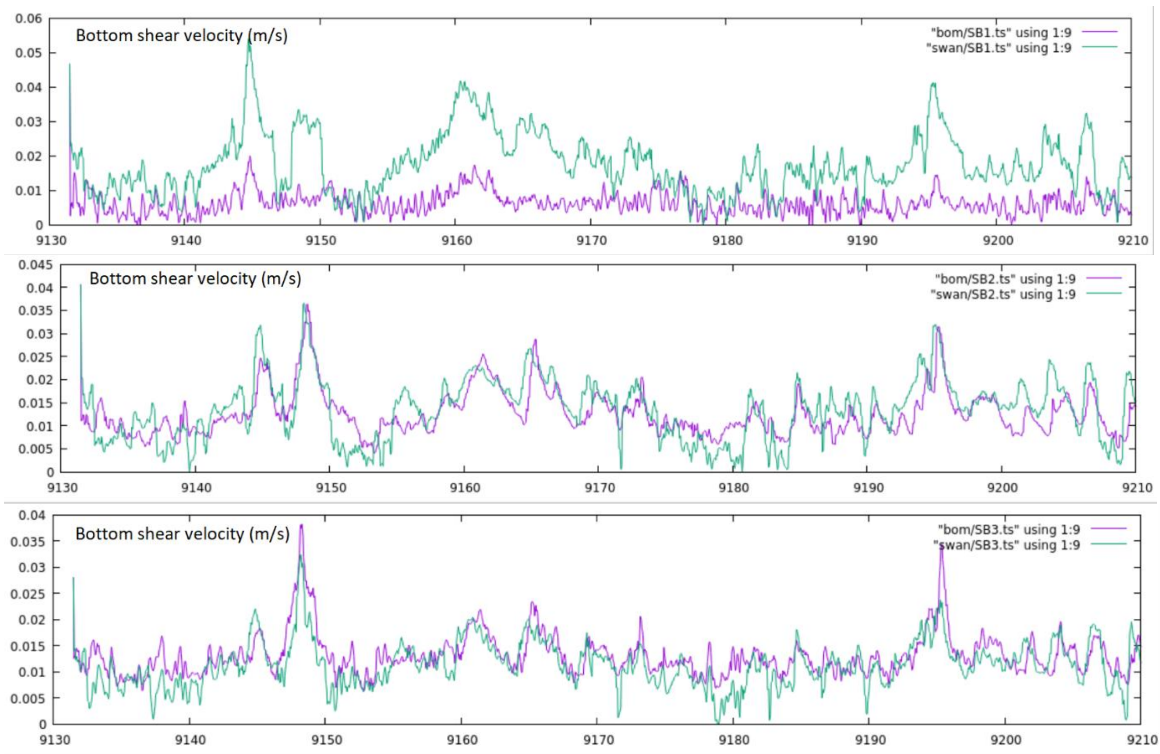
Figure A3.3a Bottom shear velocity simulated by the sediment transport mode driven by either Auswaves (BoM) or Swan waves (location map in Figure A3.1). Horizontal scale shows days since 01.01.1990.
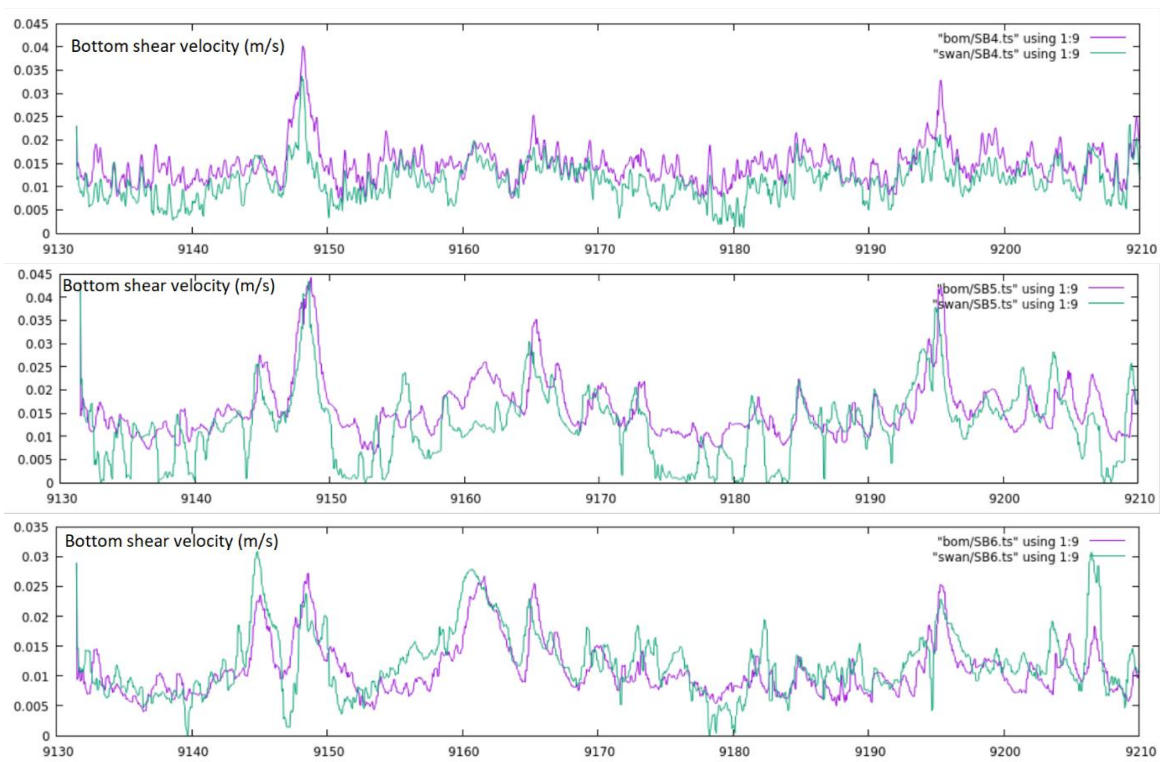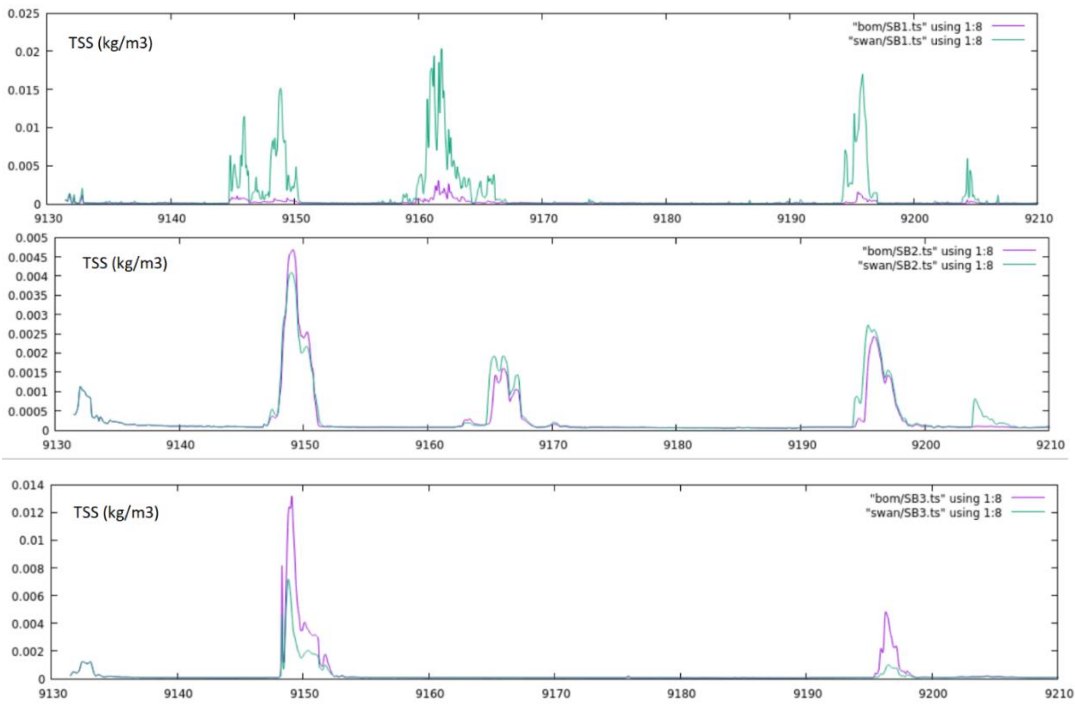

Figure A3.3b Bottom shear velocity simulated by the sediment transport mode driven by either Auswaves (BoM) or Swan waves (location map in Figure A3.1). Horizontal scale shows days since 01.01.1990.
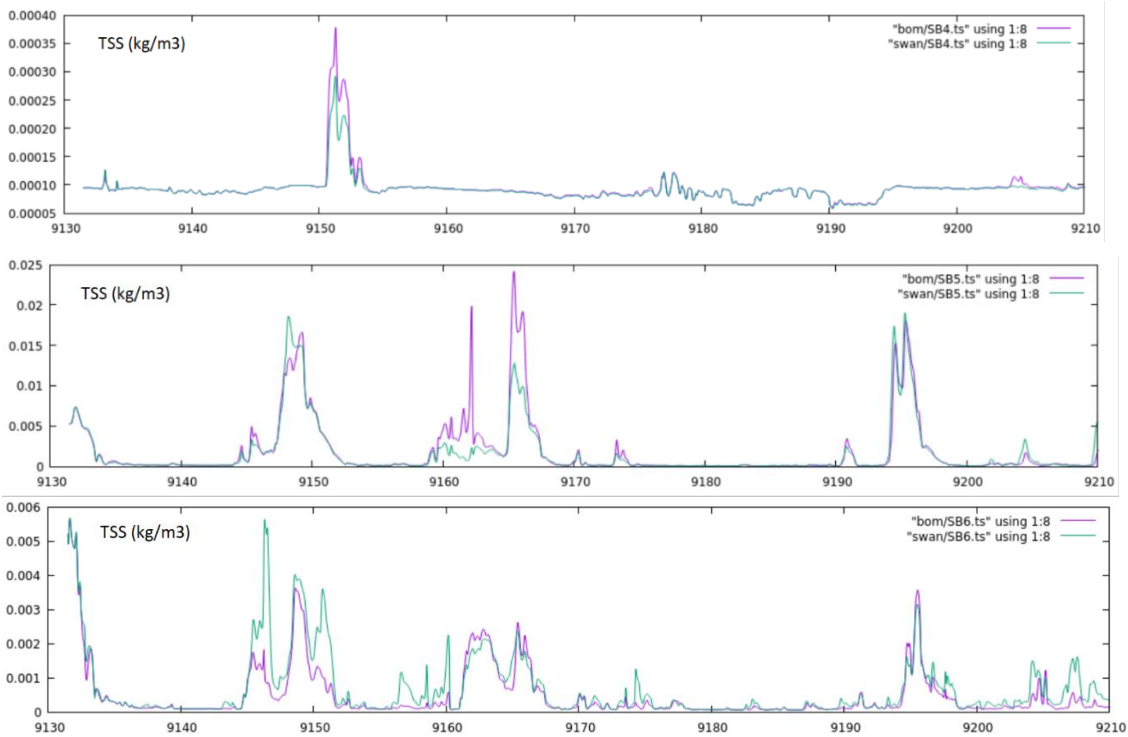
Figure. A3.4a Surface TSS simulated by the sediment transport mode driven by either Auswaves (BoM) or Swan waves (location map in Figure A3.1). Horizontal scale shows days since 01.01.1990.

Figure. A3.4a Surface TSS simulated by the sediment transport mode driven by either Auswaves (BoM) or Swan waves (location map in Figure A3.1). Horizontal scale shows days since 01.01.1990.
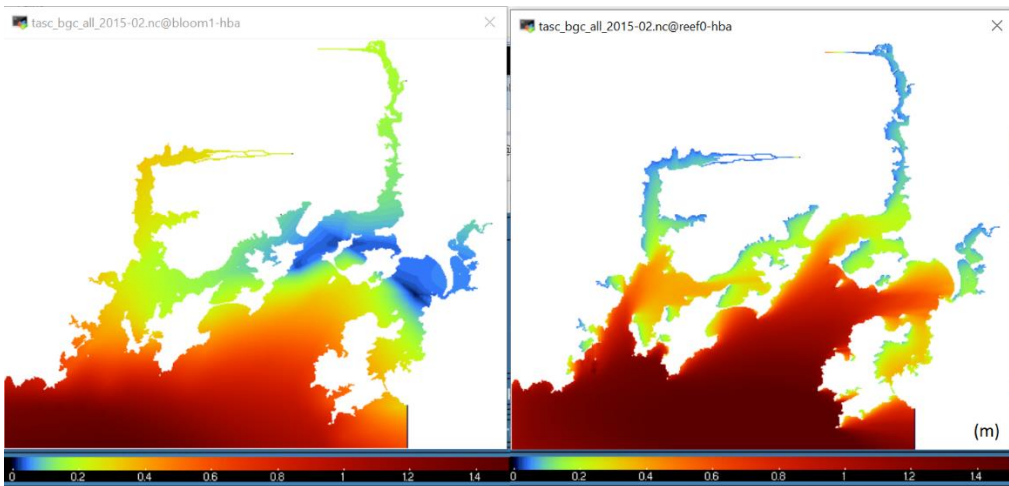
Figure A3.5 A snapshot of wave amplitude simulated by Auswaves and then interpolated inland (left) and simulated by Swan (right). The model grid is depicted in the index space.
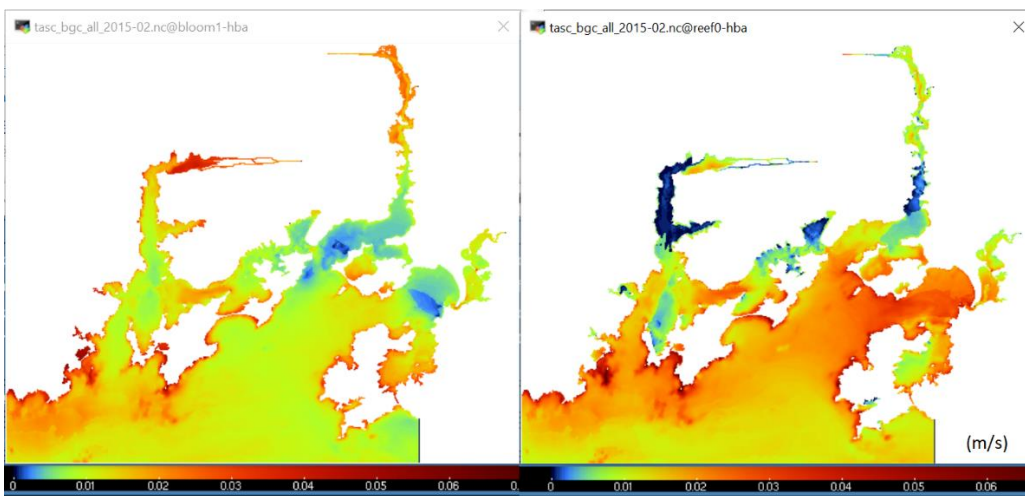

Figure A3.6 A snapshot of simulated bottom shear velocity. Auswaves (left) and Swan(right). The model grid is depicted in the index space.
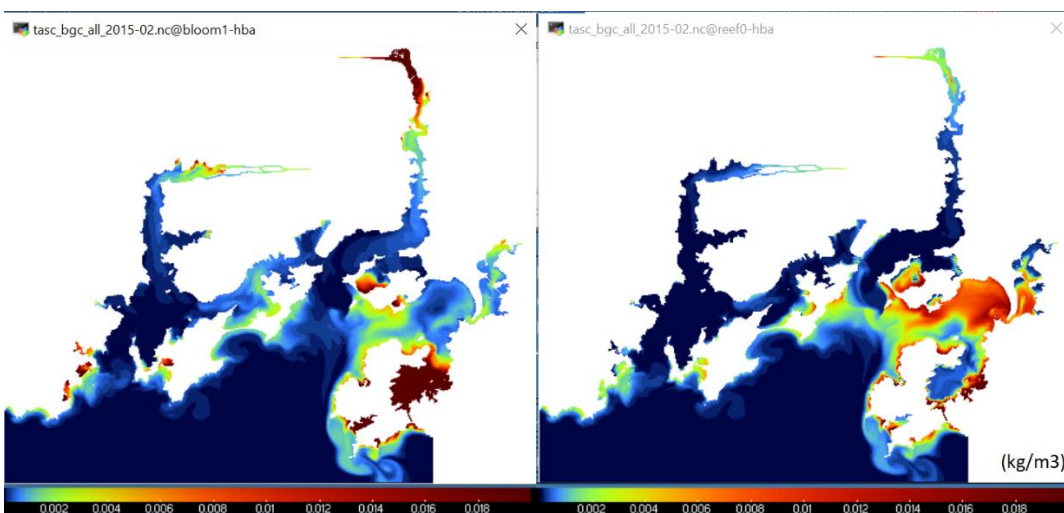

Figure A3.7 A snapshot of simulated surface TSS. Auswaves (left) and Swan (right). The model grid is depicted in the index space.

10.4 A.4 Storm Bay biogeochemical model parameters and initialisation

This appendix is provided in the supporting document of Appendices as:

Wild-Allen, K., et al., 2022 *Storm Bay Biogeochemical Modelling and Information System: supporting sustainable aquaculture in Tasmania (FRDC 2017-215) Final Report Appendices Part 1*. CSIRO Oceans & Atmosphere, Hobart, March 2023.

10.5 A.5 Biogeochemical model vs glider data including statistics

This appendix is provided in the supporting document of Appendices as:

Wild-Allen, K., et al., 2022 *Storm Bay Biogeochemical Modelling and Information System: supporting sustainable aquaculture in Tasmania (FRDC 2017-215) Final Report Appendices Part 1*. CSIRO Oceans & Atmosphere, Hobart, March 2023.

10.6 A.6 Biogeochemical model vs monitoring data including statistics

This appendix is provided in the supporting document of Appendices as:

Wild-Allen, K., et al., 2022 *Storm Bay Biogeochemical Modelling and Information System: supporting sustainable aquaculture in Tasmania (FRDC 2017-215) Final Report Appendices Part 1*. CSIRO Oceans & Atmosphere, Hobart, March 2023.

10.7 A.7 Biogeochemical model results and analysis

This appendix is provided in the supporting document of Appendices as:

Wild-Allen, K., et al., 2022 *Storm Bay Biogeochemical Modelling and Information System: supporting sustainable aquaculture in Tasmania (FRDC 2017-215) Final Report Appendices Part 2*. CSIRO Oceans & Atmosphere, Hobart, March 2023.

10.8 A.8 Scenario simulation results and analysis

This appendix is provided in the supporting document of Appendices as:

Wild-Allen, K., et al., 2022 *Storm Bay Biogeochemical Modelling and Information System: supporting sustainable aquaculture in Tasmania (FRDC 2017-215) Final Report Appendices Part 2*. CSIRO Oceans & Atmosphere, Hobart, March 2023.

AT CSIRO, WE DO THE
EXTRAORDINARY EVERY DAY

We innovate for tomorrow and help
improve today – for our customers, all
Australians and the world.

Our innovations contribute billions of
dollars to the Australian economy
every year. As the largest patent holder
in the nation, our vast wealth of
intellectual property has led to more
than 150 spin-off companies.

With more than 5,000 experts and a
burning desire to get things done, we are
Australia's catalyst for innovation.

CSIRO. WE IMAGINE. WE COLLABORATE.
WE INNOVATE.